

AGARD-R-686

AGARD-R-686

# AGARD

ADVISORY GROUP FOR AEROSPACE RESEARCH & DEVELOPMENT

7 RUE ANCELLE 92200 NEUILLY SUR SEINE FRANCE

AD A 077 420

AGARD REPORT No. 686

## Special Course on Acoustic Wave Propagation

NORTH ATLANTIC TREATY ORGANIZATION



REPRODUCED BY  
NATIONAL TECHNICAL  
INFORMATION SERVICE  
U.S. DEPARTMENT OF COMMERCE  
SPRINGFIELD, VA. 22161

NOTICE

THIS DOCUMENT HAS BEEN REPRODUCED  
FROM THE BEST COPY FURNISHED US BY  
THE SPONSORING AGENCY. ALTHOUGH IT  
IS RECOGNIZED THAT CERTAIN PORTIONS  
ARE ILLEGIBLE, IT IS BEING RELEASED  
IN THE INTEREST OF MAKING AVAILABLE  
AS MUCH INFORMATION AS POSSIBLE.

AGARD-R-686

NORTH ATLANTIC TREATY ORGANIZATION  
ADVISORY GROUP FOR AEROSPACE RESEARCH AND DEVELOPMENT  
(ORGANISATION DU TRAITE DE L'ATLANTIQUE NORD)

AGARD Report No.686  
SPECIAL COURSE ON ACOUSTIC WAVE PROPAGATION.

The material assembled in this book was prepared under the combined sponsorship of the Fluid Dynamics Panel, the von Kármán Institute and the Consultant and Exchange Program of AGARD and was presented as an AGARD Special Course at the von Kármán Institute, Rhode-St-Genèse, Belgium on 28 May – 1 June 1979.

## THE MISSION OF AGARD

The mission of AGARD is to bring together the leading personalities of the NATO nations in the fields of science and technology relating to aerospace for the following purposes:

- Exchanging of scientific and technical information;
- Continuously stimulating advances in the aerospace sciences relevant to strengthening the common defence posture;
- Improving the co-operation among member nations in aerospace research and development;
- Providing scientific and technical advice and assistance to the North Atlantic Military Committee in the field of aerospace research and development;
- Rendering scientific and technical assistance, as requested, to other NATO bodies and to member nations in connection with research and development problems in the aerospace field;
- Providing assistance to member nations for the purpose of increasing their scientific and technical potential;
- Recommending effective ways for the member nations to use their research and development capabilities for the common benefit of the NATO community.

The highest authority within AGARD is the National Delegates Board consisting of officially appointed senior representatives from each member nation. The mission of AGARD is carried out through the Panels which are composed of experts appointed by the National Delegates, the Consultant and Exchange Programme and the Aerospace Applications Studies Programme. The results of AGARD work are reported to the member nations and the NATO Authorities through the AGARD series of publications of which this is one.

Participation in AGARD activities is by invitation only and is normally limited to citizens of the NATO nations.

The content of this publication has been reproduced.  
directly from material supplied by AGARD or the authors.

Published August 1979

Copyright © AGARD 1979  
All Rights Reserved

ISBN 92-835-0248-5



Printed by Technical Editing and Reproduction Ltd  
Harford House, 7-9 Charlotte St, London, W1P 1HD.



REPORT DOCUMENTATION PAGE			
1. Recipient's Reference	2. Originator's Reference	3. Further Reference	4. Security Classification of Document
	AGARD-R-686	ISBN 92-835-0248-5	UNCLASSIFIED
5. Originator	Advisory Group for Aerospace Research and Development North Atlantic Treaty Organization 7 rue Ancelle, 92200 Neuilly sur Seine, France		
6. Title	SPECIAL COURSE ON ACOUSTIC WAVE PROPAGATION		
7. Presented	as an AGARD Special Course at the von Kármán Institute, Rhode-St-Genèse, Belgium on 28 May - 1 June 1979.		
8. Author(s)/Editor(s)	Various		9. Date August 1979
10. Author's/Editor's Address	Various		11. Pages 234
12. Distribution Statement	This document is distributed in accordance with AGARD policies and regulations, which are outlined on the Outside Back Covers of all AGARD publications.		
13. Keywords/Descriptors			
Elastic waves Acoustic scattering Sound transmission Acoustic measurement		Atmospheric attenuation Aircraft noise Noise (sound)	
14. Abstract.			
<p>The Special Course dealt with the propagation of acoustic waves in inhomogeneous and moving media of both unlimited and finite extent. Recent theoretical and experimental work was reviewed, with particular emphasis on modelling of the phenomena involved and on prediction methods, as well as standardization aspects. The fundamental phenomena treated include: reflection, refraction, scattering, diffraction and attenuation. Measurement techniques and data analysis were also considered. Applications of the material presented occur in aeroacoustics, industrial acoustics and atmospheric propagation.</p> <p>The material assembled was presented at the AGARD-Von Kármán Institute Special Course on Acoustic Wave Propagation.</p>			

# CONTENTS

	Page
PREFACE	iii
	Reference
APERCU GENERAL DES ETUDES SUR LA PROPAGATION DES ONDES ACOUSTIQUES par M Perulli	1
ACOUSTIC EQUATIONS IN MOVING FLUIDS by P.E.Doak	2
FUNDAMENTALS OF SOUND REFLECTION AND REFRACTION IN INHOMOGENEOUS MEDIA by R.Stuff	3
MATHEMATICAL TECHNIQUES FOR ACOUSTIC PROPAGATION PROBLEMS by P.E.Doak	4
DIRECTIVITY OF ACOUSTIC RADIATION FROM SOURCES by D.L.Lansing	5
PROPAGATION DANS LES CONDUITS par M.Perulli	6
PROPAGATION IN ACOUSTICALLY ABSORBENT MATERIALS by M.Perulli and P.E.Doak	7
ACOUSTIC ENERGY by C.L.Morfey	8
ABSORPTION OF SOUND WAVES IN THE ATMOSPHERE by C.L.Morfey	9
EXPERIMENTAL MEASUREMENTS OF MOVING NOISE SOURCES by L.Maestrello and T.D.Norum	10
PROPAGATION FROM MOVING SOURCES IN FLOWS by C.L.Morfey	11
APPLICATIONS OF DIFFRACTION THEORY TO AEROACOUSTICS by D.L.Lansing, C.H.Liu and T.D.Norum	12
RANDOM PROPAGATION AND RANDOM SCATTERING by C.Gazanhes	13
UNDERWATER ACOUSTIC PROBLEMS by C.Gazanhes	14
EXPERIMENTAL AND NUMERICAL RESULTS OF SOUND SCATTERING BY A BODY by L.Maestrello	15
FINITE-AMPLITUDE WAVE PROPAGATION by L.Björnø	16
NONLINEAR INTERACTION OF FINITE-AMPLITUDE SOUND WAVES by L.Björnø	17
AEROACOUSTIC MEASURING TECHNIQUE IN OR OUTSIDE TURBULENT FLOWS by H.V.Fuchs	18

APERCU GENERAL DES ETUDES SUR LA PROPAGATION  
DES ONDES ACOUSTIQUES

M. PERULLI

Office National d'Etudes et de Recherches Aérospatiales  
92320 Châtillon - France

et

Université de Technologie de Compiègne  
60206 Compiègne - France

oooOooo

RESUME

Les études tant théoriques qu'expérimentales sur la propagation des ondes acoustiques ont fait l'objet de travaux depuis de nombreux siècles. Après un bref aperçu historique de ces études on présente quelques uns des différents thèmes qui seront abordés dans le but de faire l'état des connaissances dans ce domaine particulier de l'acoustique.

1 - INTRODUCTION

Les études théoriques et expérimentales sur la propagation des sons dans les fluides ont fait l'objet de travaux à la fois anciens et modernes.

En effet, des textes anciens qui ont pu traverser les siècles et nous parvenir, le premier relatif à l'acoustique est d'Aristote (384-322 av. J.C.) qui a effectué une classification des différentes branches de l'acoustique en consacrant une part importante à la propagation des ondes sonores. Il a pressenti d'une part qu'il existait une forte analogie entre la propagation des ondes acoustiques dans les liquides et dans les gaz et, d'autre part que le milieu avait une influence non négligeable sur cette propagation (effets de réfraction). Seulement, la notion de vitesse de propagation des sons indépendante de la fréquence le gênait et, en particulier dans le cas des sons purs de basse fréquence, Aristote considérait que la célérité du son était dépendante de la fréquence.

Vraisemblablement sur la base de ces travaux, Vitruve [1] (1er siècle av. J.C.) a défini des formes de résonateurs (en forme d'amphores) qui ont eu pour conséquence la réalisation de théâtres antiques dont la qualité acoustique est difficilement imitable [2].

Aux 16ème et 17ème siècles différents travaux sur l'acoustique ont donné lieu à un certain nombre d'ouvrages. Ceux-ci étaient plutôt orientés vers l'audition des sons. En ce qui concerne la propagation on peut, entre autres, retenir les étapes suivantes :

- Cassendi (1592-1655) qui a démontré que la célérité du son est indépendante de la fréquence,
- Newton (1643-1722) qui a rédigé une première théorie de propagation des sons dans les fluides [3] en s'aidant de travaux de Galilée [4] et de Mersenne [5]. (A titre d'anecdote rappelons que Mersenne a défini les sons foliens dus à l'interaction du vent et de fils).

Puis aux 18ème et 19ème siècles, la propagation des sons continue à intéresser des savants plutôt connus pour d'autres travaux. Citons par exemple Young (1773-1829) pour sa théorie de la lumière et du son, Laplace (1749-1827) qui, le premier, donne une expression correcte de la vitesse du son dans l'air.

Enfin, vers la fin du 19ème siècle les premiers véritables traités d'acoustique sont publiés presque simultanément par Helmholtz (1821-1894) [6] et par Lord Rayleigh (1842-1919) [7].

La première guerre mondiale, de 1914 à 1918, a relancé les études d'acoustique et de propagation des sons dans les fluides sous deux aspects :

- le premier, lié à la localisation de sous-marins [8],
- le second, lié à l'acoustique des canons et des projectiles [9].

Ce dernier ouvrage (référence [9]) nous intéresse au plus haut chef.

En effet, uniquement sur la base de la géométrie dans l'espace appliquée aux équations de la mécanique analytique, Esclangon, dans son ouvrage, a étudié en détail :

- l'acoustique géométrique : ondes de bouches des canons et ondes balistiques, propriétés géométriques, cas des bolides et étoiles filantes ;

- l'acoustique physique : audition physiologique et audition auditive ; sons, bruits, détonations, infra-sons ; notions auditives de direction et de distance ; infra-sons engendrés par les canons et appareils de détection ; réfraction et réflexion atmosphériques des ondes sonores ; zones de silence ; acoustique et balistique.

Depuis la seconde guerre mondiale de très nombreux travaux sur la propagation acoustique dans les fluides et dans les solides ont vu le jour.

Les progrès obtenus ne concernent que peu les fondements physiques des phénomènes mais permettent de résoudre, grâce aux ordinateurs et aux développements des méthodes numériques, des systèmes d'équations représentant le mieux possible les problèmes rencontrés.

L'objet de la série des exposés qui rempliront cette semaine a pour ambition de faire le point sur les dernières études relatives à la propagation des ondes acoustiques dans les fluides.

Auparavant nous allons, de façon schématique, tenter de définir les classes d'ondes susceptibles de se propager dans un milieu, en fonction des propriétés physiques du milieu considéré, cela dans le but de faire apparaître les mécanismes physiques qui agissent sur la structure spatio-temporelle de l'onde.

## II - MILIEU IDEALISE

Considérons une onde plane qui se propage le long de l'axe  $x$ , avec la vitesse  $c$ , sans subir de distorsion ou d'atténuation.

Après un instant  $t$  cette perturbation aura parcouru la distance  $ct$ . L'amplitude  $p$  de cette perturbation est fonction de  $(ct - x)$  ou de  $(ct + x)$  selon que l'on considère la propagation le long de la direction des  $x$  positifs ou négatifs. Les deux fonctions :

$$(1) \quad p = f(ct - x) \quad \text{et} \quad p' = f(ct + x)$$

sont toutes deux solutions de l'équation d'ondes :

$$(2) \quad \frac{1}{c^2} \frac{\partial^2 p}{\partial t^2} - \frac{\partial^2 p}{\partial x^2} = 0$$

Admettre cette représentation équivaut à admettre que l'une des deux perturbations (1) :  $p$  ou  $p'$  ou les deux se transmettent dans le milieu, de proche en proche à condition que ce milieu possède les deux propriétés fondamentales suivantes :

- son élasticité est telle que la transmission est possible
- son inertie est telle que l'onde ne se déforme pas.

Au sens de la mécanique des milieux continus cela sous-entend que le milieu propagatif possède les propriétés suivantes :

- (1) il est continu et homogène, c'est-à-dire qu'en l'absence de perturbation le milieu est en état d'équilibre : il possède partout les mêmes propriétés physiques ;
- (2) c'est un fluide parfait : il n'y a pas de contraintes de cisaillement tangentielles à la direction du mouvement, donc il n'y a pas de friction interne (de viscosité) ;
- (3) c'est un fluide d'élasticité parfaite : après le passage de la perturbation il retrouve, sans inertie, son état initial ;
- (4) son inertie thermique est nulle ;
- (5) la conductivité thermique est nulle (ou infinie suivant le caractère thermodynamique du milieu considéré).

Dans ces conditions, on appellera  $p_0, \rho_0, T_0$  respectivement la pression, densité et température moyennes du milieu en l'absence de perturbations.

Pour aboutir à l'équation des ondes (2) deux voies sont possibles :

- linéariser les équations de conservation de la mécanique des milieux continus.
- considérer la relation fondamentale de la mécanique ( $\vec{F} = m\vec{a}$ ) et la déformation de l'élément de volume soumis à la perturbation tout en effectuant l'hypothèse des petites perturbations. En appelant  $\vec{u}$  le vecteur déformation, le vecteur vitesse  $\vec{v}$  associé à la perturbation de pression  $p$  est défini par :

$$(3) \quad \vec{v} = \frac{d\vec{u}}{dt}$$

Dans le cadre de cette théorie linéaire des sons en milieu idéalisé on démontre aisément que le champ de vitesse  $\vec{v}$  dérive d'un potentiel  $\phi$  :

$$(4) \quad \vec{v} = -\vec{\nabla}\phi$$

(cf. [10], par exemple).

Dans ce cas l'équation linéarisée de conservation de la quantité de mouvement conduit à l'expression suivante de la pression acoustique (de la perturbation) :

$$(5) \quad p = \rho_0 \frac{\partial \phi}{\partial t}$$

d'où l'équation d'ondes tridimensionnelles équivalentes à (2) :

$$(6) \quad \frac{1}{c^2} \frac{\partial^2 \phi}{\partial t^2} + \Delta \phi = 0$$

L'existence de ce potentiel acoustique  $\phi$  implique que nécessairement le champ de vitesse est irrotationnel. Parfois on appelle ce champ d'ondes de compression : ondes longitudinales.

En se référant aux raisonnements de la mécanique des milieux continus ([10] par exemple, § 2.6) on peut établir l'équation de conservation de l'énergie de l'onde qui s'écrit, en appelant

$$\frac{1}{2} \rho_0 v^2 \quad : \text{la densité d'énergie cinétique}$$

$$\frac{p^2}{2\rho_0 c^2} \quad : \text{la densité d'énergie potentielle}$$

$$\vec{q} = \rho \vec{v} \quad : \text{la densité du flux d'énergie de l'onde :}$$

$$(7) \quad \frac{\partial}{\partial t} \left( \frac{1}{2} \rho_0 v^2 + \frac{p^2}{2\rho_0 c^2} \right) + \vec{\nabla} \cdot \vec{q} = 0$$

Dans cette équation de conservation de l'énergie, la quantité  $\rho \vec{v}$  est l'analogue du vecteur de Poynting utilisé en électromagnétisme.

Il est, à ce stade, intéressant de rappeler que l'intensité sonore  $I$  est définie par :

$$(8) \quad \vec{I} = \frac{1}{T} \int_0^T \rho \vec{v} dt.$$

où  $T$  représente la période d'une onde monochromatique, ou bien dans le cas d'un bruit à large bande :

$$(8') \quad \vec{I} = \lim_{T \rightarrow \infty} \frac{1}{2T} \int_{-T}^T \rho \vec{v} dt.$$

Pour conclure ce paragraphe relatif à la propagation en milieu idéalisé, on donne dans le tableau ci-dessous, l'expression de grandeurs caractéristiques de l'onde solution de (6) et de l'impédance spécifique  $Z$  de l'onde définie par le rapport :

$$(9) \quad Z = p/v$$

dans le cas de :

I'onde plane	I'onde sphérique	I'onde cylindrique
$\phi = P \cos(\omega t - kx)$	$\phi = \frac{P'}{r} \cos(\omega t - kr)$	$\phi = \frac{P''}{\sqrt{r}} \cos(\omega t - kr)$
$v = -kP \sin(\omega t - kx)$	$v = -\frac{kP'}{r} \left(1 + \frac{1}{k^2 r^2}\right)^{1/2} \times \sin(\omega t - kr - \psi)$	$v = -\frac{kP''}{\sqrt{r}} \left(1 + \frac{1}{4k^2 r^2}\right)^{1/2} \times \sin(\omega t - kr - \psi)$
$p = kPZ \sin(\omega t - kx)$	$p = -\frac{kP'Z}{r} \sin(\omega t - kr)$	$p = -\frac{kP''Z}{\sqrt{r}} \sin(\omega t - kr)$
$u = \frac{P}{c} \cos(\omega t - kx)$	$u = \frac{P'}{cr} \left(1 + \frac{1}{k^2 r^2}\right)^{1/2} \times \cos(\omega t - kr - \psi)$	$u = \frac{P''}{c\sqrt{r}} \left(1 + \frac{1}{4k^2 r^2}\right)^{1/2} \times \cos(\omega t - kr - \psi)$
$Z = \rho_0 c = Z$	$Z = \frac{Z_0}{1 + \frac{1}{k^2 r^2}} \left(1 + \frac{j}{kr}\right)$	$Z = \frac{Z_0}{1 + \frac{1}{4k^2 r^2}} \left(1 + \frac{j}{2kr}\right)$
$\tan \psi = 0$	$\tan \psi = \frac{1}{kr}$	$\tan \psi = \frac{1}{2kr}$

### III - MILIEUX NON IDEALISES (quelques exemples)

Toujours dans le but d'introduire les exposés qui vont suivre, nous indiquons certaines situations physiques qui pourraient présenter un réel intérêt pratique et qui conduisent à des classes d'ondes parfois non négligeables.

#### III.1 - Ondes de gravité

Ces ondes se rencontrent dans le cas des gaz liquides (air-eau par exemple) et elles se propagent à la surface du liquide.

Dans ce cas l'on a :

$$(10) \quad \vec{\nabla} p = \rho \left[ \vec{\nabla} \left( \frac{\partial \phi}{\partial t} \right) + \vec{g} \right]$$

Sans entrer dans le détail des calculs indiquons simplement que l'amplitude du potentiel des vitesses décroît exponentiellement, avec la cote  $z$  du milieu (l'axe  $z$  étant perpendiculaire au plan de l'interface air-eau) :

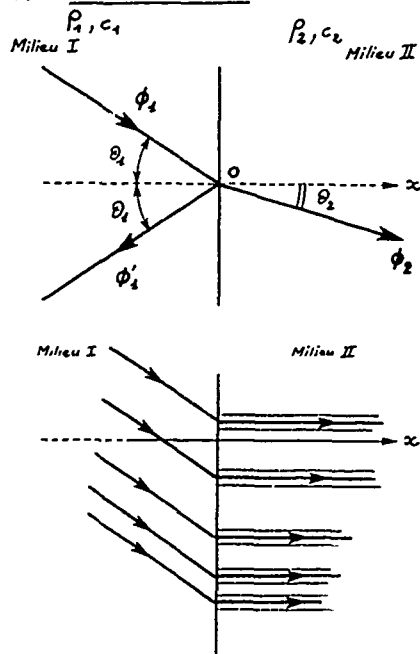
$$\phi = \phi_{0max} \exp(-k_z z) \exp j(\omega t - k_x x).$$

avec

$$k_z = \omega/c_s \quad \text{où } c_s \text{ représente la célérité de ces ondes de surface :}$$

$$(11) \quad c_s = g/\omega.$$

### III.2 - Réflexion des ondes



Ce problème de réflexion des ondes sur une surface, ou à l'interface de deux milieux, est l'un des plus vieux problèmes qui ait été étudié. Dans le cas où l'interface, définie sur le schéma ci-contre par  $x = 0$ , a un comportement parfaitement rigide au sens acoustique ( $|Z| \rightarrow \infty$ ) nous savons bien qu'il n'y a pas d'ondes transmises (onde  $\phi_2 = 0$ ) et que l'onde incidente  $\phi_1$  subit une réflexion totale  $|\phi_1| = |\phi_1'|$ .

Maintenant supposons que le milieu II corresponde à un milieu localement réactif (schéma ci-dessous), dans ce cas, dans le milieu II les ondes se propagent seulement dans la direction normale aux conditions aux limites, c'est-à-dire que les ondes transmises sont guidées et en choisissant judicieusement les impédances des milieux I et II on peut montrer que dans le milieu I il n'y a pas d'ondes réfléchies.

Cette propriété est, de façon évidente, importante pour les applications pratiques.

Les architectes de l'époque gothique connaissaient certainement sous forme empirique cette propriété d'ondes guidées par des milieux localement réactifs. En effet et si vous en avez l'occasion, vous devriez visiter le Cloître gothique (fin du 14ème siècle) de la Chaise-Dieu (cf un guide sur l'Auvergne) et plus particulièrement la "Salle de l'Echo" où deux personnes se plaçant dans des angles opposés et se tournant le dos, peuvent parler à voix basse et s'entendre de façon parfaitement intelligible.

### IV - REMARQUES

Les deux exemples choisis pour présenter des milieux non idéalisés ne comptent pas parmi les plus importants. Des cas plus complexes vous seront traités par les différents spécialistes qui interviendront au cours de cette semaine :

- en généralisant le cas de deux milieux à  $n$  milieux dont les impédances varient continûment on aboutit à l'étude des effets de réfraction, effets, très importants dans la nature, qui conduisent à des zones de silence et à des zones de renforcement de bruit ;
- en considérant l'effet de transport par un fluide on aboutit à l'étude de l'effet de convection ;
- en considérant des milieux semi-infini, ou des milieux finis on aboutit à des effets de guidage et de filtrage des ondes sonores et en fonction de l'impédance acoustique des parois à l'absorption possible de certaines ondes acoustiques ;
- en considérant la présence d'obstacles on aboutit à l'étude d'effets de diffraction ;
- en considérant des grandeurs moyennes du milieu variables au cours du temps on aborde l'étude des effets de diffusion, effets complexes et non encore bien étudiés.

Enfin, l'aspect non linéaire sera abordé sous deux formes :

- la première concerne la propagation d'ondes de fortes amplitudes,
- la seconde les mécanismes de couplage non linéaire, générateurs de sources de bruit.

On doit rester conscient de ce que cette branche de l'acoustique, relative à la propagation des ondes sonores, est vaste et que seuls certains de ses aspects sont traités, aspects considérés comme constituant la base des études de propagation en milieu inhomogène.

## V - REFERENCES

- [1] VITRUVIUS (découvertes de ses travaux aux environs du 15ème siècle, première édition 14-6), de Architectura libri decem. 40 years of Soviet Acoustics (1957), Akust. Zh. 3, 299.
- [2] CANAC R. - L'acoustique des théâtres antiques, ses enseignements, Editions du Centre National de la Recherche Scientifique, 1967.
- [3] NEWTON I. - Philosophiae naturalis principia mathematica (1686).
- [4] GALILEE G. - Discorsi e dimostrazioni matematiche (1638), Leyden.
- [5] MERSENNE F.M. - Harmonicarum libri XII, Paris (1648).
- [6] HELMHOLTZ H.L. - Die lehre von den tonempfindungen. Vieweg, Braunschweig (1877).
- [7] Lord RAYLEIGH (J.W. STRUTT) - The theory of sound (première édition en 1878).
- [8] LANGEVIN M.P., CHILANSKY M.C. - Procédé et appareils pour la production de signaux sous-marins dirigés et pour la localisation à distance d'obstacles sous-marins, Brevet n° 502913 (1918).
- [9] ESCLANGON E. - L'acoustique des canons et des projectiles, Gauthier-Villars et Cie, éditeurs 1925.
- [10] MALECKI I. - Physical foundation of technical acoustics, Pergamon Press, 1969.
- [11] KELLER J.B., PAPADAKIS J.S. - Wave propagation and underwater acoustics, Springer-Verlag, 1977.
- [12] ACHENBACH J.D. - Wave propagation in elastic solids, North-Holland, 1976.
- [13] Lord LIGHTHILL J. - Waves in fluids, Cambridge University Press, 1978.
- [14] RUDENKO O.V., SOLUYAN S.I. - Theoretical foundations of non-linear acoustics, Consultants Bureau, New York and London, 1977.

# ACOUSTIC EQUATIONS IN MOVING FLUIDS

P.E. Doak, Institute of Sound and Vibration Research, The University, Southampton SO9 5NH, England

2-1

The full transport equations of mass, momentum and energy of an arbitrarily moving, thermally inhomogeneous, fluid are considered, and also appropriate definitions of "acoustic motion" in such circumstances, leading to the partial differential equations and boundary conditions governing such motion. The fundamental nature of the convective, refractive, diffractive and diffusive effects of the fluid motion and thermal inhomogeneity on the acoustic motion is made evident. A classification is made of types of problems that have been, and can be, solved, and of the kinds of interactions that can occur between acoustic and other kinds of motions.

## 1. INTRODUCTION: SMALL AMPLITUDE FLUCTUATIONS OF A LOSSLESS FLUID ABOUT AN EQUILIBRIUM REST STATE

The human ear functions as a detector of certain pressure fluctuations in the air, and thus acoustic motion, in a general dynamical sense, is a class of mechanical stress fluctuations. The fundamentals of the dynamics of a lossless, ideal fluid, which is in a state of fluctuating motion of small amplitude relative to a uniform rest state of thermodynamic equilibrium, have long been well understood. Under such conditions, in the absence of any external force fields, the equations of mass and linear momentum transport, to first order in the small fluctuating quantities which constitute the only motion, reduce to

$$\partial p' / \partial t + \rho_0 \partial v_i' / \partial x_i = 0$$

and

$$\rho_0 \partial v_i' / \partial t + \partial p' / \partial x_i = 0,$$

respectively. Here  $\rho$  is the mass density,  $p$  the pressure and  $v_i$  ( $i = 1, 2, 3$ ) the particle velocity. Cartesian vector and tensor notation is used here and in what follows, with the usual convention of a repeated suffix indicating summation. A subscript zero indicates a constant reference value (here the equilibrium rest state value) and a prime the purely fluctuating part of a quantity: i.e.,  $\phi' = \phi(x_i, t) - \phi_0$ , etc.,  $\phi'$  being of zero time average over a period of the motion, if it is periodic, or over a suitably long interval if it is effectively random.

The momentum transport equation shows that  $v_i'$  is irrotational, so that it can be derived from a scalar potential,  $v_i' = -\partial \phi' / \partial x_i$ , and further, since then  $\partial(\rho' - \rho_0 \partial \phi' / \partial t) / \partial x_i = 0$ , one has  $p' = \rho_0 \partial \phi' / \partial t$ , apart from a function of time only which space-time causality considerations require to be zero. If the fluctuations are rapid enough so that there is not time for any fluid element to exchange heat with its surroundings by the usually relatively slow process of thermal diffusion, then  $p'$  will be adiabatically related to  $\phi'$ : i.e.,  $p' = c^2 \rho'$ , where  $c^2 = 1/\rho$ ,  $\rho$  being  $(\partial \rho / \partial p)_S$ , where  $S$  is the entropy (this subscript notation for thermodynamic partial derivatives is used throughout). The quantity  $c$  is called the speed of sound. In an ideal gas,  $c = \sqrt{\gamma p / \rho}$  and is thus proportional to  $T^{1/2}$ , where  $\gamma$  is the ratio of specific heats and  $T$  is the absolute temperature. With these relations among  $p'$ ,  $\rho'$  and  $\phi'$ , and  $c = c_0$ , being evaluated in the quiescent reference state, the mass transport equation becomes

$$\partial^2 \phi' / \partial x_i^2 = (1/c_0^2) \partial^2 \phi' / \partial t^2,$$

the homogeneous scalar wave equation, which has the primitive wave solutions  $f_{\pm}(t \mp r/c_0)/4\pi r$ , where  $r = |x_i|$ . These solutions show that any small, adiabatic pressure, density, or velocity potential fluctuation in an otherwise quiescent equilibrium fluid is composed of waves of unchanging form propagating at constant speed  $c_0$  relative to the fluid in its equilibrium rest state. Such waves are commonly called "acoustic waves".

The mean energy density associated with this acoustic wave motion is

$$(1/2) \rho_0 \overline{v_i'^2} + (1/2) \overline{p'^2} / \rho_0 c_0^2,$$

the sum of the kinetic and potential energy densities (an overbar indicates an appropriate time average). The potential energy density, of course, is the energy stored elastically in the adiabatic compression of the fluid (not isothermal). These energy densities, for any individual travelling wave, are "locked" into the wave and travel with it. Since the fluid has been assumed lossless, the total energy must be conserved, and hence the mean intensity vector (energy flux)  $\overline{J_i} = \overline{p' v_i'}$  is solenoidal: i.e.,  $\partial \overline{J_i} / \partial x_i = 0$ . Since the wave equation is linear, the Principle of Superposition applies: any sum of solutions is also a solution. Thus constructive or destructive interference occurs among waves arriving at an observation point by different paths (due to reflections, say) or from different sources. Finally the Principle of Reciprocity also applies: i.e., e.g.,  $f_{\pm}(t - |x_i - y_i|/c_0)/4\pi |x_i - y_i| = f_{\pm}(t - |y_i - x_i|/c_0)/4\pi |y_i - x_i|$ ; the wave observed at  $x_i$  from a "point" source at  $y_i$  is identical to that observed at  $y_i$  from the same "point" source at  $x_i$ . Since  $\rho_0$  and  $c_0$  are the only material parameters involved, it is evident that such wave motion is a characteristic behavioural property of any material having inertial mass and linear (Hookean) elasticity, the speed of propagation being determined by the square root of the ratio of the elastic modulus, here  $\gamma p$ , to the mass density.

If the fluid is in uniform motion at a constant velocity,  $(v_{10}, 0, 0)$ , say, then since the wave motion is relative to the fluid equilibrium state, the wave equation again applies but in a co-ordinate system having the same uniform motion: i.e.,  $(\xi_1 = x_1 + v_{10}t, x_2, x_3)$ . A Galilean transformation of co-ordinates for a wave field  $\phi'(\xi_1, x_2, x_3, t)$  into  $\phi'(x_1 + v_{10}t, x_2, x_3, t)$  then describes the uniformly convected wave motion in the fixed  $(x_i, t)$  co-ordinates. Thus, the appropriate "acoustic" wave equation in the fixed



1-2 coordinates for a fluid in uniform thermodynamic equilibrium but in uniform motion with constant velocity  $v_{10}$  is

$$\partial^2 \phi' / \partial x_1^2 = (1/c_0^2) \bar{D}^2 \phi' / Dt^2,$$

$$\text{where here } \bar{D}/Dt = \partial/\partial t + v_{10} \partial/\partial x_1.$$

It is therefore evident that the case of uniform fluid motion can be easily transformed into formal identity with that of a quiescent fluid. For this case of uniform motion, the relationships between  $p'$  and  $\rho'$  and between  $v'_i$  and  $\phi'$  remain the same, but  $p' = \rho_0 \bar{D}\phi'/Dt$ .

## 2. THE GENERAL CASE: THE TRANSPORT EQUATIONS

The situation can be essentially different from that for a quiescent equilibrium reference state, therefore, only if the reference state is one of non-uniform motion, or is thermally non-uniform. The possibility of the existence of some recognizable form of "acoustic" wave motion in the general case clearly must be considered in the context of the full transport equations of the fluid for mass, linear momentum and energy. These are, respectively, for a homogeneous fluid subject to conservation of mass,

$$\partial \rho / \partial t + \partial (\rho v_i) / \partial x_i = 0, \quad (1)$$

$$\partial (\rho v_i) / \partial t + \partial (\rho v_i v_j + p_{ij}) / \partial x_j = \rho f_i, \quad (2)$$

$$\frac{\partial}{\partial t} (\rho U + \frac{1}{2} \rho v_i^2) + \frac{\partial}{\partial x_j} \{ (\rho U + \frac{1}{2} \rho v_i^2) v_j + p_{ij} v_i + \theta_j \} = \rho f_i v_i + Q_T, \quad (3)$$

in which  $p_{ij}$  is the stress tensor,  $f_i$  the external force per unit mass,  $U$  the internal energy per unit mass,  $\theta_j$  the heat flux and  $Q_T$  the rate of external addition of heat per unit volume. According to the macroscopic laws of physics, the external ("body") force per unit volume,  $f_i$ , can be only gravitational or electromagnetic in nature, and thus it is zero if forces of these types are not appreciable. The electromagnetic external force is, of course, the Lorentz force, and thus is zero if the fluid has no electrical charge. The stress tensor is taken as  $p_{ij} = p \delta_{ij} - S_{ij}$ , where  $p$  is the thermodynamic pressure (i.e., for  $U = U(S, \rho)$ , then  $p = -(\partial U / \partial (1/\rho))_S$ ), and  $\delta_{ij}$  is the Kronecker delta,  $\delta_{ij} = 0$ ,  $i \neq j$ , and  $\delta_{ij} = 1$ ,  $i = j$ . Then, for a Stokesian fluid,  $S_{ij}$  is the usual viscous stress tensor, involving both shear and bulk viscosity coefficients,  $\mu$  and  $\eta$ , respectively:

$$S_{ij} = \mu \left( \frac{\partial v_i}{\partial x_j} + \frac{\partial v_j}{\partial x_i} \right) - 2 \frac{\partial v_k}{\partial x_k} \delta_{ij} + \left( \frac{4}{3} \mu + \eta \right) \frac{\partial v_k}{\partial x_k} \delta_{ij}. \quad (4)$$

This definition of pressure in the general case is not a trivial matter for acoustical purposes. From equation (4) it is evident that  $\frac{1}{\rho} \partial p_{ij} / \partial x_j \neq 0$  and thus for a Stokesian fluid with bulk viscosity the thermodynamic pressure  $p$  is not equal to the average normal stress,  $\frac{1}{3} \partial p_{ij} / \partial x_j$ . As thermodynamically defined, the pressure  $p$  is the independent variable for reversible changes in the enthalpy,  $h = U + p/\rho$ , through  $\delta h = T \delta S + (1/\rho) \delta p$ . Also, it is well established that for a travelling pressure wave in a viscous fluid, the decrease in amplitude per unit amplitude per unit distance due to all viscous effects is proportional to  $(4/3)\mu + \eta$ , and that only in pure monatomic fluids is the bulk viscosity  $\eta$  negligible. In polyatomic fluids and mixtures, its effective value, due to internal relaxation processes on the molecular levels, is very often much greater than that of the shear viscosity coefficient  $\mu$ .

Elimination of the terms in  $\rho v_i$  only between equations (1) and (2) gives

$$\partial^2 p / \partial x_1^2 - \partial^2 \rho / \partial t^2 + \partial^2 (\rho v_i v_j - S_{ij}) / \partial x_i \partial x_j = \partial (\rho f_i) / \partial x_i, \quad (5)$$

or, with the double divergence carried out explicitly,

$$\frac{\partial^2 p}{\partial x_1^2} - \frac{\partial^2 \rho}{\partial t^2} - 2 v_i \frac{\partial^2 \rho}{\partial x_i \partial t} + \left( \frac{\partial v_i}{\partial x_j} \frac{\partial v_j}{\partial x_i} + \frac{\partial v_i}{\partial x_i} \frac{\partial v_j}{\partial x_j} \right) \rho - \frac{\partial^2 S_{ij}}{\partial x_i \partial x_j} = \frac{\partial}{\partial x_i} (\rho f_i). \quad (6)$$

If the thermodynamic state of the fluid can be specified by the two independent thermodynamic variables entropy,  $S$ , and pressure,  $p$ , so that  $\delta p = \rho_0 \delta p + \rho_0 \delta S$ ,  $\rho_0$  being  $1/c^2$ , as before, then for small fluctuations about a reference state of uniform mean velocity  $v_{10}$ , uniform mass density  $\rho_0$ , and uniform temperature, the fluctuating part of equation (4) becomes, to first order,

$$\frac{\partial^2 p'}{\partial x_1^2} - \frac{1}{c_0^2} \frac{\partial^2 p'}{\partial t^2} - \rho_{S0} \frac{\partial^2 S'}{\partial t^2} - \frac{\partial^2 S_{ij}}{\partial x_i \partial x_j} = \frac{\partial}{\partial x_i} (\rho f_i)', \quad (7)$$

which, for negligible entropy fluctuations, internal losses and external forces, reduces to the previously obtained uniformly convected wave equation. However, in the general case, the term  $-v_i v_j \partial^2 \rho / \partial x_i \partial x_j$  in equation (6) includes not only convection of fluctuating density gradients by the mean flow but also convection of mean density gradients by the fluctuating flow, and the fifth term in equation (6) is similarly a complicated mixture of both mean and fluctuating density and velocity gradient components. Since, on an intuitive basis, and because the ear responds to pressure, it would be attractive to suppose that the fluctuating pressure, or some part of it, might be still interpretable as "acoustic" in the general case, it is natural to ask whether or not some part of the velocity could be associated with this pressure, and thus also regarded as acoustic. In the quiescent reference frame case the velocity derivable from the fluctuating scalar potential was associated with the pressure fluctuations in this way. The particle velocity, of course, according to Helmholtz' Theorem, can always be represented in terms of a scalar and a vector potential:  $v_i = V_i(x_k, t) - \partial \phi(x_k, t) / \partial x_i$ ,  $V_i(x_k, t)$  being the solenoidal component obtained from the vector potential. Consideration of the mass transport equation shows immediately, however, that this association does not extend advantageously to the general case. It is

$$\partial \rho / \partial t + (v_i - \partial \phi / \partial x_i) \partial \rho / \partial x_i = \rho \partial^2 \phi / \partial x_i^2 = 0. \quad (8)$$

In this form, the equation is non-linear and involves product terms of exactly the type it was hoped to avoid, with both mean and fluctuating solenoidal velocity components present. Also it appears that the scalar velocity potential may have both mean and fluctuating parts, and that both these can be present.

2-3

### 3. THE GENERAL CASE: DEFINITIONS OF ACOUSTICAL, TURBULENT AND THERMAL MOTION

If, however, the linear momentum density, rather than the particle velocity, is regarded as the primary dependent vector field to be determined, and it is represented in terms of solenoidal and irrotational components,  $\rho v_i = B_i - \partial\psi/\partial x_i$ ,  $\partial B_i/\partial x_i = 0$ , then the mass transport equation becomes simply

$$\partial\rho/\partial t - \partial^2\psi/\partial x_i^2 = 0, \quad (9)$$

which is linear, involves only  $\rho$  and the scalar momentum potential  $\psi$ , and with  $\rho = \rho(S, p)$  immediately suggests and permits definitions, in the general case, of "acoustical" (i.e., "adiabatic") and "thermal" (i.e., "isobaric") components of both  $\rho$  and  $\psi$ :

$$\frac{\partial\rho}{\partial t} = \frac{1}{c^2} \frac{\partial p}{\partial t} + \rho_s \frac{\partial S}{\partial t} = \frac{\partial^2\psi_A}{\partial x_i^2} + \frac{\partial^2\psi_T}{\partial x_i^2} = \frac{\partial^2\psi}{\partial x_i^2}. \quad (10)$$

These definitions are wholly consistent with the linearly independent acoustic and thermal diffusion types of motion that are well known to apply for small amplitude fluctuations about a uniform quiescent reference state. Furthermore, since  $\partial^2\psi/\partial x_i^2 = 0$  for a time stationary motion (i.e., when  $\rho = \bar{\rho}(x_i) + \rho'(x_i, t)$ , with  $\rho'$  having a zero time average over suitable time intervals), then  $\partial\psi/\partial x_i$  is both irrotational and solenoidal, so that  $\psi$  can be taken to be zero without further loss of generality, with the entire solenoidal mean momentum being represented by  $\bar{B}_i$ . (A vector which is both irrotational and solenoidal can be represented either as the gradient of a scalar potential satisfying Laplace's equation or as the curl of a vector potential each of whose Cartesian components satisfies Laplace's equation.) The uniqueness of the fluctuating momentum components,  $B_i'$  and  $-\partial\psi'/\partial x_i$ , is subject only to an appropriate allocation to one or the other of any fluctuating momentum field component which turns out to be both solenoidal and irrotational, in any particular case.

These definitions lead directly to an expression for the total linear momentum density, in the general case, that is a linear superposition of a uniquely defined mean component and similarly uniquely defined fluctuating "turbulent", "acoustical" and "thermal" components:

$$\rho v_i(x_k, t) = \bar{B}_i(x_k) + B_i'(x_k, t) - \partial\psi_A'(x_k, t)/\partial x_i - \partial\psi_T'(x_k, t)/\partial x_i. \quad (11)$$

Note, with reference to equations (10) and (11), that since  $\bar{\psi} = 0$  then, even if  $\bar{\psi}_A$  and  $\bar{\psi}_T$  are not zero, nevertheless  $\bar{\psi}_A + \bar{\psi}_T = 0$ . Note also that, as in this general case no other precise definition of turbulent, acoustical and thermal fluctuations has been previously proposed and accepted, the terms usually having been used loosely, without consistent definition - and this applies to both "turbulent" and "acoustical" - these definitions do not necessarily correspond exactly to motions previously described elsewhere by similar words.

In terms of  $\psi'$  and  $B_i'$ , the momentum transport equation becomes

$$\frac{\partial B_i'}{\partial t} + \frac{\partial}{\partial x_i} (p - \frac{\partial\psi'}{\partial t}) + \frac{\partial}{\partial x_j} \left\{ \frac{1}{\rho} (B_i B_j + \frac{\partial\psi'}{\partial x_i} \frac{\partial\psi'}{\partial x_j}) - \frac{B_i}{\rho} \frac{\partial\psi'}{\partial x_j} - \frac{B_j}{\rho} \frac{\partial\psi'}{\partial x_i} - S_{ij} \right\} = \rho f_i. \quad (12)$$

With  $B_i = \bar{B}_i + B_i'$  and  $\rho = \bar{\rho} + \rho'$ , and with  $\delta\rho = \rho_s \delta p + \rho_s \delta S$ , all the non-linear terms in equation (12) which represent  $\partial(\rho v_i v_j)/\partial x_j$ , as well as all the linear terms, are now explicitly classified as comprised of specific mean, turbulent, acoustical and thermal factors, as also are, of course, the terms in equations (10) and (11).

### 4. THE GENERAL CASE: ACOUSTICAL MOTION EQUATIONS

For investigating the nature of the fluctuating part of equation (12) it is notationally convenient to consider its time derivative so that all fluctuating terms will be clearly visible. With coefficients in a mixed notation, for compactness, this can be written as

$$\begin{aligned} \frac{\partial^2 B_i'}{\partial t^2} + \frac{\partial}{\partial x_i} \left( \frac{\partial p}{\partial t} - \frac{\partial^2\psi'}{\partial t^2} \right) + \frac{\partial}{\partial x_j} \left\{ -v_i v_j \frac{\partial p}{\partial t} + 2v_j \left( \frac{\partial B_i}{\partial t} - \frac{\partial^2\psi'}{\partial x_i \partial t} \right) - \frac{\partial S_{ij}}{\partial t} + v_i \frac{\partial}{\partial t} (\rho v_j) \right. \\ \left. - v_j \frac{\partial}{\partial t} (\rho v_i) \right\} = \frac{\partial}{\partial t} (\rho f_i). \end{aligned} \quad (13)$$

The last two terms on the left hand side of equation (13), taken together, are solenoidal. The divergence of equation (13) is thus, after elimination of  $p$  and  $\rho$  by use of equation (10),

$$\begin{aligned} \frac{\partial^2}{\partial x_i \partial x_j} \left\{ (c^2 \delta_{ij} - v_i v_j) \frac{\partial^2\psi'}{\partial x_k^2} - \frac{\partial^2\psi'}{\partial t^2} \delta_{ij} - 2v_j \frac{\partial^2\psi'}{\partial x_i \partial t} - \frac{\partial S_{ij}}{\partial t} - \rho_s c^2 \frac{\partial S}{\partial t} \delta_{ij} + 2v_j \frac{\partial B_i}{\partial t} \right\} \\ = \frac{\partial^2}{\partial x_i \partial t} (\rho f_i). \end{aligned} \quad (14)$$

This is a fourth order inhomogeneous equation for  $\psi'$ , with some obvious partial similarities to a convected wave equation. The equation would be expected to be fourth order, for two reasons. First, apart from the  $\partial B_i/\partial t$  term, the left hand side terms should be of the form, as it were,  $(\partial^2/\partial x_i^2 + L_A)(\partial^2/\partial x_i^2 + L_T)\psi'$ , where  $L_A$  is the differential operator corresponding to the acoustic part of the scalar potential,  $\psi_A'$ , and  $L_T$  that corresponding to the thermal part,  $\psi_T'$ , this form being also obtained, of course, in the well-understood case of small amplitude motion of a Stokesian fluid about an equilibrium rest state. Second, the fluid motion, through the coefficients involving the velocity  $v_i$ , makes the propagation of both acoustical and thermal disturbances anisotropic.

For purposes of physical interpretation, equation (14) expressed in terms of  $p$  and  $\rho$ , insofar as possible, is of particular interest. It is

$$\frac{\partial^2}{\partial x_1^2} \left( \frac{\partial p}{\partial t} \right) - \frac{\partial^2}{\partial t^2} \left( \frac{\partial p}{\partial t} \right) - \frac{\partial}{\partial x_1} \left( 2v_1 \frac{\partial}{\partial t} \left( \frac{\partial p}{\partial t} \right) \right) - \frac{\partial^2}{\partial x_1 \partial x_j} (v_1 v_j \frac{\partial p}{\partial t} + \frac{\partial S_{1j}}{\partial t}) + \frac{\partial}{\partial x_1} \left( 2 \frac{\partial v_1}{\partial x_j} \frac{\partial B_1}{\partial t} - \frac{\partial^2 \psi'}{\partial x_j \partial t} \right) = \frac{\partial^2}{\partial x_1 \partial t} (\rho f_1). \quad (15)$$

The special dynamical role of the velocity gradients,  $\partial v_1 / \partial x_j$ , is evident from equation (15). The other terms involving  $v_1$  are generalized convection terms for density fluctuations, but the last term represents an "acceleration" (second time derivative) of the rate of mass density change which depends on the divergence of a vector composed of products of velocity gradients by the momentum rate of change. This "acceleration" of density rate depends on all three fluctuating momentum components, turbulent, acoustical and thermal, and the acoustical component cannot readily be expressed in terms of  $p'$ , because it involves the gradient of  $\psi'$  and not its Laplacian. From the momentum equation (12), it is evident that  $\partial \psi' / \partial t$  could be written as  $p' + \partial \psi_1' / \partial t$ , where

$$\frac{\partial^2}{\partial x_1^2} \left( \frac{\partial \psi_1'}{\partial t} \right) = \frac{\partial^2}{\partial x_1 \partial x_j} (\rho v_1 v_j - S_{1j})' + \frac{\partial}{\partial x_1} (\rho f_1)'. \quad (16)$$

The component  $\psi_1'$  thus would depend on the irrotational effective force fluctuations arising from the Reynolds and viscous stresses, and the external force. However, its source terms in the Poisson equation (16) are simply the integral with respect to time of all the terms in equation (15) except the first two. Therefore, attempts at elimination of the  $\partial \psi' / \partial x_1$  term in equation (15) would lead only to an integro-differential equation, of a form much more complicated than the fourth order equation (14) for  $\psi'$ .

It is clear from equation (15), then, that pressure fluctuations in an arbitrarily moving fluid are not governed by any simple form of convected wave equation. The presence of velocity gradients of appreciable magnitude prevents this, by introducing a single term which can locally strongly couple momentum fluctuations of all three types, turbulent, acoustical and thermal, to the pressure fluctuations, which would otherwise propagate in a recognizable "acoustic-wave-like" manner relative to the moving fluid.

For the reasons stated and other obvious ones, the fourth order equation (14) for  $\psi'$ , rather than the second order equation (15) for  $\partial p / \partial t$ , must be regarded as the fundamentally correct basis for analyzing the interrelationships among turbulent, acoustical and thermal types of motion in an arbitrarily moving fluid. However, a "mixed" expression for  $\partial p / \partial t$  can be obtained from equation (15), which can be useful and of interest in some situations, and which, for the most common case of zero external forces, is relatively simple. By using the momentum equations (2) and (12), with  $f_1 = 0$ , the last term on the left of equation (15) can be written as

$$- \frac{\partial}{\partial x_1} \left( 2 \frac{\partial v_1}{\partial x_j} \left( \frac{\partial p'}{\partial x_j} - \frac{\partial S_{jk}}{\partial x_k} \right) + 2 \frac{\partial v_1}{\partial x_j} \frac{\partial}{\partial x_k} (\rho v_j v_k)' \right).$$

Equation (15) thus can be put in the form

$$\begin{aligned} \frac{\partial^2}{\partial x_1^2} \left( \frac{\partial p}{\partial t} \right) - \frac{\partial^2}{\partial t^2} \left( \frac{\partial p}{\partial t} \right) - \frac{\partial}{\partial x_1} \left( 2v_1 \frac{\partial}{\partial t} \left( \frac{\partial p}{\partial t} \right) + 2 \frac{\partial v_1}{\partial x_j} \left( \frac{\partial p'}{\partial x_j} - \frac{\partial S_{jk}}{\partial x_k} \right) \right) - \frac{\partial^2}{\partial x_1 \partial x_j} (v_1 v_j \frac{\partial p}{\partial t} + \frac{\partial S_{1j}}{\partial t}) \\ = \frac{\partial}{\partial x_1} \left( 2 \frac{\partial v_1}{\partial x_j} \frac{\partial}{\partial x_k} (\rho v_j v_k)' \right). \end{aligned} \quad (17)$$

The validity and usefulness of such an expression depends wholly on whether or not the right side source term can be evaluated, or estimated to a sufficient approximation, independently of the left side terms. In the general case this obviously is not possible, as the "Bernoulli pressure gradients" in  $\partial(\rho v_1 v_k) / \partial x_k$  of the right side can "cancel out" appreciable components of the total pressure gradient  $\partial p' / \partial x_1$  on the left side. Also it is evident that in its present form (selected for simplicity at this stage) the right side includes a term  $-\partial(2(\partial v_1 / \partial x_j) v_j \partial p / \partial t) / \partial x_1$ , "doubly" cancelling the term of half that value and identical form on the left side (from  $\partial^2(v_1 v_j \partial p / \partial t) / \partial x_1 \partial x_j$ ). With this term extracted, the remainder of the right side is  $\partial(2(\partial v_1 / \partial x_j) (\rho v_1 \partial v_1 / \partial x_j)) / \partial x_1$ , and the linearized forms of this are of interest for cases of "parallel" sheared, or only slightly divergent, mean flows. For the "parallel" mean flow case, where  $\bar{v}_1 = (v_1(x_2), 0, 0)$ , say, it becomes, to first order, simply

$$\frac{\partial}{\partial x_1} \left( 2 \frac{\partial v_1}{\partial x_2} \left( \frac{\partial v_2}{\partial x_k} \rho v_k \right)' \right) = \frac{\partial}{\partial x_1} \left( \rho \frac{\partial v_1}{\partial x_2} \frac{\partial v_2}{\partial x_1} \right),$$

since  $\bar{v}_2 = 0$ . In such a case, then, the "source" term depends on only one of the fluctuating velocity components. Note that if  $\rho$  is similarly stratified,  $\rho = \rho(x_2)$ , the source term becomes  $\partial^2(\rho (\partial v_1^2 / \partial x_2) v_2') / \partial x_1^2$ . For an axisymmetric divergent mean flow, a rather similar result would be obtained, but with both fluctuating transverse velocity components involved.

As the simplest of the "mixed" equation formulations, equation (17) can be notationally compressed down to the "acoustical analogy" form:

$$\frac{\partial^2}{\partial x_1^2} \left( \frac{\partial p}{\partial t} \right) - \frac{\partial^2}{\partial t^2} \left( \frac{1}{c^2} \frac{\partial p}{\partial t} \right) = \frac{\partial^2}{\partial x_1 \partial t} (\rho f_1) + \frac{\partial^2}{\partial t^2} (\rho S \frac{\partial S}{\partial t}) - \frac{\partial^3}{\partial x_1 \partial x_j \partial t} (\rho v_1 v_j - S_{1j}), \quad (18)$$

the last two terms on the right being regarded as independently estimable (to some degree of approximation) forcing terms.

## 5. BOUNDARY CONDITIONS

Boundary conditions are derived from the transport equations as limiting cases. As mass, linear

momentum and energy densities, and their rates of change, and also external forces and rates of heat addition, must be everywhere finite, integration of the three transport equations (1-3) across any fixed surface in a region containing the fluid, in the direction  $n$  normal to the surface, shows that  $\rho v_n$ ,  $\rho v_n v_n + p_{nn}$  and  $(\rho U + \frac{1}{2} \rho v^2) v_n + p_{nn} v_n + \theta_n$  all must be continuous across the surface. At a mutually impenetrable interface between two dissimilar continua, moving or fixed, the conditions become continuity of particle displacement (so that no "vacuum" can be formed at the interface), Newton's Third Law of action and reaction for the internal stresses  $p_{nn}$ , and continuity of stress energy and heat flux,  $p_{nn} v_n + \theta_n$ . In fluid mechanics the former conditions, the Rankine-Hugoniot conditions in general form, are appropriate across near-discontinuities in fluid properties, such as shock waves, or thin shear layers. The latter conditions, however, are the appropriate ones at the moving interfaces between fluids and solids (or other immiscible fluids) which are common in acoustics.

## 6. MEAN ENERGY FLUX

The momentum potential formulation also leads to definitions of mean, turbulent, acoustical and thermal energy fluxes, and to certain significant relationships among these. The transport equation for total (or "stagnation") enthalpy,  $H = h + (1/2) v_i^2 = U + (p/\rho) + (1/2) v_i^2$ , is

$$\frac{\partial}{\partial t} (\rho H) + \frac{\partial}{\partial x_j} (\rho H v_j - S_{ij} v_i + \theta_j) = \frac{\partial p}{\partial t} + \rho f_j v_j + Q_T \quad (19)$$

Time averaging shows that

$$\frac{\partial}{\partial x_j} (\overline{\rho H v_j - S_{ij} v_i + \theta_j}) = \overline{\rho f_j v_j} + \overline{Q_T} \quad (20)$$

that is, that the mean flux  $\overline{\rho H v_j - S_{ij} v_i + \theta_j}$  has only the external sources  $\overline{\rho f_j v_j}$  and  $\overline{Q_T}$  and is solenoidal everywhere that these are zero. The mean flux  $\overline{\rho H v_j}$  can be written as the sum of a flux carried by the mean momentum and a flux carried by the fluctuating momentum,  $\overline{\rho H v_j} = \overline{H} \overline{\rho v_j} + \overline{H'(\rho v_j)'}$ , or, by virtue of the expression for  $(\rho v_j)'$  as a sum of turbulent, acoustical and thermal parts, equation (11), as

$$\overline{\rho H v_j} = \overline{H} \overline{\rho v_j} + \overline{H' B_j} + \overline{H'(-\partial \psi_A' / \partial x_j)} + \overline{H'(-\partial \psi_T' / \partial x_j)} \quad (21)$$

As for the momentum, then, unique mean, turbulent, acoustical and thermal components of the total mean energy flux  $\overline{\rho H v_j}$  can be identified, and  $\overline{\rho H v_j}$  is a linear superposition of these.

From the momentum equation in the form

$$\frac{\partial v_j}{\partial t} + (\Omega_k x v_i)_j + \frac{\partial H}{\partial x_j} - T \frac{\partial S}{\partial x_j} - \frac{1}{\rho} \frac{\partial S_{jk}}{\partial x_k} = f_j \quad (22)$$

where  $\Omega_k$  is the vorticity (the curl of the velocity), a separate expression for  $\overline{H'(\rho v_j)'}$  can be obtained. Taking the time average of equation (22), and multiplying it scalarly by  $(\rho v_j)$  gives, after some rearrangement,

$$\begin{aligned} \frac{\partial}{\partial x_j} \{ \overline{H'(\rho v_j)'} \} + \overline{(\rho v_j)(\Omega_k x v_i)_j} - \overline{\rho v_j T \frac{\partial S}{\partial x_j}} - \overline{v_j \frac{\partial S_{jk}}{\partial x_k}} + \overline{(\rho v_j)' (T \frac{\partial S}{\partial x_j})'} + \overline{(\rho v_j)' (\frac{1}{\rho} \frac{\partial S_{jk}}{\partial x_k})'} \\ = \overline{\rho v_j f_j} \end{aligned} \quad (23)$$

Then, subtracting equation (23) from equation (20), combining and rearranging terms, with use of the time average of the entropy transport equation and the fact that, since the triple scalar product  $(\rho v_j)(\Omega_k x v_i)_j$  is identically zero,  $(\rho v_j)(\Omega_k x v_i)_j = -(\rho v_j)'(\Omega_k x v_i)_j'$ , gives, exactly,

$$\frac{\partial}{\partial x_j} \{ \overline{H'(\rho v_j)'} \} = -(\rho v_j)'(\Omega_k x v_i)_j' - (T \frac{\partial S}{\partial x_j})' - (\frac{1}{\rho} \frac{\partial S_{jk}}{\partial x_k})' + (\rho T)' \frac{\partial S}{\partial t} + \overline{(\rho v_j)' f_j'} \quad (24)$$

The sources of the mean energy flux carried by the fluctuating momentum are thus, like  $\overline{H'(\rho v_j)'}$  itself, time averages of quadratic products of fluctuating quantities. Note also that the external heat addition,  $Q_T$ , does not appear in equation (24). In the absence of external forces, and when irreversible effects are small, the only source is  $-(\rho v_j)'(\Omega_k x v_i)_j'$ , representing creation of a mean flow of fluctuating energy by fluctuating Coriolis accelerations. It can be positive or negative, corresponding, respectively, to a source or sink of such a mean energy flow. As previously mentioned, it is identically equal to  $+\rho v_j(\Omega_k x v_i)_j$ , and in the case of an internally wholly lossless fluid

$$\frac{\partial}{\partial x_j} \{ \overline{H'(\rho v_j)'} \} = -(\rho v_j)'(\Omega_k x v_i)_j' = (\rho v_j)(\Omega_k x v_i)_j = -\frac{\partial}{\partial x_j} \overline{H(\rho v_j)}, \quad (25)$$

showing that sources of the mean energy flux carried by the fluctuating momentum are locally sinks of that carried by the mean momentum, and vice versa.

In terms of the specific vorticity,  $\Omega_k/\rho$ , the fluctuating Coriolis acceleration source term is

$$-(\rho v_j)'(\Omega_k/\rho)'x(\rho v_i)_j' = (\rho v_j)'(\Omega_k/\rho)'x(\rho v_i)_j' \quad (26)$$

which shows that it depends on the mean momentum, and on each component of the momentum fluctuations. Thus, both the mean intensity associated with the fluctuations and its sources are expressed in terms of the turbulent, acoustical and thermal fluctuations.

## 7. POSSIBILITIES FOR SOLUTIONS

Because of their complexity and non-linearity, the equations for the fluctuating pressure and other

field variables in an arbitrary fluid flow are not in general amenable to analytic solution. The only case for which analytical methods are readily available and applicable is that of small amplitude fluctuations about an equilibrium quiescent (or uniformly moving) reference state, and for fluids of relatively small viscosity and thermal conductivity. In this case the equations can be reduced to a set of three uncoupled partial differential equations with linear coefficients which are readily solved by standard analytical methods: i.e., separation of variables, special functions, Green functions, etc. For this case the turbulent vector momentum (or velocity) potential and the thermal scalar potential satisfy diffusion equations and the acoustic scalar potential satisfies a form of scalar wave equation with attenuation due to viscosity and thermal conductivity.

For analytic solutions for more general cases, the most usual analytic approach is some form of perturbation method, with the diffusion and scalar wave equations of the equilibrium quiescent reference state problem used as starting points. Such methods, including those of geometrical acoustics, are particularly well suited to problems in which the variable coefficients in the full governing equations can be regarded as slowly varying. For cases where these variable coefficients are rapidly varying, but only in regions of relatively limited extent, these regions can often be effectively replaced by discontinuities and the corresponding complicating terms in the equations by appropriate "jump" (boundary) conditions.

Finally, recourse can be had to numerical computation, either by finite difference methods or general weighted residual methods (Galerkin, finite element, etc.). By such methods, with digital computers, solutions of the linearized forms (i.e., with the coefficients replaced by their mean values) of equations such as equations (14) or (17) are possible, so that the convective effects on the fluctuations of mean velocity and mean temperature can be calculated for particular cases.

#### 8. BIBLIOGRAPHY

The literature on the formulation of problems of fluctuating fluid flow is vast. Only a few suggestions for further reading are therefore given, in which there are further references.

A.C. ERINGEN 1967 Mechanics of Continua. New York: John Wiley and Sons.

W.P. MASON (Editor) 1963- Physical Acoustics (a continuing series of volumes. New York, London: Academic Press. See initially Volume 1, Part A, Chapter 1.

P.E. DOAK 1975 in Progress in Aeronautics and Astronautics, Volume 37: Aeroacoustics: Jet and Combustion Noise; Duct Acoustics (H.T. Nagamatsu, editor), 65-78. A concise formulation of momentum potential theory of fluctuating fluid motion and internally generated sound. Cambridge, Massachusetts: AIAA in cooperation with the MIT Press.

FUNDAMENTALS OF SOUND REFLECTION AND  
REFRACTION IN INHOMOGENEOUS MEDIA

3-1

Roland STUFF  
Visiting Professor, von Karman Institute  
Chaussée de Waterloo, 72  
B-1640 Rhode Saint Genèse, Belgium  
on leave from DFVLR-AVA, Göttingen, Germany

SUMMARY

Starting with a historical review of geometrical acoustics, a treatment of sound wave propagation is given including the effects of temperature and wind gradients. In section 4, analytical solutions of the wave equation are presented for an isothermally and a polytropically stratified still atmosphere and for an atmosphere with wind gradients and wind direction changes as well. These solutions are valid beyond the scope of geometrical acoustics. Finally, dispersion of infrasound is dealt with.

1. INTRODUCTION

The propagation of noise in a real atmosphere is a matter of different phenomena. Temperature and wind gradients, gravity stratification, air viscosity, humidity, finite amplitude effects and nonequilibrium behaviour of air lead to reflection, refraction, scattering, diffraction, dispersion, absorption, nonlinear propagation and relaxation and to an almost unlimited variety in the possible geometry of the wave fronts and the rays. In the limiting case of zero wavelength, this geometry can be described by means of geometric acoustics. This approximation neglects the effects of viscosity, heat conduction and gravity, though it can be applied in most cases of practical interest since sound absorption in the air is very small and the state of the atmosphere in general does not change considerably over a distance of a wavelength. Then, due to the fact that in the so-called "ray tubes" the acoustic energy is conserved, the acoustic intensity at any point of the atmosphere can be calculated. From the scientific point of view geometric acoustics now is in its final stage of development. However, application of geometric acoustics often fails for different reasons. Thus, it requires in most cases more knowledge about the atmosphere than is available. The numerical ray tube area method is very cumbersome and probably therefore not often used. On the other hand, there are severe cumulative effects over long distances, ranging from 700 to 7000 m. Geometric acoustics is also limited in range of application, diffraction, scattering and dispersion of low frequency waves are most interesting under conditions for which the basic assumption of geometric acoustics is not valid. All this implies the need for much greater care in the application of analytical techniques. That means analytical solutions of the wave equation are required, which describe long range effects as there are refraction, reflection and dispersion. Once available, these solutions can serve as initial solutions for methods describing diffraction, scattering and absorption and for characteristic methods describing nonlinear effects. This paper deals with geometric acoustics in paragraph 2 and with analytical solutions of the wave equation available at this stage in paragraph 3.

2. GEOMETRIC ACOUSTICS

2.1 Historical development

A wind gradient as a cause of refraction of sound waves was suggested by Stokes (1857) [1]. Reynolds (1874) [2] pointed out that changes in air temperature would also cause refraction of sound. One of the first theoretical accounts of these two effects was given by Rayleigh (1896) [3]. Barton (1901) [4] pointed out that in the presence of wind the direction of a sound ray in space is not necessarily along the wave front normal. He considered the case of a linear increase of wind speed with height and derived the equation of sound rays from a source at the origin. In the case where the wave front is horizontal initially, the ray paths are parabolas, and the wave front remains horizontal during propagation. Parabolic sound rays have been obtained also by Matthiesen (1899) [5], Mohn (1892, 1893, 1895) [6,7,8] and Jäger (1896) [9]. The inverse problem of deducing atmospheric properties from observations on sound wave propagation was dealt with by Löwy (1919) [10]. Abnormal propagation of sound waves has been investigated by Borne (1910) [11], Fujiwhara (1912) [12], Everdingen (1915) [13] and Nölke (1917) [14]. Kommerell (1916) [15] and Lamb (1925) [16] applied geometric acoustics to a model atmosphere with a linear temperature profile. Emden (1918) [17] and Milne (1921) [18] gave the first generalized treatments of sound propagation. Emden detected that the path of the wave front normal is a curve of single curvature whereas the ray is a curve of double curvature, if wind force and wind direction are functions of altitude only. Using Milne's paper, Groves (1955) [19] presented an even more generalized treatment of sound propagation by means of geometric acoustics. Some years



In presence of tangential components of  $\vec{u}$  to the wave front any particular wave front element propagates with the ray velocity, which is not in the direction of the wave front normal and can be obtained by substituting (10) into (7) giving

3-3

$$\vec{r} = \frac{\partial \omega}{\partial \vec{k}} = a \cdot \frac{\vec{k}}{k} + \vec{u} = \vec{a}_r \quad (12)$$

This is the vector sum of the local sound velocity in the direction of the wave front normal and the velocity  $\vec{u}$  with which the sound is carried along by the moving fluid. A ray is then a line such that the tangent to it at any point is in the same direction as the ray velocity given by equation (12).

The wave number vector  $\vec{k}$  is always in the direction of the wave front normal  $\vec{n}$  of the wave front and not necessarily into the direction of the ray velocity. The relation between  $\vec{n}$  and  $\vec{k}$  is given by

$$\frac{\vec{k}}{k} = \vec{n} \quad (13)$$

where

$$k = (\vec{k} \cdot \vec{k})^{1/2} \quad (14)$$

According to (13) and (14), the change in direction of  $\vec{n}$  is given by

$$\frac{\partial \vec{n}}{\partial t} = \frac{\partial}{\partial t} \left( \frac{\vec{k}}{k} \right) = \frac{1}{k} \frac{\partial \vec{k}}{\partial t} - \vec{n} \left( \vec{n} \cdot \frac{1}{k} \frac{\partial \vec{k}}{\partial t} \right) \quad (15)$$

On the other hand, it follows from (9) and (7) that

$$\begin{aligned} \frac{1}{k} \frac{\partial \vec{k}}{\partial t} &= -\text{grad } a - \left( \frac{\vec{k}}{k} \cdot \text{grad } a \right) \vec{n} - \left( \frac{\vec{k}}{k} \times \text{curl } \vec{u} \right) \\ &= -\text{grad } a_{ph} \end{aligned} \quad (16)$$

With (16) equation (15) can be rewritten to give :

$$\frac{\partial \vec{n}}{\partial t} = -\text{grad } a_{ph} + \vec{n} (\vec{n} \cdot \text{grad } a_{ph}) \quad (17)$$

which coincides with equation (19) of Groves [19] paper. The curve of the wave front normal is then defined as a line such that the tangent to it at any point is in the same direction as the wave front normal. Introducing the element of length along this curve  $d\vec{z} = a_{ph} dt$ , we can rewrite (17) to give

$$\frac{d\vec{n}}{d\vec{z}} = -\frac{1}{a_{ph}} \text{grad } a_{ph} + \frac{\vec{n}}{a_{ph}} (\vec{n} \cdot \text{grad } a_{ph}) \quad (18)$$

In steady propagation of sound in an inhomogeneous medium at rest ( $\vec{u} = 0$ ) the curve of the wave front normal coincides with the ray and the phase velocity with the ray velocity as well. Furthermore, the phase velocity then is equal to the local sound velocity

$$a_{ph} = a \quad (19)$$

where  $a$  is a given function of the coordinates

$$\frac{d\vec{n}}{d\vec{z}} = -\frac{1}{a} \text{grad } a + \frac{\vec{n}}{a} (\vec{n} \cdot \text{grad } a) \quad (20)$$

As is known from differential geometry, the derivative  $d\vec{n}/d\vec{z}$  along the ray is equal to  $\vec{N}/R$ , where  $\vec{N}$  is a unit vector along the principal normal and  $R$  is the radius of curvature of the ray. The right hand side of equation (20) is apart from the factor  $1/a$ , the derivative of the sound velocity along the principal normal. Therefore (20) can be rewritten to give

$$\frac{1}{R} = -\frac{1}{a} (\vec{N} \cdot \text{grad } a) \quad (21)$$

which means that the rays are bent towards the region where  $a$  is smaller. However, in the general case when  $\vec{u}$  is nonzero, the equations (12) and (17) have to be solved simultaneously in terms of the initial form of the wavefront in order to obtain the geometry of the wave front at a later time. The procedure of solving (12) and (17) can be simplified by using trace velocities introduced by Groves [19] as defined in the next chapter.

### 2.3 Groves method of trace velocities

The initial wavefront at time  $t = 0$  is given by

$$r = r(\alpha, \beta, 0) \quad (22)$$



and by

$$r = r(\alpha, \beta, t) \quad (23)$$

at a later time (See figure 2).  $\alpha$  and  $\beta$  are taken as parametric coordinates to the points of the wavefront. The unit normal at the point  $(\alpha, \beta)$

$$\vec{n} = \vec{n}(x, y, z) = \vec{n}(\alpha, \beta, t) \quad (24)$$

can also be defined as  $\vec{n}(\lambda, \mu, \nu)$  where  $\lambda, \mu, \nu$  are the direction cosines of  $\vec{n}$ :

$$\vec{n}^2 = 1 = \lambda^2 + \mu^2 + \nu^2 \quad (25)$$

The velocity  $\vec{u}$  of the medium then is

$$\vec{u} = (u, v, w) \quad (26)$$

Groves now introduced the trace velocities

$$\lambda v_\lambda = v_y \mu = \nu v_z = a_{ph} \quad (27)$$

which can be interpreted after Groves (see figure 2). The tangent plane at the point  $(\alpha, \beta)$  of the wavefront at time  $t$  cuts the  $x$ ,  $y$  and  $z$ -axis at the points  $X, Y, Z$  respectively. These intersection points move with the velocities  $a_{ph}/\lambda, a_{ph}/\mu, a_{ph}/\nu$ , i.e.,  $v_x, v_y, v_z$  along the  $x$ -,  $y$ -,  $z$ -axis respectively. Now replacing the direction cosines of the wavefront normal by the trace velocities the phase velocity (10,13) can be rewritten

$$a_{ph} = a + \frac{\left(\frac{u}{v_x} + \frac{v}{v_y} + \frac{w}{v_z}\right)}{\left(\frac{1}{v_x^2} + \frac{1}{v_y^2} + \frac{1}{v_z^2}\right)^{1/2}} = \frac{1}{\left(\frac{1}{v_x^2} + \frac{1}{v_y^2} + \frac{1}{v_z^2}\right)^{1/2}} \quad (28)$$

Now, introducing the new vector  $h(\alpha, \beta, t)$  defined by

$$\vec{h} = \left(\frac{1}{v_x}; \frac{1}{v_y}; \frac{1}{v_z}\right) \quad (29)$$

with some rearrangement Groves rewrote equation (17) as

$$\frac{\partial \vec{h}}{\partial t} + (\vec{h} \cdot \vec{h} \cdot \vec{u}) \vec{h} + \text{grad}(\vec{h} \cdot \vec{h} \cdot \vec{u}) = 0 \quad (30)$$

Here  $\vec{h}$  and  $\vec{u}$  are the local changes with the time of sound velocity and wind velocity respectively. However, since a sound wave is very fast, these changes in general can be neglected. The vector  $h$ , of course, depends on the choice of reference axis. Now, equation (30) has to be solved simultaneously with (12)

#### 2.4 Sound propagation in the atmosphere

For the sound wave propagation in the atmosphere, the following simplifying assumptions can be made:

- 1) As explained at the end of the above chapter sound velocity  $a$  and wind velocity  $\vec{u}$  are independent of time.
- 2) Furthermore,  $\vec{u}$  and  $a$  are independent of horizontal displacements. This means that the distribution of meteorologic lows and anticyclones is neglected and the curvature of the earth as well.

Thus, wind velocity and sound velocity are functions of altitude only. If the  $z$ -axis is taken in the vertical direction the relation

$$\vec{u} = \vec{u}(z) \quad a = a(z) \quad (31)$$

holds.

From (30) it then follows that

$$\begin{aligned} v_x &= d(\alpha, \beta) \\ v_y &= b(\alpha, \beta) \end{aligned} \quad (32)$$

which means that along any ray  $(\alpha, \beta)$ ,  $v_x$  and  $v_y$  remain constant. Following Groves [19]  $d$  and  $b$  are introduced as new parametric coordinates

$$\begin{aligned} d &= d(\alpha, \beta) \\ b &= b(\alpha, \beta) \end{aligned} \quad (33)$$

A characteristic velocity

$$a_c = \frac{1}{\left(\frac{1}{d^2} + \frac{1}{b^2}\right)^{1/2}} \quad (34)$$

is introduced. To an observer on the ground receiving the ray (d,b), the sound appears to be travelling along the ground with velocity  $a_c$ .

With the abbreviation

$$a_z = a_c \left[ 1 - \frac{u(z)}{d} - \frac{v(z)}{b} \right] \quad (35)$$

and using (28), (32), (34), the trace velocity in the vertical direction is found to be

$$v_z = a_c \frac{\left[ wa_z \pm a(a_z^2 + w^2 - a^2)^{1/2} \right]}{a_z^2 - a^2} \quad (36)$$

The phase velocity reads in terms of the new coordinates :

$$a_{ph} = a_c \frac{\left[ aa_z \pm (a_z^2 + w^2 - a^2)^{1/2} \right]}{a_z^2 + w^2} \quad (37)$$

#### 2.4.1 Law of refraction

The law of refraction is found by formulating first the direction cosines of the wavefront normal in terms of the new coordinates by means of (25), (27), and (32) and then substituting  $a_{ph}$  from (10)

$$\frac{\{a(z) + \lambda u(z) + \mu v(z) + w(z)\}}{\lambda} = a \quad (38)$$

$$\frac{\{a(z) + \lambda u(z) + \mu v(z) + w(z)\}}{\mu} = b$$

For every particular ray, i.e.; fixed values of d and b, these relations give together with (25) the direction cosines of the wavefront normal along the ray. When the wavefront is parallel to the y-axis ( $\mu = 0$ ), and when there is no vertical component of the wind ( $w(z) = 0$ ) (38) becomes

$$\frac{a(z)}{\lambda} + u(z) = d \quad (39)$$

This formula also has been deduced by Rayleigh [3]. When  $u(z) = 0$ , Snell's law of geometrical optics is obtained

$$\frac{\lambda}{\lambda_0} = \frac{a(z)}{a_0} \quad (40)$$

where  $\lambda_0$  and  $a_0$  are the initial values of direction cosine of the wavefront normal with the x-axis and sound velocity respectively.

From (40) again it can be seen that, as stated with equation (21), the rays are bent towards the region where the sound velocity is smaller.

From the equations (38) the relation

$$\frac{\lambda}{\mu} = \frac{b}{d} \quad (41)$$

can be deduced. This means, as stated already by Milne [18], that along any ray the wavefront normal remains parallel to the same vertical plane.

#### 2.4.2 Solution for wavefront and rays

The ray velocity (12) can be written in components as

$$\begin{aligned} \frac{\partial x}{\partial t} &= u(z) + a(z)\lambda(d,b,z) \\ \frac{\partial y}{\partial t} &= v(z) + a(z)\mu(d,b,z) \\ \frac{\partial z}{\partial t} &= w(z) + a(z)v(d,b,z) \end{aligned} \quad (42)$$

3-6

where the direction cosines  $\lambda$ ,  $\mu$ ,  $\nu$  can be found from (38) or by means of (23), (27) and (32). The integration of (42) yields the equation of the wavefront at a later time.

$$x = x(a, b, z) = x_0(a, b) + \int_{z_0(a, b)}^z \frac{u(z) + a(z)\lambda(a, b, z)}{w(z) + a(z)\nu(a, b, z)} dz$$

$$y = y(a, b, z) = y_0(a, b) + \int_{z_0(a, b)}^z \frac{v(z) + a(z)\mu(a, b, z)}{w(z) + a(z)\nu(a, b, z)} dz \quad (43)$$

$$t = t(a, b, z) = t_0 + \int_{z_0}^z \frac{dz}{w(z) + a(z)\nu(a, b, z)}$$

The above equations can be evaluated for special forms of  $a(z)$  and  $\vec{u}(z)$  only. In other cases, numerical methods would have to be utilized, see also [28], [29] and [30]. In chapter 2.3 to 2.4.2, I make considerable use of the results obtained by Groves [19]. Further details can be studied in [19].

#### 2.4.3 Still atmosphere with constant decay of sound velocity

For aircrafts flying at high altitudes in general, the temperature stratification is more important than the vertical distribution of wind face and wind direction. Furthermore, the model of the atmosphere can be simplified by assuming the sound velocity to be a linear function of altitude  $z$ , that is,

$$a(z) = a_0 - mz \quad \vec{u} = 0 \quad (44)$$

where  $z$  denotes altitude above ground, the constant  $a_0$  is the speed of sound at the ground and the constant  $m$  the decrease of sound with altitude. This variation agrees substantially with measured data at the atmosphere up to altitudes between 35 000 and 40 000 feet. For a standard atmosphere,  $a_0 \approx 1,116$  ft/sec, and  $m \approx 0,0040$  ft/sec per foot. These values were used by Lansing and considerable use of the results obtained in his paper [21] is made in this chapter. Now, Randall [31] and Lansing [21] applied Fermat's principle of least time in order to obtain the rays. Introducing (44) in (43) gives the same result. For this particular atmosphere the rays are circles:

$$(\sqrt{x^2 + y^2} + \frac{a_0}{m} \tan c)^2 + (z - z_0 - \frac{a_0}{m})^2 = \frac{a_0^2}{m^2} \sec^2 c \quad (45)$$

where  $a_0 = a_0 - mz_0$  and  $c$  is the inclination of the ray to the horizontal at the origin of the sound source. These circles are lying in vertical planes through the origin of the disturbance having their centers located at the altitude  $a_0/m = 279,000$  feet, the so-called height of the virtual atmosphere which is the theoretical altitude at which the speed of sound vanishes. In the standard atmosphere, the speed of sound decreases up to an altitude of about 40,000 feet. Above this altitude there is the stratosphere with constant sound velocity (i.e., isothermal atmosphere), for which the geometry of rays and wavefronts is the same as in a homogeneous atmosphere.

For the lowest layer of the atmosphere between ground and an altitude of about 40,000 feet, the so-called troposphere, the above assumption (44) is a very good approximation. Then, the shape of the wavefronts associated with a still point source is obtained by the system of surfaces which are orthogonal to all the rays (45) through the position of the point source. The shape and growth of a wavefront in an atmosphere with linear decrease of the speed of sound with altitude is (see references 31 and 21):

$$(x - x_0)^2 + (y - y_0)^2 + \left[ z - z_0 + \frac{a_0}{m} (\cosh mt - 1) \right]^2 = \frac{a_0^2}{m^2} \sinh^2 mt \quad (46)$$

where  $(x_0, y_0, z_0)$  are the coordinates of the position of the sound source. The wavefronts form a system of spheres with centers lying on the  $z$ -axis through the origin of the disturbance. Figure 3, taken from [21] shows a vertical cross section of some rays and wavefronts.

The center of the wavefront gradually moves down the  $z$ -axis as time increases, because the sound speed gradient causes the sound to propagate more rapidly in the direction of the ground. If the sound source moves through the atmosphere, it can be represented by an infinite number of fixed sources located on the flight path each having a nonzero time dependent source strength only when the moving source just passes its position, e.g. lights switched on and off in a series to advertise something. Then the position of the acting source is a function of the retarded time given by the flight path,  $x_0(\tau)$ ,  $y_0(\tau)$ ,  $z_0(\tau)$ . In the case of supersonic source speed the spherical wavefronts form an enveloping surface. To illustrate this an accelerated source at supersonic speeds in a homogeneous atmosphere

is chosen, figure 4. For axisymmetric flow, the y- and z-axis collapse into the  $\sqrt{y^2+z^2}$  - axis, so that three dimensional unsteady axisymmetric flow can be represented with three coordinates only. The growth of the spheres then is represented by the Le Monge cones, see figure 4. Every Le Monge cone is fixed with its apex end to the flight path. Due to Huygen's principle applied to three dimensional unsteady flow, the areas of dependence and of influence collapse into the surfaces of these Le Monge cones. The envelope formed by the distribution of these cones is also known as Mach wave. The tangent between Le Monge cone and Mach wave is known as bicharacteristic. The intersection lines between Mach wave and planes of constant time are for constant source speed the characteristics. It is obvious that different vertical stratifications of the atmosphere in combination with different flight paths (straight, inclined, longitudinally or laterally accelerated) lead to an almost unlimited variety in the possible geometry of Mach waves. For the particular case of constant decay of sound speed with altitude, Lansing [21] has plotted the intersection line of the Mach wave (i.e., shock wave) with the ground, see figure 5.

3-7

#### 2.4.4 Atmospheric wind gradients near the ground

The case of an isothermal atmosphere with a horizontal wind is now considered. Then, as the wind velocity increases linearly with altitude, it follows that the ray travelling in the direction of the wind is deflected towards the earth (Figure 6), while a ray travelling against the wind is deflected upward. The observer at P will not receive the ray leaving the source in his direction. Only a small number of rays will arrive at P due to diffraction. However, in the atmospheric wind boundary layer, there is not only a decrease of wind force while approaching to the ground but also a change of wind direction. In the case of a stably stratified atmosphere, the wind direction changes by 45 degrees. This is the so called laminar Ekman wind boundary layer, see figure 7. In practice, the wind shear may vary from 0 to 180 degrees in dependence of different weather conditions. It seems to the author of this paper that windward and leeward sound propagation cannot be understood without the vertical distribution of wind direction. Measurements done in the past scatter considerably around a theoretical line calculated from vertical wind force distribution only, see figure 8, taken from [32]. Due to wind shear atmospheric sound wave propagation becomes much more complicated because the rays will be a curve of double curvature.

#### 2.4.5 Simultaneous wind and sound velocity gradients

In a real atmosphere wind gradients and temperature gradients act simultaneously. Small gradients lead to considerable curvature of sound rays. The illustrations in figures 9 and 10 are taken from a paper by Emden [17]. Figure 9 illustrates sound propagation, if temperature drops by 6.2° per kilometer. There is no wind between ground and 370 meters, above this altitude wind increases linearly by 4 meters per second per kilometer. The rays travelling windward are deflected upward by the temperature gradient and by the wind gradient, whereas the rays propagating along with the wind initially are deflected upward by the temperature gradient and then due to the wind gradient are deflected towards the earth. A large zone of sound shadow is created extending up to 159 kilometers on the leeward side of the sound source. Figure 10 shows sound propagation if temperature drops by 3 degrees from ground up to 910 meters and wind increases by 2.13 meters per second within this altitude. Above this altitude temperature drops by 3.65°C and the wind by 3.28 meters per second both within 1 kilometer.

#### 2.4.6 Worst case of ground to ground sound propagation

Even though geometry of sound wave propagation in atmosphere is manifold the worst case probably can be reduced to one simplified model of the atmosphere: that is, the midwind sound propagation during night, when there is a temperature inversion near the ground, so that both wind and temperature gradients bend the ray downward. Investigations [33] indicate that the rays then are segments of circles with a radius of 5 km, see figure 11. This also has been taken into account for German standard regulations [34] for outdoor sound propagation. It can be seen from figure 11 that the shielding effect of walls around an airport does not exist in this worst situation, since the sound jumps along a circular segment over the wall. Walls only contribute to reduction of sound emission if they are close to the sound source. Furthermore, there is a boundary layer at the wall, see figure 12, bending in addition to the above effects the ray towards the earth on the leeward side. Thus, Maekawa's [35] sophisticated diffraction theory for a still atmosphere cannot be applied to this situation.

#### 2.5 Conservation law of acoustic energy

In absence of viscosity and heat conductivity the sound is propagating by isentropic compressions and expansions of the medium and the distribution of acoustic energy can be determined after ray and wavefront geometry. In a motionless medium conservation of the acoustic energy density E defined by Rayleigh [3] :

$$E = \frac{\rho_0 q^2}{2} + \frac{p^2}{2\rho_0 a_0^2} \quad (47)$$

gives the desired intensity.  $\frac{\rho_0 q^2}{2}$  is the kinetic acoustic energy and  $\frac{p^2}{2\rho_0 a_0^2}$  is the potential acoustic energy. Then there are no more complications than those involved in the ray geometry. Guiraud (1965) [36] presented a quadrature along the ray in order to calculate the acoustic energy. The law of the conservation of acoustic energy was extended by Blokhintzev (1946) [26,27] to a medium with steady motion. Blokhintzev considered a modified energy density  $E \omega' / \omega$ , where  $\omega'$  is the frequency for a fixed observer and  $\omega$  the frequency for an observer moving with the undisturbed medium. Garrett (1967) [37] has given an interpreta-

38

tion of the Blokhintzev invariance in terms of another invariant  $E/\omega'$ , which is of the type introduced by Whitham (1965) [38], but Garrett restricted his consideration to a medium with undistributed steady motion. Ryzhov and Shefter (1962) [39] applied the Blokhintzev invariance to ray tubes and considered weak shock waves.

The same method was applied by Hayes (1969) [40] to the calculation of the sonic boom in a stratified atmosphere. Hayes [41] [42] showed that volume integrals of  $E/\omega$  are conserved with the undistributed flow unsteady and applied this result to a wave tube. He obtained the basic law in the form of Garrett:

$$\frac{\partial}{\partial t} \left( \frac{E}{\omega} \right) + \nabla \cdot \left( \frac{Ea_r}{\omega} \right) = 0, \quad (48)$$

where  $\nabla$  is the del operator. The integral of  $E/\omega$  over any volume whose boundary points move with velocity  $a_r$  is invariant. This result was also mentioned by Bretherton and Garrett (1968) [43]. The acoustic energy is conserved in ray tubes, see figure 13.

A ray tube is formed by sound rays associated with a specific value of the phase. With  $A_0$  being the area of a ray cut by a wavefront, Hayes [42] found that the quantity  $Ea_r/\omega^2$  is constant along a ray, a function only of phase. This is a generalization of Blokhintzev's [26] result. For further details Blokhintzev's [26], Hayes' [42] and Candel's [44] paper may be used. It is evident that in an atmospheric boundary layer, when the ray is a curve of double curvature, the ray tube is difficult to determine since it is generated by rays. For this reason it is desirable to find closed form solutions of the wave equation describing the effects of temperature, wind force and wind direction gradients.

### 3. ANALYTIC SOLUTIONS OF THE WAVE EQUATION

The atmospheric sound wave propagation often is under conditions for which a treatment by geometric acoustics would not be valid as there are for example the effects of gravity on infrasound propagation, scattering and diffraction of sound. It is therefore, not only for convenience, desirable to use a complete wave theory, rather than that theory of geometric acoustics.

#### 3.1 Homogeneous atmosphere

The analytical solution for the wave propagation in a homogeneous atmosphere is well known, see for example [45] or [46]. The general solution for plane waves is given by

$$\phi = f^+(at-x) + f^-(at+x) \quad (49)$$

representing the propagation of independent waves in the positive ( $f^+$ ) and negative ( $f^-$ )  $x$ -direction with the sound velocity  $a$ . The arguments  $(at-x)$  and  $(at+x)$  are retarded times. The potential  $\phi$  is retarded to that time at which the perturbation was produced. The general solution for spherical waves is

$$\phi = \frac{f^+(at-r)}{r} + \frac{f^-(at-r)}{r} \quad (50)$$

where  $r$  is the distance of the observer from the origin of the perturbation. The two terms on the right hand side of (50) represent the radially outward and the radially inward travelling wave respectively. Acoustical dipoles and quadrupoles can be found by linear superposition of acoustical monopoles given by (50), see for example Lighthill's paper (1952) [47].

#### 3.2 Isothermal atmosphere

In the terrestrial atmosphere, due to the influence of gravity, the static pressure  $p_0$  drops with increasing altitude. The vertical distribution of  $p_0$  is given by the fundamental equation of static meteorology

$$\frac{1}{\gamma p_0} \frac{dp_0}{dz} = - \frac{g}{a^2} \quad (51)$$

where  $g$  is the gravity acceleration,  $\lambda$  the wavelength and  $\gamma$  the ratio of the specific heats. Equation (51) states that at every local altitude the static pressure of the atmosphere corresponds to the weight of the air above this altitude. The vertical density distribution, due to the isothermal stratification, is given by the vertical static pressure distribution (51). The stratification parameter

$$\alpha_{\text{isotherm}} = \frac{g\lambda}{a^2} \quad (52)$$

is, except for infrasound, a quantity of a small value, i.e., wavelength divided by 8 km. The analytical solution for the wave propagation in an isothermal atmosphere has been given by Schrödinger (1917) [48]. It follows from his theory that the kinetic and potential energy associated with a plane sound wave remain constant separately while travelling upward or downward. That means that the amplitude of the particle velocity  $q$  due to the sound wave, see also equation (47), must change with the inverse square root of the density:

$$q = \sqrt{\frac{\rho_0}{\rho(z)}} \bar{q} \quad (53)$$

3-9

where  $\rho_0$  is the density at the altitude where the sound wave is given and  $\rho(z)$  the density at that altitude where the sound wave is observed. However, the sound pressure (47) changes with the square root of the density :

$$p' = \sqrt{\frac{\rho(z)}{\rho_0}} \bar{p} \quad (54)$$

The sound intensity remains unchanged compared to that one in a homogeneous atmosphere, since the density cancels in the product of (53) and (54) :

$$J = q \cdot p' = \bar{q} \cdot \bar{p}' \quad (55)$$

This is also in accordance with the fact that in an isothermal atmosphere the geometry of the wavefronts and rays is the same as in a homogeneous atmosphere. The result (55) therefore would also follow from the conservation law of the acoustic energy in a ray tube. Schrödinger [48] also taught us that there are additional terms due to gravity in the particle velocity (see figure 14). The air particle is then circling on an elliptic path. The ratio of the small axis divided by the large axis is of magnitude of  $\alpha$ , so that except for infrasound, this effect can be neglected. From figure 14 the relationship between infrasound waves and gravity waves can be seen. It has already been stated by Schrödinger [48] that dispersion must occur. However, the main effects of isothermal stratification on sound wave propagation in the usual frequency range is described by the factor  $\sqrt{\rho(z)}/\rho_0$  which can be replaced by the square root of the static pressure ratio :

$$\sqrt{\frac{\rho(z)}{\rho_0}} = \sqrt{\frac{p(z)}{p_0}} \quad (56)$$

which is more common in literature. A lot of papers on the sonic boom [49], [50], [51] are dealing with an isothermal atmosphere. Due to the constant temperature the characteristic method itself remains unchanged. The increasing static pressure and density while approaching to the ground result in a finite asymptotic distance between a leading and a trailing shock of a finite body, see also [52], whereas in a homogeneous atmosphere there is no finite asymptotic value for this distance. Furthermore, shock waves in an isothermal atmosphere are damped with an error function, see also [51]. Because of convenience, the isothermal atmosphere is often used to make preliminary studies of the gravity stratification effects on sound and shock wave propagation.

### 3.3 Polytopic atmosphere

In a polytopic atmosphere the fundamental law of static meteorology (51) still applies. Due to vertical transport of heat during some periods of instability the vertical distribution of temperature in a real atmosphere in general is somewhere between the indifferent stratified isentropic and the stably stratified isothermal atmosphere. The polytopic atmosphere can be well approximated by a constant decay of sound velocity with altitude, compare chapter 2.4.3.

With  $a_p$  and  $p_p$  as sound velocity and static pressure at source altitude, a transformation similar to equation (56) is made :

$$\frac{\bar{q}}{a} = \left( \frac{a_p p_p}{a p_0} \right)^{1/2} \frac{q_{red}}{a_p}; \quad \frac{p'}{p_0} = \left( \frac{a_p p_p}{a p_0} \right)^{1/2} \frac{p'_{red}}{p_p} \quad (57)$$

and a reduced particle velocity  $q_{red}$  and a reduced sound pressure  $p'_{red}$  will be obtained. With (57), the sound intensity is given by

$$J = \bar{q} \cdot p' = q_{red} \cdot p'_{red} \quad (58)$$

which means that the acoustic intensity is invariant to the transformation (57). The system of differential equations is in formal accordance with the corresponding system for the isothermal atmosphere solved by Schrödinger, see also [48] and [51]. The complete solution for  $q_{red}$  and  $p'_{red}$  can be taken from [53]. There a velocity potential is introduced given by

$$\phi = - \frac{f(t - \int_0^s \frac{a_p}{a(s)} ds)}{4\pi \frac{a}{a_p} R}$$

where  $R$  is the instantaneous radius of curvature of the wavefront and  $s$  is the distance measured along the ray from the origin of the source.

The quadrature  $\int_0^s \frac{a_p}{a(s)} ds$  represents a distorted ray, so that same units of distance cor-

respond to same units of time. Furthermore, the distortion allows the choice of two sets of bicharacteristics which are perpendicular to each other, see [53]. For the particular atmosphere with a constant decay of sound velocity with altitude, see chapter 2.4.3, the radius of curvature of the wavefront and the distorted distance along the ray can be given explicitly :

$$R = (x^2 + y^2 + z^2)^{1/2} \frac{a_p}{a_0} \left[ \frac{a_0}{a_p} + \frac{1}{4} \Lambda^2 (x^2 + y^2 + z^2) \right]^{1/2} \quad (60)$$

and

$$\int_0^s \frac{a_p}{a(s)} ds = \frac{1}{A} \operatorname{ar sinh} |AR| \quad (61)$$

where

$$A = \frac{1}{a_p} \frac{da}{dz} \quad (62)$$

is given by the rate of decay of  $a$  with altitude. The geometry of  $R$  and  $s$  also can be seen from figure 3. Of course, the correct formula for the acoustic intensity (58) can be derived using the analytical solution given in [53]. In order to show the deviation of the acoustic intensity from its value in a homogeneous atmosphere, a thumb rule is found by comparison of equation (59) with equation (58) :

$$I_{\text{polytropic}} \cdot J_{\text{homogeneous}} \frac{a^2}{a^2} = J_{\text{homogeneous}} \frac{I_p}{T_0} \quad (63)$$

where  $T_p$  is the absolute temperature at source altitude and  $T_0$  the absolute temperature at the observer's altitude. In figure 15 the sound pressure radiated by an acoustic monopole is shown. At the origin, it radiates the same acoustic pressure into all directions, the local sound pressure is modified only by the ratio of the sound velocities  $a_p/a_0$  and the local acoustic intensity by the ratio of the absolute temperatures  $T_p/T_0$ . This means that only the acoustic intensity from very high acoustic monopoles is affected by the vertical temperature distribution, when  $T_p/T_0$  reaches a maximum value of 0.75. For low acoustic monopoles there is almost no influence of temperature distribution on the acoustic intensity, since the temperature changes at most by ten degrees celcius only. The above statement does no longer hold for higher order acoustical sources such as acoustical dipoles, figure 16, and acoustical quadrupoles, figure 17. In these cases, there are two or four directions of zero intensity. These directions of zero intensity, of course, follow the ray and therefore are reflected upward or downward as a function of the temperature gradients. This may be important for high directivity noise sources such as jet noise. In this connection it might be worthwhile noting that near airports in months with different major weather conditions, there are different average noise levels taken from the same microphone positioned under the flight path.

The stratification factor for a polytropic atmosphere contains in addition to the gravitational term, given in equation (52), a contribution from the sound velocity gradient, see also [53] :

$$\alpha_{\text{polytropic}} = \frac{gz}{a \cdot a_p} \frac{2-\gamma}{2} + \frac{1}{2a_p} \frac{da}{dz} \quad (64)$$

Again the air particles circle during the passage of a sound wave on an elliptic path; see figure 14. The magnitude of the small axis is then given by the one of the large axis multiplied with  $\alpha_{\text{polytropic}}$ . Except for infrasound,  $\alpha_{\text{polytropic}}$  is very small. One more time the relationship to gravity waves is seen. Equation (64) is also consistent with Bergmann's statement [54] that there is also dispersion in the absence of gravity due to density gradients.

#### 3.4 Atmospheric wind boundary layer

Due to the combined action of meteorologic pressure gradient, ground friction and Coriolis force, there is a wind force gradient and a wind direction change in the atmospheric wind boundary layer, see figure 7. A sound wave cannot have much effect on the wind boundary layer, since a sound pressure level of 100 dB causes a particle velocity of 0.5 cm/s only, whereas the wind velocity ( $u(u_E, v_E, 0)$ ) is often greater than 50 cm/s. Thus, the velocity distribution in the combined wind and incident sound field is approximately the same as that in the wind boundary layer without the sound field. The first order equations therefore are obtained by subtracting the equations for the wind field from the ones for the combined wind and sound field. One then obtains for the conservation of mass :

$$\frac{d}{dt} \left( \frac{p'}{\gamma p_0} \right) + \frac{\partial q_x}{\partial x} + \frac{\partial q_y}{\partial y} + \frac{\partial q_z}{\partial z} = 0 \quad (65)$$

3-11

and momentum

$$\begin{aligned} \frac{d}{dt} q_x &= -a^2 \frac{\partial}{\partial x} \left( \frac{p'}{\gamma p_0} \right) - q_z \frac{\partial u_E}{\partial z} \\ \frac{d}{dt} q_y &= -a^2 \frac{\partial}{\partial y} \left( \frac{p'}{\gamma p_0} \right) - q_z \frac{\partial v_E}{\partial z} \\ \frac{d}{dt} q_z &= -a^2 \frac{\partial}{\partial z} \left( \frac{p'}{\gamma p_0} \right) \end{aligned} \quad (66)$$

where  $u_E$  and  $v_E$  are the wind components in the x- and y-directions and

$$\frac{d}{dt} = \left( \frac{\partial}{\partial t} + u_E \frac{\partial}{\partial x} + v_E \frac{\partial}{\partial y} \right) \quad (67)$$

is a substantial derivation indicating that the sound is carried along with the wind. For  $u_E$  and  $v_E$  any vertical distribution of wind can be taken.

To illustrate the effects of wind gradient, a plane sound wave ( $q_y = 0$ ) with the front inclined moving into a boundary layer with constant wind direction ( $v_E = 0$ ) is studied first, see figure 18. The coordinate system is moving with the uniform wind above the boundary layer. For this particular case the solution of (65) and (66) is given by

$$\begin{aligned} \frac{p'}{\gamma p_0} &= -\frac{1}{a} \left( \frac{\partial}{\partial t} + u_E \frac{\partial}{\partial x} \right) F \\ q_x &= a \frac{\partial F}{\partial x} + \frac{\partial u_E}{\partial z} N_z F \end{aligned} \quad (68)$$

$$q_y = a \frac{\partial F}{\partial y}$$

with

$$F = \left( \frac{N_{z0}}{N_z} \right)^{1/2} f \left( t - \int_0^s \frac{d\bar{n}}{a_{ph}(\bar{n})} \right), \quad (69)$$

and  $N_z$  and  $N_x$  as direction cosines of the wavefront in the boundary layer

$$N_x^2 + N_z^2 = 1 \quad (70)$$

and  $N_{x0}$  and  $N_{z0}$  as direction cosines of the wavefront outside of the boundary layer

$$N_{x0}^2 + N_{z0}^2 = 1 \quad (71)$$

With

$$N_{x0} = \sin \alpha_0 \quad \text{and} \quad N_x = \sin \alpha \quad (72)$$

Emden's [17] refraction law of the wavefront normal can be written as

$$\frac{1}{\sin \alpha} = \frac{1}{\sin \alpha_0} - \frac{u_E}{a} \quad (73)$$

The wavefront also can be regarded as a Mach wave of a plane profile at supersonic speed. The direction cosines (71) are then related to the Mach number  $M_0$  of that profile

$$N_{x0} = \sin \alpha_0 = \frac{1}{M_0} \quad (74)$$

From Emden's [17] refraction law (73) it can be found with

$$N_x = \frac{1}{M} \quad (75)$$



that

$$M = M_0 - \frac{U_L}{a} \quad (76)$$

$M$  is a local effective Mach number determined by the relative velocity of the profile relative to the moving particle in the boundary layer. The argument of the retarded function in (69) represents a phase. Therefore, in the quadrature along the path of the wavefront normal  $\bar{n}$ , compare chapter 2.3, the phase velocity  $a_{ph}$  and not the ray velocity is required. The quadrature also can be rewritten in terms of the Mach number or the direction cosines

$$\int_0^{\bar{n}} \frac{d\bar{n}}{a_{ph}(\bar{n})} = \frac{1}{a} \int_0^{\bar{n}} \frac{N_{x0}}{N_x(\bar{n})} d\bar{n} = \frac{1}{a} \int_0^{\bar{n}} \frac{M(\bar{n})}{M_0} d\bar{n} \quad (77)$$

Thus the character of the plane sound wave, see figure 18, depends on the local effective Mach number given by (75). This phenomenon has been used by Makino (1974) [55] to describe the effect of steady wind on the sonic boom.

Due to the interaction of the particle velocity due to the sound with the wind gradient an additional velocity in the  $x$ -direction occurs, see equation (68). This additional velocity obviously belongs to the sound field, since it is propagated with the sound, see also [56] and [57].

In the general case, when the wind direction changes with altitude ( $v_E \neq 0$ ), Emden's law [17] reads

$$\frac{1}{\sin \alpha} = \frac{1}{\sin \alpha_0} - \frac{\sqrt{u_E^2 + v_E^2} \cos \phi}{a} \quad (78)$$

where  $\phi$  is the angle between wind vector and horizontal component of the wavefront normal. The wind is supposed to be a function of altitude only. The solution of (65), (66) and (67) under the condition (78) reads for a planar wave, see also [57]:

$$\frac{p'}{\gamma p_0} = -\frac{1}{a} \left( \frac{\partial}{\partial t} + u_E \frac{\partial}{\partial x} + v_E \frac{\partial}{\partial y} \right) F \quad (79)$$

$$\begin{aligned} u_x &= a \frac{\partial F}{\partial x} + \frac{\partial u_E}{\partial z} N_z F \\ u_y &= a \frac{\partial F}{\partial y} + \frac{\partial v_E}{\partial z} N_z F \end{aligned} \quad (80)$$

$$u_z = a \frac{\partial F}{\partial z}$$

with

$$F = \left( \frac{N_{z0}}{N_z} \right)^{1/2} f \left( t - \int_0^{\bar{n}} \frac{d\bar{n}}{a_{ph}} \right) \quad (81)$$

and

$$a_{ph} = a + N_x u_E + N_y v_E \quad (82)$$

Emden [17] showed for this case that the path of the wavefront normal is a curve of single curvature. Therefore, the argument of the retarded potential (81) can be handled much easier than the ray required for the ray tube area method, because the ray is a curve of double curvature.

### 3.5 Infrasound waves

Internal gravity waves and infrasound waves have been dealt with in the literature since a long time. Early work by Rayleigh (1890) [58], Lamb (1908, 1910) [59, 60], G.J. Taylor (1929, 1936) [61, 62] and Pekeris (1938, 1939) [63, 64] was concerned with waves from the Krakatoa eruption, see also Symond (1888) [65], and from the great Siberian meteorite, see also Whipple (1930) [66]. Recent studies are on the interpretation of nuclear explosion waves, see Harkrider (1964) [67] and Pierce, Moo and Posey (1973) [68]. Other papers are

concerned with infrasound waves generated in the troposphere during severe weather [69] or during the passage of Concorde supersonic transport [70] or during deceleration of big ocean waves on beaches. A bibliography [71] published in 1971 lists over 600 titles. All these papers deal with wavelengths shorter than the Brunt-Väisälä wavelength, see also Väisälä (1925) [72] and Brunt (1927) [73]. On the other hand, studies on internal gravity waves, whose time period is longer than the Brunt-Väisälä period exclude compressibility effects, see also [74] and [75]. However, there are coupled gravity and infrasound waves as described by Keck (1977) [76]. Keck investigated one dimensional wave propagation in a compressible stratified fluid including a gravity field, see figure 19. He derived a wave equation for the vertical component of the particle velocity due to a wave travelling horizontally :

$$\frac{\partial^2}{\partial t^2} \left( \frac{\partial^2 q_z}{\partial t^2} + \tilde{N}^2 q_z \right) - a^2 \frac{\partial^2}{\partial x^2} \left( \frac{\partial^2 q_z}{\partial t^2} + \tilde{N}^2 q_z \right) = 0 \quad (83)$$

where

$$\tilde{N} = \sqrt{\frac{g}{\rho} \left( -\frac{d\rho}{dz} \right)} \quad (84)$$

is the Brunt-Väisälä frequency of an incompressible fluid and

$$N = \sqrt{\tilde{N}^2 - \frac{g^2}{a^2}} \quad (85)$$

that one of a compressible fluid. For vanishing gravity ( $g \rightarrow 0$ ) equation (83) reduces to

$$\frac{\partial^2 q_z}{\partial t^2} - a^2 \frac{\partial^2 q_z}{\partial x^2} = 0, \quad (86)$$

the well known sound wave equation and for an incompressible fluid ( $a \rightarrow \infty$ ,  $\tilde{N} = N$ ) to the gravity wave equation

$$\frac{\partial^2 q_z}{\partial t^2} + \tilde{N}^2 q_z = 0, \quad (87)$$

that is for the case when the buoyancy forces as like as a force of a spring, try to put the particle back into its original position. For a harmonic dependence of  $q_z$

$$q_z = q_0 \exp[i(\omega t - kx)] \quad (88)$$

Keck [76] obtained the following relation between angular frequency  $\omega$  and wave number  $k$  from (83)

$$k^2 = \frac{\omega^2}{a^2} \frac{\omega^2 - \tilde{N}^2}{\omega^2 - N^2} \quad (89)$$

A series expansion for large wave numbers ( $\tilde{N}^2 / a^2 k^2 \ll 1$ ) clearly shows two types of waves

$$\omega_1^2 = a^2 k^2 + \tilde{N}^2 - N^2 \left\{ \left( 1 - \frac{\tilde{N}^2}{a^2 k^2} + \dots \right) + \frac{N^2}{a^2 k^2} + \dots \right\} \quad (90)$$

where after Keck [76]  $\omega_1$  can be understood as the angular frequency of a sound wave modified by gravity effects and the angular frequency  $\omega_2$ , given by

$$\omega_2^2 = N^2 \left\{ \left( 1 - \frac{\tilde{N}^2}{a^2 k^2} + \dots \right) + \frac{N^2}{a^2 k^2} + \dots \right\} \quad (91)$$

as an angular frequency of a gravity wave modified by compressibility effects. The two waves are also shown in the dispersion diagram, figure 20, taken from [76], where  $\omega^2$  is plotted as a function of  $k^2$ . The slope

$$\frac{\partial \omega^2}{\partial k^2} = \frac{\omega}{k} \frac{\partial \omega}{\partial K}$$

is the product of phase velocity given by equation (10) and groupe velocity  $a_{gr} = \frac{\partial \omega}{\partial K}$  as given by equation (7). The dispersion diagram is for a stably stratified atmosphere. For the modified sound wave, the frequency is above the Brunt-Väisälä frequency ( $\omega^2 > N^2$ ). These waves asymptotically approach the line  $\omega^2 = k^2 a^2 + g^2/a^2$ . For the gravity wave modified by compressibility effects the highest possible frequency is, obviously, the Brunt-Väisälä frequency  $N$  for a compressible fluid. A generalization of the analytical solution given in chapter 3.3 to encompass the modified sound wave as given by Keck seems to be possible.

#### 4. REFERENCES

- 3-14
1. STOKES, G.G.: On the effect of wind in the intensity of sound. Brit. Ass. Rep. 22, 1857.
  2. REYNOLDS, O.: Proc. Roy. Soc. 22, 1874, p. 531.
  3. RAYLEIGH, Lord: The theory of sound, vol. II. MacMillan & Co, 1978; reprint of 2nd ed., Dover Publications, New York, 1945, p. 289.
  4. BARTON, E.H.: On the reflection of sound by wind. Phil. Mag. 1, 1901, p. 159.
  5. MATTHIESEN, E.: Theorie der atmosphärischen Refraktion der Schallwellen. Nov. Act. Ac. Leopoldinae 74, 1899, p. 459.
  - 6,7,8. MOHN, H.: Studien über Nebelsignale. Ann. d. Hydr., 1892, 1893, 1895.
  9. JÄGER, G.: Über die Fortpflanzung des Schalles in bewegter Luft. Sitzungsbericht der Wiener Akademie 105, Abt IIIa, 1896.
  10. LÖWY, H.: Zur Erforschung der Atmosphäre bei unsichtigem Wetter. Physik. Zeitsch. 20, 1919, pp 115-182.
  11. BORNE: Über die Schallverbreitung bei Explosionskatastrophen. Physik. Zeitsch., 11, 1910, pp 483-488.
  12. FUJIIHARA, S.: On the abnormal propagation of sound waves in the atmosphere. Bull. Centr. Meteor. Observ. of Japan, Vol. 2, No 1, 1912.
  13. EVERDINGEN, E.V.: The propagation of sound in the atmosphere. Koninkl. Akad. van Wetenschappen te Amsterdam, Vol. 18, no 6, 1915.
  14. NÖLKE, B.F.: Über die bei heftigen Explosionen und beim Geschützdonner beobachteten Anomalien der Schallausbreitung. Physik. Zeitsch. 18, 1917, p. 501.
  15. KOMMERELL, V.: Die Bahn der Schallstrahlen in der Luft unter dem Einfluss der Temperatur. Physik. Zeitsch. 17, 1916, pp 172-175.
  16. LAMB, H.: Dynamical theory of sound. 2nd ed., 1925, p. 221;
  17. ENDEN, R.: I. Beiträge zur Thermodynamik der Atmosphäre. II. Über die Ausbreitung des Schalles in einer windbewegten, polytropen Atmosphäre. Meteorologische Zeitsch. 35, 1918, pp 13-29, pp 74-81, pp 114-123.
  18. MILNE, E.A.: Sound waves in the atmosphere. Phil. Mag. 42, 1921, pp 96-114.
  19. GROVES, G.V.: Geometrical theory of sound propagation in the atmosphere. J. Atmosph. and Terrest. Physics, 7, 1955, pp 113-127.
  20. KELLER, J.B.: Geometrical acoustics. I. The theory of weak shock waves. J. Appl. Physics, 25, 8, 1954, pp 938-947.
  21. LANSING, D.L.: Application of acoustic theory to prediction of sonic boom ground patterns from manoeuvring aircraft. NASA TM D 1860, 1964.
  22. TARNOGRODZKI, A.: Propagation of the sonic boom in the still atmosphere with temperature gradient. Arch. Mech. Stosowanej, 3, 21, 1969, pp 271-280.
  23. DELANY, M.E.: Sound propagation in the atmosphere: a historical review. Acustica, 38, 1977, pp 201-223.
  24. PIERCY, J.E. & EMBLETON, T.F.W.: Review of noise propagation in the atmosphere. J. Acoust. Soc. Am., 61, 6, 1977, pp 1403-1418.
  25. LANDAU, L.D. & LIFSHITZ, E.M.: Fluid mechanics. Pergamon Press, 1963, pp 256-261.
  26. BLOKHINTZEV, D.: The propagation of sound in an inhomogeneous and moving medium. J. Acoust. Soc. Am., 18, 1946, pp 322-334.
  27. BLOKHINTZEV, D.: Acoustics of a nonhomogeneous moving medium. NACA TM 1399, 1956.
  28. SABY, J.S. & NYBERG, W.L.: J. Acoust. Soc. Am., 18, 1946, p. 316.
  29. ROTHWELL, P.: J. Acoust. Soc. Am. 19, 1947, p. 205.
  30. SCHUBERT, L.K.: Numerical study of sound radiation by a jet flow. I. Ray acoustics. J. Acoust. Soc. Am. 51, 1972, p. 439.
  31. RANDALL, D.G.: Methods for estimating distributions and intensities of sonic bangs. ARC R&M 3113, 1959.
  32. ABRAHAMSON, A.L.: Sound propagation over long distances. Progress in Astronautics and Aeronautics, 46, 1975, pp 3-15.
  33. THOMASSEN, : Untersuchungen zur Bestimmung der Verteilung von Schallpegeln bedingt durch meteorologische Einflüsse in der unteren Atmosphäre. Bericht des Ministers für Arbeit, Gesundheit und Soziales des Landes Nordrhein-Westfalen, 4 Düsseldorf, 1, Postf. 1134, Bericht Nr 326007.
  34. VEREIN DEUTSCHER INGENIEURE: VDI Richtlinie Schallausbreitung im Freien. VDI 2714, 1975.
  35. MAEKAWA, Z.: Noise shielding on highway. Proc. Noise Control Conf., Warschau, 1976, published by Wroclawska Drukarnia Naukowa, Warszawa, Poland, pp 55-64.
  36. GUIRAUD, J-P: Acoustique géométrique, bruit ballistique des avions supersoniques et focalisation. J. de Mécanique, 4, 1965, pp 215-267.
  37. GARRETT, C.J.R.: The adiabatic invariant for wave propagation in a nonuniform moving medium. Proc. Roy. Soc. Ser. A, 299, 1967, pp 26-27.
  38. WHITHAM, G.B.: A general approach to linear and non linear dispersive waves using a Lagrangian. J. Fl. Mech. 22, 1965, pp 273-283.
  39. RYZHOV, O.S. & SHEFTER, G.M.: On the energy of acoustic waves propagating in moving media. Appl. Math. Mech. (PMM), 26, 1962, pp 1293-1309.
  40. HAYES, W.D.: Sonic boom propagation in a stratified atmosphere. NASA CR 1299, 1969.
  41. HAYES, W.D.: Inst. for Defense Analysis, Jason Div., Res. Pap. P-50, 1963.
  42. HAYES, W.D.: Energy invariant for geometric acoustics in a moving medium. Phys. of Fluids, 11, 1968, pp 1654-1656. Erratum Phys. Fl. 11, 1968, p. 2/80.
  43. BRETHERTON, B.P. & GARRETT, C.J.R.: Wavetrains in inhomogeneous moving media. Proc. Roy. Soc. Ser. A, 302, 1968, pp 529-554.
  44. CANDEL, S.: Numerical solution of conservation equations arising in linear wave theory: applications to aeroacoustics. J. Fl. Mech. 83, 1977, pp 465-493.
  45. RAYLEIGH, Lord: The theory of sound. Repr. 2nd ed. Dover Publ. 1945, paragraphs 245 and 279.
  46. MORSE, P.M. & INGARD, K.U.: Theoretical acoustics. McGraw Hill, New York, 1968, p. 309.
  47. LIGHTHILL, M.J.: On sound generated aerodynamically, I. General theory. Proc. Roy. Soc., Ser. A 211, 1952, pp 564-587.

48. SCHRÖDINGER, E.: Zur Akustik der Atmosphäre. Phys. Zeitsch., 18, 1917, pp 445-453.
49. SEEBASS, A.R. & GEORGE, A.R.: Sonic boom reduction through aircraft design and operation. AIAA 11th Aerospace Sciences Meeting, Washington DC 1973; Paper 73-241.
50. GEORGE, A.R. & PLOTKIN, K.J.: Sonic boom waveforms and amplitude in a real atmosphere. AIAA J., Vol. 7, No 10, 1969, pp 1978-1981.
51. STUFF, R.: Die Theorie der Knallausbreitung in einer geschichteten Atmosphäre. Z. für Flugwiss., 17, 5, 1969, pp 156-164.
52. HAYES, W.D.: Sonic boom. Ann. Rev. Fluid Mech., 3, 1971, pp 269-290.
53. STUFF, R.: Closed form solution for the sonic boom in a polytropic atmosphere. AIAA J. of Aircraft, 9, 8, 1972, pp 556-562.
54. BERGMANN, P.G.: The wave equation in a medium with a variable index of refraction. J. Acoust. Soc. Am., 17, 4, 1946, pp 329-333.
55. MAKINO, M.: The effect of steady wind on sonic boom intensities. Transact. Japan Soc. Aero. Space Sci., 17, 37, 1974, pp 123-135.
56. MÖHRING, W.: Über Schallwellen in Scherströmungen. Fortschritte der Akustik, DAGA 76. VDI-Verlag 1976, pp 543-546.
57. STUFF, R.: Analytic solution for the sound propagation through the atmospheric wind boundary layer. Proc. Noise Control Conf., Warszawa 1976, published by Wroclawska Drukarnia Naukowa, Warszawa, Poland, pp 377-381.
58. RAYLEIGH, Lord: On the vibrations of an atmosphere. Phil. Mag. 29, 1890, pp 173-180.
59. LAMB, H.: On the theory of waves propagated vertically in the atmosphere. Proc. London Math. Soc. 7, 1908, pp 122-141.
60. LAMB, H.: On atmospheric oscillations. Proc. Roy. Soc. Series A84, 1910, pp 551-572.
61. TAYLOR, G.J.: Waves and tides in the atmosphere. Proc. Roy. Soc. Series A 126, 1929, pp 169-183.
62. TAYLOR, G.J.: The oscillations of the atmosphere. Proc. Roy. Soc. Series A 156, 1936, pp 318-326.
63. PEKERIS, C.L.: Atmospheric oscillations. Proc. Roy. Soc. A 158, 1937, pp 650-671.
64. PEKERIS, C.L.: The propagation of a pulse in the atmosphere. Proc. Roy. Soc. A 171, 1939, pp 434-449.
65. SYMOND, G.J.: The eruption of Krakatoa and subsequent phenomena. Trubner & Co Publ., London, 1888.
66. WHIPPLE, F.J.W.: The great Siberian meteor and the waves, seismic and aerial, which it produced. Qua. J. Roy. Meteor. Soc., 56, 1930, pp 287-304.
67. HARKRIDER, D.G.: Theoretical and observed acoustic-gravity waves from explosive sources in the atmosphere. J. Geophys. Res., 69, 1964, pp 5295-5321.
68. PIERCE, A.D.; MOO, C.A.; POSEY, J.W.: Generation and propagation of infrasonic waves. US Air Force, Bedford, Mass. 01730, AFCRL-TR 73-0135, 1973.
69. MOO, C.A. & PIERCE, A.D.: Generation of anomalous ionospheric oscillations by thunderstorms. AGARD CP 115, 1972, pp 17-1 - 17-6.
70. DONN W.L.: Exploring the atmosphere with sonic booms. Am. Scientist, 66, 1978, pp 724-733.
71. THOMAS, J.E.; PIERCE, A.D.; FLINN, E.A.; CRAINE, L.B.: Bibliography on infrasonic waves. Geophys. J. Roy. Astr. Soc., 26, 1971, pp 399-426.
72. VÄISÄLÄ, V.: On the effect of wind oscillations on the pilot observations. Soc. Scient. Fennica, Commun. Phys.-Math. II, 19, 1925, p. 1.
73. BRUNT, D.: The period of simple vertical oscillations in the atmosphere. Qua. J. Roy. Meteor. Soc., 53, 1927, pp 30-31.
74. PHILLIPS, O.M.: The dynamics of the upper ocean. Cambridge Univ. Press, 1966.
75. TURNER, J.S.: Buoyancy effects in fluids. Cambridge Univ. Press, 1973.
76. KECK, H.: Über die eindimensionale Ausbreitung kleiner Störungen in einem kompressiblen, geschichteten Medium im Schwerfeld. Zeitsch. Flugwiss.-Weltraumforsch. 1, 1, 1977, pp 42-46.

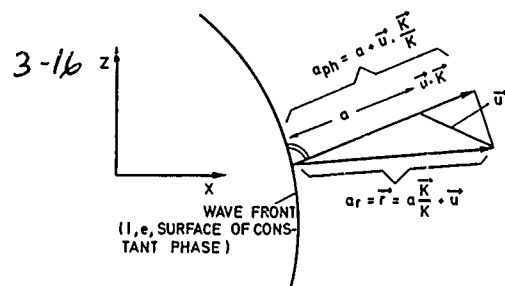


FIG 1 - PHASE VELOCITY  $a_{ph}$  AND RAYVELOCITY  $a_r$  OF A WAVE FRONT IN PRESENCE OF WIND  $\vec{u}$

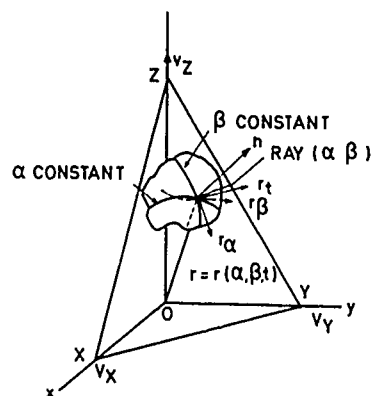


FIG. 2 - GROVES NOTATION USED FOR WAVE-FRONT AND RAYS.

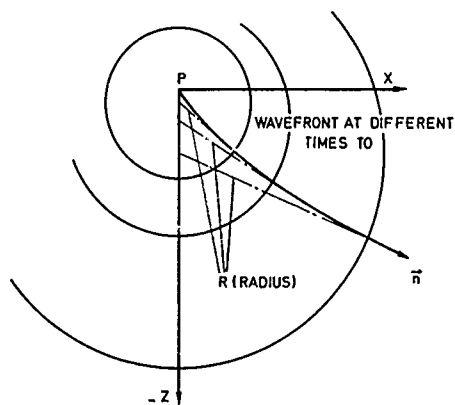


FIG 3 - THE WAVEFRONTS OF A SPHERICAL SOURCE IN A POLYTROPIC ATMOSPHERE

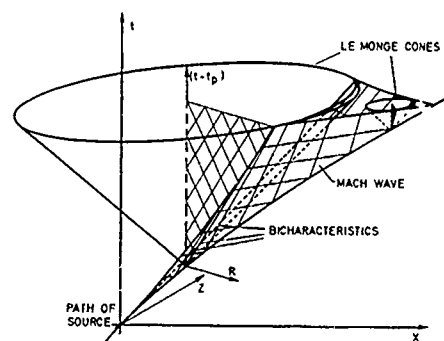


FIG 4 - MACH WAVE OF AN ACCELERATED SOURCE IN A HOMOGENEOUS ATMOSPHERE

SHOCK FRONTS AT DIFFERENT TIMES.

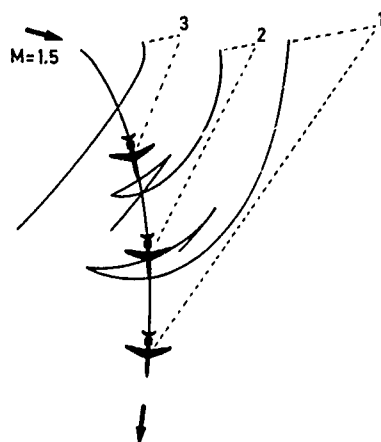


FIG. 5 - GROUND SHOCK WAVE FOR AN ELLIPTICAL RIGHT TURN AFTER LANSING (21).

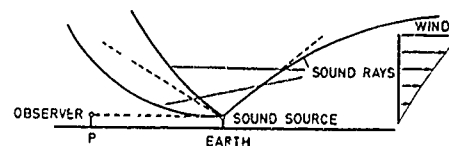


FIG 6 - EFFECT OF WIND FORCE GRADIENT ON SOUND WAVE PROPAGATION

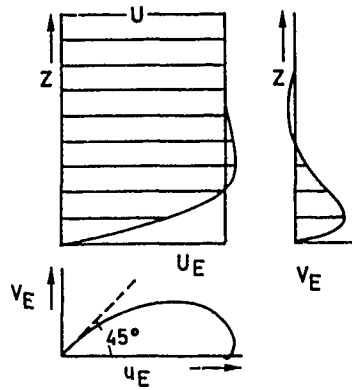


FIG. 7 - LAMINAR EKMAN LAYER.  
WIND DIRECTION CHANGES  
BY 45°.

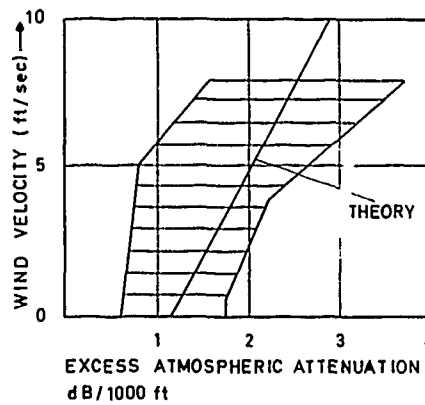


FIG. 8 - UPWIND SOUND PROPAGATION MEASUREMENTS AND THE LINE PREDICTED FROM THEORY TAKEN FROM (32)

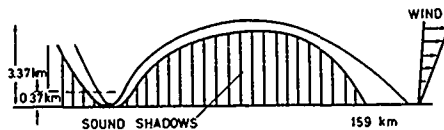


FIG. 9 - SOUND RAYS IF TEMPERATURE DECREASES WITH ALTITUDE AND WIND INCREASES ABOVE 370 m, SEE EMDEN (17)

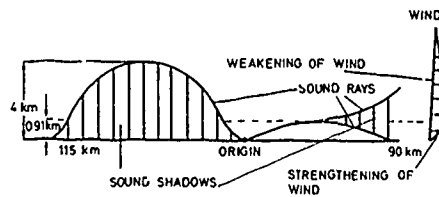


FIG. 10 - SOUND RAYS IF TEMPERATURE DROPS WITH ALTITUDE AND WIND FIRST INCREASES AND THEN DECREASES SEE EMDEN (17)

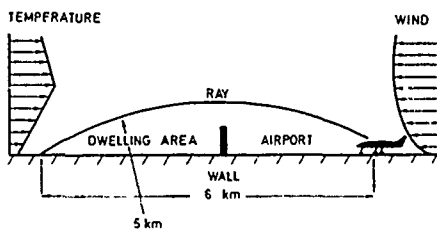


FIG. 11 - DOWNWIND SOUND PROPAGATION DURING NIGHT

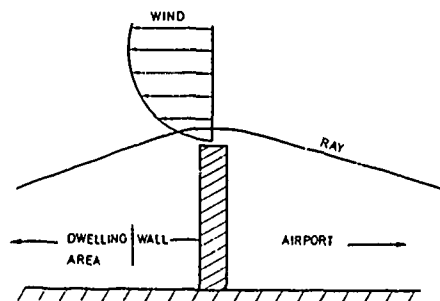


FIG. 12 - REFRACTION OF SOUND IN A BOUNDARY LAYER ABOVE A WALL

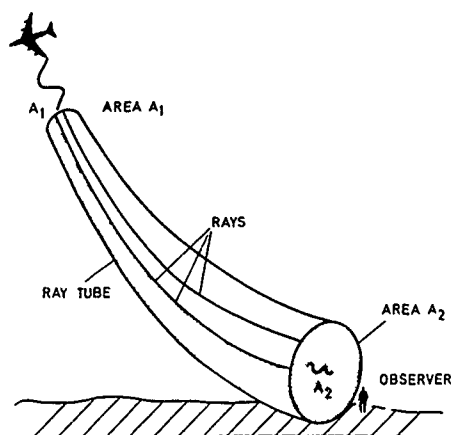


FIG 13 - THE ACOUSTIC ENERGY IS CONSERVED IN RAY TUBES

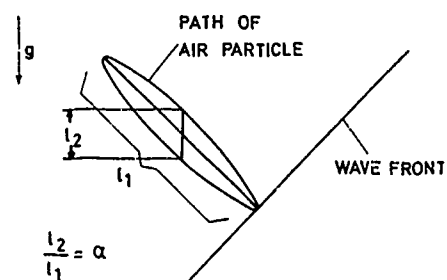


FIG. 14 - TRANSVERSAL COMPONENT OF PARTICLE VELOCITY DUE TO GRAVITY ACCELERATION,  $g$ .

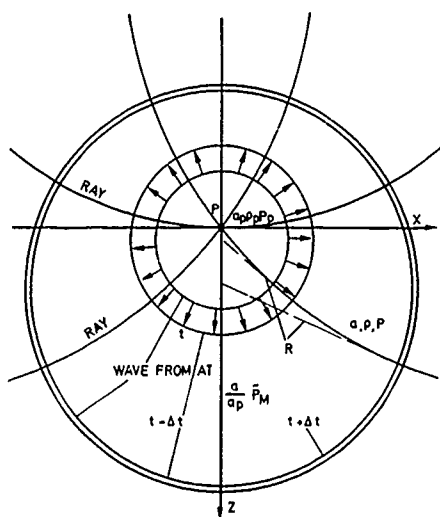


FIG 15 - RADIATION OF SOUND PRESSURE ( $\frac{a}{a_p} \bar{p}_M$ ) FROM AN ACOUSTICAL MONOPOLE

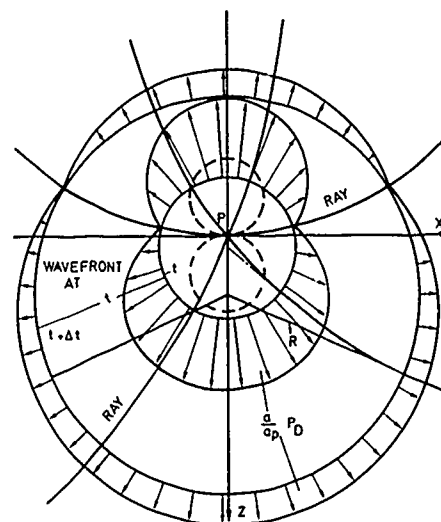


FIG 16 - RADIATION OF SOUND PRESSURE ( $\frac{a}{a_p} \bar{p}_D$ ) FROM AN ACOUSTICAL DIPOLE

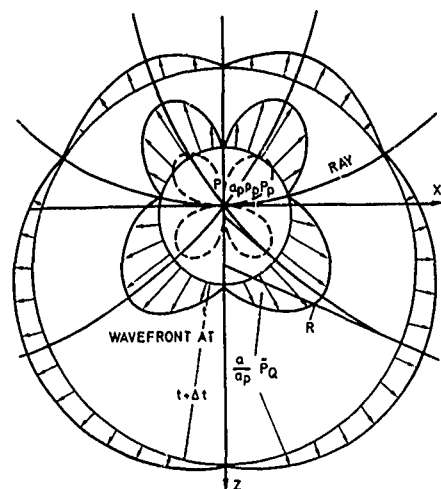


FIG 17 - RADIATION OF SOUND PRESSURE ( $\frac{a}{a_p} \bar{p}_Q$ ) FROM AN ACOUSTICAL QUADRUPOLE

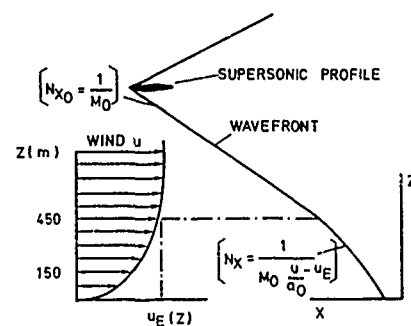


FIG 18 - DIRECTION COSINE OF A PLANE WAVE FRONT IN A BOUNDARY LAYER

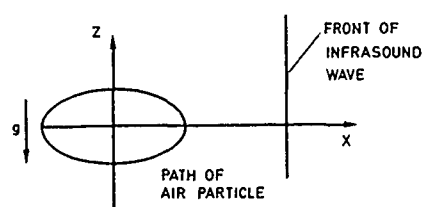


FIG 19 - HORIZONTAL INFRASOUND WAVE

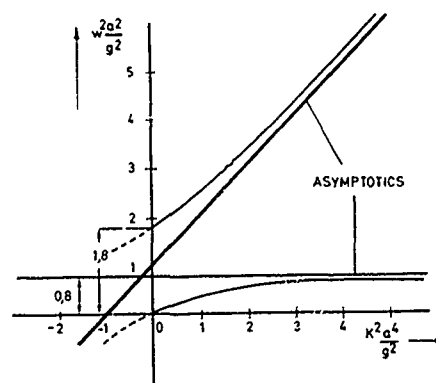


FIG 20 - DISPERSION DIAGRAM FOR  $\bar{N}^2 \frac{a^2}{g^2} = 1.0$  AND  $\bar{N}^2 \frac{a^2}{g^2} = 0.8$  (STABLY STRATIFIED)  
FOR  $\bar{N}^2 > w^2 > N^2$  NO FREQUENCY POSSIBLE  
TAKEN FROM KECK (76)



# MATHEMATICAL TECHNIQUES FOR ACOUSTIC PROPAGATION PROBLEMS

P.E. Doak, Institute of Sound and Vibration Research, The University, Southampton SO9 5NH, England

4-1

The principal mathematical techniques for solution of both steady state and transient acoustic propagation and boundary value problems, for both forced and free motion, are reviewed. These include separation of variables methods and the associated techniques for the resulting ordinary differential equations, Green function methods, Fourier, Laplace and other transform methods, finite element and other numerical methods, and certain special techniques including Wiener-Hopf. Emphasis is placed on the relative merits of the various methods for specific types of problems.

## 1. INTRODUCTION

In its relatively simple "acoustic analogy" form, the equation governing the thermodynamic pressure fluctuations  $p'(x_k, t)$  in a time stationary but otherwise arbitrary flow of a homogeneous fluid, can be written as

$$\frac{\partial^2 p'}{\partial x_i^2} - \frac{\partial}{\partial t} \left( \frac{1}{c^2} \frac{\partial p'}{\partial t} \right) = \frac{\partial}{\partial t} (\rho_s \frac{\partial S}{\partial t}) + \frac{\partial}{\partial x_i} (\rho f_i)' - \frac{\partial^2}{\partial x_i \partial x_j} (\rho v_i v_j - S_{ij})', \quad (1)$$

where  $p(x_k, t)$  is the thermodynamic pressure,  $1/c^2 = \rho_s = (\partial \rho / \partial p)_s$ ,  $\rho$  being the mass density and  $S$  the entropy per unit mass (similar subscript notation is used for other thermodynamic derivatives),  $f_i$  is the external force per unit mass (only the electromagnetic Lorentz force and/or a gravitational force are physically possible),  $v_i$  is the particle velocity and  $S_{ij}$  is the "viscous" stress tensor: i.e., the total internal stress tensor  $P_{ij}$  is given by  $P_{ij} = p \delta_{ij} - S_{ij}$ , where  $\delta_{ij}$  is the Kronecker delta,  $\delta_{ij} = 0$ ,  $i \neq j$  and  $\delta_{ii} = 1$ ,  $i = j$ . Cartesian vector and tensor notation is used,  $i, j, \dots = 1, 2, 3$ , with the usual convention that summation is indicated by a repeated index. A prime indicates the purely fluctuating part of a quantity and an overbar the time averaged, mean, part. By the time stationary hypothesis, any function  $f(x_k, t)$  can be written as  $f(x_k, t) = \bar{f}(x_k) + f'(x_k, t)$ , with  $f'$  having zero time average over an appropriate interval (a period, if the motion is periodic, or a suitably long time if it is random). Equation (1) is an inhomogeneous scalar wave equation with a wave speed,  $c(x_k, t)$ , which in general may be variable in both space and time. Analytical solution methods are readily available if  $c^2$  is a constant,  $c_0^2$ . In a physical case,  $c_0^2$  would naturally be selected as an average of  $c^2$  over an appropriate space-time region. With variable terms in  $c^2$  thus transferred to the right side equation (1) becomes of the form

$$\frac{\partial^2 p}{\partial x_i^2} - (1/c_0^2) \frac{\partial^2 p}{\partial t^2} = -q(x_k, t), \quad (2)$$

where  $-q(x_k, t)$ , the source term of this inhomogeneous scalar wave equation with a constant wave speed  $c_0$ , represents all the terms on the right side of equation (1) plus  $\partial \{ (1/c^2) - (1/c_0^2) \} (\partial p / \partial t) / \partial t$ . For simplicity, the primes indicating that the fluctuating part of  $p$  is being sought are omitted in equation (2), which in any case is formally correct even without them.

## 2. FORMAL GREEN FUNCTION SOLUTIONS

A formal solution of equation (2), appropriate for any fluid filled space  $V$  with any boundary surface  $S$ , and satisfying the condition of space-time causality (i.e., that the cause precedes the effect), can be obtained by using the free space Green function (the "point-impulse" response)  $G_\infty(x_k, t; y_k, \tau)$ , which is the particular solution of equation (2), satisfying radiation conditions, when  $q(x_k, t) = \delta(x_k - y_k) \delta(t - \tau)$ , where  $\delta(x_k - y_k) = \delta(x_1 - y_1) \delta(x_2 - y_2) \delta(x_3 - y_3)$ ,  $\delta(\cdot)$  being the Dirac delta function, and  $x_k, t$  and  $y_k, \tau$  being observer and source space time co-ordinates, respectively. This Green function is the impulsive primitive spherical wave  $G_\infty = \delta(\tau - (t - r/c_0)) / 4\pi r$ , where  $r = |x_k - y_k|$  is the source to observer distance. The problem can always be formulated on the hypothesis that  $q, p'$  and all its derivatives are zero up to, say, time  $t = 0$ , so that the complementary function for equation (2) is zero, and the forced particular integral solution due to  $q$  is then

$$p(x_k, t) = \int_V \frac{q(y_k, \tau - r/c_0)}{4\pi r} dy_k + \int_S \frac{1}{4\pi r} \left[ \frac{\partial p}{\partial n}(y_k, \tau) + \frac{\cos(n, r)}{r} \left( 1 + \frac{r}{c_0} \frac{\partial}{\partial \tau} \right) p(y_k, \tau) \right] dS(y_k), \quad (3)$$

Here  $n$  is the normal to  $S$  outward from  $V$ , and  $\cos(n, r)$  is the cosine of the angle between  $n$  and  $r$ . The volume integral in equation (3) represents the superposition of the primitive spherical waves propagating out from each point in the source distribution  $q(y_k, \tau)$ , each contribution arriving at an observation point a time  $r/c_0$  after it was emitted. The surface integral represents the effects of scattering of these original waves at the boundary  $S$ , and/or, since  $S$  could be simply any "fictitious" geometric surface drawn arbitrarily in the fluid, the effects of any sources outside  $V$ . The first term in the surface integral shows that the pressure gradient on  $S$  acts like a surface source layer. The second term, which is

$$- \int_S \int_\tau p(y_k, \tau) \frac{\partial G_\infty}{\partial n} dS d\tau,$$

shows that the pressure on  $S$  acts like a dipole surface layer, or, what is the same thing, a distribution of normal force per unit area on the fluid at the surface.

In addition to  $G_\infty$ , the Green function can include an arbitrary complementary function,  $G = G_\infty + G_c$ , and this in principle can be selected so that the Green function satisfies an "impedance" boundary condition of the form  $AG + \partial G / \partial n = 0$  on the surface  $S$ , the quantity  $A$  being specified on the surface. This form obviously includes the homogeneous boundary condition cases of  $G = 0$  or  $\partial G / \partial n = 0$  on  $S$ . The general Green function expression for  $p(x_k, t)$  can be written as

$$p(x_k, t) = \int_V \int_\tau q(y_k, \tau) G dy_k d\tau + \int_S (G \frac{\partial p}{\partial n} - p \frac{\partial G}{\partial n}) dS d\tau. \quad (4)$$

4.2

Evidently, if  $p$  satisfies an impedance boundary condition then if  $G$  is selected so that  $G$  satisfies the same condition the surface integral in equation (4) will vanish. In physical terms this means that the complementary function part of 3 represents the "scattering" from the actual impedance surface  $S$  of the incident impulse  $G$ . It is possible in many situations to construct appropriate Green functions, either exactly or approximately, by using the method of images, or expansions in suitable base functions, or otherwise. Also, the choice  $\partial G / \partial n = 0$  on  $S$  is often useful, corresponding to total in-phase reflection of the incident waves. On a rigid boundary of a fluid, of course,  $\partial p / \partial n = \partial S_{in} / \partial n$ , and insofar as the fluctuating viscous normal stresses are relatively negligible, this choice can lead to effective vanishing of the surface integral. As equation (4) for  $p(x_k, t)$  is independent of the choice of boundary condition for  $G$ , the volume integral in it always contains the "free field" contribution (i.e., the volume integral term of equation (3)) but the  $G$  contributions to the volume and surface integrals are interchangeable, as it were, being transferred from one to the other by the boundary condition choice.

If  $S$  is a surface in the fluid coinciding with a wavefront, then the surface integral in equation (3), or equation (4), is the complete formal expression of Huyghens' Principle.

### 3. SEPARATION OF VARIABLES

Image constructions for  $G$  are possible in certain problems involving plane boundaries. When the boundaries are not plane, recourse must be had to the method of separation of variables, or other methods. Fourier (or Laplace) transformation on time provides separation for time:

$$p(x_k, \omega) = \frac{1}{2\pi} \int p(x_k, t) e^{-i\omega t} dt, \quad p(x_k, t) = \int p(x_k, \omega) e^{i\omega t} d\omega. \quad (5)$$

With again a quiescent unforced system for  $t < 0$ , application of the Fourier transform to equation (2) gives

$$\nabla^2 p(x_k, \omega) / \partial x_k^2 + k^2 p(x_k, \omega) = -q(x_k, \omega), \quad (6)$$

where  $k^2 = \omega^2 / c_0^2$ . Equation (6) is the scalar Helmholtz equation, and it is separable in eleven orthogonal curvilinear co-ordinate systems: rectangular Cartesian, circular, elliptic and parabolic cylinder, spherical, conical, parabolic, prolate and oblate spheroidal, ellipsoidal, and paraboloidal. It is also separable in a few non-orthogonal systems (e.g., triangular). Thus, in these co-ordinate systems, series solutions of the homogeneous form of equation (6) can be found:

$$p(x_k, \omega) = \sum_{l,m,n} \{ C_{l,m,n}^{(1)} F_{l,m,n}^{(1)}(\xi_1; k_{l,m,n}) + C_{l,m,n}^{(2)} F_{l,m,n}^{(2)}(\xi_1; k_{l,m,n}) \}, \quad i = 1, 2, 3, \quad (7)$$

where the  $\xi_i$  are the three co-ordinates, the  $C_{l,m,n}^{(i)}$ 's are constants, the  $k_{l,m,n}$ 's are the associated wave-numbers,  $k_{l,m,n}^2 = k_{2l,m,n}^2 + k_{3l,m,n}^2 = k^2$ , whose relative proportions are determined by boundary conditions, including those at infinity, if any, and the superscripts correspond to the two linearly independent solutions of the second order ordinary differential equations produced by the separation process. The total wavenumber eigenvalues,  $k^2$ , may be selected equal to  $k^2$ , or not, according to the type of problem. This selection is possible, and desirable, according to circumstance, because for the orthogonal co-ordinate systems suitable combinations of the  $F_{l,m,n}$ 's can be constructed to form a complete orthonormal set of base functions over an interval along a co-ordinate curve, or on a co-ordinate surface,  $\xi_i = \text{constant}$ , or over a volume bounded by co-ordinate surfaces. The case of rectangular Cartesian co-ordinates is the simplest for illustration, and is representative of the general case. Here, for the co-ordinate surfaces  $x_1 = 0, a$ ,  $x_2 = 0, b$ ,  $x_3 = 0, d$ , the (un-normalized) base functions are, for curve interval, surface and volume cases,

$$\begin{aligned} & \cos \left( \frac{l\pi x_1}{a} \right), \quad \cos \left( \frac{l\pi x_1}{a} \right) \cos \left( \frac{m\pi x_2}{b} \right), \quad \cos \left( \frac{l\pi x_1}{a} \right) \cos \left( \frac{m\pi x_2}{b} \right) \cos \left( \frac{n\pi x_3}{d} \right), \\ & \sin \left( \frac{l\pi x_1}{a} \right), \quad \sin \left( \frac{l\pi x_1}{a} \right) \sin \left( \frac{m\pi x_2}{b} \right), \quad \sin \left( \frac{l\pi x_1}{a} \right) \sin \left( \frac{m\pi x_2}{b} \right) \sin \left( \frac{n\pi x_3}{d} \right), \end{aligned}$$

with the corresponding  $k_{l,m,n}$ 's as  $k_{1l}^2 = (l\pi/a)^2$ ,  $(k_{1l}, k_{2m}) = (l\pi/a, m\pi/b)$  and  $k_{l,m,n}^2 = (l\pi/a)^2 + (m\pi/b)^2 + (n\pi/d)^2$ . Evidently when such sets of base functions are constructed, the wavenumber eigenvalues are geometrically determined, quite independently of the fluid's sound speed or density, and of any applied forcing frequencies.

By means of such sets of base functions, series expressions for any functions defined in the volume, or on its surfaces or edges, can be found. By virtue of the orthonormality of the base functions,  $\psi_{l,m,n}(\xi_i)$  for the volume case, for example,

$$\int_V \psi_{l,m,n} \psi_{l',m',n'}^* dV = \begin{cases} (0, & l,m,n \neq l',m',n', \\ (1, & l,m,n = l',m',n', \end{cases} \quad (8)$$

and hence for any function  $f(\xi_i)$ ,

$$f(\xi_i) = \sum_{l,m,n} a_{l,m,n} \psi_{l,m,n}, \quad a_{l,m,n} = \int_V f \psi_{l,m,n}^* dV, \quad (9)$$

and similarly for the surface and co-ordinate curve cases. By use of such expansions matching of boundary conditions on co-ordinate surfaces can be readily accomplished, and also the particular solution of the inhomogeneous equation (6) can be obtained.

The case of a sphere in a fluid ( $\rho, c$ ) of infinite extent, the sphere having a small amplitude normal velocity  $v_n(a, \theta, \phi) e^{i\omega t}$  on its surface  $r = a$ , provides an illustration of boundary condition matching. In spherical polar co-ordinates  $(r, \theta, \phi)$  with origin at the sphere's centre, the normalized (i.e., on a sphere of unit radius) surface base functions are the spherical harmonics  $S_n^m(\theta, \phi) = N_n^m P_n^m(\cos \theta) e^{im\phi}$ ,  $P_n^m$  being the associated Legendre functions and  $N_n^m$  the normalization constants. The radial functions satisfying outgoing wave radiation conditions at infinity are the spherical Hankel functions of the second kind,  $h_n^{(2)}(kr)$ . Thus the pressure for  $r > a$  can be written as

$$p(r, \theta, \phi) e^{i\omega t} = e^{i\omega t} \sum_{mn} p_{mn} S_n^m(\theta, \phi) h_n^{(2)}(kr), \quad (10)$$

with the constants  $p_{mn}$  remaining to be determined by application of the boundary conditions at  $r = a$ . For small amplitudes,  $\rho \partial v_{mn} / \partial t + \partial p / \partial r = 0$  so that at  $r = a$  one must have  $(1/ik\rho_0 c_0) \partial p / \partial r + v_r(a, \theta, \phi) = 0$ . Expansion of  $v_r(a, \theta, \phi)$  in the spherical harmonics gives

$$v_r(a, \theta, \phi) = \sum_{mn} v_{mn} S_n^m, \quad v_{mn} = \frac{2\pi}{0} \int_0^\pi \int_0^{2\pi} v_r(a, \theta, \phi) S_n^m \sin\theta d\theta d\phi.$$

The boundary condition therefore is

$$e^{i\omega t} \sum_{mn} \{ (1/ik\rho_0 c_0) h_n^{(2)}(ka) p_{mn} + v_{mn} \} S_n^m(\theta, \phi) = 0, \quad (11)$$

where the prime indicates differentiation with respect to the argument. Since the  $S_n^m$ 's are orthogonal, equation (11) can be satisfied only if the coefficient of each  $S_n^m$  vanishes. Hence the coefficients  $p_{mn}$  are determined:

$$p_{mn} = \rho_0 c_0 i h_n^{(2)}(ka) v_{mn}. \quad (12)$$

The quantity  $\rho_0 c_0 i h_n^{(2)}(ka)$  is evidently the "mn-modal" impedance at the radiating surface  $r = a$ .

An illustration of how particular solutions can be similarly obtained is provided by the case of scattering of an incident plane wave by a rigid sphere, again of radius  $r = a$ . Suppose first that a point simple harmonic pressure source of unit strength is located at  $z = h$  ( $h > a$ ) on the polar axis of the  $(r, \theta, \phi)$  co-ordinate system with origin at the centre of the sphere. The pressure from this source then can be expressed as  $e^{i\omega t - ikR/4\pi R}$ ,  $R = \sqrt{x^2 + y^2 + (z - h)^2}$ , in which, of course,  $x = r \sin\theta \cos\phi$ ,  $y = r \sin\theta \sin\phi$  and  $z = r \cos\theta$ . This potential is the particular solution of the inhomogeneous equation

$$(\partial^2 / \partial x_i^2 + k^2) p_0 = -\delta(x) \delta(y) \delta(z - h) e^{i\omega t} \quad (13)$$

and is thus a free space Green function for simple harmonic motion. The small amplitude boundary conditions of zero pressure gradient on the rigid sphere  $r = a$  evidently can be satisfied if the source term, or, what is the same thing, the pressure field from it, can be expressed in terms of the wave functions  $S_n^m(\theta, \phi) h_n^{(1,2)}(kr)$  appropriate to the co-ordinates with origin at the sphere's centre. Such expansions of base functions in one co-ordinate system in terms of those of another are obviously possible in any region in which the domains of the base functions overlap (since both sets are complete and orthonormal). They are sometimes called "addition formulas". In the case of  $e^{-ikR}/4\pi R$ , with the point  $R = 0$  being on the polar axis at  $z = h$ , the expansion is

$$\frac{e^{-ikR}}{4\pi R} = -\frac{ik}{4\pi} h_0^{(2)}(kR) = -\frac{ik}{4\pi} \sum_{n=0}^{\infty} (2n+1) P_n(\cos\theta) \begin{cases} j_n(kr) h_n^{(2)}(kh), & r < h \\ j_n(kh) h_n^{(2)}(kr), & r > h \end{cases}. \quad (14)$$

Here  $P_n$  are the Legendre polynomials and  $j_n$  the spherical Bessel functions. By proceeding to the limit  $h \rightarrow \infty$ , one obtains

$$p_i = e^{ikr \cos\theta} = \sum_{n=0}^{\infty} (-i)^{-n} (2n+1) P_n(\cos\theta) j_n(kr), \quad (15)$$

a representation for the incident plane wave in the negative  $z$ -direction. With the incident pressure wave,  $p_i$ , thus represented in terms of the appropriate base functions, the boundary condition that the total normal pressure gradient be zero at  $r = a$  can easily be applied as before. The scattered field can conveniently be represented as

$$p_s(r, \theta, \phi) e^{i\omega t} = e^{i\omega t} \sum_{sn} p_{sn} (-i)^{-n} (2n+1) P_n(\cos\theta) h_n^{(2)}(kr), \quad (16)$$

satisfying radiation conditions. The boundary condition then is

$$\left( \frac{\partial p_i}{\partial r} + \frac{\partial p_s}{\partial r} \right)_{r=a} = 0 = \sum_{n=0}^{\infty} (-i)^{-n} (2n+1) P_n(\cos\theta) \{ k j_n'(ka) + p_{sn} k h_n^{(2)}(ka) \},$$

which gives, by equating each coefficient to zero as before,

$$p_{sn} = -j_n'(ka) / h_n^{(2)}(ka).$$

The case of a hard-walled rectangular room containing a simple harmonic point source provides an interior problem example. With the  $e^{i\omega t}$  factor omitted, and the point source at  $y_1$ , the pressure satisfies

$$(\partial^2 / \partial x_i^2 + k^2) p(x_i) = -\delta(x_i - y_i) \quad (17)$$

in the room ( $0 < x_1 < a$ ,  $0 < x_2 < b$ ,  $0 < x_3 < d$ ), and  $\partial p / \partial n = 0$  on the walls. The normalized (over the room volume) base functions satisfying these boundary conditions are

$$\psi_{lmn}(x_i) = (1/abd) (2 - \delta_{0l}) (2 - \delta_{0m}) (2 - \delta_{0n}) \cos(l\pi x_1/a) \cos(m\pi x_2/b) \cos(n\pi x_3/d).$$

The formal expansion of the delta function in these base functions is

$$\delta(x_i - y_i) = \sum_{lmn} \psi_{lmn}(x_i) \psi_{lmn}(y_i),$$

and similarly the pressure can be written as

$$p(x_i) = \sum_{lmn} p_{lmn} \psi_{lmn}(x_i),$$

with the  $p_{lmn}$ 's to be determined by substituting both of these expansions into equation (17). This gives, again term by term,

4-4

$$((k^2 - k_{lmn}^2)p_{lmn} + \psi_{lmn}(y_i))\psi_{lmn}(x_i) = 0,$$

whence  $p_{lmn} = \psi_{lmn}(y_i)/(k^2 - k_{lmn}^2)$ . The coefficients  $p_{lmn}$  thus turn out to be infinite when  $k$  is equal to one of the wavenumber eigenvalues  $k_{lmn} = \sqrt{((\pi/a)^2 + (m\pi/b)^2 + (n\pi/d)^2)}$ . This is only to be expected as the fluid in the room has been assumed lossless and there are no losses at the walls. If, realistically, viscous, thermal and relaxation losses in the fluid are taken into account  $k$  will be a complex function of frequency, which, in itself, of course, is sufficient to remove the singularity. Small losses at the walls similarly can be taken into account; they will provide imaginary parts to the  $k_{lmn}$ 's, without affecting the base functions to a first approximation.

With the wavenumber eigenvalues  $k_{lmn}$ , one can associate frequency eigenvalues,  $\omega_{lmn} = c_0 k_{lmn}$ . These are the normal frequencies of free vibration of the fluid in the room and the functions  $\psi_{lmn}$  are the normal modes of vibration. A general free vibration of the fluid in the room is thus represented by

$$p(x_i) = \sum_{lmn} p_{lmn} \psi_{lmn}(x_i) e^{i\omega_{lmn} t},$$

where the constants  $p_{lmn}$  are determined from initial conditions.

By the same procedures as in these three examples, formal series solutions for radiation, scattering and interior problems can be obtained in any of the eleven orthogonal curvilinear co-ordinate systems in which the scalar Helmholtz equation is separable, the differences from one system to another being only in the specific functions used.

Obtaining numerical results from such formal solutions is dependent on the rapidity of convergence and on the availability of appropriate asymptotic or other approximate representations of the functions, or of efficient computer programs for calculating them. The limitations here are very real in practice; except when asymptotic formulas can be used to greatly simplify the series the labour of calculation is almost invariably orders of magnitude greater than that of obtaining the formal solution. In many boundary value problems where numerical values are required, it is often simpler to return to the Green function solution, equation (3), and either integrate it directly or treat it by integral equation methods - it can be regarded, of course, as an integral equation. Such approaches are of relatively new general use, their increase in popularity coinciding with the increased interest in obtaining numerical results in specific cases with the aid of computers.

There are two general analytical properties of solutions of the homogeneous scalar wave equation and homogeneous scalar Helmholtz equation, respectively, that are of particular interest, in connection with any solutions, analytic or numerical. The first is that, in consequence of energy conservation, the mean intensity vector  $\bar{J} = \bar{p} \nabla \psi$  is solenoidal,  $\nabla \cdot \bar{J} = 0$ . The mean energy flow contours therefore are relatively simple, and reasonable estimates of them can sometimes be made in the absence of full information on the values of  $p$  and  $\psi$ . The second property, relevant only to the scalar Helmholtz equation, is that for both the real part and the imaginary part of  $p(x_i, \omega)$  separately, the average value over any sphere of one-half wavelength radius is zero. (This result comes from the analog for the scalar Helmholtz equation of the well known mean value theorem for Laplace's equation.) Consequently, whatever the particular boundary conditions or source distribution, both the real and imaginary parts of  $p(x_i, \omega)$  must be oscillatory functions of space with an "average" distance between nodal surfaces of one-half wavelength. Evidently this property, like the energy conservation one, is available for use as a "control" on any assumed solutions.

#### 4. MULTIPOLE EXPANSIONS

The relative ease with which exact formal solutions for the general inhomogeneous scalar wave equation can be obtained is in strong contrast with the subsequent difficulties one can have in numerical evaluation of the solutions. These difficulties are inevitable in the general case, because of two inherent properties of the wave motion itself. The first of these properties is that the motion propagates and the second is that superposition results in interference. Contributions to the motion at any point in space from different regions of a source distribution interfere with one another, and with the waves from the same origins which have been scattered from the obstacles in the fluid. The range of characteristic impedances,  $\rho c$ , of common materials is very large: for example, the  $\rho c$  of air is of the order of  $10^{-3}$  to  $10^{-5}$  those of water and the many other liquids and solids of comparable densities and compressibilities, but porous fibrous or granular materials can have characteristic impedances of magnitudes comparable to that of air. Scattering, therefore, can vary from being very strong to very weak, and in general can result in changes in wave form. As the Green function formula (3) shows, to calculate the pressure at any point at any time  $t$ , if the source began emitting at  $t = 0$ , one has to know what the field was on all scatterers within a radius  $c_0 t$  of the source distribution at the respectively appropriate earlier times. For the steady state case, one has to know the field everywhere on all scattering surfaces, for all time, as it were. In general, then, calculations for only localized space-time regions are not possible.

Even if scatterers are not present, calculation of the volume integral in the Green function formula (3) is rendered difficult by interference. Variation of the source function  $q$  with position and time means that there will be interference at an observation point between contributions from different parts of the source region even if they are equidistant from the observation point. Second, even if different parts of the source region are emitting the same signals at the same times, their contributions at the observation point can interfere because of different travel times. The multipole expansion technique permits separate assessment of these two kinds of interference, due to source non-uniformity and source size, respectively.

Formal expansion of the integrand of the volume integral of the Green function formula (3) in a triple Maclaurin's series in  $y_k$ , but with only  $r = |x - y_k|$  regarded as varying (i.e.,  $q(y_k, t - r/c_0)$  is formally regarded as varying with  $y_k$  only through the retarded time,  $t - r/c_0$ ), followed by use of the fact that

$\partial r / \partial y_k = -\partial r / \partial x_k$  and term by term integration, leads to the result

$$r(x_k, t) = \sum_{l+m+n=0} D_{lmn}(|x_k|, \frac{\partial}{\partial x_k}) M_{lmn}(t - |x_k|/c_0), \quad (18)$$

where the  $D_{lmn}$  are the multipole operators, defined by

$$D_{lmn} = \frac{(-\partial)^{l+m+n}}{\partial x_1^l \partial x_2^m \partial x_3^n} \left( \frac{1}{4\pi|x_k|} \dots \right) \quad (19)$$

and the  $M_{lmn}$  are the overall instantaneous multipole moments of the source distribution, defined by

$$M_{lmn}(t) = \int_V \frac{y_1^l y_2^m y_3^n q(y_k, t)}{l!m!n!} dy_1 dy_2 dy_3. \quad (20)$$

The moment  $M_{000}$  is called the (scalar) monopole moment,  $M_{lmn}$  with  $l+m+n = 1$  the (vector) dipole moment,  $M_{lmn}$  with  $l+m+n = 2$  the (tensor) quadrupole moment, etc. When the monopole moment is zero, the field radiated by an equivalent dipole source strength density  $m_1$ , such that  $q(y_k, t) = -\partial m_1(x_k, t) / \partial x_1$ , is the same as that radiated by the actual source distribution: i.e.,

$$p(x_k, t) = -\frac{\partial}{\partial x_1} \int_V \frac{m_1(y_k, t - r/c_0)}{4\pi r} dy_1 dy_2 dy_3. \quad (21)$$

Similarly, if both monopole and dipole moments are zero, then, with  $q(x_k, t) = -\partial^2 m_{1j}(x_k, t) / \partial x_1 \partial x_j$ ,  $m_{1j}$  being the equivalent quadrupole source strength density,

$$p(x_k, t) = \frac{\partial^2}{\partial x_1 \partial x_j} \int_V \frac{m_{1j}(y_k, t - r/c_0)}{4\pi r} dy_1 dy_2 dy_3, \quad (22)$$

and so on. Note that unless the source distribution is bounded in space difficulties of convergence of the original Green function formula integral and the subsequent multipole moment integrals may arise.

In the radiation field, far from the source distribution, with terms of order higher than the first in  $1/|x_k|$  neglected in the multipole contributions  $D_{lmn} M_{lmn}$ , the pressure becomes

$$P_{rad}(x_k, t) = \sum_{l+m+n=0} \frac{(x_1/|x_k|)^l (x_2/|x_k|)^m (x_3/|x_k|)^n}{4\pi|x_k|} \left( -\frac{1}{c_0} \frac{\partial}{\partial t} \right)^{l+m+n} M_{lmn}(t - |x_k|/c_0). \quad (23)$$

Equation (23) is a fourfold inverse Fourier transform,

$$P_{rad}(x_j, t) = \frac{1}{4\pi|x_j|} \iiint_{-\infty}^{\infty} q(y_k, \omega) \exp\{i(\omega t - k|x_j| + k \frac{x_1}{|x_j|} y_1)\} d\omega dy_1 dy_2 dy_3, \quad (24)$$

where  $q(y_k, \omega)$  is the Fourier transform (time to frequency) of the source distribution function  $q(y_k, t)$ . The distribution of the far field pressure in angle and time,  $4\pi|x_j|P_{rad}(x_j, t)$ , is thus in a unique, one-to-one relationship with the source distribution  $q(y_k, \omega)$ , by the uniqueness property of Fourier transform pairs. The paired transform variables are  $(t, \omega)$  and  $(k_1, y_1)$ , where  $k_1$  is the wavenumber vector  $kx_1/|x_j|$ . By performance of the paired inverse fourfold Fourier transform on  $4\pi|x_j|P_{rad}(x_j, t)$  the source distribution  $q(y_k, t)$  is recovered. In this sense a given (complete) far field has a unique source distribution, in both space and time, and vice versa. Since scattering surfaces, according to the Green function formula (3), are equivalent to certain surface (monopole and dipole) source distributions, it follows that the same one-to-one relationship exists between the far field and a distribution of sources and scatterers (in a bounded volume). This property is the ab initio basis of acoustic holography, and of source identification and location procedures.

As a representative illustration of the multipole expansion technique, equation (24) can be used to obtain, very easily, the pressure radiation field of a single frequency uniform source distribution, of equivalent multipole moment frequency spectral density  $m_{lmn}(\omega)$ , the distribution being confined to a volume in the form of a rectangular parallelepiped of edge lengths  $2a$ ,  $2b$  and  $2d$ , respectively, in the  $x_1$ ,  $x_2$  and  $x_3$  directions. With the origin at the centre of the parallelepiped, the result can be written as

$$4\pi|x_j|P_{rad}(x_j, t) = 8abd m_{lmn}(\omega) \exp\{i\omega(t - |x_j|/c_0)\} (-ik \frac{x_1}{|x_j|})^l (-ik \frac{x_2}{|x_j|})^m (-ik \frac{x_3}{|x_j|})^n \times \\ \times \frac{\sin(kax_1/|x_j|)}{(kax_1/|x_j|)} \frac{\sin(kbx_2/|x_j|)}{(kbx_2/|x_j|)} \frac{\sin(kdx_3/|x_j|)}{(kdx_3/|x_j|)}.$$

The three factors of  $(\sin \xi)/\xi$  form are independent of the multipole order and thus represent the effect of path length interference. Similarly, the effect of source non-uniformity interference (here phase variation across the source distribution) is represented solely by the three  $(-ikx_i/|x_j|)^l \dots$  factors. Radiation fields for other source distributions can be similarly obtained and all show comparable separate factors for the interference effects of source distribution non-uniformity and source size, respectively.

##### 5. TRANSFORM AND INTEGRAL EQUATION METHODS

Since the inhomogeneous scalar wave equation is linear, it is suitable for analysis by integral transform methods. The fourfold Fourier wavenumber-frequency transform pair,

$$p(\kappa_1, \omega) = \left(\frac{1}{2\pi}\right)^4 \iiint_{-\infty}^{\infty} p(x_1, t) e^{-i\kappa_j x_j - i\omega t} dx_1 dx_2 dx_3 dt,$$

$$p(x_1, t) = \iiint_{-\infty}^{\infty} p(\kappa_1, \omega) e^{i\kappa_j x_j + i\omega t} d\kappa_1 d\kappa_2 d\kappa_3 d\omega,$$

is perhaps most commonly used, particularly in situations where space and/or time "correlation-type" data processing or analysis is to be employed, because of the well known Fourier pair relationships between certain correlation functions and power spectral densities, use of which readily provides formulas for overall power output.

Mathematically, with  $i\omega$  interpreted as a complex variable (often called  $s$  or  $p$ ), Fourier transformation on  $\omega$  is equivalent to Laplace transformation on  $s$ . Other transforms are occasionally useful, such as those of Mellin and Hilbert.

The principal useful property of integral transforms is that real variable differential equations - including both the wave equation and boundary conditions - can be transformed into complex variable algebraic equations, from which eigenvalues or other key parameters such as scattering coefficients can more easily be deduced. Advantage then can often be taken of contour integration techniques in evaluating the inversion integrals to recover the real solution.

Other complex variable methods, such as Wiener-Hopf and various integral equation techniques, can often be used to advantage to obtain solutions of certain types of boundary value problems. For all these integral transform, integral equation, and other complex variable techniques, the integral equation to be solved is a form of the general Green function result, equation (4), with  $G = G_0 + G_1$ , and the objective, in essence, is equivalent to determining the complementary part of the Green function so that the surface integral vanishes everywhere except where  $p$  and  $\partial p/\partial n$  have pre-specified non-zero values.

As closed form solutions are very much the exception rather than the rule, and convergence of base function series as obtained by separation of variables methods is reasonably rapid only for low frequencies (or, in their asymptotic forms, for high frequencies in some cases), integral forms of solution equivalent to the Green function formulas (3) and (4) can be particularly advantageous when numerical computations are to be performed. These integral forms, in effect, permit selection of that  $G_0$  which inspection indicates may be most appropriate for the economical numerical evaluation of the integral for each particular source-receiver-scatterer situation. Integral transform, integral equation and other sophisticated complex variable techniques generally, however, are inevitably the province of mathematical specialists. If they are to be used, their details and intricacies must be studied and mastered by reference to textbooks and research publications for specialist expositions of their principles and applications.

#### 6. PERTURBATION METHODS

Perturbation methods, like the integral transform and other complex variable techniques, are primarily the province of specialist mathematicians, but they usually can be more closely related to physical considerations. Questions of dynamical stability of the reference and perturbed states of motion naturally arise, and physical considerations are primary in selection of the perturbation variables. In perturbation schemes, the convergence of the iterative procedure is usually of an asymptotic nature, rather than absolute, and this can be an advantage when it comes to numerical evaluation. The most widely applicable, and commonly used, perturbation techniques for acoustic propagation problems belong to the class of matched asymptotic expansion methods, which might also be called the WKBJ methods (Wentzel-Kramers-Brillouin-Jeffreys-Langer), originated by Jeffreys and first given a sound mathematical basis and generalized by Langer. The idea of such techniques is simple. Given that valid solutions can be found in regions of the field to be determined that are close to opposite boundaries, as it were, one devises, for the governing equation concerned, an asymptotically valid solution in the intermediate region which at least correctly matches, in an asymptotic sense, the extreme "inner" and "outer" solutions at appropriate "boundaries" of their respective regions of validity. Thus the solution as a whole may satisfy both the governing differential equation and the boundary conditions in only an asymptotic sense. The procedure can be very effective in producing good first order (and sometimes second order as well) analytic approximations to the exact solution, but it is a general rule that the labour involved in obtaining higher order approximations by perturbation methods is usually prohibitive. The advantage, from the numerical point of view, of asymptotic expansions is of course that the errors can be easily estimated. (The error in the representation of a function by  $n$  terms of an asymptotic series is less than one-half the  $(n+1)$ -th term.)

Perturbation methods can be used for variations in boundary conditions, as well as in the governing differential equations, from those for which solutions are known.

#### 7. GEOMETRIC ACOUSTICS

For low frequencies, separation of variables techniques involving base function series, together with perturbation methods as necessary, often constitute the most satisfactory approach, as convergence is relatively rapid. At high frequencies, however, this is not the case, and it is then often more effective, and even necessary, to proceed on the basis of the geometric, "ray-tube", propagation of the waves that would occur in the infinite frequency limit. The propagation of the wavefronts can be calculated on the basis of Fermat's principle of least time (or, what is in effect the same thing, Huyghens' principle). With the wavefronts known, and hence their trajectories, the "rays", the problem is reduced to determining the pressure amplitudes along each selected bundle of rays - the ray-tube. At this stage the geometric acoustic assumption is made, that of conservation of wave energy along each ray-tube, and the corresponding pressure amplitudes obtained in accordance with the appropriate formulas derived on the basis of this assumption.

The most powerful energy conservation principle of this kind developed to date appears to be the "wave action principle" of Bretherton and Garrett. Computation methods based on this principle have recently been developed and used successfully for prediction of propagation of relatively small amplitude pressure disturbances in fluids of inhomogeneous mean velocity and/or temperature - e.g., in the atmosphere, the sea and jet flows. More detailed information is provided elsewhere in these Lecture Course Notes.

#### 8. VARIATIONAL AND NUMERICAL METHODS

The most direct approach to numerical calculation in acoustic propagation problems, applicable to fluids in arbitrary motion and thus of inhomogeneous thermodynamic state, is to reduce the partial differential equations of transport of mass, momentum and energy to finite difference equations, as appropriate for the problem of interest, and to integrate these numerically by standard methods, with the aid, of course, of a large digital computer programmed for the purpose. In physical terms, this is a lumped parameter approach. Since for accuracy space step differences must be small compared with the acoustic wavelength and time step differences small compared with the period, this approach, although it can and has been used to good effect, is usually prohibitively or impossibly expensive in terms of machine time and capacity.

Considerable machine time and capacity economies are possible if instead one of the general weighted residual methods is used. These can be regarded as including methods based traditionally, for vibration problems, on variational principles, such as the Rayleigh-Ritz, Galerkin and finite element methods. Adaptation of weighted residual methods to acoustic propagation problems, for purposes of practical calculation, is relatively very new, still being in the research and development stage, and for details of the particular and effective methods (i.e., computer programs) available to date reference must be made to current research publications.

#### 9. BIBLIOGRAPHY

As the research and pedagogical literature on mathematical techniques for acoustic propagation problems, even in only fluids, is so large, and most of the techniques are so sophisticated mathematically, it has not been possible to do more in the preceding sections than to provide specific information for only a very few of the most well-established methods, those which, for the most part, provide relative maxima of physical insight. Similarly, it is appropriate to list only a very few selected references as suggested further reading, these being the monographs which, in the author's opinion, provide the most effective, fundamental and comprehensive introductions to the methods available. No suitably up to date monographs are yet available on the subjects of weighted residual methods and geometric acoustic methods for acoustic propagation problems. For these, and indeed for information on recent developments in all the various techniques, especially insofar as efficient procedures for numerical computations are required, regular reference to contemporary research publications is necessary.

L. BRILLOUIN 1946 Wave Propagation in Periodic Structures. New York: McGraw-Hill Book Company.

P.M. MORSE and H. FESHBACH 1953 Methods of Theoretical Physics (two volumes). New York: McGraw-Hill Book Company.

L.A. CHERNOV 1960 Wave Propagation in a Random Medium. New York: McGraw-Hill Book Company. (Translated from the Russian by R.A. Silverman.)

S.G. MIKHILIN 1965 Multidimensional Singular Integral Equations. Oxford: Pergamon Press.

A.H. NAYFEH 1973 Perturbation Methods. New York: John Wiley and Sons.

## DIRECTIVITY OF ACOUSTIC RADIATION FROM SOURCES

Donald L. Lansing  
Head, Aeroacoustics Branch  
NASA Langley Research Center  
Hampton, Virginia 23665

5-1

### SUMMARY

This paper will describe the radiation properties of acoustic monopoles and dipoles. The directivity of radiation from these sources in a free field and in the presence of an absorptive surface is described. The kinematic effects on source radiation due to translation and rotation are discussed. Experimental measurements of sound from an acoustic monopole in motion and the characteristics of helicopter rotor and propeller noise are reviewed. The paper provides an introduction to several essential concepts required by noise control engineers making measurements of noise from moving sources in the proximity of the ground.

### INTRODUCTION

When a noise source is brought near a surface or put into motion, a complex radiation pattern results which may be wholly unlike that of the source at rest in a free field. Acoustic measurements made of moving sources near surfaces for the purpose of characterizing the source behavior or understanding noise generating mechanisms must accordingly be corrected for motion and surface effects. A common example of this situation occurs when making measurements of noise from moving ground vehicles or aircraft during takeoff and landing. The effects of reflection and absorption of sound by the ground and the kinematic and dynamic effects of forward motion must be considered in the data analysis and subsequent interpretation.

This paper will survey the effects of the proximity of surfaces and the kinematic effects of motion, both translatory and rotational, on the directivity of radiation from acoustic monopoles and dipoles. The interference patterns and attenuation of sound from a source near an absorbing ground surface are explained. Three kinematic effects associated with uniform rectilinear motion, namely: retarded time, convective amplification, and Doppler shift, are described. An experimental study of the measurement of sound from an acoustic monopole in motion is discussed to illustrate the concurrence of surface and motion effects under controlled conditions. The paper surveys rotating blade noise radiation. The characteristic directivity patterns produced by blade thickness and aerodynamic forces, statically and in flight, are discussed to illustrate the features of propeller and rotor noise. General introductions to the kinematics of moving sources and helicopter noise are contained in references 1 and 2 respectively. The paper concludes with a brief review of several recent significant contributions to the theory of source radiation and its various applications. This paper provides useful background to the paper in this lecture series by Maestrello and Norum entitled, "Experimental Measurements of Moving Sources," and provides an introduction to several essential concepts required by engineers making and interpreting field measurements of noise from moving sources.

### SOURCES OF SOUND

The sources of sound in a fluid can be introduced by considering the field equations of linearized acoustic theory. These equations, shown in Figure 1, are the continuity equation which expresses the conservation of mass, the momentum equation which describes the balance forces in the fluid, and the pressure-density relation which expresses the proportionality between the acoustic pressure and density perturbations. The term  $Q$  in the continuity equation accounts for the time rate of production of mass within the fluid. The vector whose components  $F_i$  appear in the momentum equation is any externally applied body force. These three equations can be combined into a single well known inhomogeneous wave equation.

In addition to the field quantities  $p$ ,  $\rho$ , and  $u_i$  several quantities relating to energy and energy flux in the acoustic field need to be mentioned. These quantities are the acoustic intensity and acoustic power defined in Figure 2. The acoustic intensity is the time rate of sound energy flow across a unit area and is calculated by taking the time average of the product of the pressure and velocity component normal to the area. The acoustic power is the time rate of total energy flow through a closed surface completely surrounding the noise source and is a measure of the overall energy in the propagating sound field.

The nomenclature and definition of symbols given in Figures 1 and 2 will be used throughout the rest of this paper.

Figure 3 summarizes the principle sources of sound which occur within a completely linearized acoustic theory and present some practical examples of these sources. The differential operator on the left-hand side of the inhomogeneous wave equation describes the propagation of sound through a quiescent medium whose ambient speed of sound is  $c$ . The right-hand side of the equation consists of two terms which act as forcing functions to the wave equation and can be interpreted as producers of sound. These two terms represent the unsteady injection of mass into the medium and spatially varying applied body forces. Examples of the former type of sound source are unsteady or transient air jets and vibrating surfaces. Every element of a vibrating surface can be modelled as a piston which appears to insert and withdraw mass from the surrounding medium during its vibration. An important general class of examples of the second source is aerodynamic forces which develop upon bodies moving through a fluid. If nonlinear terms are included in the field equations, a third type of noise source arising from velocity fluctuations within the fluid itself can be derived. Examples of this noise source are turbulent fluid motions such as occur in jets, wakes and boundary layers. Thus, this type of source is central to flow noise generation. The production of noise by shear stresses will not be discussed in any great detail in this paper. The list of sound sources given here is not exhaustive. Other sources of sound in a fluid such as convecting density homogeneities, viscous shear stresses and enthalpy fluctuations are known. The reader is referred to the specialized literature for details.



5-2

The radiation from an acoustic monopole serves as a convenient reference to use in illustrating the effects of surfaces and motion on source directivity. The monopole represents the acoustic field produced by periodically injecting and withdrawing mass at a point in space with an angular frequency  $\omega$ . The strength of the source,  $Q_0$ , is the time rate of mass injection. The acoustic pressure, radial velocity component, intensity and power are presented in figure 4 for convenience and will be referred to frequently throughout the paper to illustrate the changes surfaces and motion have upon the directivity of sources. A fact that will be used repeatedly is that the amplitude of the acoustic pressure for a monopole is constant on a sphere whose center is at the location of the monopole. Point harmonic generators of sound such as monopoles and dipoles (to be discussed subsequently) are central to the theory of acoustics since more complicated spatial and temporal distributions can be built up from these idealized sources by linear superposition. One expects then that the radiation properties of these point sources will then be carried over to more complicated distributions.

#### THE EFFECTS OF SURFACES ON SOURCE DIRECTIVITY

Consider first of all the influence of a nearby surface upon the directivity of sound from a monopole. A simple representation of this situation is shown in Figure 5 in which the surface is represented by a very large flat and perfectly reflecting plane. The boundary condition at the plane surface then is that the normal component of the acoustic velocity vanish at the surface. This situation in which a sound source is in the proximity of a large flat surface occurs for example during the landing approach or take-off operations of a commercial jet transport.

The mathematical solution of this radiation problem contains two terms, as shown in Figure 5. The first term represents the radiation field of the given monopole. The second term represents the radiation field of an image monopole placed directly below the actual source at an equal distance on the opposite side of the surface. At large distances from the source the equation for the radiation field can be considerably simplified as shown at the bottom of Figure 5. For the purposes of this discussion it is convenient to measure the distance  $R$  from the foot of the perpendicular from the source to the reflecting plane. If one compares the pressure fields obtained in this case with that of a free field monopole shown in Figure 4, it is seen that the amplitude of the pressure still falls off inversely with distance  $R$  but that the two equations differ by the directivity function  $d(\theta)$  which is defined at the top of Figure 6. The pressure is no longer constant over a sphere of constant radius but is also a function of the observer's angular position  $\theta$ , the source height  $h$  and the source frequency  $k$ . This nonuniform directivity comes about as a result of the superposition of the wave fields from the direct and image sources. The combined field has localized reinforcements and cancellations which produce a complex sound pattern.

The sketches at the bottom of Figure 6 illustrate the variation of the directivity function with observer angle and source frequency. The sketch on the left is a polar plot of the directivity function for a fixed source height and frequency. For a free space monopole the "directivity function" is a circle of unit radius. As the sketch shows the radiation field of a monopole near a surface produced by cancellations and reinforcements exhibits a lobed pattern for which pressure amplitudes can be locally twice as much as in the absence of the ground; moreover, there are angles at which the pressure amplitude drops completely to zero. The sketch at the right shows how the directivity function varies for fixed source and observer position as a function of frequency. It is seen that different frequencies undergo varying amounts of reinforcements and cancellation. Some frequencies experience complete reinforcement with pressure doubling; other frequencies show complete cancellation.

Ground surfaces such as grassland, or tilled soil are not perfectly rigid as is the idealized surface in the preceding example. Most ground surfaces exhibit some degree of compliance to an incident acoustic wave. As suggested in Figure 7, an acoustic wave reflected from such a surface shows a decrease in amplitude due to sound absorption and a phase change produced by time lags in the sound-surface interaction process. These two physical phenomena are represented mathematically by a quantity known as the specific acoustic impedance which is characteristic of the particular type of surface. The specific acoustic impedance is a complex number which contains both amplitude and phase information. The real and imaginary parts of the impedance are known as the acoustic resistance and acoustic reactance, respectively. It is convenient to define a quantity called the specific acoustic admittance as the inverse of the specific acoustic impedance.

An alternate method of characterizing an acoustically absorbing surface is presented by L. Maestrello in the lecture entitled, "Experimental Measurements of Moving Sources." This method makes use of the notion of an acoustic transfer function between incident and reflected waves rather than that of an acoustic impedance. The two approaches are equivalent but the former technique appears to have the advantage in that the transfer function is more easily evaluated than the impedance over a broad frequency range.

Some measurements of the acoustic impedance of dry sand and grassland, taken from Reference 3, are shown in Figure 8. For these surfaces the acoustic resistance is nearly independent of frequency. The reactance on the other hand decreases significantly with increasing frequency over the range of measurements. The impedance of a surface may also vary with the angle of incidence of the sound wave. This effect is sometimes taken into account by defining an "effective" impedance as the product of the normal acoustic impedance and the cosine of the angle of incidence.

The far-field acoustic pressure for a source above an absorbing surface having a specific admittance is shown in Figure 9. The directivity function becomes considerably more complicated than for the perfectly reflecting surface. Directivity now depends on the surface properties as well as the source height and frequency and the observer location.

Some calculations of the directivity function  $d'(\theta)$  for an absorbing surface are shown in Figure 10 and compared with the directivity for a perfectly reflecting surface. On the left is a polar plot of the directivity function for a fixed height and frequency and on the right is a plot as a function of frequency. The specific acoustic impedance used in the calculations,  $4 - 4i$ , is typical of the measurements shown in Figure 8. As can be seen from the two sketches, the effect of an absorbing surface on the directivity is

to reduce wave reinforcements so that pressure doubling does not occur. The frequencies at which pressure maxima and minima occur are increased significantly.

5-3

In summary then, there are several observations to be made regarding the effects of a surface upon the radiation from a source. The surface will produce a nonuniform directivity pattern due to the interference of sound waves from the source with waves reflected from the surface. These two wave fields interact with each other producing reinforcements at which the pressure is greater (up to two times) than the pressure in the free field and cancellations where the pressure can go nearly to zero. Compliant surfaces such as sand, soil, and grass tend to smooth out these reinforcements and cancellations somewhat and shift the frequency of their occurrence depending upon the impedance properties characteristic of that surface.

#### KINEMATIC EFFECTS OF MOTION ON SOURCE DIRECTIVITY

When a noise source is put into motion its radiation characteristics may be significantly different from those of the source at rest. There are two reasons for such differences: kinematic effects due solely to moving the source about in space and dynamic effects which may alter the noise generating process or radiation efficiency of the source. This section of the paper will consider the kinematic effect of uniform rectilinear motion on the directivity of source radiation. A second important class of moving sources, that is sources in rotation, will be considered subsequently in the paper. Moving sources occur frequently in noise measurement and noise control problems associated with transportation noise sources such as automobiles and aircraft.

Consider then the situation indicated in Figure 11. An aircraft is in constant velocity, constant altitude flight over an observer on the ground (for simplicity the surface effects discussed in the previous part of the paper will not be included in the discussion of this section). As the aircraft moves along the flight path beyond point A, the sound emitted at point A travels along the straight line joining point A to the observer. The aircraft arrives at point B when the sound emitted at point A arrives at the observer. That is, the observer simultaneously sees the aircraft at point B and hears the sound emitted at point A. Thus, for a moving source two source positions must be distinguished: the position at which the source is observed and the position of the source at which the detected sound was emitted. Let  $R$  be the distance between the observer and the emission point. The time taken for sound to travel this distance is  $\frac{R}{c}$ . Consequently the sound heard at time  $t$  by the observer was actually emitted at an earlier time  $t - \frac{R}{c}$ . This quantity  $t - \frac{R}{c}$  referred to as the retarded source time. The retarded time is the time at which the observed sound was emitted by the source. In order to deduce information about a moving noise source from far-field sound measurements one must associate the measured acoustic signatures at time  $t$  with the position and condition of the source at the corresponding retarded time.

Figure 12 gives the mathematical relationships between observation quantities and emission quantities and presents some sample calculations. The Mach number of the moving source is seen to be a fundamental parameter in the transformations. The sketch in the lower left shows the difference between the observation and emission angles as a function of the observation angle. The sketch at the right shows the ratio of the emission and observation distances. It can be seen that the difference between emission and observation quantities increases as the source Mach number increases. The difference between the source and observer angles is the greatest for overhead positions of the source. The ratio  $\frac{R}{R_0}$  is most sensitive to positions when the source is approaching and less sensitive when the source is departing in the distance.

Figure 13 shows the mathematical expression for the far-field acoustic pressure of a monopole in motion. This expression should be compared to that shown in Figure 4 for a stationary monopole. It is convenient in this situation to express the pressure in terms of the emission quantities  $R$  and  $\theta$ . The pressure still falls off inversely with distance from the point of emission. However, the equation contains an additional directivity factor which is referred to as the "convective amplification factor." This factor is a function of the source Mach number and the emission angle  $\theta$ . The equation implies that a monopole of fixed strength  $Q_0$  will acquire directional radiation according to the convective amplification factor when it is set into uniform motion.

Figure 14 shows the effect of source Mach number upon the monopole directivity. It is convenient to consider the difference in sound pressure level between the moving monopole and the stationary monopole. The sketch gives a polar plot of this sound pressure level difference as a function of the emission angle for various Mach numbers. It can be seen that the sound pressure level increases significantly with Mach number in the direction of motion. There is a 16 dB increase for example directly ahead of the source at a Mach number of .6. There is also a decrease in the sound pressure levels behind the source. Note that convection effects are absent at 90° to the emission point. Far-field noise measurements for moving sources are frequently made at this 90° position in order to eliminate convection effects from the measured data.

The effects of source motion on the radiated acoustic power are shown in Figure 15. This figure shows a plot of the ratio of the power radiated at subsonic Mach number  $M$  to the value at zero forward speed (a quantity given in Figure 4) as a function of the source Mach number  $M$ . The simple algebraic expression for this ratio is given in the figure. The acoustic power associated with the moving monopole is calculated by determining the time average of the energy flux through a cylinder completely enclosing the path of motion as suggested by the sketch. It is seen from the plot that as the Mach number increases the radiated acoustic power also rapidly increases becoming infinite at sonic speed.

Another kinematic effect of motion on the radiation from a source is illustrated in Figure 16. This is the shift in the observed frequency of the radiation. The phase of the far-field acoustic pressure is determined by the expression  $kR - \omega t$ . Introduce a cylindrical coordinate system  $(x, r)$  with the  $x$  axis coinciding with the line of source motion and the origin coinciding with the position of the source at time zero. In terms of these coordinates and the source velocity  $U$  and Mach number  $M$  the emission distance  $R$  can be written out explicitly as shown. The  $x, r$  coordinate system is a fixed set of coordinates in

5-4

space which then designate the observer position. In terms of these observer coordinates the phase of the acoustic pressure along the line of motion simplifies as indicated. Directly ahead of the source an observer will detect a frequency  $\omega/(1 - M)$  where  $\omega$  is the frequency of the moving source. This observed frequency is larger than the actual source frequency. Behind the source the observed frequency decreases by a factor of  $1/(1 + M)$ . For a general observation position the observed frequency is the time rate of change of the phase of the pressure. When the algebra is worked through the general expression for the observer frequency is that given at the bottom of figure 16. It is seen that in general the frequency is increased ahead of the emission point and is decreased aft of the emission point. Convective changes in frequency vanish at the  $90^\circ$  to the emission point.

In summary there are three kinematic effects of motion upon radiation from a source. There is the notion of retarded time, that is, that the observed sound was emitted at a time before it is measured at a point which is different from where the source is observed. The directivity of radiation from a source changes with the sound energy generally beamed in the direction of motion. And finally the observed frequency of a moving sound source may be larger than or less than the true source frequency depending upon the position of the observer with respect to the source.

It is important to reemphasize that these effects are solely due to the forward motion of the source and are independent of the nature and strength of the source. These effects must be corrected out of far-field acoustic data when the latter are used to diagnose the nature and condition of a complex unknown moving source. In particular convection effects must be distinguished from fundamental changes in the noise generation process which can come about due to forward motion. Far-field acoustic measurements are frequently used to diagnose the presence of such changes in the source. As seen from the equations in Figures 13 and 16, convection effects can be eliminated from the far-field directivity and Doppler shifts in frequency by making acoustic measurements at  $90^\circ$  to the emission point.

#### MEASUREMENTS OF SOUND FROM AN ACOUSTIC MONOPOLE IN MOTION

A moving source problem of considerable interest in connection with aircraft noise is the effect of forward motion upon the generation of jet noise. Changes in jet noise with forward motion occur due to both kinematic and dynamic effects. In an effort to understand kinematic effects as they occur in actual practice and to evaluate a theoretical model for predicting these effects an experimental study was carried out of the effects of forward speed upon radiation from a monopole, Reference 4. Both motion and surface effects which have been discussed individually in the previous sections of the paper make their appearance in this experimental study.

The monopole source was mounted on top of an automobile 7.9 meters above the ground atop a mast supported with guy wires as indicated in Figure 17. The source consisted of a 60 watt acoustic driver necked down through a 1.52 centimeter diameter tubular opening. The source radiated approximately uniformly in all directions when at rest. The output of this source consisted of tones of discrete frequency  $f$ . The automobile was driven at constant speeds  $U$  ranging from 13.4 to 44.4 meters per second.

Figure 18 shows a schematic of the experimental test setup. The automobile was driven along a straight track at constant velocity. The experiment was performed over an aircraft runway consisting of an asphalt surface. Sideline microphones were positioned at heights,  $h_0$ , of 3.05 meters and 6.10 meters above the ground surface. Pressure signals were measured with 1.3 centimeter diameter condenser microphones and recorded on magnetic tape.

A mathematical analysis of this problem was carried out for comparison with the experiment. The solution was obtained by the use of Fourier integral techniques and an application of the Lorentz transformation. The solution contains both surface reflection effects and convection effects. The next three figures show some results of the measurements and analysis made in this investigation.

Figure 19 shows a comparison between the calculated and measured noise time histories. The specific acoustic impedance of the runway surface used in the calculation is taken as  $4 - 4i$ . The sound pressure level in dB is plotted on the vertical scale. The horizontal scale is time normalized by means of the source velocity  $U$  and the source to observer distance at closest approach  $\sigma$ . The measured and computed curves are not superimposed here because of the many oscillations in the SPL's which are due to reinforcements and cancellations which come about due to ground reflection.

The smooth computed curve at the top of the figure is the predicted variation in the sound pressure level in the absence of a surface. As the source approaches the microphone the sound pressure level increases smoothly, reaches a maximum level at the point of closest approach, and then decreases gradually as the source moves away. In the presence of the ground surface both the computed and measured sound pressure levels show this general trend. However, superimposed upon this mean trend is a strong modulation due to the motion past the microphone of the complicated pattern of reinforcements and cancellations produced by ground reflection.

Figures 20 and 21 show the variation of the computed and measured noise time histories with observer height  $h_0$  and source frequency. It can be seen that as either the observer height or the frequency of the source is increased the measured and computed SPL's become more and more oscillatory as the distance between successive reinforcements and cancellations grows smaller.

#### ROTATING BLADE NOISE

Noise from rotating blades is a pervasive problem associated with ground transportation. Blade induced noise may cause vibration to vehicle structures, malfunction of onboard instrumentation and equipment, annoyance in passengers, vibration in nearby ground structures, and interference with crew performance. Aircraft having rotating blade components include CTOL, VTOL, general aviation, and supersonic transport vehicles. Examples of rotating blade components which produce noise are shown in Figure 22. These components include ducted fans and compressors as well as free rotors such as helicopter rotors and general aviation propellers. This section of the paper will survey the fundamentals of noise production and radiation from rotating sources.

The noise sources for rotating blades are shown in Figure 23. These sources are the aerodynamic forces such as torque, thrust, and coning which develop on the rotating blades and the thickness distribution of the blades. Thus, in general, rotating blades produce both monopole and dipole type noise. Both steady and unsteady aerodynamic forces may be generated on the blades. The former may occur for example on a rotor in hover having a very smooth and uniform inflow. The latter are produced for example by skewed inflow, or blade-vortex interaction. The sound field from a system of rotating blades is periodic in time with a period  $\frac{1}{B\Omega}$  and periodic around the axis of rotation with period  $\frac{1}{B}$  where B is the number of blades and  $\Omega$  is the shaft speed. Therefore, the far-field acoustic pressure can be represented as a Fourier series as indicated at the bottom of Figure 23 in which  $P_n$  are the Fourier harmonics. The remainder of the paper will discuss the effects of blade operating conditions on the radiation shapes associated with these individual sound harmonics. 5-5

Since some of the noise radiated from rotating blades is generated by blade aerodynamic loads, Figure 24 which summarizes the properties of radiation from a stationary dipole is included for reference. An acoustic dipole represents the acoustic effect due to the application at a point of a concentrated applied force which varies harmonically with time at angular frequency  $\omega$ . In this figure the force is applied at the origin in the direction of the z axis. The resulting acoustic pressure is given by the z derivative of the pressure for a monopole. The directivity function in the far field is given by the cosine of the angle  $\psi$  between the axis of the force and the position vector to the observer. As indicated by the sketch at the bottom of Figure 24, the radiated noise is a maximum along the line of action of the force. The pressure vanishes everywhere in a plane normal to the force axis and passing through the point of application of the force.

The basic equation for the classical theory of propeller and rotor noise is shown in Figure 25. In this theory it is assumed that the inflow to the rotor is extremely clean and smooth so that the blade load distribution does not vary with time and that the rotor is stationary with respect to the surrounding air. An element of area of the rotor disc receives an impulse each time a blade passes. These impulses are represented by a distribution of monopoles and dipoles over the disc properly phased to take into account the time interval between successive blade passages. The amplitudes of the monopoles are determined by the blade thickness distribution whereas the amplitudes of the dipoles are obtained from the rotor thrust and torque distributions. The amplitude of the nth sound harmonic,  $P_n(R, \psi)$  depends upon the rotor operating conditions and the observer position as shown in the equation.

The characteristic directivity patterns for these harmonics are shown in Figure 26. This figure contains schematic diagrams of the rotational noise radiation patterns for the thickness, thrust, and torque terms contained in the equation. These radiation patterns should be compared with those for a stationary monopole and dipole shown in Figures 4 and 24 respectively. For these sketches the rotor orientation illustrated at the top of the figure applies, that is, the axis of rotation is vertical and the plane of rotation is horizontal. The noise due to torque and thickness is a maximum in the plane of rotation and a minimum on the axis. The noise due to thrust has a four leaf clover pattern with pressure minima in the plane of rotation and on the axis.

The theory of propeller and rotor noise was modified by Garrick and Watkins to include the effects of propeller forward speed, Reference 5. The expression for the nth sound harmonic is given in Figure 27. The equation again assumes a clean inflow to the rotor which is in uniform forward motion at a Mach number M. The equation is expressed in terms of the emission distance  $\bar{R}$  and angle  $\bar{\psi}$  of the observer. A convective amplification factor is evident for each harmonic for thickness, thrust, and torque noise. Additional changes in the far-field directivity result from the presence of the forward Mach number in the argument of the Bessel function.

Figure 28 shows the changes which result in rotor noise radiation patterns due to forward motion. Sketches are given of the torque and thickness component and the thrust component of noise for three different low subsonic Mach numbers. The rotor orientation is as indicated at the top of the figure. The rotor is moving from left to right. The plane of rotation is vertical. For simplicity only half of the radiation pattern is shown. The complete pattern is of course symmetric about the axis of rotation. Even at relatively modest forward speeds very significant beaming of the sound in the direction of motion occurs. Noise produced by torque and thickness is also increased in and behind the plane of rotation. There is little change in noise produced by thrust in the aft quadrant.

#### RECENT DEVELOPMENTS IN SOURCE RADIATION THEORY

The ideas described in the previous part of this paper have been well known and accepted for many years. Several more recent developments in the fundamental theory and application of source radiation deserve mention. The work of References 6 through 12 is recommended to the reader who wishes to familiarize himself with some of the current directions, controversies, and problems relating to source radiation.

Lowson, Reference 6, has developed an analysis for the radiation from monopoles, dipoles, and quadrupoles in arbitrary motion. His theory has been applied to explaining noise radiation from rotors due to unsteady blade loads, Reference 7. Unsteady blade loads result from rotor-stator interaction in turbofan aircraft engines or from blade-vortex interaction in free rotors. Unsteady blade loads have been found to be a very significant source of noise whenever they occur.

F. Farassat has derived expressions for the acoustic field of bodies of arbitrary shape and motion, Reference 8. Required parameters for noise prediction are the body geometry, time history of the motion, and surface pressure distribution. The compactness of the sources is not assumed. The analysis is carried out in the time domain and does not require decomposing the noise field into harmonics. The theory is particularly suitable for the prediction of impulsive noise from bodies such as high speed blade slap from helicopter rotors, Reference 9. Such noise is particularly difficult to handle and understand using Fourier analysis because of the presence of many high harmonics.

Lansing and Drishler, References 10 and 11, have obtained expressions for the sound field of a ducted propeller or rotor. The acoustic field within the duct due to rotating blades is expressed as a superposition of modes appropriate to the duct geometry. Corrections to account for the radiation into the free field are derived. This work is useful in analyzing the problem of aircraft engine noise propagation and radiation from internal rotating machinery.

A. Dowling, Reference 12, has recently published a new analysis of the radiation from a convecting monopole. The monopole is represented as a pulsating compact body which interacts with the surrounding fluid to produce both a mass and a momentum flux. The sound field from such a body has both a monopole and dipole component. Stronger convective amplification effects are obtained than for the simple monopole. It is also found that amplification in the direction perpendicular to the emission point may occur. The results raise some perplexing questions regarding the proper modeling of noise sources of practical importance.

#### CONCLUDING REMARKS

This paper has discussed the influence of the ground surface and motion - both rectilinear and rotational - on the directivity of radiation from acoustic sources. It was shown that interference patterns are produced by reflection and absorption at a surface and that consequently the far-field directivity of an acoustic source near the ground can be substantially altered from its free field value. The kinematic effects of motion which have been described are the beaming of sound in the direction of source motion and the shifting of the observer source frequency in a manner which is directionally dependent. Experimental data were shown to illustrate these effects. These phenomena explain some of the problems encountered in measuring noise from moving sources and the characteristics of noise from rotating blades. Reflection phenomena and kinematic effects of motion must be removed from noise data for moving sources near the ground in order to determine the characteristics of an unknown noise source and to investigate the dynamic effects of motion upon noise generation.

#### REFERENCES

1. Morse, Philip M.; and Ingard, K. Uno: *Theoretical Acoustics*. McGraw-Hill Book Company, 1968.
2. Richards, E. J.; and Mead, D. J.: *Noise and Acoustic Fatigue in Aeronautics*. John Wiley & Sons, Ltd., 1968.
3. Dickinson, P. J.; and Doak, P. E.: Measurements of the Normal Acoustic Impedance of Ground Surfaces. *J. Sound & Vibration*, vol. 13, no. 3, Nov. 1970, pp. 309-322.
4. Norum, T. D.; and Liu, C. H.: Point Source Moving Above a Finite Impedance Reflecting Plane - Experiment and Theory. *J. Acoust. Soc. Am.*, vol. 63, no. 4, April 1978, pp. 1069.
5. Garrick, I. E.; and Watkins, Charles E.: A Theoretical Study of the Effect of Forward Speed on the Free-Space Sound-Pressure Field Around Propellers. National Advisory Committee for Aeronautics Report 1198, 1954.
6. Lawson, M. V.: The Sound Field for Singularities in Motion. *Proc. Roy. Soc. (London)*, ser. A, vol. 286, no. 1407, Aug. 1965, pp. 559-572.
7. Lawson, M. V.; and Ollerhead, J. B.: A Theoretical Study of Helicopter Rotor Noise. *J. Sound & Vibration*, vol. 9, no. 2, 1969, pp. 197-222.
8. Farassat, F.: Theory of Noise Generation from Moving Bodies with an Application to Helicopter Rotors. NASA TR R-451, December 1975.
9. Farassat, F.; and Brown, T. J.: A New Capability for Predicting Helicopter Rotor and Propeller Noise Including the Effect of Forward Motion. NASA TM X-74037, June 1977.
10. Lansing, Donald L.: Exact Solution for Radiation of Sound from a Semi-Infinite Circular Duct with Application to Fan and Compressor Noise. Analytical Methods in Aircraft Aerodynamics. Symposium held at Ames Research Center, NASA SF-228, Oct. 28-30, 1969, pp. 323-334.
11. Drishler, Joseph A.: Analytical Studies of Sound Pressures Inside the Duct of Ducted Propellers. NASA TN D-6345, September 1971.
12. Dowling, Ann: Convective Amplification of Real Simple Sources. *J. Fluid Mech.* vol. 74, part 3, 1976, pp. 529-546.

#### ACKNOWLEDGEMENT

The author would like to thank Ms. Jean Mason for her help in carrying out many of the calculations shown in the figures.

CONTINUITY.  $\frac{\partial \rho}{\partial t} + \rho_0 \frac{\partial u_i}{\partial x_i} = Q$

MOMENTUM:  $\rho_0 \frac{\partial u_i}{\partial t} = F_i - \frac{\partial p}{\partial x_i}$

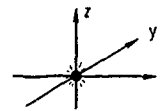
PRESSURE-DENSITY RELATION.  $p = c^2 \rho$

INHOMOGENEOUS WAVE EQUATION  $\frac{1}{c^2} \frac{\partial^2 p}{\partial t^2} - \frac{\partial^2 p}{\partial x_i \partial x_i} = \frac{\partial Q}{\partial t} - \frac{\partial F_i}{\partial x_i}$

$\rho$  DENSITY PERTURBATION  $\rho_0$  c AMBIENT DENSITY AND SPEED OF SOUND  
 $p$  PRESSURE PERTURBATION  $Q$  TIME RATE OF PRODUCTION OF MASS PER UNIT VOLUME  
 $u_i$  VELOCITY COMPONENTS  $F_i$  COMPONENTS OF BODY FORCE PER UNIT VOLUME

Figure 1.- The Field Equations of Linearized Acoustics.

$Q = Q_0 \delta(x) \delta(y) \delta(z) e^{-i\omega t}$



$p = \frac{\omega Q_0}{4\pi i} \frac{e^{i(kR - \omega t)}}{R}$   $R^2 = x^2 + y^2 + z^2$ ,  $k = \frac{\omega}{c}$

$u_R = \frac{1}{i\omega \rho_0} \frac{\partial p}{\partial R} = \frac{Q_0}{4\pi \rho_0} e^{i(kR - \omega t)} \left[ \frac{1}{R^2} - \frac{ik}{R} \right]$

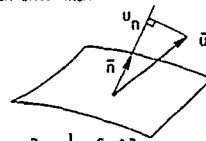
$I_R = \frac{1}{2\rho_0 c} \left( \frac{\omega Q_0}{4\pi R} \right)^2 = \frac{1}{2\rho_0 c} |p|^2$

$\Pi = \frac{\omega^2 Q_0^2}{8\pi \rho_0 c}$

Figure 4.- Radiation from a Monopole.

#### ACOUSTIC INTENSITY

TIME RATE OF ENERGY FLOW PER UNIT AREA



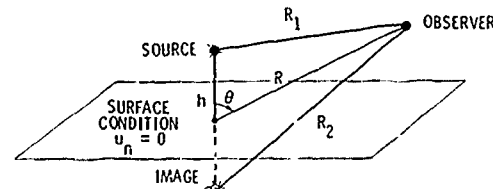
$I_n = \text{TIME AVERAGE OF } [\text{Re}(p) \text{Re}(u_n)] = \frac{1}{2} \text{Re}[p u_n^*]$

#### ACOUSTIC POWER

TIME RATE OF TOTAL ENERGY FLOW THROUGH A CLOSED SURFACE

$\Pi = \iint_S I_n dS$

Figure 2.- Energy Equations of Linearized Acoustics.



$p = \frac{\omega Q_0}{4\pi i} \left\{ \frac{e^{ikR_1}}{R_1} + \frac{e^{ikR_2}}{R_2} \right\} e^{-i\omega t}$   
 ACTUAL SOURCE IMAGE SOURCE

IN THE FAR FIELD:

$R_1 \approx R - h \cos \theta$   $R_2 \approx R + h \cos \theta$

$p \approx \frac{\omega Q_0}{2\pi i} \cos(kh \cos \theta) \frac{e^{i(kR - \omega t)}}{R}$

Figure 5.- Monopole Near a Reflecting Surface.

#### LINEAR ACOUSTIC THEORY

$\frac{1}{c^2} \frac{\partial^2 p}{\partial t^2} - \frac{\partial^2 p}{\partial x_i \partial x_i} = \frac{\partial Q}{\partial t} - \frac{\partial F_i}{\partial x_i}$

SOUND PROPAGATION SOUND PRODUCTION

MATHEMATICAL EXPRESSION	PHYSICAL MEANING	EXAMPLES
$\frac{\partial Q}{\partial t}$	MASS INJECTION	UNSTEADY JETS VIBRATING SURFACES
$\frac{\partial F_i}{\partial x_i}$	BODY FORCES	AERODYNAMIC FORCES ON MOVING BODIES
IF NONLINEAR TERMS ARE INCLUDED IN THE EQUATION		
$\frac{\partial^2 (\rho u_i u_j)}{\partial x_i \partial x_j}$	SHEAR STRESSES	TURBULENT FLUID MOTIONS, JETS, WAKES, BOUNDARY LAYERS

Figure 3.- Sources of Sound.

DIRECTIVITY FUNCTION  $d(\theta) = |2 \cos(kh \cos \theta)|$

FIXED SOURCE HEIGHT AND FREQUENCY  
 $f = 200 \text{ Hz}$   $h = 2.5 \text{ m}$   $kh = 9.1$

FIXED SOURCE AND OBSERVER POSITION  
 $h = 2.5 \text{ m}$   $\theta = 80^\circ$

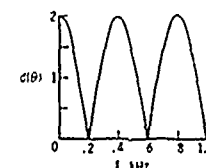
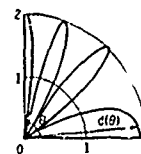
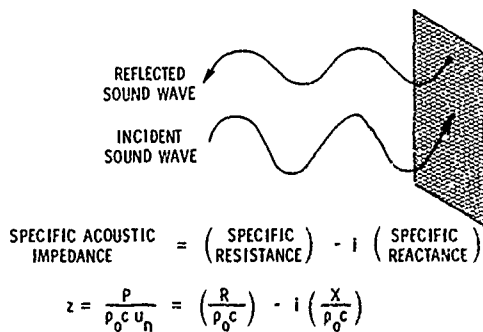


Figure 6.- The Directivity Function for a Monopole Near a Reflecting Surface.



SPECIFIC ACOUSTIC ADMITTANCE:  $y = 1/z$

Figure 7.- The Impedance of an Absorbing Surface.

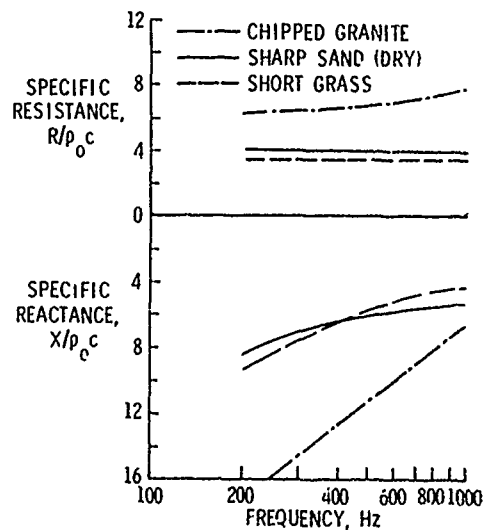
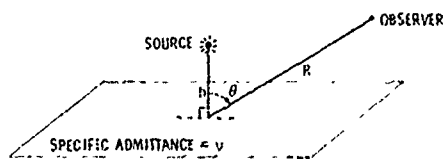


Figure 8.- Measured Acoustic Impedance of Ground Surfaces.



IN THE FAR FIELD:

$$P = \frac{\omega Q_0}{2\pi i} \left\{ \frac{\cos \theta \cos \theta h \cos \theta h - i v \sin \theta h \cos \theta h}{\cos \theta + v} \right\} \frac{e^{i \omega R - \omega t}}{R}$$

Figure 9.- Monopole Near an Absorbing Surface.

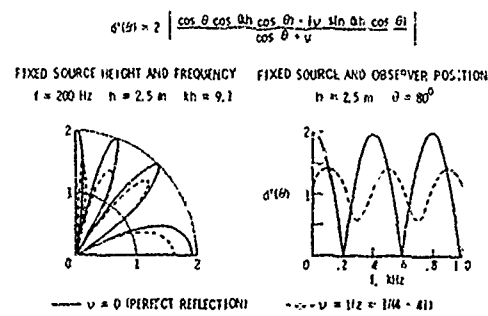


Figure 10.- The Directivity Function for a Monopole Near an Absorbing Surface.

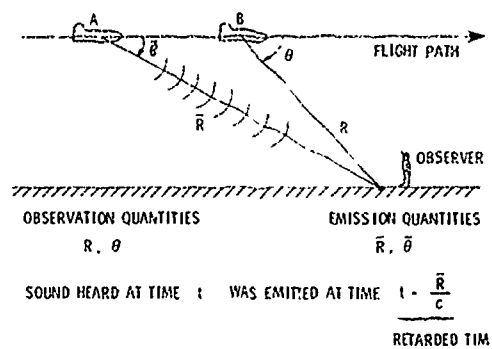


Figure 11.- The Effects of Motion on Source Radiation for Constant Altitude and Velocity Flight.

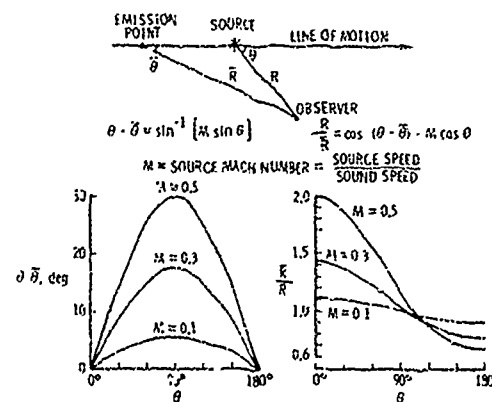
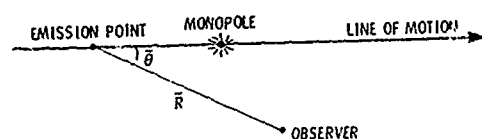


Figure 12.- Observer and Emission Quantities for Various Flight Mach Numbers.



FARFIELD ACOUSTIC PRESSURE:

$$P \approx \frac{\omega Q_0}{4\pi r} \frac{1}{(1 - M \cos \theta)^2} \frac{e^{i(kR - \omega t)}}{R}$$

CONVECTIVE AMPLIFICATION FACTOR

Figure 13.- Directivity of Radiation for a Monopole in Motion.

$$P \sim e^{i(kR - \omega t)} \quad \text{WHERE } \bar{R} = \frac{M(x - Ut) + \sqrt{(x - Ut)^2 + (1 - M^2)r^2}}{1 - M^2}$$

AHEAD OF THE SOURCE

$$\theta = 0, r = 0, x > Ut$$

$$P \sim e^{i\left[\frac{k}{1-M}x - \frac{\omega}{1-M}t\right]}$$

OBSERVER FREQUENCY

BEHIND THE SOURCE

$$\theta = 180^\circ, r = 0, x < Ut$$

$$P \sim e^{i\left[\frac{k}{1+M}x - \frac{\omega}{1+M}t\right]}$$

FOR A GENERAL LOCATION THE OBSERVER FREQUENCY,  $\omega_o$ , IS

$$\omega_o = \frac{d}{dt}(\omega t - k\bar{R}) = \frac{\omega}{1 - M \cos \theta}$$

Figure 16.- Doppler Shift in Observation Frequency.

$$\Delta SPL = 20 \log \left[ \frac{\text{MOVING SOURCE PRESSURE}}{\text{STATIONARY SOURCE PRESSURE}} \right] = -40 \log (1 - M \cos \theta)$$

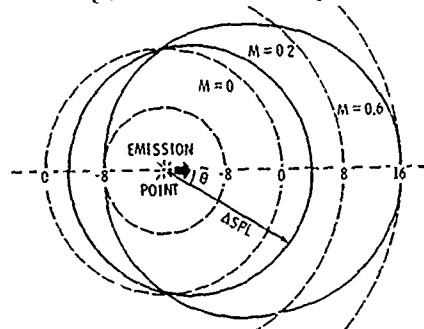


Figure 14.- Convective Amplification of Monopole Radiation.

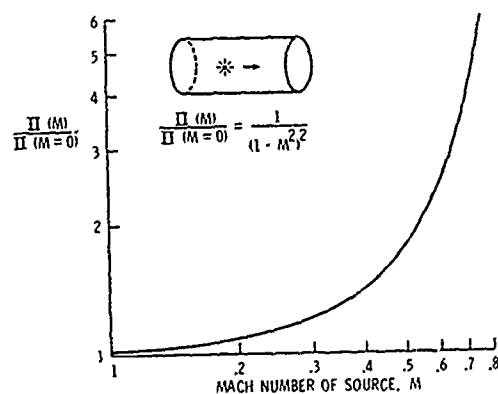


Figure 15.- Convective Amplification of Monopole Power.

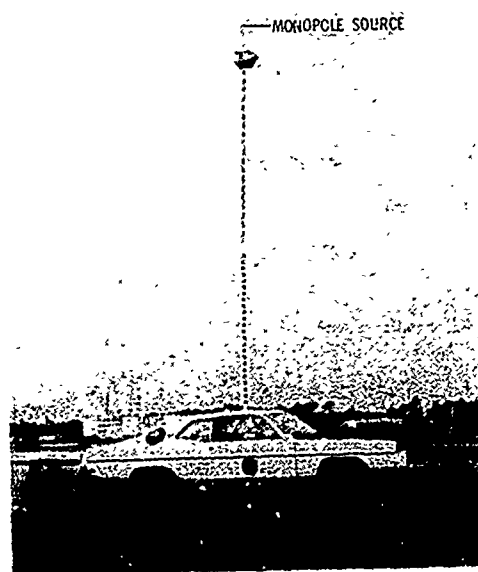


Figure 17.- Moving Monopole Source Experiment.

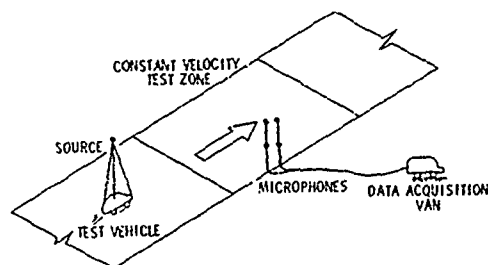


Figure 18.- Schematic of Test.



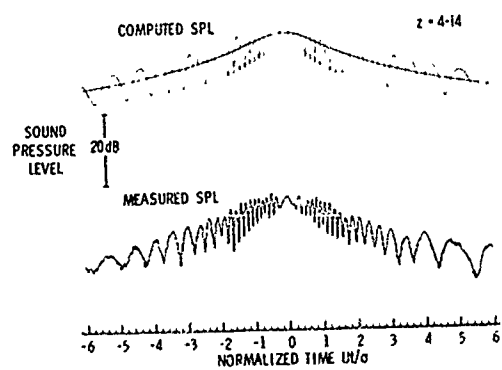


Figure 19.- Comparison of Theoretical and Experimental Noise Time Histories.

$f = 1230 \text{ Hz}$ ,  $U = 13.4 \text{ m/s}$ ,  $h_0 = 6.10 \text{ m}$ .

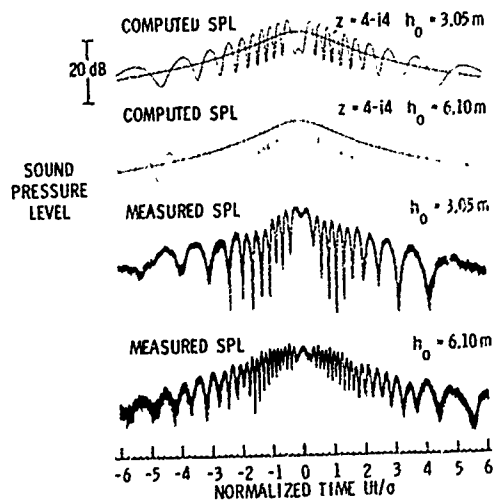


Figure 20.- Variation of Computed and Measured Noise Time Histories with Observer Height.  $f = 1230 \text{ Hz}$ ,  $U = 13.4 \text{ m/s}$ .

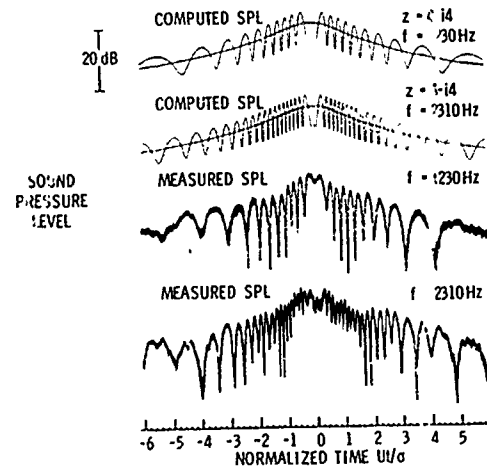
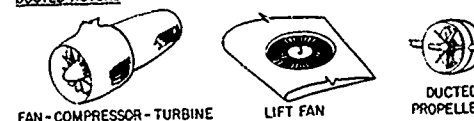


Figure 21.- Variation of Computed and Measured Noise Time Histories with Frequency.

$U = 13.4 \text{ m/s}$ ,  $h_0 = 3.05 \text{ m}$ .

#### DUCTED ROTORS



#### FREE ROTORS:

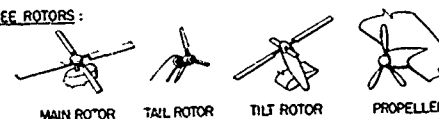
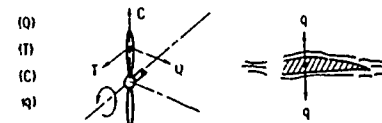


Figure 22.- Rotating Blade Components.

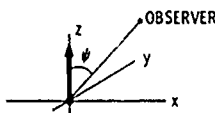
TORQUE  
THRUST  
CONING  
THICKNESS



THE SOUND FIELD IS PERIODIC IN TIME AND SPACE AND THEREFORE BE DEVELOPED IN A FOURIER SERIES

$$P = \sum_{n=-\infty}^{+\infty} P_n e^{in(\theta - \Omega t)}$$

Figure 23.- Noise Sources for Rotating Blades.

$$\vec{F} = F_z \delta(x) \delta(y) \delta(z) e^{-i\omega t} \vec{e}_z$$


$$P = -\frac{3F_z}{4\pi} \frac{\partial}{\partial z} \left[ \frac{e^{i(kR - \omega t)}}{R} \right] e^{-i\omega t} \approx \frac{3kF_z}{4\pi} \cos \psi \frac{e^{i(kR - \omega t)}}{R}$$

IN THE FAR FIELD

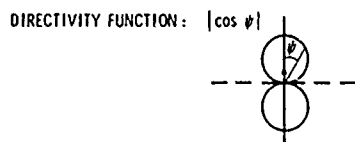
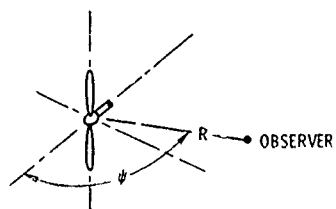


Figure 24.- Radiation from a Dipole.



$$P_n(R, \psi) = \frac{nB\Omega}{2\pi cR} \left[ cq + T \cos \psi - \frac{Q}{M_1 R_e} \right] J_n B (nB M_1 \sin \psi)$$

n	HARMONIC NUMBER	T	THRUST
B	BLADE NUMBER	Q	TORQUE
Ω	SHAFT SPEED	R <sub>e</sub>	EFFECTIVE RADIUS
M <sub>1</sub>	TIP MACH NUMBER	q	THICKNESS

Figure 25.- Noise Radiation Equations for Clean Inflow to a Hovering Rotor.

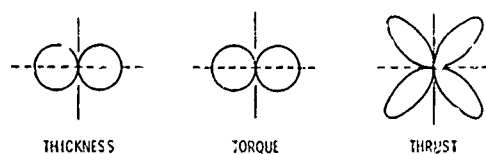
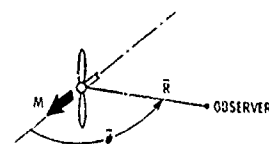


Figure 26.- Rotor Noise Radiation Patterns for Clean Inflow to a Hovering Rotor.



5-11

$$\vec{E}_n(R, \psi) = \frac{nB\Omega}{2\pi c R (1 - M^2)^{1/2} (1 - M \cos \psi)^{3/2}} \left[ cq + T \cos \psi - \frac{Q}{M_1 R_e} \right] J_n B \left[ nB M_1 \frac{\sin \psi}{1 - M \cos \psi} \right]$$

Figure 27.- Noise Radiation Equations for Clean Inflow to a Rotor in Forward Motion.

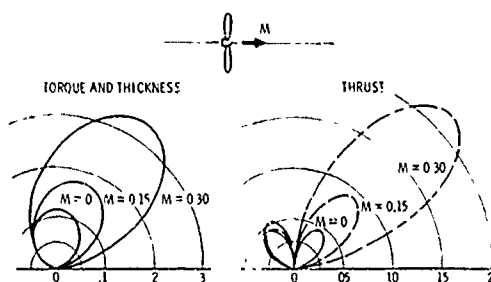


Figure 28.- Rotor Noise Radiation Patterns for Clean Inflow to a Rotor in Forward Motion.

PROPAGATION DANS LES CONDUITS

M. Pérulli  
Office National d'Etudes et de Recherches Aéronautiques  
92320 Châtillon - France

et

Université de Technologie de Compiègne  
60206 Compiègne - France

RESUME

L'étude de la propagation d'ondes acoustiques dans les conduits s'effectue à partir d'une équation d'ondes dans laquelle intervient :

- la géométrie du conduit,
- les grandeurs moyennes et fluctuantes caractérisant le fluide,
- les propriétés acoustiques des parois.

Généralement cette équation ne peut être résolue qu'à l'aide de méthodes numériques complexes et, à ce jour, on ne sait traiter analytiquement que des cas particuliers qui correspondent à des géométries simples.

Afin de mettre en évidence un grand nombre de propriétés physiques on discute le cas d'un conduit infini de section quelconque mais constante dans lequel s'écoule un fluide uniformément homogène, l'impédance acoustique des parois pouvant être ou non absorbante. Puis on donne l'expression du champ de pression pour différentes géométries types (conduits rectangulaires, annulaires, cylindriques).

1 - HYPOTHESES

Les équations de continuité et de conservation de la quantité de mouvement de la mécanique des milieux continus s'écrivent :

$$(1) \quad \frac{\partial \rho_1}{\partial t} + \vec{\nabla} \cdot (\rho_1 \vec{v}_1) = 0$$

$$(2) \quad \rho_1 \frac{\partial \vec{v}_1}{\partial t} + \rho_1 (\vec{v}_1 \cdot \vec{\nabla}) \vec{v}_1 + \vec{\nabla} p_1 = 0$$

dans la mesure où l'on néglige les effets de viscosité, d'inertie, de gravité, d'échanges thermiques.

Dans ces équations :  $\rho_1$ ,  $p_1$ ,  $\vec{v}_1$  représentent respectivement la densité, la pression et la vitesse totales. De plus, en supposant le milieu isentropique on a la relation :

$$(3) \quad p_1 = c^2 \rho_1$$

où  $c$  est la célérité du son dans le milieu.

Posons, afin de linéariser les équations (1) à (3) :

$$\rho_1 = \rho_0 + \rho$$

$$\frac{p_1}{\rho_1} = \frac{p_0 + p}{\rho_0 + \rho} \quad , \quad \text{avec} \quad \vec{\nabla} \cdot \vec{v}_0 = 0 \quad (\text{écoulement homogène})$$

$$c_1 = c_0 + c$$

$$\text{avec : } |\rho| \ll \rho_0, \quad |p| \ll p_0, \quad |\vec{v}| \ll |\vec{v}_0|$$

et en supposant de plus que :

$$\langle \rho_1 \rangle = \rho_0, \quad \langle p_1 \rangle = p_0, \quad \langle \vec{v}_1 \rangle = \vec{v}_0$$

(  $\langle A \rangle$  : indique que l'on considère la valeur moyenne dans le temps de la grandeur entre crochets ).

Compte tenu de ces définitions, à l'ordre un, les équations (1) à (3) s'écrivent :

$$(4) \quad \frac{\partial \rho}{\partial t} + \vec{v}_0 \cdot \vec{\nabla} \rho + \rho_0 \vec{\nabla} \cdot \vec{v} = 0$$

$$(5) \quad \rho_0 \left( \frac{\partial \vec{v}}{\partial t} + \vec{v}_0 \cdot \vec{\nabla} \vec{v} \right) + \vec{\nabla} p = 0$$

$$(6) \quad p = c_0^2 \rho$$

En formant la combinaison  $\frac{\partial}{\partial t}(4) - \vec{V}_0(s) = 0$  on obtient, compte tenu de (6), une équation équivalente aux équations (4), (5) et (6) qui constituent un système complet.

Tous calculs effectués, cette combinaison conduit à :

$$(7) \left\{ \frac{1}{C_0^2} \left( \frac{\partial}{\partial t} + \vec{V}_0 \cdot \vec{\nabla} \right)^2 - \Delta \right\} p(\vec{r}, t) = 0$$

où  $p(\vec{r}, t)$  représente la pression acoustique perçue par un observateur fixe par rapport à l'écoulement de vitesse moyenne

Considérons (Fig. 1) un conduit admettant l'axe  $\vec{z}$  dont la direction positive est colinéaire à  $\vec{V}_0$ . Nous supposons que la section droite de ce conduit est de section, de forme et de dimension constante, et, enfin qu'il est de longueur infinie. Ces hypothèses non forcément réalistes sont parfois valables localement. En effet, si les variations de section sont petites devant les longueurs d'ondes acoustiques axiales, alors l'hypothèse de section constante est localement acceptable. Si les variations axiales de l'écoulement, c'est-à-dire si le gradient axial de l'écoulement est petit devant le nombre d'onde axiale, alors l'hypothèse d'écoulement localement uniforme est également acceptable.

Nous allons chercher à dégager les principes essentiels attachés à l'équation (7). Pour cela décomposons le vecteur tridimensionnel  $\vec{r}$  en deux composantes :

- l'une  $\vec{r}_1$  évidemment dirigée le long de l'axe  $\vec{z}$
- l'autre  $\vec{r}_2$  située dans un plan perpendiculaire à cet axe.

$$\text{De plus posons : } p(\vec{r}, t) = p(\vec{r}_1) p(z, t)$$

Avec ces conditions, (7) est équivalent à :

$$(8) p(z, t) \left[ \Delta_1 p(\vec{r}_1) \right] - p(\vec{r}_1) \left[ \frac{1}{C_0^2} \left( \frac{\partial}{\partial t} + V_0 \frac{\partial}{\partial z} \right)^2 - \frac{\partial^2}{\partial z^2} \right] p(z, t) = 0$$

soit encore :

$$\frac{1}{p(\vec{r}_1)} \Delta_1 p(\vec{r}_1) = \frac{1}{p(z, t)} \left[ \frac{1}{C_0^2} \left( \frac{\partial}{\partial t} + V_0 \frac{\partial}{\partial z} \right)^2 - \frac{\partial^2}{\partial z^2} \right] p(z, t) = 0$$

Pour que cette égalité soit satisfaite, quel que soit  $\vec{r}_1$ ,  $z$  et  $t$ , il faut et il suffit que chacun des deux membres soit égal à une même quantité constante que l'on appellera  $-T^2$ , où  $T^2$  est réel. Ce choix est dicté par des considérations énergétiques qui seront explicitées au paragraphe

Dans ces conditions, nous avons à résoudre le système équivalent :

$$(9a) \left\{ \Delta_1 + T^2 \right\} p(\vec{r}_1) = 0$$

$$(9b) \left\{ \frac{1}{C_0^2} \left[ \frac{\partial}{\partial t} + V_0 \frac{\partial}{\partial z} \right]^2 - \frac{\partial^2}{\partial z^2} + T^2 \right\} p(z, t) = 0$$

Résoudre l'équation (9a) équivaut à rechercher, pour la forme particulière donnée de l'opérateur  $\Delta_1$ , l'ensemble des valeurs propres  $(-T^2)$  associées aux fonctions propres  $p(\vec{r}_1)$  de cet opérateur. Ce problème peut être traité de façon générale (c'est-à-dire pour un conduit de section quelconque), compte tenu de conditions aux limites fixées à la paroi du conduit. On peut résoudre l'équation (9b) suivant deux méthodes.

La première consiste à considérer un paquet d'ondes qui se propage dans le conduit le long de l'axe. Ce paquet est défini par la double transformée de Fourier  $\tilde{p}(\omega, k_z)$  de  $p(z, t)$  où  $k_z$  est le nombre d'onde axial et  $\omega$  la fréquence angulaire :

$$\tilde{p}(\omega, k_z) = \iint p(z, t) \exp[i(\omega t - k_z z)] dz dt,$$

et,

$$p(z, t) = \frac{1}{(2\pi)^2} \iint \tilde{p}(k_z, \omega) \exp[-i(\omega t - k_z z)] d\omega dk_z.$$

Toute transformation effectuée, (9b) s'écrit, avec  $K \equiv \omega/C_0$  et  $M_0$ , nombre de Mach axial de l'écoulement, égal à  $V_0/C_0$

$$(10a) \left[ k_z^2 - (K - M_0 k_z)^2 + T^2 \right] \tilde{p}(k_z, \omega) = 0$$

Pour que la relation (10a) admette une solution non triviale, c'est-à-dire, pour qu'elle soit satisfaite pour une onde d'amplitude non identiquement nulle, il faut et il suffit que :

$$(11) \left[ k_z^2 - (K - M_0 k_z)^2 + T^2 \right] = 0$$

La relation (11) est la relation de dispersion des ondes d'amplitude  $\tilde{p}(k_z, \omega)$ . Cette relation pour chaque valeur propre de l'opérateur  $\Delta_\perp$ , et chaque fréquence  $\omega$  impose la valeur de  $k_z$ . Elle est donc de la forme :  $R(k_z, \omega) = 0$ . On dit aussi que (10a) est l'image de Fourier dans l'espace et dans le temps de (9b).

La seconde méthode, cas particulier de la première, consiste à rechercher des solutions harmoniques de (9b), c'est-à-dire des solutions de la forme :  $\exp i(\omega t - k_z z)$ , multipliée éventuellement par une constante arbitraire  $P$  qui représente l'amplitude de l'onde (indépendante de  $z$ ).

On trouve, tout calcul effectué :

$$(10b) \quad [T^2 + k_z^2 - (K - M_0 k_z)^2] P \exp i(\omega t - k_z z) = 0$$

Cette relation est satisfaite par toute onde harmonique de la forme, proposée dont les  $k_z$  et les  $\omega$  satisfont la relation de dispersion (11) :

$$(11) \quad T^2 + k_z^2 - (K - M_0 k_z)^2 = 0$$

La différence physique de ces deux méthodes est évidente :

- la première conduit à la notion de paquets d'ondes d'amplitude  $\tilde{p}(k_z, \omega)$  satisfaisant la relation (11)
- la seconde, à des ondes harmoniques, cas particulier de la première forme et satisfaisant la même relation. De même, on aurait pu définir ces modes harmoniques (en  $\exp i\omega t$ ) en décomposant en série de Fourier  $p(\vec{r}, t)$ . Nous trouverions le même résultat, chaque fréquence  $\omega$  devant vérifier (11).

Dans ces conditions :  $p(\vec{r}, t) = p(\vec{r}_\perp) \exp i(\omega t - k_z z)$ .

où  $p(\vec{r}_\perp)$  est solution de :

$$(12) \quad \Delta_\perp p(\vec{r}_\perp) + [(K - M_0 k_z)^2 - k_z^2] p(\vec{r}_\perp) = 0.$$

Dans le repère lié à l'écoulement, c'est-à-dire pour un observateur porté par l'écoulement, l'onde est (au facteur  $C_0$  près) de fréquence  $K' = K - M_0 k_z$  donc,  $p(\vec{r}_\perp)$  est solution de :

$$(13) \quad \Delta_\perp p(\vec{r}_\perp) + (K'^2 - k_z^2) p(\vec{r}_\perp) = 0.$$

L'équation (13) a une forme qui correspond à celle qui serait obtenue dans le cas où la vitesse  $V_0$  de l'écoulement serait nul. Avec  $\omega' \equiv \omega - k_z V_0$ ,  $\omega'$  fréquence de l'onde dans le repère mobile, et, comme  $K' \equiv \omega'/C_0$  représente le nombre d'ondes total et  $k_z$  le nombre d'ondes axial, les valeurs propres de l'opérateur  $\Delta_\perp$  représentent le vecteur d'ondes transversal  $\vec{K}_\perp$  tel que :

$$(11bis) \quad K'^2 = k_z^2 + |\vec{K}_\perp|^2.$$

De même dans le repère fixe (ou en présence d'écoulement ayant toutes les propriétés mentionnées ci-dessus) on a :

$$(11ter) \quad (K - k_z M_0)^2 = k_z^2 + |\vec{K}_\perp|^2.$$

La relation (11bis) est paire en  $K'$  et en  $k_z$ . Il n'en est pas de même pour (11ter).

#### Conditions aux limites

De l'équation de conservation de la quantité de mouvement :

$$\rho_0 \left( \frac{\partial}{\partial t} + V_0 \frac{\partial}{\partial z} \right) \vec{v} + \vec{\nabla} p = 0,$$

on déduit :

$$(14) \quad \vec{v} = \frac{i}{\rho_0 C_0 (K - M_0 k_z)} \vec{\nabla} p.$$

D'où le résultat fondamental suivant :

la vitesse et la pression acoustique ne sont en phase que si, et seulement si,  $\vec{\nabla} p$  est de la forme  $i \vec{k} p$  où  $p$  est indépendant des coordonnées d'espace.

Les conditions aux limites imposent que, à la paroi, le rapport de la pression acoustique à la vitesse normale à la paroi soit égal à l'impédance acoustique de la paroi  $Z$ , avec  $Z = Z_0 / C_0$ .

6-4

Appelons  $\vec{v}_n = \vec{v} \cdot \vec{N}$  le produit de la vitesse de l'onde acoustique  $\vec{v}$ , par le vecteur unitaire normale à la paroi considérée.

La condition aux limites s'écrit :

$$(15) \quad (p = Z_1 v_n) \quad \text{à la paroi}$$

De (14), on déduit que :

$$(16) \quad \vec{v} \cdot \vec{N} = v_n = \frac{i}{\rho_0 c_0 (K - M_0 k_z)} \vec{N} \cdot \vec{\nabla} p.$$

Donc, (15) est équivalent à :

$$(17) \quad (p = \frac{iZ}{(K - M_0 k_z)} \vec{N} \cdot \vec{\nabla} p) \quad \text{à la paroi}$$

Rappelons que la vitesse  $\vec{v}$  de l'onde peut être déduite du vecteur déplacement  $\vec{u}$  qui, en présence d'écoulement, conduit à la relation  $\vec{v} = \frac{d\vec{u}}{dt}$ , soit  $\vec{v} = i(\omega - V_0 k_z) \vec{u}$  et, en l'absence d'écoulement :  $\vec{v} = i\omega \vec{u}$ .

Au niveau de la paroi on a, à l'intérieur du conduit :

$$\lim \vec{N} \cdot \vec{v} = (i\omega \vec{N} \cdot \vec{u}_p) \quad \text{et} \quad \lim \vec{N} \cdot \vec{v} = [i(\omega - k_z V_0) \vec{N} \cdot \vec{u}_p].$$

(dans l'épaisseur de la paroi)

(pour l'onde elle-même)

D'où, en écrivant la continuité des déplacements :

$$(18) \quad (p = \frac{iKZ}{(K - M_0 k_z)^2} \vec{N} \cdot \vec{\nabla} p) \quad \text{à la paroi}$$

Les relations (17) et (18) sont différentes, quoique voulant représenter le même phénomène. En réalité, nous avons effectué une erreur de raisonnement due au fait, qu'à la paroi, la vitesse est simultanément d'amplitude  $|\vec{v}_0|$  et d'amplitude nulle. Il faudrait écrire en toute rigueur que le vecteur déplacement lié à l'onde acoustique et arrivant à la paroi est égal en amplitude et en phase à celui de la paroi, c'est-à-dire écrire de façon très détaillée les conditions aux limites. Ce point particulier a conduit à de nombreuses discussions qui perdent de leur intérêt pour les applications pratiques pour lesquelles seuls des calculs numériques à l'aide d'ordinateur permettent de résoudre convenablement la relation des conditions aux limites en prenant en compte le réel profil de vitesse, ce qui permet de lever toute ambiguïté. Dans ce travail nous ne considérerons que la relation (17) mais nous avons tenu à attirer l'attention sur ce point, à cause des différentes formes que l'on peut trouver dans la littérature. Ce point de discussion est sans intérêt dans le cas de parois parfaitement rigides pour lesquelles  $|E_s| = |\infty| \Rightarrow v_n = 0$  ainsi qu'en l'absence d'écoulement, puisque  $V_0 = 0$  entraîne l'identité des relations (17) et (18).

Enfin, lorsqu'il existe réellement une discontinuité de vitesse, la solution proposée de l'équation de Helmholtz est fautive puisqu'elle ne tient pas compte de cette discontinuité. Dans ce cas il faut résoudre cette équation au sens des distributions.

## 2 - VITESSE DE PHASE : VITESSE DE GROUPE (Fig. 2)

La vitesse de phase  $v_p = \omega/k_z$  représente la vitesse avec laquelle les plans de phase constante  $\Phi_0$  définie par  $(\omega t - k_z z) = \Phi_0$  se déplacent.  $(\frac{1}{c_0} v_p = \frac{1}{c_0} \frac{\omega}{k_z} = \frac{K}{k_z} \equiv M_p)$

Dans le cas d'une onde dispersive, (où  $k_z$  est fonction de  $\omega$ , relation (11) par exemple), la vitesse de groupe  $v_g = \delta\omega/\delta k_z$  représente la vitesse avec laquelle l'onde se déplace. Nous verrons que dans le cas où les parois du conduit sont parfaitement rigides, cette vitesse s'identifie avec la vitesse de transport de l'énergie. Dans le cas de paquets d'ondes la vitesse de groupe correspond à la vitesse avec laquelle les ondes élémentaires composant le paquet d'ondes n'interfèrent pas de manière destructive autour du point de phase stationnaire (défini par la relation de dispersion) :  $(M_g \equiv \frac{v_g}{c_0} = \frac{1}{c_0} \frac{\partial \omega}{\partial k_z} \equiv \frac{\partial K}{\partial k_z})$

La relation de dispersion (11) implique :

$$(19) \quad M_g \equiv \frac{\partial K}{\partial k_z} = M_0 + \frac{k_z}{(K - M_0 k_z)}.$$

Or, dans le repère lié à l'écoulement, de la relation (11bis) on déduit :

$$(20) \quad \frac{\partial K'}{\partial k_z} = \frac{k_z}{K'} = \frac{k_z}{K - M_0 k_z},$$

d'où :

$$(20bis) \quad \frac{\partial K}{\partial k_z} = M_0 + \frac{\partial K'}{\partial k_z}.$$

La vitesse du groupe se comporte comme une vitesse "classique" de la mécanique puisque :

$$\begin{array}{ccccc} M_g & = & M_o & + & M_g' \\ \text{(vitesse dans} & & \text{(vitesse} & & \text{(vitesse dans} \\ \text{repère absolu)} & = & \text{d'entraînement)} & + & \text{repère relatif)} \end{array}$$

6-5

### 3 - EQUATION DE CONSERVATION DE L'ENERGIE

Le système d'équation (4), (5) et (6) étant complet, l'équation de conservation de l'énergie n'est qu'une conséquence de ces équations. Pour l'obtenir calculons  $\vec{v} \cdot (\nabla) = 0$ , et compte tenu de (4) et de (6), on obtient tous calculs effectués :

$$\frac{\partial}{\partial t} \left( \frac{1}{2} \rho_o v^2 + \frac{p^2}{2\rho_o c_o^2} \right) + \vec{\nabla} \cdot \left[ \left( \frac{1}{2} \rho_o v^2 + \frac{p^2}{2\rho_o c_o^2} \right) \vec{V}_o + p \vec{v} \right] = 0,$$

$\Leftrightarrow$

$$\frac{\partial W}{\partial t} + \vec{\nabla} \cdot [W \vec{V}_o + p \vec{v}] = 0,$$

$\Leftrightarrow$

$$\frac{\partial W}{\partial t} + \vec{\nabla} \cdot \vec{I} = 0$$

Cette équation a la forme d'une équation de Poynting où  $W$  est la densité d'énergie totale :

$$W = \frac{1}{2} \rho_o v^2 + \frac{p^2}{2\rho_o c_o^2}$$

où  $\frac{1}{2} \rho_o v^2$  est la densité d'énergie cinétique,

et  $\frac{1}{2\rho_o c_o^2} p^2$  la densité d'énergie potentielle

$\vec{I}$  est la densité de flux d'énergie totale :  $\vec{I} = W \vec{V}_o + p \vec{v}$

$W \vec{V}_o$  est la densité d'énergie totale convectée par l'écoulement (à la vitesse  $\vec{V}_o$ ),

$p \vec{v}$  est la densité d'énergie de l'onde.

La vitesse de transport d'énergie  $\vec{V}_e$  qui représente la vitesse avec laquelle le flux d'énergie traverse la section droite du conduit est, par définition, égale à :

$$\vec{V}_e = \frac{\langle \vec{I} \rangle}{\langle W \rangle}$$

où  $\langle AB \rangle$  représente la valeur moyenne dans le temps de AB

et  $\overline{AB}$  représente la valeur moyenne de AB sur la section droite du conduit.

Dans notre cas, l'axe  $\vec{z}$  représente une direction privilégiée puisque  $\vec{z}$  est un axe de symétrie, donc  $\vec{V}_e$  est colinéaire à l'axe des  $\vec{z}$ , et :

$$V_e = V_o + \frac{\langle p v_z \rangle}{\langle W \rangle}$$

Rappelons que si A et B sont écrites en notation complexe,

$$\langle AB \rangle = R_e A \cdot R_e B = \frac{1}{4} (AB^* + A^* B)$$

$$\text{Calcul de } \langle p v_z \rangle : \quad \langle p v_z \rangle = \frac{1}{4} (p v_z^* + p^* v_z)$$

$$\text{avec } p(\vec{r}, t) \equiv p(\vec{r}_\perp) \exp i(\omega t - k_z z),$$

$$\text{et : } v_z(\vec{r}, t) = \frac{k_z}{\rho_o c_o (K - M_o k_z)} p(\vec{r}, t)$$

$$\text{donc : } \langle p(\vec{r}, t) v_z(\vec{r}, t) \rangle = \frac{1}{2} \cdot \frac{k_z}{\rho_o c_o (K - M_o k_z)} |p(\vec{r}, t)|^2$$

$$= \frac{1}{2} \cdot \frac{k_z}{\rho_o c_o (K - M_o k_z)} |p(\vec{r}_\perp)|^2$$

$$\text{d'où : } \langle p(\vec{r}, t) v_z(\vec{r}, t) \rangle = \frac{1}{2} \cdot \frac{k_z}{\rho_o c_o (K - M_o k_z)} \cdot P$$

$$\text{avec : } P \equiv \int_S |p(\vec{r}_\perp)|^2 dS.$$

Remarque : calcul de  $\vec{I} \equiv \langle \rho \vec{v}_1 \rangle$  :

6-6 Comme :  $\vec{v}(\vec{r}, t) = \frac{i}{\rho_0 c_0 (K - k_z M_0)} \vec{\nabla} P(\vec{r}, t)$ ,

$$\vec{v}_1(\vec{r}, t) = \frac{i \exp[i(\omega t - k_z z)]}{\rho_0 c_0 (K - M_0 k_z)} \vec{\nabla} P(\vec{r}_1) \equiv \vec{v}(\vec{r}_1) \exp i(\omega t - k_z z),$$

et :

$$\langle \rho(\vec{r}, t) \vec{v}_1(\vec{r}, t) \rangle = \frac{1}{4} (\rho \vec{v}_1^* + \rho^* \vec{v}_1) = \frac{1}{4} \left\{ \frac{-i}{\rho_0 c_0 (K - k_z M_0)} + \frac{i}{\rho_0 c_0 (K - k_z M_0)} \right\} \rho(\vec{r}_1) \vec{\nabla}_1 P(\vec{r}_1)$$

d'où :  $\vec{I}_1 \equiv \langle \rho \vec{v}_1 \rangle = 0$  et, a fortiori :  $\vec{I}_1 \equiv \langle \rho \vec{v}_1 \rangle = 0$ .

On en conclut que dans ce genre de conduit :

- section de forme quelconque mais constante,
- écoulement homogène uniforme,
- milieu non dissipatif ( $\omega$  et  $k_z$  réels)

l'énergie de l'onde se propage, en moyenne, colinéairement à l'axe  $\vec{z}$  du conduit.

Calcul de  $\langle W \rangle$  :  $W \equiv \frac{1}{2} \rho_0 \vec{v}^2 + \frac{\rho^2}{2 \rho_0 c_0^2} = \frac{1}{2} \rho_0 \vec{v}_1^2 + \frac{1}{2} \rho_0 v_z^2 + \frac{\rho^2}{2 \rho_0 c_0^2}$

$$\langle W \rangle = \langle \frac{1}{2} \rho_0 \vec{v}_1^2 \rangle + \langle \frac{1}{2} \rho_0 v_z^2 \rangle + \langle \frac{\rho^2}{2 \rho_0 c_0^2} \rangle.$$

$$\frac{1}{2 \rho_0 c_0^2} \langle \rho^2 \rangle = \frac{1}{4 \rho_0 c_0^2} \langle |P(\vec{r}_1)|^2 \rangle = \frac{P}{4 \rho_0 c_0^2};$$

$$\frac{1}{2 \rho_0} \langle v_z^2 \rangle = \frac{1}{4 \rho_0 c_0^2} \cdot \frac{k_z^2}{(K - M_0 k_z)^2} P$$

$$\frac{1}{2 \rho_0} \langle v_1^2 \rangle = \frac{1}{4 \rho_0 c_0^2} \cdot \frac{1}{(K - M_0 k_z)^2} \int_S |\vec{\nabla}_1 P(\vec{r}_1)|^2 dS.$$

Nous allons évaluer  $\int_S |\vec{\nabla}_1 P(\vec{r}_1)|^2 dS$  :

(compte tenu de la relation de dispersion (11) et des conditions aux limites pour un conduit parfaitement rigide. Dans ce cas la vitesse de l'onde normale à la paroi est nulle).

Sachant que :  $\Delta_1 P(\vec{r}_1) = -T^2 P(\vec{r}_1)$

On déduit :  $P^*(\vec{r}_1) \Delta_1 P(\vec{r}_1) = -T^2 |P(\vec{r}_1)|^2$

$$\Rightarrow \int_S P^*(\vec{r}_1) \Delta_1 P(\vec{r}_1) dS = -T^2 P,$$

d'où en intégrant par partie à gauche et en tenant compte de la condition aux limites qui impliquent que  $(\vec{n} \cdot \vec{\nabla}_1 P(\vec{r}_1)) \equiv 0$  à la paroi :

$$-\int_S |\vec{\nabla}_1 P(\vec{r}_1)|^2 dS = -T^2 P$$

d'où :

$$\frac{1}{2} \langle \rho_0 \vec{v}_1^2 \rangle = \frac{1}{4 \rho_0 c_0^2} \cdot \frac{T^2}{(K - M_0 k_z)^2} P$$

(Ce résultat justifie le choix de la classe des valeurs propres pour la forme choisie de  $\Delta_1$  puisque l'énergie cinétique est un scalaire défini positif).

d'où :  $\langle W \rangle = \frac{P}{4 \rho_0 c_0^2} \left\{ 1 + \frac{T^2 + k_z^2}{(K - M_0 k_z)^2} \right\} = \frac{1}{2 \rho_0 c_0^2} P$

Ce résultat remarquable mérite un commentaire.

En effet :  $\langle W \rangle = \langle \frac{1}{2} \rho_0 v^2 \rangle + \langle \frac{1}{2} \frac{\rho^2}{\rho_0 c_0^2} \rangle$

avec :  $\langle \frac{1}{2} \rho_0 v^2 \rangle = \frac{1}{4 \rho_0 c_0^2} \cdot \frac{k_z^2 |P(\vec{r}_1)|^2 + |\vec{\nabla}_1 P(\vec{r}_1)|^2}{(K - M_0 k_z)^2}$

et :  $\langle \frac{1}{2} \frac{\rho^2}{\rho_0 c_0^2} \rangle = \frac{1}{4 \rho_0 c_0^2} |P(\vec{r}_1)|^2.$

Ces relations montrent d'une façon évidente que :

La densité d'énergie potentielle est toujours différente de la densité d'énergie cinétique, en tout point  $\vec{r}$  de l'espace et à tout instant  $t$ . Cette propriété est encore vraie en moyenne dans le temps.



Cette remarque est effectivement valable en tout point de l'espace, que l'on tienne ou non compte des conditions aux limites.

Pour que la densité d'énergie cinétique égale la densité d'énergie potentielle, il faut et il suffit que :

$$|\vec{\nabla}_1 P(\vec{r}_1)|^2 = |\vec{k}_1|^2 |P|^2 \iff \Delta_1 P(\vec{r}_1) = |\vec{k}_1|^2 P,$$

où  $P$  est indépendant de  $\vec{r}_1$  et, dans ce cas :

$$\langle \frac{1}{2} \rho_0 v^2 \rangle = \frac{1}{4\rho_0 c_0^2} \frac{k_z^2 + |\vec{k}_x|^2}{(K - M_0 k_z)^2} |P|^2 = \frac{1}{4\rho_0 c_0^2} |P|^2 = \langle \frac{1}{2} \frac{P^2(\vec{r}, t)}{\rho_0 c_0^2} \rangle$$

Dans ce cas, on a bien l'égalité des densités d'énergie cinétique et potentielle et l'onde est de la forme générale :

$$P(\vec{r}, t) = P \exp i(\omega t - \vec{k} \cdot \vec{r})$$

où l'amplitude  $P$  est une constante et :  $|\vec{k}| = \omega/c_0$

$$\vec{k} \cdot \vec{r} \text{ est décomposé en } \vec{k}_x \cdot \vec{r}_x, k_z \cdot \vec{z}, (\vec{v}_0 \equiv v_0 \frac{\vec{z}}{|\vec{z}|})$$

pour tenir compte de la direction privilégiée imposée par l'écoulement  $\vec{v}_0$ .

Cette onde est une onde plane, seul cas d'onde pour laquelle les densités d'énergie cinétique et potentielle sont égales.

On comprend alors pourquoi le résultat précédent est remarquable, à savoir :

$$\langle W \rangle = \frac{1}{4\rho_0 c_0^2} \left\{ 1 + \frac{k_z^2 + T^2}{(K - k_z M_0)^2} \right\} P^2 = \frac{1}{2\rho_0 c_0^2} P^2.$$

En effet, ce résultat montre que pour un guide de section quelconque : cylindrique, annulaire, rectangulaire, ..., mais non évolutive dans l'espace et seulement dans le cas où les parois sont parfaitement rigides, alors dans toute section droite du conduit l'énergie cinétique est égale à l'énergie potentielle. C'est-à-dire que les valeurs moyennes, dans le temps et sur la section droite du conduit des densités d'énergie cinétique et potentielle sont égales.

L'hypothèse "parois parfaitement rigides" est essentielle car c'est elle qui nous a permis d'évaluer la grandeur :

$$\int_S |\vec{\nabla}_1 P(\vec{r}_1)|^2 dS$$

Pour des parois d'impédance quelconque, ce résultat est mis en défaut, il reste cependant acceptable pour des parois quasi-rigides, telles que pour tout mode, la longueur d'amortissement est supérieure à la longueur d'onde axiale (hypothèse de parois "localement quasi-rigides" qui implique que :

$$\frac{R_a(z)}{I_m(z)} \ll 1 \iff \frac{I_m(k_z)}{R_a(k_z)} \ll 1.$$

Ces considérations étant faites, revenons à l'objet du calcul :

$$V_a = V_0 + \frac{\langle P v_z \rangle}{\langle W \rangle} \quad (\vec{v}_a \equiv V_a \frac{\vec{z}}{|\vec{z}|})$$

$$\iff V_a = V_0 + c_0 \frac{k_z}{(K - k_z M_0)}$$

soit à :

$$(21) \quad M_a = M_0 + \frac{k_z}{(K - k_z M_0)} = M_0 + M'_g,$$

soit à :

$$(21bis) \quad V_a = V_0 + \frac{k_z}{(\omega - k_z V_0)} = V_0 + v'_g.$$

Nous reconnaissons dans cette dernière relation, l'expression de la vitesse du groupe  $v'_g$ , calculée dans le repère absolu, puisque  $k_z/(\omega - k_z V_0)$  est la vitesse de groupe dans le repère lié à l'écoulement.

D'où le second résultat important de ce paragraphe,

la vitesse de groupe s'identifie à la vitesse de transport de l'énergie de l'onde pour tout conduit de section quelconque, constante, à parois parfaitement rigides et en présence d'un écoulement uniforme.

#### 4 - ETUDE DE LA RELATION DE DISPERSION (11), DEFINITION DES MODES

$$\begin{aligned}
 6-8 \quad (11) \quad T^2 + k_z^2 - (K - M_0 k_z)^2 &= 0 \\
 \Leftrightarrow (1 - M_0^2) k_z^2 + 2 K M_0 k_z - (K^2 - T^2) &= 0 \\
 (22) \quad \delta' &= K^2 - (1 - M_0^2) T^2 \\
 (23) \quad k_z^{\pm} &= \frac{-K M_0 \pm \sqrt{K^2 - (1 - M_0^2) T^2}}{(1 - M_0^2)}
 \end{aligned}$$

Nous allons étudier des formes particulières de (23).

4.1 - En l'absence d'écoulement ( $M_0 = 0$ ):

$$(24) \quad k_z = \pm \sqrt{K^2 - T^2}.$$

La forme de la relation de dispersion est présentée sur la figure 3. Cette courbe est symétrique par rapport à l'axe des K (des fréquences). Au point  $K = T$ ,  $k_z = 0$  donc  $(\lambda_z = 2\pi/k_z) \rightarrow \infty$ , et la tangente en ce point est infinie, donc  $v_g \equiv 0$ .

Pour  $K < T$ ,  $k_z$  est imaginaire pur. Posons  $k_z \equiv i\alpha$  donc  $\exp i(\omega t - k_z z) = \exp[i\omega t + \alpha z]$ . Pour  $\alpha > 0$ ;  $\alpha z$  est d'amplitude croissante avec  $z$ , ce qui n'a aucun sens physique, puisque par hypothèse, le milieu ne contient pas de "réservoir d'énergie" permettant tout mécanisme d'amplification, et,  $-\alpha z$  est d'amplitude décroissante avec  $z$ , c'est-à-dire : onde évanescence, ou onde non propagative.

$K = T$  définit la fréquence de coupure  $\omega_c = T_c$ . Le conduit se comporte comme un filtre passe-haut en fréquence pour la valeur propre  $T$  considérée.

Pour  $K > T$ ,  $k_z$  est réel, l'onde acoustique monochromatique de fréquence  $\omega$  oscille le long de l'axe  $z$  avec la longueur d'onde :

$$\lambda_z = 2\pi/k_z.$$

Sur la figure 3, nous remarquons que le produit  $M_g \cdot M_p$  est positif ou nul, quel que soit  $K$ . Donc  $M_g$  et  $M_p$  sont de même signe.

Pour  $\omega = \omega_c$ , fréquence de coupure,  $M_g \equiv 0$  et,  $M_p = \infty$ ;

(l'inverse de la tangente à la courbe de dispersion représente la vitesse de groupe).

On appellera mode aval les modes tels que  $M_g$  et  $M_p$  soient tous deux positifs. Ces modes se déplacent dans le sens de l'écoulement. On appellera mode amont les modes tels que  $M_g$  et  $M_p$  soient tous deux négatifs. Ces modes remontent l'écoulement (Fig. 4).

4.2 - En présence d'un écoulement subsonique ( $M_0 < 1$ ):

$$k_z^{\pm} = \frac{-K M_0 \pm \sqrt{K^2 - (1 - M_0^2) T^2}}{(1 - M_0^2)}$$

$k_z^{\pm}$  est purement réel pour  $K \geq T\sqrt{1 - M_0^2}$  donc l'amplitude oscille continuellement le long de  $z$ . La relation de dispersion des ondes subsoniques est tracée sur la figure 5.

Pour chaque valeur de  $K$  on a deux valeurs de  $k_z$ .

$$k_z^+ \geq 0 \Leftrightarrow K \geq T: M_g M_p > 0; M_g, M_p > 0:$$

ce qui définit un mode aval :

$$\text{Soit : } \sqrt{1 - M_0^2} T \leq K \leq T \quad \text{alors : } -\frac{K M_0}{(1 - M_0^2)} \leq k_z^+ < 0$$

et,  $M_g M_p \leq 0$  avec  $M_g \geq 0$  et  $M_p < 0$

On appellera un tel mode : mode amont inverse, car bien que l'énergie de l'onde se déplace dans le sens de l'écoulement ( $M_g > 0$ ), les plans de phase constante, se déplacent à contre-courant ( $M_p < 0$ ).

$$\text{Soit } k_z^- < -\frac{K M_0}{(1 - M_0^2)} \quad \text{pour } K > T\sqrt{1 - M_0^2},$$

alors :

et :  $M_g M_p > 0$  avec  $M_g$  et  $M_p$  tous deux négatifs, ce qui définit bien un mode amont (Fig. 6).

$k_z$  est complexe pour :  $K < T \sqrt{1-M_0^2}$ .

dans ce cas l'onde est d'amplitude décroissante d'autant plus rapidement que  $K$  est petit devant  $T \sqrt{1-M_0^2}$  tout en oscillant avec le nombre d'onde  $(-KM_0/(1-M_0^2))$ . C'est une onde oscillante amortie.  $\omega_c = c_0 T \sqrt{1-M_0^2}$  définit la fréquence de coupure de l'onde oscillante considérée, le conduit, se comporte encore comme un filtre passe-haut pour la valeur propre choisie :

$$T \sqrt{1-M_0^2} \cdot (R_e(k_z) = -KM_0/(1-M_0^2) ; I_m(k_z) = [(1-M_0^2)T^2 - K^2]^{1/2}/(1-M_0^2))$$

#### 4.3 - En présence d'un écoulement sonique ( $M_0 = 1$ )

Lorsque  $M_0 = 1$ ,

alors :

$$(11a) \Leftrightarrow 2Kk_z - (K^2 - T^2) = 0$$

$$\text{d'où : } k_z = \frac{K^2 - T^2}{2K}$$

Sur la figure 7, on constate que : à une valeur de  $K$ , correspond une seule valeur de  $k_z$  et non deux valeurs de  $k_z$  comme précédemment.

La fréquence de coupure  $\omega_c$  tend vers zéro, comme le montre la relation  $\omega_c = c_0 \sqrt{(1-M_0^2)T^2}$  dans laquelle  $M_0 \rightarrow 1$ .

Nous remarquerons sur cette figure, comme sur la figure 8, que la tangente à la courbe de dispersion  $k_z(\omega)$  est toujours positive contrairement aux deux cas précédents où elle pouvait être également négative.

$$\forall k_z : M_0 \geq 0 \text{ et } k_z \geq 0 \Rightarrow M_0 > 0 \Leftrightarrow \text{mode aval}$$

$$k_z < 0 \Rightarrow M_0 \leq 0 \Leftrightarrow \text{mode amont inverse (Fig. 8)}$$

#### 4.4 - En présence d'un écoulement supersonique ( $M_0 > 1$ ) (Fig. 9)

$$k_z^2 = \frac{-KM_0^2 \sqrt{K^2 + (M_0^2 - 1)T^2}}{(1-M_0^2)}$$

où  $(M_0^2 - 1)$  est strictement positif. Donc  $k_z$  est purement réel, et, dans ce cas, l'onde est purement oscillante le long de l'axe  $Z$  pour toute valeur de  $K$ .

Dans ce cas, la notion de fréquence de coupure disparaît

$$\forall k_z : M_0 > 0 \quad \text{puisque la courbe est monotone croissante.}$$

$$k_z \geq 0 \Rightarrow M_0 \geq 0 \Leftrightarrow \text{mode aval}$$

$$k_z < 0 \Rightarrow M_0 < 0 \Leftrightarrow \text{mode amont inverse.}$$

Une onde acoustique ne peut remonter un écoulement sonique, a fortiori, supersonique (Fig. 10).

#### 5 - CALCUL DES FONCTIONS PROPRES DE L'OPERATEUR

Pour calculer les fonctions propres de l'opérateur bidimensionnel  $\Delta_{\perp}$ , il est nécessaire d'en expliciter sa forme. Nous choisirons pour ce faire, des formes classiques de conduit : conduit rectangulaire, annulaire et circulaire. Dans le cas du conduit circulaire et à titre d'exemple nous expliciterons des solutions analytiques dans le cas de parois quasi-rigides. Pour les autres formes de la section droite du conduit nous nous contenterons de donner les relations à résoudre numériquement.

##### 5.1 - Conduit rectangulaire bidimensionnel : $P(x, y, z, t) = \sum_n P_n(x, z, t)$ (Fig. 11).

Avec des parois parfaitement rigides

$$P_n(x, z, t) = \frac{1}{\sqrt{L_x}} \cos \frac{n\pi x}{L_x} \exp i(\omega t - k_z z) \quad \text{avec } n \begin{cases} \text{pair} \\ \text{impair} \end{cases}$$

Le coefficient  $\frac{1}{\sqrt{L_x}}$  a été introduit pour que la norme de  $P(x, z, t)$  soit égale à 1  $\Leftrightarrow \int_{-L_x/2}^{L_x/2} |P(x, z, t)|^2 dx = 1$ . Cela est parfois utile.

Relation de dispersion :

$$n^2 \pi^2 + k_z^2 L_x^2 = (KL_x - k_z L_x M_0)^2$$

Avec des parois non rigides

Posons pour  $x = \pm \frac{L_x}{2}$  :  $Z_1 = \rho_0 c_0 Z$ . On a :

$$P(x, z, t) = \frac{1}{\sqrt{L_x}} \left( 1 + \frac{\sin 2\rho_0^2}{2\rho_0^2} \right)^{1/2} \cos \left( 2\rho_0^2 \frac{x}{L_x} \right) \exp i(\omega t - k_z z)$$

où  $\rho_n^{\pm}$  est une des racines de  $\text{Cotg } T \frac{L_x}{2} = -2E \frac{X}{(K_{L_x} - k_z L_x M_0)} \left( T \frac{L_x}{2} \right)$   
 6-10 avec  $E = -1$  pour  $T \frac{L_x}{2} \in \mathbb{R}^+$  et,  
 $E = 1$  pour  $T \frac{L_x}{2} \in \mathbb{R}^-$  et où l'on a posé  $Z = -iX$  afin que  $\rho_n^{\pm}$  et  $k_z$  soient réels pour  $\omega$  réel (cf § 5.5). Il est à remarquer que  $\rho_n^{\pm}$  est de la forme :

$$\rho_n^{\pm} = n \frac{\pi}{2} + q_n^{\pm} \quad \text{où } n = (2p+1), p \in \mathbb{Z} \text{ et } |q_n^{\pm}| \leq \frac{\pi}{2}.$$

Autre forme de la solution :

$$P_n(x, z, t) = \frac{1}{\sqrt{L_x}} \left( 1 - \frac{\sin 2\rho_n^{\pm}}{2\rho_n^{\pm}} \right)^{-1/2} \sin \left( 2\rho_n^{\pm} \frac{x}{L_x} \right) \exp i(\omega t - k_z z)$$

où  $\rho_n^{\pm}$  est l'une des double racines de :

$$\text{tg} \left( T \frac{L_x}{2} \right) = -2E \frac{X}{(K_{L_x} - k_z L_x M_0)} \left( T \frac{L_x}{2} \right)$$

avec les mêmes définitions que précédemment et,

$$\rho_n^{\pm} = n\pi + q_n^{\pm} \quad \text{où } n = 2p, p \in \mathbb{Z}, \text{ et } |q_n^{\pm}| \leq \frac{\pi}{2}$$

Relation de dispersion :  $\left( \frac{2\rho_n^{\pm}}{L_x} \right)^2 + k_z^2 = (K - k_z M_0)^2$

5.2 - Conduit rectangulaire tridimensionnel (Fig. 12)

Avec des parois rigides

$$P_{n,m}(x, y, z, t) = \frac{1}{\sqrt{L_x L_y}} \cos n\pi \frac{x}{L_x} \cos m\pi \frac{y}{L_y} \exp i(\omega t - k_z z) \quad \text{avec : } n \text{ et } m \begin{cases} \text{pairs} \\ \text{impairs} \end{cases}$$

ou bien :

$$P_{n,m}(x, y, z, t) = \frac{1}{L_x L_y} \cos n\pi \frac{x}{L_x} \sin m\pi \frac{y}{L_y} \exp i(\omega t - k_z z) \quad \text{avec : } n \begin{cases} \text{pair} \\ \text{impair} \end{cases} \text{ et } m \begin{cases} \text{impair} \\ \text{pair} \end{cases}$$

On obtient 4 cas qui correspondent aux combinaisons des modes pairs et impairs suivant les axes  $x$  et  $y$ , puisque Cos et Sin sont tous deux solutions de  $\frac{\partial^2 f}{\partial x^2} + T^2 f(x) = 0$

Relation de dispersion :  $\frac{n^2 \pi^2}{L_x^2} + \frac{m^2 \pi^2}{L_y^2} + k_z^2 = (K - k_z M_0)^2$

Avec des parois non rigides

Appelons  $Z_{x,x} = \rho_0 c_0 Z_x$  avec  $Z_x = -iX_x$  l'impédance des parois situées en  $x = \pm \frac{L_x}{2}$  et  $Z_{y,y} = \rho_0 c_0 Z_y$  avec  $Z_y = -iX_y$  celles qui sont situées en  $y = \pm \frac{L_y}{2}$ . En s'inspirant de 5.1, on déduit aisément les 4 combinaisons possibles entre des modes pairs et impairs suivant les axes  $x$  et  $y$  :

$$P_{n,m}(x, y, z, t) = \frac{1}{\sqrt{L_x L_y}} \left[ \left( 1 + \frac{\sin 2\rho_{x,n}^{\pm}}{2\rho_{x,n}^{\pm}} \right)^{-1/2} \cos 2\rho_{x,n}^{\pm} \frac{x}{L_x} \right] \left[ \left( 1 + \frac{\sin 2\rho_{y,m}^{\pm}}{2\rho_{y,m}^{\pm}} \right)^{-1/2} \cos 2\rho_{y,m}^{\pm} \frac{y}{L_y} \right] \exp i(\omega t - k_z z)$$

où  $\rho_{x,n}^{\pm}$  solution de :  $\text{cotg} \left( T \frac{L_x}{2} \right) = -2E \frac{X_x}{(K_{L_x} - k_z L_x M_0)} \left( T \frac{L_x}{2} \right)$   
 ou encore :

$$P_{n,m}(x, y, z, t) = \frac{1}{\sqrt{L_x L_y}} \left[ \left( 1 + \frac{\sin 2\rho_{x,n}^{\pm}}{2\rho_{x,n}^{\pm}} \right)^{-1/2} \cos 2\rho_{x,n}^{\pm} \frac{x}{L_x} \right] \left[ \left( 1 + \frac{\sin 2\rho_{y,m}^{\pm}}{2\rho_{y,m}^{\pm}} \right)^{-1/2} \sin 2\rho_{y,m}^{\pm} \frac{y}{L_y} \right] \exp i(\omega t - k_z z)$$

Relation de dispersion :  $\left( \frac{2\rho_{x,n}^{\pm}}{L_x} \right)^2 + \left( \frac{2\rho_{y,m}^{\pm}}{L_y} \right)^2 + k_z^2 = (K - k_z M_0)^2$

5.3 - Conduit annulaire (Fig. 13)

Appelons  $Z_{a,a}$  l'impédance de la paroi interne du rayon  $a$  et  $Z_{b,b}$  l'impédance de la paroi externe de rayon  $b$  ;  $Z_{a,a} = \rho_0 c_0 Z_a$ ,  $Z_{b,b} = \rho_0 c_0 Z_b$  en posant :

$$C_m(T_{mn}r) = A_n J_m(T_{mn}r) + B_n Y_m(T_{mn}r),$$

la pression de chaque mode  $(m, n)$  est définie par :

$$P_{m,n}(r, \theta, z, t) = C_m(T_{mn}r) \exp i[\omega t - (m\theta + k_z z)]$$

où les  $T_{mn}$  sont définis par les solutions simultanées des deux relations :

$$\frac{C_m(T_{mn}a)}{C'_m(T_{mn}a)} = \frac{i T_{mn} a Z_a}{(K_a - k_{z,a} M_0)} \quad \text{et} \quad \frac{C_m(T_{mn}b)}{C'_m(T_{mn}b)} = \frac{i T_{mn} b Z_b}{(K_b - k_{z,b} M_0)}$$



Comme  $|T_i/T_r| \ll 1$  et  $|da/\beta a| \ll 1$ , il faut établir une relation entre  $X$  et  $R$  afin que ces deux relations soient homogènes :

6-12

- le membre de gauche de (29b) est d'ordre un, car homogène  $(T_i a)$
- le membre de droite doit l'être, donc nécessairement  $|R/X| \ll 1$ .

Dans ces conditions,

$$(29) \quad \frac{J_m(T_r a)}{J'_m(T_r a)} \approx - \frac{X T_r a}{(K a - \beta a M_0)} \quad (29a')$$

$$T_r a \left\{ 1 - \frac{J_m(T_r a)}{J'_m(T_r a)} \cdot \frac{J''_m(T_r a)}{J'_m(T_r a)} \right\} \approx \frac{R T_r a - X T_r a}{(K a - \beta a M_0)} \quad (29b')$$

Supposons la relation (29a') résolue, alors  $\beta$  et  $\alpha$  sont calculés par les relations (29b') et (28) pour les valeurs choisies de  $X, R, K, M_0$ . En particulier, remarquons que si  $|X| \rightarrow \infty$  alors  $J_m(T_r a) \rightarrow 0$  et  $(T_r a)$  est égal aux valeurs des zéros de  $J_m(z)$  notés  $\chi_{mn}$ . Pour chaque valeur de  $m$ , il existe une suite infinie de zéro de  $J'_m$ .

#### 5.5 - Résolution graphique de (29a')

$$\text{De (28bis) on déduit : } \beta^2 a = - \frac{K a M_0 \pm \sqrt{K^2 a^2 - T_r^2 a^2 (1 - M_0^2)}}{(1 - M_0^2)}$$

En régime subsonique  $M_0 < 1$

$(\beta^2 a)$  est purement réel pour  $T_r a \leq \frac{K a}{\sqrt{1 - M_0^2}}$  (30) ce qui permet de définir la fréquence de coupure du conduit qui se comporte comme un filtre passe-haut. Compte tenu de (30) :

$\beta^2 a$  est strictement négatif

$\beta a$  est  $\begin{cases} \text{strictement positif pour : } T_r a < K a \\ \text{nul pour : } T_r a = K a \\ \text{strictement négatif pour : } \frac{K a}{\sqrt{1 - M_0^2}} \geq T_r a > K a. \end{cases}$

En régime supersonique  $M_0 > 1$

$$\beta^2 a = + \frac{K a M_0 \pm \sqrt{K^2 a^2 - (M_0^2 - 1) T_r^2 a^2}}{(M_0^2 - 1)}$$

$\forall K a, T_r a : \beta^2 a$  est purement réel.

$\beta^2 a$  est strictement positif

$\beta a$  est  $\begin{cases} \text{strictement positif pour : } K a > T_r a \\ \text{nul pour : } K a = T_r a \\ \text{strictement négatif pour : } K a < T_r a. \end{cases}$

Pour résoudre graphiquement (29a'), posons :

$$f_1(T_r a) = \frac{J_m(T_r a)}{J'_m(T_r a)} \text{ et } f_2(T_r a) = - \frac{X T_r a}{(K a - \beta^2 a M_0)}$$

D'où, résoudre (29a') équivaut à résoudre :

$$(29a'') \quad f_1(T_r a) = f_2(T_r a)$$

La fonction  $f_1(T_r a)$  a même forme que  $f_2$  :  $f_1(T_r a) = 0$  pour  $T_r a \in \{E_{mn}\}$  où  $E_{mn}$  est un des éléments de la suite des zéros de  $J'_m$ .  $(J'_m(T_r a) = J'_m(E_{mn}) = 0 \iff$  amplitude de la pression nulle à la paroi ;  $f_1(T_r a) \rightarrow \infty$  pour  $T_r a \in \{\chi_{mn}\}$  où  $\chi_{mn}$  est un des éléments de la suite des zéros de  $J_m$ .  $(J_m(T_r a) = J_m(\chi_{mn}) = 0 \iff$  amplitude de la vitesse normale à la paroi,  $v_n$ , nulle à la paroi.

Rappelons que  $m$  repère l'ordre de la fonction de Bessel et  $n$  le rang du zéro. En particulier :  $\chi_{0,0} = 0, E_{0,0} = 2,40$ . De plus, pour tout couple  $(m,n)$ , on a  $\chi_{mn} < E_{mn}$ , car, à  $m$  fixé et pour chaque  $m$ , les suites des zéros de  $J'_m$  et de  $J_m$  sont imbriquées.

#### 5.5.1 - En l'absence d'écoulement $M_0 = 0$

$f_2(T_r a) = - \frac{X T_r a}{K a}$  est une droite de pente négative lorsque la réactance  $(I_m(Z))$  est positive (Fig. 15).

Pour chaque valeur de  $K a$  (pour chaque fréquence  $\omega$ ), (29a'') a un nombre fini de solutions, notées  $P_{mn}$ , telles que :

$$P_{mn} \in [\chi_{mn}, E_{mn}]$$

Sur nombre fini de  $P_{mn}$  correspond un nombre limité de modes propagatifs à la fréquence choisie ( $K a$ )

Pour  $T_r a = P_{mn}$ , c'est-à-dire pour le  $(m,n)^{\text{ième}}$  mode considéré, le conduit se comporte comme un filtre passe-haut puisque nécessairement :

$$\omega \geq \frac{c_0 P_{mn}}{a} \sqrt{1 - M_0^2} \equiv \omega_c \quad (31)$$

Par analogie on pourrait dire que pour la fréquence  $\omega$  considérée ( $K_a$  fixé) le conduit se comporte comme un filtre spatial passe-bas puisque les modes de rang supérieur au dernier mode  $(m, n)$  tel que  $p_{mn} \leq K_a$ , sont évanescents. On dit aussi que seuls les modes de rang peu élevé sont propagatifs.

- " Cette propriété de filtrage du conduit qui se comporte
- " comme un véritable guide d'ondes, est générale lorsque
- "  $M_0 \leq 1$  et pour  $Z$  quelconque.

Lorsque  $X \rightarrow \infty$  alors  $p_{mn} \sim X_{mn}$  : on retrouve le résultat caractéristique des parois parfaitement rigides.

Lorsque  $X \rightarrow 0$  (avec  $R \rightarrow 0$  plus rapidement que  $X$  afin que les développements limités adoptés restent valables), alors  $p_{mn} \rightarrow E_{mn}$  : on retrouve le résultat caractéristique des parois parfaitement molles.

- " Ces conclusions restent vraies quelle que soit la valeur
- "  $M_0$  comme on pourra aisément le vérifier à la lecture
- " des paragraphes qui suivent.

Pour  $X$  borné,  $p_{mn}$  est fonction de  $K_a$ , donc de la fréquence (Fig. 16). De ce fait, la courbe de dispersion  $\beta_a = \beta(K_a)$  reste de forme hyperbolique (Fig. 3) mais sera d'autant plus distordue que  $K_a$  est proche de  $p_{mn}$ .

#### 5.5.2 - En présence d'un écoulement subsonique

$$f_1^\pm(T_r a) = - \frac{X T_r a (1 - M_0^2)}{K_a \pm M_0 \sqrt{K_a^2 - T_r^2 a^2} (1 - M_0^2)}$$

pour  $T_r a \in [0, \frac{K_a}{\sqrt{1 - M_0^2}}]$  :  $f_1^\pm(T_r a) \in [0, -X]$ ,

avec :  $f_1(T_r a) = -X$  lorsque  $T_r a = K_a$

L'allure de la fonction  $f_1^\pm$  est présentée sur la figure 3. On remarquera en particulier que :

- le point C est défini par  $K_a = T_r a$  et  $f_1^- = -X$ . Il correspond au changement de signe de  $\beta_a$  soit de  $\sigma_{\beta}$  (Fig. 5).
- le point A est défini par  $T_r a = K_a / \sqrt{1 - M_0^2}$ , ce qui définit la fréquence de coupure (point A, Fig. 5).

Lorsque  $M_0 \rightarrow 0$ ,  $A \rightarrow C$  :  $f_1^\pm$  est d'autant plus "ventrue" que  $M_0$  est plus proche de l'unité.

Les  $f_{mn}^\pm$  sont fonctions de  $K_a$ , soit de la fréquence  $\omega$ , lorsque  $X$  est borné, non nul. De ce fait, la relation de dispersion  $(\beta^2 a) = f(K_a)$  est semblable à celle tracée sur la figure 5, mais est déformée par la dépendance en  $K_a$  des  $p_{mn}^\pm$ , sauf dans la région des  $(K_a)$  très supérieurs aux valeurs des  $p_{mn}^\pm$ . Il est évident qu'à chaque mode  $(m, n)$  défini par  $f_{mn}^\pm(K_a)$  à  $X$  et  $M_0$  fixés, correspond une courbe de dispersion.

Il est à remarquer que pour  $m = 0$ ,  $n = 1$ , et  $X = \infty$  :  $T_r a = X_{01} = 0$ . Dans ce cas :

$$J_m(T_r r) = J_m\left(p_{mn} \frac{X}{a}\right) = J_0\left(X_{01} \frac{n}{a}\right) = J_0(0) = 1$$

Le mode (0,1) pour  $X \rightarrow \infty$  est un mode plan puisque le long du rayon l'amplitude et la phase de la pression acoustiques sont constantes.

- " C'est le seul mode plan possible dans un conduit. Cette
- " propriété est vraie quelle que soit la valeur de  $M_0$ .
- " En conséquence : lorsque  $|X| < \infty$  il n'existe pas de
- " modes plans dans un conduit. (Cette propriété est indé-
- " pendante de la valeur de  $M_0$ ).

#### 5.5.3 - En présence d'un écoulement sonique

$$f_2(T_r a) = - \frac{2X K_a T_r a}{K_a^2 a^2 + T_r^2 a^2}$$

pour  $T_r a \in [0, +\infty[$  :  $f_2(T_r a) \in [0, X]$ , avec :

$$f_2(T_r a) = -X \quad \text{pour } T_r a = K_a$$

Aux points d'intersection des courbes  $f_1(T_r a)$  et  $f_2(T_r a)$  correspond une suite infinie de solutions  $p_{mn}$  telles que  $p_{mn} \in [X_{mn}, E_{mn}]$ , figure 18.

#### 5.5.4 - En présence d'un écoulement supersonique $M_0 > 1$ : (Fig. 19)

$$f_2^\pm(T_r a) = + \frac{X T_r a (M_0^2 - 1)}{K_a \pm M_0 \sqrt{K_a^2 - T_r^2 a^2} (1 - M_0^2)}$$

pour  $T_r a \in [0, +\infty[$  :  $f_1^\pm(T_r a) \geq 0$ ,  $f_2^\pm(T_r a) \in [0, X \frac{\sqrt{M_0^2 - 1}}{M_0}]$

et :  $f_1^-(\tau a) = 0$ , avec :  $f_1^-(0) = 0$ ;  $f_1^-(\kappa a) = -x$ ;

et :  $\lim_{\tau a \rightarrow \infty} f_1^-(\tau a) = -x \sqrt{\frac{H_0^2 - 1}{H_0}}$

On trouve une double suite infinie de solutions,  $p_{mn}^{\pm}$ , telles que :  $p_{mn}^- \in [\chi_{mn}, \varepsilon_{mn}]$  et  $p_{mn}^+ \in [\varepsilon_{mn}, \chi_{mn}]$

avec :

pour  $x \rightarrow \infty$  :  $p_{mn}^- \rightarrow \chi_{mn}$ ;  $p_{mn}^+ \rightarrow \chi_{mn+1}$

c'est-à-dire qu'à la condition de modifier la notation il n'y a qu'une valeur de  $p_{mn}$  à considérer pour calculer  $(\beta_{mn}^{\pm})$

pour  $x \rightarrow 0$  :  $p_{mn}^-$  et  $p_{mn}^+$  tendent vers  $\varepsilon_{mn}$

## 6 - RAPPEL DES PROPRIÉTÉS ESSENTIELLES

En guise de conclusion rappelons et résumons les propriétés essentielles mises en évidence et qui sont presque toutes générales malgré le caractère apparemment restrictif des hypothèses.

### 6.1 - Conditions aux limites

à la paroi :  $p = Z \sigma_N$

AMBIGUÏTÉ : que choisir ?

- la relation 17

ou ?

- la relation 18

Pas d'ambiguïté apparente pour :

$$H_0 = 0 ; |Z| = \infty ; |Z| = 0$$

Et pour  $|Z|$  fini ? deux attitudes sont possibles :

. le problème est mal posé car, à la paroi, l'écoulement ne peut être simultanément d'amplitude nulle et d'amplitude  $V_0$ , d'où nécessité d'introduire le vrai profil de vitesse et de résoudre par calcul numérique l'équation des ondes.

. la vitesse étant égale à  $V_0$  et 0 pour  $r = a$ , on considère  $r_c = a - \xi$ ,  $\xi \ll 1$  et  $Z$  représente l'impédance vue par l'onde au rayon  $r_c$ .

### 6.2 - Vitesse de transport de l'énergie d'une onde

. La vitesse de phase est portée par la normale au front d'ondes.

. En général pression et vitesse ne sont pas des grandeurs en phase, sauf pour une onde plane.

. La vitesse de groupe n'est pas forcément colinéaire à la vitesse de phase (sauf pour une onde plane).

. Dans un conduit ayant au moins un axe privilégié et dans lequel se déplace un écoulement donc le vecteur vitesse est porté par cet axe :

- la vitesse de propagation de l'énergie est colinéaire au vecteur vitesse de l'écoulement et : vitesse de transport de l'énergie = vitesse de groupe

d'où :

- la vitesse de groupe est une vitesse au "sens de la mécanique" et, en particulier :

vitesse de groupe = vitesse de l'écoulement + vitesse de groupe  
(dans le repère fixe) (vitesse d'entraînement) (dans le repère mobile)

De ce fait, une onde de vitesse de groupe nulle dans le repère mobile  $K_z = K/H_0$  est vue se déplaçant, portée par l'écoulement  $V_0$ , par un observateur situé dans le repère fixe, et l'amplitude de cette onde décroît comme  $\exp(-p_{mn} z)$

. En général (sauf pour des ondes planes et dans le champ lointain) :

$\left\{ \begin{array}{l} \text{la densité} \\ \text{d'énergie} \\ \text{cinétique} \end{array} \right\}$  est différente de  $\left\{ \begin{array}{l} \text{la densité} \\ \text{d'énergie} \\ \text{potentielle} \end{array} \right\}$

Mais :

$\left\{ \begin{array}{l} \text{l'énergie cinétique} \\ \text{moyenne sur la} \\ \text{surface de la section} \\ \text{droite du conduit} \end{array} \right\}$  =  $\left\{ \begin{array}{l} \text{l'énergie potentielle} \\ \text{moyenne sur la} \\ \text{surface de la section} \\ \text{droite du conduit} \end{array} \right\}$



### 6.3 - Courbes de dispersion

Sauf dans le cas de l'écoulement sonique, à une fréquence donnée (ou à  $Ka$  fixé) correspondent deux modes, puisque la relation de dispersion est un polynôme du second degré en  $\beta$  (nombre d'onde) et  $K$  (fréquence). Nous noterons  $\beta^+$  et  $\beta^-$  (ou  $K_2^+$  et  $K_2^-$ ) chacun de ces deux modes définis par chaque valeur de la solution de (29a").

6-15

. En l'absence d'écoulement à chaque valeur de  $Ka$  :  $|\beta^+a| = |\beta^-a|$  : la courbe de dispersion est symétrique par rapport à l'axe des  $(Ka)$

. En présence d'un écoulement subsonique ou supersonique, pour chaque valeur de  $Ka$  :

.  $|\beta^+a| > |\beta^-a|$  et,  $|\beta^+a| = |\beta^-a|$  seulement pour :

$\omega = \omega_{\text{coupure}}$  en régime subsonique, et

$\omega = 0$  en régime supersonique.

.  $|\beta^+a|$  et  $|\beta^-a|$  sont des fonctions croissantes de  $Ka$  (de la fréquence) ;

par contre :

lorsque la fréquence (ou  $Ka$ ) croît :

$v_g^+ \nearrow$   $v_g^- \searrow$  avec  $|v_g^+| < |v_g^-|$  ; ( $|v_g^+| = v_g^- = 0$

pour  $\omega = \omega_c$  dans un écoulement subsonique ; et,  $v_g^+ = v_g^- = \frac{M_0^2 - 1}{M_0}$  pour  $\omega = 0$  dans un écoulement supersonique).

. En particulier, le long d'une même branche de la courbe de dispersion :

$$(Ka)_1 > (Ka)_2 \implies \begin{cases} |v_g^-(Ka)_1| > |v_g^-(Ka)_2| \\ |v_g^+(Ka)_1| < |v_g^+(Ka)_2| \end{cases}$$

Pour un observateur placé dans le repère fixe et, pour chaque fréquence considérée (ou à  $Ka$  fixé),

$$|\beta^+| > |\beta^-| \iff \lambda < \lambda^-$$

où la longueur d'onde  $\lambda$  est égale à :  $2\pi/\beta$  (ou  $K_2$ ).

La distorsion de la relation de dispersion par l'écoulement, observée dans le repère absolu, explique que, pour une fréquence donnée, les longueurs d'ondes de chacun des deux modes diffèrent. Tout se passe comme si l'écoulement dilatait la longueur d'onde du mode  $\beta^-$  et contractait celle du mode  $\beta^+$ . En particulier, pour  $0 \leq M_0 < 1$  à la fréquence de coupure :  $\lambda^+ = \lambda^- = \infty$

Cela amène à donner une image représentative de la définition des modes. Considérons un voilier, ou un nageur :

- . la vitesse de phase est portée par le vecteur qui passe par l'axe du voilier (ou du nageur) et est orientée de la poupe vers la proue (des pieds vers la tête)
- . la vitesse de groupe est portée et orientée suivant la direction réelle du déplacement, du voilier ou du nageur.

Ainsi définies, la vitesse de phase  $\vec{v}_p$  et la vitesse de groupe  $\vec{v}_g$  sont observées du rivage par un observateur placé dans le repère fixe qui, de plus, connaît, dans ce repère, la direction et la force du vent ou du courant notées  $\vec{v}_0$  et définissant la direction positive.

On a alors les allures ou situations suivantes :

VENT ARRIERE ou baigneur nageant dans le sens du courant	$\vec{v}_g \cdot \vec{v}_0 > 0$ $\vec{v}_p \cdot \vec{v}_0 > 0$	Mode aval : existe quelle que soit la valeur de $M_0$
Grand large (bâbord) ou baigneur nageant de biais dans le sens du courant	$\vec{v}_p \cdot \vec{v}_0 > 0$	
au plus près (bâbord) amures ou (tribord) baigneur nageant de biais à contre-courant	$\vec{v}_g \cdot \vec{v}_0 < 0$ $\vec{v}_p \cdot \vec{v}_0 < 0$	Mode amont : existe seulement pour $0 \leq M_0 < 1$
Baigneur nageant à contre-courant	$\vec{v}_p \cdot \vec{v}_0 > 0$	
VENT DEBOUT !! ou baigneur nageant à contre- courant ... tel l'écrevisse ou baigneur naïf nageant de biais à contre-courant !!	$\vec{v}_g \cdot \vec{v}_0 > 0$ $\vec{v}_p \cdot \vec{v}_0 < 0$ $\vec{v}_g \cdot \vec{v}_p < 0$	Mode amont inverse existe lorsque $0 < M_0$

. conclusion importante : une onde telle que  $\vec{v}_p \cdot \vec{v}_0 < 0$  ne peut remonter un écoulement sonique ou supersonique.

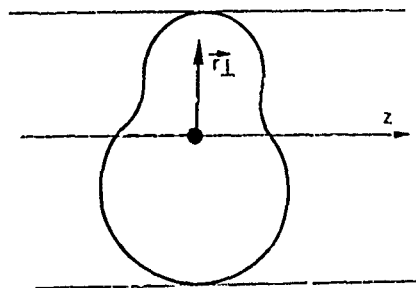
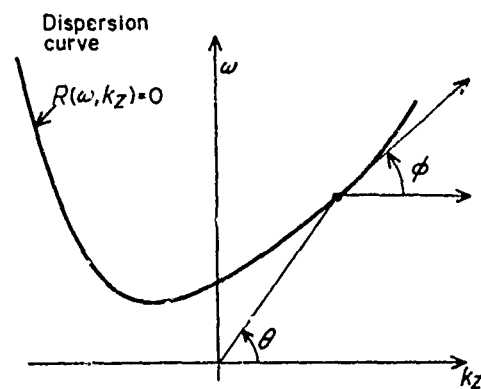
Fig. 1 - Pattern  $\vec{r} = \vec{r}_1 + \vec{z}$ 

Fig. 2 - Definition of phase and group velocities.

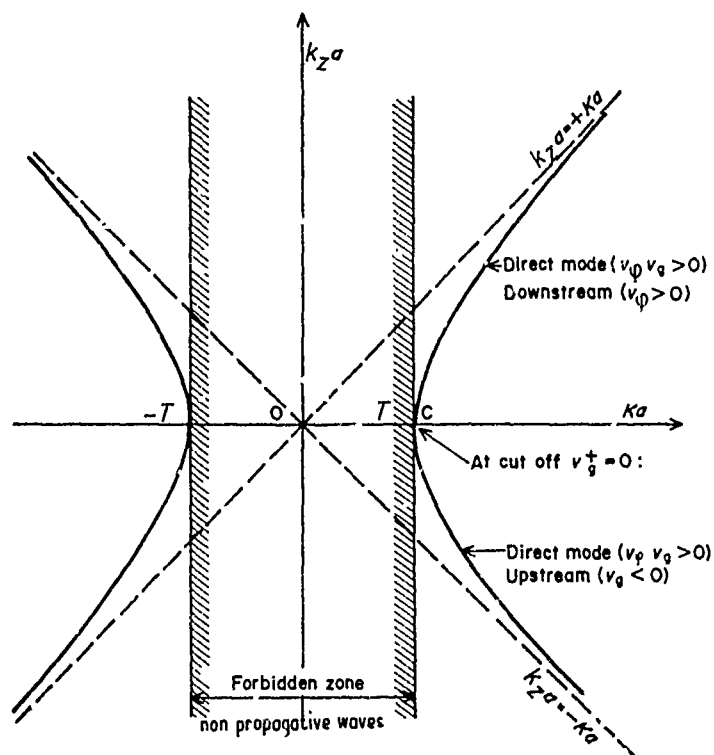


Fig. 3 - Dispersion curve of an acoustic mode in the absence of flow

6-17

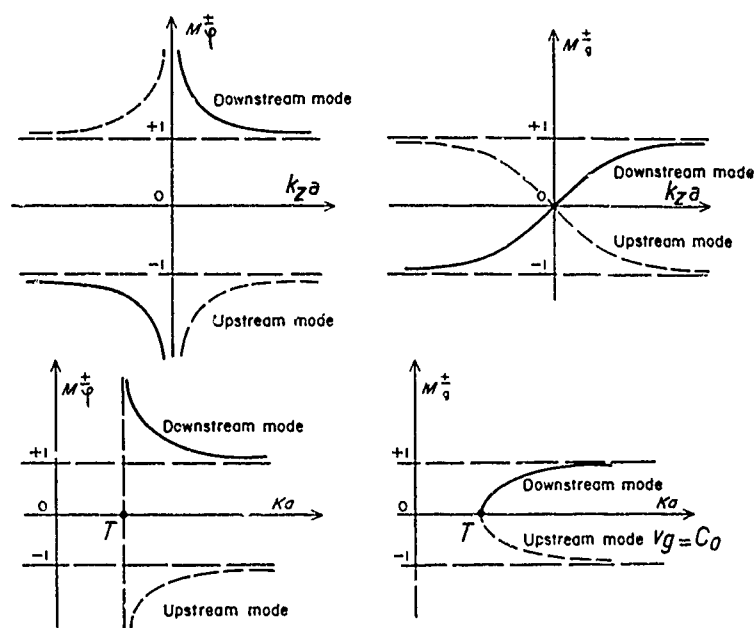


Fig. 4 - Variations of  $M_\phi^\pm$  and  $M_\theta^\pm$  for  $M_0 = 0$

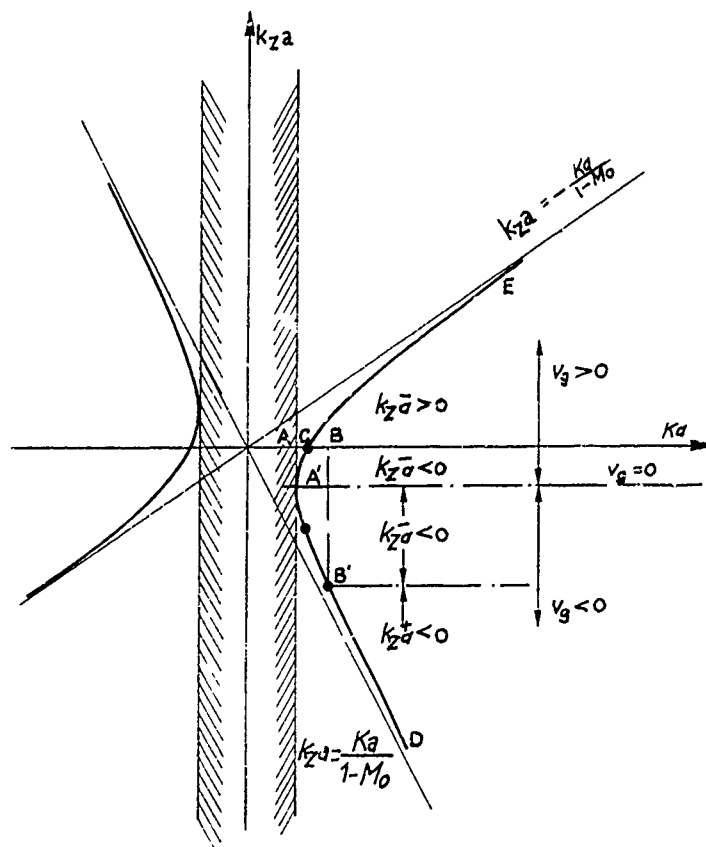
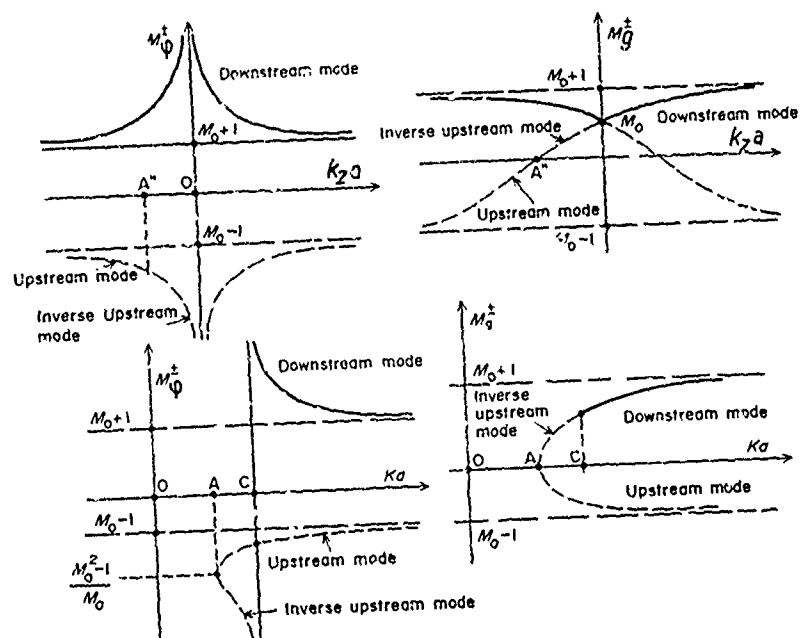
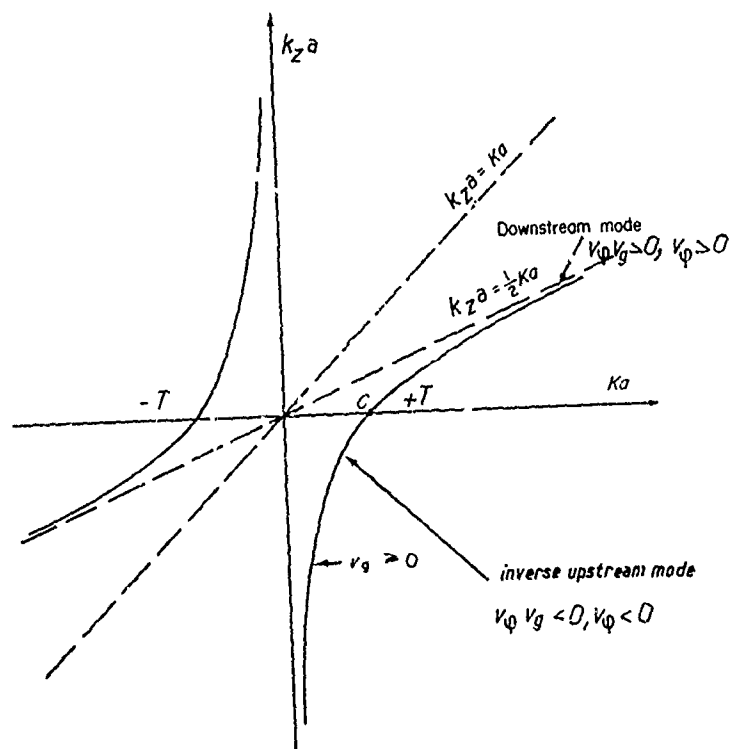


Fig. 5 - Dispersion curve for  $M_0 < 1$ .

Fig. 6 - Variations of  $M_0^+$  and  $M_0^-$  for  $K_0^2 < 1$ .Fig. 7 - Dispersion curve for  $M_0 = 1$ .

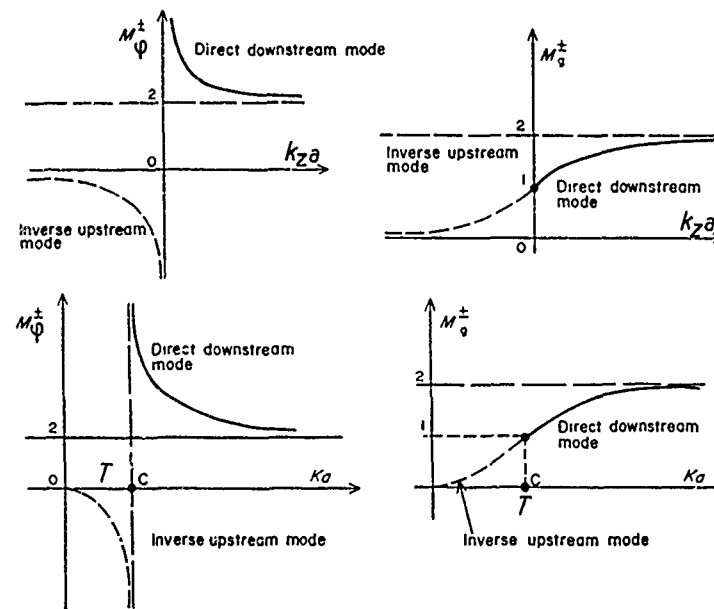


Fig. 8 - Variations of  $M_\phi^\pm$  and  $M_\theta^\pm$  for  $M_0 = 1$ .

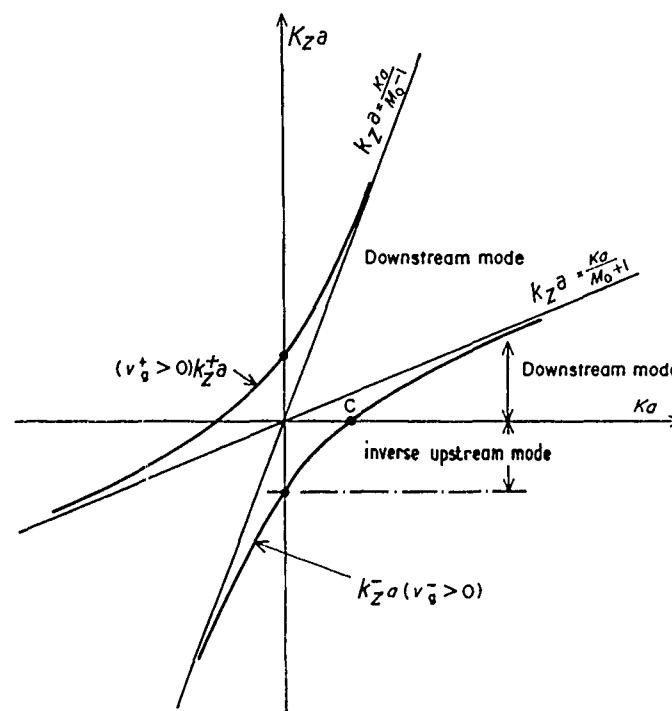


Fig. 9 - Dispersion curve for  $M_0 > 1$ .

6-20

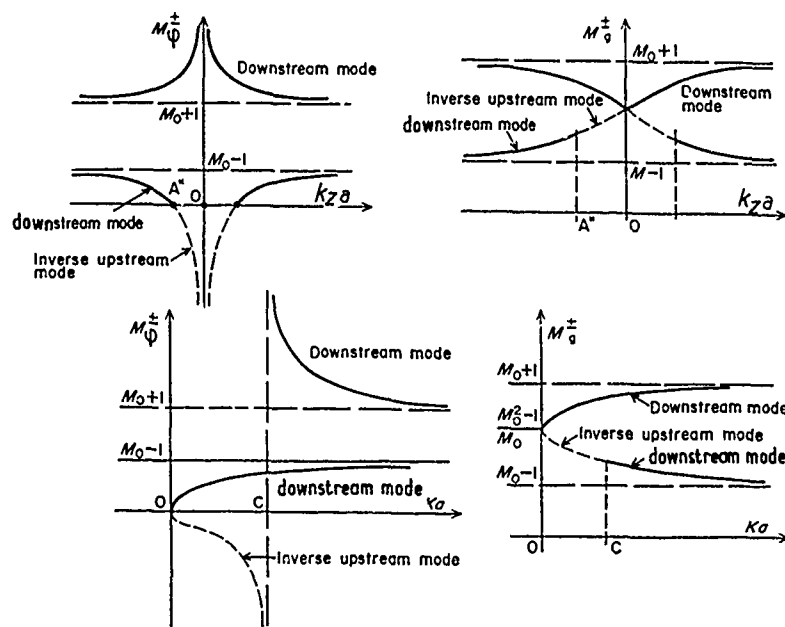


Fig. 10 - Variations of  $M_0^+$  and  $M_0^-$  for  $M_0 > 1$ .

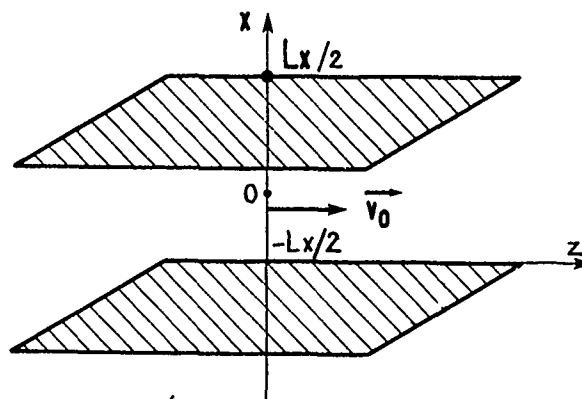


Fig 11 - Rectangular bidimensional duct

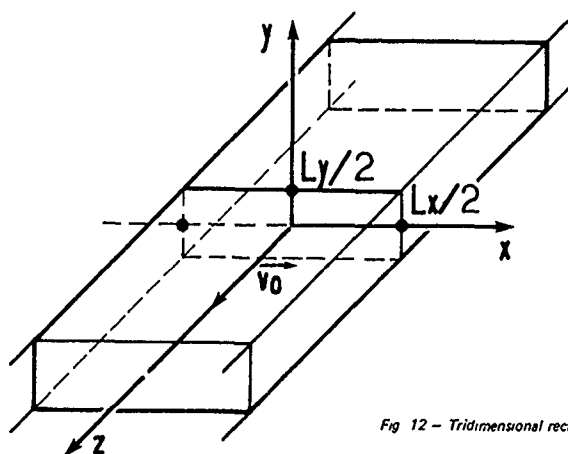
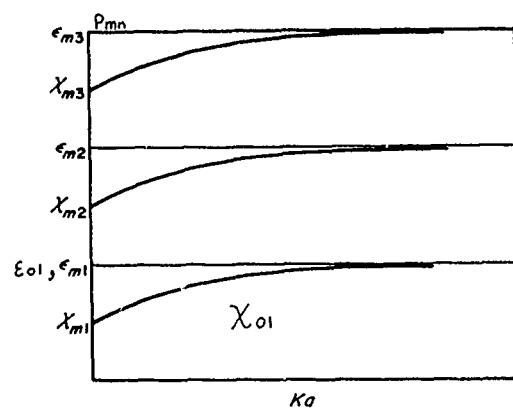
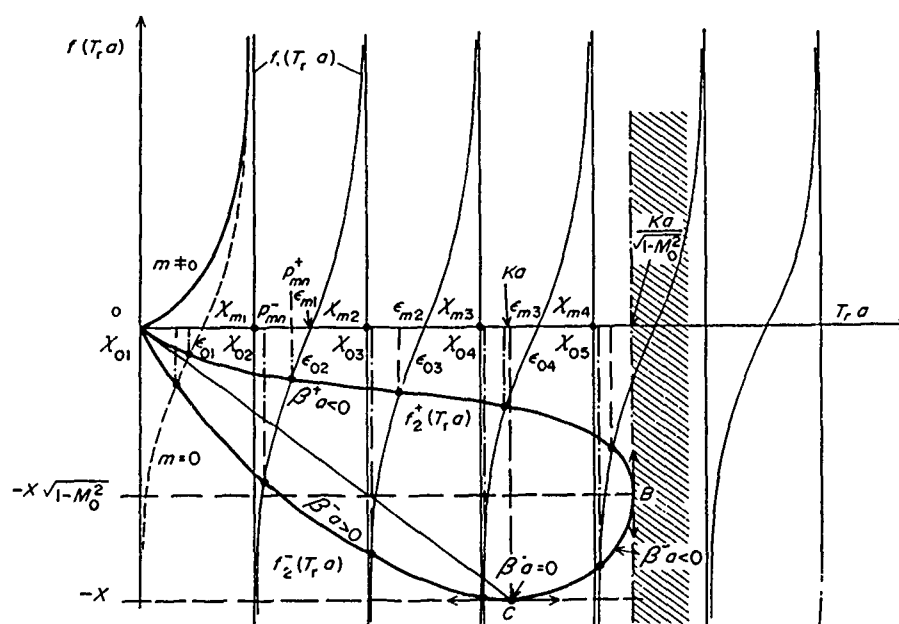


Fig 12 - Tridimensional rectangular duct.

Fig. 16 - Variation of the solution  $P_{mn}$  for  $M_0 = 0$ Fig. 17 - Graphical solution of the limit condition for  $M_0 < 1$ .





# PROPAGATION IN ACOUSTICALLY ABSORBENT MATERIALS

M. Perulli, Département de Génie Mécanique, Université de Technologie de Compiègne,  
Compiègne, France

7-1

and

P.E. Doak, Institute of Sound and Vibration Research, The University, Southampton, England

Models for representing the dynamics of porous and other acoustically absorbent materials are reviewed. A relatively detailed discussion is presented of propagation in significantly absorbent materials widely used in practice, or commonly occurring, for example, as outdoor ground surfaces. The principles governing design of composite materials for high acoustic absorption are presented. Non-linear high amplitude effects and mean flow effects are briefly described.

It is rare to find in nature, and difficult to design and synthesize "artificially", a material, composite or otherwise, in which stress waves, including sound, are rapidly attenuated when they travel in it. For example, a suitable and suitably loaded rubber material may be extremely effective as a low frequency vibration isolator but yet transmit higher frequency stress waves with practically no attenuation (i.e., no loss of energy).

As Lord Rayleigh observed, however, a few natural materials, such as a well-compacted haystack, can attenuate acoustic waves effectively, providing enough viscous and thermal dissipative retarding forces to reduce the pressure amplitude of an acoustic wave travelling through the air in the haystack "pores" by as much as a factor of 1/6 or so over a distance of travel of the order of a wavelength in the material. In contrast, the viscosity and thermal conductivity of more common substances such as atmospheric air, water, steel, concrete, etc., is sufficient to produce amplitude reductions of comparable order only over travel distances of hundreds of thousands of wavelengths, or more. Dry, or dryish, ground, on the other hand, is often porous enough to act as a reasonably good sound absorber.

In a general formal sense, whatever the mechanism ultimately responsible for the losses in an acoustic continuum, the effects on the acoustic propagation of a wave with simple harmonic time dependence can be expressed through appropriate, complex, effective, mass density and speed of sound parameters, both in general functions of frequency, and in turn one may equivalently use a complex characteristic impedance ( $\rho c$ ) and "propagation constant", or wavenumber ( $k = \omega/c$ ). With these equivalent complex parameters, mathematical forms like  $e^{-ikx}$  and  $p = \rho c u$  remain the same as for a lossless medium, but of course both real and imaginary parts of  $k$  and  $\rho c$  must be taken into account when interpreting formal results in order to obtain numbers applicable to practical problems.

A relatively simple model for sound propagation in a porous material can be devised - the original development of this model was accomplished by Lord Rayleigh (Theory of Sound, Volume 2, pp. 328-333). This model is sufficiently accurate to indicate the main features distinguishing such propagation and to provide a guide for designing the structure of "man-made" materials - such as fibreglass, mineral wool, expanded plastic foams, sintered metals, etc. - in such a way that they will have useful, and reasonably predictable, sound attenuating properties.

One proceeds as follows (see, e.g., the treatment in Morse and Ingard's book Theoretical Acoustics, pp. 252-256, 269-270, 303, 428, 569-571, but note the explanations in what follows here of the physical interpretations of Morse and Ingard's "mean velocity" and "effective density  $\rho_p$ "). The development of the model is easier to visualize if one considers first the one-dimensional case. Generalization to three dimensions is then straightforward, requiring only conceptual re-interpretation of the parameters.

The porous material can be thought of, one dimensionally, as a solid rigid material in which are bored a number of parallel holes, each of area of cross-section  $S_p$ , say. The porosity,  $\Omega$ , of the material (percentage volume of the pores) then can be defined as  $\Omega = n S_p$ , where  $n$  is the number of holes per unit area of cross-section (in a plane perpendicular to the direction of the holes, of course), or as  $S_p/S$ , where  $S$  is the area of cross-section per hole.

An equivalent particle velocity,  $u'$ , regarded as possessed by the whole region occupied by the porous material, that provides the same mass flow locally as the actual velocity,  $v'$ , in the pores may then be defined by  $S u' = S_p v'$ , or  $u' = v' \Omega$ . Then, in terms of  $u'$ , the equation of conservation of mass, which is in terms of  $v'$  simply, as usual,

$$\frac{\partial \rho'}{\partial t} + \rho \frac{\partial v'}{\partial x} = 0,$$

(primes indicate the acoustic fluctuating parts of the designated quantities), becomes, upon multiplication by  $\Omega$ ,

$$\Omega \frac{\partial \rho'}{\partial t} + \rho \frac{\partial u'}{\partial x} = 0, \quad (1)$$

since of course  $\Omega$  is a constant.

The normal adiabatic relationship between pressure fluctuations and mass density fluctuations may not apply for the material in the pores. First, if the pores are very small and the skeletal material is a relatively good heat conductor, there may be time even within the relatively small period of an acoustic oscillation for the normally adiabatic temperature fluctuations associated with the cyclic compression and

7-2

rarefaction to be conducted away into the skeleton. This has the effect, in the limit, of making the process of compression and rarefaction isothermal instead of adiabatic: in other words, for a fluid, the ratio of specific heats,  $\gamma$ , in the expression for the speed of sound,  $\sqrt{\gamma p/\rho}$ , reduces from its adiabatic value (1.4 for air, e.g.) to unity. In terms of the compressibility of the material,  $\kappa \equiv (1/\rho)(\partial\rho/\partial p)$ , this means that the effective compressibility of the material in the pores,  $\kappa_p$ , may lie between its high-frequency, large-pore adiabatic value  $\kappa_s$  as a lower limit and its low-frequency, small-pore isothermal value  $\kappa_t$  as an upper limit. Pore sizes and frequency ranges for many porous materials are such that the transition may occur from one value to another within the frequency range of interest and hence, for simple harmonic acoustic fluctuations,  $\kappa_p$  strictly should be regarded as a function of frequency (for transients, of course, this implies that  $\kappa_p$  should be replaced by an appropriate operator involving  $\partial/\partial t$ ).

Thus the usual adiabatic relationship between mass density and pressure,

$$\rho' = \rho \kappa_s p', \quad \text{or } \rho' = p'/c^2 = p'/( \gamma p/\rho), \quad (2)$$

must be replaced by

$$\rho' = \rho \kappa_p p', \quad (3)$$

it being understood that  $\kappa_p$  may be a possibly slowly varying but nonetheless significant function of frequency, (or for transients an operator in  $\partial/\partial t$ ). Whatever the variation in  $\kappa_p$ , however, it will not normally vary between large limits: again, for air, the limits would be proportional to those of  $1/\gamma$  from adiabatic to isothermal conditions i.e., 1/1.4 to 1.

Insertion of expression (3) into equation (1) gives the conservation of mass relationship between the pressure fluctuations and the effective velocity:

$$\Omega \kappa_p \partial p'/\partial t + \partial u'/\partial x = 0. \quad (4)$$

Generalization of equation (4) to three dimensions is straightforward. With  $\Omega$  interpreted as the percentage of total volume occupied by open, interconnecting pores and  $\partial u'/\partial x$  becoming the divergence of the vector effective velocity, one has

$$\Omega \kappa_p \partial p'/\partial t + \text{div } u' = 0. \quad (4a)$$

An expression for conservation of linear momentum can be similarly constructed. First, one must consider the effective inertial mass of the material in the pores. This may be somewhat greater than the actual mass, for two reasons: (i) in fibrous porous materials, like fibreglass or mineral wool, some of the fibres may move with the material (fluid) in the pores; (ii) the actual, relatively small scale, motion of the material in the pores may, according to details of the geometry, result in inertial reactions greater than those one might expect if the motion were of a quasi-steady, incompressible flow nature. Thus, for the effective mass density in the pores one should replace  $\rho$ , the actual mass density, by  $\rho_p$ , an effective mass density, which may be up to 1.5 times as great as  $\rho$ , very approximately (normally it will not be that much greater than  $\rho$ ). Second, if the pores are of very small effective diameters, then viscous retarding forces will be appreciable. The flow in such small pores can be likened to Poiseuille flow, so that, in terms of the actual velocity in the pores,  $v'$  (averaged over each pore cross-section, of course), this retarding force can be taken to be of the form  $-Rv'$ , where  $R$  is a flow resistance depending upon the viscosity of the material in the pores, the area of cross-section of the pores, and again, ultimately, especially for larger pores, on the frequency. In most applications, however, the pore size is small, and since the motion in the pores is then of Poiseuille type, although quasi-steady, the flow resistance  $R$  will have its steady flow value, and thus can be determined independently of any acoustic excitation by steady flow tests on the material.

Thus, the motion in the pores is governed by pressure forces and the assumed frictional force  $-Rv'$ , and with the effective mass density  $\rho_p$ , the equation of conservation of linear momentum (or Newton's Law, for the motion of the material in the pores can be written as  $\rho_p \partial v'/\partial t = -\partial p'/\partial x - Rv'$ . It is more convenient, for purposes of combining this expression with equation (4) (to eliminate  $p'$  or  $u'$ ), to express this linear momentum equation in terms of  $u' = \Omega v'$ : i.e.,  $(\rho_p/\Omega) \partial u'/\partial t = -\partial p'/\partial x - (R/\Omega)u'$ . The forms of the first and third coefficients suggest, finally, defining a new effective mass density,  $\rho_p$ , and flow resistance,  $\phi$ , as

$$\rho_p \equiv \rho_p/\Omega, \quad \phi \equiv R/\Omega. \quad (5)$$

The linear momentum equation then takes the form

$$\rho_p \partial u'/\partial t + \partial p'/\partial x + \phi u' = 0. \quad (6)$$

For typical porous materials for use in air - with, of course, air the material in the pores - the porosity,  $\Omega$ , may be, say, from 0.2 to 0.7, and the flow resistance  $\phi$  may be from 50 to 500  $\text{pc m}^{-1}$ . The final "effective density" in the pores,  $\rho_p$ , being  $\rho_p/\Omega$ , thus may range from, say, 1.5 to 50 (since, it will be recalled,  $\rho_p$  may range from  $\rho$  to about 1.5 $\rho$ ). Note that all these effective parameters usually must be determined by experiment for each particular porous material, and that apart from  $\phi$ , the d.c. flow resistance, the experiments must be acoustic experiments, the determinations being accomplished by fitting curves derived as solutions of the governing equations (4) and (6) of the model to experimental results. Note also, that like equation (4)'s generalization to three dimensions, the three-dimensional generalization of equation (6) can be written down at once:

$$\rho_p \partial u'/\partial t + \text{grad } p' + \phi u' = 0. \quad (6a)$$

The system of two equations (4) and (6) can readily be solved for simple harmonic motion. Insertion of the forms

$$p' = P(x)e^{i\omega t}, \quad u' = U(x)e^{i\omega t} \quad (7)$$

into the equations gives

$$i\omega\kappa_p P + dU/dx = 0, \quad dP/dx + (\phi + i\omega\rho_p)U = 0. \quad (8) \quad 7-3$$

Elimination of, say,  $U$  (by differentiating the second equation with respect to  $x$  and subtracting from it  $(\phi + i\omega\rho_p)$  times the first equation), gives the following equation for the pressure phasor  $P(x)$ :

$$d^2P/dx^2 + \omega^2\kappa_p\rho_p(1 + \phi/i\omega\rho_p)P = 0. \quad (9)$$

This can be brought into formal correspondence with the corresponding equation for acoustic pressure propagation in a lossless medium, with (real speed of sound  $c$ ), namely

$$d^2P/dx^2 + (\omega^2/c^2)P = 0,$$

by defining a complex, effective speed of sound,  $c_e$ , as

$$c_e \equiv \frac{1}{\sqrt{\kappa_p\rho_p}} \left(1 + \frac{\phi}{i\omega\rho_p}\right)^{-1/2}, \quad (10)$$

equation (9) then becoming

$$d^2P/dx^2 + (\omega^2/c_e^2)P = 0 \quad (11)$$

and evidently having the solutions

$$P = A_{\pm} e^{\pm i k_e x}, \quad (12)$$

where  $k_e$  is the effective complex wavenumber

$$k_e \equiv \omega/c_e. \quad (13)$$

From equations (8) it can be seen that the corresponding solutions for the effective particle velocity phasor,  $U(x)$ , are

$$U = \frac{\pm i k_e}{\phi + i\omega\rho_p} A_{\pm} e^{\pm i k_e x}, \quad (14)$$

or, again with an effective complex characteristic impedance,  $\rho_e c_e$ , and effective complex mass density,  $\rho_e$ , defined, respectively, as

$$\rho_e c_e \equiv (\phi + i\omega\rho_p)/i k_e = \left(\frac{\phi + i\omega\rho_p}{i\omega}\right) c_e = \frac{i\omega\rho_p(1 + \phi/i\omega\rho_p)}{i\omega(\kappa_p\rho_p)^{1/2}(1 + \phi/i\omega\rho_p)^{1/2}} = \left(\frac{\rho_p}{\kappa_p}\right)^{1/2} \left(1 + \frac{\phi}{i\omega\rho_p}\right)^{1/2}, \quad (15)$$

$$\rho_e \equiv \rho_e c_e / c_p = \left(\frac{\rho_p}{\kappa_p}\right)^{1/2} \left(1 + \frac{\phi}{i\omega\rho_p}\right)^{1/2} (\kappa_p\rho_p)^{1/2} \left(1 + \frac{\phi}{i\omega\rho_p}\right)^{-1/2} = \rho_p \left(1 + \frac{\phi}{i\omega\rho_p}\right), \quad (16)$$

equation (14) also can be put into formal correspondence with the corresponding expression for a lossless material:

$$U = \pm P/\rho_e c_e. \quad (17)$$

Thus acoustic propagation through the porous material can be characterized by the two complex parameters (functions of material properties and frequency)  $k_e$  and  $\rho_e c_e$ , just as for a lossless material in which case  $k_e$  and  $\rho_e c_e$  are real - the lossless material result now appearing as a special case of the porous, lossy material. Also, just as in the lossless case the mean intensity in the  $x$  direction can be written as

$$\overline{J}_x = \frac{1}{2} \operatorname{Re} (PU^*),$$

the overbar indicating time averaging and the asterisk the complex conjugate, one has for the porous material an identical expression

$$\overline{J}_x = \frac{1}{2} \operatorname{Re} (PU^*). \quad (18)$$

As to the magnitudes of the real and imaginary parts of the complex wavenumber  $k_e$  and the complex characteristic impedance  $\rho_e c_e$ , one can first note, from equation (10), that apart from the explicit dependence on  $\omega$ , the effective speed of sound,  $c_e$ , depends on the two parameters  $\kappa_p/\rho_p$  and  $\sqrt{\kappa_p\rho_p}$ . These two parameters similarly determine  $k_e = \omega/c_e$ . From equation (15) these same two parameters, and  $\rho_p$ , determine the characteristic impedance  $\rho_e c_e$ .

For greater insight and ease of estimation of probable values for these parameters, for a given porous material, it is helpful to re-express them in somewhat different forms. In the paragraph preceding equation (2) it was pointed out that the effective compressibility,  $\kappa_p$ , could be expected to lie between the isothermal and adiabatic compressibilities of the actual material in the pores. Also (see equations (2) and (3)) it is evident that one could use, instead of the compressibility, an "effective ratio of specific heats",  $\gamma_e$ , defined as

$$\gamma_e = 1/p \kappa_p', \quad (19)$$

where  $p$  (as always here) is the static, ambient pressure of the actual material in the pores. For air, at the isothermal limit  $\gamma_e$  would be unity, rising to 1.4 at the adiabatic (lossless) limit. Also (see the

7-4 two paragraphs following equation (4a)), the effective mass density  $\rho$  can be expressed alternatively as  $\rho_p/\Omega$ , where  $\rho_p$  is the (more physically realistic) actual mass density of the material in the pores,  $\rho$ , times a factor of again from about unity to 1.4 or 1.5, to account for added inertia due to motion of some fibres with the pore material, etc. Thus the parameter  $1/\sqrt{\Omega \rho_p}$  can be rewritten as

$$1/\sqrt{\Omega \rho_p} = 1/\sqrt{\Omega (\rho_p/\Omega) (1/\gamma_p)} = \sqrt{(\gamma_p/\rho_p)}. \quad (20)$$

It can then be seen directly that, since (for air, e.g.)  $\gamma_p$  ranges from, say, 1 to 1.4 and  $\rho_p$  from  $\rho$  (the actual density of the air in the pores) to again about 1.4 $\rho$  (or perhaps 1.5 $\rho$ ), one has the range of  $1/\sqrt{\Omega \rho_p}$  going from about  $c/\sqrt{1.4}$  to about 1.4 $c$ , where  $c = \sqrt{\gamma_p/\rho}$  is the usual adiabatic sound speed of the actual material in the pores. Thus the parameter  $1/\sqrt{\Omega \rho_p}$  is simply the usual sound speed of the material in the pores, minus or plus about 20%.

Similarly, since again  $\rho_p = \rho_p/\Omega$  and  $\phi = R/\Omega$  (see equation (5)), the parameter  $\phi/\rho_p$  can be expressed as

$$\phi/\rho_p = (R/\Omega) (\Omega/\rho_p) = R/\rho_p.$$

$R$  is the flow resistance for the actual velocity in the pores and thus is readily estimable from Poiseuille-type flow resistance formulas or data for capillaries, if one knows the actual mass density, coefficient of viscosity and approximate, representative area of cross section of the pores. From the figures quoted following equation (6), one has a range of  $\phi/\rho_p = R/\rho_p$  of from 10-300  $\text{cm}^{-1}$ , where again  $c$  is the usual speed of sound of the actual pore material. Furthermore,  $\phi/\rho_p = R/\rho_p$  of course has the dimensions of (time) $^{-1}$  and thus may be expressed as a characteristic radian frequency (inverse time constant)

$$\phi/\rho_p = R/\rho_p \equiv \omega_p. \quad (21)$$

From the range just quoted, if again the pore material is air, one obtains a range of about 300 to  $9 \times 10^4$  radians/s (i.e., about 50 to 15,000 Hz, roughly the audio frequency range, not surprisingly) as a representative "relaxation" frequency range for porous materials used as sound absorbers in air. Finally, one has the third parameter,  $\rho_p$ , and as before this can be expressed as  $\rho_p/\Omega$ , evidently a maximum typical range (for air in the pores) from about 1 to 5 $\rho$ .

In terms of these more physical quantities, then, one has, for  $k_e$  (and  $c_e$ ) and  $\rho_e c_e$ ,

$$k_e = \frac{\omega}{c_e} = \frac{\omega}{c} \cdot \frac{1}{\sqrt{\gamma_e/\gamma} (1 + \omega_p/i\omega)^{-1/2}}, \quad (22)$$

$$\rho_e c_e = \rho c (1/\Omega) \sqrt{\gamma_e/\gamma} (1 + \omega_p/i\omega)^{1/2}, \quad (23)$$

showing clearly the relationship of the complex effective quantities to the corresponding adiabatic, lossless values of  $k = \omega/c$  and  $\rho c$  for the actual material in the pores ( $\gamma$ , of course, is the "specific heat ratio" giving the usual adiabatic sound speed,  $\sqrt{\gamma p/\rho}$ , for the actual material in the pores). The factor  $1/\Omega$  appears in  $\rho_e c_e$  for the same reason that it does in  $v' = u'/\Omega$ : i.e., to express the fact that acoustic motion actually occurring only in the pores is visualized in the model as occurring over the whole cross-section of the porous material. The factor  $\sqrt{\gamma_e/\gamma}$  corrects the sound speed in the pores according to whether it is adiabatic (large pores, high frequency) or isothermal (small pores, low frequency). The explicitly imaginary quantity in expressions (22) and (23),  $\omega_p/i\omega$  (it should be kept in mind that both  $\sqrt{\gamma_e/\gamma}$  and  $\omega_p$  may, more generally, both depend on frequency and hence be complex; as mentioned previously, although this frequency dependence may in fact occur, it is often weak by comparison with the explicitly shown  $\omega_p/i\omega$  dependence, with  $\omega_p$  approximately constant), expresses the dissipative effect of the flow resistance, and the phase difference that this introduces between the acceleration and the negative pressure gradient (see equations (6) and the one preceding it earlier in the same paragraph).

The expressions (22) and (23) for  $k_e$  and  $\rho_e c_e$  can be written explicitly in terms of real and imaginary parts as follows (provided frequency dependence is only as shown explicitly):

$$k_e = k \sqrt{\frac{\gamma_e}{\gamma}} \sqrt{1 - i\omega_p/\omega} = k \sqrt{\frac{\gamma_e}{\gamma}} \left[ 1 + \left( \frac{\omega_p}{\omega} \right)^2 \right]^{1/4} e^{-i\phi}, \quad \tan 2\phi \equiv \omega_p/\omega \quad (0 < \phi < \pi/4);$$

$$\text{for } \omega_p/\omega \ll 1, \quad k_e \approx k \sqrt{\gamma_e/\gamma} (1 - i\omega_p/\omega);$$

$$\text{in general, } k_e \equiv k(\kappa - i\delta), \quad \kappa \equiv \sqrt{\gamma_e/\gamma} [1 + (\omega_p/\omega)^2]^{1/4} \cos\phi, \quad \delta \equiv \sqrt{\gamma_e/\gamma} [1 + (\omega_p/\omega)^2]^{1/4} \sin\phi;$$

$$\rho_e c_e = \rho c \frac{1}{\Omega} \sqrt{\gamma_e/\gamma} [1 + (\omega_p/\omega)^2]^{1/4} (\cos\phi - i\sin\phi);$$

$$\text{for } \omega_p/\omega \ll 1, \quad \cos\phi \approx 1, \quad \sin\phi \approx \phi \approx \omega_p/\omega;$$

$$\text{for } \omega_p/\omega \gg 1, \quad \phi \rightarrow \pi/4, \quad \cos\phi \rightarrow \sin\phi \rightarrow 1/\sqrt{2}.$$

The pressure in a plane wave in the porous material, travelling in the +x-direction, will be of the form

$$p(x,t) = A_+ e^{i\omega t - ik_e x} = A_+ e^{i\omega t - i\kappa x - \delta x},$$

where  $A_+$  is a complex constant, and the equivalent particle velocity,  $u(x,t)$ , will be  $u(x,t) = p(x,t)/\rho_e c_e$ . Since  $k = \omega/c$  the factor  $e^{i\omega t - i\kappa x}$  can be written as  $e^{i\omega(t - x/(c/\kappa))}$ , it then being evident that the phase speed of the waves (speed of propagation of the wave fronts) in the porous material is  $c/\kappa$ . Similarly,

since, for waves generally,  $\omega/c = k = 2\pi/\lambda$ , where  $\lambda$  is the wavelength, it is clear that the wavelength in the porous material is  $\lambda_e = 2\pi/k_e$ . Thus the entire exponential function can be written as

7-5

$$e^{i\omega t - i2\pi x/\lambda_e - (\delta/\kappa)2\pi x/\lambda_e}$$

From this it is clear that the wave amplitude is decreased by a factor  $e^{-2\pi\delta/\kappa}$  in each wavelength of travel.

For frequencies  $\omega$  well above the characteristic frequency parameter of the material,  $\omega_p$ , it is evident that  $\lambda_e \rightarrow \lambda/\sqrt{\gamma/\gamma_p}$ , to first order in  $\omega_p/\omega$ , which is at most some 20% less than  $\lambda$ , since  $\gamma/\gamma_p$  can be expected to lie in the range 1-1.4. Also  $2\pi\delta/\kappa + \pi\omega_p/\omega$ , which is small compared with unity, so that the attenuation per wavelength is small. For frequencies  $\omega$  well below  $\omega_p$ , however,  $\kappa \rightarrow \delta + \sqrt{(1/2)(\gamma/\gamma_p)(\omega_p/\omega)}$  and  $2\pi\delta/\kappa$  hence tends to  $2\pi$ , giving a significantly large factor for attenuation per wavelength,  $e^{-2\pi}$ . The wavelength itself,  $\lambda_e$ , becomes  $\lambda\sqrt{2(\gamma/\gamma_p)(\omega/\omega_p)}$  which can be appreciably smaller than  $\lambda$ . Thus for the frequency range  $\omega_p/\omega > 1$ , the porous material can act as an effective attenuator of sound. However, for the sound to enter the porous material from the surrounding medium, the impedances must be reasonably matched; i.e., if the outside region has the same mass density and speed of sound as the material in the pores of the porous material ( $\rho$  and  $c$ ), then  $|\rho_e c_e| \sim \rho c$ . The ratio is

$$\frac{|\rho_e c_e|}{\rho c} = \frac{1}{\Omega} \sqrt{\frac{\gamma_e}{\gamma}} \left[ 1 + \left( \frac{\omega_p}{\omega} \right)^2 \right]^{-1/2}$$

Since the porosity,  $\Omega$ , is always less than (or equal to) unity it is evident that the ratio can be appreciably larger than unity if  $\omega_p/\omega$  is too large. Thus one often has to compromise - accept a lower than maximum possible attenuation per wavelength (or per unit length) in order to achieve a reasonable impedance match of  $|\rho_e c_e|/\rho c \sim 1$ . This can often be done with an impedance ratio of around 2. A normal impedance ratio of this order, of course, gives a good impedance match if the incident waves have angles of incidence around  $\pi/4$ , and thus absorption for fields with "random incidence" can be reasonably effective.

In all the preceding discussion motion in the porous material has been assumed to be confined to the fluid in the pores, and to be of small amplitude. If the skeletal material also moves, then the situation becomes more complicated: evidently the inertia, elasticity and internal damping parameters of the skeletal material will also be involved and so at least six material parameters (instead of the three of equations (22) and (23)) will be needed to characterize the dynamical behaviour. Development of a theoretical model for this situation has recently been accomplished by Zarek (see the Bibliography); the only factors not explicitly included in Zarek's model are the thermal conductivities of the skeletal material and the fluid, but extension of the model to include them is straightforward. This model has the advantage of being based on a lumped element representation of each "cell" of fluid and skeletal material so that all the local dynamic mechanisms are directly evident. This approach has the further advantage that the quantitative form of each such local mechanism can be adjusted appropriately for each particular material and situation, and it thus is able to trace the effect of such adjustments through to the acoustic and/or vibration performance of the material. It is of particular significance that this model permits one to readily evaluate the difference in the characteristic impedance of the porous material when the excitation forces motion of the skeletal material as well as of the fluid in the pores, as occurs, for example, when a relatively impervious membrane is used to cover the surface of the material. This difference can be significant, in some cases.

In practice, of course, composite constructions for acoustic and vibration absorption purposes often include limp, massive membranes, perforated facings, relatively large scale cellular components (acting as Helmholtz resonators, for example), etc., as well as porous materials. Analysis of the performance of such composite acoustic transmission networks can be accomplished by the well known lumped element and acoustical/mechanical waveguide techniques. In this connection, since the point is often overlooked in standard texts, it is worth mentioning that the one-dimensional specific acoustic impedance ratio of an element of an acoustic medium of length  $l$ , terminated in an impedance ratio  $\zeta_l$ , is obtained by regarding it as either a "T-section" or a "pi-section" element, in parallel with the terminal impedance. For the T-section,

$$\zeta = -ikl + 1/\left(\frac{1}{1/ik\zeta_l} + \frac{1}{2ikl} + \frac{1}{\zeta_l}\right),$$

and for the pi-section,

$$\frac{1}{\zeta} = \frac{1}{1/4ikl} + \frac{1}{ikl} + \frac{1}{1/4ikl} + \frac{1}{\zeta_l}.$$

In both cases, of course, the formulas are valid only when  $kl \ll 1$ . Thus the element in question possesses both stiffness and inertia, but behaves primarily like a stiffness when rigidly terminated ( $\zeta_l \rightarrow \infty$ ) and like a mass when "short circuited" ( $\zeta_l = 0$ ). These formulas are valid for lossy acoustic media (like porous materials), where  $k$  is complex, as well as for lossless materials where  $k$  is real. When  $k$  is complex, of course, each mass-like element,  $1/ikl$ , and each stiffness-like element,  $1/ik\zeta_l$ , has a real part representing dissipation as well as an imaginary, reactive, part.

When a porous material, or perforate, is exposed to intense acoustic fields, or to flows either parallel or normal to its surface, the particle velocities in the pores, or apertures, can become substantial enough to result in vortex shedding or even turbulent flow in the fluid of the material. Breakdown of the flow in the pores, or apertures, into some kind of turbulence depends primarily on the Reynolds number based on pore or aperture diameter and the actual fluid velocity there. It thus can occur even at relatively moderate external sound pressure amplitudes for perforates with apertures of the order of millimetres in diameter, but only at very high sound intensities for microporous materials. When the fluctuating acoustic particle velocity amplitudes in the pores or apertures are large the effect is of introducing a velocity amplitude dependence of the flow resistance  $\zeta$  (or  $R$ ), which is approximately a linear one, so that large increases in the resistance occur as the Reynolds number increases. The publication of Milling (see the Bibliography) summarizes the most important work to date on this acoustic non-linearity. Qualitatively, the value of  $\zeta$  to be used remains that which would be obtained by

steady flow tests on the material at comparable flow speeds.

The situation with respect to large amplitude and mean flow effects on the reactive impedance of an aperture, or pore, is not at all well understood. There is a general tendency for the no-flow attached mass ("end-correction") of an orifice to be "blown away", as it were, so that the orifice's mass reactance can be somewhat less than in the no-flow, small amplitude, case, but no satisfactory quantitative formulas are yet available.

At very high intensities, in porous materials of good acoustic absorption, the rate of conversion of acoustic energy into heat can be sufficient to produce high temperatures inside the material, especially if its skeleton is not a good thermal conductor and is not provided with a heat sink into which the heat energy can flow. Thus in foam materials, and resin bonded glass or mineral fibre materials, charring or combustion can occur inside the material. In air this may happen at sound pressure levels around 150 dB or higher, and hence use of metal fibre porous materials can be necessary.

#### BIBLIOGRAPHY

In the several cited works, further references to the extensive literature may be found.

C.W. KOSTEN and C. ZWIKKER 1949 Sound Absorbing Materials. Amsterdam: Elsevier Publishing Company.

J.H.B. ZAREK 1978 Journal of Sound and Vibration 61, 205-234. Sound absorption in flexible porous materials.

T.H. MELLING 1973 Journal of Sound and Vibration 29, 1-66. The acoustic impedance of perforates at medium and high sound pressure levels.

## ACOUSTIC ENERGY

C.L. Morfey  
Institute of Sound and Vibration Research  
University of Southampton, England

## SUMMARY

Acoustic energy equations are shown to be a consequence of the linearized equations of motion. Definitions of acoustic energy density and flux are given for sound fields in fluids at rest, and in various types of mean flow. Several applications to flow-acoustic problems are discussed, involving the transmission of sound through jets and shear layers and along lined flow ducts.

## 1. INTRODUCTION

Acoustic energy definitions are developed in these notes from the linearized equations of fluid motion, following the general approach set out in reference [1]. The balance of acoustic energy in the absence of mean flow is considered first (section 2); in particular, nonlinear and dissipative effects are demonstrated by writing the acoustic energy equation in spectral form. Subsequent sections are concerned with acoustic energy conservation - or otherwise - in the presence of mean flow.

The discussion in section 3 is based on the definitions of acoustic energy density and energy flux given by Cantrell and Hart [2]. In irrotational flows with no entropy gradients, a generalized energy conservation law is obtained, which reduces to that of Blokhintsev [3] in the geometric acoustics approximation. Alternative energy definitions are also possible which lead to more or less general conservation laws [4,5,6]; that of Möhring [4] is particularly useful as it provides a simple method of accounting for shear layers when these are acoustically thin. This and various other problems are discussed in section 4 in order to illustrate the application of acoustic energy principles to flow acoustics.

## 2. ACOUSTIC ENERGY IN THE ABSENCE OF FLOW

Oscillating motion of an ideal fluid generally implies a mean transport of energy, as the following argument shows. Consider a material surface  $S$  in an inviscid, nonconducting fluid and let  $p, \mathbf{v}$  be the pressure and fluid velocity associated with a given fluid element on  $S$ . The local energy flux crossing  $S$  is  $p\mathbf{v}$ ; the time average of this quantity, following the same fluid element at all times, is

$$\bar{\mathbf{I}} = \langle p\mathbf{v} \rangle_L = \langle p'v' \rangle_L. \quad (1)$$

Here primes denote departures from the Lagrangian average  $\langle \rangle_L$ , and we have assumed that the motion of each particle is purely oscillatory so that  $\langle \mathbf{v} \rangle_L = 0$ , the average velocity of a particle of fluid, is zero.

In what follows we shall use local (rather than Lagrangian) time averages, denoted by  $\langle \rangle$ . Perturbations (denoted by primes) will be described by the linearized equations of motion, since we are aiming only for second-order accuracy in equations such as (1) above. Equation (1) gives the mean energy flux correct to second order (under the conditions stated above) whether the surface  $S$  is fixed or moves with the fluid, and whether exact or first-order values of  $p', v'$  are used.

## 2.1 Ideal medium at rest - linearised theory

We show in this section how an acoustic energy balance equation follows from the linearized equations of fluid motion. For an ideal fluid initially at rest, these may be written as

$$\frac{1}{c_0^2} \frac{\partial p'}{\partial t} = -\rho_0 \operatorname{div} \mathbf{v}', \quad (2)$$

$$\frac{\partial \mathbf{v}'}{\partial t} = -\frac{1}{\rho_0} \nabla p'. \quad (3)$$

Note that  $\rho_0$  may vary with position, the undisturbed density need not be uniform. Multiplying (2) by  $p'/c_0$  and adding  $\rho_0 \mathbf{v}' \cdot (3)$  gives

$$\frac{1}{c_0^2} p' \frac{\partial p'}{\partial t} + \rho_0 \mathbf{v}' \cdot \frac{\partial \mathbf{v}'}{\partial t} = -\operatorname{div}(p' \mathbf{v}'). \quad (4)$$

Equation (4) is an example of the general form

$$\partial/\partial t + \operatorname{div} \mathbf{N} = 0, \quad (5)$$

in which  $\mathbf{N}$  represents the acoustic energy density and  $\mathbf{N}$  the acoustic energy flux. In the present case we have

$$\mathbf{N} = \frac{1}{c_0^2} (p')^2 + \frac{1}{2} \rho_0 \mathbf{v}' \cdot \mathbf{v}', \quad \mathbf{N} = p' \mathbf{v}' \quad (6)$$

8-2 which are the standard definitions for an acoustic medium at rest. Note that both  $E$  and  $N$  are second-order quantities; the energy balance is accurate to second order, although based on first-order equations.

Equation (5) is often used in the time-averaged form

$$\partial D / \partial t + \text{div } \bar{I} = 0, \quad (7)$$

where  $D = \bar{E}$  and  $\bar{I} = \bar{N}$  are short-term averages of the energy density and flux. Also useful is the spectral energy equation

$$(\partial / \partial t) D(\omega) + \text{div } \bar{I}(\omega) = 0, \quad (8)$$

obtained by first Fourier transforming equations (2) and (3) over an appropriate time interval. The spectral quantities  $D(\omega)$  and  $\bar{I}(\omega)$  are related to the power spectra of  $p'$  and  $v_i'$  over the corresponding interval by

$$D(\omega) = \frac{1}{2\rho_0 c_0^2} S_p(\omega) + \frac{1}{2\rho_0} S_{ii}(\omega) \quad (S_{ij} = \text{cross spectral density of } v_i', v_j'); \quad (9)$$

$$I_i(\omega) = C_{pi}(\omega) \quad (C_{pi} = \text{co-spectral density of } p', v_i'). \quad (10)$$

## 2.2 Nonlinear effects

Inclusion of nonlinear terms in the preceding model leads to a spectral transfer term in the acoustic energy equation. We start from Westervelt's virtual source equation [7] for acoustic disturbances in an ideal uniform fluid at rest:

$$\frac{1}{c_0} \frac{\partial^2 p'}{\partial t^2} - \nabla^2 p' = \frac{\beta}{\rho_0 c_0^4} \frac{\partial^2 q}{\partial t^2} \quad (q = p'^2). \quad (11)$$

This allows for nonlinear effects up to second order. The nonlinearity coefficient  $\beta$  is a property of the fluid, equal to  $1/(\gamma + 1)$  for a perfect gas.

The Fourier transform of equation (11), taken over a suitable time interval, gives

$$(\omega/c_0)^2 \tilde{p} + \nabla^2 \tilde{p} = (\omega^2 \beta / \rho_0 c_0^4) \tilde{q} \quad (12)$$

where we define

$$\tilde{p} = \frac{1}{2\pi} \int p(t) \exp(-i\omega t) dt \quad \text{and similarly for } \tilde{q}. \quad (13)$$

We multiply equation (12) by the complex conjugate  $\tilde{p}^*$  and take the imaginary part of the result to obtain

$$\text{div } \text{Re}(\tilde{p}^* \tilde{v}) = -\frac{\omega \beta}{\rho_0 c_0^4} \text{Im}(\tilde{p}^* \tilde{q}), \quad (14)$$

where the velocity has been introduced through the momentum equation

$$\nabla \tilde{p} = -i\omega \rho_0 \tilde{v}. \quad (15)$$

Finally, taking averages of both sides gives the following nonlinear spectral equation for stationary sound fields:

$$\text{div } \bar{I}(\omega) = -\frac{\omega \beta}{\rho_0 c_0^4} Q_{pq}(\omega) \quad (Q_{pq} = \text{quad-spectral density of } p, q). \quad (16)$$

This equation has been used<sup>†</sup> by Westervelt [8] and Merklinger [9] to describe the spectral transfer of energy which accompanies high-intensity sound propagation.

## 2.3 Dissipative effects

A spectral energy equation for real fluids may be obtained by starting from the Helmholtz equation for linear waves in a uniform medium at rest. Thus we write

$$\nabla^2 \tilde{p} + K^2 \tilde{p} = 0 \quad (17)$$

where  $K(\omega)$  is a complex propagation constant.

Multiplying by  $\tilde{p}^*$  and proceeding as in section 2.2 gives the following result for stationary sound fields in weakly-dissipative media:

<sup>†</sup> In a slightly different form, appropriate for periodic signals.



$$\text{div } \mathbf{I}(\omega) = -\frac{2\alpha}{\rho_0 c_0} S_p(\omega) \quad (-\text{Im } K = \alpha \ll \omega/c_0). \quad (18)$$

The intensity in equation (18) is based on the acoustic velocity perturbation  $\mathbf{u}'$  defined by

$$\partial \mathbf{u}' / \partial t = -(1/\rho_0) \nabla p', \quad (19)$$

rather than on the actual fluid velocity  $\mathbf{v}'$ . The difference is generally negligible except near solid boundaries.

In the *radiation field* at large distances ( $r$ ) from a sound source,  $\partial \tilde{p} / \partial r \approx \tilde{p} / \rho_0 c_0$  and equation (18) reduces to the well-known result

$$\frac{\partial}{\partial r} (r^2 S_p) \approx -2\alpha r^2 S_p, \quad (20)$$

which shows the combined effects of spreading and linear attenuation on the propagation of time-stationary signals.

### 3. ACOUSTIC ENERGY IN NON-UNIFORM FLOWS

The conservation property of acoustic energy is extended to small-amplitude disturbances in irrotational uniform-entropy flow, by modifying the definitions of  $E$  and  $\mathbf{N}$  in equation (5). The presence of vorticity is shown to lead to sources (or sinks) of acoustic energy, except in the short-wavelength (geometric acoustics) limit where the conservation property holds for arbitrary flows.

#### 3.1 Irrotational uniform-entropy flow

In the absence of vorticity or entropy gradients, the linearized equations of motion may be written as

$$\partial \rho' / \partial t = -\text{div } \mathbf{m}' \quad (\mathbf{m} = \rho \mathbf{v}), \quad (21)$$

$$\partial \mathbf{u}' / \partial t = -\nabla H' \quad (H = h + \frac{1}{2} |\mathbf{u}'|^2), \quad (22)$$

where  $h$  is the specific enthalpy of the fluid. Multiplying (21) by  $H'$  and adding  $\mathbf{m}' \cdot (22)$  gives

$$H' \partial \rho' / \partial t + \mathbf{m}' \cdot \partial \mathbf{u}' / \partial t + \text{div}(\mathbf{H}' \mathbf{m}') = 0. \quad (23)$$

But

$$\mathbf{m}' = \rho_0 \mathbf{u}' + \rho' \mathbf{V} \quad (\mathbf{V} = \text{undisturbed or mean velocity}) \quad (24)$$

and since the fluid is assumed ideal,

$$\rho' = p' / c_0^2; \quad h' = p' / \rho_0. \quad (25)$$

With these substitutions, equation (23) takes the form (5), the generalized energy density and energy flux are given by

$$E = \frac{1}{2\rho_0 c_0^2} (p')^2 + \frac{1}{2}\rho_0 |\mathbf{u}'|^2 + \frac{1}{2} \mathbf{V} \cdot (p' \mathbf{u}') \quad (26)$$

and

$$\mathbf{N} = H' \mathbf{m}' = \left( \frac{1}{\rho_0} p' + \mathbf{V} \cdot \mathbf{u}' \right) (\rho_0 \mathbf{u}' + \frac{1}{c_0^2} \mathbf{V} p'). \quad (27)$$

Generalized versions of the spectral quantities  $D(\omega)$  and  $\mathbf{I}_s(\omega)$  may be written down immediately by analogy with section 2.1. Equations (26) and (27) are the definitions proposed by Cantrell and Hart [2].

#### 3.2 Energy sources in general flows

The momentum equation for arbitrary flow of an ideal fluid is

$$\partial \mathbf{v}' / \partial t = -\nabla H + T \nabla s + \mathbf{v}' \times \boldsymbol{\omega}, \quad (28)$$

where  $T$  and  $s$  are the temperature and specific entropy of the fluid and  $\boldsymbol{\omega}$  is the vorticity ( $\nabla \times \mathbf{v}$ ). Use of the linearized version of (28) in place of (22) leads to the result

$$\partial E / \partial t + \text{div } \mathbf{N} = P; \quad (P \neq 0). \quad (29)$$

In other words, acoustic energy sources (or sinks) appear in flows containing vorticity ( $\boldsymbol{\omega}$ ) or entropy gradients ( $\nabla s$ ), when  $E$  and  $\mathbf{N}$  are defined as in section 3.1; details of the analysis are given by Goldstein [10; see eqn. 1.87]. Nor is the conservation property recovered by redefining  $E$  and  $\mathbf{N}$  in terms of the irrotational part of the velocity perturbation, although the expression for  $P$  is different [1].

We conclude that the Cantrell and Hart definitions of acoustic energy density and flux are useful (i.e., yield a conservation law) only for flows of the type described in section 3.1. In the general case, Möring [4] has shown that generalized versions of  $E$  and  $N$  may be defined so as to yield acoustic energy conservation in any linearly-perturbed flow of an ideal fluid; but the generalized  $E$  and  $N$  values involve auxiliary potentials, which are not explicitly related to the local pressure and velocity perturbations.

### 3.3 Energy sources in flows of uniform entropy

In the special case where  $\nabla s$  is zero, the linearized version of equation (28) becomes

$$\partial_t \chi = -\nabla H + \chi' \quad (\chi = \chi \times \omega). \quad (30)$$

Using equation (30) in place of (22) then gives

$$P = \rho' \cdot \chi' \quad (31)$$

for the rate of acoustic energy production per unit volume.

This result offers the prospect of identifying sources of aerodynamic sound in flows with vorticity, since  $\chi'$  is zero outside the region of rotational flow. A note of caution is appropriate, however: for the integral over the flow region of  $P$  (or its average value  $\bar{P}$ ) may be almost zero as a result of cancellation between positive and negative regions. Physically,  $P$  represents a local transfer of energy from the mean flow to the unsteady disturbance; the flow as a whole exhibits energy conservation.<sup>†</sup>

The expression for  $P$  given above may be written in several different forms, all of which are equivalent to second order\*; for example,

$$P = \rho_0^2 \chi \cdot (\chi' \times \chi') = \rho_0^2 \chi' \cdot (\chi \times \chi') \quad (32)$$

where  $\chi$  denotes the ratio  $\omega/\rho$ . The last expression above is the one given by Goldstein.

### 3.4 Geometric acoustics

Although the definitions of  $E$  and  $N$  introduced above imply a non-vanishing production term ( $P$ ) for general flows, the value of  $P$  tends to zero for sound propagation in an ideal fluid in the short-wavelength limit. The one modification required to equations (26) and (27) is the replacement of  $\chi'$  by the acoustic velocity perturbation  $u'$ , defined by equation (19) in a frame of reference moving with the local mean velocity. Thus the components of  $u'$  are

$$u_n' \approx p'/\rho_0 c_0, \quad u_t' \approx 0, \quad (33)$$

normal and tangential to the local wavefront surfaces.

When these values are substituted in equations (26) and (27), we obtain the definitions of  $E$  and  $N$  given by Blokhintsev [3]. In time-averaged form,

$$D = \frac{1}{\rho_0 c_0} \left( 1 + \frac{v_n}{c_0} \right) \langle p'^2 \rangle \quad (v_n = \text{component of } \chi \text{ normal to wavefront}) \quad (34)$$

and

$$\bar{L} = \left( 1 + \frac{v_n}{c_0} \right) \langle p' u' \rangle + \frac{1}{\rho_0 c_0} \chi \langle p'^2 \rangle. \quad (35)$$

Note that these definitions are special to the geometric acoustics situation (quasi-plane wave propagation), and cannot be applied to more general sound fields.

## 4. APPLICATIONS OF ACOUSTIC ENERGY

In this section we demonstrate some applications of acoustic energy principles to flow acoustics.

### 4.1 High-frequency sound transmission through a cylindrical shear layer

Figure 1 shows a cylindrical shear layer between a jet and the surrounding flow. The energy conservation law of geometric acoustics will be used to relate the external sound field (region 2) to the incident sound field in the jet flow (region 1). Spreading of the shear layer is neglected; the wavenormal angles  $(\theta_1, \theta_2)$  are therefore related by

<sup>†</sup> An exception is discussed in section 4.3.

<sup>‡</sup> Note that  $\rho' \cdot \chi' = 0$  identically.

\* P.E. Doak, unpublished research memorandum, Lockheed-Georgia Co. (1975).

$$\frac{c_1}{\cos \theta_1} + U_1 = \frac{c_2}{\cos \theta_2} + U_2, \quad (36)$$

which expresses the fact that the axial phase speeds are equal in regions 1 and 2.

The sound power incident on the shear layer in region 1 is characterized by its distribution,  $W(\cos \theta_1)$ , with respect to  $\cos \theta_1$ ; this distribution is assumed to be known. Conservation of energy across the shear layer gives the power distribution in region (2) as

$$W(\cos \theta_2) = W(\cos \theta_1) \frac{d(\cos \theta_1)}{d(\cos \theta_2)} \quad (37)$$

$$= W(\cos \theta_1) \cdot \frac{c_1}{c_2} \left( \frac{D_2}{D_1} \right)^2;$$

the last line follows from (36), where  $D_1$  and  $D_2$  are defined by

$$D_i = \left( 1 + \frac{U_i}{c_i} \cos \theta_i \right)^{-1} \quad (i = 1 \text{ or } 2). \quad (38)$$

In order to relate the power distribution  $W(\cos \theta_2)$  to the far-field mean square pressure in region 2, we note that equation (35) gives the intensity normal to a wavefront as

$$I_n = \left( 1 + \frac{V}{c_o} \right)^2 \frac{\langle p'^2 \rangle}{\rho_o c_o} = \frac{\langle p'^2 \rangle}{\rho_o c_o D^2}. \quad (39)$$

Thus the power radiated in the conical sector  $(\theta_2, \theta_2 + d\theta_2)$  is

$$\langle p_2'^2 \rangle_\phi \cdot \frac{1}{\rho_2 c_2 D_2^2} \cdot 2\pi R_2^2 d(\cos \theta_2) = W(\cos \theta_2) d(\cos \theta_2), \quad (40)$$

where  $\langle \rangle_\phi$  denotes the azimuthal average about the jet axis and  $R_2$  is the wavefront radius in region 2. The required result then follows from equations (40) and (37):

$$R_2^2 \langle p_2'^2 \rangle_\phi = \frac{1}{2\pi} \left[ c_1 D_1^{-2} W(\cos \theta_1) \right] \rho_2 D_2^4. \quad (41)$$

Equation (41) shows how the mean square pressure radiated at any angle  $\theta_2$  depends on the external flow.† With the aid of a further assumption - that the field inside the jet is effectively radiated from a point - we may relate the mean square pressures inside and outside the jet by writing

$$W(\cos \theta_1) = \langle p_1'^2 \rangle_\phi \cdot \frac{1}{c_1^2 D_1^2} \cdot 2\pi R_1^2 \quad (42)$$

(compare equation (40) above). When equation (42) is used in (41) we obtain

$$R_2^2 \langle p_2'^2 \rangle_\phi = R_1^2 \langle p_1'^2 \rangle_\phi \cdot \frac{\rho_2 D_2^4}{\rho_1 D_1^4}. \quad (43)$$

This last result was used in reference [11] to derive an acoustic correction factor for open-jet flight simulation facilities.

#### 4.2 Energy flux discontinuity across a vortex sheet

The definition of  $N_y$  in section 3.1 implies a discontinuity in the energy flux component normal to a vortex sheet. The value of the discontinuity is calculated below; the implications for sound power in flow ducts are discussed in section 4.3.

The vortex sheet sketched in Figure 2 separates two uniform parallel flows of velocity  $U_1$  and  $U_2$ . Superimposed on the basic flow is a small-amplitude disturbance, with velocity components  $(u', v')$  in the  $(x, y)$  directions. From equation (27), the  $y$ -component energy flux in either region is

$$N_y = p'v' + \rho U u'v'. \quad (44)$$

† The corresponding angle  $\theta_1$  is assumed to be real; this limits the application of equation (41) to angles outside the cone of silence.

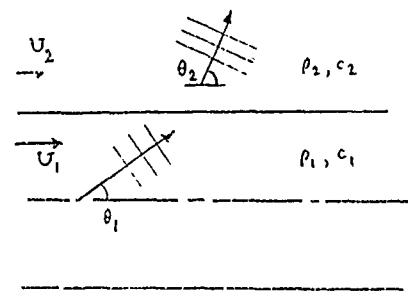


FIGURE 1. High-frequency sound transmission through a cylindrical shear layer separating two regions of uniform flow.

The physical origin of the energy loss may be understood by evaluating the energy flux expression (27) in the low-frequency limit: at the duct exit, where  $p' \rightarrow 0$ , this gives

$$N_x = Uu' \cdot \rho u' \quad (51)$$

Thus the axial flux of acoustic energy is dominated by the convection of kinetic energy perturbations, which are swept downstream in the subsonic exhaust flow without radiating significant energy to the far field.

A theoretical model of the transmission process has been studied by Munt<sup>†</sup>, in which the jet shear layer is modelled by a cylindrical vortex sheet attached to the lip of a semi-infinite thin-walled pipe. Despite the idealized representation of the shear layer, which in the experiments was turbulent and of finite thickness, the model predicts values for the plane-wave reflection coefficient ( $R_p$ ) and the power transmission coefficient

$$\alpha_{\text{rad}} = W_{\text{rad}}/W_{\text{inc}} \quad (W_{\text{rad}} = \text{power radiated in far field}) \quad (52)$$

which agree well with the various available experiments. In particular the model predicts

$$\alpha_{\text{rad}} < 1 - |R_p|^2 \left( \frac{1-M}{1+M} \right)^2 \quad (M = \text{Mach number of flow in pipe}); \quad (53)$$

i.e. an acoustic energy loss in the transmission process. It is interesting to note, however, that  $\alpha_{\text{rad}}$  is predicted to remain within 1 dB of its zero-flow value at all frequencies, provided  $U_j/c_0 < 0.5$ .

#### 4.5 Sound power radiation from a duct inlet

At a duct inlet, the flow remains irrotational (except for a thin boundary layer) provided the inlet is suitably shaped so as to avoid separation. It follows that conservation of acoustic energy may be expected for high Reynolds number inlet flows.

A further consequence of the irrotational flow is that at low frequencies  $\alpha_{\text{rad}}$  is predicted to be unaffected by the mean flow into the duct, at least at low Mach numbers.  $\alpha_{\text{rad}}$  follows from the plane-wave relation

$$\alpha_{\text{rad}} = 1 - |R_\phi|^2 \quad (R_\phi = \text{velocity-potential reflection coefficient}), \quad (54)$$

together with the prediction from Taylor's acoustic transformation [15] that  $R_\phi$  is unaltered by the inlet flow to first order in  $M$ . However, these theoretical predictions have not as yet been tested experimentally.

#### REFERENCES

1. C.L. MORFEY 1971 *Journal of Sound and Vibration* **14**, 159-170. Acoustic energy in non-uniform flows.
2. R.H. CANTRELL and R.W. HART 1964 *J. Acoust. Soc. Am.* **36**, 697. Interaction between sound and flow in acoustic cavities: mass, momentum and energy considerations.
3. D.I. BLOKHINTSEV 1946 *Acoustics of a nonhomogeneous moving medium* (in Russian). Translated as NACA TM 1399 (1956).
4. W. MÖHRING 1971 *Journal of Sound and Vibration* **18**, 101-109. Energy flux in duct flow.
5. S.M. CANDEL 1975 *Journal of Sound and Vibration* **41**, 207-232. Acoustic conservation principles and an application to plane and modal propagation in nozzles and diffusers.
6. W. EVERSMAN 1979 *Journal of Sound and Vibration* **62**, 517-532. Acoustic energy in ducts: further observations.
7. P.J. WESTERVELT 1969 in *Nonlinear Acoustics* (ed. T.G. Muir): proceedings of conference at ARL, Univ. of Texas at Austin, pp. 165-181.
8. P.J. WESTERVELT 1961 in *Proceedings of 3rd ICA*, Stuttgart (ed. L. Cremer), Vol. I, pp. 316-321. Amsterdam: Elsevier.
9. H.M. MERKLINGER 1973 *J. Acoust. Soc. Am.* **54**, 1760-1761. Fundamental-frequency component of a finite-amplitude plane wave.
10. M.E. GOLDSTEIN 1976 *Aeroacoustics*. New York: McGraw-Hill.
11. C.L. MORFEY and B.J. TESTER 1977 *Journal of Sound and Vibration* **54**, 83-106. Noise measurements in a free jet flight simulation facility: shear layer refraction and facility-to-flight corrections.
12. B.J. TESTER 1973 *Journal of Sound and Vibration* **28**, 205-215. Acoustic energy flow in lined ducts containing uniform or "plug" flow.
13. D. BECHERT, U. MICHEL and E. PFIZENMAIER 1977 *AIAA Paper No.* 77-1278. Experiments on the transmission of sound through jets.
14. C.J. MOORE 1977 *Journal of Fluid Mechanics* **80**, 321-367. The role of shear-layer instability waves in jet exhaust noise.
15. K. TAYLOR 1977 *RAE (Farnborough) Technical Report* 77109. A transformation of the acoustic equation with implications for wind tunnel and low speed flight tests.

<sup>†</sup>R.M. Munt, unpublished note to British Aeronautical Research Council (1978). To appear in *Journal of Sound and Vibration*.

## ABSORPTION OF SOUND WAVES IN THE ATMOSPHERE

C.L. Morfey,  
Institute of Sound and Vibration Research,  
The University,  
Southampton,  
SO9 5NH,  
England.

## SUMMARY

Absorption processes for sound waves in gases are described, with particular emphasis on atmospheric propagation over the frequency range  $10^3$ - $10^5$  Hz. The topics covered include molecular transport processes (viscosity, heat conduction and diffusion in mixtures); rotational relaxation in air; vibrational relaxation of  $H_2$  and  $O_2$  molecules in air and the influence of humidity; radiative heat transfer due to water vapour; viscothermal absorption due to suspended particles, and the additional effects arising from droplet evaporation in fogs. In each case, graphs or formulae for estimating atmospheric attenuation are provided, together with references to further information. The survey concludes with a brief introduction to dissipative effects in nonlinear waves; sonic boom rise times in the atmosphere are discussed, together with the spectral distortion of high-intensity noise.

## 1. INTRODUCTION

The propagation of small-amplitude sound waves in a uniform stationary atmosphere is closely described by

$$(\nabla^2 + K^2)p = 0, \quad (1)$$

where  $K(\omega)$  is a complex propagation constant for single-frequency waves (time factor  $e^{i\omega t}$ ). The approximation is good for frequencies well below the relaxation frequencies of the principal energy-containing molecular degrees of freedom (the rotational and translational modes). For air, this restricts the frequency to

$$f \ll f_{\text{rot}} \approx 0.04 \, c^2/\nu \approx \frac{1}{3} \, \text{GHz} \, (15^\circ\text{C}, 1 \, \text{atm})^\dagger; \quad (2)$$

the acoustic wavelength at  $f_{\text{rot}}$  (the rotational relaxation frequency) is only about 10 times the molecular mean free path, so the Navier-Stokes equations cease to be valid when condition (2) is not met [1,2,3].

Equation (1) implies that the pressure in a plane progressive wave is proportional to

$$e^{-iKx} = \exp[-(\alpha + i\omega/c_p)x] \quad (x = \text{coordinate in propagation direction}). \quad (3)$$

Here  $\alpha$  is the attenuation coefficient and  $c_p$  is the phase speed; dispersive propagation occurs when  $c_p$  differs from  $c_0$ , the equilibrium sound speed. At low frequencies  $K$  approaches  $\omega/c_0$ ; moreover, throughout the frequency range for which (1) is valid we have [1]

$$\frac{\alpha}{\omega} \ll \frac{1}{c_0}, \quad \sigma = \left(\frac{1}{c_0} - \frac{1}{c_p}\right) \ll \frac{1}{c_0} \quad (\alpha, \sigma \text{ positive}). \quad (4)$$

In the notes which follow, attention is focussed on the attenuation coefficient  $\alpha$  rather than  $\sigma$ . This is because for many practical purposes it is the spectral energy distribution of the received signal which is important, rather than the actual waveform. According to linear theory,  $\sigma$  has no influence on the energy distribution, since it merely alters the relative phasing of different frequency components. However, during high-amplitude propagation over large distances (e.g. aircraft jet noise and sonic boom), dispersive effects assume practical significance; this subject is briefly covered in section 6.

The attenuation of sound in uniform atmospheric air is plotted versus frequency in Figure 1, at  $20^\circ\text{C}$  and 1 atm pressure [4]. It is immediately apparent that the relative humidity (RH, %) is an important parameter. The relative humidity and the water vapour molecule ratio ( $h$ , %) are related by

$$h = (\text{percentage of } H_2O \text{ molecules in mixture}) = (RH) \cdot (p_s/p_0), \quad (5)$$

where  $p_s$  is the saturated water vapour pressure and  $p_0$  is the atmospheric pressure.

The various absorption mechanisms contributing to Figure 1 are discussed in sections 2 and 3. Two additional mechanisms not included in Figure 1 are radiative heat transfer and particulate attenuation; these are assessed in section 4 and section 5 (with particular reference to fog). Finally, nonlinear effects are introduced in section 6.

<sup>†</sup>Numerical values in this chapter refer to a temperature of  $15^\circ\text{C}$  and pressure of 1 atm as standard, unless otherwise specified.

9-2

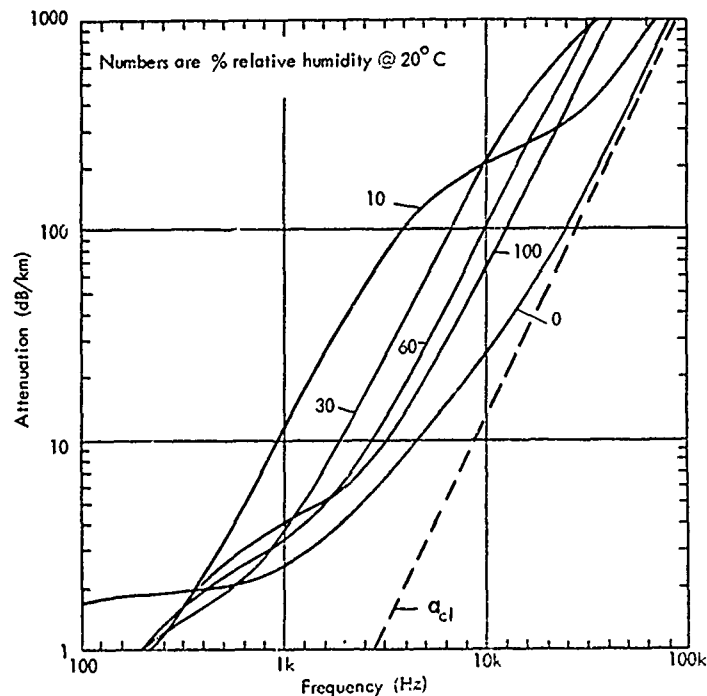


FIGURE 1. Absorption of sound in air (1 atm, 20°C) as a function of frequency and relative humidity: values calculated by Evans, Bass and Sutherland [4]. Classical absorption is shown by the broken line.

## 2. CLASSICAL AND ROTATIONAL ABSORPTION

In a gas mixture such as the atmosphere, molecular transport processes (shear viscosity, heat conduction and species diffusion) give rise to the so-called classical absorption coefficient [1,5,6,7],

$$\alpha_{cl} = \frac{1}{2} \frac{\omega^2 \nu}{c_0^3} \left( \frac{4}{3} + \frac{\gamma - 1}{Pr} + \frac{C(1-C)}{Sc} \frac{(M_1 - M_2)^2}{M_1 M_2} \right). \quad (6)$$

The first two terms represent viscous and heat conduction effects respectively; the diffusion term is calculated for a two-component mixture model, with molecular weights ( $M_1, M_2$ ). Other quantities in equation (6) are defined as follows:

- C, (1-C) mass fractions of species 1 and 2 in gas mixture
- Pr Prandtl number  $\nu/K$  ( $K$  = thermal diffusivity)
- Sc Schmidt number  $\nu/D_{12}$  ( $D_{12}$  = species diffusivity)
- $\gamma$  specific-heat ratio of mixture
- $\nu$  kinematic viscosity of mixture.

The largest contribution to  $\alpha_{cl}$  in air (about 70%) comes from the viscous term. The heat conduction term accounts for most of the remainder. The diffusion term contributes only about 0.5% to the classical absorption in air; the principal components involved are oxygen, nitrogen and argon.<sup>†</sup>

Measurements of  $\alpha$  at high frequencies (well above the vibrational relaxation frequencies discussed in the next section) show the correct  $f^2$  dependence, but yield values of  $\alpha$  about 31% greater than equation (6) predicts (compare Figure 1). The discrepancy is attributed to rotational relaxation of  $N_2$  and  $O_2$  molecules, which may be modelled as a bulk viscosity in the frequency range allowed by (2) above.<sup>‡</sup> An empirical formula due to Sutherland [8] predicts the total (classical plus rotational) absorption as

$$a(CR) = 0.159 g(T) \cdot F^2 / P \quad \text{dB/km (at frequency } F \text{ kHz).}^* \quad (7)$$

<sup>†</sup>A further contribution due to water vapour becomes comparable in hot humid air, but for air temperatures less than 40°C its effect on the total classical plus rotational absorption remains small (see remarks on equation (7) below).

\*Values of  $a$  (in dB/km) are related to  $\alpha$  (in neper/m) by  $a = 8686\alpha$ .

Equation (7) refers to dry air, at a temperature  $T(K)$  and pressure  $P(atm)$ . The presence of water vapour in significant concentrations alters the viscosity and renders the formula inaccurate, but the error is less than 3% for temperatures below  $20^\circ C$ . The temperature correction factor  $g(T)$  equals 1 at  $15^\circ C$ , and is given by

9-3

$$g(T) = \frac{1.383 T}{T + 110.4} \quad (270 < T < 320 K; \text{ see [9] for higher temperatures}). \quad (8)$$

Figure 1 shows that the classical plus rotational absorption is typically of secondary importance in humid air over most of the audio frequency range, although it becomes dominant at ultrasonic frequencies. The additional absorption shown in Figure 1 arises from vibrational relaxation processes, as described in the following section.

### 3. VIBRATIONAL RELAXATION ABSORPTION

In air at equilibrium, a small but finite fraction of the internal energy resides in vibrational modes of the  $O_2$ ,  $N_2$  and  $CO_2$  molecules. Rapid changes of pressure - as in a sound wave - cause departures from equilibrium, because of the relatively slow response of these vibrational modes to changes in translational and rotational energy of the molecules. The rate of approach to the equilibrium energy distribution is characterized by the vibrational relaxation frequency,  $f_r$ , of each mode.

The theory of molecular relaxation absorption is well set out in references [5] and [10]. It predicts the attenuation coefficient of a single relaxation process as

$$\begin{aligned} \alpha_{vib} &= Af^2/[1 + (f/f_r)^2], \\ &\rightarrow Af^2 \quad (f \ll f_r) \\ &\rightarrow Af_r^2 \quad (f \gg f_r). \end{aligned} \quad (9)$$

Thus  $\alpha_{vib}$  increases as (frequency)<sup>2</sup> initially, in the same way as  $\alpha_{cl}$ , but levels off to a constant value beyond the relaxation frequency. The  $\alpha_{vib}$  contributions from different vibrational modes are additive at atmospheric temperatures, since each mode contributes only a small fraction of the total internal energy:

$$\alpha_{vib} = \alpha_{vib}(O_2) + \alpha_{vib}(N_2) + \alpha_{vib}(CO_2, \text{ transverse}) + \dots \quad (10)$$

Only the three contributions above will be discussed here, since they account for the whole of  $\alpha_{vib}$  in air to within the accuracy of available data.

In dry air,  $f_r(O_2)$  and  $f_r(N_2)$  are very low - of order 10-20 Hz - and  $f_r(CO_2)$  is around 10 kHz. The oxygen and nitrogen absorption rates at audio frequencies are correspondingly low, levelling off at between 1 and 2 dB/km, and their contribution can be identified in Figure 1 at the low-frequency end of the 0% humidity curve. The contribution from  $CO_2$  relaxation becomes significant between 1 and 10 kHz (same curve); it is roughly comparable with the classical absorption over this range.

The addition of  $H_2O$  as water vapour, however, greatly increases  $f_r(O_2)$  and  $f_r(N_2)$ . Collisions with  $H_2O$  molecules help to couple the translational modes with the vibrational modes of  $O_2$  and  $N_2$ , so that equilibrium is reached much more quickly. A similar but relatively small effect is expected with  $CO_2$ ; this is because at the low  $CO_2$  concentration present in air, collisions with any  $H_2O$  molecules present will be relatively infrequent for  $CO_2$  as compared with  $O_2$  and  $N_2$ .

The overall effect is to increase the attenuation rate in humid air relative to dry air, particularly in the frequency range from 1 to 50 kHz. The relaxation frequencies  $f_r(O_2)$  and  $f_r(N_2)$  are moved up into the audio frequency range, while the product  $Af_r$  remains essentially unchanged; thus  $\alpha_{vib}$  rises to a much higher plateau. This may be seen in Figure 1, and more clearly in Figure 2 where the principal contributions are plotted separately.

The parameters  $A$  and  $f_r$  in equation (9) depend on temperature, water vapour concentration and pressure. The product  $Af_r$  is predictable theoretically [10], and is relatively well established for both the  $O_2$  and  $N_2$  contributions. However, values of  $f_r$  have to be determined by experiment and there is considerable scatter in the data [8]. Estimated relaxation frequencies for saturated air ( $RH = 100$ ) are plotted in Figure 3, and corresponding  $A$  values in Figure 4, but actual values may deviate by up to 15% ( $O_2$ ) or 35% ( $N_2$ ) over the temperature range given.

In order to adjust the values in Figures 3 and 4 for changes in relative humidity, the following factors may be applied:

$$\begin{aligned} (H_2) \quad f_r &\propto (RH) & A &\propto (RH)^{-1} \quad (\text{no } P \text{ dependence}), \\ (O_2) \quad f_r &\propto (RH)^{1.3p-0.3} & A &\propto (RH)^{-1.3p0.3} \end{aligned} \quad (11)$$

Here  $P$  is the pressure in atm. The scaling laws above are expected on theoretical grounds to hold down to absolute humidities of about  $h = 0.02$  (per cent.), but supporting data are scarce below  $h = 0.1$  [8,11,12].

#### 3.1 Prediction methods for relaxation absorption in air

Detailed formulae for predicting  $N_2$  and  $O_2$  vibrational absorption in air are given by Sutherland [8] and Bazley [11]. The latter report includes tables for the total absorption at frequencies from 500 Hz to 100 kHz, temperatures from 0 to  $30^\circ C$ , and relative humidities from 10 to 95 per cent. Similar tables,

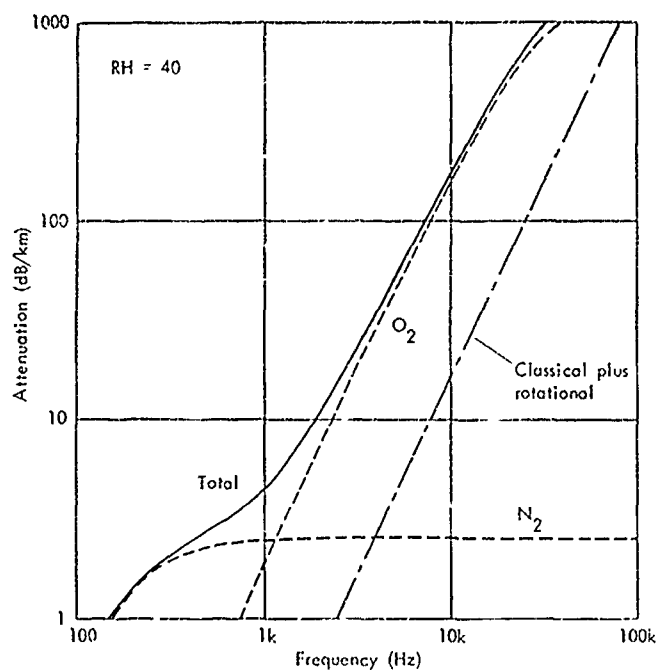


FIGURE 2. Absorption of sound in air (1 atm, 20°C) at 40% relative humidity, showing the breakdown at different frequencies [11]. The curves labelled N<sub>2</sub> and O<sub>2</sub> represent the contributions due to vibrational relaxation of nitrogen and oxygen.

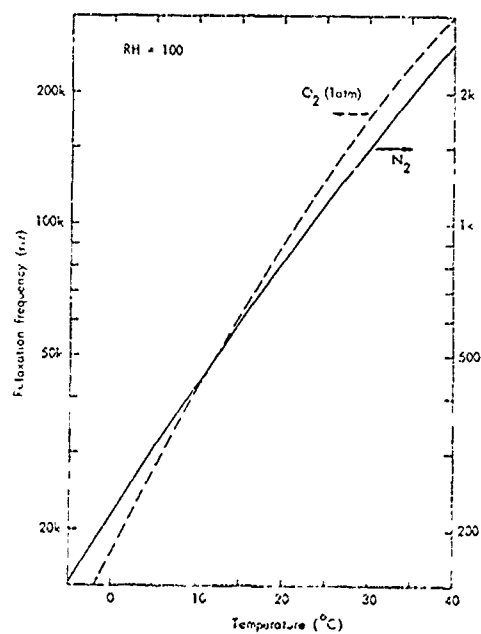


FIGURE 3. Vibrational relaxation frequencies of N<sub>2</sub> and O<sub>2</sub> in air, as a function of temperature at 100% relative humidity.

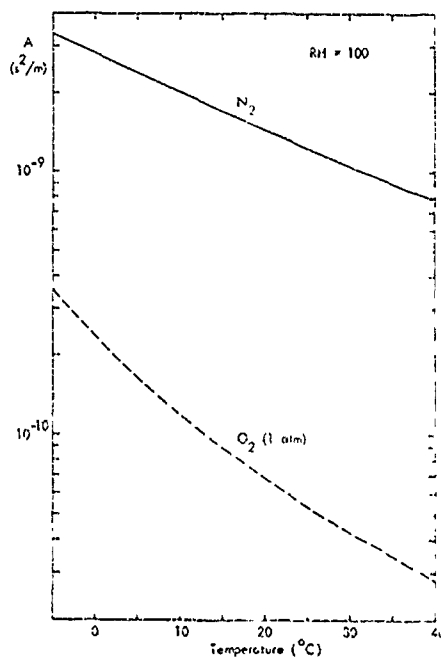


FIGURE 4. Values of the constant A in the relaxation-attenuation equation, for vibrational relaxation of N<sub>2</sub> and O<sub>2</sub> in air at 100% relative humidity.



but based on the formulae given in reference [12],<sup>†</sup> are available from the Engineering Sciences Data Unit [13]; these cover frequencies from 50 Hz to 100 kHz, temperatures from 270 to 310 K, and pressures  $P = 0.8$  to 1.1 (atm). These predictions may be taken to supersede the SAE methods of 1964 [14] and 1975 [15].

The accuracy of all the above prediction methods is limited by uncertainties in  $f_r(O_2)$  and  $f_r(N_2)$ . The scatter in the available measurements indicates that over the temperature range 0 to 40°C,  $\alpha_{vib}$  can be predicted with certainty only within a factor 1.2 (for  $O_2$  relaxation) or 1.4 (for  $N_2$  relaxation). Since these two mechanisms between them dominate the total attenuation in the audio frequency range, similar factors must be presumed to apply to the absorption tables [11,13]. This is borne out by detailed comparison of the NPL and ESDU tables, which differ by a factor of up to 1.4; the largest discrepancies occur either side of the  $N_2$  relaxation frequency (typically 500 Hz - 2 kHz) where the absolute attenuation rates are relatively small.

### 3.2 Further practical problems

When sound propagates over distances of order 1 km or more in the atmosphere, the difference in attenuation between two frequencies only one-third octave apart may amount to several dB at high frequencies. Use of 1/3-octave band analysis in such situations requires special care; it is clearly not adequate to apply an average attenuation rate, based on the band centre frequency, to the band as a whole.

Methods of estimating attenuation for finite bands of noise are presented in references [13] and [16]. They should be used with caution, however, as the need for a significant bandwidth correction indicates a rapidly-sloping spectrum which should preferably be resolved by analysis at a narrower bandwidth. Furthermore, the possibility of nonlinear spectral transfer should be borne in mind under these conditions (see section 6 below).

An additional problem encountered in atmospheric propagation is that  $\alpha$  may vary significantly along the propagation path. This is all for in principle by integrating the attenuation along each ray path of interest; because  $\alpha$  depends sensitively on temperature and humidity, meteorological data are required at points along the ray. Practical guidance in allowing for atmospheric non-uniformity is given in reference [13].

### 3.3 Dispersion of sound due to molecular relaxation

Although a knowledge of the attenuation coefficient  $\alpha$  is often all that is required, there are situations where the dispersion of sound waves is important. This is evidently the case if we need a description of the acoustic waveform  $p(t)$ . Even if we are concerned only with the power spectrum of the signal, however, dispersion becomes relevant when the propagation is nonlinear. Two examples of nonlinear propagation are discussed in section 6.

According to relaxation theory [5,16], dispersion and attenuation are related for nearly unexcited modes by

$$\left(\frac{1}{c_0} - \frac{1}{c_f}\right) = \sigma(f) = \sum_n \frac{1}{2\pi f_n} \alpha_n(f). \quad (12)$$

The summation in equation (12) is over the various relaxing modes with relaxation frequencies  $f_n$ . Thus  $\sigma(f)$  may be calculated for air from the data on  $\alpha_{vib}(O_2, N_2)$  referred to earlier.

## 4. ELECTROMAGNETIC RADIATION ABSORPTION

Although air is virtually transparent to radiation in the optical waveband, it is strongly absorbent at certain infra-red frequencies. One of the principal absorption processes involves the rotational excitation of water vapour molecules; the absorption of sound which results from this radiative transfer mechanism has been estimated by Calvert, Coffman and Querfeld [17]. The basic theory of radiative absorption which they use is set out by Smith [18].

At high frequencies (typically above 1 kHz in air) the electromagnetic absorption over one acoustic wavelength becomes small. This is the almost-transparent limit, for which the theory predicts an absorption coefficient  $\alpha(EM)$  independent of frequency and proportional to  $h/c_0$  ( $h$  is the percentage of absorbing molecules,  $H_2O$  in this case). Using the values in [17] to find the constant of proportionality gives

$$\alpha(EM) = 32 h/c_0 \text{ dB/km} \quad (\text{high-frequency limit}). \quad (13)$$

At lower frequencies the dependence of  $\alpha(EM)$  on humidity and temperature is complicated, but the numerical values in [17] indicate that down to 0.01 Hz the attenuation rate is roughly

$$\alpha(EM) = 0.011 F^{0.8} \text{ dB/km} \quad (14)$$

at  $F$  kHz, under typical atmospheric conditions.

<sup>†</sup>The differences concern the temperature dependence of  $f_r$  for  $O_2$  and  $N_2$ . Over the range 0 to 40°C, they are fairly small compared with other uncertainties in the prediction method.

Although the estimates above are for one infra-red absorption process only, they are believed to give the correct order of magnitude for radiative absorption in the atmosphere. It is interesting to compare these values with those for  $N_2$  relaxation, which is the principal absorption mechanism in humid air below about 1 kHz. Taking a relative humidity of 100% (which gives the lowest value of  $A$  in equation (9)) we find

$$\alpha(\text{EM}) < 0.03 \alpha_{\text{vib}}(N_2) \text{ for } f > 50 \text{ Hz.} \quad (15)$$

Thus radiative transfer is insignificant above 50 Hz, but may become significant at infrasonic frequencies because of its  $f^{0.5}$  dependence (as compared with  $f^2$  for vibrational relaxation).

## 5. ABSORPTION DUE TO SUSPENDED PARTICLES AND FOG

Significant increases in atmospheric absorption below 10 kHz can be caused by fog. Other suspended particles may also cause sound attenuation, although the behaviour of volatile particles such as water droplets is somewhat different from that of non-volatile particles such as smoke or dust. In all cases the additional attenuation is approximately proportional to the particle mass loading  $m$ , defined as the mass of suspended particles per unit mass of the surrounding gas.

### 5.1 Non-volatile particle suspensions

The theory of sound attenuation by non-volatile particles is summarized in references [19] and [20]. Dissipation is caused by heat conduction and viscous drag between the gas and suspended particles. For each mechanism, the attenuation coefficient varies with frequency according to the relaxation equation (9); the contributions from the different mechanisms are additive. The relaxation frequencies and high-frequency absorption limits for non-volatile aerosols are as follows.

(Heat conduction)

For particles of diameter  $d$  in a gas of thermal conductivity  $k$  the thermal relaxation frequency is

$$f_c = kd/(\text{particle heat capacity}) = \frac{6\nu}{\pi\kappa Pr} \cdot \frac{1}{\rho_1 d^2}, \quad (16)$$

where subscript 1 refers to the particle material,  $\kappa$  is the specific-heat ratio  $C_{p1}/C_{v1}$ , and  $\nu$ ,  $Pr$  are the viscosity and Prandtl number of the surrounding gas. The high-frequency absorption coefficient depends additionally on  $\gamma$  (the ratio  $C_{p0}/C_{v0}$  for the gas phase) and  $c_0$  (the equilibrium speed of sound):

$$(\alpha_\infty)_c = m \kappa \frac{6(\gamma-1)}{c_0^2 Pr} \cdot \frac{1}{\rho_1 d^2} \quad (1 \ll \frac{f}{f_c} \ll \frac{2}{3} \frac{k_1}{k}). \quad (17)$$

(Viscous drag)

$$f_d = \frac{3}{2} \mu d/(\text{particle mass}) = \frac{9\mu}{\pi} \cdot \frac{1}{\rho_1 d^2}; \quad (18)$$

$$(\alpha_\infty)_d = m \cdot \frac{9\mu}{c_0} \cdot \frac{1}{\rho_1 d^2} \quad (1 \ll \frac{f}{f_d} \ll \frac{4}{9} \frac{\rho_1}{\mu}, \frac{4}{9} \frac{\mu_1}{\mu}). \quad (19)$$

The physical significance of the upper frequency limits is that the temperature within each particle is assumed uniform (for the conduction mechanism), and the unsteady viscous length scales<sup>†</sup> are assumed large compared with the particle diameter (for the drag mechanism).

### 5.2 Evaporating particles (fog)

The possibility of phase changes (evaporation and recondensation) introduces complications into the simple non-volatile analysis. The basic equations have been formulated and simplified predictions obtained by Wooten and Marble [21,22,23]. A more detailed analysis was given by Cole and Dobbins [24] and subsequently shown to agree quite well with measurements in air/water fogs [25]. Refinements to Cole and Dobbins's theory by Davidson [26] reduced the predicted attenuation for air/water fog by about 10%, improving the agreement with experiment. The following approximations are based on the simplified analytical results of Cole and Dobbins [24].

(Heat conduction - volatile particles)

Coupling between phase changes and heat transfer modifies the relaxation frequency for the conduction mechanism to

$$f_{ce} = f_c \cdot E_v. \quad (20)$$

The factor  $E_v$  is typically of order 2-4 for atmospheric fog; it is related to the vapour mass fraction  $C_v$  in the surrounding gas by

$$E_v = 1 + \left(\frac{\gamma}{\gamma-1}\right) \frac{M_1}{M} \eta^2 C_v \quad (\text{note that } C_v = \frac{M_1}{M} \frac{p_s}{p_0}, \text{ since the vapour is assumed saturated}). \quad (21)$$

<sup>†</sup>I.e. the viscous boundary layer thicknesses in the surrounding gas and in the fluid particles.

Here  $\eta (= h_{fg}/C_p T)$  is a latent heat parameter based on the specific enthalpy of vaporization  $h_{fg}$  for the evaporating substance, and  $M, M_1$  are the molecular weights of the surrounding gas mixture and vapour respectively.

The high-frequency attenuation  $(\alpha_\infty)_c$  is not affected by evaporation, however, so equation (17) still applies.

(Viscous drag - volatile particles)

The presence of evaporation leaves equations (18) and (19) unchanged.

(Evaporation/recondensation)

An additional relaxation process, associated with the time taken to reach equilibrium between the vapour phase and the suspended particles, produces a low-frequency attenuation band with the following properties.

$$f_e \approx m \kappa f_c = m \cdot \frac{6\eta}{\pi p r} \cdot \frac{1}{\rho_1 d^2}; \quad (22)$$

$$(\alpha_\infty)_e \approx m \cdot \frac{6\eta\eta}{C_p p r} (\eta-1) \left( \frac{M_1}{M} \eta - 1 \right) \frac{C_v}{E_v} \cdot \frac{1}{\rho_1 d^2} \quad (f \ll m^{\frac{1}{2}} f_e = \frac{2m^{\frac{1}{2}}}{3Pr} f_d). \quad (23)$$

The upper frequency limit in equation (23) prevents the conduction and evaporation ranges from overlapping. It may be relaxed if the expression for  $\alpha_e(f)$  is further divided by the factor  $1 + (f/f_{ce})^2$ ; then the attenuation  $\alpha_e$  reaches a plateau between the frequencies  $f_e$  and  $f_{ce}$ , and falls off on either side.

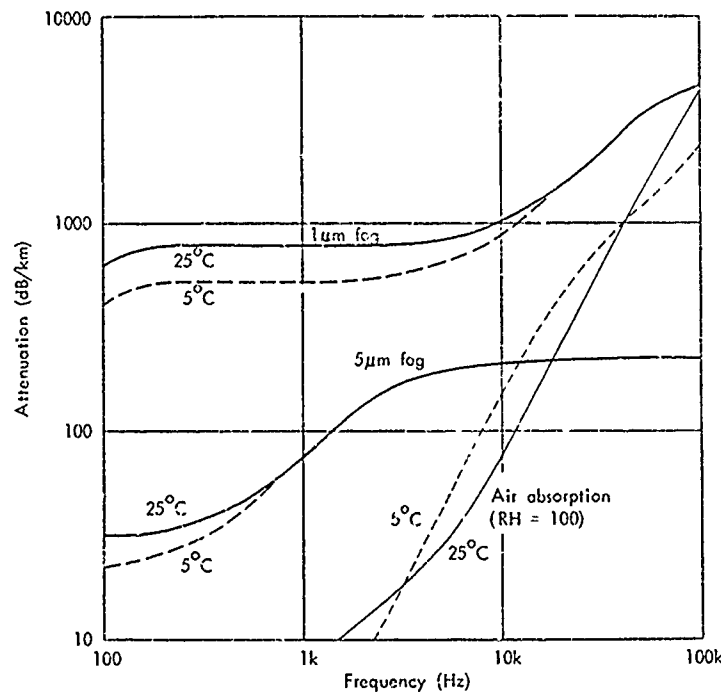


FIGURE 5. Absorption of sound in saturated air (1 atm) containing suspended water droplets, for droplet diameters of 1  $\mu\text{m}$  and 5  $\mu\text{m}$ . The droplet mass loading ( $m$ ) in each case is  $10^{-3}$ . Separate curves show the droplet and gas-phase contributions to the total attenuation.

Figure 5 shows the predicted attenuation ( $\alpha = \alpha_a + \alpha_d + \alpha_e$ ) for air/water fogs with droplet diameters of 1 and 5  $\mu\text{m}$ . This corresponds to the lower end of the size range encountered in the atmosphere; equations (17), (19) and (23) show that above each relaxation frequency, the attenuation is proportional to  $1/d^2$ . The mass loading  $m$  has been taken as  $10^{-3}$ ; atmospheric fogs range between about  $10^{-3}$  and  $10^{-4}$ , and the theoretical equations above show that the attenuation is proportional to  $m$  (except at very low frequencies where  $f < f_e$ ). Thus the values used in Figure 5 correspond to the high end of the attenuation range expected under normal atmospheric conditions.

Comparison with the air attenuation predicted for corresponding conditions ( $RH = 100$ ) shows that below 10 kHz, fog can produce very large increases in attenuation. The attenuation is relatively insensitive to air temperature, but depends strongly on the droplet diameter.

### 5.3 Summary of approximations involved in theory

- 9-8 (a) Non-continuum and surface tension effects are neglected. For air/water fogs, this requires  $d \geq 1 \mu\text{m}$ .
- (b) Suspended particles are assumed identical and spherical.
- (c) The density and bulk modulus of the particles are both large compared with the values for the surrounding gas.
- (d) The particle mass loading ( $m$ ) is small.
- (e) In the estimation of  $a_e$  (evaporation mechanism),  $C_v$  is assumed small and the latent heat parameter ( $n$ ) is assumed large. (Typically,  $n = 8-10$  for air/water fogs.)
- (f) The Lewis number for the vapour/noncondensing gas mixture ( $Le = Sc/Pr = K/D$ ) is close to unity. (For water vapour/air mixtures,  $Le \approx 0.84$ .)
- (g) The particles are small enough that departures from internal equilibrium are negligible, and are small compared with the unsteady diffusion length scales (velocity, temperature and concentration) in the surrounding gas. These requirements are reflected in the upper frequency limits of equations (17) and (19).

### 5.4 Numerical values for air/water fog

The following relaxation frequencies and high-frequency attenuation rates are estimated for  $d = 1 \mu\text{m}$ ,  $m = 10^{-3}$ , at  $15^\circ\text{C}$  and  $1 \text{ atm}$ .

$f_c$	11.5 kHz		
$f_{ce}$	42 kHz	$(a_\infty)_c$	1500 dB/km
$f_d$	51.5 kHz	$(a_\infty)_d$	4100 dB/km
$f_e$	48 Hz	$(a_\infty)_e$	650 dB/km

The valid frequency range (see (g) above) extends as far as the beginning of the high-frequency attenuation plateau shown in Figure 5. Above this range, the attenuation may be overestimated by a factor of about 1.5.

## 6. NONLINEAR PROPAGATION OF SOUND IN THE ATMOSPHERE

In an ideal (nondissipative) fluid, nonlinear propagation effects would cause sound waves to distort and eventually form shocks, as illustrated for an initially sinusoidal signal in Figure 6. The principal effect of dissipative processes - including the various relaxation phenomena described in sections 3 and 5 - is to counteract the waveform steepening. If the nonlinear effects are strong enough, recognizable shocks will still develop but will have a finite rise time. The relation between the rise time ( $t_r$ ) and the pressure jump ( $\Delta p$ ) is discussed below.

The competing effects of waveform steepening and dissipative smoothing may alternatively be viewed in the frequency domain. Nonlinear distortion of the waveform transfers part of the wave energy to higher frequencies; but the build-up of high-frequency energy is opposed by dissipation, which attenuates the higher frequencies more rapidly. A frequency domain description is convenient for studying nonlinear propagation of continuous signals; the governing equations are outlined in the second part of this section.

### 6.1 The rise time of fully-dispersed shock waves

The structure of weak shock waves in relaxing gases (including atmospheric air) is described in detail by Johannesen and Hodgson [27]. We shall limit our attention to fully-dispersed shocks, which are sufficiently weak that their speed (relative to the undisturbed gas) lies between the equilibrium sound speed ( $c_0$ ) and the frozen sound speed ( $c_f$ ). The upper limit on  $\Delta p$  is accordingly

$$\frac{\gamma + 1}{4} \frac{(\Delta p)_{\max}}{\rho_0 c_0} \leq c_f - c_0 \quad (24)$$

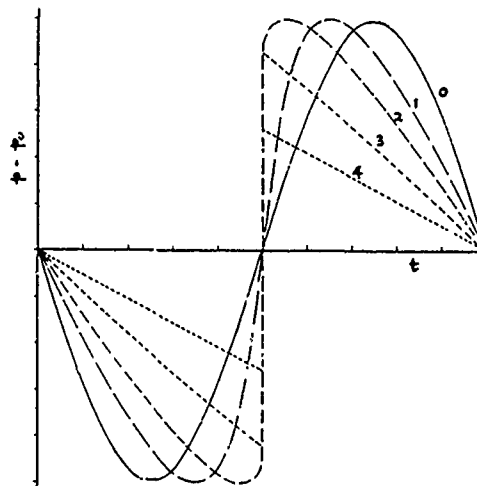


FIGURE 6. Progressive distortion of an initially-sinusoidal plane waveform in the limit of small dissipation ( $\alpha \rightarrow 0$ ). The initial waveform is labelled 0; successive waveforms (1 to 4) are shown for increasing propagation distances (doubling each time).

In atmospheric air free from suspended particles, the structure of weak shocks is determined principally by the  $N_2$  and  $O_2$  vibrational relaxation processes described in section 3. We therefore interpret  $c_f$  as the sound speed well above the  $N_2$  and  $O_2$  vibrational relaxation frequencies. The difference between the two sound speeds is given by

$$c_f - c_0 \approx c_0 \frac{(\gamma - 1)^2}{2\gamma} c' \quad (c' \ll 1); \quad (25)$$

here  $c'$  is the vibrational contribution (both  $N_2$  and  $O_2$ ) to the specific heat of air, divided by the gas constant. Typical values are  $5.0 \cdot 10^{-3}$  at  $5^\circ C$ , and  $7.75 \cdot 10^{-3}$  at  $25^\circ C$  [12].

Combining equations (24) and (25) gives the maximum shock strength for fully-dispersed shocks as

$$\left(\frac{\Delta p}{p_0}\right)_{\max} \approx \frac{2(\gamma - 1)^2}{\gamma + 1} c'. \quad (26)$$

Thus for air at  $(5-25^\circ C, 1 \text{ atm})$ ,

$$(\Delta p)_{\max} \approx 67-105 \text{ Pa}. \quad (27)$$

Typical pressure profiles, for (a) a fully-dispersed shock and (b) a shock whose strength exceeds the above limit, are shown in Figure 7. The stronger shock exhibits a rapid initial rise in pressure - with a rise

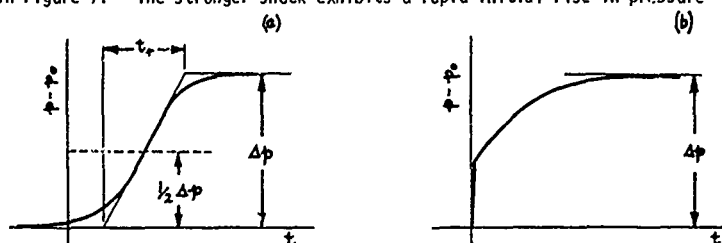


FIGURE 7. Sketch of shock profiles in a relaxing gas, showing definition of rise time. (a) Fully-dispersed weak shock; (b) partly-dispersed stronger shock (shock speed greater than frozen sound speed).

time dictated in practice by faster relaxation processes such as  $CO_2$  vibration and molecular rotation - followed by a region at the rear of the shock in which  $N_2$  and  $O_2$  vibrational relaxation control the approach to equilibrium.

Estimation of the shock rise time in air is complicated by the presence of two simultaneous ( $N_2$  and  $O_2$ ) relaxation processes, but some general statements are possible. Thus for very weak shocks, up to a limiting strength of

$$\left(\frac{\Delta p}{p_0}\right)_{\max, N_2} \approx \frac{2(\gamma - 1)^2}{\gamma + 1} c'(N_2), \quad (28)$$

the shock structure is controlled by  $N_2$  relaxation; here  $c'(N_2)$  is the nitrogen contribution to  $c'$  in air, with typical values of  $0.66 \cdot 10^{-3}$  at  $5^\circ C$  and  $1.29 \cdot 10^{-3}$  at  $25^\circ C$ . The corresponding pressure rise, for air at  $(5-25^\circ C, 1 \text{ atm})$ , is

$$(\Delta p)_{\max, N_2} \approx 9-17 \text{ Pa}. \quad (29)$$

In the nitrogen-controlled region, the shock rise time may be estimated from equation (30) below as though only  $N_2$  relaxation were present. On the other hand, shocks of more than 3 times the strength given by (28) are controlled by  $O_2$  relaxation and their rise time may be estimated from equation (30) as though only  $O_2$  relaxation were present, provided the fully-dispersed limit (26) is not exceeded.

A convenient, if somewhat arbitrary, measure of the shock rise time is one based on the slope at the mid-pressure point (Figure 7). With this definition, Hodgson and Johannesen [28] have shown that in gases with a single relaxing mode

$$t_r = \frac{4}{\gamma} \left(\frac{\gamma - 1}{\gamma + 1}\right) c_0 A \cdot \left(\frac{\Delta p}{p_0}\right)^{-1}. \quad (30)$$

Here  $A$  is the quantity plotted (for  $N_2$  and  $O_2$ ) in Figure 4. Thus in atmospheric air at  $(5^\circ C, 1 \text{ atm})$ , the following rise times are estimated for fully-developed shock waves.

$$\begin{aligned} \Delta p &= 5 \text{ Pa, } N_2 \text{ controlled: } t_r \approx 4 \text{ ms} \times (RH/100)^{-1} \\ \Delta p &= 35 \text{ Pa, } O_2 \text{ controlled: } t_r \approx 0.04 \text{ ms} \times (RH/100)^{-1.3}. \end{aligned} \quad (31)$$

The bow shock observed on the ground from high-altitude supersonic aircraft (e.g. Concorde in cruising flight) is commonly within this  $\Delta p$  range, and rise times of 2-3 ms appear to be typical under these conditions [29]. However, the rise time is sensitive to changes in atmospheric conditions (temperature and relative humidity) as well as shock strength, and it remains a matter of some controversy as to whether observed sonic-boom rise times can be fully accounted for by relaxation effects - as proposed in references [27] and [28] - or whether some other mechanism such as turbulent scattering is involved.

9-10 It is instructive to compare the estimates in (31) above, in which real-gas effects are accounted for, with the values obtained by considering classical and rotational absorption alone. The rise time in the latter case would be

$$t_r = \frac{8}{\gamma + 1} \frac{\mu'}{\Delta p} \quad (\text{modified Taylor rise time}), \quad (32)$$

where  $\mu'$  is the equivalent longitudinal viscosity  $\mu(4/3 + (\gamma-1)/Pr) + \mu_v$ , and  $\mu_v$  is the bulk viscosity representing rotational relaxation in air [5]. Equation (32) gives (5°C, 1 atm)

$$\begin{aligned} \Delta p = 5 \text{ Pa, vibrational relaxation neglected: } t_r &\approx 0.03 \text{ ms} \\ \Delta p = 35 \text{ Pa, " " " : } t_r &\approx 0.004 \text{ ms.} \end{aligned} \quad (33)$$

Comparison of estimates (31) and (33) illustrates the importance of accounting for vibrational relaxation; the classical/rotational rise times are too small by a factor of order 10 to 100 for such weak shocks.

A final comment on equation (30) is required concerning the shock development distance. The rise time given by (30) refers to the asymptotic steady-state shock waveform; but development of such a waveform from an initially discontinuous pressure jump, for example, involves spatial diffusion over a region of thickness  $\Delta \sim c_0 t_r$ . Taking as a measure of the diffusion velocity the difference in sound speeds,  $(c_f - c_0)$ , gives the diffusion time scale as  $t_d \sim \Delta / (c_f - c_0)$ . Thus the shock development distance ( $x_d = c_0 t_d$ ) is of order

$$x_d \sim c_0^2 t_r / (c_f - c_0) = \frac{8}{\pi} \lambda_r \left( \frac{\gamma}{\gamma + 1} \right) \left( \frac{\Delta p}{p_0} \right)^{-1}, \quad (34)$$

where  $\lambda_r = c_0 / f$  is the wavelength at the relaxation frequency of the dominant vibrational mode. Equation (34) predicts very large development distances for very weak ( $H_2$ -dominated) shocks; thus for the 5 Pa shock considered above,  $x_d$  is around 30 km. Such large development distances clearly cannot be calculated properly without taking account of the way the atmosphere varies with altitude; nevertheless equation (34) - which is supported by numerical calculations in [27] - is useful for indicating orders of magnitude.

## 6.2 Continuous wave propagation and spectral energy transfer

We conclude this section by examining the combined effects of dissipation and weak nonlinearity on continuous waves (i.e. waves which are statistically stationary in time, or approximately so). Of particular interest is the influence of nonlinearity on the power spectrum of the signal; as the waveform distorts, we expect sum and difference frequencies to appear, and in the case of a peaked spectrum (such as jet noise) nonlinearity will cause a transfer of energy from the peak frequency region to lower and higher frequencies.

The governing equation in the frequency domain is a modified Burgers equation, which for plane (one-dimensional) waves takes the form

$$\frac{\partial \tilde{p}}{\partial x} + \alpha' \tilde{p} = \frac{1}{2} i \omega c \tilde{q} \quad (x \text{ is the coordinate in the propagation direction}). \quad (35)$$

The Fourier-transformed variables ( $\tilde{p}$ ,  $\tilde{q}$ ) are related to the time-domain variables ( $p$ ,  $q$ ) by

$$\tilde{f}(x, \omega) = \frac{1}{2\pi} \int_0^T f(x, t') \exp(-i\omega t') dt' \quad (t' = t - x/c_0),$$

$$\text{i.e. } \tilde{f}(x, \omega) = \exp(i\omega x/c_0) \cdot \frac{1}{2\pi} \int_{x/c_0}^{x/c_0+T} f(x, t) \exp(-i\omega t) dt. \quad (36)$$

The sample length  $T$  is chosen large enough to give adequate frequency resolution of the signal. Other symbols are defined as follows:

$q = p^2(x, t)$  square of the pressure signal

$\alpha' = (\alpha - i\omega)$  complex coefficient representing frequency-dependent attenuation and dispersion

$c = \frac{1}{2}(\gamma + 1)/\rho_0 c_0^3$  nonlinearity coefficient.

An equation for the power spectral density of the pressure signal is obtained by multiplying equation (35) by the complex conjugate  $\tilde{p}^*$  and taking the real part of the result. Ensemble averaging and dividing by  $T$  gives [30]

$$\frac{d}{dx} (e^{2\alpha x} S_p) = -c \omega e^{2\alpha x} Q_{pq}, \quad (37)$$

where  $S_p$  is the power spectral density of  $p$  at any point, and  $Q_{pq}$  is the imaginary part of the cross-spectral density of  $p$  and  $p^2$ . Note that dispersion, although allowed for, does not appear explicitly in this result.

Equation (37) describes the spectral transfer process in statistical terms, for plane propagating waves. The corresponding equation for spherically spreading waves is

$$\frac{d}{dr} (r^2 e^{2\alpha r} S_p) = -c \omega r^2 e^{2\alpha r} Q_{pq} \quad (r = \text{distance from origin}). \quad (38)$$

Note that in the small-amplitude limit, the  $Q_{pq}$  terms on the right of equations (37) and (38) become negligible; the equations then reduce to the well-known linear forms. Direct measurement of the right-



16. F.D. SHIELDS and H.E. BASS 1977 NASA CR-2760. Atmospheric absorption of high frequency noise and application to fractional-octave bands.
17. J.B. CALVERT, J.W. COFFMAN and C.W. QUERFELD 1966 Journal of the Acoustical Society of America 39, 532-536. Radiative absorption of sound by water vapour in the atmosphere.
18. P.W. SMITH Jr. 1957 Journal of the Acoustical Society of America 29, 693-698. Effect of heat radiation on sound propagation in gases.
19. S. TEMKIN and R.A. DOBBINS 1966 Journal of the Acoustical Society of America 40, 317-324. Attenuation and dispersion of sound by particulate-relaxation processes.
20. C.L. MORFEY 1968 Journal of Sound and Vibration 8, 156-170. Sound attenuation by small particles in a fluid.
21. F.E. MARBLE 1969 Astronautica Acta 14, 585-614. Some gasdynamic problems in the flow of condensing vapors.
22. F.E. MARBLE and D.C. WOOTEN 1970 Physics of Fluids 13, 2657-2664. Sound attenuation in a condensing vapor.
23. F.E. MARBLE 1970 Annual Review of Fluid Mechanics 2, 397-446. Dynamics of dusty gases.
24. J.E. COLE and R.A. DOBBINS 1970 Journal of the Atmospheric Sciences 27, 426-434. Propagation of sound through atmospheric fog.
25. J.E. COLE and R.A. DOBBINS 1971 Journal of the Atmospheric Sciences 28, 202-209. Measurements of the attenuation of sound by a warm air fog.
26. G.A. DAVIDSON 1975 Journal of the Atmospheric Sciences 32, 2201-2205. Sound propagation in fogs.
27. N.H. JOHANNESEN and J.P. HODGSON 1979 Reports on Progress in Physics 42, 629-677. The physics of weak shock waves in gases.
28. J.P. HODGSON and N.H. JOHANNESEN 1971 Journal of Fluid Mechanics 50, 17-20. Real-gas effects in very weak shock waves in the atmosphere and the structure of sonic bangs.
29. J.E. FLOWERS WILLIAMS and M.S. HOWE 1973 Journal of Fluid Mechanics 58, 461-480. On the possibility of turbulent thickening of weak shock waves.
30. G.P. HOWELL 1978 M.Sc. dissertation, Institute of Sound and Vibration Research, University of Southampton. Finite-amplitude noise propagation: the virtual source approach.
31. J. GALLARD and C. GOWER 1978 British Aerospace (Weybridge) Acoustic Report 554. Study of the attenuation of sound in the atmosphere using existing in-flight aircraft noise data.
32. E.H. BROWN and S.F. CLIFFORD 1976 Journal of the Acoustical Society of America 60, 788-794. On the attenuation of sound by turbulence.
33. E.H. BROWN and F.F. HALL 1978 Reviews of Geophysics and Space Physics 16, 47-110. Advances in atmospheric acoustics.
34. P.K. KASPER, R.S. PAPPAS, L.R. KEEFE and L.C. SUTHERLAND 1975 NASA CR-2617. A study of air-to-ground sound propagation using an instrumental meteorological tower.
35. A.D. PIERCE 1968 Journal of the Acoustical Society of America 44, 1052-1061. Spikes on sonic-boom pressure waveforms.
36. A.D. PIERCE 1971 Journal of the Acoustical Society of America 49, 906-924. Statistical theory of atmospheric turbulence effects on sonic-boom rise times.
37. H.S. RIBNER, P.J. MORRIS and W.H. CHU 1973 Journal of the Acoustical Society of America 53, 926-928. Laboratory simulation of development of superbooms by atmospheric turbulence.



## EXPERIMENTAL MEASUREMENTS OF MOVING NOISE SOURCES

by

L. Maestrello and T. D. Norum  
 NASA Langley Research Center  
 Hampton, Virginia 23665

SUMMARY

This report presents results of the far-field pressures measured from three different types of moving sources. These acoustic sources consist of a point monopole, a small model jet, and an aircraft. Results for the pressure time history produced by the point source show good agreement with those predicted analytically. Both actual and simulated forward motion of the model jet show reductions in noise levels with forward speed at all angles between the source and observer. Measurement with the aircraft over both an anechoic floor and over the ground yields a method for evaluating the transfer function for ground reflections at various angles between the moving aircraft and measurement position.

INTRODUCTION

This report discusses three types of experiments on moving noise sources and the interpretation of the measured far-field pressures. The experiments consist of i) a point source moving above a finite impedance reflecting plane, ii) a model jet in actual and simulated forward motion, and iii) an airplane flyover with and without ground reflection effects. This work is an integral part of a prediction scheme for the effects of forward motion on noise radiation. From the practical point of view, one must account for the effects of motion of the sources and their location relative to nearby scattering surfaces.

In section I, preliminary information on the motion of noise sources is obtained by looking at the simplest source, the point monopole (Ref. 1). The experiment is carried out using a small monochromatic source which behaves like an acoustic monopole when stationary. The purpose of this experiment is to determine the behavior of the source when in motion at constant speed.

There are different types of sources that radiate in the same manner in a stationary medium but radiate differently when in motion. The present experimental source consists of a time rate of introduction of mass, so it should behave like an acoustic monopole in the wave equation for the velocity potential. The experiment was designed to determine if motion yields the expected changes in source directivity.

The source was positioned above an automobile via a guy wire supported mast. The automobile was driven at constant speeds over an asphalt surface past a stationary microphone. The resulting measured time histories were then compared to analytical computations of a monopole moving above a finite impedance reflecting plane.

Section II reports experiments of a model jet in both actual and simulated motion (Ref. 2). The model nozzle was first mounted above the same automobile used in the experiments reported above. The vehicle was again driven past stationary microphones in order to quantify the effects of motion on jet mixing noise. The nozzle was then tested in an anechoic environment with a free jet simulating the forward motion. The results of these two methods of obtaining forward speed effects on jet noise are compared.

In section III, tests conducted using an airplane (a T-38 NASA trainer vehicle) are reported. Measurements were taken over an anechoic floor as well as over the ground, and auto-correlations of these measurements were obtained for short time intervals corresponding to a particular position of the aircraft. These show the direct signal for the microphone over the anechoic floor as well as a combination of the direct and reflected signals for the microphone above the ground.

The simultaneous processing of the signals received by the two microphones permits one to determine the transfer function of the surface for a large range of frequencies and source positions. This approach will permit correction of flyover spectra for contamination by ground reflections.

The results of these three tests are presented and discussed together with recommendations for future work.

I. POINT SOURCE IN MOTION

The experiment was conducted by placing a point source above an automobile, and driving it over an asphalt surface past sideline microphones. An analysis for an acoustic monopole moving above a reflecting plane was made and results from the experiment and analysis are compared for different forward speeds.

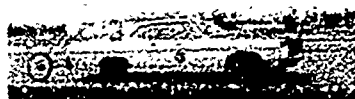
A. Description of Experiment

The experimental source consisted of a 50 watt acoustic driver necked down to a 1.52 cm diameter tubular opening. When driven by an oscillator at a discrete frequency, the output of this source consists of tones at the oscillator frequency and its harmonics. By appropriate filtering, the measured signal consists essentially of a discrete frequency.

The source was positioned 7.9 m from the ground above an automobile via a guy wire supported mast (Fig. 1). An oscillator located in the trunk of the vehicle excited the source at a frequency of either 1230 Hz or 2310 Hz. The automobile was driven at constant speeds ranging from 13.4 to 44.7 m/s which were recorded on a strip chart within the vehicle. Sideline microphones were located at a closer approach distance of 11.0 m and positioned 3.05 m and 6.10 meters from the ground surface. The experiment was performed on an aircraft runway consisting of a 16.5 cm asphalt surface on top of a concrete foundation.

POINT SOURCE

Figure 1.- Moving point source experiment.



The pressure signals were measured with 1.3 cm diameter condenser microphones and recorded on magnetic tape. In both the recording and reproduction stages the data were passed through a band pass filter set to pass all the frequency components possible due to the Doppler effect on the oscillator frequency. The analog tapes were digitized at the rate of 10,000 points per second.

The oscillator frequency was set to an accuracy of  $\pm 1$  Hz. Vehicle speed varied by no more than  $\pm 0.5$  m/s over the test zone. The frequency response of the recording and analysis system was estimated to be flat within  $\pm 0.5$  dB over all frequencies of interest.

#### D. Analysis

For the monopole of angular frequency  $\omega$  and strength  $q_0$  moving with constant velocity  $U$  in the  $x$  direction at a distance  $h$  above the  $x$ - $z$  plane (Fig. 2), the propagation is governed by:

$$\nabla^2 \psi(x, y, z, t) = -q_0 e^{-i\omega t} \delta(x-Ut) \delta(y-h) \delta(z) \quad (1)$$

where  $\nabla^2$  is the wave operator,  $\nabla^2 = \frac{\partial^2}{\partial x^2} + \frac{\partial^2}{\partial y^2} + \frac{\partial^2}{\partial z^2}$ , and  $\psi$  is the acoustic velocity potential. Specifying the  $x$ - $z$  plane to be a locally reacting surface of normal impedance  $Z$ , the velocity potential must satisfy the condition:

$$\frac{1}{c} \frac{\partial \psi}{\partial t} - Z \frac{\partial \psi}{\partial y} = 0 \quad \text{at } y = 0 \quad (2)$$

where  $Z = \zeta/\rho c$  and  $\rho c$  is the acoustic impedance of air.

Through the use of a Lorentz transformation and a subsequent Fourier transformation on the spatial variables, the solution valid at a sufficient distance above the plane is

$$\psi(x, y, z, t) \approx (q_0/4\pi) e^{-ik_Y^2(ct-Mx)} (e^{ik_Y^2 R_1/R_1} + C_R e^{ik_Y^2 R_2/R_2}), \quad (3)$$

where

$$R_1 = [(x - Mct)^2 + ((y - h)/\gamma)^2 + (z/\gamma)^2]^{1/2}, \quad (4a)$$

$$R_2 = [(x - Mct)^2 + ((y + h)/\gamma)^2 + (z/\gamma)^2]^{1/2}, \quad (4b)$$

$$C_R = \frac{Z(y + h) - \gamma^2(R_2 + M(x - Mct))}{Z(y + h) + \gamma^2(R_2 + M(x - Mct))}. \quad (4c)$$

Note that if the Mach number  $M$  is set equal to zero the solution reduces to that for the stationary source (Ref. 3) with the reflection coefficient given by

$$C_R = (Z \cos \alpha - 1)/(Z \cos \alpha + 1), \quad (5)$$

where  $\alpha = \cos^{-1}[(y + h)/(x^2 + (y + h)^2 + z^2)^{1/2}]$  is the angle of incidence. This stationary source solution is stated in reference 3 to be a very good approximation as long as the observer is not closer than a half-wavelength to the boundary surface.

Hence, in addition to the well-known convection effects on the form of the direct and reflected waves, source motion introduces a convection term into the reflection coefficient. This convection term in Eq. (4c) is seen to be more important for small values of impedance and large incidence angles (small grazing angles), and increases in significance as the source velocity increases.

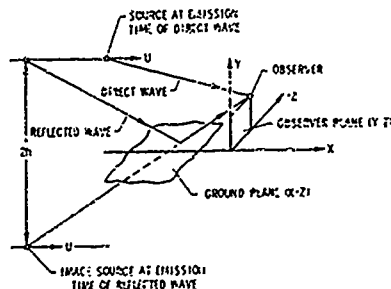


Figure 2.- Source moving at constant velocity above a ground plane.

The acoustic pressure is obtained in the usual manner from the velocity potential by

$$p(x, y, z, t) = -\rho \frac{\partial \psi(x, y, z, t)}{\partial t} \quad (6)$$

### C. Results and Comparisons

To investigate the effects of motion on the experimental point source and the extent to which the observed signal can be predicted analytically, various comparisons of the time histories were made. These comparisons are shown in figures 3-5, in which the mean square pressure in dB is plotted against the normalized time  $Ut/\sigma$ , where  $U$  is the source velocity and  $\sigma$  is the closest approach distance. The analytical mean square pressure was computed at discrete points in time from Eq. (6), whereas the experimental values were obtained by averaging the digitized data over a time interval corresponding to a given increment in the source travel distance. The comparisons below include the effect of analysis time on the perceived results and the effects of varying source velocity and observer height.

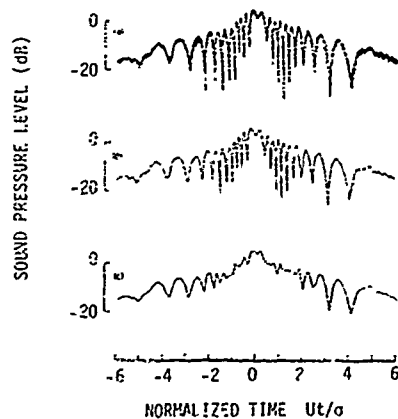


Figure 3.- Effect of analysis time on experimental noise-time history. Source frequency  $F = 1230$  Hz; source velocity  $U = 13.4$  m/s; observer height  $h = 3.05$  m; analysis time: (a) 1.52 cm/point, (b) 10.7 cm/point, (c) 152 cm/point

To see the effect of analysis time on the observed signal, one of the experimental time histories was analyzed using three different analysis times. In figure 3a, each plotted point corresponds to 1.52 cm of source travel distance (1.52 cm/point), whereas 10.7 cm/point and 152 cm/point were used in figure 3b and 3c, respectively. Each of the first two curves show the pattern of alternate reinforcements and cancellations caused by the reflected wave, although the magnitudes of the cancellations are seen to differ by as much as 10 dB between the two curves. (The same phenomena was obtainable with the theoretical results when different time intervals between computed points were used.) This not unexpected fact illustrates that little information about the reflected wave from an acoustically hard surface can be obtained from a consideration of the magnitude of the cancellations. Figure 3c shows that the details of the reflection process are lost if the analysis time is not chosen small enough.

A comparison of the theoretical and experimental results is given in figure 4 for the two different observer heights. The time interval between computed points for all the theoretical curves presented was chosen to correspond to 10.7 cm/point. Superimposed on each of these curves is the signal that would be received in the absence of the ground surface, obtained by using a value of zero for the reflection coefficient. The value chosen for the normalized ground impedance in the theoretical curves was  $Z = 4 - i4$ , a value indicative of a fairly hard ground surface. One can see a good agreement between the curves both in shape and in the time intervals between the alternate reinforcements and cancellations. Decreases in the time interval between successive reinforcements and cancellations are seen to occur in both the theoretical and experimental results with increasing ground to observer distance.

10-4 The effect of source velocity can be seen in figure 5. Since the time axis has been normalized by using the velocity, the shapes of the observed signal are the same. (The erratic nature of the experimental curves with increasing velocity is due to a smaller analysis time being used as the velocity increases.)

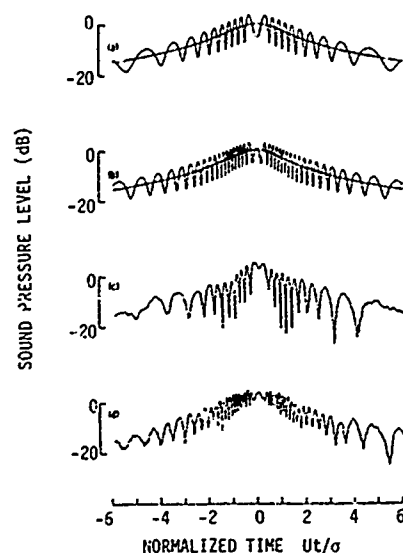


Figure 4.- Variation of theoretical and experimental noise-time histories with observer height. Source frequency  $F = 1230$  Hz; source velocity  $U = 13.4$  m/s; impedance  $Z$  for computed curves  $= 4 - i4$ ; observer height  $h$ : (a) 3.05 m (computed); (b) 6.10 m (computed); (c) 3.05 m (measured); (d) 6.10 m (measured).

Many of the above results are qualitatively predictable from a simple consideration of the time and length scales involved. The purpose of the comparisons presented is to show the good agreement in the shapes of the experimental and theoretical results. This agreement gives credence to the assumption that the experimental source indeed radiates in the same manner as a theoretical monopole in motion.

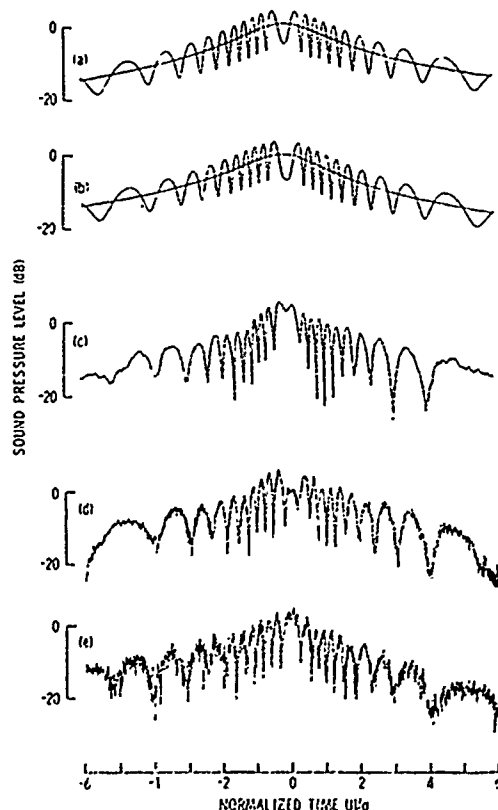


Figure 5.- Variation of theoretical and experimental noise-time histories with source velocity. Source frequency  $F = 1230$  Hz; observer height  $h = 3.05$  m; impedance  $Z$  for computed curves  $= 4 - i4$ ; source velocity  $U$ : (a) 13.4 m/s (computed); (b) 35.7 m/s (computed); (c) 13.4 m/s (measured); (d) 22.3 m/s (measured); (e) 35.7 m/s (measured).

## II. MODEL JET IN ACTUAL AND SIMULATED MOTION

The model nozzle was mounted above the automobile in the same manner as the point source and driven past fixed microphones. The nozzle was then mounted in a anechoic facility inside a large free jet simulating the forward motion. These two methods of obtaining forward speed effects on jet mixing noise are compared. 10-5

### A. Tests with the Vehicle

The noise generated by the automobile in motion was estimated from the test discussed in section I. Since the vehicle noise is predominantly low frequency, a high pass filter can be used to suppress much of this background noise. This necessitates the use of a high speed, small diameter jet to maintain the spectral peak of the jet noise above the low frequency cutoff. Hence a 2.54 cm exit diameter nozzle run at a nominal Mach number of 0.85 was chosen along with a 500 Hz high pass filter. Since the spectral peak of jet noise corresponds to a Strouhal number near 0.25, this peak should then occur around 3 kHz.

A more obvious reason for the high jet exit velocity was to obtain jet noise levels above that of the vehicle noise throughout most of the spectra. Also, the high jet levels assured minimum contamination from upstream valve noise.

The nozzle flow was provided by a high flow accumulator filled with nitrogen and mounted in the trunk of the vehicle. The gas passed through a long supply tube to the nozzle exit. For the chosen exit Mach number of 0.85, between 2 and 3 seconds of constant mass flow could be obtained from this system.

Both the nozzle and microphones were positioned approximately 7.6 m (25 ft.) above the ground and the closest approach distance between vehicle and microphones was about 11 m.

The test vehicle was driven over an asphalt surface past six sideline microphones at a constant speed within the test section. The microphones were positioned at 2 m intervals parallel to the path of the vehicle. Since the nozzle supply system was limited to about 2.5 seconds, measurements at all angles of interest could not be obtained during a single run. Hence each run was set up to obtain data for a single nozzle to microphone emission angle. The vehicle position with respect to the microphones was determined by long metal strips that functioned as electrical switches. These were placed perpendicular to the path of the vehicle and activated by its tires. The signals produced by these switches were recorded along with the microphone signals. Each microphone signal was analyzed only over 3 m of vehicle motion such that the midpoint of the signal corresponded to the desired nozzle-microphone angle at the emission time. Vehicle background noise was measured using the same procedure without the jet activated.

Static jet noise data at each emission angle were obtained from two of the six microphones, with the stationary vehicle positioned such that the two microphones were located at the extreme angles of the corresponding motion run.

Five discrete nozzle-microphone emission angles were tested, equally spaced from  $30^\circ$  to  $150^\circ$ . Vehicle Mach numbers of 0, 0.04, 0.08, and 0.12 were run at all five angles, with the exception that data were not obtained at the two upstream angles at the highest speed due to a significant masking of the jet signal by the vehicle noise. Each test condition (corresponding to a given vehicle speed and angle) was repeated a number of times, resulting in at least 2 seconds of data per condition.

Power spectral densities (PSD's) were obtained from the measurements using a constant bandwidth filter of 72 Hz over the range 500 Hz to 20 kHz. Each acceptable data segment was analyzed and those corresponding to a given test condition averaged.

The PSD's for all test conditions at a nozzle-microphone angle of  $30^\circ$  are shown in figure 6. The background vehicle noise (jet-off condition) is shown as the continuous traces in the lower part of the figure. Data at the highest speed in the frequency region near 4.5 kHz are not shown since this region was contaminated by background noise due to aeolian tones caused by the guy wires supporting the nozzle supply tube.

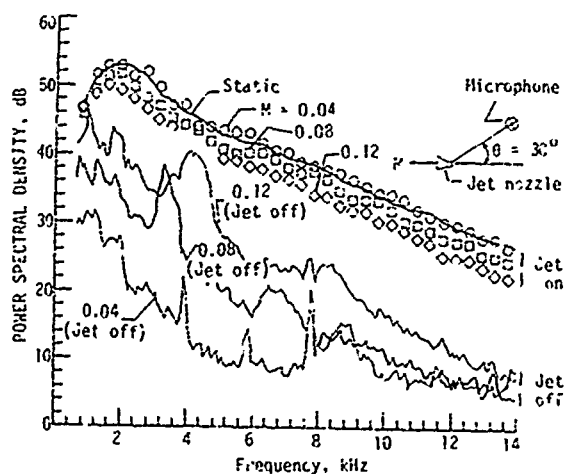


Figure 6.- Measured power spectral densities for jet and vehicle noise at  $30^\circ$  emission angle.

There is no discernable difference between the static and motion spectrum at the lowest vehicle speed. At the higher speeds, however, a level difference can be noticed over almost the entire spectrum, this difference increasing as the vehicle speed is increased. Also noted is the expected Doppler shift of the peak frequency to lower values with increasing speed.

This decrease in level across the spectrum with increasing forward speed was obtained at all angles. Details of these results can be found in reference 2.

Since portions of the measured PSD's were contaminated by background noise, the overall sound pressure levels (OASPL) were estimated from the uncontaminated portions of the spectra. The estimated OASPL's are shown in figure 7 along with the results computed from the contaminated PSD's. It can be seen that there is a consistent decrease in the estimated OASPL with increasing forward velocity at all nozzle-microphone emission angles, as one would expect from the spectral results mentioned above.

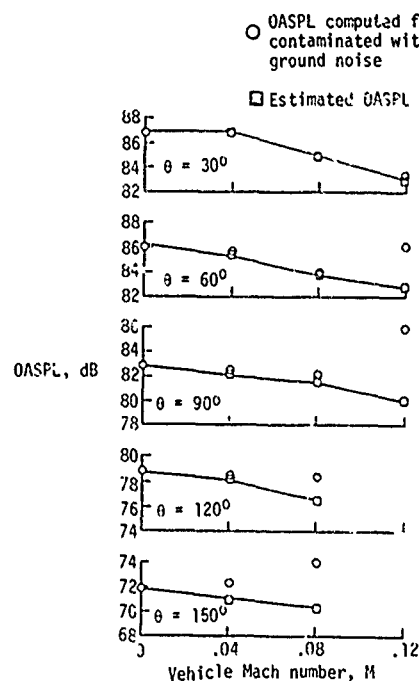


Figure 7.- Variation of overall sound pressure level with forward velocity. (Moving vehicle tests.)

#### B. Tests with the free jet

The free jet used to simulate forward motion was limited to a maximum Mach number of 0.11. Positioning of the jet in the anechoic chamber restricted measurements in the upstream direction to 120°. Other than these limitations, test conditions with the vehicle were repeated using the free jet. Air was used instead of pure nitrogen for the model jet.

The free jet exhausted vertically from a 1.2 m diameter nozzle into an anechoic environment. The 2.5 cm jet nozzle was positioned at the center of the free jet. A 1.3 cm (half-inch) condenser microphone designed for free-field linear response past 20 kHz was located on a boom that traversed an arc about the center of the model nozzle exit plane on a 3.7 m radius.

With the model jet maintained at a Mach number of 0.85 the free jet was run at the static case (no flow), and Mach numbers of 0.04, 0.08, and the maximum available, 0.11. For each test condition the microphone was held stationary at discrete angles from the downstream centerline ranging from 30° to 120°.

The noise generated above 500 Hz by the free jet was insignificant at all test conditions. Hence, the problems associated with background noise present in the vehicle tests were nonexistent during the tests with the free jet. However, the presence of the free jet shear layer requires corrections to correlate noise emission angle with observer angle.

Acoustic pressure power spectral density measurements using 400 Hz bandwidth are shown in figure 8 for the test conditions corresponding to an observer angle of 90°, the angle where the shear layer corrections are a minimum. One can make here the same observation as with the vehicle test—relative motion tends to decrease the jet noise level throughout the spectrum.

The true emission angles corresponding to the measured results were computed in the standard manner (c.f. ref. 4) under the assumption that the noise originates at the nozzle exit. (Amplitude corrections due to the shear layer were found to be less than 0.5 dB for all test conditions and hence were neglected.) The measured OASPL is given in figure 9 as a function of the computed emission angle. Again, a decrease in the OASPL is observed at all angles with increasing forward speed.

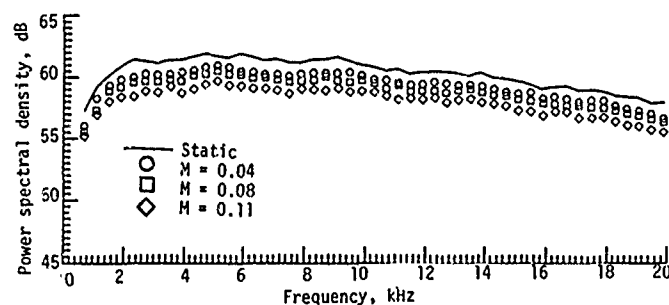


Figure 8.- Power spectral densities from free-jet at 90° observer angle.

#### C. Comparisons Between Vehicle and Free Jet Results

The difference in sound pressure level between static and motion conditions is generally correlated against the ratio of jet velocity to relative velocity (the difference between jet and forward velocities). This type of comparison should yield consistent results for flight simulation studies (free jet or wind tunnel) since there is no relative motion between the jet and the observer. However, in actual flight the Doppler effect results in a frequency shift of the entire spectrum, so this type of comparison (particularly when done on a frequency-by-frequency basis) can be misleading. Nevertheless, in order to reassert the main findings of this report in a fashion that is commonly presented, the static-to-motion OASPL differences are given in figure 10 as a function of  $10 \log M_j/M_{rel}$  for both series of tests. The effects due to convection that are sometimes subtracted from the OASPL differences before this type of correlation is made (ref. 4) were computed to be less than 0.4 dB for all test conditions and hence were neglected.

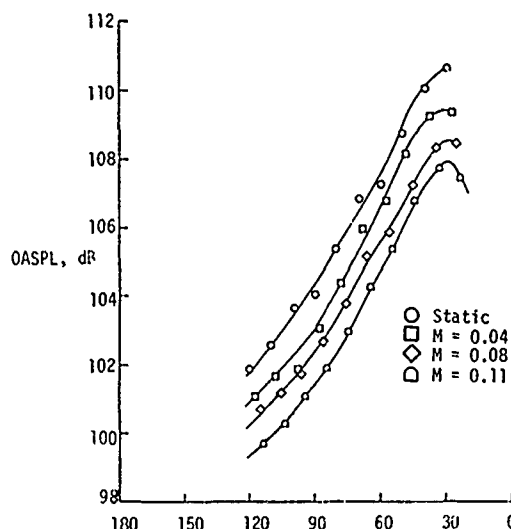


Figure 9.- Overall sound pressure levels including angular refraction correction. (Free-jet tests.)

The uncertainty due to the procedure used in estimating the OASPL for the vehicle tests leads to the considerable scatter shown in figure 10. The relative velocity exponent  $m$  lies somewhere between 3 and 6. The data uncertainty as well as the test limitations of high jet velocity/low forward speed prevent a reasonable estimate of this exponent or its variation with emission angle. Nevertheless, an increase in noise reduction with increasing forward speed is again clearly indicated at all angles at these low velocities for both testing methods.

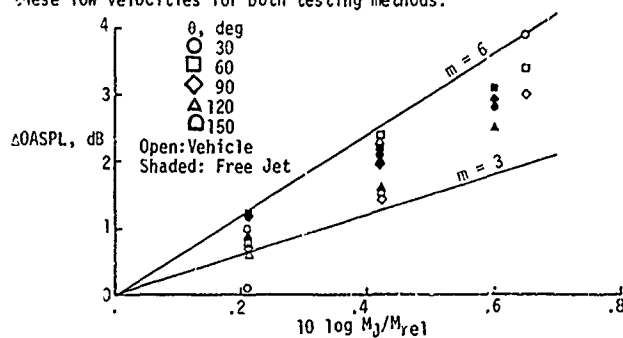


Figure 10.- Change in overall sound pressure level between static and motion conditions.

### 10-8 III. AIRCRAFT FLYOVER MEASUREMENTS

To better estimate the effect of forward motion on real engine noise, flight experiments were conducted using an actual aircraft. There are considerable difficulties to overcome before interpreting the far field data from a full scale aircraft in flight. Existing studies on forward flight have yet to address these difficulties but have concerned themselves with more obvious practical prerequisites. Since the results of aircraft flyovers are still dubious, it becomes important to establish exact techniques to quantize the sound field from a moving aircraft. This section focuses on one of the fundamental measurement problems, ground reflections. Measurements of the far field pressure from an airplane flyover were taken over both an anechoic floor and over the ground. A method is presented for evaluating the transfer function of the ground surface, which can be used for correcting data contaminated by ground reflections. These corrections are independent of the source, but depend on the geometrical orientation between the sources and observer as well as on the distance from the microphone to the ground surface.

#### A. Method of Measurements

Since the objectives of this test were to separate the effects of reflection and to establish the properties of the reflecting surface, microphones were located over both an anechoic floor and a reflecting ground. The anechoic floor is shown in Figure 11. It consists of a semicircular surface with a radius of 12.2 m composed of anechoic wedges of size 0.3 x 0.3 x 0.9 meters. The wedges are placed one meter above the ground and supported by wire mesh.

Four equally spaced microphones were placed over the anechoic floor, and an additional four over the ground (Fig. 12). The microphones were oriented along the direction of the flight path at a height of 3.36 m above the ground. The ground surface consists of packed turf, typical of surfaces used in aircraft flyover noise test. All the microphones are recorded simultaneously on magnetic tape recorder so that the measurements over the anechoic floor and over the ground surface were taken at the same time. The aircraft used was a NASA T-38 airplane (Fig. 13). One of the interesting features of this aircraft is that the two jets exhaust at the rear end of the fuselage, thus concentrating the emission over a small area. The test was conducted at an altitude of  $h = 305$  meter at velocity of  $V_f = 105$  m/sec.



Figure 11.- Outdoor anechoic test facility

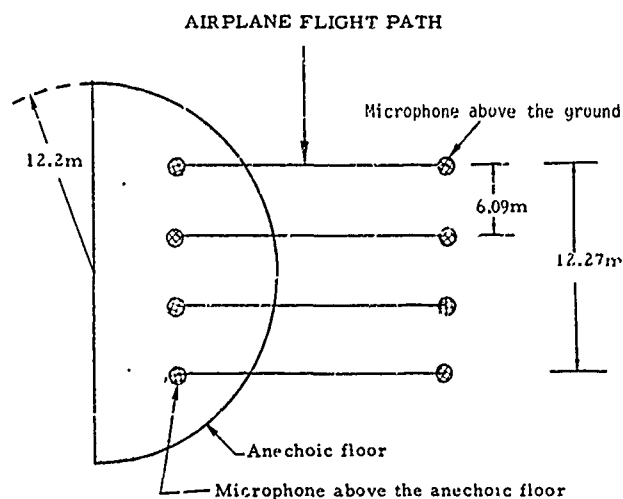


Figure 12.-Microphones positions above the anechoic floor and above the ground



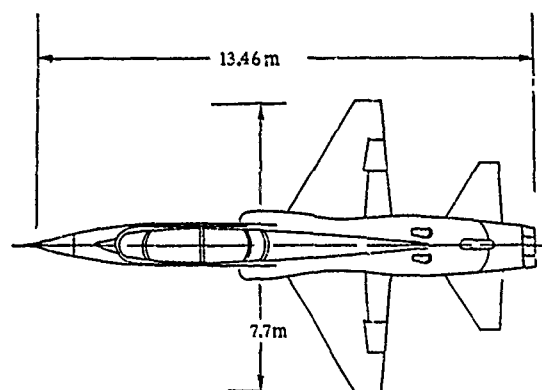


Figure 13.- Geometry of T-38 airplane

## B. Results and Discussion

The data collected in one flyover was recorded over the time period of 14 seconds. During this time the aircraft moved over a  $140^\circ$  arc with respect to the reference microphone. Seven auto-correlations were obtained, each over one record time interval, centered at the angles  $\theta = 36^\circ, 55^\circ, 90^\circ, 124^\circ, 144^\circ, 156^\circ$ , and  $160^\circ$  (Fig. 14). The overhead position of the aircraft ( $90^\circ$ ) is chosen as reference, such that at  $\theta = 36^\circ$  the airplane is four seconds ahead of the reference, and at  $\theta = 160^\circ$  is eight seconds past the reference.

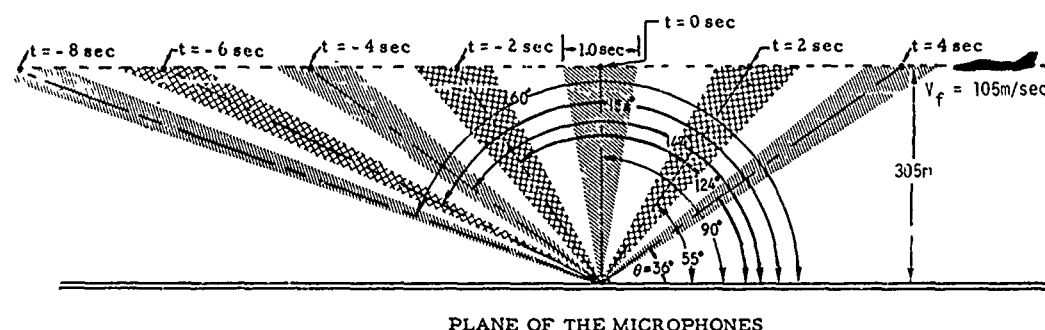


Figure 14.- Positions of the aircraft for data analysis

The auto-correlations taken over the anechoic floor are smooth while those taken over the ground contain a second peak (Figs. 15 and 16). The time delay of this peak depends on the position of the aircraft with respect to the microphone and is associated with the retarded time between the incident and reflected signals. At  $\tau = 0$ , the auto-correlation measured over the ground consists of the direct signal and the reflected signal that was emitted at an earlier time, whereas the second peak at the time delay  $\tau_0 = \pm 2h \sin \theta / c$  consists of the correlation of the direct signal with itself after reflection.

In order to separately resolve the two peaks, the time delay of the secondary peak must be large in comparison with the correlation time scale of the direct signal. The measured signal can also be deconvoluted in the frequency domain, since the auto-correlation can be interpreted as the convolution of the transforms of both direct and reflected signals (See Ref. 4).

The position of the aircraft was determined from the auto-correlations over the ground. Notice that the time delays of the secondary peaks in Figure 16 increase from  $\theta = 36^\circ$  to  $90^\circ$  and then decrease again as the angle becomes larger than  $90^\circ$ , as expected from the expression relating  $\tau_0$  to  $\theta$ . Use of this expression along with the measured value of  $\tau_0$  then yielded the aircraft position (i.e.,  $\theta$ ) at the emission time of the direct signal. In addition to using the auto-correlation to determine the position of the aircraft, the cross correlation between two adjacent microphones can also be used to estimate the speed of the aircraft.

The main objective of this experiment, however, is the evaluation of the transfer function ( $T$ ) of the reflected signal from the surface. This function is defined as the ratio between the spectrum measured over the ground ( $S_g$ ) to that measured over the anechoic floor ( $S_a$ ) over the same time interval, and depends on the angle  $\theta$ , the distance of the microphone from the ground ( $h$ ), and frequency.

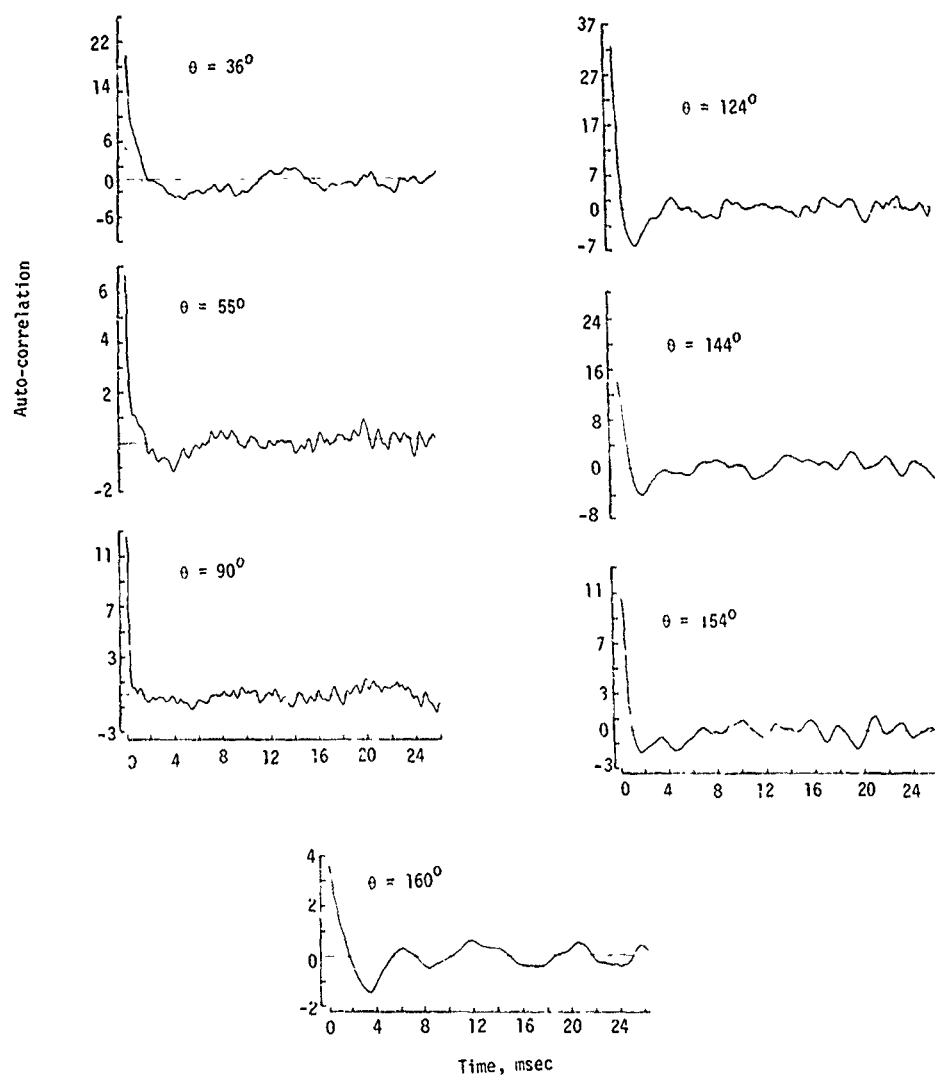


Figure 15.- Unnormalized auto-correlations over the anechoic floor.

Computed results of this transfer function are shown in Figure 17 for three different values of  $\theta$ . The oscillatory behavior is due to the fact that the spectra from which the transfer function was derived are themselves not smooth because of the short averaging time necessitated by the motion of the source. Also, the nature of reflections leads to non-smooth spectra measured over the ground. However, for the practical purpose of correcting the ground spectrum for reflections, the transfer function can be averaged as shown by the smooth lines in Figure 17. These curves show that the corrections needed for ground reflections spread out in frequency as the source approaches the overhead position.

Using the average spectrum of the transfer function, the ground spectrum for  $\theta = 36^\circ$  was corrected and shown in Figure 18 along with the two corresponding measured spectra. As can be seen from this figure, the spectrum corrected for ground reflections by the transfer function agrees well with the spectrum measured over the anechoic floor.

Pursuing ground reflection corrections utilizing the transfer function approach rather than the more common ground impedance measurements is certainly easier and more practical for any engineering approach. Measurements of surface impedance are known to be difficult and even at the present time these data are ambiguous and incomplete. In addition, discrete frequency measurements of surface impedance yields large scatter in results. The transfer function approach instead uses frequency bands so that oscillations are not as pronounced. Also, from the engineering approach it is easy to understand and simple to apply.

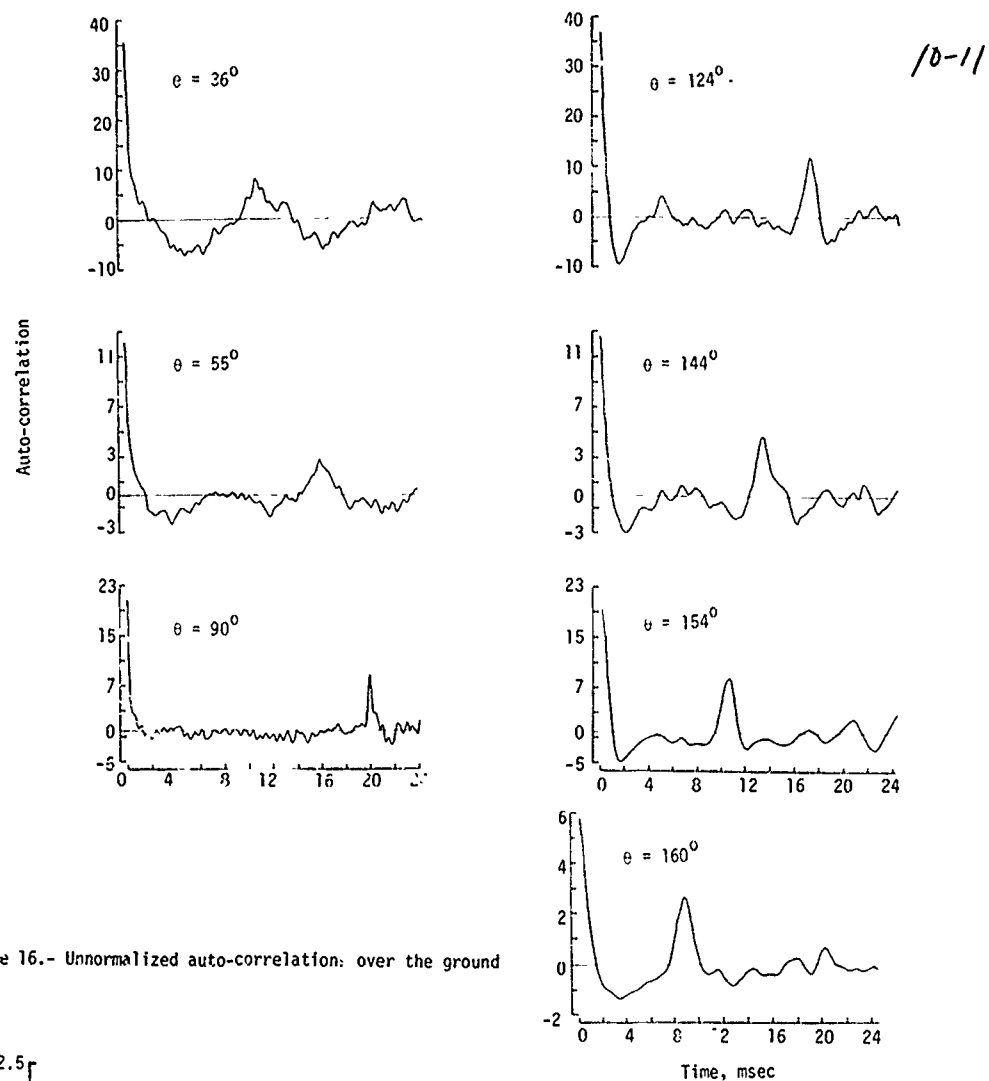


Figure 16.- Unnormalized auto-correlation: over the ground

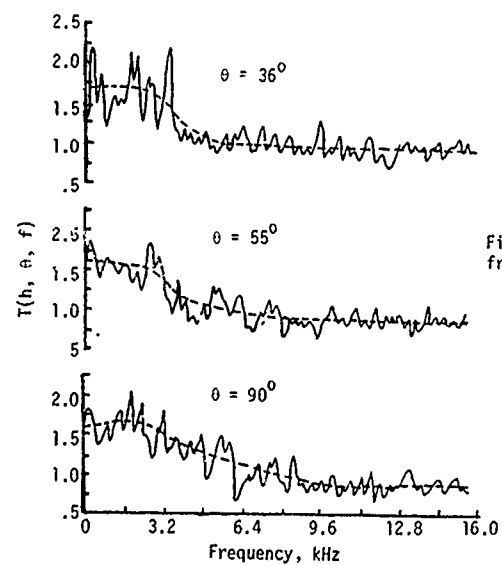


Figure 17.- Transfer function of the reflected signal from the surface of three different values of  $\theta$ .

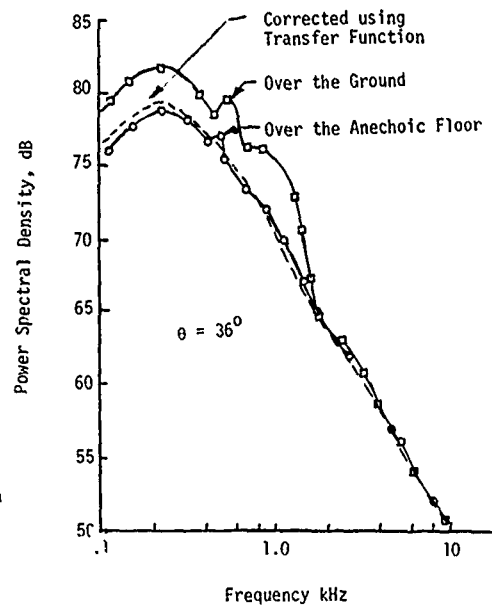


Figure 18.- Acoustic Spectra

CONCLUDING REMARKS

Experiments were conducted with three different types of noise sources in motion. A discrete frequency point source moving over a reflecting surface yields results that agree with those predicted analytically. Measurements of a model jet in actual and simulated forward motion both show that the noise decreases with increasing speed at all observation angles. The fact that observed effects in flight testing of actual jet engines do not appear in these model jet tests suggest that the flight data includes installation effects and, or sources other than pure jet mixing noise. Auto-correlations from noise measurements of an actual aircraft in flight over a ground surface gives an indication of reflections from the existence of a secondary peak in the correlation. This secondary peak also allows determination of the position of the aircraft. Simultaneous measurements over an anechoic floor and the ground permit the evaluation of the transfer function of the reflected signal from the surface and hence allow the spectrum to be corrected for ground reflections.

There is much work to be done to establish the effects of motion on aircraft noise. One step is the establishment of the temporal and spatial distribution of the sources in a jet in a fashion amenable to experimentation for both stationary and moving aircraft. This technique has been tested for a model stationary jet in reference 5. Furthermore, it is necessary to reduce the nonstationary signal (resulting from the motion of the aircraft) into an equivalent stationary one, such that comparison can be made between static and moving aircraft. A preliminary investigation of this effect is reported in reference 6.

REFERENCES

1. T. D. Norum and C. H. Liu, "Point Source Moving Above A Finite Impedance Reflecting Plane - Experimental and Theory," J. Acoust. Soc. Am. 63(4), April 1978.
2. T. D. Norum, "A Comparison of the Noise Produced By A Small Jet On A Moving Vehicle With That In A Free Jet," NASA T.P. 1326, December 1978.
3. R. K. Amiet, "Refraction of Sound By A Shear Layer," AIAA Paper 77-54, January 1977.
4. R. B. Rice, "Inverse Convolution Filters," Geophysics, Vol. 27, No. 1, 1962.
5. L. Maestrello and C. H. Liu, "Jet Noise Source Distribution from Far-Field Cross-Correlations," AIAA Journal, Vol 15, No. 6, June 1977.
6. E. McDaid and L. Maestrello, "The Estimation of Nonstationary Spectra From Moving Acoustic Source Distributions," AIAA Paper No. 72-667, June 1972.



The single-zero assumption is appropriate if  $U < c$  at all points of the source distribution; otherwise equation (6) is replaced by a summation over the zeros of  $f(\tau)$ . Differentiating equation (5) with  $(y', x, t_0)$  constant gives

$$f'(\tau) = -1 + U_r/c_0 \quad (U_r = \text{component of } U \text{ towards the observation point}); \quad (7)$$

thus the pressure follows from equations (4) and (6) as

$$p(x, t_0) = \frac{1}{4\pi} \int \frac{q(x', \tau_0)}{|D(\tau_0)|} \cdot \frac{1}{r(\tau_0)} dy' \quad (8)$$

where the Doppler factor  $D$  is defined by

$$D = 1 - U_r/c_0, \quad (D \neq 0). \quad (9)$$

Equation (8) states that when a moving coordinate source description is used, the contribution from each volume element  $dy'$  to the pressure

$p(x, t_0)$  contains a weighting factor  $|D(\tau_0)|^{-1}$ . The quantity  $\tau_0$  is the emission time corresponding to the reception time  $t_0$ , and must be determined for all points of the source distribution before the volume integral (8) can be evaluated.

For supersonically moving sources,  $D(\tau_0)$  may be zero at some point in the source distribution; the integral in (8) then contains a singularity which is usually integrable, but makes the equation unsuitable for numerical evaluation. In such cases it is more convenient to use a fixed-coordinate source description, as discussed by Hanson [1].

### 1.1 Far-field solution

Although equation (8) is valid for any observation point  $x$ , we shall limit ourselves in what follows to the acoustic far field. This allows some simplification, in that a single representative value of the factor  $1/r(\tau_0)$  may be applied to the whole source distribution when calculating the pressure received at time  $t_0$ ; the same also applies to the Doppler factor, when the source frame of reference has zero acceleration. We therefore choose the origin of  $y'$  to lie within the source distribution, and define

$$R(\tau) = r(y' = 0); \quad (10)$$

$$\tau_{00} = \tau_0(y' = 0). \quad (11)$$

Physically,  $R$  is the distance from the origin ( $y' = 0$ ) to the observation point, and  $\tau_{00}$  is the emission time at the origin corresponding to the reception time  $t_0$ . The far-field solution may then be written as

$$p(x, t_0) = \frac{1}{4\pi R(\tau_{00})} \int \frac{q(y', \tau_0)}{|D(\tau_0)|} dy'. \quad (12)$$

The implications of this result are discussed in sections 2 and 3 below.

## 2. FAR-FIELD RADIATION FROM ACCELERATED SOURCE DISTRIBUTIONS

In this section, we illustrate with some relatively simple examples the effects of accelerated source motion. The results to be discussed are all based on the far-field equation (12), and for maximum simplicity we consider the source distributions in each case to be acoustically compact.

### 2.1 Time-varying volume displacement $V(t)$

A distributed volume displacement  $z(x, t)$  per unit volume is equivalent, according to linear theory, to a source distribution

$$q = \rho_0 \frac{\partial^2 z}{\partial t^2}. \quad (13)$$

Thus the far-field pressure is given by an expression similar to (12) above, but with two extra time derivatives (with respect to observation time  $t_0$ ):

$$p(x, t_0) = \frac{\rho_0}{4\pi R(\tau_{00})} \int \left(\frac{\partial}{\partial t_0}\right)^2 \frac{z(y', \tau_0)}{|D(\tau_0)|} dy'. \quad (14)$$

The definition of  $\tau_0$ , namely

$$t_0 = \tau_0 + r(\tau_0)/c_0, \quad (15)$$

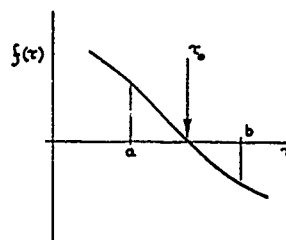


FIGURE 1. Sketch of the function  $f(\tau)$  in the vicinity of  $\tau = \tau_0$ .

gives (for constant  $x, y'$ )

$$dt_o = [1 - U_r(\tau_o)/c] d\tau_o = D(\tau_o) d\tau_o \quad (16)$$

and hence

$$(\partial/\partial t_o)_{x,y'} = \frac{1}{D(\tau_o)} (\partial/\partial \tau_o)_{x,y'}. \quad (17)$$

Thus the general far-field result, for the pressure radiated by a volume displacement distribution, is

$$p(x, t_o) = \frac{\rho_o}{4\pi R(\tau_{oo})} \int \left\{ \frac{1}{D(\tau_o)} \frac{\partial}{\partial \tau_o} \right\}^2 \frac{z(x', \tau_o)}{|D(\tau_o)|} dy'. \quad (18)$$

At this stage we introduce two simplifying assumptions:

(a) The variation of  $D(\tau_o)$  over the source region, for given observer coordinates  $(x, t_o)$ , may be neglected.

(b) Variations in emission time  $\tau_o$  over the source region, for given  $(x, t_o)$ , are small on the time scale of the source.

Assumption (b) - referred to as the *compactness assumption* - requires the typical source frequency (in the moving frame) to be small compared with  $cD/L$ , where  $L$  is the spatial extent of the source region in the radiation direction. Taken together, (a) and (b) allow  $\tau_o$  to be replaced by  $\tau_{oo}$  in the source integral, (18).

The final result for a compact volume-displacement source is therefore

$$p(x, t_o) = \frac{\rho_o}{4\pi R} \left( \frac{1}{D} \frac{\partial}{\partial \tau} \right)^2 \left( \frac{1}{|D|} V(\tau) \right), \quad (19)$$

where  $V(\tau) = \int z(y, \tau) dy$  is the total displaced volume and evaluation at  $\tau = \tau_{oo}$  is implied. Evaluating the derivatives explicitly gives

$$p(x, t_o) = \frac{\rho_o}{4\pi R} \{ (1 - M_r)^{-3} \ddot{V} + (1 - M_r)^{-4} (3\dot{M}_r + V\ddot{M}_r) + (1 - M_r)^{-5} 3V(\dot{M}_r)^2 \}, \quad (20)$$

as in reference [2]; here  $M_r = U_r/c_o$ , and time derivatives are indicated by dots (').

Equations (19) and (20) refer to the idealized case of a compact source for which the disturbance consists only of a volume displacement. We consider next a complementary source model, in which the only disturbance is a force field applied to the fluid. A compact moving body, which introduces both momentum and volume, may be represented by a superposition of the two source types.

## 2.2 Time-varying force $F(t)$

A distributed force with components  $f_i(x, t)$  per unit volume is equivalent to a source distribution

$$q = - \frac{\partial f_i}{\partial x_i} \quad (\text{summation over } i = 1, 2, 3) \quad (21)$$

in the linear wave equation for  $p$ . But in a free field, a source distribution of the form

$$q = \left( \frac{\partial^2}{\partial x_i \partial x_j} \dots \right) f_{ij} \dots \quad (\text{summation over repeated subscripts})$$

radiates the same pressure to the far field as

$$q = \left( - \frac{1}{c_o} \frac{\partial}{\partial t} \right)^n f_{rr} \dots \quad (\text{subscript } r \text{ denotes radiation direction});$$

thus the far-field pressure corresponding to (21) may be written down immediately, by analogy with the previous example, as

$$p(x, t_o) = \frac{1}{4\pi c_o R(\tau_{oo})} \int \left\{ \frac{1}{D(\tau_o)} \frac{\partial}{\partial \tau_o} \right\} \frac{f_r(x', \tau_o)}{|D(\tau_o)|} dy'. \quad (22)$$

With the simplifying assumptions (a) and (b) used previously, we obtain the compact-force result

$$p(x, t_o) = \frac{1}{4\pi c_o R} \left( \frac{1}{D} \frac{\partial}{\partial \tau} \right) \left( \frac{1}{|D|} F_r(\tau) \right), \quad (23)$$

where  $F_r(\tau) = \int f_r(y, \tau) dy$  is the total applied force in the radiation direction, and evaluation at  $\tau = \tau_{oo}$  is implied. Evaluating the derivatives explicitly gives

$$p(x, t_o) = \frac{1}{4\pi c_o R} \{ (1 - M_r)^{-2} \dot{F}_r + (1 - M_r)^{-3} F_r \dot{M}_r \}, \quad (24)$$

in agreement with Lowson [3].

### 2.3 Accelerating body of fixed volume

11-4 If a compact body of fixed volume  $V$  is accelerated through a uniform fluid at rest, it will exert a time-varying force  $\vec{F}$  on the fluid and the far-field sound pressure will be a combination of the two previous results. In the compact limit, equations (20) and (24) give

$$p(x, t) \approx \frac{\rho_0 V_0}{4\pi R} \left( \frac{\ddot{M}_r}{(1-M_r)^4} + \frac{3(\dot{M}_r)^2}{(1-M_r)^5} \right) + \frac{1}{4\pi c_0 R} \left( -\frac{\dot{r}}{(1-M_r)^2} + \frac{F_r \dot{M}_r}{(1-M_r)^3} \right);$$

$$= \frac{1}{4\pi c_0 R} \left( \frac{\dot{P}_r}{(1-M_r)^2} + \frac{P_r \dot{M}_r}{(1-M_r)^3} \right),$$

where

$$P_r = \vec{F} + \rho_0 V_0 \ddot{U} (1 - M_r)^{-2} \quad (\vec{U} = \text{velocity of body}) \quad (25)$$

is the equivalent total force including the displacement effect [2]. Equation (25) is consistent with equation (7.4) in Ffowcs Williams and Hawkings [4], although the present result was not given explicitly by these authors. The incompressible version of (25), i.e. without the  $(1 - M_r)^{-2}$  factor, was given earlier by Lighthill [5].

### 2.4 Acoustic sources in steady circular motion

The special case of steady motion in a circle has been extensively investigated in connection with models of propeller and helicopter rotor noise. Analytical predictions of mean square far-field pressure and radiated power are given for a variety of compact idealized source types in references [2], [6] and [7]. In particular, the effects of rotation on the spectral density of the far-field sound are studied in detail for broad-band sources. The reader is referred to these papers, and references cited therein, for further details.

### 2.5 Compact body of volume $V(t)$ moving at constant velocity

We conclude this section with an example in which sound is radiated as a result of a force  $\vec{F}(t)$  and volume displacement  $V(t)$ , but the force itself depends on the motion. If a body of constant shape but variable volume is moved with constant velocity  $\vec{U}$ , it will exert a time-varying force on the surrounding fluid. Dowling [9] has calculated the resulting far-field radiation on the assumption that the flow round the body is irrotational (so that the force  $\vec{F}(t)$  exerted on the fluid is given by potential flow theory): in the case of a pulsating sphere, for example, she finds

$$p(x, t_0) \approx \frac{\rho_0}{4\pi R} (1 - M_r)^{-3.5} \ddot{V}. \quad (26)$$

The Doppler index is -3.5, as compared with -3 for a pulsating body which exerts no force on the fluid (section 2.1).

## 3. FAR-FIELD RADIATION FROM UNIFORMLY MOVING SOURCE DISTRIBUTIONS

A special case with several practical applications is that of uniform steady source motion. In this situation, equation (12) which gives the far-field pressure radiated into a stationary uniform medium can be further simplified, by bringing the Doppler factor outside the volume integral. When this is done, the moving-source solution resembles the solution for a fixed source distribution with a modified time dependence. Applications to propeller and rotor thickness noise and to turbulent jet mixing noise are discussed in detail.

### 3.1 The Doppler transformation

We consider the general case of a source distribution of order  $n$ , specified by

$$q = \left( \frac{\partial}{\partial t} \right)^n f(x', t). \quad (27)$$

the far-field pressure, with arbitrary motion of the source reference frame, is

$$p(x, t_0) \approx \frac{1}{4\pi R(\tau_{00})} \int \left\{ \frac{1}{D(\tau_0)} \frac{\partial}{\partial \tau_0} \right\}^n \frac{f(x', \tau_0)}{|D(\tau_0)|} dx', \quad (28)$$

by analogy with the displacement-distribution result (18). However, the fact that  $\vec{U}$  is now steady and uniform allows  $D(\tau_0)$  to be replaced in the volume integral by the representative value  $D(\tau_{00})$ , which does not depend on  $\vec{y}'$ . Thus when the source reference frame is in steady translation, the far-field pressure is

$$p(x, t_0) \approx \frac{|D|^{-1} D^{-n}}{4\pi R} \int \left( \frac{\partial}{\partial \tau_0} \right)^n f(x', \tau_0) dx'. \quad (29)$$

Note that  $R$  and  $D$  are both evaluated at the emission time  $\tau_{00}$  in equation (29).

An expression very similar to (29) above is obtained by considering the radiation from a stationary source distribution with a modified time dependence. To simplify the argument we choose a time origin such that  $\tau_{00} = 0$ , and coordinate origins such that  $\vec{x} = \vec{x}'$  at  $t = 0$ . Comparison of the far-field pressures produced by the distributions



$$q = \left(\frac{\partial}{\partial t}\right)^n f(x', t) \quad \text{MOVING} \quad \text{and} \quad q = \left(\frac{\partial}{\partial t}\right)^n f(x, t/D) \quad \text{STATIONARY} \quad (30)$$

then shows that the only difference is the factor  $|D|^{-1}$  which appears in the moving-source result (29); a detailed derivation may be found in reference [9].

It follows that the far-field radiation from any moving source distribution of the form (27) may be found by transforming to an appropriate stationary distribution as in (30), and multiplying the far-field pressure thus obtained by a factor  $|D|^{-1}$ .

### 3.2 Application to Propeller and Rotor Thickness Noise

By thickness noise is meant the sound field arising from the blade volume displacement, as discussed in section 2.1. Nonlinear effects are not considered, and the rotating blades are regarded as acoustically compact in the direction normal to the blade surfaces, so that the radiated pressure consists of a superposition of contributions - as in equation (19) - from each blade element.

Uniform steady translation of a rotating propeller through the surrounding fluid will have the same effect on the thickness noise, under these conditions, as running the static propeller at a different rotational speed and applying a factor  $|D|^{-1}$  to the pressure. This follows from the Doppler transformation described above, since translation of the propeller leaves the thickness noise source distribution unchanged apart from the superimposed convection.

The far-field pressure at a given observation point is therefore obtained as follows.

- For any chosen reception time  $t_o$ , the emission time ( $\tau_{oo}$ ) at the centre of the propeller disk is calculated, together with the propeller position at that instant.
- An equivalent static propeller is defined which has the same dimensions but rotates at a speed  $1/D$  times the original speed, where

$$D = 1 - U_r(\tau_{oo})/c_o. \quad (31)$$

- The position of the static propeller is chosen to coincide exactly with the moving propeller at time  $\tau_{oo}$ .

The time-history of the received pressure is then multiplied by  $1/|D|$  to give the true time-history in the vicinity of  $t_o$ . For any finite observation distance  $R(\tau_{oo})$ , the emission direction will actually change with time  $\tau_{oo}$  (although slowly on the time-scale of the pressure signal) and the time-history thus calculated should be interpreted as a local approximation around  $t_o$ .

### 3.3 Application to Turbulent Jet Mixing Noise

By making certain assumptions about the similarity of static and moving jets, Michalke and Michel have been able to apply the Doppler transformation to jet mixing noise.\* The result is a method of predicting jet noise in flight from static tests (or from tests at a different flight speed) which does not rely on a specific model of the turbulent jet structure.

The application to jet noise is based on Lighthill's acoustic analogy [10], and therefore takes no account of the refraction processes known to occur in high-speed jets [11]. Also, it is limited to flight velocities parallel to the jet axis. Nevertheless, impressive agreement has been demonstrated in comparisons with aircraft flight data. An outline derivation of the main result is given below.

We begin by assuming that the mixing region between a moving jet and the ambient fluid is similar to that of a stationary jet, provided the fluid properties at the nozzle exit are the same. Specifically, we assume that at a fixed position relative to the nozzle (Figure 2), the mean shear and the turbulent velocity statistics scale on the velocity difference  $U_j - U_F$ .

It follows from the above assumption that the equivalent source distribution ( $q$ ) for the moving jet, in the Lighthill analogy, is the same as that in a static jet of exit velocity  $U_j - U_F$ . The effect of motion at  $U_F$  on the far-field pressure is reproduced - according to the Doppler transformation - by substituting  $(t/D_F)$  for  $t$  in the static source distribution  $q(x, t)$ , where  $D_F$  is the flight Doppler factor defined by

$$D_F = 1 + U_F \cos \theta / c_o. \quad (32)$$

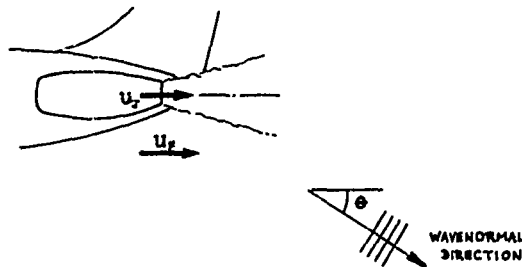


FIGURE 2. Sound radiation from a moving jet, viewed in a frame of reference moving with the nozzle.

\*Personal communication, March 1979; paper submitted to Journal of Sound and Vibration.

The appropriate change of time scale may be achieved physically by running the static jet at an equivalent exit velocity  $U_E$ , given by

11-6

$$U_E = (U_J - U_F)/D_F. \quad (33)$$

However, this has the unwanted side-effect of multiplying the far-field radiated pressure by an extra factor  $D_F^{-2}$  (relative to the original static jet with exit velocity  $U_J - U_F$ ) in view of the scaling assumption introduced earlier.\* Thus the mean-square far-field pressure from the "equivalent static jet" (exit velocity  $U_E$ ) requires a correction factor  $D_F^4$  in addition to the usual factor  $D_F^{-2}$  arising from the Doppler transformation.

The final result may be stated as

$$\overline{p^2}(U_J, U_F) = D_F^2 \overline{p^2}(U_E, 0); \quad (34)$$

it applies to the mean square pressure in the same band of observed frequencies (relative to the surrounding medium) in the two cases. There is no need to Doppler-shift the spectrum of the equivalent static jet, since this is automatically allowed for in the Doppler transformation when the source time scale is modified.

It is possible to refine the above analysis to make allowance for the stretching of the jet mixing region which occurs in flight. The simplest assumption is to regard the entire jet velocity field as being stretched in the axial direction by a factor  $\alpha$ , with local velocities remaining the same at corresponding points in the jet.

The introduction of the stretching factor  $\alpha$  has two effects. First, the increase of axial separation between corresponding pairs of points leads to increased travel-time differences for acoustic signals reaching a given observer. This change can be allowed for by a change in observation angle, if it is assumed that axial interference effects are the principal cause of jet noise directionality: it is necessary to observe the "equivalent static jet" at an angle  $\theta_E$  to the axis given by

$$\cos \theta_E = \alpha \cos \theta. \quad (35)$$

The second effect of stretching is to increase the source volume by a factor  $\alpha$ ; since the source moment densities are unchanged locally (by assumption), the mean square pressure radiated in flight is multiplied by  $\alpha^2$  relative to equation (34). Thus the final result with approximate allowance for jet stretching in flight is

$$\overline{p^2}(U_J, U_F, \theta) = \alpha^2 D_F^2 \overline{p^2}(U_E, 0, \theta_E). \quad (36)$$

#### 4. DIFFRACTION OF SOUND BY SURFACES IN STEADY MOTION

The preceding discussion is based on a free-field model in which sources are convected through an infinite uniform medium at rest. If diffracting bodies are moving along with the sources (for example, an aircraft wing in the case of aircraft noise), it is necessary to describe the diffraction of incident sound in the presence of mean flow past the body.

The typical situation is sketched in Figure 3, in a frame of reference fixed to the diffracting body. Steady translation of the body is assumed, so that the relative flow field is steady. It has been shown by Taylor [12] that if the diffraction process can be described (theoretically or experimentally) in the absence of flow, the effect of a low Mach number potential flow may be accounted for by a straightforward transformation.

Taylor's transformation uses a modified time variable

$$t' = t + \frac{\phi}{c_0^2}, \quad (37)$$

where  $\phi$  is the velocity potential of the steady flow field relative to the body (so that  $U = \text{grad } \phi$ ), and  $c_0$  is the speed of sound at infinity (where the flow is uniform). The space coordinates are left unchanged. To  $O(M)$  accuracy, the propagation of

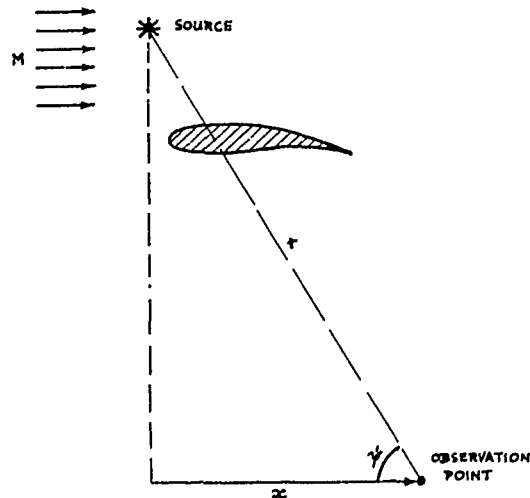


FIGURE 3. Diffraction of sound by a streamlined body embedded in a steady potential flow field.

\*The equivalent quadrupole moment density  $\rho_0 v_i v_j$  increases in proportion to the square of the static jet exit velocity; so also does the equivalent dipole moment density  $(1/\rho_0 - 1/\rho) \partial p / \partial x_i$ , with the present scaling assumption.

small-amplitude irrotational disturbances is described in  $(x, t')$  coordinates by

$$\frac{1}{c_0^2} \frac{\partial^2 \phi}{\partial t'^2} + \nabla^2 \phi = 0 \quad (\phi = \text{perturbation potential}), \quad (38)$$

as in the zero-flow case. Moreover, the rigid-body boundary condition is unaltered by the transformation (more general boundary conditions are covered in reference [12]). Thus as far as  $\phi$  is concerned, the diffracted field in the presence of flow is related to the zero-flow result by a shift in the time variable. The acoustic pressure  $p$  then follows from the relation

$$p = \rho_0 \frac{D\phi}{Dt} = \rho_0 \frac{D\phi}{Dt} + \rho_0 \nabla \phi \cdot \mathbf{U} \cdot \text{grad} \quad (39)$$

where  $\rho_0$  is the density at infinity.

Some insight into the transformation may be obtained by considering the special case where no diffracting body is present and the mean flow field is uniform. An acoustic signal which travels from the source point in Figure 3 to the observation point takes a time  $R/c_0$  to cover the distance  $r$  between the two points, where  $R$  is given by

$$R = \frac{r(1 - M^2 \sin^2 \psi)^{1/2}}{1 - M^2} = \frac{Mx}{1 - M^2} \\ = r - Mx + O(M^2). \quad (40)$$

Physically,  $R$  is the distance travelled relative to the moving fluid. Thus if we introduce the modified time variable

$$t' = t + c_0^{-2} \phi = t + c_0^{-1} Mx, \quad (41)$$

the interval  $\Delta t'$  between source and receiver is

$$\Delta t' = R/c_0 + Mx/c_0 = r/c_0 + O(M^2) \quad (42)$$

with no influence from the flow to  $O(M)$  accuracy.

The transformation described above is useful only when the incident field is given; thus if a source and a diffracting body are moving together through a uniform medium, the effect of the source motion on the incident field must be determined first (for example, by the Doppler transformation of section 3).

A further point is that the incident field must be described in reception time coordinates (e.g.,  $(r, \psi)$  in Figure 3). Thus in the situation of Figure 3, changing the incident Mach number has a somewhat complicated effect on the sound field at a fixed angle  $\psi$ . The relation between incident and diffracted pressures is altered in a predictable manner, as described above; but the alteration in the incident field for a fixed  $\psi$  value is not obtainable directly from the Doppler transformation, for example, since this applies only to the radiation at a fixed emission angle. It follows that measurements which involve moving sources and moving bodies require careful interpretation; the recommended procedure is first to deduce the incident field\* (by allowing for diffraction effects), and then to seek a connection between the incident field and the source motion.

## 5. SOUND RADIATION FROM TURBULENT JETS

The directionality of turbulent jet mixing noise - at least outside the "cone of silence" caused by refraction - is largely due to the convected nature of the turbulent velocity field. In this section we adopt a specific model of the equivalent sources in a jet, and show how this leads to "convective amplification" for static jets and also for jets in motion. We then show how the results are altered by including the mean flow field in the radiation calculation, with the aid of the geometric acoustics approximation.

### 5.1 Static Jets - Lighthill Analogy

Because of the random nature of turbulence, we seek a relation between the statistics of the source distribution ( $q$ ) and of the far-field pressure ( $p$ ). A convenient starting point is the following general equation for the power spectral density of  $p$ , in terms of the cross spectral density of  $q$  at two points  $(\mathbf{x}, \mathbf{x} + \mathbf{r})$ :

$$(4\pi R)^2 S_p(\mathbf{x}, \omega) = \int d\mathbf{y} \int d\mathbf{r} S_q(\mathbf{r}, \omega) \exp(i\frac{\omega}{c_0} \mathbf{r} \cdot \mathbf{y}). \quad (43)$$

Here  $R$  is the distance of the far-field point  $\mathbf{x}$  from the source region, and  $\mathbf{y}$  is the unit vector in the radiation direction.

\*It is assumed that no feedback occurs between the diffracting body and the source, so that the incident field is unaffected by the body. Then if the source position relative to the body is fixed, the effect of the body on the far-field radiation pattern may be deduced from experiments at a different (or zero) translation velocity.

If the source distribution is spatially coherent on a scale ( $\lambda$ ) which is small compared with the overall extent ( $L$ ) of the source region - as is expected for small-scale turbulence in jets - the inner integral in equation (43) may usefully be interpreted as a local property of the source distribution. The "local" contribution to  $S_p(\omega)$  per unit volume of the source region is

$$P(\omega) = (4\pi R)^{-2} \int d\eta \cdot S_q(\eta, \omega) \exp(i \frac{\omega}{c_0} \eta \cdot \hat{n})$$

$$= \frac{1}{4\pi R^2} [Q(k, \omega)]_{k=\omega \hat{n}/c_0} \quad (44)$$

where  $Q(k, \omega)$  is the spatial Fourier transform of  $S_q(\eta, \omega)$  and represents the source wavenumber-frequency power spectrum per unit volume.

We now restrict attention to jets of uniform density\*, and introduce a specific model of the source space-time structure. According to the Lighthill analogy, for uniform-density jets

$$q \approx \rho_0 \frac{\partial^2}{\partial x_i \partial x_j} (v_i v_j); \quad (45)$$

thus we expect a wavenumber-frequency spectrum of the form

$$Q = \rho_0^2 k_i k_j k_l k_m \phi_{ijlm}(k, \omega) \quad (46)$$

(reflecting the double space derivative in (45) above). The function  $\phi_{ijlm}$  is assumed to have ellipsoidal contours in  $(k, \omega)$  space, as shown in Figure 4; the contours are defined by the equation

$$(\omega')^2 + (k_1 U_{e1})^2 + (k_2 U_{e2})^2 + (k_3 U_{e3})^2$$

$$= \text{constant} = (\omega'')^2 \quad (47)$$

where

$$\omega' = \omega - k_1 U_c, \quad (48)$$

and the parameters  $(U_c, U_{e1}, U_{e2}, U_{e3})$  are different in general for each contour. Physically,  $U_c$  is a characteristic convection velocity for the source pattern\*\*, while the parameters  $U_{ei}$  determine the shape of each ellipsoid.

The ellipsoidal-contour assumption includes as a special case the Gaussian form assumed for  $\phi_{ijlm}$  by Ribner [13] and Ffowcs Williams [14] in their early work on jet noise. To show that it leads to the well-known convective amplification factor, we make use of equations (44) and (46): thus

$$R^2 P(\omega) = \frac{1}{4\pi} \rho_0^2 \cdot [k_i k_j k_l k_m \phi_{ijlm}(k, \omega)]_{k=\omega \hat{n}/c_0}$$

$$= \frac{\rho_0^2}{4\pi c_0^4} \alpha_i \alpha_j \alpha_l \alpha_m \phi_{ijlm}(0, \omega_m) \cdot \omega^4 \quad (49)$$

Here  $\omega_m$  is the value of  $\omega'$  corresponding to  $k = \omega \hat{n}/c_0$ , i.e. from equations (47) and (48)

$$(\frac{\omega_m}{\omega})^2 = D_m^2 = (1 - \frac{U_c}{c_0} \cos \theta)^2 + (\frac{U_{e1}}{c_0})^2 \cos^2 \theta + (\frac{U_{e2}}{c_0})^2 \sin^2 \theta, \quad (50)$$

where we have used

$$\alpha_1 = \cos \theta; \quad \alpha_2^2 + \alpha_3^2 = \sin^2 \theta \quad (\theta = \text{radiation angle relative to jet axis}) \quad (51)$$

together with the assumption that  $U_{e2} = U_{e3} = U_c$ . Equation (50) defines the modified Doppler factor  $D_m$ .

The convective amplification effect follows immediately; equation (49) is multiplied by  $\omega$  to bring it into proportional bandwidth (rather than spectral density) form, and becomes

$$R^2 \omega P(\omega) = \frac{\rho_0^2}{4\pi c_0^4} [\phi_{rrrr}(0, \omega_m) \cdot \omega_m^5]_{\omega_m}^{-5} \quad (52)$$

\*For a discussion of the general case, see reference [11].

\*\*The convection velocity is taken as parallel to the jet axis ( $x_1$  direction).

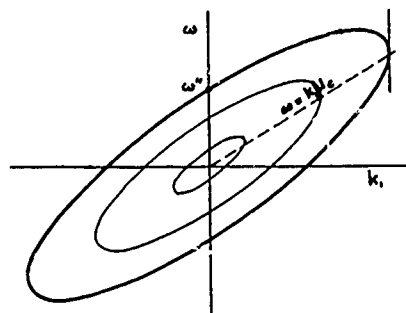


FIGURE 4. Contours of the quadrupole source spectrum  $\phi_{ijlm}$  in wavenumber-frequency space, shown for  $(k_2, k_3) = 0$ .

(the notation  $\phi_{rrrr} = \alpha_1 \alpha_2 \alpha_3 \alpha_4 \phi_{rrrr}$  has been introduced for brevity). Equation (52) may be interpreted more clearly if we compare it with the approximate form valid for a compact\* source distribution, namely,

$$R^2 \omega P(\omega) = \frac{\rho_0}{4} \frac{1}{c_0} \phi_{rrrr}(0, \omega) \omega^5 \quad (\text{acoustically compact coherent regions}). \quad (53)$$

According to equation (52), the effects of source convection and non-compactness are accounted for by

(a) Evaluating the compact-source approximation (53) with the Doppler-shifted frequency  $\omega_m$  in place of the actual frequency  $\omega$ ;

(b) Multiplying the result by  $D_F^{-5}$ .

The convective amplification factor  $D_F^{-5}$  is therefore superimposed on any directivity inherent in jet noise, and implies (for any given  $\omega_m$  value) a strong downstream bias in the far-field radiation from high-speed jets. This and other implications of equation (52) have been systematically applied by Lush [15] to the study of jet noise measurements.

## 5.2 The effect of jet motion

The preceding analysis can be extended to allow for motion of the jet as a whole (as for an aircraft in flight). We shall adopt a frame of reference moving with the nozzle, as in Figure 2, so that the ambient fluid is moving at speed  $U_p$  in the jet direction. The wavenormal direction is denoted by the unit vector  $\hat{q}$ , as previously (with  $\alpha_1 = \cos \theta$ ).

For a given wavenormal direction - i.e. a given emission angle  $\theta$  from the moving jet - the effect of the uniform flow velocity  $U_p$  may be deduced from the Doppler transformation described in section 5.1. This involves the jet-motion Doppler factor  $D_F$  based on the velocity  $\mathbf{U} = (-U_p, 0, 0)$  at which the jet moves:

$$D_F = (1 - \mathbf{U} \cdot \hat{q} / c_0) = 1 + (U_p / c_0) \cos \theta. \quad (54)$$

Motion of the jet - described in nozzle coordinates by the wavenumber-frequency source spectrum  $Q(k, \omega)$  - is allowed for by defining an equivalent stationary source distribution in which

$$\omega Q(k, \omega) \text{ is replaced by } \omega D_F Q(k, \omega D_F). \quad ** (55)$$

The pressure radiated by the moving source distribution is  $|D_F|^{-1}$  times that radiated by the equivalent stationary distribution; thus the spectral equation corresponding to (44), in a fluid-fixed reference frame, is

$$[\omega P(\omega)]_F = \frac{1}{4} \pi R^2 D_F^{-2} [\omega_F D_F Q(k, \omega_F D_F)]_{k=\omega_F \hat{q} / c_0} \quad (56)$$

The notation  $\omega_F$  is used here to denote frequencies relative to the ambient fluid.

Equation (56) may now be expressed in the frame of reference attached to the nozzle, by noting that frequencies in this frame are given by

$$\omega = \omega_F D_F. \quad (57)$$

Thus relative to the nozzle, we have

$$R^2 P(\omega) = \frac{1}{4} \pi R^2 [Q(k, \omega)]_{k=\omega \hat{q} / c_0} \quad (58)$$

note that  $R$  is used consistently to denote the distance travelled by a wavefront relative to the fluid (i.e. the source-observer distance at the emission time). This result generalizes equation (44) above, by allowing for a uniform flow field surrounding the source and extending to infinity.

When the convected-quadrupole source model described in section 5.1 is substituted in equation (58), we obtain the following result for the spectral density of the far-field pressure:

$$R^2 \omega P(\omega) = \frac{\rho_0}{4} \frac{1}{c_0} [\phi_{rrrr}(0, \omega_m) \omega_m^5] D_{m,rel}^{-5} |D_F|^{-1}. \quad (59)$$

Here the Doppler factor  $D_{m,rel}$  is defined by

$$D_{m,rel}^2 = (1 - \frac{U - U_F}{c_0} \cos \theta)^2 + (\frac{U}{c_0})^2 \cos^2 \theta + (\frac{U}{c_0})^2 \sin^2 \theta, \quad (60)$$

\*"Compact" here means that over the acoustic wavenumber range  $|k| < \omega/c_0$ ,  $\phi_{rrrr}(k, \omega) \approx \phi_{rrrr}(0, \omega)$ . Thus the coherent length scale  $l$  is small compared with the acoustic wavelength.  
\*\*This relation simply expresses the change in time scale - and hence shift in source spectrum - required by the Doppler transformation.

while the modified frequency used to define the source strength is

$$\omega_m = \omega D_F^{-1} D_{m,rel} = \omega_F D_{m,rel} \quad (61)$$

These results agree with the earlier work of Ribner [13] and Ffowes Williams [14].

Comparison of equation (59) for the moving jet with equation (52) for the static jet shows three differences:

- An extra factor  $|D_F|^{-1}$  now appears.
- The convective amplification factor  $D_m^{-5}$  becomes  $D_{m,rel}^{-5}$ .
- The source spectrum is evaluated at a frequency  $D_{m,rel}$  times the frequency relative to the surrounding fluid.

Thus if jet noise measurements from a moving aircraft were to be interpreted using (59), a frequency factor  $D_{m,rel}$  would be applied to spectra measured in proportional bands on the ground. The height of the spectrum would then be corrected for source convection and non-compactness effects by multiplying by  $D_{m,rel}^5 |D_F|$ .

### 5.3 Geometric acoustics radiation model

Recent advances in the understanding of jet noise, summarized in reference [11], have shown that the agreement between theory and experiment can be greatly improved by allowing for the jet mean flow field in the acoustic radiation model. Although the general calculation is complicated, reference [11] shows that remarkably accurate results are obtained outside the so-called "cone of silence" by using geometric acoustics (ray theory).

The application of geometric acoustics to sound radiation from a moving jet is discussed in reference [16]. Figure 5 indicates the model used: the source region is placed in a parallel-flow shear layer which represents the mixing region of a jet in forward motion. Wavenormal directions in the source and ambient regions are defined by unit vectors  $\hat{q}_s$  and  $\hat{q}_a$  respectively, with corresponding polar angles  $\theta_s$  and  $\theta$ :

$$\cos \theta_s = \alpha_{s1}, \quad \cos \theta = \alpha_1. \quad (62)$$

These are related by the condition that the axial phase speed of the wavefronts should be the same in each layer. Thus

$$c_{\phi 1} = U_s + c_s / \cos \theta_s = U_F + c_o / \cos \theta. \quad (63)$$

The radiation calculation proceeds in two stages. First the value of  $R^2 P(\omega)$  is calculated *within the source region*,\* which gives a result closely similar to equation (58) except that  $U_s$ , the source-region flow velocity, replaces  $U_F$ . Secondly, the change in  $R^2 P(\omega)$  across the shear layer is found by energy conservation, as described in references [16] and [17]; (see the notes on *Acoustic Energy* in this series). The final result, which may be compared with equation (59), is

$$R^2 \omega P(\omega) = \{ \pi D_{s,rel}^2 \frac{\rho_o \rho_s}{c} \frac{f(s)}{4 \pi r r r r} (0, \omega_m) \cdot \omega_m^5 D_{m,rel}^{-5} |D_F|^{-1} \}, \quad (64)$$

where the modified frequency has the same formal definition as previously - see equation (61) - but the modified Doppler factor is altered.

$$D_{m,rel}^2 = \left( 1 - \frac{U_c - U_F}{c_o} \cos \theta \right)^2 + \left( \frac{U_c^2 - U_F^2}{c_o^2} \right) \cos^2 \theta + \left( \frac{U_c}{c_s} \right)^2 D_{s,rel}^2. \quad (65)$$

The source-region Doppler factor  $D_{s,rel}$  which appears in these equations is defined as

$$D_{s,rel} = \left( 1 + \frac{U_s - U_F}{c_s} \cos \theta_s \right)^{-1} = 1 - \frac{U_s - U_F}{c_o} \cos \theta. \quad (66)$$

\*According to the GA approximation the source region is many wavelengths thick, so that a far field can be defined locally.

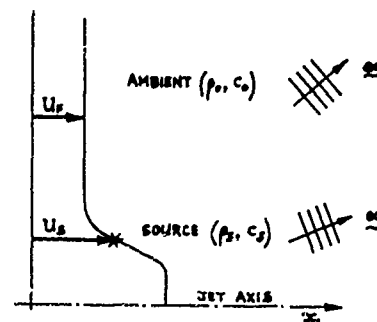


FIGURE 5. Geometric acoustics model for sound radiation from sources in a shear layer.

Apart from the different definition of  $D_{s,rel}$  above, three significant features distinguish the GA result (64) from the previous result (59) in which no account was taken of the far field in the source region.

- (a) The source term in brackets is evaluated in the emission direction  $\theta_s$ , rather than in the external radiation direction  $\theta$ . This is important if the source is inherently directional; it also limits the application of equation (64) to angles outside the cone of silence.
- (b) The mean square pressure is proportional to  $\rho_o \rho_s$ , rather than  $\rho_o^2$  as previously.
- (c) An additional flow-dependent factor  $D_{s,rel}^2$  appears in the GA result.

Finally, equation (64) gives the azimuthal average of the mean square pressure about the jet axis, which is equal to the local mean square pressure only if the jet noise field has no azimuthal directivity (e.g., a round jet).

#### 6. RADIATION THROUGH A MOVING JET FROM UPSTREAM SOURCES

As a final example of propagation from moving sources, we consider the situation sketched in Figure 6. A parallel round jet pipe contains upstream sound sources which are characterized by the wave field incident at the open end of the pipe. The fluid outside the pipe is in uniform motion at speed  $U_F$ , simulating steady motion of the jet pipe through the atmosphere in the opposite direction.

Two limiting cases are discussed in turn below, corresponding to high-frequency (multimode) and low-frequency (plane wave) sound fields arriving at the open end of the pipe. The aim is to describe the effect of the external flow  $U_F$  on the external far-field radiation.

##### 6.1 Geometric acoustics approximation

In the high-frequency limit, two approximations are possible which simplify the analysis.

- (a) Reflection of sound at the open end of the pipe may be neglected.
- (b) The jet shear layer may be regarded as acoustically passive, so that the radiated sound power equals the incident sound power.

In order to quantify the external flow effect, let  $S_i(\omega, \theta_J)$  be the power spectral density of the  $P_i$  external farfield pressure (for a given wavenormal angle  $\theta_J$  in the jet) when

$$U_F = U_J, \quad \rho_o = \rho_J, \quad c_o = c_J \quad (\text{reference case}). \quad (67)$$

In the general case, radiation incident at angle  $\theta_J$  to the jet axis will emerge at a different angle, given by

$$\cos \theta = \frac{U_J - U_F}{c_o} + \frac{1}{\cos \theta_J} \frac{c_J}{c_o} - 1 \quad (68)$$

(obtained by assuming a stratified mean flow and equating axial phase speeds); the power spectral density of the azimuthally-averaged far-field pressure is then given by the energy relation

$$R^2 S_p(\omega, \theta) = R_i^2 S_{pi}(\omega, \theta_J) \cdot (\rho_o / \rho_J) D_{J,rel}^{-4} \quad (69)$$

where  $R_i$  and  $R_{J,rel}$  are the radiation distances (relative to the fluid) in the two cases. The Doppler factor  $D_{J,rel}$  is defined by an equation similar to (56) above:

$$D_{J,rel} = \left(1 + \frac{U_J - U_F}{c_J} \cos \theta_J\right)^{-1} = \left(1 - \frac{U_J - U_F}{c_o} \cos \theta\right)^{-1} \quad (70)$$

Equation (69) is based on acoustic energy conservation in a frame of reference attached to the jet pipe, and the frequencies are all expressed relative to this frame. Conversion to other reference frames (e.g., one moving with the ambient fluid) is facilitated by expressing the equation in proportional-band form:

$$R^2 \omega S_p(\omega, \theta) = [P_i^2 \omega S_{pi}(\omega, \theta_J)] \cdot (c_o / \rho_J) D_{J,rel}^{-4} \quad (71)$$

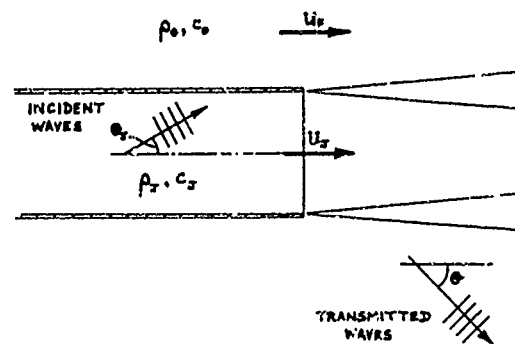


FIGURE 6. Geometric acoustics model for sound transmission through a jet flow.

Equation (71) may be interpreted as follows. For given jet pipe conditions (flow plus incident sound) and a given value of  $\theta_j$ , the quantity in brackets remains constant regardless of external flow conditions. Thus if the far-field radiation is observed at an angle  $\theta$  given by equation (68) - which varies according to the external flow - the influence of the external flow field is entirely contained in the density factor  $\rho_o/\rho_j$  and the Doppler factor  $D_{j,rel}^{-4}$ .

The effect of  $U_F$  on the Doppler amplification factor becomes clearer if we write

$$D_{j,rel} = (1 + \frac{U_j}{c_j} \cos \theta_j)^{-1} D_F, \quad (72)$$

where  $D_F$  is the flight Doppler factor defined in equation (54). Thus for fixed jet-pipe conditions and a given angle  $\theta_j$ , the relation

$$R^2 \omega_p^2(\omega, \theta) \propto \rho_o D_F^{-4} \quad (73)$$

expresses the dependence of the far-field pressure spectrum on the flight speed and ambient fluid properties; note that the jet parameters ( $U_j$ ,  $\rho_j$ ,  $c_j$ ) do not enter into this result.

Two ways in which equation (73) might be applied to aircraft noise are.

- As a method of normalizing engine internal-noise measurements, for given engine operating conditions and different flight speeds  $U_F$ . Measured far-field spectra, multiplied by  $D_F^4/\rho_o$ , should collapse at a given value of  $\theta_j$ .
- As a method of predicting engine internal noise in flight from static measurements.

For these purposes it may be more convenient to use the static situation ( $U_F = 0$ ) as a reference case, and instead of introducing  $\theta_j$  as a parameter, to use the static radiation angle  $\theta_E$  defined by

$$\cos \theta_E = D_F^{-1} \cos \theta. \quad (74)$$

The inverse of (74), which gives  $\theta$  (and  $D_F^{-1}$ ) in terms of  $\theta_E$  and therefore corresponds to equation (68), is

$$\cos \theta = D_F \cos \theta_E; \quad D_F = 1 - \frac{U_F}{c_o} \cos \theta_E. \quad (75)$$

Thus the effect of changing  $U_F$ , all other conditions remaining constant, may be obtained from the present model by using (73) and (75), without introducing the jet parameters.

## 6.2 Low-frequency approximation

Below the cut-off frequency of the lowest transverse acoustic mode in the jet pipe, the only sound waves which can propagate are plane (axial) waves. The external sound field due to plane waves in the pipe has been calculated by Munt [18], who accounted for the interaction between the end of the pipe and the jet by representing the jet shear layer as a vortex sheet attached to the lip of the pipe.

The effect of the external flow velocity  $U_F$  in this situation is more complicated than at high frequencies, and cannot be expressed as a simple factor of the type  $D_F^{-n}$ . Nevertheless, the general trends are the same; the radiation is amplified in the forward direction (wavenormal angles  $\theta > 90^\circ$ ) and reduced in the rear arc, with a sector in the rear arc (similar to the cone of silence in the CA model) where the model breaks down. Over most of the angle range, the flight effect is roughly equivalent to a Doppler index of  $-3$ , as opposed to  $-4$  in the high-frequency limit; there is no change in the radiation at  $\theta = 50^\circ$ .

Experimental support for Munt's predictions, based on model tests with an unheated subsonic jet, is described in reference [19].

## 7. CONCLUDING REMARKS

The theory of sound radiation from sources moving through a uniform medium is well established, and detailed accounts may be found in the books by Morse and Ingard [20] and Goldstein [21]. An outline is presented in sections 1 and 2 of these notes, using a frame of reference in which the medium appears stationary; conversion to any other convenient reference frame is straightforward since all results are given in terms of pressure, which (unlike intensity) is unaffected by motion of the coordinates. The principal difficulty in applying these results lies in defining an appropriate source model to represent the noise source of interest.

If it is required simply to predict the effect of steady motion on the radiated sound field, the source model need not be prescribed in full detail. The Doppler transformation described in section 3 allows the effects of source motion to be predicted with minimal information about the source structure, by relating the moving-source field to the field of an equivalent stationary source.

The problem of sound radiation from sources in non-uniform steady flows is less well understood. Analytical predictions are available only in certain idealized situations, such as irrotational low Mach number flow (section 4), slowly-varying flows (sections 5, 6) and uniform flow regions separated by vortex sheets (section 6). Such predictions nevertheless provide useful insight into practical problems, for example the radiation of exhaust mixing noise and engine internal noise from aircraft in flight.



A final comment is worth making about the interpretation of measurements on moving noise sources, such as aircraft: should the data be presented in terms of the source position at the time the sound was emitted, or the source position at the time of reception? If the source is accelerating, the latter has no physical relevance; but for steady uniform motion, the use of reception time coordinates offers some advantage in dealing with diffraction effects (such as the shielding of aircraft engine noise by the wing). This point is discussed further in section 4; it seems to be the main exception to the general rule, that far-field sound radiation measurements are more easily interpreted in emission time coordinates.

## REFERENCES

1. D.B. HANSON 1976 AIAA Paper No. 76-565. Near field noise of high tip speed propellers in forward flight.
2. H.K. TANNA and C.L. MORFEY 1971 Journal of Sound and Vibration **16**, 337-348. Sound radiation from point sources in circular motion.
3. M.V. LOWSON 1965 Proc. Roy. Soc. (London) **A 286**, 559-572. The sound field for singularities in motion.
4. J.E. FLOWES WILLIAMS and D.L. HAWKINGS 1969 Trans. Roy. Soc. (London) **A 264**, 321-342. Sound generation by turbulence and surfaces in arbitrary motion.
5. M.J. LIDTHILL 1962 Proc. Roy. Soc. (London) **A 267**, 147-182. The Bakerian Lecture, 1961: Sound generated aerodynamically.
6. C.L. MORFEY and H.K. TANNA 1971 Journal of Sound and Vibration **15**, 325-351. Sound radiation from a point force in circular motion.
7. H.K. TANNA 1971 Journal of Sound and Vibration **16**, 349-363. Sound radiation from point acoustic stresses in circular motion.
8. A.P. DOWLING 1976 Journal of Fluid Mechanics **74**, 529-546. Convective amplification of real simple sources.
9. C.L. MORFEY 1972 Journal of Sound and Vibration **23**, 291-295. The sound field of sources in motion.
10. M.J. LIDTHILL 1963 AIAA Journal **1**, 1507-1517. Jet noise.
11. C.L. MORFEY, V.M. SZEWCZYK and B.J. TESTER 1978 Journal of Sound and Vibration **61**, 255-292. New scaling laws for hot and cold jet mixing noise based on a geometric acoustics model.
12. K. TAYLOR 1977 RAE (Farnborough) Technical Report 77109. A transformation of the acoustic equation with implications for wind tunnel and low speed flight tests.
13. H.S. RIBNER 1964 Advances in Applied Mechanics **8**, 103-182. The generation of sound by turbulent jets.
14. J.E. FLOWES WILLIAMS 1963 Phil. Trans. Roy. Soc. (London) **A 255**, 469-503. The noise from turbulence convected at high speed.
15. P.A. LUSH 1971 Journal of Fluid Mechanics **46**, 477-500. Measurements of subsonic jet noise and comparison with theory.
16. H.E. PLUMBLEE (Ed.) 1976 NASA CR - 2702. Effects of forward velocity on turbulent jet mixing noise.
17. C.L. MORFEY and B.J. TESTER 1977 Journal of Sound and Vibration **54**, 83-106. Noise measurements in a free jet flight simulation facility: shear layer refraction and facility-to-flight corrections.
18. R.M. MUNT 1977 Journal of Fluid Mechanics **83**, 609-640. The interaction of sound with a subsonic jet issuing from a semi-infinite cylindrical pipe.
19. R.A. PINKER and W.D. BRYCE 1976 NGTE (Preston) Note. No. NT 1024. The radiation of plane-wave duct noise from a jet exhaust, statically and in flight. (See also 1977 AIAA Journal **15**, 133-134).
20. P.M. MORSE and K.U. INGARD 1968 Theoretical Acoustics. New York: McGraw-Hill.
21. M.E. GOLDSTEIN 1976 Aeroacoustics. New York: McGraw-Hill.

## APPLICATIONS OF DIFFRACTION THEORY TO AEROACOUSTICS

Donald L. Lansing  
 Head, Aeroacoustics Branch  
 Chen-Huei Liu  
 Aero-Space Technologist  
 Thomas D. Norum  
 Aero-Space Technologist  
 NASA Langley Research Center  
 Hampton, Virginia 23365

## SUMMARY

This paper reviews the fundamentals of diffraction theory and the application of the theory to several problems of aircraft noise generation, propagation, and measurement. The general acoustic diffraction problem is defined and the governing equations set down. Diffraction phenomena are illustrated using the classical problem of the diffraction of a plane wave by a half-plane. Infinite series and geometric acoustic methods for solving diffraction problems are described. Four applications of diffraction theory are discussed: the selection of an appropriate shape for a microphone, the use of aircraft wings to shield the community from engine noise, the reflection of engine noise from an aircraft fuselage and the radiation of trailing edge noise.

## INTRODUCTION

There is a growing appreciation for the role of diffraction phenomena in aircraft noise research. Diffraction occurs for example in the propagation and radiation of engine noise from internal ducts, the scattering of engine noise from aircraft wing, fuselage and tail surfaces, and the design and calibration of special sensors for acoustic measurements. While diffraction theory is a branch of classical mathematical physics with a voluminous literature, most available results are for pure tone plane wave, line, or point sources diffracted by simple shapes. Aeroacousticians are presented with severe challenges in extending this body of work to broadband, distributed noise sources and complex aircraft geometry in the presence of a turbulent moving medium.

This paper is a blend of textbook results on diffraction theory and some current problems in noise generation and measurement. The literature on diffraction is vast. Excellent bibliographies and comprehensive introductions to the theory can be found in references 1, 2, and 3. To lay a foundation for understanding the later examples the paper begins by reviewing the essentials of diffraction theory. The governing equations are set out, the important physical phenomena are reviewed, and two solution methods used in the practical applications are described. Four applications of diffraction theory to aircraft noise related problems are discussed: selection of an appropriate shape for a pressure gradient microphone, the reduction of community noise through wing shielding effects, the reflection of engine noise from aircraft fuselage surfaces, and the radiation of trailing edge noise. The paper provides useful background information for the lecture by L. Maestrello and A. Bayliss in this series entitled "Acoustic Scattering from an Elliptical Body."

## BASIC EQUATIONS OF ACOUSTIC DIFFRACTION THEORY

A sketch of the general acoustic diffraction problem and the field equations and auxiliary conditions of diffraction theory are shown in Figures 1 and 2, references 2 and 3. An incident sound field from either an incoming wave or a source distribution  $Q$  impinges upon a body. Due to the presence of the body a secondary or scattered field is produced. The complete wave field is a superposition of the incident and scattered fields. The basic mathematical problem is to predict the scattered and total acoustic wave fields.

The inhomogeneous wave equation is the partial differential equation which governs the incident and scattered sound fields. The source distribution  $Q$ , when it occurs, appears on the right hand side of this equation. The physically measurable quantities in the sound field, that is the acoustic pressure  $p$  and the acoustic velocity vector  $u$ , are determined from the velocity potential  $\phi$  by taking the time derivative and gradient respectively as indicated at the bottom of Figure 1. For a solution of the field equations to be acceptable from a physical viewpoint, the pressure and velocity must be continuous throughout the wave field.

In addition to satisfying the inhomogeneous wave equation, the solution must also satisfy several auxiliary conditions listed in Figure 2. The first of these is the surface boundary condition which states that the ratio of the normal acoustic velocity to the pressure at any point on the surface must equal the prescribed surface admittance  $\nu$ . On a hard surface  $\nu = 0$ . Nonzero and generally complex values of  $\nu$  designate various degrees of absorption and compliance for nonrigid surfaces.

The second condition called the radiation condition, assures that, with the exception of a prescribed incident wave, the solution consists only of outgoing waves at large distances from the body. That is, in the acoustic far field the additional disturbance produced by the presence of the scattering object must appear to originate at the object and produce waves which propagate away from it. Another way to state the radiation condition is that the pressure and radial component of acoustic velocity must be in phase in the far field. The third condition, the edge condition, is required to ensure the uniqueness of solutions for problems in which the scattering body has very sharp edges as when, for example, the body is a thin screen or disc of zero thickness. From a physical point of view the edge condition assures that no sound energy is generated at a sharp edge.

## PLANE WAVE DIFFRACTION BY A HALF PLANE

12-2

Considerable insight into diffraction phenomena can be had by considering the problem of the diffraction of a plane acoustic wave by a very large flat surface idealized as a semi-infinite half plane. A two-dimensional formulation of this problem is shown in Figure 3. The half plane or screen is perfectly rigid so that the normal component of the acoustic velocity on the screen is zero.

Consider, first of all, a description of the sound field from the standpoint of geometric acoustics in which it is assumed that sound travels along straight rays. Then the sound field may be decomposed into three principle regions. Region I, called the geometric shadow, receives none of the incident sound and is completely silent. The sonified region, that is, the region in which sound can be received along straight rays from the source, consists of two subregions. Within region II sound is received only from the incident plane wave. Region III, however, receives not only direct radiation from the incident plane wave but also sound which is reflected from the lower half of the screen.

This description is mathematically discontinuous across both the shadow boundary and the reflected edge ray. Thus, the geometric acoustic solution exhibits discrete jumps which are unacceptable physically and theoretically. The complete solution requires an additional wave field called the "diffracted wave" which provides a smooth transition between all of the regions and makes for a solution which is continuous everywhere. The table at the bottom of Figure 3 summarizes the wave constituents in these three regions.

The exact mathematical solution of this diffraction problem is shown in Figure 4, see references 2 and 4. The origin of the polar coordinates ( $r, \theta$ ) of the observer is at the edge of the half plane.  $k = \omega/c$  is the wave number of the incident wave in which  $\omega$  is the angular frequency and  $c$  is the speed of sound. The mathematical expression is a solution of the wave equation whose normal derivative vanishes at the surface of the half plane and which represents the prescribed incident plane wave. The function  $\phi(x)$  is called a Fresnel integral. These functions appear in many diffraction problems involving sharp edges. Because of their frequent occurrence in wave propagation problems they have been extensively tabulated and computational subroutines have been devised for evaluating them accurately on high speed computing machines. By replacing the Fresnel integrals by their approximations for very large values of  $kr$  one recovers precisely the geometric acoustic solution to this problem.

A calculation of the mean square pressure in the sound field is shown in Figure 5. The calculation is for a normally incident sound wave as indicated in the sketch. The calculation is made along an arc defined by  $kr = 6\pi$  which corresponds to a radial distance equal to three times the wavelength of the incident sound. The three regions described in Figure 3 are indicated at the top of the plot. For reference it is useful to note the square of the pressure in the incident wave field is unity. The intensity is very low but nonzero in the shadow region. As one crosses the shadow boundary into the sonified region the intensity increases smoothly, overshoots the intensity in the incident wave, and then settles down after several oscillations to the incident wave value. Well into region III the intensity is characterized by a number of large oscillations which are caused by the constructive and destructive interference between the incident wave and waves reflected from the screen. The intensity maxima and minima occur at the same angles as though the half plane was infinitely large in both directions.

## SOLUTION METHODS FOR DIFFRACTION PROBLEMS

Obtaining a solution to the inhomogeneous wave equation which satisfies the appropriate auxiliary conditions for complex shapes and general source distributions over a wide range of frequencies is an extremely difficult problem for which there is no single comprehensive method. Diffraction theory is a highly mathematical theory which is rich in subtle detail and great ingenuity. Diffraction methods include for example the Kirchhoff approximation, integral equation formulations, function theoretic methods, series expansions, variational formulations, and ray theories. In this paper two solution techniques will be briefly described which are suitable for fairly broad classes of diffraction problems: The series method, which provides exact solutions for certain standard geometric shapes in the form of infinite series; and geometric theory, which gives an approximate solution for quite general shapes at high frequencies. The details of these two methods will be illustrated for the diffraction of a plane wave by a rigid circular cylinder.

**Series Solution Method** - Consider the two-dimensional problem of the diffraction of an incident plane wave by a rigid circular cylinder of radius  $a$  as indicated in Figure 6, reference 4. The velocity potential  $\phi$  must be a solution of the homogeneous Helmholtz equation which represents an incoming plane wave and a system of outgoing scattered waves whose combination satisfies the boundary condition that the normal acoustic velocity at the surface of the cylinder vanishes. A time factor  $e^{-i\omega t}$  will be used in this paper.

The velocity potential  $\phi$  is represented as the sum of two potentials:  $\phi_i$  corresponding to the incident plane wave and  $\phi_s$ , the scattered potential, corresponding to the sum of all reflected and diffracted waves. Choosing the plane wave to be incident on the cylinder from the negative  $x$  direction  $\phi_i$  takes the form shown in Figure 6 in which  $e_0 = 1$  and  $e_2 = e_3 = \dots = 2$ . An appropriate form for  $\phi_s$  is given by the series at the bottom of the figure in which the  $A_n$ 's are undetermined coefficients. Each term in this infinite series is a solution of the wave equation which is finite and continuous everywhere outside of the cylinder and which represents sound waves radiating away from the cylinder. The sum  $\phi_i + \phi_s$  satisfies all the conditions of the problem with the exception of the surface boundary condition on the cylinder.

The complete expression for  $\phi$  is shown in Figure 7. The unknown coefficients  $A_n$  are now determined by applying the boundary condition to this series expression. This leads to the requirement that the Fourier series in  $\theta$  be equal to zero which requires that each coefficient of the series be equal to zero. The final equation for  $A_n$  is shown in the middle of Figure 7.

By substituting these values for the  $A_n$ 's back into the series expression for  $\phi$ , one has the complete solution to the diffraction problem. The acoustic pressures and velocities can be calculated at any point within the wave field by evaluating the appropriate infinite series expressions. The infinite series is a

useful means for obtaining the numerical values of the solution for small values of  $ka$  but converges very slowly and requires many terms when  $ka$  is large, that is when the wavelength is much shorter than the cylinder radius. In the acoustic far field the series for the scattered pressure can be approximated as shown at the bottom of Figure 7.

12-3

Some calculations of the mean square pressure in the scattered wave obtained from this series are shown in Figure 8. The sketches are polar plots of  $|P|^2$  for values of  $ka = 1, 3$ , and  $5$ . These calculations were made using a maximum of 30 terms in the series which was found to be sufficient for values of  $ka$  as high as 10. The origin of each polar plot, indicated by the heavy black dot in the center of each sketch, corresponds to the center of the cylinder. For values of  $ka$  less than 1, there is considerable backscatter from the cylinder in the direction of the incoming plane wave and relatively little sound scattered in the forward direction. As  $ka$  increases, there is a tendency for the scattered wave to be beamed in the forward direction with a decrease, but a growing number of lobes, in the relative amplitude of the back scattered field.

**Geometric Theory** - A wave theory solution requires solving the wave equation. Numerous methods have been devised for finding wave solutions, but these methods generally only apply to simple geometries and are not always useful for practical applications. Keller, reference 5, introduced the geometric theory of diffraction for solving approximately problems of wave propagation. The method is intended to apply to high frequency waves, or, more precisely, to problems in which the wavelength  $\lambda$  is small compared to the dimensions of the scattering body. In many practical cases it has been found that the method also gives useful results down to frequencies for which  $\lambda$  is comparable to scatter dimensions. An important advantage of the geometrical theory is that it does not depend upon the separation of variables or any similar analytical procedure. The shapes of objects to which it can be applied are quite general.

The basic idea of the theory is that short acoustic waves propagate along straight rays as in geometrical optics. However, the theory introduces new kinds of rays called "diffracted" rays. In applying the geometric theory of diffraction the field at a point is calculated from the sum of fields from all the geometrical acoustics rays, i.e., the direct and reflected rays, and all the diffracted rays. The solution of the problem of the diffraction of a plane wave by a circular cylinder in two-dimension will now be derived using the geometric theory.

First, it is necessary to calculate the wave field produced by the reflection of the incident plane wave from the cylinder, see Figure 9. The notation of the preceding section of the paper is used. Let  $P_r(0)$  denote the reflected field at a point  $O$ . One determines the amplitude  $A_r$  and the phase  $\phi$  of this wave as follows. The amplitude of the reflected wave is determined by the conservation of energy along the incident and reflected rays at point  $O'$ . That is, the energy flux in the tube of rays incident upon and reflected from this point must be the same at all points along the tube. The energy density along the tube is inversely proportional to the cross-sectional area of the tube, which can be determined from the Jacobian of the transformation between the physical variables  $(x, y)$  and the ray variables  $s$  and  $\theta$ . The  $(x, y)$  phase  $\phi$  is assumed to be a linear function of the distance  $s$  along the reflected ray. The constant  $s_0$  is determined by requiring that the phase of the reflected pressure at  $O'$  be identical to the phase of the incident pressure there. The final expression for the reflected pressure is shown at the bottom of Figure 9 where it has been simplified for an observer in the acoustic far field. In the geometric shadow  $P_r(0) = 0$  since there are no reflected rays there.

It is now necessary to calculate the diffracted field induced by the cylinder. The result of this calculation is shown in Figure 10. Behind this calculation is significant extension of classical geometrical acoustics introduced by Keller who postulates that there exists a class of diffracted rays which account for the phenomena of diffraction. These rays are produced when incident rays hit edges or corners of the scattering surface or when the incident ray impinges tangentially upon a smooth curved surface. Some of the diffracted rays penetrate into the shadow regions and describe the diffracted field there. Other rays modify the field in the sonified regions. The value of the field on a diffracted ray is obtained by multiplying the field on the incident ray at the point of diffraction of a so called "diffraction coefficient." Diffraction coefficients are determined entirely by the local properties of the field and the boundary in the immediate neighborhood at the point of diffraction and hence may be determined from the solution of simple boundary value problems having these local properties.

For the cylinder, diffracted rays emanate tangentially from all points of the cylinder surface. These rays are produced by "creeping" waves or surface waves which appear to originate at points  $O_1$  and  $O_2$  on the upper and lower surface of the cylinder. These waves encircle the cylinder in both directions and continuously radiate energy so that they steadily decay as they propagate. The series for the diffracted pressure may be interpreted as the sum of infinitely many creeping waves. The various orders of creeping waves are determined by the number of times the wave has encircled the cylinder. The complete solution is therefore given by  $P_i(0) + P_r(0) + P_d(0)$  which enables one to calculate the field at any point which does not lie on a caustic or a shadow boundary.

The expression developed in Figures 9 and 10 will now be used to calculate the diffraction of a plane wave by a cylinder. The amplitude of the field divided by the amplitude of the incident field is plotted along the  $x$ -axis for  $ka = 10$  in Figure 11. The solid curve is computed using the series method from the preceding section of the paper. The dot points are just the solution from the geometrical theory of diffraction. (Noted that  $P_r = 0$  in the forward direction) The comparison is seen to be quite acceptable.

The remainder of this paper will consider four problems in applied acoustics in which diffraction phenomena play a central role. The two solution methods just described have been used to obtain theoretical insight into these problems.

#### DIFFRACTION BY PRESSURE GRADIENT MICROPHONES

A photograph of a pressure gradient microphone and a sketch indicating its operation are shown in Figure 12. The type of microphone shown in the photograph has the shape of a thick disc of diameter about 2.36 cm. The purpose of this pressure sensor is to measure the pressure gradient in an incident wave field

12-4

as indicated in the sketch at the right. The microphone consists of two pressure sensitive elements separated by a distance  $\Delta Z$ . The pressure gradient at the center of the microphone 0, is then given approximately by the ratio  $(P_T - P_B)/\Delta Z$  in which  $P_T$  and  $P_B$  are the pressures measured on the top and bottom sides of the microphone. The actual pressures measured on the surfaces of the pressure gradient microphone will not be the desired free-field pressures because of diffraction effects. The scattering factor  $\sigma$  defined at the bottom of the figure is a measure of the degree to which the measured pressure difference divided by the microphone thickness approximates the true free-field pressure gradient and is therefore a figure of merit for the operation of a pressure gradient microphone. An analytical and experimental investigation was undertaken in order to determine an optimal shape which would minimize diffraction effects.

In order to assess the effects of microphone shape upon the measured surface pressures and thereby determine shapes which introduce minimum distortion one needs a validated analytical procedure for predicting the surface pressures on a variety of microphone shapes. The shape of the pressure gradient microphone in Figure 12 can be approximated as an oblate spheroid. The wave equation is separable in oblate spheroidal coordinates and the diffraction of plane waves by such a spheroid can be solved using the series method described earlier in this paper, reference 6. Some coordinate lines for oblate spheroidal coordinates  $(\xi, \eta)$  are shown in Figure 13. The curves  $\xi = \text{constant}$  are ellipses which generate oblate spheroids when rotated about the Z axis. The curves  $\eta = \text{constant}$  are hyperbolas. Compared to polar coordinates, the coordinate  $\xi$  varies from the surface of the spheroid into the acoustic far field analogous to the radial coordinate  $r$  whereas  $\eta$  varies around the spheroid analogous to the angular coordinate  $\theta$ . As a matter of reference the coordinate  $\eta$  decreases from +1 on the positive Z axis to 0 in the mid-plane of the spheroid to -1 on the negative Z axis.

The equation for calculating surface pressures at any point  $\eta$  on the surface of an oblate spheroid  $\xi = \xi_1$  due to an incident plane wave traveling in the negative Z direction is shown in the bottom of Figure 13. The series converges rapidly enough to be conveniently evaluated by computer for values of  $ka \leq 10$ . The functions  $S_{on}(-ika, \eta)$  and  $R_{on}(-ika, i\xi_1)$  are oblate spheroidal wave functions.

In order to determine the accuracy of the series solution for predicting surface pressures an experimental investigation of the diffraction of a plane wave by an oblate spheroid was conducted in an anechoic chamber. The spheroid used in the test had a major diameter of 25.4 cm and a thickness of 8.08 cm which corresponds to a value  $\xi_1 = .336$ . The details of these measurements and a description of the experiment are given in reference 6. The spheroid was instrumented with seven surface pressure gauges on one side which were used to map the surface pressures in detail on both the sonified and shadow sides of the spheroid. The incident wave was generated by a loud speaker placed at a distance of 3.5 m from the center of the spheroid. Figure 14 shows a comparison between measured and predicted values of the ratio  $|P_s/P_f|$  for several values of  $ka$ .  $P_s$  is the surface pressure at a point on the spheroid and  $P_f$  is the free-field pressure at the same point in the absence of the spheroid. At  $ka = 0.43$  the pressure distribution around the spheroid is quite uniform varying only slightly from that in the incident wave. At  $ka = 2.0$  constructive interference more than doubles the pressure in the center of the top side of the spheroid, and a shadow begins to form on the bottom side. At  $ka = 7.5$  a large region of uniform pressure doubling extends on the top side of the surface and a more distinct and widespread shadow region characterized by pressures less than those in the incident wave begins to spread over the bottom side. The overall agreement between theory and experiment is quite good over this range of  $ka$  values. One can now proceed to apply the theory to calculating surface pressures and evaluating the scattering factor for a family of spheroidal shapes with confidence.

The results of such a parameter study are shown in Figure 15. The parameter  $\xi_1$  was varied from 0 to 1 producing a family of oblate spheroids. The value  $\xi_1 = 0$  corresponds to a flat thin disc whereas  $\xi_1 = 1$  corresponds to a sphere. The scattering factor measures the extent to which the finite difference approximation using measured surface pressures approximates the desired free-field pressure gradient at the center of the spheroid. The smaller the magnitude of the scattering factor the better the approximation. The criterion chosen to identify an optimum shape is:  $|\sigma| < 1$  over the largest possible range of the frequency parameter  $F$ . It can be seen from the figure that for the four shapes shown the spheroid corresponding to  $\xi_1 = .826$  is the best shape allowing measurement up to a value of the frequency parameter of 1.7. An extension of these optimum shape studies to bodies of more general shapes has been carried out in reference 7 using a finite element technique.

#### WING SHIELDING OF AIRCRAFT ENGINE NOISE

One method for reducing the aircraft noise received by the airport community during landing approach and takeoff operations is to place the aircraft engine above the wing. Observers on the ground may thereby be shielded from the direct radiation of some engine noise by the presence of the wing surface. Three current engine over-the-wing aircraft configurations for which wing shielding may reduce community noise are shown in Figure 16. The QSRA is a NASA research aircraft. The YC-14 is a STOL transport designed for military use by the Boeing Commercial Aircraft Company. The jet engine exhaust close to the nozzle is then above the wing which tends to block off the downward radiation of jet noise from this part of the flow. The VFW-614 has its two engines mounted completely above the wing on pylons. The engine inlet is placed about over the mid-chord of the wing resulting, one would expect, in some shielding of ground observers from the forward radiated turbomachinery noise.

An experiment to measure the potential shielding effects of an aircraft wing was reported in reference 8. The test model and test arrangement are shown in Figure 17. The model consisted of a simulated wing and flap system having a chord-length of about 0.37 meters. The wing was very long in the span-wise direction, so as to simulate a two-dimensional arrangement. The noise source was a broadband point source placed at two positions above the wing, at 20 percent and 50 percent chord. Measurements of the diffracted sound field were made at increments of  $10^\circ$  from  $20^\circ$  to  $160^\circ$  below the wing as indicated in the sketch at the right of the figure. The measurements, made along an arc of radius 0.65 meters were taken in one-third octave bands at frequencies from 800 to 10,000 Hz. The measurements were made both with and without the wing in place and the results subtracted to obtain a change in sound pressure level,  $\Delta SPL$ , due to the

presence of the wing in the field of the point source. A positive  $\Delta$ SPL indicates the decrease in the measured sound pressure level due to the shielding produced by the wing.

Measurements of the wing shielding effect are shown in Figures 18 and 19. Figure 18 shows the difference in the shielding effect for the two different source positions at a frequency of 800 Hz. The shielding effect for position II, which is at the mid-chord location, is symmetric about 90°. Although there is a 5 dB shielding directly beneath the wing the maximum shielding effect, about 14 dB, occurs symmetrically ahead of and behind the overhead position at angles of 60° and 120°. The shielding effect produced for the source at position I is unsymmetric about 90°. The maximum shielding of about 13 dB is seen to occur at about 80°. These directivity patterns come about as a result of the constructive and destructive interference which results from the superposition of waves diffracted around the leading and trailing edges of the airfoil. The results of the figure show that achieving a desired shielding effect requires properly locating the wing relative to the noise source.

Figure 19 shows measurements of the wing shielding effect for source position II for frequencies of 800, 1600, and 5,000 Hz. In general, as the frequency increases the amount of shielding obtained below the wing increases. As frequency increases, the shadow produced under the wing intensifies and for these experiments, produces nearly 25 dB of noise shielding directly below the wing at 5000 Hz.

Shielding effects are therefore seen to depend both upon source frequency and source position. Jet engine noise is both broadband in nature and is produced in a region which extends for considerable distance downstream of the jet nozzle. It is evident, therefore, that designing for a optimum amount of engine noise shielding will require very careful design procedures. The results of a flight test program to study shielding utilizing a delta wing fighter aircraft are reported in reference 9.

#### DIFFRACTION BY AN AIRCRAFT FUSELAGE

It is of practical interest to know whether the diffraction of aircraft noise by the fuselage, wing and tail surfaces must be accounted for in aircraft noise prediction. This is a difficult question to answer since it involves multiple distributed sources and complex geometries. The possibility of such installation effects is suggested by the fact that the wavelengths of aircraft noise can be comparable to or smaller than the characteristic dimensions of the wing and fuselage surfaces. A preliminary analytical study of the importance of scattering from the aircraft fuselage was conducted using a prolate spheroid with acoustic point sources on one major axis, reference 10. The geometry and coordinate system for this problem are shown in Figure 20.

Several approaches for calculating the diffracted field of a point source near a prolate spheroid are available, see for example reference 1, including the series expansion method. The method of geometric acoustics discussed earlier in the paper was selected because of the relative simplicity of the solution. Expressions for the sound field are obtained which can be quickly evaluated on a computer.

The solution of the diffraction problem using geometric acoustics is given in Figure 21. A point source is at Q on the major axis of the prolate spheroid. The incident velocity potential  $\phi_i$  at the point P<sub>1</sub> on the surface of the spheroid is given in equation 1 in which  $QP_1$  indicates the distance between points Q and P<sub>1</sub>.

The reflected field  $\phi_r$  at a point P along a reflected ray is given by equation 2 in which  $\theta$  is the angle of incidence,  $\rho_1$  is the radius of curvature of the spheroid in the plane of incidence at P<sub>1</sub>, and  $\rho_2$  is the radius of curvature in the plane perpendicular to the plane of incidence and containing the normal to the spheroid at P<sub>1</sub>. In order to calculate  $\phi_r$  using equation 2 when Q and P are given, three computations must be made: the reflection point P<sub>1</sub> must be located, the angle of incidence  $\theta$  must be determined, and finally the two radii of curvature must be computed. The details of this process are given in reference 10.

To complete the calculation one must determine the diffracted field,  $\phi_d$ . The diffracted field is given in equation 3 in which  $\xi$  and  $\eta$  denote prolate spheroidal coordinates of points on the spheroid surface as indicated in Figure 4 of reference 10, and  $a$  is the interfocal distance. The functions  $f_n(\eta)$  and  $x_n(\alpha, \beta)$  are defined in reference 10. This formulation for the diffracted field is valid provided  $ka(\frac{b}{a})^2 \gg 1$ . The complete solution for the acoustic velocity potential is:  $\phi_d$  in the shadow region and  $\phi_i + \phi_r + \phi_d$  in the sonified region.

Sample calculations were made of the diffracted sound field for a spheroid which is the approximate size and shape of a commercial aircraft fuselage and for frequencies typical of aircraft noise. Some results of these calculations are shown in Figure 22. The value  $ka = 1000$  corresponds, for example, to a frequency of about 3500 Hz and a major axis of 30 meters. The sketches show contours of equal sound pressure level on an imaginary observer plane below and parallel to the x, y plane, see Figure 20), at  $\frac{z}{a} = 20$ . The intersection of the z axis with this observer plane is the origin of the plots. All sound pressure levels are normalized with respect to the SPL at this reference point.

The sketch at the top of Figure 22 shows the circles of constant SPL produced by a simple stationary point source in the absence of the scattering body. The sketch at the lower left shows the distortion produced by these contours by adding the spheroid. The source is placed at a distance equal to 0.028a aft of the spheroid on the extension of the major axis. The sketch at the lower right shows contours for the case of correlated sources on the major axis of the spheroid. The greater distortion of the equal SPL contours in the case of one source is evident. The complex patterns shown here resulting from diffraction by the fuselage are considered severe enough to warrant giving more attention to the possible effects of scattering of aircraft noise by the airframe.

12-5

12-6

A comparison of the geometric acoustic solution with other experimental and numerical results is shown in Figure 23. The integral equation solution method and the details of the experiment are discussed in the lecture entitled, "Acoustic Scattering from an Elliptic Body" by L. Maestrello and A. Bayliss in this lecture series. The calculations are for a value  $ka = 164$  which is considered sufficiently large for the geometrical theory to be applicable. The comparison with the more exact solution of Bayliss and the experimental data of Maestrello is seen to be quite acceptable except at small angles within the geometrical shadow region.

#### TRAILING EDGE NOISE RADIATION

Trailing edge noise is a frequently occurring source of aircraft noise which has been found for instance on the STOL, VTOL, and CTOL configurations shown in Figure 24. Trailing edge noise is an aerodynamic noise source caused by the turbulent flow shed off the trailing edges of wings, flaps, or rotating blades. The readjustment process which the flow makes as it transitions from being constrained by a surface to being a free shear flow results in the radiation of noise. The turbulent flow may be either a boundary layer flow or a wall jet flow. Thus, trailing edge noise has been encountered in connection with blown flaps used for the generation of powered lift, wings and flaps, from which it is a source of airframe noise, and rotating blades for which it is a broadband noise source.

The currently accepted theory of trailing edge noise generation is shown in Figure 25. see reference 11. The airfoil is idealized as a semi-infinite flat rigid surface in a uniform stream,  $U_0$ , parallel to the plate. A boundary layer flow develops over the upper and lower surfaces. A typical turbulent eddy in the flow field, with vorticity of  $\bar{\omega}$ , travels downstream parallel to the plate at a velocity  $\bar{V}$ . As this eddy passes across the trailing edge of the plate a counterrotating eddy is generated with a circulation  $\bar{\Gamma}$  which then proceeds to travel downstream at the velocity  $\bar{W}$ . The vorticity  $\bar{\Omega}$  of the induced eddy is determined by the condition imposed upon the flow field at the trailing edge of the plate. Two extreme conditions have been considered: a full Kutta condition, which stipulates that there will be no pressure difference across the plate at the trailing edge and the contrary condition in which no vorticity at all is shed into the wake in which case the pressure difference at the trailing edge of the plate becomes infinite.

The partial differential equation governing the generation and propagation of sound by turbulent trailing edge eddies is shown in the center of Figure 25. The equation consists of a convective wave operator which describes the propagation of sound through the externally moving medium and an inhomogeneous term on the right hand side of the equation which is responsible for the generation of sound by the eddies. The two vectors  $\bar{\omega} \times \bar{V}$  and  $\bar{\Omega} \times \bar{W}$  each lie in the plane of the sketch normal to the plate. These vectors play the role of externally applied body forces in the turbulent fluid surrounding the trailing edge which act normal to the trailing edge. Thus, the trailing edge noise source may be interpreted as a distribution of dipoles in the wake whose strength is related to the vorticity in the fluid and the convection speed of the turbulent eddies. In the formulation of this theory it was found to be convenient to use as the principal acoustic variable the stagnation enthalpy  $B$  in the flow field which is related to the far-field acoustic pressure as indicated in the equation at the bottom of the figure in which  $M_0$  is the component of the free stream Mach number in the direction of the observer. On the plate the normal derivative of  $B$  vanishes.

Trailing edge noise is generated then by dipole, located near the trailing edge of the plate and normal to the plane of the plate. Because of the presence of the plate the directivity pattern of a trailing edge dipole will be different than that of a free-field dipole as a result of acoustic diffraction phenomenon. The directivity of a trailing edge dipole is shown in Figure 26. The angles  $\alpha$  and  $\theta$  defining the observer position are shown in the sketch. The mean square pressure in the acoustic far field is proportional to  $\sin^2 \alpha \sin^2 \frac{\theta}{2}$ . Several cross sections through the radiation pattern of such a baffled dipole are shown in the sketches at the bottom of the figure. This dipole has its maximum radiation amplitude in the plane of the plate in contrast to the radiation from the free-field dipole which achieves its maximum along the axis of the applied force and has no radiation perpendicular to the force axis. The theory predicts that the amplitude of the mean square pressure depends upon the boundary conditions imposed at the trailing edge.

A comparison between measured and predicted directivity patterns of trailing edge noise, taken from reference 12, is shown in Figure 27. The trailing edge noise was produced by placing a thin plate in a jet exhaust as indicated by the sketch in the middle of the figure. Measurements of the radiated noise were then taken in narrow bands at the six frequencies between 100 and 3,000 Hz. Note that the dB levels on the upper and lower halves of the figure are different. There is a consistent and appreciable decrease in amplitude with increasing frequency. At any frequency there is a clear tendency for the radiated noise to peak in the upstream direction, as predicted by the theory. This type of evidence supports the general correctness of the theoretical prediction of trailing edge noise radiation. The additional diffraction which may be expected from the leading edge of a plate of finite length is discussed in references 12 and 13.

#### CONCLUDING REMARKS

This paper has provided an introduction to the concepts and methods of diffraction theory and has presented several examples of diffraction phenomena arising in the study of aircraft noise. It has been shown how the diffraction theory was used to select the shape of a microphone so as to extend its usefulness over the widest possible frequency range. Experiments on wing shielding of engine noise show the potential for considerable reduction of the community noise through proper engine placement. The scattering of sound from an aircraft fuselage was studied using a geometrical theory of diffraction. Severe distortions of equal sound pressure level contours were observed suggesting that the scattering of noise from the airframe deserves more attention. Experiments and theory on trailing edge noise indicate that the diffracting effect of the wing explains the unusual cardioid radiation pattern of this noise source. The need for more powerful theoretical methods to calculate diffraction phenomena for complex shapes and broadband distributed sources is clear.

## REFERENCES

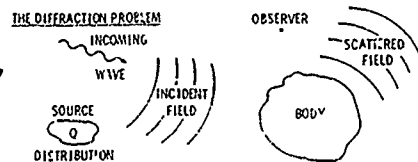
1. Asvestas, J. S.; Bowman, J. J.; Christiansen, P. L.; Einarsson, O.; Kleinman, R. E.; Sengupta, D. L.; Senior, T. B. A.; Sleator, F. B.; Uslenghi, P. L. E.; Zitron, N. R.: Electromagnetic and Acoustic Scattering by Simple Shapes. North-Holland Publishing Company, Wiley Interscience Division, John Wiley & Sons, Inc.- New York, 1969.
2. Bouwkamp, C. J.: Reports on Progress in Physics (Diffraction Theory), Vol. XVII, 1954, published by The Physical Society, London.
3. Morse, Philip M.; Feshbach, Herman: Methods of Theoretical Physics. Part II, Chapter 11, McGraw-Hill Book Company, Inc., 1953.
4. Morse, Philip M.; Ingard, K. Uno: Theoretical Acoustics. Chapter 8, McGraw-Hill Book Company, 1968.
5. Lewis, Robert M.; Keller, Joseph B.: Asymptotic Methods for Partial Differential Equations: The Reduced Wave Equation and Maxwell's Equation. Research Report No. EM-194, New York University, Courant Institute of Mathematical Sciences, January 1964, Contract No. AF 19(604)5238, Project No. 5635, Task No. 563502.
6. Maciulaitis, Algirdas; Seiner, John M.; Norum, Thomas D.: Sound Scattering by Rigid Oblate Spheroids, with Implication to Pressure Gradient Microphones. NASA TN D-8140, May 1976.
7. Norum, Thomas D.; Seiner, John M.: Shape Optimization of Pressure Gradient Microphones. NASA TM 78632, December 1977.
8. Sears, Frederick M.: The Acoustic Shielding of Noise by a Jet Wing. Submitted in partial fulfillment of the requirements for the degrees of Bachelor of Science and Master of Science at the Massachusetts Institute of Technology, May 1975.
9. Jeffery, R. W.; Holbeche, T. A.: An Experimental Investigation of Noise-Shielding Effects for a Delta-Winged Aircraft in Flight, Wind Tunnel and Anechoic Room. Tech. Memo AERO 1621, Royal Aircraft Establishment, February 1975.
10. Padula, S. L.; Liu, C.H.: Acoustic Scattering of Point Sources by a Moving Prolate Spheroid. AIAA 4th Aeroacoustics Conference, Atlanta, Georgia, October 3-5, 1977, Paper No. 77-1326.
11. Howe, M. S.: A Review of the Theory of Trailing Edge Noise. NASA Contractor Report 3021, June 1978.
12. Hayden, Richard E.; Fox, Herbert L.; Chanaud, Robert C.: Some Factors Influencing Radiation of Sound from Flow Interaction with Edges of Finite Surfaces. Bolt Beranek & Newman Report No. 2797, July 1976.
13. Tam, Christopher K. W.; Yu, J. C.: Aeroacoustics: STOL Noise; Airframe and Airfoil Noise (Trailing Edge Noise). Volume 45, Progress in Astronautics and Aeronautics, 1976.

## ACKNOWLEDGEMENT

The authors would like to acknowledge the assistance of Ms. Jean Mason with various calculations presented in this paper.



12-8



INHOMOGENEOUS WAVE EQUATION

$$\frac{1}{c^2} \cdot \frac{\partial^2 \varphi}{\partial t^2} - \nabla^2 \varphi = q$$

 $\varphi$  ACOUSTIC VELOCITY POTENTIAL $p = \rho_0 \frac{\partial \varphi}{\partial t}$  ACOUSTIC PRESSURE $c$  AMBIENT SPEED OF SOUND $\vec{u} = -\nabla \varphi$  ACOUSTIC VELOCITY VECTOR

Figure 1 - Basic Equations of Acoustic Diffraction Theory - Field Equation

## SURFACE BOUNDARY CONDITION

$$\rho_0 c u_n = \nu p; \nu = \text{SPECIFIC SURFACE ADMITTANCE.}$$

$$\nabla \varphi \cdot \vec{n} + \frac{\nu}{c} \frac{\partial \varphi}{\partial t} = 0 \text{ ON THE BODY SURFACE.}$$

## RADIATION CONDITION

OUTGOING WAVES AT LARGE DISTANCES

$$\frac{\partial \varphi}{\partial r} + \frac{1}{c} \frac{\partial \varphi}{\partial t} \rightarrow 0 \text{ OR } p \approx \rho_0 c u_r \text{ AS } r \rightarrow \infty.$$

## EDGE CONDITION

NO ENERGY IS GENERATED AT SHARP EDGES.

$$\iint_{\text{FINITE REGION}} (\nabla \varphi \cdot \nabla \varphi) dv \text{ IS FINITE.}$$

Figure 2 - Basic Equations of Acoustic Diffraction Theory - Auxillary Conditions

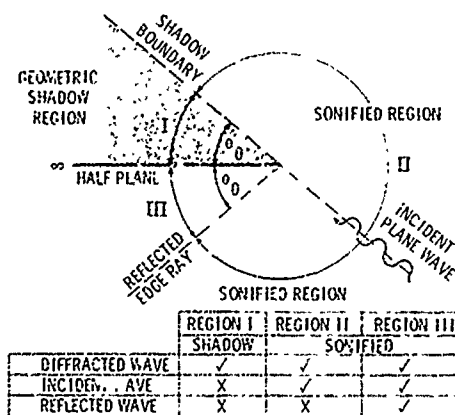
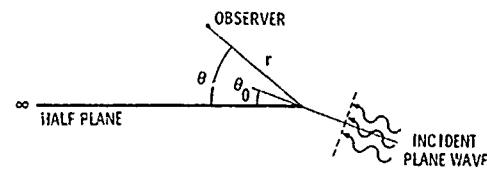


Figure 3 - Plane Wave Diffraction by a Half Plane - Interpretation of Solution



$$p = \frac{e^{-i\pi/4}}{\sqrt{\pi}} \left\{ e^{ikr \cos(\theta - \theta_0)} \Phi \left( \sqrt{2kr} \sin \frac{1}{2} (\theta - \theta_0) \right) + e^{ikr \cos(\theta + \theta_0)} \Phi \left( -\sqrt{2kr} \sin \frac{1}{2} (\theta + \theta_0) \right) \right\}$$

$$\Phi(x) = \int_{-\infty}^x e^{it^2} dt = \text{FRESNEL INTEGRAL}$$

Figure 4 - Plane Wave Diffraction by a Half Plane - Exact Mathematical Solution

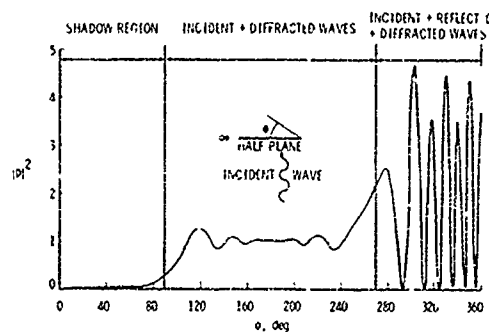
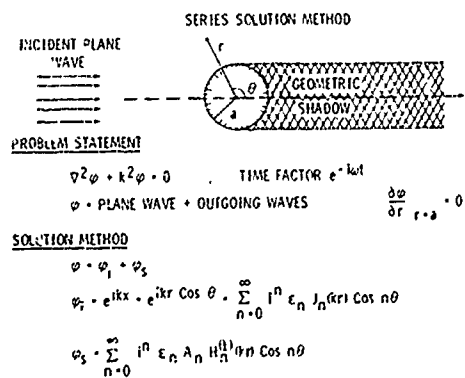
Figure 5 - Mean Square Pressure in the Sound Field for Plane Wave Diffraction by a Half Plane - Normal Incidence:  $kr = 6\pi$ 

Figure 6 - Diffraction of a Plane Wave by a Cylinder - Series Solution Method

# **SOLUTION METHOD**

$$\varphi = \sum_{n=0}^{\infty} |n| \epsilon_n \left[ J_n(kr) + A_n H_n^{(1)}(kr) \right] \cos n\theta$$

$$\left. \frac{\partial \varphi}{\partial r} \right|_{r=a} = 0 = \sum_{n=0}^{\infty} |n| \epsilon_n \left[ J_n'(ka) + A_n H_n^{(1)'}(ka) \right] \cos n\theta$$

$$\therefore A_n = -J_n'(ka) / H_n^{(1)'}(ka)$$

$$P = P_i + P_s = -i k \rho_0 c \varphi \quad ; \quad \bar{u} = \bar{u}_i + \bar{u}_s = -\nabla \varphi$$

# **ACOUSTIC FAR FIELD**

$$\text{FOR } kr \rightarrow \infty : P_s \approx \rho_0 c (i k r)^{-1/2} \sqrt{\frac{k}{r}} e^{i(kr + \frac{\pi}{4})} P(ka, \theta)$$

$$P(ka, \theta) = \sqrt{\frac{2}{\pi}} \sum_{n=0}^{\infty} \epsilon_n \frac{J_n'(ka)}{H_n^{(1)'}(ka)} \cos n\theta$$

Figure 7 - Diffraction of a Plane Wave by a Cylinder - Far-Field Acoustic Solution

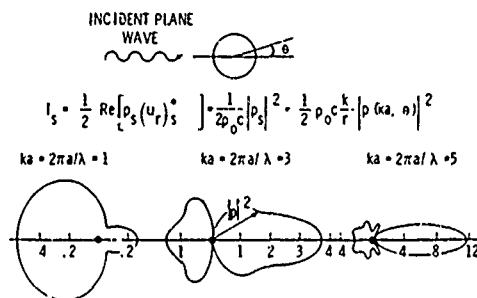


Figure 8 - Scattered Intensity for Diffraction of a Plane Wave by a Cylinder

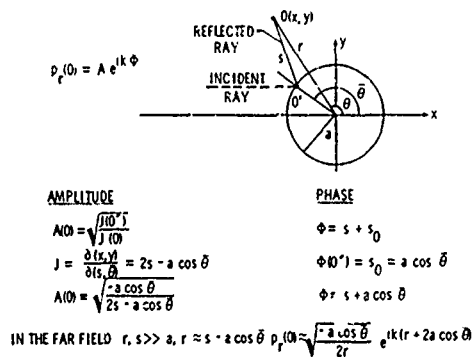


Figure 9 - Plane Wave Diffraction by a Circular Cylinder-Geometric Theory: Reflected Waves

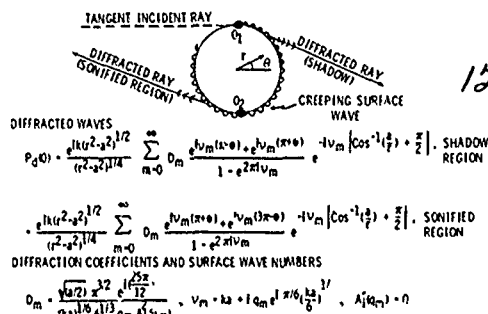


Figure 10 - Plane Wave Diffraction by a Circular Cylinder-Geometric Theory: Diffracted Waves

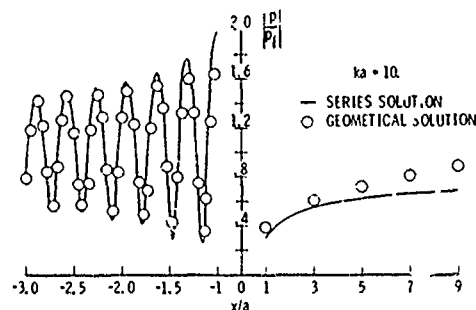


Figure 11 - Comparison Between Series Solution and Geometric Acoustics

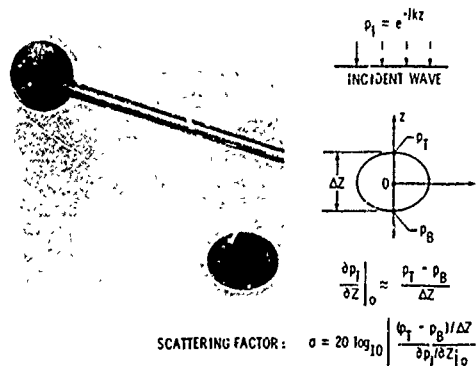
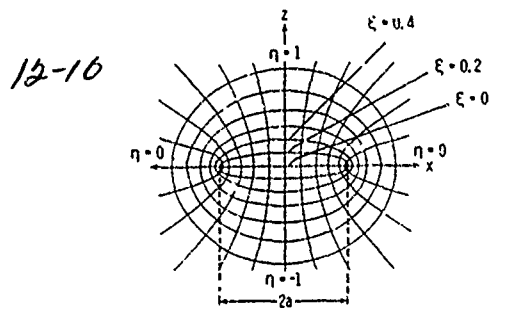


Figure 12 - Pressure Gradient Microphone - Appearance and Function



SURFACE PRESSURES ON AN OBLATE SPHEROID

$$\frac{p_s(\eta, \xi_1)}{p_i} = \frac{2}{ka(1 + \xi_1^2)} \sum_{n=0}^{\infty} \frac{S_{on}(-ika, -1) S_{on}(-ika, \eta)}{N_{on}(ika) R_{on}^{(3)}(-ika, 1, \xi_1)}$$

Figure 13 - Oblate Spheroidal Coordinates

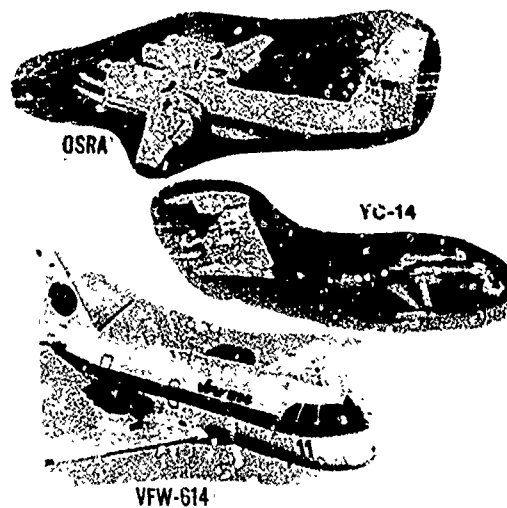


Figure 16 - Engine Over the Wing Aircraft Configurations

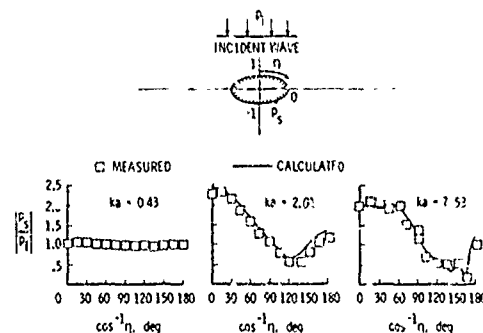


Figure 14 - Comparison of Measured and Calculated Surface Pressures

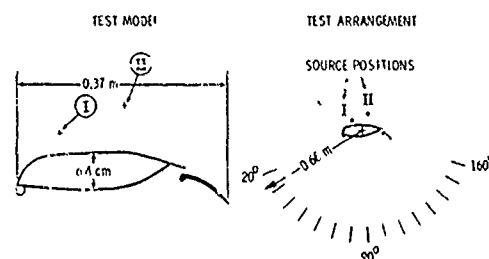


Figure 17 - Wing Shielding Experiment

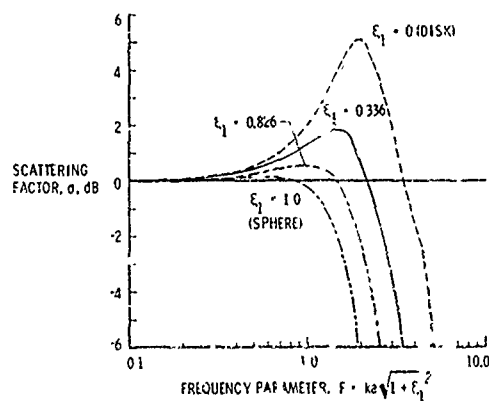


Figure 15 - Variation of Scattering Factor with Frequency Parameter

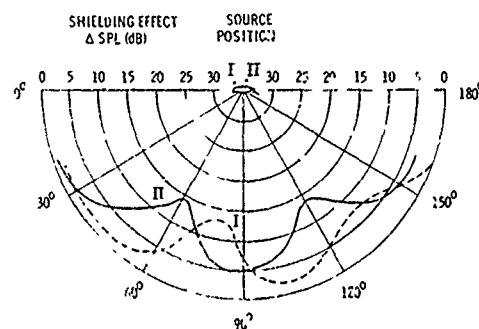


Figure 18 - Measured Wing Shielding Effect  
C/c d/wave length = 0.85, f = 800 Hz

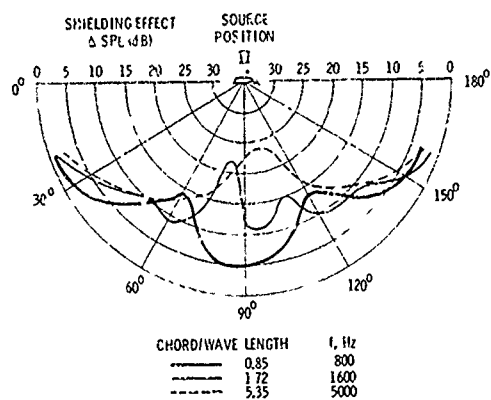


Figure 19 - Measured Wing Shielding Effect

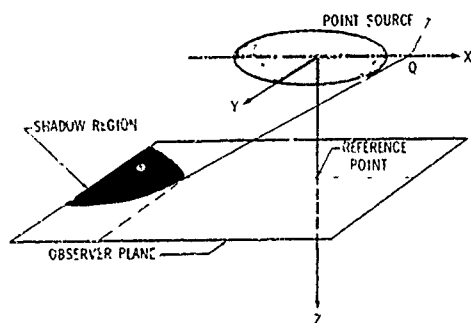


Figure 20 - Acoustic Scattering of Point Source by an Aircraft Fuselage

PLANE OF INCIDENCE

OBSERVER PLANE

X, Y, Z

$$\varphi_1 = \exp \left\{ i k \left( \frac{r_1}{a} \right) \right\} \left\{ \frac{1}{a} \left( \frac{r_1}{a} \right) \right\}^{1/2} \quad (1)$$

$$\varphi_2 = \exp \left\{ i k \left( \frac{r_2}{a} \right) \right\} \left\{ \frac{1}{a} \left( \frac{r_2}{a} \right) \right\}^{1/2} \left[ 1 + \frac{(P_1 P_2)}{(Q P_1)} + \frac{2(P_1 P_2)}{P_1 \cos \theta} \right]^{-1/2} \quad (2)$$

$$\varphi_3 = \frac{2^{3/2} \exp \left\{ \frac{i \pi}{12} \right\} \left\{ \frac{\epsilon_1 \epsilon_2}{\epsilon_0} \right\}^{1/6}}{\pi^{1/2} (2 k d)^{1/6}} \cdot \frac{\exp \left\{ i k d \sqrt{\epsilon_0^2 - 1} \sqrt{\epsilon_0^2 - \epsilon_1^2} \right\}}{\left[ \epsilon_0^2 - \epsilon_1^2 \epsilon_0^2 - 1 \right] \sqrt{\epsilon_0^2 - 1} \sqrt{\epsilon_0^2 - \epsilon_1^2}} \quad (3)$$

Figure 21 - Geometrical Theory of Scattering by a Prolate Spheroid

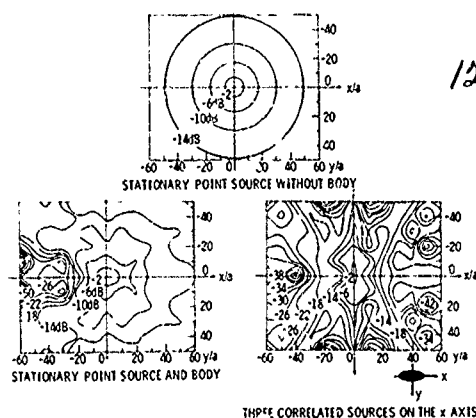


Figure 22 - Sound Pressure Level Contours on Observer Plane  
ka = 1000, b/a = 0.14, z/a = 20

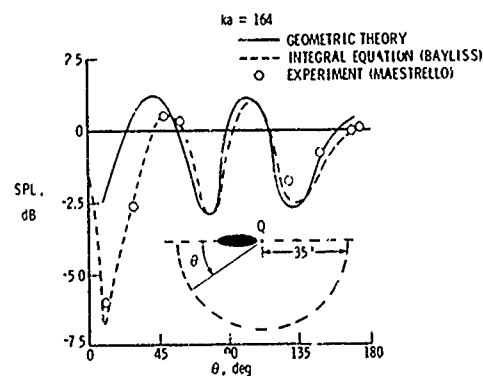


Figure 23 - Validation of Computational Method  
ka = 164

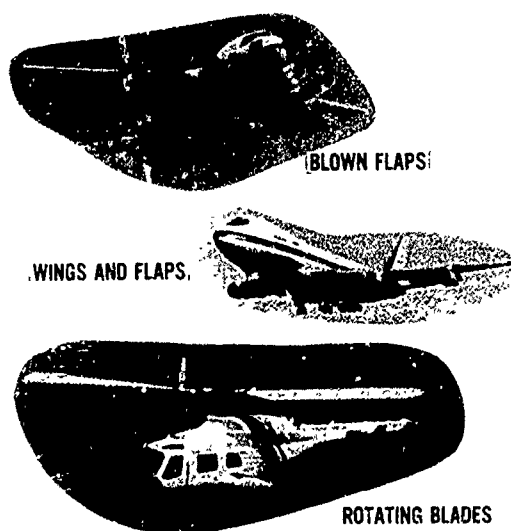
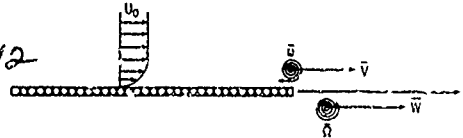


Figure 24 - Aircraft Trailing Edge Noise Sources

12-12



$$\left[ \frac{1}{c^2} \left( \frac{\partial}{\partial t} + U_0 \frac{\partial}{\partial x} \right)^2 - \nabla^2 \right] \rho = \text{div} (\bar{\omega} \times \bar{v} + d\bar{h} (\bar{\Omega} \times \bar{v}))$$

CONVECTED WAVE OPERATOR EDGE DIPOLE DISTRIBUTION

$$\mathbf{g} = \mathbf{h} + \frac{1}{2} \bar{v} \cdot \bar{v} \sim \mathbf{Q} + \bar{M}_0 \frac{\mathbf{r}}{r_0} \quad \text{IN THE FAR FIELD}$$

Figure 25 - Howe Trailing Edge Noise Theory

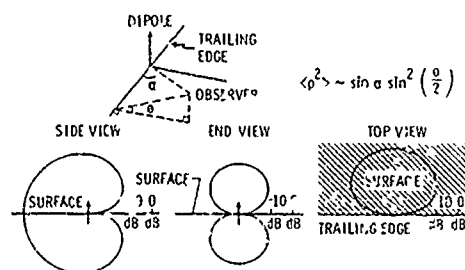


Figure 26 - Directivity of a Trailing Edge Dipole

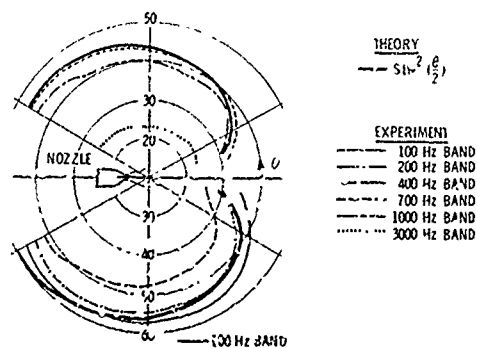


Figure 27 - Measured Directivity of Trailing Edge Noise

RANDOM PROPAGATION AND RANDOM SCATTERING  
C. Gazanhes, Maître de Recherche  
Department of Acoustics, C.N.R.S., Marseille, France

SUMMARY

Acoustic wave propagation through atmosphere (or ocean) undergoes amplitude and phase fluctuations because the random nature of the medium.

The purpose of this course is to provide a review of the principal methods : geometrical optics, Born approximation, Rytov method, parabolic equation, ... which allow us to treat the random propagation problems.

Finally we consider the case of the scattering by a cloud of random scatterers.

INTRODUCTION

The random nature (in space and time) of real media (atmosphere, ocean) has a strong influence on the propagation of acoustic waves. In particular, it produces amplitude and phase fluctuations of the received signals. In the case of a long range propagation, because of a cumulated effect, these fluctuations can become very important even if the medium fluctuations are weak.

Depending the fluctuations scale, two points of view /1/ can be distinguished. First, the macroscopic point of view, where one assimilates the medium to a continuous random medium, of which the properties vary in function of time and space. Second, the microscopic point of view where we assimilate the medium to a random medium containing randomly distributed scatterers. We are going to study these two points of view in the following chapters.

1. PROPAGATION IN RANDOM MEDIA

1.1. Description of the medium

In the hypotheses of a temporal harmonic dependance, the simplest equation which governs the waves propagation is the Helmholtz's equation :

$$(1-1) \quad \Delta U(\vec{r}) + k_0^2 n^2(\vec{r}, \omega) U(\vec{r}) = 0$$

$\vec{r}$  specifies the space coordinates

$k_0$  represents the wave number in free space

$n(\vec{r}, \omega)$  is a random function which describes the properties of the medium (for example, the index of refraction).

We suppose :  $n(\vec{r}) = 1 + \mu(\vec{r}) \quad (\mu \ll 1)$

and for an homogeneous and stationary medium, we write :

$$E[n(\vec{r})] = 0 \quad (\text{Average value})$$

$$E[\mu^2(\vec{r})] = \bar{\mu}^2 \quad (\text{Variance})$$

$$\Gamma(\rho) = E[\mu(\vec{r}_1) \mu(\vec{r}_2)] = \bar{\mu}^2 C(\rho)$$

$\rho = \vec{r}_2 - \vec{r}_1$

where

To fit the experimental results, we choose an analytic model for  $C(\rho)$ . For instance an exponential model :

$$C(\rho) = e^{-\frac{|\rho|}{L}}$$

or a Gaussian model ;

$$C(\rho) = e^{-\left(\frac{\rho}{L}\right)^2}$$

13.2

$\ell$  is the correlation length of the refractive index.

We schematise the medium fluctuations by blobs the dimensions  $c^2$  which would be approximately  $\ell$ .

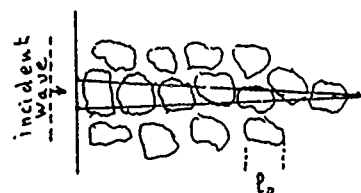
For a sound wave of high frequency each diffusing blob reacts as a lens of an angular opening  $\lambda/\ell$ . The energy is diffused in a cone in which the angle at the vertex would be centered on the receiver. If  $L$  is the wave path length in the medium, the maximal opening of the diffusion cone takes the value  $L\lambda/\ell$ .

We now have to consider the two following situations :

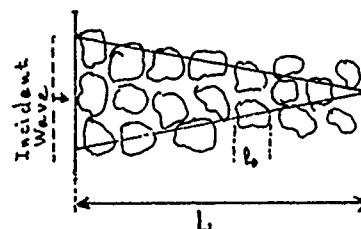
a)  $\sqrt{L\lambda} \ll \ell_0$  diffraction effects can be ignored (Figure 1a) this corresponds to ray propagation and the geometrical optics-approach can be used.

b)  $\sqrt{L\lambda} \gg \ell_0$  diffraction effects become important and it is necessary to solve the waves equation. (figure 1b)

The problem is more complex, because there are a number of many possible values for  $\ell$ . For example in the atmosphere, (Figure 2) shows a turbulent spectrum traced in function of the wave number  $k = 2\pi/\ell$ .



(a) Geometrical Optics  $\sqrt{L\lambda} \ll \ell_0$



(b) Diffraction Effects  $\sqrt{L\lambda} \gg \ell_0$

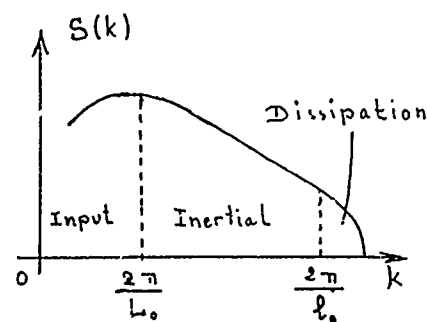


Figure 2

Figures 1a - 1b

We distinguish three regions delimited by the wave numbers  $k_0$  and  $k_m$ .

a)  $0 < k < k_0$

In this range the turbulence (wind or convection streams) is created. the turbulent blobs are large (100 meters). The turbulence is anisotropic : is called the outer scale of turbulence.

b)  $k_0 < k < k_m$

This range is characterized by the progressive subdivision of blobs, the energy is transferred to the smaller and smaller blobs. The turbulence is isotropic.

c)  $k > k_m$

From a certain value  $k_m = 2\pi/\ell_c$  the energy loss by viscosity becomes preponderant. could be of the order of millimeters. In the atmosphere the blobs are the most stable.

#### 1.2. Geometrical optic method

This method is only valid in the high frequencies domain with the condition :  $\lambda \ll \ell_0$ . We then consider a ray propagation and the scalar wave equation has an asymptotic solution in the form :

$$U(\vec{r}) = A(\vec{r}) \cdot e^{iS(\vec{r})}$$

Where  $A(\vec{r})$  is the amplitude and  $S(\vec{r})$  the phase of the wave. It satisfies the Eikonal equation.

13.3

(1-2)

$$|\text{grad } S|^2 = n^2$$

The surfaces  $S = \text{Cte}$  are the wave front and orthogonal curves to these surfaces are the rays. In random medium, the equation (1-2) can be written :

$$\frac{d}{ds} \left[ n \frac{d\vec{r}}{ds} \right] = \text{grad } n(\vec{r})$$

where  $s$  is the path along the ray. Chernov /2/ shows that the mean square lateral displacement of a ray is in the form :

$$\langle d^2 \rangle = \frac{4}{3} \sqrt{\pi} \bar{\mu}^2 L^3 / \ell_0$$

For a weak random medium, we can consider that the rays are only slightly deviated, from the propagation direction  $ox$ . Chernov /2/ shows then that the phase fluctuations take the value :

$$\bar{S}^2 = 2 \bar{\mu}^2 k^2 L \int_0^\infty C(x, 0) dx$$

and the logarithmic amplitude fluctuations

$$\bar{\chi}^2 = \left( \text{Log} \frac{A}{A_0} \right)^2 = \frac{8}{3} \sqrt{\pi} \bar{\mu}^2 L^3 / \ell_0^3$$

### 1.3. Born's approximation

The geometrical optic doesn't allow us to take into account the diffraction problems. To introduce the diffraction we can resolve the equation (1-1) in developing the solution  $U(\vec{r})$  in perturbation series in the form /3/.

The equation (1-1) can be written :  $U = U_0 + U_1 + U_2 + \dots$

(1-5)

$$(\Delta + k_0^2) U = -k_0^2 \delta n U$$

after writing :

$$\delta n = (1 + \mu)^2 - 1 = 2\mu + \mu^2$$

A general solution (1-5) is given by the integral equation

$$U(\vec{r}) = U_0(\vec{r}) + k_0^2 \int_V G(\vec{r} - \vec{r}') \delta n(\vec{r}') U(\vec{r}') dV'$$

$\vec{r}$  locates the receiver and  $\vec{r}'$  the scattering volume  $V'$ .  $U_0(\vec{r})$  is the field in the absence of fluctuation ( $\delta n = 0$ ) and  $G(\vec{r} - \vec{r}')$  is the Green function for the free space.

(1-7)

$$G(\vec{r} - \vec{r}') = \frac{e^{ik_0 |\vec{r} - \vec{r}'|}}{4\pi |\vec{r} - \vec{r}'|}$$

The Born approximation consists of replacing  $U(\vec{r}')$  by  $U_0(\vec{r}')$  in the equation (1-6). We then get the solution of Born which is an approximation of single scattering.

Let us now calculate the mean scattered intensity, in the far field conditions. We choose the origine of the coordinates at the center of the scattering volume. The Green function (1-7) is then given by

$$G(\vec{r} - \vec{r}') \approx \frac{e^{ik_0 \vec{r}}}{4\pi |\vec{r}|} e^{-i\vec{k}_d \cdot \vec{r}'}$$

where

$$\vec{k}_d = k_0 \frac{\vec{r}}{|\vec{r}|}$$

represents the scattered wave number. For an incident plane wave defined by  $e^{ik_0 \vec{r}}$  Prish /1/ derives the mean scattered intensity in the form :



if

$$(1-13) \quad |\nabla \psi_1| \ll |\nabla \psi_0|$$

and

$$(1-14) \quad \mu^2 \ll 2\mu$$

The equation (1-11) can be written :

$$(1-15) \quad (\nabla^2 + k_0^2)(U_0 \psi_1) = [(\nabla \psi_1)^2 + k_0^2 \delta \mu] U_0$$

which is the inhomogeneous wave equation, the solution of which can be written :

$$(1-16) \quad \psi_1(\vec{r}) = \frac{1}{U_0(\vec{r})} \int_V G(\vec{r} - \vec{r}') [(\nabla \psi_1)^2 + k_0^2 \delta \mu] U_0(\vec{r}') dV'$$

By iteration we obtain the general solution. For the first iteration we choose the value

 $\psi_1 = 0$  in the integral and we get :

$$(1-17) \quad \psi_1(\vec{r}) = \frac{k_0^2}{U_0(\vec{r})} \int_V G(\vec{r} - \vec{r}') \delta \mu U_0(\vec{r}') dV'$$

This is the first solution of Rytov. Hence :

$$(1-18) \quad U(\vec{r}) = U_0(\vec{r}) e^{\frac{k_0^2}{U_0(\vec{r})} \int_V G(\vec{r} - \vec{r}') \delta \mu U_0(\vec{r}') dV'}$$

which gives the Born approximation for the weak variations of the signal.

Let us write :

$$U(\vec{r}) = A(\vec{r}) e^{iS(\vec{r})}$$

if

$$\psi_1(\vec{r}) = \chi + iS = \text{Log} \frac{A}{A_0} + i(S - S_0)$$

We can see that the real part :  $\chi = \text{Log} \frac{A}{A_0}$ of  $\psi_1(\vec{r})$  represents the fluctuations of the logarithmic amplitude A.

It seems that the Rytov method doesn't apply any longer when the propagation distances become greater (approximately one kilometer). We then verify a very clear divergence between the experimental and theoretical results. The method known as the parabolic equation allows us to go further.

### 1.5. The Parabolic Equation

We obtain it from the wave equation (1-1) by looking for a solution in the form of /6/.

$$(1-19) \quad U(\vec{r}) = u(\vec{r}) e^{ikx}$$

We then obtain the equation

$$(1-20) \quad \Delta u(\vec{r}) + 2ik \frac{\partial u(\vec{r})}{\partial x} + 2k^2 \mu(\vec{r}) u(\vec{r}) = 0$$

13-6

In the case of a propagation following  $o x$ .

If  $u(\vec{r})$  is a function, slightly variable to  $x$  and if  $\lambda \ll l$  (correlation of index) we have

$$\left| \lambda \frac{\partial u}{\partial x} \right| \gg \left| \frac{\partial^2 u}{\partial x^2} \right|$$

In these conditions we can substitute for the Laplacian  $\Delta$  the transverse Laplacian

$$\Delta_{\perp} = \frac{\partial^2}{\partial y^2} + \frac{\partial^2}{\partial z^2}$$

We then obtain the simplified equation :

$$(1-21) \quad \Delta_{\perp} u(\vec{r}) + 2ik \frac{\partial u(\vec{r})}{\partial x} + 2k^2 \nu(\vec{r}) u(\vec{r}) = 0$$

This equation is only valid in the approximation of slightly inclined rays from the propagation direction  $x$ .

R.H. Clark /7/ proposes to resolve the equation (1-21) in a way similar to the proceeding one. He considers two separated steps :

In the first step, we suppose an homogeneous medium such as  $\mu = 0$  and in the half plan  $x > 0$  we represent the acoustic field by the integral

$$(1-22) \quad U_0(y, x) = \int_{-\infty}^{+\infty} F_0(s) e^{ik[y\delta + xc]} d\delta$$

where  $s = \sin \theta$  and  $c = \cos \theta$ .

$F_0(s)$  represents the plane waves spectrum of  $U_0(y, x)$ .

We have :

$$(1-23) \quad c = \cos \theta \approx 1 - \frac{1}{2} \theta^2$$

and we can write the field in a plane located at  $\Delta x$  from the origin :

$$(1-24) \quad U_0(y, \Delta x) = e^{ik\Delta x} \int_{-\infty}^{+\infty} F_0(s) e^{-\left(\frac{1}{2} ik\Delta x s^2\right)} e^{iky\delta} d\delta$$

In the second step we look for a solution of the parabolic equation, supposing that the medium is slightly heterogeneous. We then neglect the second order derivative in such a way that in (1-21).

The solution of the first order differential equation that remains can be written as :

$$(1-25) \quad u(y, \Delta x, t) = u(y, 0) e^{ik \int_0^{\Delta x} \nu(y, x, t) dx}$$

In these condition the medium is divided into homogeneous slabs at the same width  $\Delta x$  (Figure 5), but the refractive index can be different from one slab to another.

$u(y, 0)$  represents the distribution of the acoustic field on the plane  $x = 0$

$u(y, t, \Delta x)$  represents the same distribution on the plane  $x = \Delta x$

affected by the phase shift introduced by propagation along a ray of length  $\Delta x$ .

To finish, we combine the two types of solution (1-24) and (1-25) by writing

$$(1-26) \quad U(y, \Delta x, t) = U_0(y, \Delta x) e^{i\Phi(y, \Delta x, t)}$$

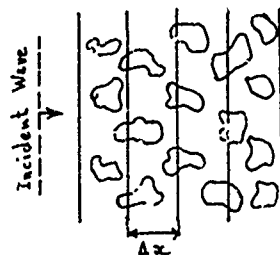


Figure 5

in which  $U_0$  is the solution corresponding to the homogeneous medium. (1-23) allows us to pass from the plan  $x = x$  to the next one  $x = x + \Delta x$  and so on.

The first type of solution (1-24) takes into account the diffraction effects. The second type of solution (1-25) takes into account the random irregularities of the medium.

## 2. THE MULTIPLE SCATTERING

### 2.1 Fundamental equations

Let a volume  $V$  containing  $N$  particles located at points  $r_1, r_2, r_j, r_N$ .

Let us consider an observation point  $A$  and let  $\psi$  be the acoustic field at this point. (Figure 6).

It verified the wave equation :

$$(2-1) \quad \Delta \psi + k_0^2 \psi = 0$$

where  $k_0 = 2\pi/\lambda_0$  is the wave number in the medium surrounding the scatterers. Let us call  $\psi_0$  the incident field at the point  $A$ , in absence of scatterers and  $F(r, r_j)$  the wave scattered by the  $j$ th scatterer at the point  $A$ . The total field will be under the form (Figure 7a).

$$(2-2) \quad \psi(\vec{r}) = \psi_0(\vec{r}) + \sum_{j=1}^N F(\vec{r}, \vec{r}_j)$$

The scattered wave  $F(\vec{r}, \vec{r}_j)$  can be expressed by the means of the incident wave  $\psi_0$  on the scatterer and the scattering coefficient  $u_j(\vec{r}_j, \vec{r})$  characterises the scatterer. The wave transmitted by the  $j$ th scatterer can then be written :

$$(2-3) \quad F(\vec{r}, \vec{r}_j) = u_j(\vec{r}_j, \vec{r}) \psi_j(\vec{r}_j)$$

It is important to notice that (2-3) is a symbolic writing which represents a product only with an incident plane wave. In these conditions

$$\psi_j(\vec{r}) = e^{ik_0 \vec{r}}$$

and when the distance between  $\vec{r}_j$  and  $\vec{r}$  is large we have (Figure 7b)

$$(2-4) \quad u_j(\vec{r}_j, \vec{r}) = g_j(\vec{r}_j) \frac{e^{-ik_0 |\vec{r} - \vec{r}_j|}}{|\vec{r} - \vec{r}_j|} = g_j(\vec{r}_j) E(\vec{r}, \vec{r}_j)$$

$g_j(\vec{r}_j)$  is the scattering pattern of the considered scatterer.

The wave impinging on the scatterer  $j$  is then the sum on the incident wave  $\psi_0(\vec{r}_j)$  and the waves scattered by all the other scatterers different from the scatterer  $j$  (Figure 7c).

We can write :

$$(2-5) \quad \psi_j(\vec{r}_j) = \psi_0(\vec{r}_j) + \sum_{i=1, i \neq j}^N g_i(\vec{r}_i) \psi_i(\vec{r}_i) E(\vec{r}_j, \vec{r}_i)$$

The equations (2-2) and (2-5) are the fundamental equations of the multiple scattering /9 - 10 - 5/

Let us write against :

$$(a) \quad \psi(\vec{r}) = \psi_0(\vec{r}) + \sum_{j=1}^N g_j(\vec{r}_j) \psi_j(\vec{r}_j) E(\vec{r}, \vec{r}_j)$$

$$(b) \quad \psi_j(\vec{r}_j) = \psi_0(\vec{r}_j) + \sum_{\substack{i=1 \\ (i \neq j)}}^N g_i(\vec{r}_i) \psi_i(\vec{r}_i) E(\vec{r}_j, \vec{r}_i)$$

For a given incident wave  $\psi_0(\vec{r})$  one can eliminate  $\psi_j(\vec{r})$  and calculate the resultant wave  $\psi(\vec{r})$ .

By successive iteration, we obtain the series :

$$\begin{aligned} \psi(\vec{r}) &= \psi_0(\vec{r}) + \sum_{j=1}^N g_j(\vec{r}_j) E(\vec{r}, \vec{r}_j) \left[ \psi_0(\vec{r}_j) + \sum_{\substack{i=1 \\ (i \neq j)}}^N g_i(\vec{r}_i) \psi_i(\vec{r}_i) E(\vec{r}_j, \vec{r}_i) \right] \\ &= \psi_0(\vec{r}) + \sum_{j=1}^N \mu_j(\vec{r}, \vec{r}_j) \left[ \psi_0(\vec{r}_j) + \sum_{\substack{i=1 \\ (\lambda \neq j)}}^N \mu_i(\vec{r}_j, \vec{r}_i) \psi_i(\vec{r}_i) \right] \\ &= \psi_0(\vec{r}) \\ &+ \sum_{j=1}^N \mu_j(\vec{r}, \vec{r}_j) \psi_0(\vec{r}_j) \\ &+ \sum_{j=1}^N \sum_{\substack{i=1 \\ (i \neq j)}}^N \mu_j(\vec{r}, \vec{r}_j) \mu_i(\vec{r}_j, \vec{r}_i) \psi_0(\vec{r}_i) \\ &+ \sum_{j=1}^N \sum_{\substack{i=1 \\ (i \neq j)}}^N \sum_{\substack{m=1 \\ (m \neq i)}}^N \mu_j(\vec{r}, \vec{r}_j) \mu_i(\vec{r}_j, \vec{r}_i) \mu_m(\vec{r}_i, \vec{r}_m) \psi_0(\vec{r}_m) \\ &+ \dots \dots \dots \end{aligned} \quad (2-7)$$

where the successive terms represent the incident wave and single, double, triple scattering waves. (Figure 8).

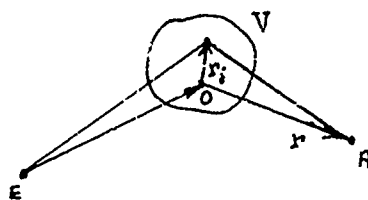
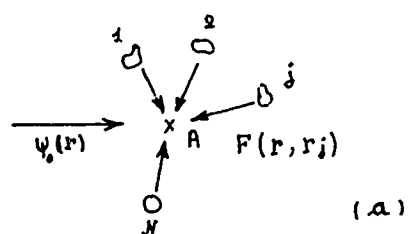
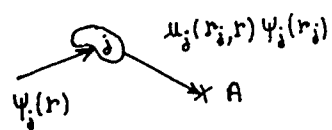


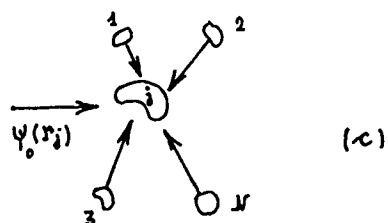
Figure 6



(a)

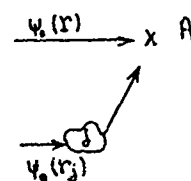


(b)

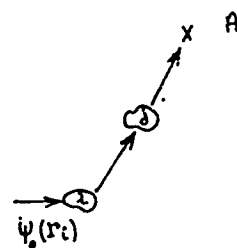


(c)

Figure 7



(a): Single Scattering



(b): Double Scattering

Figure 8

13-10

## 2.2. Randomly distributed scatterers

A random distribution of  $N$  scatterers contained in a volume  $V$  can be described by a multiple probability density in the form :

$$(2-8) \quad p_N(\vec{r}_1, \vec{r}_2, \vec{r}_3, \dots, \vec{r}_N; \lambda_1, \lambda_2, \lambda_3, \dots, \lambda_N)$$

$\vec{r}_j$  is the position of the particle  $j$  characterised by a scattering parameter  $s_j$ . If the scatterers are not correlated, the probability density (2-8) is written :

$$(2-9) \quad p_N = \left(\frac{1}{N}\right)^N p(\vec{r}_1, \lambda_1) p(\vec{r}_2, \lambda_2) \dots p(\vec{r}_N, \lambda_N)$$

## 2.3. Average acoustic field

In these conditions L.L. Foldy /9/ shows that the average acoustic field scattered by a set of  $N$  scatterers can be written : (average value of 2-2).

$$(2-10) \quad \langle \psi(\vec{r}) \rangle = \psi_0(\vec{r}) + \int_V G(\vec{r}, \vec{r}') \langle \psi(\vec{r}') \rangle E(\vec{r}, \vec{r}') d\vec{r}'$$

with

$$(2-11) \quad G(\vec{r}) = \int g(\lambda) n(\vec{r}, \lambda) d\lambda$$

where  $n(\vec{r}, s)$  is the average number of scatterers per unit volume in the neighbourhood of the point  $\vec{r}$  having the scattering parameter lying between  $s$  and  $s + ds$ .

The equation (2-10) is the solution of the heterogeneous equation :

$$(2-12) \quad \nabla^2 \langle \psi(\vec{r}) \rangle + k^2(\vec{r}) \langle \psi(\vec{r}) \rangle = 0$$

or again

$$(2-13) \quad k^2(\vec{r}) = k_0^2 + 4\pi G(\vec{r})$$

The mean value  $\langle \psi(\vec{r}) \rangle$  satisfies the general wave equation. The results (2-12) and (2-13) can be compared to (1-5) and (1-6).

## REFERENCES

- /1/ FRISCH U. - La propagation des ondes en milieu aléatoire et les équations stochastiques. Annales d'Astrophysique. Part I - 1966 29 (6) (645-682)  
Part II - 1967 30 (3) (565-601)
- /2/ CHERNOV L.A. - Wave propagation in a random medium. Mc Graw-Hill Book New-York 1960.
- /3/ FORTUIN L. - Wave propagation in random media. Saclantzen Technical Report N° 221. La Spezia 1973.
- /4/ WHEELON A.D. - Radio wave scattering by tropospheric irregularities. Journal of Research of the National Bureau of Standards. 63 D N° 2 sept-Oct 1959. (205-233).
- /5/ ISHIMARU E. - Wave propagation and scattering in random media (Volume 2) Academic Press New-York 1978.
- /6/ TATARSKI V.I. - The effects of the turbulent atmosphere on wave propagation. Israel Program for Scientific translations - Jerusalem 1971.
- /7/ CLARKE R.H. - Acoustic and electromagnetic waves propagation in a tenuous random medium. Nato Institute on "Signal Processing with Emphasis on underwater acoustics. Vol 1 (4.1 - 4.7) sept 1976. La Spezia Italy

- /8/ PROKHOROV A.M. et al., Laser irradiance propagation in turbulent media.  
Proc. IEEE 63 5 1975 790-811.
- /9/ FOLDY L.L. The multiple scattering of waves. Physical Review 67 1 (107-119) 1945.
- /10/ LAX M. Multiple scattering of waves. Reviews of modern physics 23 4 (287-310) 1951.

# SUMMARY

The acoustic study of underwater medium is very complex. The basic principles which give a simplified approach to the problem are reviewed.

In the first part, we give a static description of the medium and we define the transmission loss.

In the second part we consider the propagation problems from ray and mode concepts view point.

Finally we discuss some effects that fluctuations of the medium has on acoustical transmission.

## INTRODUCTION

Among the studies connected with oceanography, underwater acoustics is becoming more and more important because only the acoustic waves propagate well through the sea. Like the atmosphere, the sea is essentially a heterogeneous medium. It is characterized by parameters which differ from one point to another. (sound velocity, absorption, ...) It contains many inhomogeneities. (tiny suspended particles, gas bubbles, shoals of fish ...) which scatter acoustic waves.

We also have to take into account the presence of close boundaries (surface and bottom) and the fluctuating nature of some parameters with time that cause distortion and fluctuation of the received signal.

The internal structure of the ocean and of the atmosphere present notable analogies. Comparison between records obtained by using echo-sounders in the ocean and in the atmosphere, is enough to convince us.

Since world-war I the field of applications of underwater acoustics has not stopped developing. Let us quote some examples :

- Echo-sounder, navigation sonar
- Underwater telecommunication, telemetry, telemesures ...
- Off-shore petroleum research and exploitation
- Sediments and underwater bottom study
- Studies of gravity waves, currents, microstructure of ocean etc ...

## 1. STATIC DESCRIPTION OF UNDERWATER MEDIUM

### 1.1. The velocity profile

The acoustic waves velocity is an essential parameter for propagation calculations. In underwater medium it varies in space and it depends on temperature, salinity and hydrostatic pressure. Temperature plays an essential role in velocity variations. If in normal conditions, sound velocity is at the average of  $1500 \text{ ms}^{-1}$ , different relations have been proposed to express it in function of basic quantities : temperature  $\theta$ , salinity  $s$ , and depth  $d$ . For example, between  $6-17^\circ \text{C}$ , we can apply the relation :

$$(1-1) \quad c_{(\text{cm s}^{-1})} = 1410 + 4,21\theta - 0,037\theta^2 + 1,14s + 0,018d$$

for a temperature variation of  $10^\circ \text{C}$ , the relation gives a velocity variation of  $3840 \text{ cm s}^{-1}$ .

Usually, one plots velocity variations, in function of the depth, on a diagram called velocity profile (Figure 1).

Generally we distinguish 3 principal regions :

- The region of the thin mixed layer where the temperature is practically constant.
- The main thermocline region where the temperature and the velocity, quickly decrease with depth.
- The deep isothermal layer where the temperature is constant. The velocity increase is only due to the hydrostatic pressure.

### 1.2. Transmission losses

#### a) Absorption of sound in sea

The intensity of plane wave which travels through an absorptive medium decreases under the equation :

$$I = I_0 e^{-2\alpha x}$$

where  $\alpha$  represents the absorption coefficient of the medium. In sea water, this coefficient is more important than in pure water, especially for low and intermediate frequencies, because of the molecular relaxation of dissolved magnesium sulfate. Figure 2 shows  $\alpha$  plotted against frequency. At HF ( $> \text{MHz}$ )  $\alpha$  is very high and varies like  $f^2$  ; so these frequencies have few applications in underwater acoustic.

One may represent the frequency dependence of the coefficient  $\alpha$  in the form :

$$(1-2) \quad \alpha = Af^2 + B \frac{f_r f}{f_r^2 + f^2} \quad (\text{dB cm}^{-1})$$



14-2

where  $f_r$  is the relaxation frequency in kHz.

For sea water we have the following values of the parameters :

$$A = 3,2 \cdot 10^{-7} \quad B = 6 \cdot 10^{-4} \quad f_r = 64 \text{ kHz}$$

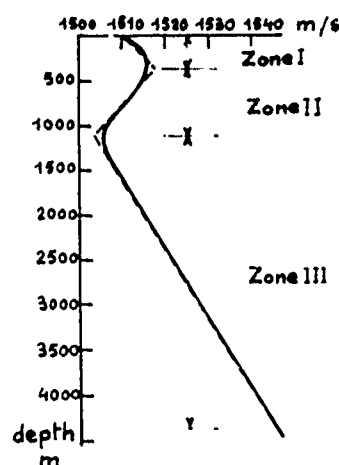


Figure 1

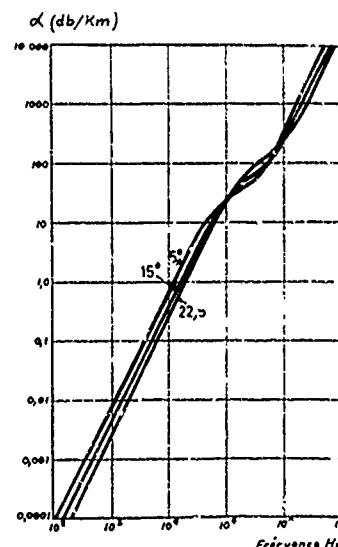


Figure 2

#### b) Spreading loss

Let a small source of sound which transmits spheric waves, in a homogeneous, unbounded and lossless medium. Following figure 3, if there is conservation of energy through spheres of radius  $r$ , we have :

$$4 \pi r_1^2 I_1 = 4 \pi r_2^2 I_2 = \dots$$

the geometrical spreading loss is then :

$$(1-3) \quad \frac{I_1}{I_2} = \left( \frac{r_2}{r_1} \right)^2$$

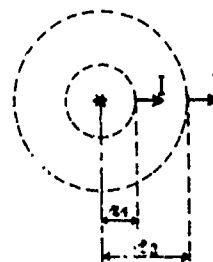


Figure 3

#### c) Transmission loss

If we now consider the absorption loss of the medium, the expression (1-3) takes the form :

$$(1-4) \quad \frac{I_2}{I_1} = \left( \frac{r_2}{r_1} \right)^2 e^{-2d(r_2 - r_1)}$$

or

$$N = 10 \log I_1 - 10 \log I_2 = 20 \log \frac{r_2}{r_1} + 8.7d(r_2 - r_1)$$

$N$  represents the transmission loss but it is impossible to define the relation  $r_1/r_2$ , because we have to calculate the losses between the source  $r_1 = 0$  and a point situated at a distance  $r = r_2$ . To overcome this difficulty we can choose a point  $r_1$  at one meter from the source ; in these conditions, omitting the term  $r_1$ , the transmission losses can

be written :

$$(1-5) \quad N = 20 \log \frac{r}{r_1} + \alpha r \quad \text{dB/m}$$

14-3

where  $\alpha$  is the absorption coefficient in  $\text{dBm}^{-1}$ . Figure 4 gives the family of curves relative to a spherical wave running into sea water.

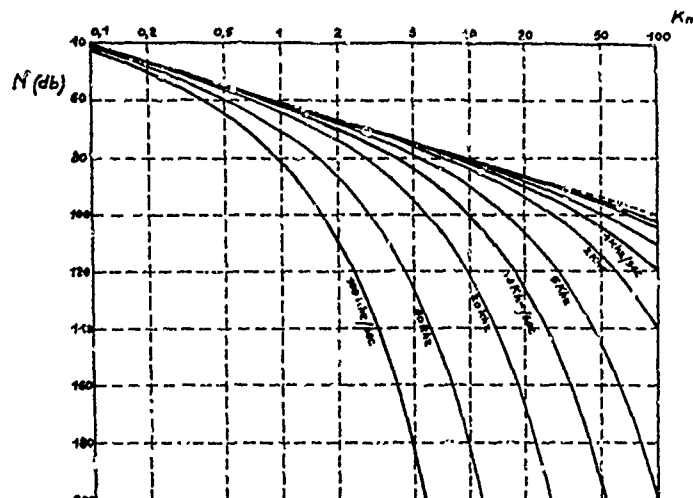


Figure 4

### 1.3. Boundary reflexion

#### a) Sea surface reflexion

The acoustic emission of a source situated close the surface is affected by its presence. If the surface is not disturbed, it acts as a perfect reflector and it provokes interferences between the direct emission of the source S and its image S' (figure 5).

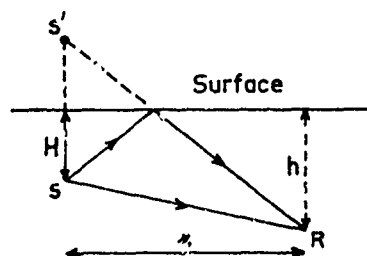


Figure 5

The receiver R receives a direct path SR and a surface reflected path emanating from the image S' of the source S in the surface. One shows that  $2/$  the combined intensity at R can be written :

$$(1-6) \quad \frac{I}{I_0} = 1 + \mu^2 - 2\mu \cos \frac{4\pi Hh}{r\lambda}$$

The reflexion coefficient  $\mu$  depends on the sea state surface.

Figure 6 represents the fluctuations of  $I/I_0$  in function of  $r$  and for different values of  $\mu$ .

#### b) Bottom reflexion

The reflexion coefficient on the bottom, (figure 7) is given by Rayleigh's formula :

$$(1-7) \quad \frac{I}{I_0} = \left[ \frac{m \sin \theta_1 - n \sin \theta_2}{m \sin \theta_1 + n \sin \theta_2} \right]^2$$

where  $m = \rho_2/\rho_1$  et  $n = c_1/c_2$ . If  $c_2 > c_1$  a critical angle  $\theta_c$  exists such as :

$$\sin \theta_c = \frac{c_1}{c_2}$$

For an incidence  $\theta_1 < \theta_c$  a transmission in the bottom takes place and weakens the reflected wave. For  $\theta_1 > \theta_c$  the reflexion is total, but the waves undergo a phase change in function of the incidence (figure 8).

14-14

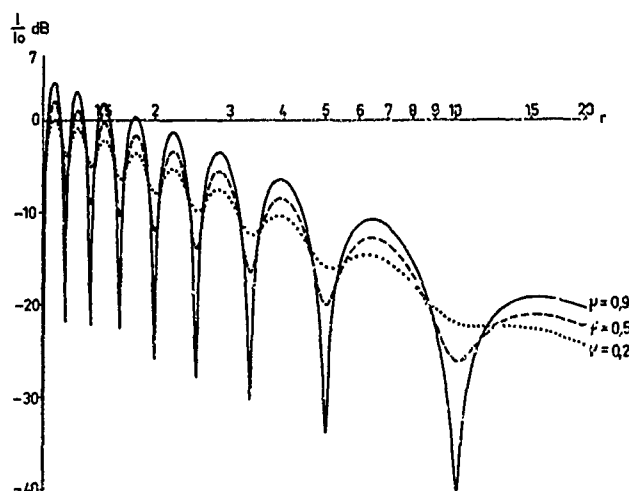
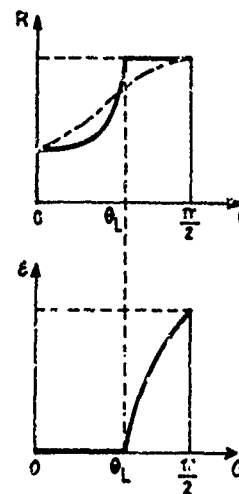


Figure 6



Figures 7 et 8

## 2. UNDERWATER PROPAGATION OF SOUND

### 2.1. Normal mode and ray propagation

The waves propagation in underwater medium is governed by the wave equation :

$$(2-1) \quad \Delta \Phi - \frac{1}{c^2} \frac{\partial^2 \Phi}{\partial t^2} = 0$$

where  $\Phi(x, y, z, t)$  specifies a quantity describing the acoustic field and  $c(x, y, z, t)$  represents the sound velocity which depends on the space coordinate and time. In the particular case of a monochromatic wave, let

$$(2-2) \quad \Phi(x, y, z, t) = \varphi(x, y, z) e^{j\omega t}$$

substitute in the equation (2-1) it becomes :

$$(2-3) \quad \Delta \varphi + k^2 \varphi = 0$$

and the propagation problem is then governed by the Helmholtz equation (2-3).

From that point, there are two possible points of view for the equation (2-3). If the boundaries play a dominant part, the problem is the following :

Find a function  $\varphi$  describing the acoustic field at any point and any time, which is a solution of the equation (2-3) and fits the boundary and source conditions. From the first point of view, the general solution  $\varphi(x, y, z)$  is given from a method of superposition of particular related solutions, which are called modes.

The total field is composed of a discrete sum of propagation modes

$$(2-4) \quad \varphi(x, y, z) = \sum_n \varphi_n(x, y, z)$$

On the other hand, if we forget the boundary problems, we end up with the second point of view, and the propagation problem looks like the search of paths on which the energy is propagating, and the study of signal evolution on these paths.

For this we look for a solution of the equation (2-3) under the form :

$$(2-5) \quad \Phi(x, y, z, t) = A(x, y, z) e^{jS(x, y, z)}$$

where  $A$  and  $S$  denote amplitude and phase. The

surfaces of constant phase  $S = \text{cte}$  are the wave-front, and the orthogonal curve to these surfaces are the sound rays.

### 2.2. Ray theory

Let us now consider the point of view of the Ray Theory.

#### 2.2.1. Ray Equation

Let us substitute (2-5) in (2-3) and separate the real and imaginary parts ; we get the system :

$$(2-6) \quad \Delta A - A(\nabla S)^2 + k^2 A = 0$$

$$(2-7) \quad 2\nabla A \cdot \nabla S + A \Delta S = 0$$

the resolution which poses serious difficulties.

The geometrical approximation is written :

$$(2-8) \quad \left| \frac{\Delta A}{A} \right| \ll k^2 \quad \text{so (2-6) is reduced to} \quad (\nabla S)^2 = k^2 \quad (2-9)$$

which is known as the eikonal equation for which the condition (2-8) is equivalent to :

$$(2-10) \quad \frac{1}{2\pi} \frac{\lambda}{c} \text{grad} c \ll 1 \quad (\lambda \rightarrow 0)$$

and expresses the high frequency character ( $\lambda \rightarrow 0$ ) of the approximation or also a weak gradient.

It means that we can neglect the velocity variations on a path length comparable to the wave length.

### 2.2.1. Rays equation

We suppose that the propagation velocity  $c$  is a function of the only immersion  $z$ , so that we can write :  $c = c(z)$ . In this case the rays always lie in the vertical plane  $(x, z)$ . With fixed end points, the rays are always paths of stationary time, (Fermat principle). In these conditions, any variation  $\delta$  between two fixed end points will be that as :

$$(2-11) \quad \delta \int \frac{d\ell}{c} = 0$$

and according to figure 9.

$$(2-12) \quad \delta \int \frac{1}{c(z)} \left[ 1 + \left( \frac{dx}{dz} \right)^2 \right]^{1/2} dz = 0$$

Applying to (2-12) the Euler - Lagrange equation, we get :

$$(2-13) \quad - \frac{1}{c(z)} \frac{dx/dz}{[1 + (dx/dz)^2]^{1/2}} = - \frac{1}{\gamma} = c_0$$

and since  $\frac{dx}{dz} = \cot \theta$ , consequently :

$$(2-14) \quad \frac{c}{c_0 \sin \theta} = \frac{c_0}{c_0 \sin \theta_0} = \gamma$$

which is Descartes law in which  $c_0$  and  $\theta_0$  are the parameters at the source. The equation (2-12) immediately gives :

$$(2-15) \quad -dx = \pm \frac{c}{(\gamma^2 - c^2)^{1/2}} dz \quad \text{if } x = 0 \text{ and } z = z_0 \text{ are the coordinates of the}$$

source :

$$(2-16) \quad dx = \pm \int_{z_0}^z \frac{c(z) dz}{(\gamma^2 - c^2(z))^{1/2}}$$

we take the sign + for a ray going down to the bottom and the sign - for a ray going up to the surface, so that  $x$  is always positive. We get the turning point of a ray when the condition  $c(z_m) = \gamma$  is fulfilled, therefore when  $dz/dx = 0$ .

We can easily determine the ray path in the case of a velocity linear profile. Let  $c(z) = gz$  and substituting in (2-16) it immediately becomes :

$$x = c_0^2 \pm \frac{\gamma}{g} \left( 1 - \left( \frac{g}{\gamma} \right)^2 z^2 \right)^{1/2}$$

if we take 0 for the constant, it comes :

$$(2-17) \quad R^2 = x^2 + z^2 = \left( \frac{\gamma}{g} \right)^2$$

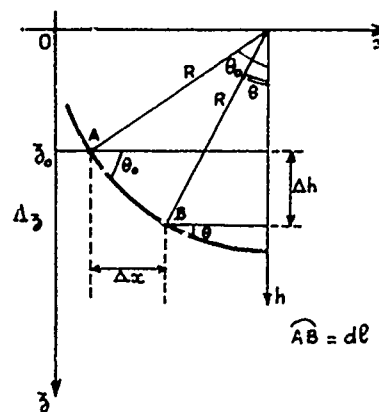


Figure 9

14-6

The ray path are circles of radius :

$$(2-18) \quad R = \frac{\gamma}{g} = \frac{c_0}{g \cos \theta_0} \quad \text{centered on the horizontal line of zero sound velocity.}$$

For digital ray computation one can divide the velocity profile into horizontal layers of constant gradient velocity. (figure 9)

Figures 10 and 11 give examples of ray diagram in the case where there are caustics, shadow zones and a sound channel.

### 2.3. Modes theory

Modes theory is often preferred when we have to take the boundaries into account. This problem occurs in the propagation studies in the case of shallow water. In this case, the ratio  $H/\lambda$  water height on wave length is small. In shallow water propagation numerous reflexions on the surface and on the bottom takes place. The solution by modes represents the waves interference phenomena, rays theory on the contrary requires a certain independence between the different rays.

#### 2-3-1 Mode Interference

An omnidirectional source set in the water transmits waves which reflect numerous times on the surface and the bottom. (figure 12). At a sufficiently large distance from the source, the waves interfere and give a standing wave pattern. Only the ones which interfere in a constructive way and which propagate under incidence angles for which the reflexion on the bottom is theoretically equal to one, will contribute to the field.

There is constructive interference effects between the rays (1) and (3) if:

$$(2-23) \quad \frac{4\pi f H}{c_1} \cos \theta - \varepsilon = (2n-1)\pi$$

where  $f$  is the emission frequency,  $c_1$  the waves velocity in water,  $\theta$  the incidence angle and  $\varepsilon$  the phase change undergone by the waves at the reflexion on the bottom.

The constructive interference condition (2-23) gives us the characteristic equation :

$$(2-24) \quad \frac{1}{g} \left( \frac{2\pi f}{c_1} H \cos \theta \right) = \frac{p_2}{p_1} \frac{\cos \theta}{[\sin^2 \theta - (c_1/c_2)^2]^{1/2}}$$

The number of possible modes is determined by the number of discrete roots of the characteristic equation (2-24).

The graphic resolution of (2-24) is given by tracing in function of  $\theta$  the curves corresponding to each member, for a determined frequency ;  $\theta$  varying from 0 to  $\pi/2$ . The curves take the aspect given by figure 13. The intersection points of these curves determine the real solutions  $\theta_n$  of the characteristic equation. The corresponding wave number is given by :

$$k_n = \frac{2\pi f}{c_1} \sin \theta_n$$

At each value of  $\theta_n$ , there is only one mode of propagation for a given frequency  $f$  and the water height  $H$ .

In addition from the equation (2-24), we can obtain for a given frequency, the cut-off depth of the  $n^{\text{th}}$  mode.

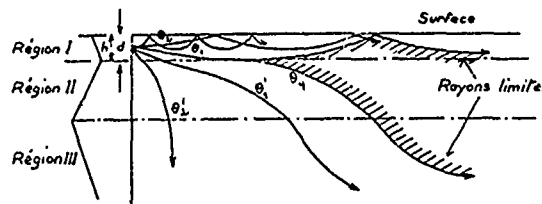


Figure 10

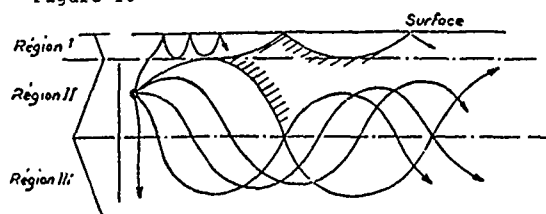


Figure 11

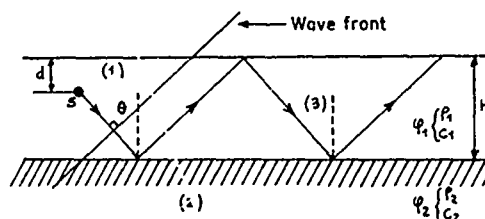


Figure 12

14-8

The expression (2-32) lets us calculate the acoustic field at any point of the medium.

a) Vertical field distribution

In function of the depth of the source, the modes excitation vary as the factor  $\sin(\gamma_{1n} d)$  of the expression (2-32). It varies as the factor  $\sin(\gamma_{1n} z)$  of this same expression in function of the depth of the receiver. Figure 14 shows for the two first modes the evolution of the vertical distribution of the pressure amplitude in function of the frequency.

b) Mode interference

For a given frequency, the propagation shows a vertical standing wave pattern along the oz axis, and a mode interference pattern along the horizontal axis or. For example a two-mode interference pattern shows successive minima and maxima which are spaced one interference wavelength apart.

$$(2-33) \quad L_{ij} = 2\pi / (k_i - k_j)$$

Figure 15 corresponds to the case where two modes are present and equally excited. The field oscillations are regular and the interference wavelength can be calculated from (2-33).

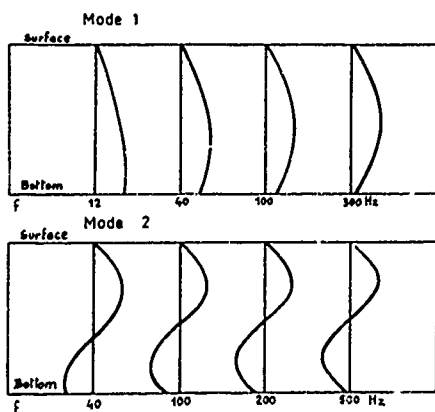


Figure 14

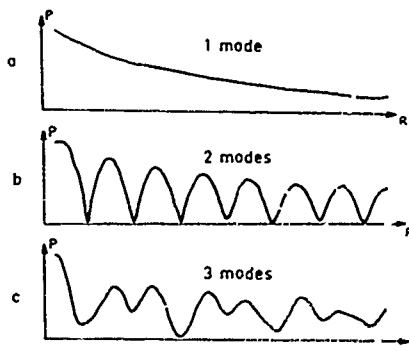


Figure 15

### 3. UNDERWATER MEDIUM FLUCTUATIONS

Ocean is a fluctuating medium in which the results obtained in chapter "Random scattering" can be applied.

3.1. Fluctuations of sound velocity are due to the turbulence of the medium, the water current and the small temperature fluctuations.

These fluctuations can be schematised by irregular blobs of water of different sound velocity. These blobs are in motion relative to each other.

In general, if  $(\Delta c)^2$  is the standard deviation of the velocity fluctuations, the relative sound velocity

$$N = [(\overline{\Delta c} / c)^2]^{1/2}$$

is about  $8 \cdot 10^{-10}$ .

We define the pressure fluctuations by the coefficient of variation :

$$\gamma_v = [(\overline{P - \bar{P}})^2 / (\bar{P})^2]^{1/2}$$

Different studies allowed to connect  $\gamma_v$  to the characteristic of the microstructure of the medium.

For a high frequency signal received at short range  $r$ , the rays theory gives :

$$\gamma_v = \left( \frac{4}{15} \pi^{1/2} \frac{\mu^2 r^3}{\rho^3} \right)^{1/2}$$

where  $r$  is the range and  $l$  is the correlation radius of fluctuations (velocity for example).

In this case, the fluctuations of the signal are essentially due to the focusing and defocusing of the sound beam.

For a low frequency signal received at long range  $r$ , the wave theory gives :

$$\chi_{\text{w}} = \left( \frac{\sqrt{\pi}}{2} \rho^2 k^3 \ell r \right)^{1/2}$$

with the condition  $r \gg kl^2$

In this case, the fluctuations are due to the scattering by the heterogeneous structure.

### 3.2. Fluctuations due to the reflexion on the surface

We show /5/ that the fluctuation of the signal reflected by the sea surface decreases when the signal frequency decreases and when amplitude of surface fluctuations decreases (Figure 16).



Figure 16

### REFERENCES

- /1/ URICK F.J. - Principles of underwater sound for engineers. Mc Graw-Hill book New-York 1967.
- /2/ TOLSTOY L. - Wave propagation. Mc Graw-Hill New-York 1973.
- /3/ Gazanhes C. et al., Etude de la propagation sonore en eau peu profonde à l'aide de modèles réduits. Revue du CETHEDC- Paris - n°54, 1978.
- /4/ Gazanhes C. - Random scattering special course on "Acoustic wave propagation".
- /5/ Gazanhes C. et al., Propriétés statistiques d'une onde sonore diffusée par une surface aléatoire. Application à la réflexion sous-marine de surface. ACUSTICA 30 1. (12-19), 1974.

# EXPERIMENTAL AND NUMERICAL RESULTS OF SOUND SCATTERING BY A BODY

by

L. Maestrello  
NASA Langley Research Center  
Hampton, Virginia 23665

A. Bayliss  
Institute for Computer Application in Science and Engineering  
NASA Langley Research Center  
Hampton, Virginia 23665

## SUMMARY

This paper presents two different facets of the interaction of aerodynamic noise with a fuselage shaped body. The first problem is the effect of scattering of an acoustic source by a body at rest. A numerical technique is presented which permits the computation of this scattering for frequencies of aeroacoustic interest. A parallel experiment is described which confirms the results of the computations. A numerical study of varying the geometry of the scattering is presented. The second problem is to simulate the effect of forward motion on the mean velocity and static pressure profiles in the wake of such a body with a jet exiting from it. Experimental results are presented and a similarity law is given. Directions for future research in this field are discussed.

## I. INTRODUCTION

This paper is concerned with the effect of a body on nearby acoustic sources. The motivation for this is the effect that an airplane fuselage has on the sources of jet noise. Previous work has ignored the effect of the fuselage on farfield sound patterns. It will be seen that the effect of the body is to substantially alter the far field acoustic pattern and that this neglect is not justified.

The airplane fuselage will be modeled by an elongated ellipsoid. The acoustic sources will be modeled by point sources placed on the major axis of the ellipsoid.

This paper will consider static effects and simulated flight in an open wind tunnel. The static effects will consist of measurements and numerical computation of the far field scattering due to the body. A numerical technique will be discussed which will permit the accurate computation of the scattered field at reasonably high frequencies. Experimental results will be given for comparison with the numerical methods. The availability of an accurate numerical scheme permits the study for a wider range of parameters than could be obtained experimentally.

The forward motion effect over the body will consist of experiments on the mean velocity and static pressure profiles for a body in a uniform flow with the point sources replaced by a jet exiting along the major axis. This is a realistic simulation of flight effects, however the acoustic measurements and the numerical calculations, being much more difficult than in the static case, are presently being developed.

In section II, the static effects are discussed, and in section III, the forward motion effect is considered. In section IV, the current state of the present research is discussed together with plans for future work.

## II. SCATTERING BY A FUSELAGE SHAPED BODY

We consider the problem of determining the scattering by an airplane fuselage, of the sound of a jet engine mounted on the axis and behind the body. This problem is modeled by a rigid elongated ellipsoid (prolate spheroid) with point sources on the major axis. (See fig. 1 and ref. 1).

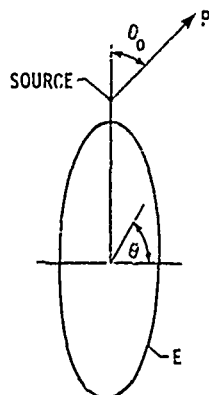


Figure 1. Coordinate system of the ellipsoid and for the farfield observation angles.



15-2

The farfield sound is a superposition of the incident field and the scattered field due to the presence of the body. A complete treatment of this problem requires the computation of the scattering with a variable flow over the body. This will permit the computation of the noise generated by an airplane in motion. Here we consider only the case of zero flow. The case of constant flow can be reduced to the case of zero flow by a Galilean transformation. A discussion of the effect of constant flow based on geometrical optics is given in Reference 2.

Several techniques are available for the numerical computation of the scattered field. These are discussed in section II.a. After comparing these methods, it was found that for the frequencies of interest, the integral equation method, using appropriate coordinate stretching, was best able to provide accurate solutions over the entire farfield. This method and the stretching transformation which is crucial to its success is discussed in section II.b.

An experiment was conducted to verify the accuracy of the numerical scheme. An experimental point source was placed near the tip of a spheroid with a shape that conforms to that of a typical airplane fuselage. The experiment is described in section II.c. and the results are given in section II.d. Additional numerical results for different ellipsoids and source configurations are presented in section II.e.

The principle conclusion from this research is that the scattered field is a significant component of the acoustic far field and can not be neglected in any realistic noise prediction scheme.

#### a. Equations and Numerical Techniques

The acoustic potential will be a solution of the wave equation, which reduces to the Helmholtz equation

$$\Delta\phi + k^2\phi = 0 \quad (1)$$

in the frequency domain. Here  $k$  is  $2\pi$  times the reciprocal wavelength. In order to work with non-dimensional quantities we introduce the term  $ka$  where  $a$  is the semimajor axis. The solution to Eq. 1 becomes more difficult as  $ka$  increases because of the oscillatory behavior of the solutions. For aeroacoustic applications, however,  $a$  is required to be large, such that the solutions for  $ka \geq 100$  will be required.

Three techniques are currently used to compute the scattered field:

- (1) Expansion in eigenfunctions,
- (2) Integral equation methods,
- (3) Asymptotic methods.

The expansion in eigenfunctions, which is restricted to special bodies, is based on the fact that the Helmholtz equation is separable in the prolate spheroidal coordinate system. Thus, the solution can be written as an infinite series of the eigenfunctions of the separated operators (see Ref. 3). This series converges very slowly unless  $ka$  is small and thus this method is not suitable for the computation of aeroacoustic scattering and will not be considered further.

The integral equation method involves solving a Fredholm equation of the second kind over the surface of the scatterer. A general discussion of this method is given in Ref. 4 and a detailed discussion of its application to the present problem is given in section II.b. The numerical solution of the equation for large values of  $ka$  can only be done efficiently if new coordinates are introduced on the body. If done properly, accurate solutions for values of  $ka$  of interest can be obtained. This method was used to generate the basic numerical results of this paper and for reasons to be described below, it is believed that this is the best of the three methods in obtaining solutions at aeroacoustic frequencies.

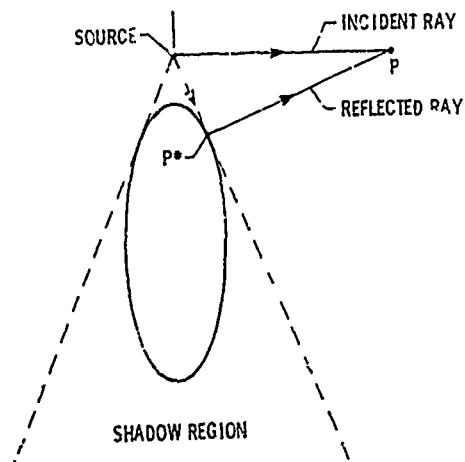


Figure 2. Geometrical optic ray paths and the illuminated and shadow regions.

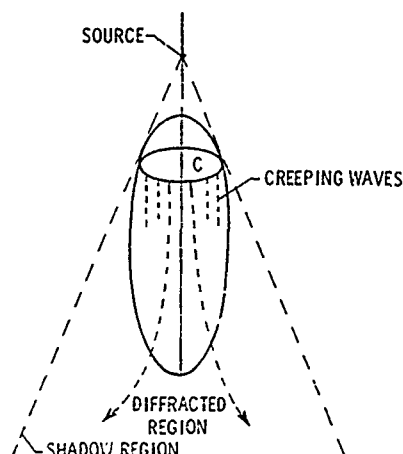


Figure 3. Geometrical diffraction showing the creeping waves on the body and diffracted rays.

The third method, asymptotic expansion, includes both the conventional geometrical optics expansion and the theory of geometrical diffraction of J. Keller (see Ref. 5).

Geometrical optics involves obtaining the solution to the scattering problem by the method of ray tracing. Referring to Figure 2, the total field at the point  $P$  is found by assuming a solution of the form

$$\phi = z(P) \frac{\exp(ik|P - P^*|)}{4\pi|P - P^*|} + \phi_{inc},$$

where  $\phi_{inc}$  is the incident wave. Here  $P^*$  is the origin of the reflected wave going through  $P$  (see Fig. 2) and  $z(P)$  is obtained through a principle of "conversion of energy" along ray tubes (see Ref. 3 for more details).

It is apparent from Figure 2 that there is a region of space where no wave can penetrate. This is called the shadow region and the geometrical optics approximation is  $\phi = 0$  in the shadow region. An improved approximation is obtained by the theory of geometrical diffraction as described in Reference 5.

Referring to Figure 3, rays incident on the curve of tangency  $C$ , excite surface rays (also called creeping waves) from which real waves are shed off tangent to the body. Analytical formulas have been developed for these diffracted waves (see, for example, Ref. 3).

Both these expansions are valid as  $k \rightarrow \infty$ . Geometrical optics requires  $ka$  large where  $a$  is the semimajor axis. Geometric diffraction, however, is based on the radius of curvature at the tip of body and requires the wavelength to be small with respect to this length scale. Since any model of an airplane fuselage will be an elongated ellipsoid, this will have a relatively small radius of curvature and thus geometric diffraction will have a more restricted domain of validity than geometrical optics.

Results to be presented indicate that geometric diffraction is very inaccurate at frequencies of aeroacoustic interest. At the highest frequencies considered errors of the order of 5 dB have been found. Geometrical optics also becomes inaccurate as the far field point approaches the shadow region. Furthermore, it is found that the effect of the scattering is strongest in and near the shadow region. Thus, the integral equation method although more expensive than the asymptotic methods, is the only presently known method able to provide accurate numerical solutions in all regions of the far field, for the frequencies considered.

#### b. Numerical Scheme

The scattering problem described previously can be described mathematically as the solution to the following problem:

$$\Delta_p \phi + k^2 \phi = -\delta(p - q), \quad (2a)$$

$$\frac{\partial \phi}{\partial n} = 0 \text{ on } E, \quad (2b)$$

$$\frac{\partial \phi}{\partial r} - ik\phi \rightarrow 0 (r \rightarrow \infty), \quad (2c)$$

where  $\phi$  is the velocity potential. Here  $p$  represents the independent variables and  $\Delta_p$  refers to the Laplacian with respect to the variables  $p$ . The point  $q$  is the source point and  $k = \omega/c$  is the wave number. The notation  $\partial/\partial n$  represent the normal derivative on the spheroid  $E$  which models the airplane fuselage. We consider only axial sources so that the problem (2a, 2c) is symmetric in the azimuthal direction (see Fig. 1). The condition (2b) expresses the fact that the scattering is hard (zero normal velocity on the surface). The condition (2c) (the radiation condition) ensures that the problem (2a, 2c) has a unique solution.

The problem (2a, 2c) is set up for numerical solution by writing

$$\phi = \phi' + \phi^S,$$

where  $\phi^S$  is the singular part of the solution

$$\phi^S = \frac{\exp(ik|p - q|)}{4\pi|p - q|}$$

and  $\phi'$  is the scattered field and will be a solution to the problem

$$\Delta \phi' + k^2 \phi' = 0, \quad (3a)$$

$$\phi'_n = -\frac{\partial \phi^S}{\partial n} \text{ on } E, \quad (3b)$$

$$\phi'_r - ik\phi' \rightarrow 0(r \rightarrow \infty). \quad (3c)$$

The problem (3a, 3c) is converted to an integral equation using the single layer potential method (see Ref. 4). One assumes a solution  $\phi'$  of the form

$$\phi'(p) = \int_E \sigma(q) G(p, q) dA_q, \quad (4)$$

where  $G$  is the free space Green's function

$$G(p, q) = \frac{\exp(ik|p - q|)}{4\pi|p - q|},$$

and  $\sigma$  is to be determined. The physical interpretation of (4) is of a distribution of point sources with density  $\sigma$  such that the total field is the superposition of the field from each of the point sources.

On taking the normal derivative of (4) and letting the point  $p$  approach the surface  $E$  one obtains the surface Fredholm equation of the second kind for the unknown function  $\sigma$  (see Ref. 4)

$$\frac{\phi(q)}{2} - \iint \sigma(q') G_{n_q}(q, q') dA_{q'} = -\phi_n(q), \quad (5)$$

where  $\phi_n$  is the prescribed Neumann condition [from 3b].

If  $\theta$  denotes the polar angle of the ellipsoid  $E$  (see Fig. 1) then by the axial symmetry (5) can be converted into a one-dimensional equation

$$\frac{\phi(\theta)}{2} - \int_{-\pi/2}^{\pi/2} d\theta' \sigma(\theta') H(\theta, \theta') = -\phi_n(\theta), \quad (6)$$

where the kernel function  $H(\theta, \theta')$  is the kernel in (5) integrated in the azimuthal direction and multiplied by the area factors.

There are two main difficulties associated with the equation (6). It is known that the equation will become singular if  $k$  is an eigenvalue of the interior Dirichlet problem. This problem of the interior resonances has been considered by various authors and the reader is referred to Reference 4 for a comprehensive discussion of techniques for dealing with this problem.

It has been found that these singularities do not extend over a wide frequency range, and for the purpose of obtaining a power spectrum, this is not an important problem.

A much more critical problem is that of adequately resolving the solution at high frequencies. A measure of the oscillatory behavior of the solution is the nondimensional quantity  $ka$  where  $a$  is some length scale associated with the body. We will take  $a$  as the semimajor axis. The study of aeracoustic scattering requires  $ka \sim 100$  and at these frequencies many grid points are required. In order to obtain solutions at these frequencies, appropriate coordinates must be introduced.

Using an evenly spaced grid Equation 6 is converted to a linear system

$$\frac{\phi(\theta_j)}{2} - h \sum_i \sigma(\theta_i) H(\theta_j, \theta_i) = -\phi_n(\theta_j), \quad (7)$$

Pressure signals were measured with a 1.3-cm-diam condenser microphone and the data were passed through a bandpass filter, with the oscillating frequency set to an accuracy of  $\pm 1$  Hz. The error of the electronic system, including readout, was estimated as within 0.5 dB. The microphones were mounted level with the body on an especially designed arc support to minimize possible reflection from the mounting. The long distances between the microphones and source made precise positioning very difficult using conventional positioning methods. Because of this error, phases could not be accurately determined and are not reported.



Figure 4. Experimental configuration on the anechoic floor.

#### 4. Discussion of Results

Data was taken over the anechoic floor at a sequence of observation angles as shown in Figure 5. Figures 6-10 are graphs of the decibel level change for the total field as a function of the observation angle  $\theta_0$  for a sequence of ascending frequencies. The graphs show the comparison between measured and computed results. The measured data were averaged over five readings taken at different times.

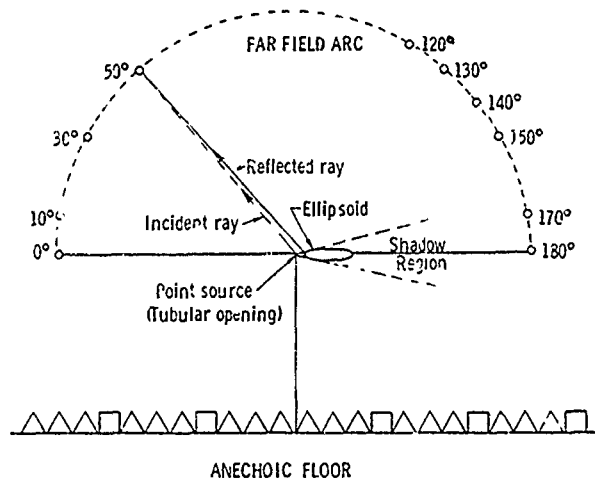


Figure 5. Measurements configuration on the anechoic floor.

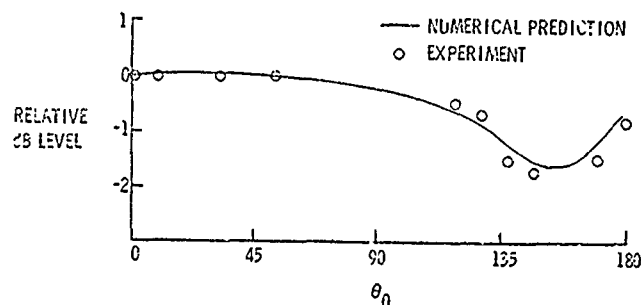


Figure 6. Sound pressure levels relative to the axial direction for  $f = 1.41$  kHz ( $ka = 14$ ).

Numerically it is found that at low frequencies the scattered field is very small relative to the incident field except in the vicinity of the shadow region. Since the incident field is omnidirectional on circles centered at the source, Curves 6 and 7 would be completely flat if there were no scattered field. Thus the measured flatness of Curves 6 and 7 near  $\theta_0 = 0$  confirms the numerical results. This effect is due to the slenderness of the body. Computations with wider spheroids at constant frequency show that scattering in directions near the axis increases as the body becomes spherical. Such results will be shown in section II.e.

15.7

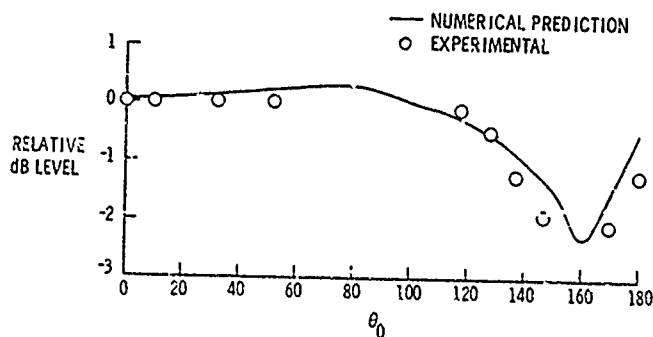


Figure 7. Relative level dB for  $f = 2.22$  kHz ( $ka = 22$ ).

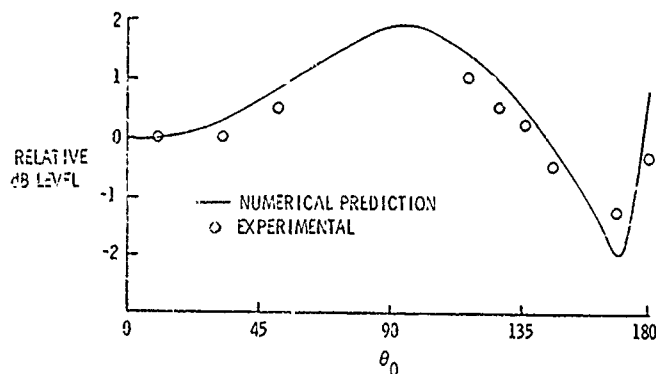


Figure 8. Relative level dB for  $f = 4.11$  kHz ( $ka = 41$ ).

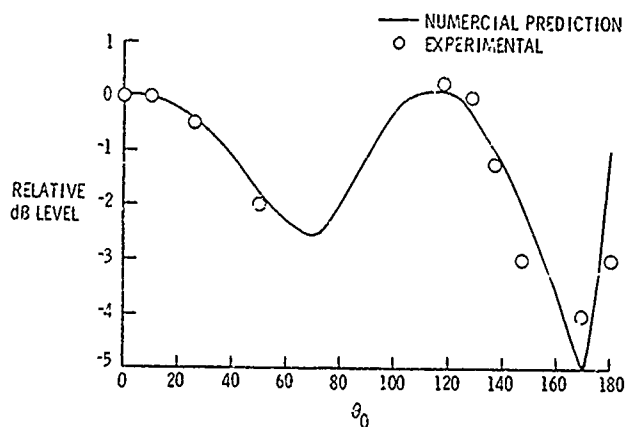


Figure 9. Relative level dB for  $f = 8.22$  kHz ( $ka = 82$ ).

As the frequency varied from 1.4 to 16.5 kHz ( $ka = 14$  to 166) the dip in the shadow region increased by 5 dB. This is the region of largest experimental difficulty because of the sharpness of the dip, which increases with frequency and is sensitive to the angular position. Agreement even near this point is within experimental error except for the highest frequency where the dip is extremely sharp. The experimental data will, in general, give a smaller dip, because the microphones average a relatively large angular spread.

15-8

We note that as the wavelength decreases, the difference between minimum and maximum pressure increases and the pressure field itself becomes more oscillatory as a function of the farfield angle. For example, at 16.4 kHz the difference is of the order of 8 dB, and this is roughly consistent with the measurements; for still higher frequencies the present measurement technique will have to be improved in order to resolve the rapidly oscillating acoustic pressure. At the lowest frequency of 1.41 kHz, the difference is only 2 dB, and in the illuminated region the pressure is essentially flat. Thus, the scattered field in all regions of space becomes stronger as the frequency increases.

At the highest frequency considered here the position of the sources with respect to the body is crucial in determining the location in the dips and peaks in the sound pressure level. This is because small changes in the source position, at this frequency, correspond to a significant change with respect to the acoustic wavelength. In the illuminated region where the total field is the superposition of two different waves the change in the phase of the two waves causes substantial difference in the total wave. In the shadow region where the field is basically composed of only one wave, the farfield sound is much less sensitive to the source position. A numerical study of the effect of varying the source position will be given in section II.e.

For the experiment body, the frequency of 16.4 kHz corresponds to a  $ka$  of 166. For a typical fuselage 70 m long, this corresponds to a frequency of approximately 0.3 kHz which is near the peak of the jet noise spectra. Thus, the major conclusion is that scattering cannot be ignored for any aeroacoustic application and must be included in any prediction scheme.

The plot for 16.4 kHz includes comparison of results obtained by experiment, integral equation, and geometrical optics. The errors due to the geometrical optics approximation near the shadow region can be clearly seen. As stated previously computations of the geometrical diffraction approximation show discrepancies of the order of 5 dB from the measured results. This was considered unacceptable for aeroacoustic applications.

The 16.4 kHz solution could be generated in core because of a proper choice of the stretching parameter. A grid of 169 points was used on a Cyber 175 machine. The computation of the matrix (see (7)) required 105 sec while the solution in the farfield can be computed in 0.9 sec/point. From the figure for 16.4 kHz and from comparisons discussed in Reference 6 it is apparent that geometrical optics provides accurate solutions except near the shadow region. Thus the solution by the integral equation method is required only in a restricted region of space and since the cost of computing the matrix must be spread over fewer points the effective cost per point becomes greater.

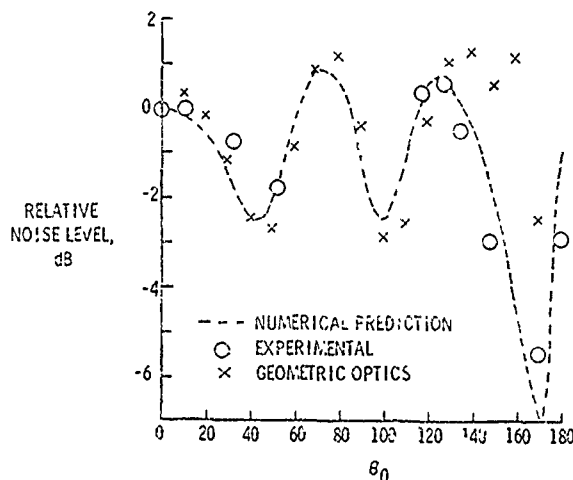


Figure 10. Relative level dB for  $f = 16.44$  kHz ( $ka = 166$ ).

#### e. Numerical Study of the Scattering Problem

Since the previous results show excellent agreement between the measurements and the computations, the numerical scheme can be used to study the scattering problem for a wide range of different parameters. Such a variation would be too costly for an experimental study.

We consider variations in the following parameters

- (1) Aspect ratio of the ellipsoid
- (2) Distance of the source from the body
- (3) Number of sources.

In practical application other considerations generally determine the choice of these parameters, but this study will clarify the effect of the scattering and give guidance to design criteria.

In Figure 11 the relative sound pressure level is plotted for two ellipsoids of aspect ratio 4:1 and 10:1. All other parameters are the same as in Figure 10.

The figure indicates that the forward scattering is greatly increased as the aspect ratio is decreased (the body becomes blunter). This result is consistent with the asymptotic theory. The dip in the shadow region is drastically increased as the bluntness increases (i.e. the body becomes more opaque to sound). 15-9

The figure is plotted with an angular spacing of  $10^\circ$ . This is sufficient to provide the gross features of the scattering. In the shadow region ( $\theta_0 \geq 170^\circ$ ) the asymptotic theory predicts that the total field is a superposition of two waves of roughly equal strength (see references 3 and 5 for more details). It is well known that this causes interference patterns which are manifested by rapid variations of the acoustic pressure over small angles. This is confirmed by the numerical computations and in Figure 11, these oscillations are plotted on a finer grid between  $170^\circ$  and  $180^\circ$ , for the 10-1 ellipsoid. Experimentally these variations are difficult to resolve by microphones and the measured pressure corresponds to a spatial average of the point wise pressure. This has been verified in the experiment discussed previously.

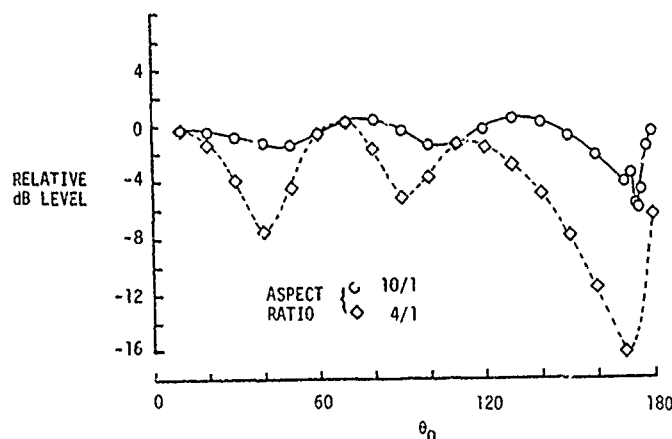


Figure 11. Computed sound pressure levels relative to the axial direction for different ellipsoids ( $ka = 166$ )

In Figure 12 computations for three different source positions are shown. The sources were placed at 3.12, 4.45, and 5.71 cm from the tip of the body. The aspect ratio was 7.0833 and the non-dimensional wavelength ( $ka$ ) was 166. Note that the effect of the scattering becomes much stronger as the source approaches the body. This is true in both the forward illuminated region and also in the shadow region. This result is to be expected based on the asymptotic theory.

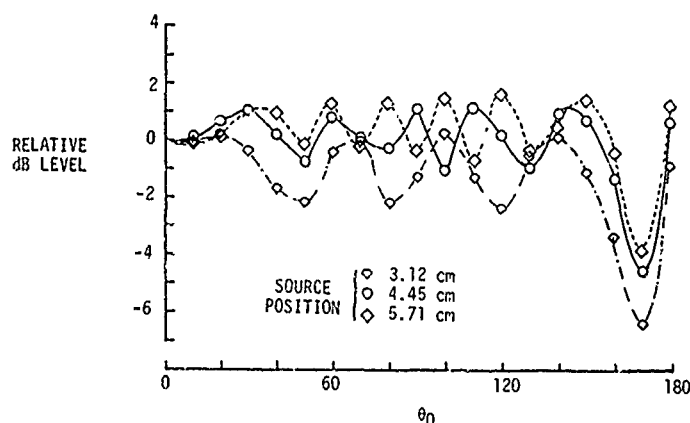


Figure 12. Computed sound pressure levels for three different source positions with respect to the body (aspect ratio = 7.0833,  $ka = 166$ )

In Figure 13 the sound pressure level for five axial sources placed 0.625 cm apart and with the first one at 1.9 cm is shown. The other parameters are the same as in Figure 12. The result of this computation is typical of the smoothing effect caused by replacing point sources by line sources. The effect of the scattering is now predominantly in the shadow region and is still quite substantial. The flatness of the curve in the illuminated region can be changed by rearranging the position of the sources with respect to the wavelength. Therefore, one can not always expect the scattering by line sources to be so negligible in the illuminated region.

These computations are not meant to be exhaustive but to indicate the trend caused by varying the different parameters. Such variation of parameters is not generally feasible experimentally, but can be obtained efficiently by numerical simulation with a code whose reliability has been checked experimentally.

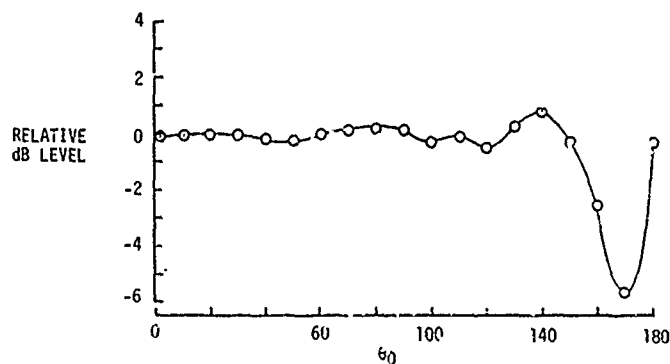


Figure 13. Combined sound pressure level for five axial sources at a spacing of 0.625 cm with first source placed at 1.0 cm. (aspect ratio = 7.083,  $k\lambda = 166$ ).

### III. VELOCITY AND STATIC PRESSURE PROFILE FOR SIMULATED FORWARD MOTION

The forward motion effect was simulated in the NASA Langley 2.44 m diameter jet facility in an anechoic chamber. The same ellipsoid as used in the previous experiment was mounted in the 2.44 m jet with a 2.5 cm diameter exiting along the major axis. The configuration is shown in Figure 14.

The 2.44 m jet has a mean velocity of 36.57 m/sec. The 2.5 cm jet had an exit Mach number of 0.50. The mean velocity profile and static pressure was measured at various X and Y stations as indicated in the Figure 14. Measurements were made at 11 stations with X/d varying between 1 and 17 where d is the exit jet diameter.

The mean velocity profile follows a similarity law which we now describe. Define  $Y_{1/2}$  as the point where

$$Y_{1/2} = U - U_e = 1/2(U_c - U_e)$$

where U is the local mean velocity,  $U_e$  is the free stream velocity of the 2.44 m jet and  $U_c$  is the centerline velocity. If we set

$$\gamma = Y/Y_{1/2}$$

then the following similarity law holds

$$f(\gamma) = \frac{U - U_e}{U_c - U_e}$$

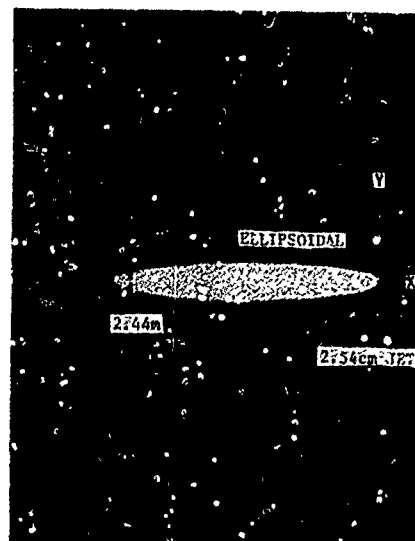


Figure 14. Test configuration for the mean flow measurements.



Figure 15 shows the mean velocity plotted in terms of the similarity variable  $\gamma$ . Because of the nature of the potential flow and core of the jet, this similarity law is not satisfied within the potential core. However, beyond  $X/d = 5$  there is excellent agreement.

15-11

The static pressure variation has a similarity law given by

$$g(\gamma) = \frac{P}{P_C} ; \quad \gamma = Y/\gamma_{1/2}$$

where  $P_C$  is the centerline pressure (Fig. 16). This also clearly valid outside the potential core ( $X/d \geq 5$ )

It has been shown in the literature that a different similarity law can be obtained inside the potential core. Functional forms for the functions  $f(\gamma)$  and  $g(\gamma)$  can easily be obtained by curve fitting this data. It is planned to utilize this velocity and static pressure profile to determine the effect of simulated forward motion in a realistic environment, since the real acoustic sources will come from the jet itself. Eventually, these results will be tested with a real flyover experiment by an airplane.

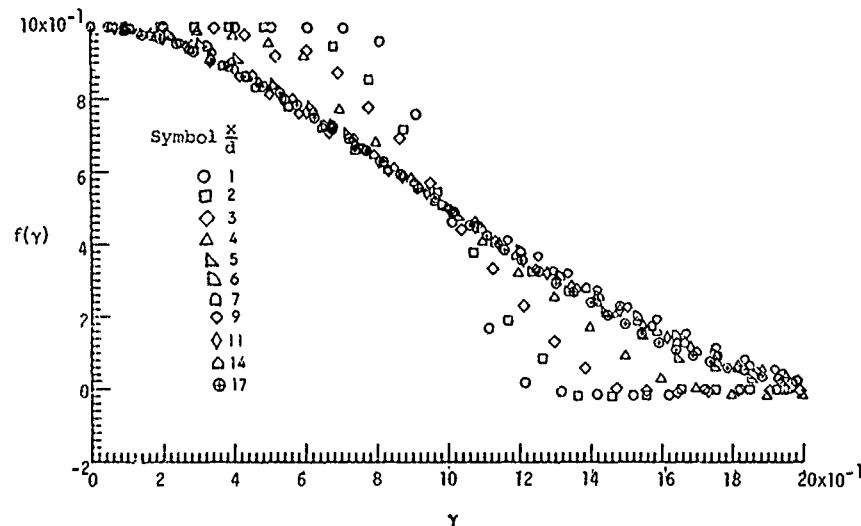


Figure 15. Similarity law of the mean velocity profile.

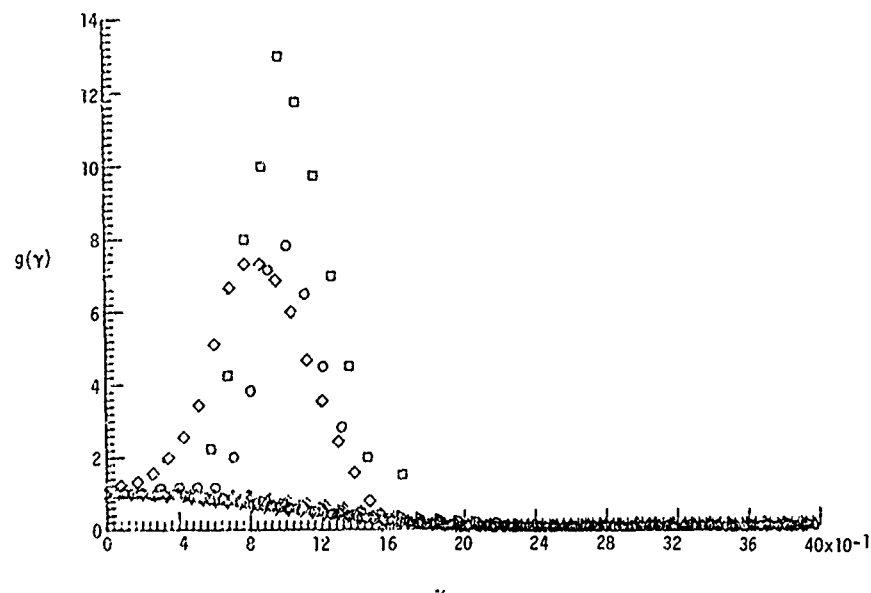


Figure 16. Similarity law of the static pressure profile.

## IV. CONCLUSION

The effect of scattering by a body at rest with point sources on the axis has been handled both numerically and experimentally. The next step is to include the effect of the mean flow on the acoustic field. Computations for a point source in a jet without a body, have been conducted (see Ref. 9). This includes more realistic effects such as sources in motion and non-harmonic sources. The program can be modified to compute the sound field in the mean flow described in Figures 14 and 15 which corresponds to the jet in the wake of a body. The addition of the body, so that the scattering can be computed is feasible at the present time.

These numerical computations can only be obtained for axially symmetric sources flows and bodies. The computation of three-dimensional effects, such as off-axis sources are not within the power of present day computers for frequencies of interest. Thus such effects can only be studied experimentally at the present time.

Future experimental work in this field will consist first of measuring the scattered field of a body placed in an open wind tunnel with the point sources behind it. This will simulate the effect of forward motion on the scattering. Following this, experiments will be made with a real jet behind the body. This will be a realistic flight effect simulation, because it contains the body, the wake, its mean flow and the jet as the noise sources. It is hoped that in the not too distant future these measurements can be confirmed numerically. Then there will be a realistic method of predicting flight effects for this geometry.

## ACKNOWLEDGEMENT

This paper was prepared as a result of work performed under NASA Contract No. NAS1-14101 while the second author was in residence at ICASE, NASA Langley Research Center, Hampton, VA 23665.

## REFERENCES

1. A. Bayliss and L. Maestrello, "Measurements and analysis of farfield scattering from a prolate spheroid," J. Acoust. Soc. Am. 64(3), September 1978, p. 896-900.
2. S. L. Padula and C. H. Liu, "Acoustic Scattering of Point Sources by a Moving Prolate Spheroid," AIAA Fourth Aeroacoustic Specialists Conference, Paper No. 77-1326, Atlanta, GA, October 1977.
3. J. J. Bowman, Sr. and P. L. E. Uslenghi, Electromagnetic and Acoustic Scattering by Simple Shapes (North Holland, Amsterdam, 1969).
4. A. J. Burton, "Numerical Solution of Scalar Diffraction Problem," in Numerical Solution of Integral Equations, edited by Delves and Walsh (Clarendon, Oxford, 1974).
5. B. R. Levy and J. B. Keller, "Diffraction by a Smooth Object:" Commun. Pure Appl. Math. 12, 59-209 (1959).
6. A. Bayliss, "On the Use of Coordinate Stretching in the Numerical Computation of High Frequency Scattering," J. Sound Vib. (to be published in 1979).
7. L. L. Beranek, Acoustic (McGraw-Hill, New York, 1954).
8. M. M. Myles, I. L. Ver, and H. R. Henderson, "Effects of Outdoor Exposure on Sound Absorption Material," J. Sound Vib. 2(6), 24-27 (1977).
9. A. Bayliss and E. Turkel, "Computation of Acoustic Waves in a Jet," ICASE Report 78-22, Dec. 1978.

## FINITE-AMPLITUDE WAVE PROPAGATION

Leif Bjørnø  
Professor, Ph.D., DIC.  
The Acoustics Laboratory  
Technical University of Denmark  
Building 352  
DK-2800 Lyngby, Denmark

16-1

### SUMMARY

A brief view is given of the historical development of finite-amplitude wave propagation in fluids. The theoretical basis for the propagation of plane, cylindrical or spherical finite-amplitude waves through lossless, thermoviscous or relaxing fluids is presented and characteristic features of the distortion course observed by finite-amplitude waves in various regions of propagation are emphasized. Some experimental procedures and results are mentioned.

### INTRODUCTION

The non-linearity of Nature is a fact that has frequently been recognized by physicists, geologists, and engineers when considering motion in fluids and in solids. Nevertheless, a linearization of the governing equations has in a number of cases led to mathematically more simple expressions with solutions showing surprisingly good agreement with experimental results. Rather early it was recognized that the validity of the solutions was limited, especially for cases of strong nonlinearity of the material, represented for instance by its equation of state, and for cases of high amplitude of the disturbances propagating in the material.

The propagation of acoustic waves of finite, but moderate, amplitude in media of various degrees of nonlinearity will be discussed in this chapter, thus excluding the consideration of strong shocks. The finite-amplitude wave propagation is comprised by the special field of acoustics termed "Nonlinear Acoustic", which includes waves with amplitudes ranging from infinitesimal - covered by the linear theory - to a magnitude leading to the formation of weak shocks.

Finite-amplitude wave phenomena influence a great number of acoustic topics of both theoretical and practical character. Steady and unsteady finite-amplitude waves in supersonic aerodynamics, weak-shock theory, finite-amplitude wave propagation in gases, liquids and solids, finite-amplitude bubble pulsations and cavitation in liquids, etc. Moreover, finite-amplitude wave propagation influences are found by high-power ultrasonic cleaning, filtering and welding processes, by high-intensity sound agglomeration of aerosols, trapping of fog and drying of powder. Furthermore, finite-amplitude waves are used for mixing of difficultly miscible materials, production of emulsions, dispersion of solids in liquids, coagulation processes, degassing of liquids and melts, etc.

Noise generation and propagation by high-powered jet engines and noise propagation in motor silencers are influenced by finite-amplitude wave phenomena leading to a change in the spectral composition of the noise.

A field of practical application and of great theoretical interest too which has developed very fast during recent years is underwater utilization of finite-amplitude waves in for instance the parametric acoustic array, which will be discussed in the next chapter.

Only wave propagation in unlimited fluids will be considered in this chapter. Therefore, discussion of influence of free surfaces, solid walls, etc. on wave propagation in fluids will be omitted in what follows. This restriction further implies that reflection of finite-amplitude waves, standing waves and resonances, acoustical boundary layers, and finite-amplitude waves in tubes and horns in general will not be discussed, though fundamental solutions and conclusions derived from studies of these topics will be discussed to the extent that they may serve the purpose of explaining basic concepts of nonlinear acoustics. The same limitations will apply to nonlinear impedance materials and nonlinear acoustic resonators.

The convective acceleration terms in the equations of motion and the nonlinear pressure-density relationship found by fluids and solids describe and contribute to the finite-amplitude wave distortion course where their cumulative, rather than merely their local, effect, eventually may produce steep wavefronts. These nonlinear processes are counteracted by linear processes like attenuation, dispersion, molecular relaxation and diffraction. It is this conflict between cumulative nonlinear wave distortion and the competing linear processes leading to a pronounced change in waveform which forms the key to the contents of this chapter.

Like the development within about all scientific fields, the development within finite-amplitude wave propagation is based on works done by earlier generations. Although the greatest development in this field has taken place within the last quarter of a century - as evidenced by the still-increasing number of papers published on problems relat-

16-2 ing to the propagation of finite-amplitude waves through nonlinear media - the basic research and early developments in nonlinear acoustics can be traced back some hundred years.

# 1. HISTORICAL DEVELOPMENT

A brief survey of the history of finite-amplitude wave propagation might appropriately begin with Euler's formulation of the conservation equations for a fluid: the equation of continuity (1) and the equations of motion (2), respectively.

$$\frac{\partial \rho}{\partial t} + \frac{\partial}{\partial x_i} (\rho u_i) = 0, \quad (1)$$

$$\rho \frac{Du_i}{Dt} = \rho \left( \frac{\partial u_i}{\partial t} + u_j \frac{\partial u_i}{\partial x_j} \right) = - \frac{\partial p}{\partial x_i} + F_i, \quad (2)$$

where  $\rho$  and  $p$  are the fluid density and the static pressure, respectively.  $u_i$  is the particle velocity vector (with components  $u_1, u_2$  and  $u_3$ );  $t$  and  $x_i$  are the time and the cartesian spatial coordinate (with components  $x_1, x_2$  and  $x_3$ ), respectively.  $F_i$  denotes a body force per unit volume vector. Equations 2 ( $i=1,2,3; j=1,2,3$ ) are known as the Euler equations for frictionless flow. The character of a system of nonlinear partial differential equations appears from the second (convective) term, in the parentheses in Eq. (2).

Euler's interest in lossless flow led to his study of the propagation of both infinitesimal-amplitude and finite-amplitude waves in fluids [1]. In 1765 he published a nearly correct version of the nonlinear wave equation for finite-amplitude wave propagation in an ideal fluid:

$$h^2 \frac{\partial^2 \xi}{\partial a^2} - \left( 1 + \frac{\partial \xi}{\partial a} \right)^2 \frac{\partial^2 \xi}{\partial t^2} = 0, \quad (3)$$

where  $h$  is the "isothermal" (Newtonian) sound velocity and  $a$  is the identification coordinate in a Lagrangian coordinate system.  $\xi$  denotes the particle displacement. Euler did not solve Eq. (3), but he briefly concluded that, because of the nonlinear term, the wave propagation velocity would be higher than the isothermal sound velocity.

Lagrange in 1761 [2] also considered the propagation of finite-amplitude waves, and although he based his calculations on a wave equation having the parentheses in Eq. (3) in the first power, he was able to draw reasonable conclusions as to the general form of the solution to the equation. His conclusion that the propagation velocity of the finite-amplitude wave should depend on the original wave amplitude shook his confidence in his own calculations, and led to his conclusion that the only possible means of wave propagation was the linear one governing the propagation of infinitesimal-amplitude waves.

In 1808 Poisson [3] worked on a one-dimensional, nonlinear wave equation in Eulerian (or spatial) coordinates of the form

$$h^2 \frac{\partial^2 \eta}{\partial x^2} - \frac{\partial^2 \eta}{\partial t^2} = 2 \frac{\partial \eta}{\partial x} \frac{\partial^2 \eta}{\partial x \partial t} + \left( \frac{\partial \eta}{\partial x} \right)^2 \frac{\partial^2 \eta}{\partial x^2}, \quad (4)$$

where  $\eta$  denotes a velocity potential, and he found an exact solution to this equation given by

$$\frac{\partial \eta}{\partial x} = F \left( x - \left( h + \frac{\partial \eta}{\partial x} \right) t \right) \quad (5)$$

for finite-amplitude wave propagation in the direction of increasing  $x$ .

In order to be able to obtain the total solution to the differential Eq. (4) Poisson coupled the solution (5) to an auxiliary relation:

$$\frac{\partial \eta}{\partial t} + h \frac{\partial \eta}{\partial x} + \frac{1}{2} \left( \frac{\partial \eta}{\partial x} \right)^2 = 0 \quad (6)$$

which is a reduced version of the wave equation for finite-amplitude waves propagating in the positive  $x$ -direction in a lossless fluid.

During the years around 1848, while revolution spread across Europe, there was an increase in nonlinear acoustics research. It is hard to say whether there was any connection between these incidents, but they were certainly both characterized by a breakthrough of new ideas. After a discussion between Airy and Challis about the existence of plane sound waves, Stokes [4] published the first sketches showing how waveform distortion might occur due to the different phase velocity of different parts of a finite-amplitude

16-3  
 wave. Stokes even traced the waveform in the limit of distortion - the shock wave - but because he considered a lossless fluid he omitted the thermodynamic consequence of shock formation. Little was known about thermodynamics in 1648, and it was to be another 20 to 30 years before the significance of energy loss for shock propagation was recognized and generally accepted.

The year 1860 could be considered as the end of the era of wave propagation in lossless fluids. The last essential contributions to the theory of lossless wave propagation, completing the period of development started by Euler, were made by Earnshaw [5] and Riemann [6]. Earnshaw established a connection between the thermodynamics represented by the thermodynamical expression  $\lambda$  in Eq. (7) and the original mathematical basis for one-dimensional, finite-amplitude wave propagation represented by the equation of continuity (8), the equation of motion (9) and an equation of state (10):

$$\lambda = \int_{p_0}^p \left( \frac{c}{\rho} \right) d\rho ; \quad (7)$$

$$\frac{\partial \rho}{\partial t} + u \frac{\partial \rho}{\partial x} + \rho \frac{\partial u}{\partial x} = 0 ; \quad (8)$$

$$\frac{\partial u}{\partial t} + u \frac{\partial u}{\partial x} + \frac{1}{\rho} \frac{\partial p}{\partial x} = 0 ; \quad (9)$$

$$p = p(\rho) . \quad (10)$$

$\lambda$  is the local thermodynamic state of the fluid, and  $c$  is the local "isentropic" velocity of sound. Insertion of Eq. (7) into Eqs. (8) and (9) yields

$$\frac{\partial \lambda}{\partial t} + u \frac{\partial \lambda}{\partial x} + c \frac{\partial u}{\partial x} = 0 , \quad (11)$$

$$\frac{\partial u}{\partial t} + u \frac{\partial u}{\partial x} + c \frac{\partial \lambda}{\partial x} = 0 ; \quad (12)$$

which led to Earnshaw's conclusion for simple waves that the "phase" velocity of a point of a wave having particle velocity  $u$  is given by  $(u \pm c)$ , + for waves propagating in the positive  $x$ -direction and - for waves propagating in the negative  $x$ -direction. Earnshaw further showed that the local velocity of sound in a gas might be written as

$$c = c_0 \pm \left( \frac{\gamma - 1}{2} \right) u , \quad (13)$$

where  $c_0$  is the velocity of sound for infinitesimal-amplitude waves, while the correction terms  $\pm ((\gamma - 1)/2)u$  arises from the nonlinearity of the pressure-density relation of the gas.  $\gamma$  is the ratio of specific heats of the gas.

For wave propagation in the positive  $x$ -direction the phase velocity of a point of the wave having particle velocity  $u$  might therefore be written

$$\left( \frac{dx}{dt} \right)_{u=\text{constant}} = u + c = c_0 + \left( \frac{\gamma + 1}{2} \right) u , \quad (14)$$

which involves the two fundamental contributions to finite-amplitude wave distortion, the thermodynamic contribution  $((\gamma - 1)/2)u$  and the convective contribution arising from the fact that the local velocity of sound  $c$  is being convected along with the local particle velocity  $u$  [7].

Earnshaw's theory for simple waves was generalized by Riemann [6] to comprise a non-simple wave region, i.e. a region for wave propagation in two directions. Riemann's results form the basis for the method of characteristics used, for instance, by solving the hyperbolic partial differential equations describing supersonic flow.

Rather incorrectly Riemann assumed that the transition across a shock is adiabatic and reversible, an error which was corrected some years later by Rankine (1870) after a development of the thermodynamics had taken place [8]. A contribution to a better understanding of the nature of a shock was published by Hugoniot (1889) who showed that an adiabatic, reversible transition in a shock would violate the principle of conservation of energy, and further that, in the absence of viscosity and heat conduction in the fluid outside the shock, the conservation of energy implied conservation of entropy across the shock [9]. The conservation equations connecting the thermodynamic and kinematic quantities on the two sides of a shock, the so-called Rankine-Hugoniot equations, thus found their final form.

16-4

A deeper appreciation of the processes occurring in a shock was obtained through the work of Lord Rayleigh [10] and G.I. Taylor [11] published in 1910. Viscosity and heat conductivity had now been included in the equations governing finite-amplitude wave propagation. The problem was now to solve the nonlinear wave equations subjected to specific initial or boundary conditions considering the influence of the loss sources.

During the nineteen thirties development in nonlinear acoustics research was brought a great step forward by Fay's (1931) publication of a solution for a periodic finite-amplitude wave in a viscous fluid and by Fubini's (1935) explicit solution to the wave equation for finite-amplitude wave propagation in a lossless fluid.

Fay [12] published a solution to the wave equation valid for the propagation of plane, finite-amplitude waves in a viscous fluid in the region showing a comparatively stable wave form:

$$\frac{p-p_0}{\rho_0 c_0^2} = \frac{2\alpha c_0}{\beta \omega} \sum_{n=1}^{\infty} \frac{\sin n(\omega t - kx)}{\sinh n\alpha(x+x_0)}, \quad (15)$$

where

$$\alpha = \frac{2}{3} \frac{\omega^2 \eta}{\rho_0 c_0^3}$$

and

$$\beta = \frac{\gamma + 1}{2}.$$

$\eta$  and  $\omega$  are the shear viscosity and the angular frequency, respectively.  $n$  is the harmonics number.  $x_0$  is a constant related to the discontinuity distance, which is the distance from the wave source for the formation of a discontinuity in a plane sine wave of angular frequency  $\omega$  propagating in a dissipationless medium.

While Fay's solution does not satisfy the boundary conditions of a sinusoidal source, the explicit solution to the wave equation obtained by Fubini [13] some years later does. Fubini's solution shows how an original sinusoidal wave of finite-amplitude will distort by formation of higher harmonics during propagation:

$$u = 2u_0 \sum_{n=1}^{\infty} \frac{J_n(n\sigma)}{n\sigma} \sin(n(\omega t - kx)), \quad (16)$$

where

$$\sigma = \left( \frac{\gamma + 1}{2} \right) \frac{u_0}{c_0} kx.$$

The discontinuity is attained for a value of the dimensionless distance parameter  $\sigma = 1$ . While Fubini's solution describes the finite-amplitude wave distortion close to the source and before shock formation, Fay's solution describes the waveform towards which the finite-amplitude wave tends if the original amplitude is high enough for shock formation.

The development of theoretical solutions for finite-amplitude wave propagation has since the Second World War mainly followed two tracks: (1) solutions based upon Burgers' equation, and (2) solutions based upon the theory of weak shocks, which permit the solution of finite-amplitude wave propagation problems, when the waveform contains shocks of not too high amplitude. Both main approaches will be discussed in detail in the following.

## 2. FINITE-AMPLITUDE WAVE PROPAGATION OF TODAY

Owing to the fact that the wave propagation in a fluid is completely determined once the particle velocity vector  $u$ , and the three thermodynamic properties are specified as a function of space and time, six independent equations are needed. These are usually: (a) the equation of continuity expressing the conservation of mass, (b) the three components of the equation of motion expressing the conservation of momentum, (c) an energy equation expressing the conservation of energy, and (d) an equation of state, a constitutive relation characterizing the fluid and its response to thermal or mechanical stress. For a number of fluids, constitutive equations expressing the dependence of other physical fluid properties, for instance viscosity, on temperature and pressure, and through it on space and time, may be needed. Very often these constitutive equations are of an empirical character.

The derivation of the basic equations of finite-amplitude wave propagation may for instance be found in [7] and they are:

Let the displacement of a piston at  $a = 0$  be given by:

$$\xi = f(t) \quad (24)$$

The Taylor series expansion about the equilibrium density  $\rho_0$  of the square of the local sound velocity  $c$  in Eq. (23), retaining terms through second-order only, leads by Eq. (25) to the following approximate form of the exact wave

$$\frac{\partial^2 \xi}{\partial t^2} = c_0^2 \frac{\partial^2 \xi}{\partial a^2} - 2c_0^2 \left[ 1 + \frac{\rho_0}{c_0} \left( \frac{dc}{d\rho} \right) \right] \frac{\partial \xi}{\partial a} \frac{\partial^2 \xi}{\partial a^2} \quad (25)$$

By substitution, a general solution to Eq. (25) can be found:

$$\xi(a, t) = f\left(t - \frac{a}{c_0}\right) + \frac{a}{2c_0^2} \left[ 1 + \frac{\rho_0}{c_0} \left( \frac{dc}{d\rho} \right) \right] \left[ f'\left(t - \frac{a}{c_0}\right) \right]^2 \quad (26)$$

where the term  $f(t - a/c_0)$  is a solution to the infinitesimal amplitude wave equation for one-dimensional wave propagation. The second term in Eq. (26) is proportional to  $a$  and to the square of the ratio of the piston velocity to the velocity of sound. This ratio, being dimensionless, forms an acoustic Mach-number which frequently in practice may be exceedingly small. Nevertheless, the second term may become of increasing importance during the wave propagation owing to the factor  $a$  in this term. It is therefore to be expected that, for continuous propagation of the wave under the lossless conditions concerned, the neglect of terms of third and higher order will no longer be justified.

If the fluid considered is a perfect gas the solution (Eq. (26)) may be written:

$$\xi(a, t) = f\left(t - \frac{a}{c_0}\right) + \frac{\gamma+1}{4c_0^2} a \left[ f'\left(t - \frac{a}{c_0}\right) \right]^2 \quad (27)$$

For a simple harmonic piston motion given by:

$$f(t) = A \cos \omega t \quad (28)$$

Eq. (27) yields:

$$\xi(a, t) = A \cos \omega \left( t - \frac{a}{c_0} \right) + \frac{(\gamma+1)}{8c_0^2} \omega^2 A^2 a \left[ 1 - \cos 2\omega \left( t - \frac{a}{c_0} \right) \right] \quad (29)$$

Eq. (29) shows that the displacement of any particle in the wave motion is no longer simple-harmonic, but is made up of a term independent of  $t$  and of two simple harmonic terms, one with the piston frequency and one with twice this frequency. The occurrence of the factor  $a$  in the term of twice the piston frequency implies that the energy being supplied at the piston frequency will gradually be transferred to the second and higher harmonic components, leading to a progressively steeper front of a condensation wave during its propagation. This transfer of energy, from the fundamental frequency to its higher harmonics, is one of the basic features of nonlinear acoustics and it will under lossless conditions result in the formation of a shock wave at a distance from the piston given by:

$$l = \frac{2c_0^2}{(\gamma+1)\omega u_0} = \frac{2}{(\gamma+1)kM} \quad (30)$$

where  $u_0$  is the peak value of the particle velocity and where  $M = u_0/c_0$  is the acoustic Mach number;  $k (= \omega/c_0)$  is the propagation constant in the wave propagation with fundamental frequency  $\omega$ .

The distance  $l$  is often called *discontinuity distance*, and is, as given by Eq. (30), connected to a lossless wave propagation.

It should be noted that, even for  $M \ll 1$ , the cumulative nonlinear effect of the second term of Eq. (26) may lead to serious wave distortions. If dissipative mechanisms are taken into account, the increasing absorption for increasing frequencies - for a number of liquids and gases the absorption is proportional to the square of the frequency for broad frequency ranges - implies that the wavefront will attain a maximum steepness, when the distance of propagation is such that the rate of energy transfer to higher harmonics, due to the nonlinearities, is just equalized by the increase of absorption at the higher harmonics.

The stabilization of the wave profile thus taking place is only relative. It does not mean that by further propagation no change of the wave profile will take place. The damping of the wave amplitude will reduce the strength of the nonlinear effects, and an original sinusoidal wave profile for instance will experience a gradual smoothing out of the steep wavefront and the wave will at longer distances again return to its original sinusoidal shape.

The transfer of energy to higher harmonics appears as an attenuation of the funda-

mental frequency wave in excess of the attenuation due to absorption at the fundamental frequency.

Let us consider the propagation of a plane, finite-amplitude wave in a dissipative fluid. It is assumed that heat conduction (constant heat conductivity) and viscous dissipation (constant viscosities) are the only sources contributing to the entropy production. Further, it is assumed that the acoustic Mach number  $M \ll 1$ , which is the most interesting case due to the interaction between nonlinearities and dissipation. Then the equation of motion (18) without body forces may be written:

$$\rho \left( \frac{\partial u}{\partial t} + u \frac{\partial u}{\partial x} \right) = - \frac{\partial p}{\partial x} + \left( \frac{4}{3} \eta + \zeta \right) \frac{\partial^2 u}{\partial x^2} \quad (31)$$

and the energy equation may through the 2'nd law of thermodynamics be written:

$$\rho T \left( \frac{\partial s}{\partial t} + u \frac{\partial s}{\partial x} \right) = \kappa \frac{\partial^2 T}{\partial x^2} + \phi \quad (32)$$

By inserting Eq. (20a) in Eq. (32), linearizing the diffusion terms due to viscosity and heat conductivity, and by insertion of the result in the equation of motion (31), this equation may be written in the following approximate form:

$$\rho \frac{\partial u}{\partial t} = - \frac{\partial p}{\partial x} + b \frac{\partial^2 u}{\partial x^2} \quad (33)$$

with

$$b = \frac{4}{3} \eta + \zeta + \kappa \left( \frac{1}{c_v} - \frac{1}{c_p} \right) \quad (34)$$

where  $\zeta$  and  $\kappa$  denote the bulk viscosity and heat conductivity coefficients, respectively.

Here  $p$ , by means of Eq. (20a), is given as:

$$p = p_0 + A \left( \frac{\rho - \rho_0}{\rho_0} \right) + \frac{B}{2} \left( \frac{\rho - \rho_0}{\rho_0} \right)^2 \quad (35)$$

with  $A$  and  $B$  being expressed by Eq. (20b).

If we introduce the thermodynamic function:

$$\lambda = \int_{p_0}^p \frac{dp}{\rho}$$

together with a velocity potential  $\phi$  we may write the equation of continuity (17) as:

$$\frac{\partial \lambda}{\partial t} + \frac{\partial \phi}{\partial x} \frac{\partial \lambda}{\partial x} + c^2 \frac{\partial^2 \phi}{\partial x^2} = 0 \quad (36)$$

Analogously, Eqs. (33) and (35) may be transformed by  $\lambda$  and  $\phi$ , and their results, when inserted in Eq. (36), lead to:

$$\frac{\partial^2 \phi}{\partial x^2} - \frac{1}{c_0^2} \frac{\partial^2 \phi}{\partial t^2} + \frac{b}{\rho_0 c_0^2} \frac{\partial}{\partial t} \left( \frac{\partial^2 \phi}{\partial x^2} \right) + \frac{1}{c_0} \left( \frac{B}{A} + 2 \right) \frac{\partial \phi}{\partial x} \frac{\partial^2 \phi}{\partial x^2} = 0 \quad (37)$$

which is an approximation correct to the squared term in  $M$  inclusive.

Transforming the variable  $t$  to the variable  $t' = t - x/c_0$  and by returning to the velocity  $u = \partial \phi / \partial x$ , Eq. (37) reduces to:

$$\frac{\partial u}{\partial x} - \left( \frac{B}{2A} + 1 \right) \frac{u}{c_0^2} \frac{\partial u}{\partial t'} = \frac{b}{2\rho_0 c_0^2} \frac{\partial^2 u}{\partial t'^2} \quad (38)$$

Eq. (38) is of the same type as the Burgers' equation, and by omission of the nonlinear term (38) reduces to an equation of the diffusion type. Eq. (38) describes with sufficient accuracy, in spite of its approximate character, both the nonlinear and the dissipative processes during the propagation of finite-amplitude plane waves in a viscous, heat conducting fluid. Owing to the reduction of the retarded time  $t'$  to  $t$  for  $x=0$ , Eq. (38) is well adapted for use with boundary-value problems, and it may be termed the boundary-value form of the Burgers' equation.

Using a characteristic distance  $x_0$  in the sound field together with the peak value of the particle velocity  $u_0$  (source value), the following dimensionless ratios can be established:

$$y = \frac{u}{u_0} ; \quad \sigma = \left( \frac{B}{2A} + 1 \right) M \frac{x}{x_0} \quad \text{and} \quad y = \frac{c_0 t'}{x_0} \quad (39)$$

which inserted in Eq. (38), yields the dimensionless form of the Burgers equation suitable for boundary-value problems.

$$\frac{\partial y}{\partial \sigma} - y \frac{\partial y}{\partial y} = \Gamma^{-1} \frac{\partial^2 y}{\partial y^2} \quad (40)$$

with



$$\Gamma = \left( \frac{B}{A} + 2 \right) \frac{u_0 \rho_0}{b} x_0 = \left( \frac{B}{A} + 2 \right) (\text{Re}_a) \quad (41)$$

where  $\text{Re}_a = \frac{u_0 x_0}{b/\rho_0}$  constitutes an acoustic Reynolds number analogous to the hydrodynamic one.

The coefficient  $\Gamma$  is an essential parameter in nonlinear acoustics. It describes the ratio of the influence of nonlinearity (including "equation of state" and "convective" nonlinearity contributions), represented by the nonlinear strength term  $(1+B/2A)M$ , to the influence of dissipation.

$\Gamma$  was first introduced by Gol'berg [16] as a criterion such that shock formation is not likely to take place if  $\Gamma \gg 1$ . For an originally sinusoidal wave, it will be appropriate to choose the characteristic distance  $x_0$  of the wave propagation as:

$$x_0 = \frac{c_0}{\omega} = \frac{1}{k} = \frac{\lambda}{2\pi}$$

where  $\lambda$  is the wavelength. This leads to the expression:

$$\Gamma = \frac{B/2A+1}{\pi} \frac{u_0 \rho_0 \lambda}{b} = \left( \frac{B}{A} + 2 \right) \frac{p_0}{b\omega} \quad (42)$$

where  $p_0$  is peak pressure of the finite-amplitude sinusoidal wave (measured at the source).

Further, by the choice of  $x_0 = 1/k$ , the value  $\sigma=1$  of the spatial coordinate  $\sigma$  will correspond to a propagation distance equal to the discontinuity length  $l$  given by Eq. (30) for the lossless propagation.

Eq. (40) has formed the basis for a number of theoretical analyses of finite-amplitude wave propagations in dissipative fluids. A complete steady-state solution to Eq. (40) can for instance be found in [17] and [18] for plane waves giving:

$$v = \left( \frac{2}{\Gamma} \right) \frac{\partial}{\partial y} \dots \quad (43)$$

where  $\tilde{v} = \sum c_n (-1)^n I_n \left( \frac{\Gamma}{2} \right) \exp(-n^2 \eta / \Gamma) \cos n\eta$  with  $c_n$  the Neumann factor ( $c_0=1$ ,  $c_n=2$  for  $n \geq 1$ ), and,  $I_n$  the Bessel function of imaginary argument:  $I_n(x) = i^{-n} J_n(iz)$ .

The reduction of the hydrodynamical equations and the equation of state to one single equation for the approximate description of the propagation of cylindrical and spherical waves of finite amplitudes, analogous to the plane wave case expressed in Eq. (38) may be written:

$$\frac{\partial}{\partial r} + n \frac{u}{r} - \left( \frac{B}{2A} + 1 \right) \frac{u}{c_0^2} \frac{\partial u}{\partial t} = \frac{b}{2\rho_0 c_0^3} \frac{\partial^2 u}{\partial t^2} \quad (44)$$

where  $n=1$ ,  $\frac{1}{2}$  and  $0$  for spherical, cylindrical and plane wave, respectively. For  $n=1$  and  $\frac{1}{2}$ , Eq. (44) is valid only in the domain  $kr \gg 1$ , and  $t' = t \mp (r-r_0)/c_0$  for divergent and convergent waves, respectively.

Using dimensionless quantities, Eq. (44) can be reduced to the dimensionless boundary value form of Burgers' equation given by:

$$\frac{\partial W}{\partial f} - W \frac{\partial W}{\partial y} = \Gamma^{-1} \frac{\partial^2 W}{\partial y^2} \quad (44a)$$

where

$$W = (\sigma/\sigma_0)^n v = (r/r_0)^n v = (r/r_0)^n (u/u_0) \\ J = 2\sqrt{\sigma_0} (\sqrt{\sigma} - \sqrt{\sigma_0}) = 2\sigma_0 [\sqrt{r/r_0} - 1] \quad \text{for cylindrical waves } (n=\frac{1}{2}) \\ \Gamma = \Gamma_0 (1+f/2\sigma_0)^{-1}$$

$$f = \sigma_0 \ln(\sigma/\sigma_0) = \sigma_0 \ln(r/r_0) \quad \text{for spherical waves } (n=1) \\ \Gamma = \Gamma_0 e^{-f/\sigma_0}$$

$$y = \omega_0 t' = \omega_0 [t - (r-r_0)/c_0]$$

$$J_0 = \left( \frac{B}{2A} + 1 \right) \frac{u_0}{c_0} k_0 r_0$$

$$\Gamma_0 = \left( \frac{B}{A} + 2 \right) \frac{\rho_0 u_0 c_0}{b\omega}$$

The similarities between the form of Eq. (44a) and the form of Eq. (40) for plane waves should be noted. The two equations differ in respect of the spatial coordinate dependence of  $\Gamma$  in Eq. (44a). This is a very interesting feature and owing to it the propagation of a finite-amplitude cylindrically or spherically divergent wave in a thermoviscous fluid is mathematically equivalent to the propagation of a plane finite-amplitude wave in a fluid which has a thermoviscous loss coefficient that grows respectively linearly or exponentially with range.

Thus, for a diverging wave Eq. (44a) shows that viscous effects will dominate and reduce nonlinear effects sooner than for plane waves, or alternatively, the spreading loss incurred in diverging waves reduces their amplitudes and thus the nonlinear effects. Conversely, an amplification of the nonlinear effects may for instance be found for finite-amplitude waves propagating upward in the atmosphere owing to exponential variation in atmospheric thermodynamic properties. 16-9

Calculations based on the above equations and supported by experimental findings show that the propagation path of an original sinusoidal finite-amplitude wave in a dissipative fluid roughly may be divided into three regions. In the first region - in what follows termed region I - the dissipative effects are small compared to the prevailing nonlinear effects. Thus the nonlinear effects by accumulation during the wave propagation distort the sinusoidal wave and lead to an increasing steepness of the wave fronts, eventually resulting in the formation of a "sawtooth" wave. But before the wave shape becomes a sawtooth the first discontinuity of the wave front (or maximum steepness) has formed at its zero-crossings at a source distance termed the discontinuity length. This distance must, owing to the dissipative effects in region I, be greater for wave propagation in a thermoviscous fluid than for wave propagation in a lossless fluid, Eq. (30), if the same initial wave amplitude is considered. The discontinuity length may appropriately form the boundary between region I and the subsequent region II, where the effects of nonlinear and dissipative processes cancel one another, leading to a stabilization of the wave shape. In region II a relatively stable sawtooth shape of the original sinusoidal wave may be obtained.

Owing to the relatively strong dissipation of energy in a sawtooth wave profile, the finite-amplitude wave gradually loses its wavefront steepness and the shock thickness of the weak periodic shock wave (the sawtooth wave) increases. Finally, the wave profile returns to its original sinusoidal shape at a distance from the source forming the beginning of region III, the so-called "old-age-region" in which the amplitude of the wave will become of second order of smallness and in which further amplitude reduction is governed by small-amplitude (linear) absorption rules.

The question of whether the shape of an original sinusoidal wave will change according to the three-region scheme outlined above depends on the initial pressure amplitude of the wave, its frequency, and the strength of the dissipative properties of the fluid; all these properties are incorporated in the Gol'dberg number  $\Gamma$  which according to Gol'dberg [16] may lead to shock formation only for  $\Gamma > 1$ .

Thus, for the propagation in a thermoviscous fluid of a sinusoidal wave of not too high an initial amplitude the dissipative effects may lead to a direct transition from region I to region III without the occurrence of region II.

Only higher initial amplitudes lead to the relatively stable wave shapes of region II.

At a sufficiently high initial pressure, the later amplitude of the distorted originally sinusoidal wave becomes relatively independent of the initial amplitude, an effect termed *acoustical saturation*.

Description of finite-amplitude wave distortion in a thermoviscous fluid has been done by the use of Burgers' Eq. (40) and its plane wave solution (43). Eq. (43) can be simplified and reduced to:

$$v = \frac{2}{\Gamma} \sum_{n=0}^{\infty} \frac{\sin ny}{\sinh n(l+\sigma)/\Gamma} \quad (45)$$

which is a form of Fay's frequency domain solution [12] for a nearly stable periodic waveform in a viscous perfect gas (region II solution). A region I solution to Eq. (40) for  $\Gamma \gg 1$  has been given by Khokhlov et al. [19] for an initial sinusoidal waveform:

$$u = u_0 \sin \omega t \text{ (at } x = 0 \text{)}. \quad (46)$$

Their solution for the distortion of the travelling plane wave has the form:

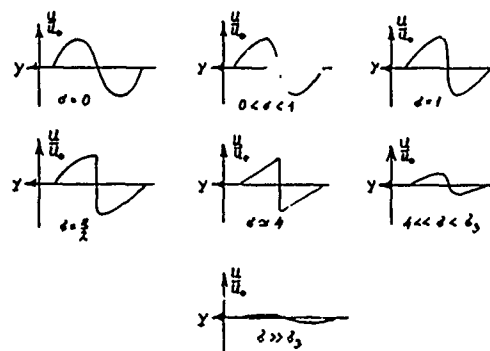
$$y = \arcsin(u/u_0) - \sigma(u/u_0) \quad (47)$$

where

$$\sigma = \left( \frac{\gamma+1}{2} \right) \frac{u_0}{c_0} \frac{\omega}{c_0} x \text{ and } y = \omega(t - x/c_0).$$

Figure 1. The different "milestones" in the change of the shape of an originally sinusoidal finite-amplitude wave, including all three characteristic regions, are shown in Fig. 1.

Eq. (47) may be used for a graphical construction of the waveform in region I since it consists of the sum of two functions,  $\arcsin(u/u_0)$  and a straight line making an angle  $\phi = \arctan \sigma$  with the  $u/u_0$  axis (see Fig. 2).



16-10

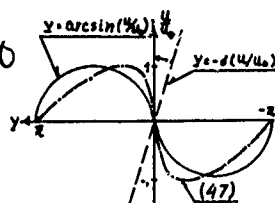


Figure 2. Graphical construction of the waveform distortion according to Eq. (47).

An exact solution to Eq. (40) describing the structure of one period of a sawtooth wave, i.e., a periodic shock wave in region II, can be written:

$$V = \frac{u}{u_0} = \frac{1}{1+\sigma} \left\{ -y + \pi \tanh \frac{y}{\Delta} \right\} \quad (-\pi \leq y \leq \pi) \quad (48)$$

where the dimensionless quantity  $\Delta$  is a measure for the shock thickness given by:

$$\Delta = \frac{2}{\pi} \frac{1+\sigma}{\Gamma} \quad (49)$$

Thus the shock thickness will decrease for increasing  $\Gamma$ , leading to  $\Delta \rightarrow 0$  for  $\Gamma \rightarrow \infty$ . In this limit the solution becomes discontinuous at  $y=0$  and describes a real sawtooth expressed by:

$$V = \frac{1}{1+\sigma} (-y \pm \pi). \quad (50)$$

The plus sign corresponds to  $0 < y < \pi$  and the minus sign to  $-\pi < y < 0$ . If the particle velocity amplitude is designated  $u_p$  for  $y=0$ , Eq. 50) gives:

$$\frac{u_p}{u_0} = \frac{\pi}{1+\sigma} \quad (51)$$

which determines the reduction of the peak amplitude of an originally sinusoidal wave, when the wave during its propagation has attained a sawtooth shape.

The onset of region II for lossless propagation of plane waves was given previously by  $\sigma=1$ . Owing to the dissipation influences in a thermoviscous fluid, changing the steepness of the wavefronts, it is more appropriate to choose a somewhat higher value of  $\sigma$  for the start of region II. Blackstock [7] selected  $\sigma = \pi/2$  to determine the onset of region II. This  $\sigma$ -value corresponds to the distance from a sinusoidal source where the peak amplitude of the wave just reaches the steep wavefront (see Fig. 1), and after which a sawtooth wave is formed.

We have seen that the dissipation of energy and the increase of entropy taking place during the irreversible compression processes in the wavefront reduces the amplitude of the sawtooth wave according to Eq. (51). Thus  $\Gamma$  will decrease for increasing  $\sigma$ , giving rise to an increase in the dimensionless quantity  $\Delta$  for the shock thickness. This increase in  $\Delta$  creates the basis for a determination of the end of region II for waves in a thermoviscous fluid, leading to an upper limit in dimensionless distance  $\sigma$  (the end of region II) on  $\sigma < 0.6\Gamma - 1 = \sigma_3$ , which for large  $\Gamma$ -values may reduce to  $\sigma < 0.6\Gamma$ , or

$$\sigma < 0.6 \left( \frac{2\rho_0 c_0^3}{\omega^2 b} \right) < 0.6/\alpha \quad (52)$$

where  $\alpha$  is the dimensional low-frequency, small-amplitude attenuation coefficient.

In order to bridge between the solutions discussed above for regions I and II, establishing an inner relation between the solutions, Blackstock [20] suggested a connection between the Fubini and the Fay solutions for plane sound waves of finite amplitudes. By use of the theory for weak non-uniform shock waves he developed a general solution that contains the Fubini and the sawtooth solutions as limiting cases, and which also covers the transition region between the two solutions. The solution was given as a Fourier series representation of the waves in the two regions:

$$B_n = (2/n\pi) V_p \int_{\phi_{\min}}^{\pi} \cos n(\phi - \sigma \sin \phi) d\phi \quad (53)$$

where  $B_n$  is the Fourier coefficient for the  $n$ th harmonic,  $V_p = u_p/u_0$  is the shock amplitude given by Eq. (51), and  $\phi$  is a function of  $y = \omega t - kx$ .

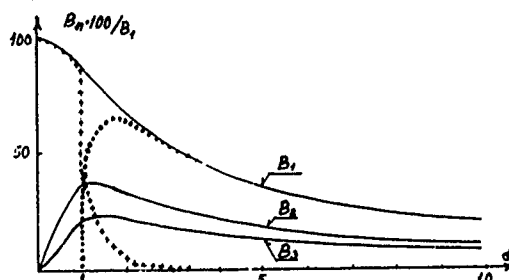


Figure 3. Dimensionless amplitude (Fourier coefficient) variation as a function of the dimensionless distance parameter  $\sigma$  for the fundamental  $B_1$  and for the second and third harmonics  $B_2$  and  $B_3$ , respectively, in an originally sinusoidal wave: +) Fourier coefficient contribution to  $B_1$  arising from the Fubini solution (Eq. (16)); ●) Fourier coefficient contribution to  $B_1$  arising from the sawtooth solution (Eq. (54)).

In the range  $0 \leq \sigma < 1$ ,  $V_p = 0$ , Eq. (53) reduces to the Fourier coefficient  $B_n = (2/n\sigma) J_n(n\sigma)$  of the Fubini solution (Eq. (16)), while for  $0 \gg 1$ ,  $V_p$  is given by Eq. (51) and Eq. (53) reduces to a sawtooth solution given by:

$$B_n = \frac{2}{n(1+\sigma)} \quad (54)$$

which is the Fourier coefficient of the Fay solution (Eq. (15)) in the lossless limit ( $\Gamma \rightarrow \infty$ ) of this equation.

Analogous to the propagation of plane waves of finite-amplitude in a thermoviscous fluid described by the use of Burgers' equation, the cylindrical and the spherical wave cases show characteristic regions I-III of propagation [7].

16-11

### 3. THE WEAK-SHOCK THEORY

In Burgers' equation discussed above the nonlinear and the dissipative effects were attached to individual terms in the equation which then formed the basis for analytical or approximate solutions in region I or in region II. An analytical method, which more quickly and more easily leads to results in region II, is the *weak-shock theory*. The basic features of the weak-shock theory are that the diffusion effects (viscosity and heat conduction effects) are disregarded except within the shock themselves, where they account for the entropy increase, and that the continuous parts of the wave in the regions between the shocks are governed by the Earnshaw solution for simple waves, thus assuming isentropic flow in these regions.

The Rankine-Hugoniot relations will be the bridging functions which connect the continuous parts of the wave by relating the values of the kinematic and the thermodynamic quantities at both sides of a surface of discontinuity. These relations may for one-dimensional wave propagation (normal shocks) be written:

$$u_1 - u_2 = [(p_2 - p_1)(1/\rho_1 - 1/\rho_2)]^{1/2} \quad (55)$$

$$h_2 - h_1 = \frac{1}{2}(p_2 - p_1)(1/\rho_1 + 1/\rho_2) \quad (56)$$

where  $u$  denotes the particle velocity and  $h$  denotes the enthalpy per unit mass. The subscripts 1 and 2 refer to the conditions just ahead of the shock and just behind the shock, respectively.

It should be noted that dissipation is accounted for indirectly by Eq. (56). If this equation is transformed by expanding it in powers of small differences  $(s_2 - s_1)$  and  $(p_2 - p_1)$ , retaining terms to third order in  $(p_2 - p_1)$  and to first order in  $(s_2 - s_1)$ , we obtain, after insertion of  $(\partial h / \partial s)_p = T$  and  $(\partial h / \partial p)_s = 1/\rho = v$ , the following expression for the entropy increase across the shock:

$$s_2 - s_1 = \frac{1}{12T_1} \left( \frac{\partial^2 v}{\partial p^2} \right)_s (p_2 - p_1)^3 \quad (57)$$

Thus, the discontinuity of entropy in a weak-shock wave is of the third order of smallness relative to the discontinuity of pressure.

This very essential expression (57) justifies the adoption of isentropy for infinitesimal wave propagation, and shows that even finite, but small, amplitude waves lead to approximately isentropic conditions.

Friedrichs [21] concluded from Eq. (57) that if changes up to only the second order of smallness in the shock strength  $\delta = (p_2 - p_1)/p_1$  are considered, no change of entropy will be observed. This may lead to a theory for the isentropic lossless fluid.

As already shown by Earnshaw [5] the propagation of a finite-amplitude wave in a perfect gas may subject to the boundary conditions:

$$u(0, t) = G(t) \quad (58)$$

be written in terms of a parameter  $\phi$  as:

$$u(x, t) = G(\phi) \quad (59)$$

where

$$\phi = t - \frac{x}{c_0 + [(\gamma + 1)/2]G(\phi)}$$

The parameter  $\phi$  may be interpreted as the time the "wavelet" of particle velocity  $u$  left the origin  $x = 0$ .

If the continuous waveform solution represented by Eq. (59) leads to a shock formed at a distance  $x$  from the origin and at the time  $t$ , then this shock will arrive at any subsequent point at a time  $t_s$  given by:

$$t_s = t + \int_x^\infty \frac{d\xi}{U} \quad (60)$$

$U$  is the velocity of propagation of the shock, which according to the Rankine-Hugoniot relations depends on the particle velocity values  $u_1$  and  $u_2$  on either side of the shock, and thus may be written:

$$U = c_0 + \frac{1}{2} \left( \frac{\gamma + 1}{2} \right) (u_1 + u_2) \quad (61)$$

Eq. (61) shows that weak shock propagate with a velocity which is the mean value of the phase velocities just ahead of and just behind the shock.

By use of the retarded time  $t' = t - x/c_0$  and by insertion of Eq. (61) into Eq. (60) the following first-order expression is obtained:

16-12 
$$t'_s = t' - \frac{1}{2} \left( \frac{\gamma+1}{\gamma} \right) \frac{1}{c_0^2} \int_{-\infty}^x (u_1 + u_2) d\xi \quad (62)$$

which may be converted to a differential equation for the path and amplitude of the shocks expressed by:

$$\frac{dt'_s}{dx} = - \frac{1}{2} \left( \frac{\gamma+1}{\gamma} \right) \frac{1}{c_0^2} (u_1 + u_2) \quad (63)$$

$u_1$  and  $u_2$  are determined by the continuous solution given by Eq. (59) for the wave parts between the shocks, thus giving together with the Eq. (63) a system of equations to be solved giving  $u_1$ ,  $u_2$  and  $t'_s$  within the weak-shock theory.

At very great distances from the origin the formulas derived by the use of weak-shock theory will be inaccurate owing to reduction in the shock strength leading to a dispersed shock, which no longer may be approximated by a discontinuity. In order to estimate the point beyond which the weak-shock theory gives inaccurate results, the decay rates of a sawtooth wave and a small-signal wave may be equated leading to the following approximate expression for the maximum distance  $x_m$  at which the sawtooth solution, and thus the weak-shock theory, is valid:

$$x_m = 1/\alpha \quad (64)$$

which shows good agreement with the upper limit of the sawtooth region given by Eq. (52).

It should be noted that, in order to use the weak-shock theory at all, the nonlinear effects must prevail over the dissipative effects. This may, by the use of the acoustic Reynolds number  $\Gamma$ , be written as:

$$\Gamma \gg 1 \text{ or } \left( \frac{\gamma+1}{2} \right) \frac{u_0}{c_0} k \gg \alpha \quad (65)$$

where  $\alpha$  is given by Eq. (52).

The formulas given above for the weak-shock theory applied to the plane wave case may be generalized for  $kr \gg 1$  also to comprise cylindrical and spherical finite-amplitude waves [7].

### 3. PROPAGATION IN A RELAXING FLUID

The reestablishment of thermodynamic equilibrium in a fluid normally takes place very fast, i.e. the time scale for the processes leading to reestablishment of equilibrium is normally much smaller than the time scale characterizing the variation of properties within acoustical waves. Therefore, in most cases it is a good approximation to consider that the fluid remains in equilibrium during the wave propagation.

Some molecular processes are, however, so slow that the time for establishing the new thermodynamic equilibrium, the so-called *relaxation time*  $\tau$ , becomes comparable to the period of the propagating disturbance. This is the case in, for instance, energy transport from external to some retarded internal degrees of freedom for some chemical reactions taking place between the components of the fluid.

The intensity of the irreversible processes taking place during the restoration of the thermodynamic equilibrium and leading to a dissipation of energy depends on the relation between  $\tau$  and the angular frequency  $\omega$  of the propagating wave. It is characteristic for all relaxation processes that an acoustic wave with a frequency high enough to yield  $\omega\tau \gg 1$  will propagate with a phase velocity  $c_\infty$  which is higher than the phase velocity  $c_0$  with which a wave satisfying  $\omega\tau \ll 1$  propagates. The high-frequency signal ( $\omega\tau \gg 1$ ) suffers no increased absorption due to the presence of relaxation, i.e. the internal degrees of freedom act as if "frozen", while the low-frequency signal ( $\omega\tau \ll 1$ ) attains thermodynamic equilibrium at all times during the wave motion due to the slow change of state in the long period wave.

Owing to the lack of thermodynamic equilibrium during the relaxation processes, it is necessary to specify one more thermodynamic variable in the equation of state for a fluid. Such a variable  $\xi$ , characterizing the state of non-equilibrium considered, may for small deviations from equilibrium be determined by the simple first-order reaction equation:

$$\frac{\partial \xi}{\partial t} = \frac{\xi_0 - \xi}{\tau} \quad (66)$$

where  $\xi_0$  is the equilibrium value of  $\xi$ .

Thus, the equation of state for a relaxing fluid may instead of Eq. (20) be written as:

$$p = p(\rho, s, \xi) \quad (67)$$

On the basis of the equations of continuity and motion correct to second order, the following two equations governing the propagation of finite-amplitude waves in a relaxing fluid may be derived:

$$\frac{\partial u}{\partial x} - \frac{1}{c_0^2} \left( \frac{B}{2A} + 1 \right) u \frac{\partial u}{\partial t} = - \frac{B_0 \tau}{2\rho_0 c_0^2} \frac{\partial^2 \xi}{\partial t^2} \quad \tau \frac{\partial \xi}{\partial t} + \xi = - \frac{m\rho_0 c_0}{B_0} u \quad (68)$$

where  $B_0 = (\partial p / \partial \xi)_{\rho_0}$  is a small quantity of the order  $M = u_0 / c_0$  and where  $m = (c_0^2 - c^2) / c_0^2 \ll 1$  represents the dispersion.

Eqs. (68) can be merged into the form of a single equation similar to Burgers' equation, which may be written:

$$\left( \tau \frac{\partial}{\partial t'} + 1 \right) \left( \frac{\partial u}{\partial x} - \frac{1}{c_0^2} \left( \frac{B}{2A} + 1 \right) u \frac{\partial u}{\partial t'} \right) = \frac{\pi \tau}{2 c_0} \frac{\partial^2 u}{\partial t'^2} \quad (69)$$

For  $\omega \tau \ll 1$  and by assuming  $\partial u / \partial x = 0$ , a steady-state solution to the Eqs. (68) can be found describing the structure of single steady compression jump of amplitude  $2u_0$  by:

$$\frac{t' + t'_0}{\tau} = \ln \frac{(u_0 + u)^{\kappa-1} u_0^2}{(u_0 - u)^{\kappa+1}} \quad (70)$$

where  $\kappa = m c_0 / [ (B/A + 2) u_0 ]$  and  $t'_0$  is a constant of integration.

$\kappa$  is a characteristic quantity for wave propagation in relaxing fluids. It expresses the ratio of the relaxing to the nonlinear effects, and thus it serves for a relaxing fluid the same purpose as  $\Gamma$  does for the thermoviscous fluid case.

If  $\kappa \gg 1$ , a relatively mild nonlinear effect exists and the solution Eq. (70) reduces to:

$$u = u_0 \tanh(t' / 2 \kappa \tau) \quad (71)$$

for the amplitude of the velocity jump.

For a periodic finite-amplitude wave in region II, where the nonlinear and the relaxing effects are of importance, an approximate solution of Eqs. (68) can be obtained by combining the solution in Eq. (70) or Eq. (71) with the solution describing a sawtooth wave (Eq. (48)).

$$u = \frac{u_0}{1 + \sigma_r} \left( -y + \pi \tanh \frac{y}{\Delta} \right)$$

where

$$\Delta = \frac{1 + \sigma_r}{\pi} \frac{1}{(B/2A + 1) \text{Re}} \quad (72)$$

with

$$\sigma_r = (B/2A + 1) (\omega u_0 x / c_0^2)$$

$$y = \omega t' = \omega (t - x / c_0)$$

$$\text{Re} = u_0 / c_0 \omega \tau m \text{ (Reynolds' number for relaxing fluid)}.$$

For  $\kappa > 1$  and  $\kappa < 1$ , i.e. stronger nonlinear effects, the factor  $\tanh(y/\Delta)$  should be replaced by  $u = u(y)$  found from the solution of Eq. (70). The form of one period of a finite-amplitude wave for  $\kappa > 1$  and  $\kappa < 1$ , respectively, is given in Fig. 4.

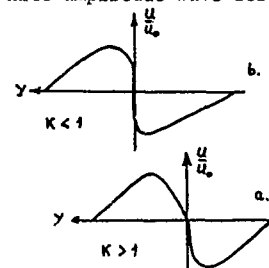


Fig. 4. The region II shape of one period of a finite-amplitude wave propagating in a relaxing fluid in the case of  $\omega \tau \ll 1$ : (a) for the case of  $\kappa > 1$  and (b) for the case of  $\kappa < 1$ .

Thermoviscous effects, relaxation effects, nonlinear effects and diffraction effects may all be included in a compound equation which for a quasi-plane wave case may be written in dimensionless form [22] as:

$$\frac{\partial}{\partial y} \left( \frac{\partial V}{\partial \sigma} - V \frac{\partial V}{\partial y} - G \frac{\partial^2 V}{\partial y^2} - D \frac{\partial}{\partial y} \int_{-\infty}^y \frac{\partial V}{\partial y'} e^{-\frac{y-y'}{\omega \tau}} dy' \right) = \frac{N}{4} \left( \frac{\partial^2 V}{\partial \xi^2} + \frac{1}{\xi} \frac{\partial V}{\partial \xi} \right) \quad (73)$$

where  $V = u/u_0$  and  $\xi$  is a diffraction variable.

Eq. (73) has the following properties:

- (i) for  $G \neq 0$  and  $D=N=0$ , it reduces to Burgers' Eq. (40) for a thermoviscous medium ( $G = \Gamma^{-1}$ );
- (ii) for  $D \neq 0$  and  $G=N=0$ , in the limit of  $\omega \tau \ll 1$ , it reduces to a symbiosis of the Korteweg-de-Vries equation involving nonlinearity and dispersion and Burgers' equation involving nonlinearity and dissipation (see also Eqs. (68));
- (iii) for  $N \neq 0$  and  $G=D=0$ , it reduces to the equation governing the diffraction influence on the nonlinear wave propagation.

#### 4. EXPERIMENTAL STUDIES

A great number of experiments have during recent years been carried out in order to verify theories discussed above or in order to seek clear experimental information concerning different aspects of finite-amplitude wave propagation without the purpose of verifying a theory. A number of tests have further been oriented towards the development of new experimental equipment and procedures for its use.

The subjects for experimental investigations may roughly be divided into three main groups. (1) The nonlinearity of the pressure-density relation of the fluid expressed by

16-14 the nonlinearity ratios  $B/A$  (second-order terms, see Eq. (21) and  $C/A$  (third-order terms, see Eq. (22)). (2) The growth and decay of the harmonic content of the finite-amplitude waves during propagation. (3) Absorption measurements.

Determination of the parameters of nonlinearity  $B/A$  and  $C/A$  has mainly been performed using static, thermodynamic or finite-amplitude waveform distortion methods, of which the thermodynamic method has been the one mostly used. Knowing from experiments how the sound velocity in a fluid depends on pressure and temperature the sound velocity derivatives in Eqs. (21) and (22) may be determined. These derivatives form the most crucial factors of the equations for  $B/A$  and  $C/A$  and the other terms may be found through standard thermodynamic laboratory procedures. Some  $B/A$  and  $C/A$  values for various fluids are given in table 1.

Fluid ( at atmos- pheric pressure)	$T(^{\circ}\text{C})$	$B/A$	Fluid	$T(^{\circ}\text{C})$	$C/A$
Distilled water	0	4.16	Water		
Distilled water	10	4.63	$10^5 \text{ N/m}^2$	30	32.0
Distilled water	20	4.96	$2 \times 10^6 \text{ N/m}^2$	30	38.6
Distilled water	30	5.22	$4 \times 10^6 \text{ N/m}^2$	30	32.5
Distilled water	40	5.38	$8 \times 10^6 \text{ N/m}^2$	30	26.0
Distilled water	50	5.55			
Distilled water	60	5.67			
Distilled water	80	5.96	1 Propanol		
Distilled water	100	6.11	$10^5 \text{ N/m}^2$	30	75.0
Carbon tetrachloride	30	11.54	$8 \times 10^6 \text{ N/m}^2$	30	25.0
Glycerine	20	8.80			
Mercury	40	8.33			
Methyl alcohol	30	9.62			
Ethyl alcohol	30	10.57			
Propyl alcohol	30	10.70			
Liquid nitrogen	-199	9.69			
Liquid oxygen	-199	9.56			
Monatomic gas	20	0.67			
Diatomic gas	20	0.40			

Table 1.  $B/A$  and  $C/A$  values for various fluids.

Investigation of the growth and decay of the harmonic contents of finite-amplitude waves during propagation is very much tied up with the determination of  $B/A$  and  $C/A$ , both optical and electro-mechanical devices have been used for the experimental study of finite-amplitude wave distortion in various fluids. A detailed account of these studies and their results may be found in Reference [7].

Nonlinear absorption, i.e. energy transport from the fundamental to its higher harmonics and the higher dissipation rate at the higher harmonics, appears from Eq. (74) for the effective absorption coefficient  $\alpha_e$ .  $\alpha$  is the absorption coefficient for waves having the infinitesimal displacement amplitude  $\xi_0$ .

$$\frac{\alpha_e}{\alpha} = 1 + \frac{3\omega^2 \xi_0 / B}{4\alpha c^2} \left( \frac{B}{2A} + 1 \right) \exp(-2\alpha x) (1 - \exp(-2\alpha x))^2 + \text{higher order terms.} \quad (74)$$

The effective absorption is compared with the infinitesimal amplitude absorption (linear relation) in Figure 4, which shows the relative pressure amplitude measured at various distances  $x$  from a finite-amplitude wave source for a number of source amplitudes  $P_1(0)$ . These experimental results published by Lester [23] show the existence of a definite upper limit to the sound pressure amplitude which can be transmitted across a given distance, i.e. the existence of acoustical saturation.

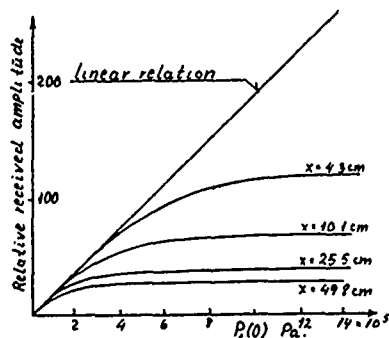


Fig 5. Relative pressure amplitudes of finite-amplitude waves measured at various distances  $x$  from a source of amplitude  $P_1(0)$ .

#### CONCLUSIONS

The development of nonlinear acoustics began in 1755; because of its ability to subsume different physical processes with its methodology and to contribute solutions to practical problems, it has been strengthened during the years. It is therefore to be expected that the growing recognition of the importance of this field of research might result in a situation where an increasing number of research and development centres around the world are involved in solving problems comprising elements of finite-amplitude wave propagation.

## REFERENCES

1. Euler, L. "Principes généraux du mouvement des fluides". Hist. de l'Acad. de Berlin. Vol. 11 (1757), p. 274.
2. Oeuvres de Lagrange. Vol. 1, Gauthier-Villars, Paris 1867.
3. Poisson, S.D. "Mémoire sur la théorie du son". Journal de l'Ecole Polytechnique. Vol. 7 (1808), p. 319.
4. Stokes, G.G. "On a difficulty in the theory of sound". Phil. Mag. Ser. 3, Vol. 32 (1848), p. 349.
5. Earnshaw, S. "On the mathematical theory of sound". Phil. Trans. (1860), p. 133.
6. Riemann, B. "Über die Fortpflanzung ebener Luftwellen von endlicher Schwingungsweite". Gött. Abhandlungen, Vol. 8 (1860), p. 43.
7. Bjørnø, L. "Nonlinear acoustics". In Stephens, R.W.B. & Leventhall, H.G. (Eds), Acoustics and Vibration Progress. Chapman & Hall Ltd., London, Vol. II (1976).
8. Rankine, W.J.M. "On the thermodynamic theory of waves of finite longitudinal disturbance". Trans. Roy. Soc., London, Vol. 160 (1870), p. 277.
9. Hugoniot, H. "Sur la propagation du mouvement dans les corps et spécialement dans les gaz parfaits". Journal de l'Ecole Polytechnique. Vol. 58 (1889), p. 1.
10. Lord Rayleigh. "Aerial plane waves of finite amplitude". Proc. Roy. Soc. Vol. A84 (1910), p. 247.
11. Taylor, G.I. "The conditions necessary for discontinuous motion in gases". Proc. Roy. Soc. Vol. A84 (1910), p. 371.
12. Fay, R.D. "Plane sound waves of finite amplitude". J. Acoust. Soc. Amer. Vol. 3 (1931), p. 222.
13. Fubini, E. "Anomalia nella propagazione de onde acustiche di grande ampiezza". Alta Frequenza IV, Vol. 5 (1935), p. 530.
14. Coppens, A.B., Beyer, R.T., Seiden, M.B., Donoghue, J., Guepin, F., Hudson, R.H. and Townsend, C. "Parameter of nonlinearity in fluids II". J. Acoust. Soc. Amer. Vol. 38 (1965), p. 797.
15. Eckart, C. "Vortices and streams caused by sound waves". Phys. Rev. Vol. 73 (1948), p. 68.
16. Gol'dberg, Z.A. "On the propagation of plane waves of finite amplitude". Soviet Phys. (Acoust.), Vol. 2 (1956), p. 346.
17. Mendousse, J.S. "Nonlinear dissipative distortion of progressive sound waves of moderate amplitudes". J. Acoust. Soc. Amer. Vol. 25 (1953), p. 51.
18. Blackstock, D.T. "Thermoviscous attenuation of plane, periodic, finite-amplitude sound waves". J. Acoust. Soc. Amer. Vol. 36 (1964), p. 534.
19. Khokhlov, R.V. and Soluyan, S.K. "Propagation of acoustic waves of moderate amplitude through dissipative and relaxing media". Acustica, Vol. 14 (1964), p. 241.
20. Blackstock, D.T. "Connection between the Fay and Fubini solutions for plane sound waves of finite amplitude". J. Acoust. Soc. Amer. Vol. 39 (1966), p. 1019.
21. Friedrichs, K.O. "Formation and decay of shock waves". Comm. Pure. Appl. Math. Vol. 1 (1948), p. 211.
22. Rudenko, O.V., Soluyan, S.I. and Khokhlov, R.V. "Problems of the theory of nonlinear acoustics". Paper No. 1.15 in "Finite-amplitude wave effects in fluids". L. Bjørnø (Ed.), JPC Science and Technology Press, London 1974.
23. Lester, W.W. "Experimental study of the fundamental frequency component of a plane, finite-amplitude wave". J. Acoust. Soc. Amer. Vol. 40 (1966), p. 847.



# NONLINEAR INTERACTION OF FINITE-AMPLITUDE SOUND WAVES

Leif Bjørnø  
Professor, Ph.D., DIC.  
The Acoustics Laboratory  
Technical University of Denmark  
Building 352, DK-2800 Lyngby, Denmark

17-1

## SUMMARY

A brief account of the history and the fundamental theory of nonlinear interaction of finite-amplitude sound waves is given leading to the introduction of the concept: "Parametric acoustic arrays". Low-amplitude wave interactions in absorption and spreading-loss limited parametric transmitting arrays are discussed for continuous and pulsed primaries and for field points outside or inside the interaction region. High-amplitude wave interactions leading to nearfield saturation limited parametric transmitting arrays are further treated for field points outside and inside the interaction region. The parametric receiving array for low- and high-amplitude pump waves is discussed and finally is given an exposition of the possibilities for obtaining an improvement of the parametric conversion efficiency for low- and high-amplitude wave interactions.

## INTRODUCTION

The generation of sum- and difference-frequencies by the interference between two finite-amplitude sound waves has been the subject of discussion for more than two hundred years. Helmholtz [1] and Lamb [2] credit the original observation of difference-frequency tones to Sorge (1745) and Tartini (1754). Since then the subject of difference-frequency wave generation has received the attention of several authors but only the last 15 years have brought a strong development in the practical exploitation of the finite-amplitude wave interaction products, in particular the difference- and frequency waves, while earlier works seem to have considered the effect as an occasional, undesirable nuisance or as a rather academic subject. The practical exploitation of the nonlinear sum- and difference-frequency wave generation in particular for underwater sound purposes has particularly through the last 10 to 15 years went through a rapid development, and the spectrum of fields of underwater applications now includes parametric transmitting and receiving arrays for echo-ranging, for bottom and subbottom profiling, for marine archeological detection of buried artifacts, for selected mode excitation in shallow water sound propagation and for ultrasonic imaging in medical diagnostics. The development hitherto in the field of parametric acoustic arrays gives no basis at all for an expectation of a future reduced research activity in studying and developing new fields of application of the parametric acoustic arrays and in improving the parametric acoustic arrays aiming at a better adaptation to fields where it already is being used.

### 1. HISTORY AND FUNDAMENTAL THEORY

The theoretical work on nonlinear interaction of two sound beams - or, in different words, the scattering of sound by sound - begins with the papers of M.J. Lighthill on sound produced by turbulence [3], [4]. He transformed the basic equations of fluid mechanics into a form being particularly suited for the study of sound generated aerodynamically. Lighthill's exact equation for arbitrary fluid motion can be written as:

$$\frac{\partial^2 \rho}{\partial t^2} - c_0^2 \nabla^2 \rho = -c_0^2 \nabla^2 \rho = \frac{\partial^2 T_{ij}}{\partial x_i \partial x_j} \quad (1)$$

where  $T_{ij} = \rho u_i u_j + p_{ij} - c_0^2 \rho \delta_{ij} + D_{ij}$ , with  $D_{ij}$  comprising the viscous stresses.

$\rho u_i u_j$  is the instantaneous Reynolds stress tensor,  $p_{ij}$  the non-viscous stress tensor and  $\delta_{ij}$  the Kronecker delta. In effect, the sound field radiated by fluid flow - including the interacting sound beams - is equivalent to one produced by a static distribution of acoustic quadrupoles with source strength density given by  $T_{ij}$ .

In the far field Eq. (1) reduces to:

$$\rho - \rho_0 = \frac{1}{4\pi c_0^2} \frac{r_i r_j}{r^3} \int \frac{1}{c_0^2} \frac{\partial^2}{\partial t^2} T_{ij} \left( \mathbf{R}, t - \frac{r-R}{c_0} \right) dV \quad (2)$$

where  $\mathbf{R}$  and  $\mathbf{r}$  denote the position vectors from the origin to the location of the observer (i.e. the field point) and to the differential volume  $dV$  of the zone of volume integration  $V$ , respectively.

In their analysis, Ingard and Fridmore-Brown [5] began with this equation, neglected viscous losses and derived the following expression for the far field amplitude of the pressure at the sum frequency,  $p_+$ :

$$p_+ = \frac{4\pi a^3}{\rho_0 c_0^4} (f_1 + f_2)^2 \frac{p_1 p_2}{r} \left( \sin 2\theta + 2 \frac{B}{A} \right) \frac{\sin \alpha}{\alpha} \frac{\sin \beta}{\beta} \quad (3)$$

Here  $f_1, f_2$  are the primary beam frequencies,  $a$  the radius of each source,  $p_1, p_2$  the primary beam pressure amplitude at the centre of the interaction region,  $r$  the distance from

the interaction region to the receiver,  $\theta$  = angle between the first incident beam and the receiver, and the angles  $\alpha$ ,  $\beta$  are defined by

$$\alpha = \frac{2\pi a}{c_0} [f_1 - (f_1 + f_2) \cos \theta] \quad \beta = - \frac{2\pi a}{c_0} [(f_1 + f_2) \sin \theta - f_2] .$$

In their attempts to verify the theory, Ingard and Pridmore-Brown obtained an intensity of the scattered signals being about 10 dB below those expected theoretically. Westervelt [6] developed another theory for the interaction. He used the expansion of the pressure in terms of the density and deduced the following equation for the lowest order in the scattering process:

$$\nabla^2 p_s = - \frac{1}{c_0^2} \frac{\partial^2}{\partial x_i \partial x_j} \left[ \rho_0 u_i u_j + \frac{1}{2} \left( \frac{\partial^2 p}{\partial \rho^2} \right)_{\rho=\rho_0} \rho^2 \delta_{ij} \right] . \quad (4)$$

where  $\rho_s$  is the density in the scattered wave and the nonlinearity parameter  $B/A$  is represented through the term:  $(2c_0^2)^{-1} (\partial^2 p / \partial \rho^2)_{\rho=\rho_0} = B / (\rho_0 A)$ .

For the case of two mutually perpendicular beams, Eq. (4) reduces for harmonic initial waves to:

$$\nabla^2 p_s = \nabla^2 \left[ \frac{1}{c_0^2} \left( \frac{c_0^2 \rho_1 \rho_2}{\rho_0} - \frac{\rho_0}{2\omega_1 \omega_2 c_0^2} \left( \frac{\partial^2 p}{\partial \rho^2} \right)_{\rho=\rho_0} \cdot \nabla^2 \left( \left( \frac{c_0^2}{\rho_0 \omega_1 \omega_2} \right) \left( \frac{\partial \rho_1}{\partial t} \right) \left( \frac{\partial \rho_2}{\partial t} \right) \right) \right] \quad (5)$$

where the quantities  $\rho_1$  and  $\rho_2$  refer to the excess density in each of the primary sound beams. In a subsequent paper Westervelt [7] generalized his theory to comprise the case of two collimated sound beams intersecting at an arbitrary angle.

The case of two collinear sound beams was treated by Westervelt [8] in a paper where he noted that the nonlinear terms made the beam act as a distribution of sources for the modulating frequency. In [8] and in particular in [9] Westervelt formulated his now classical theory for the parametric acoustic array, a name given to the collinear sound beam interaction region due to its resemblance to the corresponding sonar array. The following simplifying assumptions and approximations underlie Westervelt's work:

- The equation of motion for an ideal fluid is used and the attenuation effect is introduced in an "ad hoc" way.
- The two superimposed, high-frequency, plane primary waves are assumed to form beams so narrow and so perfectly collimated that the volume distribution of sources may adequately be represented by a line distribution located along the axis of the primary waves. The cross-sectional dimensions of the primary wave interaction region are assumed to be small compared with the wavelength at the difference frequency.
- No attenuation of the difference-frequency wave is assumed to occur.
- The amplitude attenuation coefficients for each of the two primary waves are equal and assumed to be one or more orders of magnitude less than the wave number of the difference-frequency wave.
- Nonlinear attenuation is negligible.

Rewriting (1) on the basis of the assumptions (a) to (e) and using a perturbation analysis retaining terms to second order in the field variables only, Westervelt's quasi-linear approach led to the following inhomogeneous wave equation for the pressure amplitude  $p_s$  of the difference-frequency wave:

$$\nabla^2 p = - \rho_0 \frac{\partial q}{\partial t} \quad (6)$$

where

$$q = \frac{\beta}{\rho_0^2 c_0^4} \frac{\partial}{\partial t} p_1^2 \quad (7)$$

$q$  is the source strength density responsible for the generation of acoustic energy through the nonlinear interaction of the primary waves in which the instantaneous pressure at a source point is  $p_1$ .  $\beta$  is related to the second order nonlinearity ratio  $B/A$  of the fluid through:  $\beta = 1 + B/A$ , while expression (7) is valid for plane waves travelling in the same direction, a general expression for the source strength density  $q$  of a primary field of any configuration may be found in [10].

The general solution to the equation (6) may be written as a volume integral by:

$$p_s(R, t) = - \frac{\rho_0}{4\pi} \int_V \frac{\partial}{\partial t} \frac{e^{j\omega_s |R-r|}}{|R-r|} dV . \quad (8)$$

The volume integral (8) was used by Westervelt for a derivation of the difference-frequency sound field generated by the nonlinear interaction of the two perfectly collimated, plane, monochromatic, collinear, primary waves of equal source amplitude  $p_0$ . His expression for the pressure amplitude  $p_s$  as a function of the distance  $R$  from the projector emitting the primary waves to the observation point and as a function of the angle  $\theta$  between the observation point and the acoustic axis of the projector may be written as:

$$p_s(R, \theta) = \frac{\omega_s^2 p_0^2 S \beta}{8\pi \rho_0 c_0^4 \alpha_0} \left( \frac{1}{\left( 1 + \frac{k_s^2}{\alpha_0^2} (\sin^2 \frac{\theta}{2}) \right)^{\frac{1}{2}}} \right) \quad (9)$$

where the time and phase dependences have been omitted.  $\omega_s$  is the angular frequency of the difference-frequency wave,  $S$  denotes the cross-sectional area of the collimated wave re-

gion and  $k_s$  denotes the wave number of the difference-frequency wave.  $\alpha_0$  is the mean absorption coefficient of the primary waves for infinitesimal wave amplitudes.

Westervelt's solution (9) is restricted to the farfield of the scattered wave by the condition:  $k_s R > (k_s/\alpha_0)^2$ . 17-3

The bracket in (9) leads to the half-power beamwidth  $\theta_h$  of the difference-frequency wave given by:

$$\theta_h \approx 2(\alpha_0/k_s)^{1/2} \quad (10)$$

which shows that a narrowing of the beam takes place for a decrease in the primary wave frequency, opposite to what is the case for a conventional linear projector. Further, a narrowing of the beam will follow an increase in the difference-frequency. It should be noted that the influence of the primary frequencies on (9) and (10) is only through the absorption coefficient  $\alpha_0$ .

The difference-frequency signal amplitude  $p_s$  may be considered to be radiated from an array of sources distributed continuously throughout the interaction region, being bounded by the collimated beams and extending a distance along the acoustic axis determined by the small signal absorption of the carrier waves. The parametric array is shaded by virtue of the naturally smooth decay in the conversion of the carrier frequency waves to the difference-frequency wave with increasing distance from the signal source. The shading of the array, being due to the carrier wave absorption and diffraction within the interaction region, gives rise to a monotonically decaying angular response of the difference-frequency wave with increasing  $\theta$ -values, thus avoiding the undesirable minor lobes that are common in conventional piston type transducers. Due to the small width of the interaction region compared to its length the parametric array produces a field of radiation much narrower than the one which would be produced by a conventional underwater sound source operating linearly at the difference frequency. Moreover, the wide band character of the parametric conversion process enables one to remedy some of the disadvantages of the rather low efficiency of the nonlinear conversion process by the use of wide-band signal processing techniques. In spite of the low source level efficiency - ranging from 10% down to  $10^{-5}\%$  - systems employing parametric arrays can be superior to conventional linear systems when the reduction of the beamwidth, the transducer size or the absorption - due to the low difference frequency - are taken into account.

Since Westervelt's publication of his quasilinear approach leading to his asymptotic solution being valid at long ranges from the interaction region, a great deal of theoretical and experimental work has been done in order to improve the understanding of the characteristics of the parametric acoustic arrays.

The aperture effect due to the finite size of the projector, which should be taken into account when the interaction volume is substantially limited to the nearfield of the projector by the rate of absorption of the primary waves has been discussed by Naze & Tjøtta [11] and by Berktaay [12]. Berktaay assumed a rectangular projector of sides  $2b$  and  $2d$  situated in the  $y$ - $z$ -plane and he obtained the following expression for the difference-frequency pressure amplitude produced by the nonlinear interaction of two collimated, plane waves of initial pressure amplitudes  $p_1$  and  $p_2$ :

$$p_s = \frac{p_1 p_2 \omega^2 S \beta}{4\pi \rho_0 c_0^4 R} \frac{\psi(b, d, k_s, \gamma, \theta) e^{-\alpha_s R}}{(\alpha_T^2 + 4k_s^2 \sin^2(\frac{\theta}{2}))^{1/2}} \quad (11)$$

where the aperture effect is represented by the expression:

$$\psi(b, d, k_s, \gamma, \theta) = \frac{\sin(d k_s \cos \gamma) \sin(b k_s \sin \gamma \sin \theta)}{d k_s \cos \gamma \cdot b k_s \sin \gamma \sin \theta} \quad (12)$$

with  $S = 2b \cdot 2d$ .

$\alpha_T$  denotes an absorption coefficient determined by:

$$\alpha_T = \alpha_1 + \alpha_2 - \alpha_s \cos \theta \approx \alpha_1 + \alpha_2 - \alpha_s \quad \text{for } \theta \ll 1.$$

$\alpha_1$ ,  $\alpha_2$  and  $\alpha_s$  are the absorption coefficients of the primary waves and the difference-frequency wave, respectively.  $\gamma$  is the angle between the  $z$ -axis and the radial distance  $R$  from the centre of the projector ( $x, y, z = 0, 0, 0$ ) to the observation point.

For a circular projector the  $(\sin(N)/(N))$  in (12) will be replaced by  $(2J_1(N)/(N))$ .

For spherically spreading primary waves confined to a cone of angular width  $2\psi_1$  and by assuming a uniform intensity distribution across the cone, Berktaay found for the difference-frequency pressure amplitude along the axis of symmetry:

$$p_s(R, 0) = \frac{p_1 p_2 \omega^2 \beta e^{-\alpha_s R}}{2\rho_0 c_0^4 R k_s} \left\{ \left( \frac{1}{2} \ln(1 + \psi_h^4) \right)^2 + \left( \tan^{-1} \psi_h^2 \right)^2 \right\}^{1/2} \quad (13)$$

where  $\psi_h$  is given by:

$$\psi_h^4 = (\psi_1/\theta_h)^4 \approx (k_s/\alpha_T) (1 - \cos(\psi_1))^2$$

and where the half-power beamwidth  $\theta_h$  (for the expressions (11) and (13) is given by:

$$\theta_h \approx 2(\alpha_T/2k_s)^{1/2}, \quad \text{for } \alpha_T/2k_s \ll 1. \quad (14)$$

17-4

$\alpha_T$  is for the spherical wave case given by:

$$\alpha_T = \alpha_1 + \alpha_2 - \alpha_s \cos \theta \cos \psi \approx \alpha_1 + \alpha_2 - \alpha_s.$$

Berklay's asymptotic solutions (11) and (13) are valid for the field point at long ranges from the interaction region.

The plane and spherical waves hitherto discussed form parts of the wave field arising from a piston source embedded in an infinite, rigid baffle. Some characteristic source distances shall briefly be defined in the following due to the fact that piston sources have most frequently been used for primary wave transmission by the nonlinear interaction between two finite-amplitude waves taking place in the parametric acoustic array. For a piston source of area  $S$ , embedded in an infinite, rigid baffle, operating simultaneously at the angular frequencies  $\omega_1$  and  $\omega_2$  (wave numbers  $k_1$  and  $k_2$ ) the wave fields can be treated as plane collimated waves within a distance - the Rayleigh distance or the collimation distance forming the nearfield of the primary wave source - expressed by:

$$R_r = k_2 S / (2\pi) = S / \lambda_0 \quad (15)$$

where  $k_2 = \frac{1}{2}(k_1 + k_2)$ . At distances greater than  $R_r$  the primary wave field can be represented as spherically spreading waves.

The Fresnel distance may analogously be expressed by:

$$R_f = S / (4\lambda_0) \quad (16)$$

Empirically [13], it has been found that a source radius  $R_0 = S / (2\lambda_0)$  provides acceptable agreement with experimental results, thus forming an effective radius of a spherical wave source.

Using the down-shift-ratio  $H_s = k_2 / k_1 = \omega_2 / \omega_1$ , (with  $\omega_0 = \frac{1}{2}(\omega_1 + \omega_2)$ ), the difference-frequency wave collimation distance may be defined through:

$$R_s = R_r / H_s \quad (17)$$

The half-power beamwidth  $\theta_h$  of the difference-frequency wave may under certain circumstances asymptotically approach that of the primary wave at a source distance given by:

$$R_0 = R_r H_s \quad (18)$$

The possibility of shock formation in the primaries necessitates the definition of a dimensionless "saturation number"  $\chi$  [14], being expressed by:

$$\chi = R_r / \ell, \quad (19)$$

where  $\ell$  is the "discontinuity distance".

## 2. LOW-AMPLITUDE WAVE INTERACTIONS IN PARAMETRIC TRANSMITTING ARRAYS

### ABSORPTION AND SPREADING-LOSS LIMITED ARRAYS

Low-amplitude (finite-amplitude) waves are waves whose peak amplitudes are below their respective shock formation threshold by means of which nonlinear absorption can be neglected.

Westervelt's farfield approximation, treated in section 1, for the difference-frequency signal generated by nonlinear interaction of infinitely plane, unsaturated primary waves of finite-amplitude only subject to viscous absorption and the extension of Westervelt's theoretical approach to include the difference-frequency signal generation by the nonlinear interaction between two monochromatic, unsaturated spherical waves emitted by a circular piston projector discussed by Muir [15] and Muir & Willette [16] are examples on low-amplitude wave interaction parametric transmitting arrays.

If the nearfield primary wave absorption loss ( $\alpha_T R_r \gg 1$  Np) to ensure that the primary waves are sufficiently absorbed within  $R_r$  to such an extent that no further nonlinear interactions take place beyond  $R_r$ , the parametric array is termed: absorption limited, and Westervelt's solution can be used for a determination of the difference-frequency signal. If  $\alpha_T R_r$  is very small, the primary wave interactions take place predominantly beyond  $R_r$  and the array is essentially spreading-loss limited, which demands the use of a spherical wave solution for the difference-frequency signal.

While the absorption limited arrays are characterized by a farfield half-power beamwidth of the difference-frequency signal given by expression (14), spreading-loss limited arrays (also including some viscous absorption effects) will show a half-power beamwidth increasing with the source distance  $r$  and asymptotically approaching the half-power beamwidth of the product of the primary beam directivity patterns. The two half-power beamwidths may become equal at the source distance  $R_0$ .

The validity of the asymptotic solution derived for the parametric array (using Rutherford's scattering formula) demands that the field point (point of observer) is far outside the interaction region, but volume integral solutions have been derived for field points in the interaction region. The use of continuous or pulsed primaries will influence the parametric wave generation process. Further, the question whether most difference-frequency signal generation takes place in the near- or in the farfield of the primary wave projector - or is shared between the two fields - can be replied to when the primary wave frequencies, their source level and the size of the projector are known.

The subsequent discussion may therefore appropriately be subdivided into discussion

of procedures and results arising from (a) field point outside or inside the primary wave interaction region, (b) continuous or pulsed primaries and (c) predominant near- or far-field interactions.

175

a. Field point outside the interaction region

(i) Continuous primaries

The absorption limited, predominant nearfield interaction, arrays are represented by Westervelt's [9] and Berkta's [12] approaches discussed in section 1. Another method for predicting the performance of parametric transmitters, published by Mellen & Moffet [18], [21], uses  $\alpha_m R_0$  as the basic parameter for absorption/spreading-loss limited arrays. Their model combines the simple plane and spherical solutions by adding the difference-frequency wave contributions from sources in a well-collimated end-fire array ( $r < R_0$ ) and from sources in a spherical region ( $r > R_0$ ) having a directivity given by the product of the primary directivity functions.

This model has proved to be of considerable use for calculation of the parametric efficiency in cases when the field point is sufficiently far from the source for all points in the interaction region for which diffraction is important to be represented as being at the same range. Their general expression for the parametric sonar source level efficiency (i.e. the ratio of the difference-frequency to the primary source levels) can be written as:

$$\left| \frac{R_{p_s}}{R_{p_0}} \right| = \frac{\chi \left( \frac{k_s}{k_0} \right)^2}{2} \int_0^\infty \frac{dr}{R_r} \left( 1 + \left( \frac{k_s}{k_0} \right)^2 \left( \frac{r}{R_r} \right)^2 \right)^{\frac{1}{2}} \frac{e^{-2\alpha_0 r}}{\left( 1 + \left( \frac{\chi}{2} \right) \sinh^{-1} \left( \frac{r}{R_r} \right)^2 \right)} \quad (20)$$

where it is assumed that the primary waves were of the same initial amplitude  $p_0$ . Neglecting finite-amplitude absorption ( $\chi < 1$ ) and assuming that the parametric array is absorption limited at  $r < R_0$ , (20) reduces asymptotically to the Westervelt case, which may be easily verified by insertion of:

$$\chi = \frac{\beta p_0 k_0 R_0}{\rho_0 c_0^2}$$

and by the use of (15).

The square dependence of  $p_s$  on the down-shift-ratio ( $p_s \propto \omega^2$ ) and on the primary wave amplitude  $p_0$  for interactions in the collimated beam region should be noted by (20).

For  $\chi < 1$  and  $2\alpha_0 R_0 < 1/H$ , i.e. the array is spreading loss limited in the farfield of the primaries where most of the difference-frequency generation takes place, expression (20) reduces to:  $|R_{p_s}/(R_{p_0})| \propto \chi/2 (k_s/k_0) E(2\alpha_0 R_0)$  where  $E()$  is the well-known exponential integral function. The linear dependence on the down-shift-ratio, i.e.  $p_s \propto \omega_s$ , represented by this expression for the farfield interaction should be noted. In the general case, when both near- and farfield interactions contribute to  $p_s$ , the exponent of the down-shift-ratio is between 1 and 2, which also has been experimentally verified [20], [21].

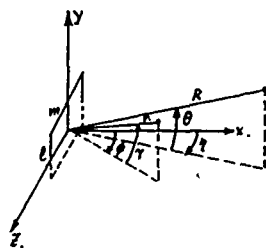


Figure 1. Geometry according to ref. [19].

Numerous authors have contributed to our knowledge about the spreading-loss limited arrays ( $\alpha_m R_0 < 1$  Np) where farfield interaction predominates. Two ways of handling the geometry of the array have been prevailing. The first is to approximate the interacting signals as one-dimensional propagating waves [19] and the second is to perform a three-dimensional integration [16].

Berkta & Leahy [19] considered the interaction taking place in the farfield of a piston projector. Their geometry with the projector surface in the y-z-plane is shown in Figure 1. The far field beam patterns of the primary waves of angular frequencies  $\omega_1$  and  $\omega_2$  can be represented in the form:

$$p_{1,2} = \frac{\bar{p}_{1,2}}{Y} D_{1,2}(Y, \phi) e^{-(\alpha_{1,2} + jk_{1,2})R} \quad (21)$$

where  $D_{1,2}(Y, \phi)$  are the normalized directivity functions of the primaries.  $\bar{p}_{1,2}$  denote the source amplitudes of the primaries.

The difference-frequency pressure at the field point  $(R, \theta, \eta)$  in Figure 1 can now be written as:

$$p_s(R, \theta, \eta) \approx \frac{\omega_s^2 \bar{p}_1 \bar{p}_2 \beta}{4\pi \rho_0 c_0^4 R} e^{-(\alpha_s + jk_s)R} \int_{-\pi/2}^{\pi/2} \int_{-\pi/2}^{\pi/2} \frac{D_1(Y, \phi) D_2(Y, \phi)}{(\alpha_s + jk_s(1-v))} \cos \gamma \, d\gamma \, d\phi \quad (22)$$

where  $v \approx 1 - \frac{1}{2}(\gamma - \theta)^2 - \frac{1}{2}(\phi - \eta)^2$ .

The double integral in (22) is the two-dimensional convolution of the product of the primary directivity patterns (weighted by  $\cos \gamma$ ) with directivity function

17-6

$D(\theta, \eta) = (1 + j(k/a_s(1 - \cos\theta \cos\eta)))^{-1}$ , which is the Westervelt directivity function (9) transferred to the coordinate system given in Figure 1. For extremely narrow primary beams and for  $D_1() = D_2()$ , (22) reduces to the Westervelt case, and when  $\theta_h$  given by (14) is much smaller than the beamwidth associated with the product  $D_1()D_2()$ , the difference-frequency beam patterns become the product of the primary-frequency directivity functions.

Evaluation of (22) for both a rectangular and a circular projector embedded in an infinite, rigid baffle has been given in [19]. For a rectangular projector with the dimensionless side lengths  $L$  and  $M$  (normalized by use of  $\lambda_0$ ) parallel with the  $y$ - and  $z$ -axis, respectively, (22) may be rewritten as:

$$P_S(R, \theta, \eta) \approx P_W(R, 0) V(\psi_y, \psi_z, \theta', \eta') \quad (23)$$

where

$$P_W(R, 0) = - \frac{\omega^2 (W_1 W_2)^{1/2} \beta}{2\pi c_0^3 R \alpha_T} e^{-(\alpha_s + jk_s)R}$$

$W_1$  and  $W_2$  are the acoustic power transmitted at the primary frequencies and

$$V() \approx LM \theta_h^2 \int_{-\pi/2}^{\pi/2} \int_{-\pi/2}^{\pi/2} \frac{\sin^2(\sqrt{2}\gamma'/\psi_y)}{(\sqrt{2}\gamma'/\psi_y)^2} \frac{\sin^2(\sqrt{2}\phi'/\psi_z)}{(\sqrt{2}\phi'/\psi_z)^2} N d\gamma' d\phi'$$

where  $N = [1 + j(\theta' - \gamma')^2 + (\eta' - \phi')^2]^{-1}$ .

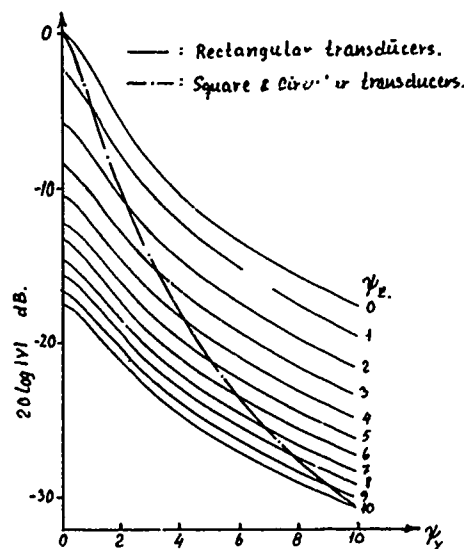


Figure 2. Pressure reduction factor,  $|V|$ , for rectangular, squared and circular transducers.  $\theta' = \eta' = 0$ .

If  $\chi$  is put equal to 1 ( $\lambda = R_0$ ), high, but not too high for the continued omission of strong finite-amplitude distortion and absorption effects, initial primary amplitudes occur. The use of  $B/A = 5$ ,  $\rho = 10^3$  kg/m<sup>3</sup> and  $c = 1500$  m/s will then lead to the maximum obtainable difference-frequency source level given by:

$$SL_m \approx 20 \log(f_s) - 40 \log(f_0) + 20 \log(|V|/\alpha_T R_0) + 274 \text{ dB re } 1 \mu\text{Pa} \cdot \text{m} \quad (25)$$

#### (ii) Pulsed primaries

Besides the nonlinear interactions between continuous (monochromatic) primary waves, also pulsed carriers have been studied.

Berkday [12] considered primary waves which at the source were of the form:

$$p_i(t) = p_0 F(t) \cos(\omega t) \quad (26)$$

where  $F(t)$  is an envelope function assumed to vary slowly compared with the  $\cos(\omega t)$ -term, thus covering a relatively narrow band (no components higher than  $\omega/3$ ) in order to avoid overlap in the frequency spectra of the scattered and the primary waves. The time-domain solution for the scattered wave may for plane waves, along the axis of the array be expressed by:

$$p_s(R, t) \approx \frac{p_0^2 \beta S}{16\pi \rho_0 c_0^4 R \alpha_T} \frac{\partial^2}{\partial t^2} F^2(t') \quad (27)$$

where viscous absorption of the primary has been introduced.  $t' = t - R/c_0$ , is the retarded

All angles are normalized with respect to  $\theta_h$  and the half-power beamwidths  $2\gamma_1$  and  $2\phi_1$  of the primary beams in the two planes of symmetry are given by:  $\pi L \gamma_1 = \pi M \phi_1 \approx \sqrt{2}$ .  $\gamma' = \gamma/\theta_h$ ,  $\phi' = \phi/\theta_h$ ,  $\psi_y = \gamma_1/\theta_h$  and  $\psi_z = \phi_1/\theta_h$ . A calculation of  $h_V()$  along the acoustic axis ( $\theta' = \eta' = 0$ ) has been performed [19] and is given in Figure 2. Using  $B/A = 5$  for water, the RMS source level at the difference-frequency can be calculated by (23) through the expression:

$$SL_m \approx 137 + 20 \log(f_s) - 40 \log(\theta_h^0) + 10 \log(W_1) + 10 \log(W_2) + 20 \log|V|, \text{ dB re } 1 \mu\text{Pa} \cdot \text{m} \quad (24)$$

(24) can be used for an evaluation of the far-field response of a parametric transmitter.  $f_s$  is the difference-frequency in kHz,  $\theta_h$  is in degrees,  $W_1$  and  $W_2$  are in watts and  $20 \log|V|$  is obtained from Figure 2, where a circular projector of radius  $a$  gives:  $\psi_d = 92.5/(k_0 a \theta_h^0)$  and a rectangular projector of sides  $l$  and  $m$  gives:  $\psi_y = 163/(k_0 l \theta_h^0)$  and  $\psi_z = 163/(k_0 m \theta_h^0)$ .

A comparison between the farfield difference-frequency amplitudes calculated by means of (20) and by means of (23) can be performed for both circular and rectangular projectors through the use of:  $\alpha_T R_0 = 0.650/\psi_d^2$  (for circular projectors) and  $\alpha_T R_0 = 0.635/(\psi_y \psi_z)$  (for rectangular projectors).

time.

Experiments have shown that pulsed carriers yield a scattered component being about 2 dB greater than in a two-frequency parametric array [21], [22], [23]. The use of pulsed carriers demands that the projector bandwidth must be much wider than the scattered wave frequency, in order to avoid interpulse distortion. (27) stresses the wide band character of the parametric array at the scattered wave frequency.

#### b. Field point inside the interaction region

The full consequence of the asymptotic theory for parametric arrays cannot be met with the field point in the interaction region, which is frequently the case for laboratory tank experiments. Two different theoretical approaches have been used in order to calculate the difference-frequency signal level at points in the interaction region. The first approach is based on numerical integration of a volume integral [16] and the second is based on the introduction of a correction factor to the asymptotic theory [24].

Muir & Willette [16] investigated the generation in fresh-water of the sum- and difference-frequency signal of two high-frequency primaries (418 and 482 kHz) transmitted by a 3-in-diameter, circular piston projector. In their theoretical approach they only considered contributions from farfield interactions and they derived the following volume integral expression for the (sum- or) difference-frequency pressure amplitude, valid for  $R \gg r$ , but approximately valid for the field point in the interaction region:

$$p_s(R, \theta) = \frac{2p_1 p_2 \omega_s^2 \beta R^2}{\pi \rho_0 c_0^4 k_1 k_2 a^2} \int_{R_r}^R \int_0^{\phi_e + \theta} \int_0^\pi \frac{J_1(k_1 a \sin \sigma) J_1(k_2 a \sin \sigma)}{\sin^2 \sigma} \times \\ \times \frac{e}{r'} - ((\alpha_1 + \alpha_2) - jk_s) r - (jk_s - \alpha_s) r' \sin \phi d\psi d\phi dr' \quad (28)$$

with:  $\sin \sigma = [(\sin(\theta - \phi) + \sin \phi \cos \theta (1 - \cos \psi))^2 + \sin^2 \phi \sin^2 \psi]^{\frac{1}{2}}$  and  $r' = (R^2 + r^2 - 2Rr \cos \phi)^{\frac{1}{2}}$ .  $\phi_e$  is an effective array angle and  $R' = 3a^2/4\lambda_0$  with  $a$  being the projector radius. The geometry of expression (28) is shown in Figure 3.

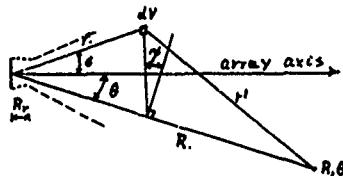


Figure 3. Geometry used in [16].

### 3. HIGH-AMPLITUDE WAVE INTERACTIONS IN PARAMETRIC TRANSMITTING ARRAYS

#### SATURATION EFFECTS

Finite-amplitude effects, i.e. wave distortion and finite-amplitude absorption, in parametric transmitting arrays have been dealt with by Muir [15], Mellen & Moffett [17], [18], Merklinger [25], Bartram [26] and Fenlon [27], [28]. In all cases, quasi one-dimensional models were utilized among other things due to the fact that the treatment hitherto of finite-amplitude effects in parametric arrays is generally based on one-dimensional models and frequently on theories originally formulated for a monochromatic wave source. General effects of finite-amplitude distortion and absorption in a parametric array is an effective shortening of the array length leading to a broadening of the difference-frequency beam and a reduction in the difference-frequency source level relative to the source level values calculated through the use of expressions given in section 2. If a parametric source is saturation limited, almost certainly the saturation will occur within the nearfield, rather than the farfield, of the primary beam. For  $\chi > 1$  in (20) the parametric array will be saturation limited in the nearfield and (20) will reduce to:

$$\left| \frac{R p_s}{R_p p_0} \right| = \frac{\pi}{2} \left( \frac{k_s}{k_0} \right)^2 \quad (29)$$

which shows a linear relation between  $p_s$  and  $p_0$  at an observation point outside  $s$

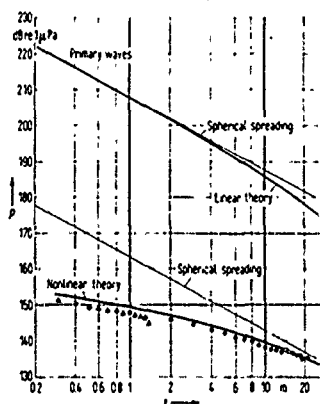


Figure 4. Sound pressure levels measured and calculated in [21]. The curve marked "Nonlinear Theory" arises from the numerical integration of a modified version of (28).

the interaction region.

(17-8)

The original Mellen & Moffett equation for the parametric source level efficiency involving a finite-amplitude effect taper function:

$$T_f = (1 + (\sigma/2)^2)^{-1/2}$$

where  $\sigma = \chi \sin^{-1}(r/R_p)$ , together with the small amplitude taper  $T_s = \exp(-\alpha r)$ , can be numerically integrated for particular values of the down-shift-ratio  $(k_0/k_s)$  and of  $\alpha_0 R_p$ .

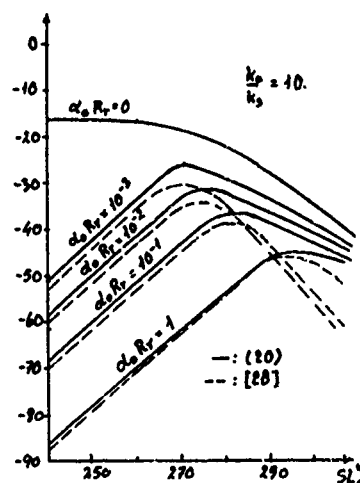


Figure 5. Abscissa: Scaled mean primary wave source level  $SL_0^*$  (dB re 1  $\mu$ Pam kHz, RMS).

Ordinate: Parametric conversion efficiency.  $20 \log |R_p / (R_p p_0)|$  (dB).

in the sidelobe levels relative to the level of the major lobe. These phenomena are due to the finite-amplitude absorption dependence on the primary wave amplitudes, which in the farfield of a directive source are greatest on the acoustic axis.

#### 4. PARAMETRIC RECEIVING ARRAYS

The possibility of developing a parametric receiving array was first mentioned by Westervelt [9] and in spite of the fact that most efforts in developing parametric arrays have been laid down into the transmitting arrays in order to obtain highly directional, low frequency sources using relatively small transducers, the parametric receiving array has recently received considerable interest. In a parametric receiver, the nonlinear interaction process may take place between a low-frequency, plane signal wave of low intensity and a high-frequency pump wave of higher intensity being generated locally. The sum- or difference-frequency signal are then received by a transducer on the acoustic axis of the pump wave.

A discussion of parametric receiving arrays may appropriately be divided into (a) low-amplitude and (b) high-amplitude parametric receiving arrays. The difference between the two approaches lay in the inclusion or not of finite-amplitude effects in the pump wave. Farfield reception was considered by Barnard et al. [29] who studied a first-order sound field consisting of a "low-amplitude", spherical, harmonic pump wave of frequency  $f_1$  and a plane, harmonic signal wave of frequency  $f_2$ , ( $f_1 > f_2$ ). No nearfield effects of the pump were assumed to be involved and only the pump wave was assumed undergoing absorption (viscous).

In polar coordinates  $((r, \psi, \phi))$ , where  $\phi$  is the polar angle and  $\psi$  is the azimuthal angle) their first-order sound field can be written as:

$$P_f = p \left( \frac{r_0}{r} \right) \left( \frac{2J_1(k_1 a \sin \phi)}{k_1 a \sin \phi} \right) e^{-\alpha_1 r} \cos(\omega_1 t - k_1 r) + p_2 \cos(\omega_2 t - k_2 z) \quad (32)$$

where  $p_1$  is the peak sound pressure level of the pump wave at a distance  $r_0$  and  $p_2$  is the sound pressure level of the signal wave at input to the parametric receiving array.  $a$  is the radius of the piston pump and  $k_2 z$  is defined as the plane-wave phase at  $r$ , where:  $z = r(\sin \nu \cos \phi - \sin \phi \cos \psi)$ . The angle  $\nu$  in the horizontal plane is the acute angle between the acoustic axis of the array and the plane wave front. Insertion of (32) into

Curves for the difference-frequency source level efficiency as a function of the scaled-mean primary source level  $SL_0^*$  for the down-shift-ratio  $k_0/k_s = 10$  with  $\alpha_0 R_p$  as a parameter are given in Figure 5. The primary source level  $SL_0$  is defined as the mean level of the two components:  $SL_0 = \frac{1}{2}(SL_1 + SL_2)$ , leading to the 1 kHz scaled value  $SL_0^*$  through:

$$SL_0^* = SL_0 + 20 \log(f_0) \text{ dB re 1 } \mu\text{Pam} \quad (30)$$

where  $f_0 = \frac{1}{2}(f_1 + f_2)$  (kHz).

Using  $SL_0^*$  from (20) in Figure 5 leads for an appropriate  $\alpha_0 R_p$ -value (and for  $k_0/k_s = 10$ ) to the parametric source level efficiency (conversion efficiency), which added to  $SL_0$  gives the difference-frequency source level  $SL_-$  by:

$$SL_- = SL_0 + 20 \log |R_p / (R_p p_0)| \text{ dB re 1 } \mu\text{Pam} \quad (31)$$

The asymptotic cases (20) and (29) are reflected in the shape of the curves in Figure 5. The absorption effect terminates the growth of the difference-frequency wave amplitude, leading to the square law dependence of  $p_u$  on  $p$  given by (20) for input levels below a certain value.

No higher order spectral interactions are included in the derivation of (20), but these interactions will in general give rise to enhanced finite-amplitude effects, thus causing a more rapid decrease in the parametric conversion efficiency. This rapid decrease can be seen by the dotted line curve in Figure 5.

The shortening of the parametric array length due to finite-amplitude effects at high primary source levels leads to a blundering of the difference-frequency beam patterns around the array axis with an increase



(8) and introduction of the viscous absorption in an "ad hoc" way, lead to the following volume integral expression for the pressure amplitude of the sum- or difference-frequency signal:

$$P_s(R_o, \nu) = \frac{8\omega_s^2 p_1 p_2 r_o}{2\pi \rho_o c_o^2 a k_1} \int_0^R \int_0^{\phi_{eff}} \int_0^\pi J_1(k_1 a \sin \phi) e^{j(k_1 r + k_2 z + j\alpha_1 r)} \cdot \frac{e}{r'} j(k_s + j\alpha_s) r' r d\phi d\theta dr \quad (33)$$

where  $\omega_s = \omega_1 \pm \omega_2$ , and  $r' = (r^2 + R^2 - 2rR \cos \phi)^{1/2}$ , while  $\phi_{eff}$  is the angle between the acoustic axis and the first null of the pump farfield radiation pattern.  $R_o$  is the distance along the acoustic axis between the pump and the receiving transducer. (33) has been solved numerically and the results have been tested against experiments for the sum-frequency wave [29] showing a good agreement, both concerning beam patterns and range ( $R_o$ ) for various signal frequencies. Later works along the line introduced by (33) have been published in [30] and nearfield reception has been treated theoretically by Rogers et al. [31].

The half-power beamwidth of the parametric receiver is completely determined by:

$$\theta_h = 1.9 (\lambda_2 / R_o)^{1/2} \quad (34)$$

Only a small amount of work has been done in analyzing finite-amplitude effects in parametric receiving arrays. In general some serious problems still have to be overcome before a practical system can be realized. For instance, motion of the pump and the transducer during reception, water noise at the signal frequency or at the sum- or difference-frequencies, electronic noise in the equipment, etc., can create serious problems for full-scale reception. But the promising results hitherto obtained point to solutions to the problems to be obtained in a not too distant future.

#### 5. IMPROVEMENT OF THE CONVERSION EFFICIENCY OF THE PARAMETRIC ACOUSTIC ARRAY

The low conversion efficiency of the parametric acoustic arrays previously mentioned is its capital weakness. The second-order effects on which it is based limit the energy transfer from the primary beams to the difference- and sum-frequency beams.

It was pointed out by Merklinger [22] that if the necessary bandwidth of the transmitter was available, a pulsed carrier type of transmission would give an improvement in conversion efficiency of between 2 and 6 dB depending on the system constraints. Experimental evidence for this prediction has later been created [21]. 100% amplitude modulation of a primary wave was shown in [21] and in [23] to lead to a 2.5 dB increase in the difference-frequency sound pressure level compared to a two-component primary of the same total power.

From the parameters involved in the expressions (9), (11), (20) and (22) for low-amplitude wave interactions in parametric transmitting arrays it may be concluded, that an increase in the virtual source strength and thus in  $p_o$  may be obtained primarily by the following procedures: a. An increase in the peak amplitudes of the carrier waves, and b. an increase in  $\beta$  and a decrease in  $\rho_o$  and in particular in  $c_o$  in the fluid. The influence of these parameters on the conversion efficiency of a parametric transmitting array has been studied in theory and through experiments in [21]. By putting the nearfield of the projector under pressure, cavitation effects could be avoided and the nearfield liquid was replaced by liquids showing more appropriate  $\beta$ ,  $\rho_o$  and  $c_o$  values (methyl and ethyl alcohols), which led to an about 15 dB increase in the difference-frequency sound pressure level. Further, it was shown in [21] that some essential dB's at the difference-frequency sound pressure level could be gained through the use of an acoustic lens effect and through the use of a slow-waveguide antenna effect in the nearfield liquid cylinder, a subject which also recently has been studied by Ryder et al. [32] for a silicone rubber cylinder in contact with the projector. The increase in  $\beta$  by using air-bubbles in the interaction region of the primaries has been attempted by Lockwood et al. [33], but without considerably success.

The disappearance of  $\beta$  in the expression for  $p_o$  by high-amplitude wave interactions (29) points against an increase in the conversion efficiency for nearfield saturation limited arrays may be obtained through a decrease in the velocity of sound of the liquid in contact with the projector, a decrease in the primary mean frequency  $\omega_o$  or an increase in the projector size (normally attempted to be kept small), which can be seen from the transformation of (29) into:

$$|P_s| \propto \omega_s^2 S p_o (4R c_o \omega_o)^{-1} \quad (35)$$

The last expression in (35) was also found by Bartram [26] through a consideration of the absorption in repeated shocks.

The increase in the conversion efficiency of the parametric acoustic arrays belongs to a research field into which more theoretical and experimental work must be invested before an optimum exploitation of the parametric array can be achieved.

#### CONCLUSION

The nonlinear interaction between finite-amplitude sound waves has due to intensive studies went through a fast development, leading into a practical exploitation, since it was first suggested only about 20 years ago. Some problems, certain nearfield effects [34], [35], [36], certain saturation effects, improvement of the conversion efficiency etc.,

still have to find their solutions, but the promising results obtained in theoretical studies and in laboratory and full-scale tests have long ago established the significance of this "corner" of acoustic wave propagation.

## REFERENCES

1. Helmholtz, H., Die Lehre von den Tonempfindungen als physiologische Grundlage für die Theorie der Musik. Brunswick 1862.
2. Lamb, H., The dynamical theory of sound. Dover, New York, 1960.
3. Lighthill, M.J., Proc. Roy. Soc. (London), Vol. 211A (1952), p. 564.
4. Lighthill, M.J., Proc. Roy. Soc. (London), Vol. 222A (1954), p. 1.
5. Ingard, K.U. and Fridmore-Brown, D.C., J. Acoust. Soc. Amer. Vol. 28 (1956), p. 367.
6. Westervelt, P.J., J. Acoust. Soc. Amer. Vol. 29 (1957), p. 199.
7. Westervelt, P.J., J. Acoust. Soc. Amer. Vol. 29 (1957), p. 934.
8. Westervelt, P.J., J. Acoust. Soc. Amer. Vol. 32 (1960), p. 8.
9. Westervelt, P.J., J. Acoust. Soc. Amer. Vol. 35 (1963), p. 535.
10. Bjørnø, L., Ultrasonics International 1975, Conference Proceedings, IPC Science and Technology Press Ltd., London 1975.
11. Naze, J. and Tjøtta, S., J. Acoust. Soc. Amer. Vol. 37 (1965), p. 174.
12. Berkta, H.O., J. Sound and Vib. Vol. 2 (1965), p. 435.
13. Skooter, J.A., Muir, T.G. and Blackstock, D.T., J. Acoust. Soc. Amer. Vol. 55 (1974), p. 54.
14. Mellen, R.H. and Moffett, M.B., Naval Underwater Systems Center, Technical Memo, 1971. PA4-229-71.
15. Muir, T.G., Ph.D. thesis, University of Texas at Austin, ARL-TR-71-1.
16. Muir, T.G. and Willette, J.G., J. Acoust. Soc. Amer. Vol. 52 (1972), p. 1481.
17. Mellen, R.H. and Moffett, M.B., NUSC Technical Memo. PA4-229-71, 1971.
18. Moffett, M.B., NUSC Technical Memo, PA4-234-71, 1971.
19. Berkta, H.O. and Leahy, D.J., J. Acoust. Soc. Amer. Vol. 55 (1974), p. 539.
20. Muir, T.G. and Blue, J.E., J. Acoust. Soc. Amer. Vol. 46 (1969), p. 227.
21. Bjørnø, L., Christoffersen, B. and Schreiber, M.P., Acustica, Vol. 35 (1976), p. 99.
22. Merklinger, H.M., Proceedings of Symposium on Nonlinear Acoustics, University of Birmingham, April 1971.
23. Eller, I.A., J. Acoust. Soc. Amer. Vol. 56 (1974), p. 1935.
24. Lockwood, J.C. and Frandsdal, L.A., AMETEK/STRAZA R&D Rept. 11-730004-00000E-11, 1973.
25. Merklinger, H.M., Ph.D. thesis, University of Birmingham, 1971.
26. Bartram, J.F., J. Acoust. Soc. Amer. Vol. 52 (1972), p. 1042.
27. Fenlon, F.H., in Finite-Amplitude Wave Effects in Fluids, L. Bjørnø (Ed.), IPC Science & Technology Press Ltd., London, 1974.
28. Fenlon, F.H., Parametric scaling laws, Westinghouse Res. Labs., No. 0014-14-c-0214, 1974.
29. Barnard, G.R., Willette, J.G., Truchard, J.J. and Shooter, J.A., J. Acoust. Soc. Amer. Vol. 56 (1972), p. 1437.
30. Truchard, J.J., ibid. Ref. 27.
31. Rogers, P.H., van Buren, A.L., Williams, Jr., A.O. and Barber, J.M., ibid. Ref. 27.
32. Ryder, J.D., Rogers, P.H. and Jarzynski, J., J. Acoust. Soc. Amer. Vol. 59 (1976), p. 1977.
33. Lockwood, J.C. and Smith, D.P., AMETEK/STRAZA Techn. Rept., 11-1354E-74-1, 1974.
34. Rolfeigh, R.L., J. Acoust. Soc. Amer. Vol. 58 (1975), p. 964.
35. Mellen, R.H., J. Acoust. Soc. Amer. Vol. 61 (1977), p. 883.
36. Mellen, R.H. and Moffett, M.B., J. Acoust. Soc. Amer. Vol. 63 (1978), p. 1622.

# AEROACOUSTIC MEASURING TECHNIQUES IN OR OUTSIDE TURBULENT FLOWS

by

Helmut V. Fuchs \*

Deutsche Forschungs- und Versuchsanstalt für Luft- und Raumfahrt E.V.  
Institut für Experimentelle Strömungsmechanik  
Abteilung Turbulenzforschung  
Müller-Breslau-Straße 8, 1000 Berlin 12

18-1

## SUMMARY

These lecture notes deal with a fundamental phenomenon in aero-acoustics: the motion of aerodynamic or acoustic sources relative to the fluid and/or to the measuring instrument. Some practically important effects on the pressure and velocity fields in and outside the active source region are deduced from linearized wave equations with simple source functions. The possibility of and limitations on fluctuating aerodynamic and acoustic pressure measuring techniques employing special microphone probes are discussed. Applications of current interest are, for instance, (i) the pressure pulsations induced in the near fields of jet, wake, and duct flows and (ii) the effects of source convection and forward speed on the far field radiation characteristics of jets or other aeroacoustic sources in motion.

## LIST OF CONTENTS

	<u>Page</u>
1. Introduction	2
2. Near and far fields of sources in uniform motion	2
2.1 Galilean and Lorentz transformations of linear wave equations	
2.2 The field of a source moving relative to the observer and the flow	
2.3 The various practical effects of relative motion	
2.4 Three special cases of relative motion	
2.4.1 Moving source problem	
2.4.2 Moving observer problem	
2.4.3 Co-moving source and observer problem	
3. Jet noise radiated under static and under flight conditions	11
3.1 Jet noise source convection effect	
3.2 Jet noise forward speed effect	
4. Aerodynamic pressure measurements in turbulent flow	14
4.1 The near field induced by convected flow inhomogeneities	
4.2 Possible sources of error in aerodynamic pressure measurements	
4.3 Survey of pressure coefficients measured in various shear flows	
4.3.1 Circular model jets	
4.3.2 Co-annular model jets	
4.3.3 Two-stream plane shear layer	
4.3.4 Axisymmetric wake behind circular disk	
4.3.5 Two-dimensional wake behind circular cylinders	
4.3.6 Fully developed turbulent duct flows	
4.3.7 Grid generated turbulence	
4.4 Limitations on measuring techniques employing inserted microphone probes	
4.4.1 Acoustic contamination of the flow	
4.4.2 Resolution error due to finite transducer dimensions	
4.4.3 Flow-affected sensitivity of the microphone	
4.4.4 Acceleration response due to probe vibrations	
4.4.5 Probe-flow interaction effects	
4.4.6 Fluctuating cross flow error	
4.4.7 Response to axial velocity fluctuations	
5. Aerodynamic pressure fields in wakes and in jets	24
6. Sound pressure measurements in turbulent flow	25
References	25-27
List of Symbols	28

\*Present address:  
Fraunhofer-Institut für Bauphysik, 7000 Stuttgart 70, Germany

## 1. INTRODUCTION.

Over more than two decades of extensive research in the field of flow noise an immense variety of experimental measuring techniques have evolved. These may be grouped into three main categories,

- (1) Techniques applicable in the aerodynamic *near field* inside the active source region, e.g.,
  - hot-wire anemometers
  - probe microphones
  - optical Laser techniques
- (2) Techniques applicable in the acoustic *far field* at some distance from the active source region, e.g.,
  - single microphone
  - pressure gradient
  - intensity meter
- (3) Techniques trying to relate certain *radiation* features to specific *source* characteristics and vice versa, e.g.,
  - causality correlations
  - directional microphones
  - source location and identification techniques

It is impossible to discuss all these highly different techniques together. Rather is it intended to concentrate here on a peculiarity of aerodynamic noise in general: the majority of aeroacoustic sources are not fixed in space but move relative to the observer and/or the fluid in which they are embedded. One may think, e.g., of

- boundary layer noise radiated from a high-speed train (*pass-by* measurement)
- fan noise radiated into a flow channel (*in-duct* measurement)
- air frame noise radiated from an aircraft in flight (*fly-over* measurement)
- jet noise generated by convected flow inhomogeneities.

This typical relative motion of sources gives rise to a number of practically important effects on the pressure and velocity fields in and outside the actual source region which are worth to be considered in the specific context of this Short Course on wave propagation. Proceeding from this more general scope of this lecture, we shall give a few examples of aeroacoustic measuring techniques applicable in or outside turbulent flows.

## 2. NEAR AND FAR FIELDS OF SOURCES IN UNIFORM MOTION

Before dealing with complicated aerodynamic sources in arbitrary relative motion, it may be helpful to recall here what basic acoustic equations can tell us about the motion of simple point sources. The propagation of small disturbances through an otherwise unperturbed (laminar) flow is governed by wave equations. For a general non-uniform mean flow and a unidirectional, transversely sheared flow these were derived in Ref. [1]. In the simplest of all flows with a constant, uniform flow ( $\bar{c}_j$ ) in just one direction these reduce to what is usually termed a "convected wave equation" of the form

$$\frac{\partial^2 \phi}{\partial t^2} - a_0^2 \frac{\partial^2 \phi}{\partial x_i^2} = \frac{\partial^2 \phi}{\partial t^2} + 2 \bar{c}_j \frac{\partial^2 \phi}{\partial x_j \partial t} + (\bar{c}_i \bar{c}_j - a_0^2 \delta_{ij}) \frac{\partial^2 \phi}{\partial x_i \partial x_j} = 0 \quad (2.1)$$

It differs from the ordinary wave equation (for  $\bar{c}_i = 0$ ) in that the partial time derivatives  $\partial/\partial t$  have been replaced by the substantive derivatives

$$\frac{D}{Dt} = \frac{\partial}{\partial t} + \bar{c}_j \frac{\partial}{\partial x_j}.$$

## 2.1 Galilean and Lorentz transformations of linear wave equations

In Ref. [2] it was shown that a general Galilean transformation of coordinates,

$$x_i = \bar{x}_i + a_{ij} x_j^0 + \bar{c}_i t^0; \quad t = t^0, \quad (2.2)$$

performing a translation ( $\bar{x}_i$ ), rotation ( $a_{ij}$ ) and dilatation ( $\bar{c}_i t$ ) of the  $x_i$ -system does not change the character of the differential equation (2.1). It transforms into

$$\frac{\partial^2 \phi}{\partial t^2} + 2 \bar{c}_j^0 \frac{\partial^2 \phi}{\partial x_j^0 \partial t^0} + (\bar{c}_i^0 \bar{c}_j^0 - a_0^2 \delta_{ij}) \frac{\partial^2 \phi}{\partial x_i^0 \partial x_j^0} = 0 \quad (2.3)$$

with

$$\bar{c}_j^0 = a_{jj} (\bar{c}_i - \bar{c}_i^0). \quad (2.4)$$

We may now just as well specify the arbitrary velocity  $\bar{c}_1$  so that in a system (a) moving with the mean flow:

$$\bar{c}_1^a = 0; \quad \bar{c}_1 = \bar{c}_1; \quad x_1 = \bar{x}_1 + a_{1j}x_j^a + \bar{c}_1 t^a; \quad t = t^a \quad (2.5) \quad 18.3$$

The origin  $x_1^a = 0$  of these new flow coordinates transforms like

$$x_1 = \bar{x}_1 + \bar{c}_1 t \quad (2.6)$$

in the observer coordinates  $x_1$  (compare Fig. 1). Eq. (2.3) then assumes the form of an ordinary wave equation,

$$\frac{\partial^2 \phi}{\partial t^2} - a_0^2 \frac{\partial^2 \phi}{\partial x_1^2} = 0 \quad (2.7)$$

It was also shown in Ref. [2] that Eq. (2.7) is invariant under a Lorentz transformation of coordinates,

$$x_1^a = \frac{x_1^* - \bar{c} t^*}{\sqrt{1 - (\bar{c}/a_0)^2}}; \quad t^a = \frac{t^* - \bar{c} x_1^*/a_0^2}{\sqrt{1 - (\bar{c}/a_0)^2}}; \quad x_2^a = x_2^*; \quad x_3^a = x_3^* \quad (2.8)$$

$$\frac{\partial^2 \phi}{\partial t^{*2}} - a_0^2 \frac{\partial^2 \phi}{\partial x_1^{*2}} = 0 \quad (2.9)$$

To illustrate the usefulness of the above transformations, we will consider the sound field of a single point source which is convected parallel to a uniform mean flow ( $\bar{c} = \text{const}$ ) at a constant speed  $\bar{u} \neq \bar{c}$  (see Fig. 2).

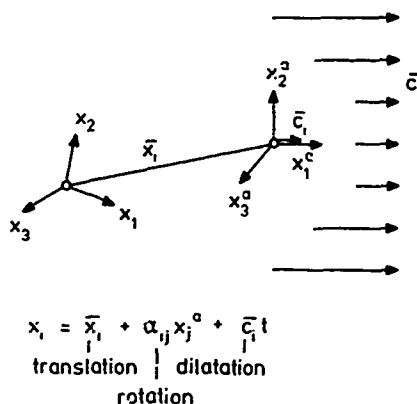


Fig. 1: Sketch illustrating general Galilean transformation of coordinates.

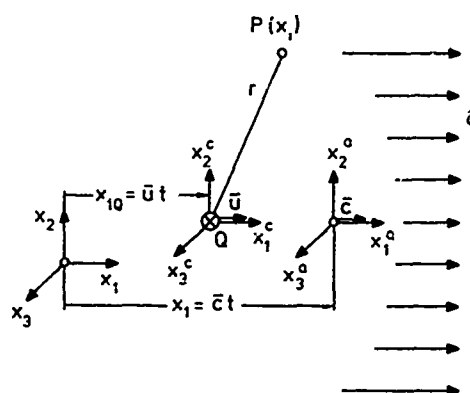


Fig. 2: Point source Q moving relative to observer P and uniform flow  $\bar{c}$ .

## 2.2 The field of a source moving relative to the observer and the flow

When  $\bar{c}_1$  is in the  $x_1$ -direction, with flow Mach number  $M = \bar{c}/a_0$ , the Galilean transformation (2.5) relating the observer and flow coordinates may be simplified to yield

$$x_1 = x_1^a + a_0 M t^a; \quad x_2 = \bar{x}_2 + x_2^a; \quad x_3 = \bar{x}_3 + x_3^a; \quad t = t^a \quad (2.10)$$

If the arbitrary constant  $\bar{c}$  is specified as

$$\bar{c} = \bar{c} - \bar{u} = a_0 M_c \quad (2.11)$$

the origin of the system (b) of Lorentz coordinates,

$$x_1 - a_0 M t = x_1^a = \frac{x_1^b - a_0 M_c t^b}{\sqrt{1 - M_c^2}}; \quad x_2 - \bar{x}_2 = x_2^a = x_2^b; \quad x_3 - \bar{x}_3 = x_3^a = x_3^b \quad (2.12)$$

$$t = t^a = \frac{t^b - M_c x_1^b/a_0}{\sqrt{1 - M_c^2}},$$

moves at the speed  $\bar{u}$  in the observer's system,

$$x_1 = x_1^a + a_0 M t = a_0 M_c t - a_0 M_c t = \bar{u} t \quad (2.13)$$

just as we have required for the source point in Fig. 2 with

$$x_{1Q}(t=0) = (0, \bar{x}_2, \bar{x}_3) \quad (2.14)$$

18-4 The system (b) is thus found to be unique in the sense that in it the source Q is fixed in space and the ordinary wave equation,

$$\frac{\partial^2 \phi}{\partial t^2} - a_0^2 \frac{\partial^2 \phi}{\partial x_1^2} = 0 \quad (2.15)$$

is valid.

By contrast, in another Galilean system (c) moving with the source,

$$x_1 = x_1^c + \bar{u}t^c; \quad x_2 = \bar{x}_2 + x_2^c; \quad x_3 = \bar{x}_3 + x_3^c; \quad t = t^c \quad (2.16)$$

the convected type of a wave equation would be valid,

$$(1-M_c^2) \frac{\partial^2 \phi}{\partial x_1^{c2}} + \frac{\partial^2 \phi}{\partial x_2^{c2}} + \frac{\partial^2 \phi}{\partial x_3^{c2}} - 2 \frac{M_c}{a_0} \frac{\partial^2 \phi}{\partial x_1^c \partial t^c} - \frac{1}{a_0^2} \frac{\partial^2 \phi}{\partial t^{c2}} = 0. \quad (2.17)$$

In this system (c) of source coordinates the potential field  $\phi$  generated by the source would not easily be found. With the aid of system (b), however, this problem is solved straightforwardly.

Harmonic solutions of Eq. (2.15) read

$$\phi = \frac{\phi^b}{r^b} \exp i\omega^b(t^b - r^b/a_0) \quad (2.18)$$

with

$$r^b = |x_1^b - x_{1Q}^b| = \sqrt{x_1^{b2} + x_2^{b2} + x_3^{b2}}.$$

The physical meaning of the arbitrary constants  $\phi^b$  and  $\omega^b$  can best be uncovered after re-transformation of solution (2.18) into the source system  $(x_1^a, t)$ , flow system  $(x_1^c, t)$  or observer system  $(x_1^b, t)$ , whose physical character is more obvious than that of the Lorentz system  $(x_1^b, t^b)$ , by means of

$$\begin{aligned} x_1^b &= \frac{x_1^a + a_0 M_c t^a}{\sqrt{1-M_c^2}} = \frac{x_1 - \bar{u}t}{\sqrt{1-M_c^2}} = \frac{x_1^c}{\sqrt{1-M_c^2}} \\ x_2^b &= x_2^a = x_2 - \bar{x}_2 = x_2^c \\ x_3^b &= x_3^a = x_3 - \bar{x}_3 = x_3^c \\ t^b &= \frac{t^a + M_c x_1^a/a_0}{\sqrt{1-M_c^2}} = \frac{t(1-M_c^2) + M_c x_1/a_0}{\sqrt{1-M_c^2}} = \frac{t^c(1-M_c^2) + M_c x_1^c/a_0}{\sqrt{1-M_c^2}} \end{aligned} \quad (2.19)$$

The distance between the source and the observer transforms like

$$\begin{aligned} r^b &= \frac{1}{\sqrt{1-M_c^2}} \sqrt{(x_1^a + a_0 M_c t^a)^2 + (1-M_c^2)(x_2^{a2} + x_3^{a2})} \\ &= \frac{1}{\sqrt{1-M_c^2}} \sqrt{(x_1 - \bar{u}t)^2 + (1-M_c^2)[(x_2 - \bar{x}_2)^2 + (x_3 - \bar{x}_3)^2]} \\ &= \frac{1}{\sqrt{1-M_c^2}} \sqrt{x_1^{c2} + (1-M_c^2)(x_2^{c2} + x_3^{c2})}. \end{aligned} \quad (2.20)$$

From the transformed exponential function in the source system (c),

$$\begin{aligned} \exp i\omega^b(t^b - r^b/a_0) &= \\ &= \exp i\omega^b \sqrt{1-M_c^2} \left\{ t^c + \frac{M_c}{a_0(1-M_c^2)} x_1^c - \frac{1}{a_0(1-M_c^2)} \sqrt{x_1^{c2} + (1-M_c^2)(x_2^{c2} + x_3^{c2})} \right\}, \end{aligned} \quad (2.21)$$

it becomes evident that the actual frequency  $\omega_a$ , which would be received by an observer moving with the source, is given by

$$\omega_a = \omega^b \sqrt{1-M_c^2}. \quad (2.22)$$

This enables us to attribute to  $\omega^b$  a definite physical meaning.

Next we will relate the second arbitrary constant in (2.18),  $\phi^b$ , to the other characteristic source quantity, namely its pulsation amplitude. The velocity field  $v_i$  is easily derived from the potential  $\phi$  according to

$$v_i = -\frac{\partial \phi}{\partial x_i} = -\frac{\partial \phi}{\partial x_i^a} = -\frac{1}{\sqrt{1-M_c^2}} \left( \frac{\partial \phi}{\partial x_i^b} + \delta_{i1} \frac{M_c}{a_0} \frac{\partial \phi}{\partial t^b} \right) = -\frac{\partial \phi}{\partial x_i^c} \quad (2.23)$$

with, e.g., the streamwise component

$$v_1 = \left\{ i \frac{\omega^b}{a_0} \left( \frac{x_1^c}{\sqrt{1-M_c^2}} - M_c \right) + \frac{x_1^c}{\sqrt{1-M_c^2}} \right\} \frac{\phi^b}{\sqrt{1-M_c^2} r^b} \exp i\omega^b(t^b - r^b/a_0) \quad (2.24)$$

or the transverse component

$$v_2 = \left\{ i \frac{\omega^b}{a_0} \frac{x_2^c}{r^b} + \frac{x_2^c}{r^b} \right\} \frac{\phi^b}{r^b} \exp i\omega^b(t^b - r^b/a_0) \quad (2.25)$$

This flow field includes the limit case of quasi-steady linear perturbations of an ideal compressible fluid. The corresponding condition,

$$\frac{\omega^b}{a_0} \ll \frac{1}{r^b} \quad \text{or} \quad \frac{\omega^b}{a_0} \ll \frac{1-M_c^2}{\sqrt{x_1^2 + (1-M_c^2)(x_2^2 + x_3^2)}} \quad (2.26)$$

defines a near field close to the source in which the pulsation amplitude of the source can be determined directly from

$$v_2(x_1^c = x_3^c = 0) = \frac{\phi^b}{x_1^c} \exp i\omega^b t^c \quad (2.27)$$

For doing so, we compare this with the radial velocity of a simple source (of strength  $A_0$ ) in a uniform medium at rest,

$$v_r = \frac{A_0}{4\pi r^2} \exp i\omega_0 t \quad (2.28)$$

where now  $r$  is the radial distance from the source. When equating

$$\phi^b = \frac{A_0}{4\pi} \quad (2.29)$$

it should be born in mind, however, that for  $M_c \neq 0$  the pulsation amplitude of the source as we have defined it is no longer uniform in all three directions. In the streamwise direction,

$$v_1(x_2^c = x_3^c = 0) = \frac{\sqrt{1-M_c^2} A_0}{4\pi x_1^c} \exp i\omega_0 t, \quad (2.30)$$

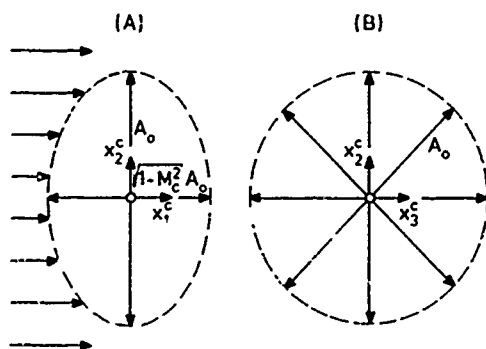


Fig. 3: Structure of monopole source in the Lorentz-transformed system (b) as observed in system (c) moving with source, (A) in plane  $x_2 = 0$  (B) in plane  $x_1 = 0$ .

the source issues fluid into its immediate vicinity (outwards and inwards) at a flow rate that is reduced by a factor  $\sqrt{1-M_c^2}$  relative to that issued in a direction normal to the flow as illustrated in Fig. 3. What was initially assumed a simple monopole type of a source or a pulsating sphere in the Lorentz transformed system (b) may now be identified as a pulsating ellipsoid in the physically more obvious system (c) moving with the source. That simply means that we had to assume a slightly different point source in the system (b) with a correspondingly modified potential function instead of Eq. (2.18) if we were particularly interested in a source of which we unambiguously knew that it behaved like a monopole in system (c).

After the constants  $\omega^b$  and  $\phi^b$  in Eq. (2.18) have been specified, we may derive the pressure field as

$$p(x_1, t) = p_0 \left( \frac{\partial \phi}{\partial t} + \bar{c} \frac{\partial \phi}{\partial x_1} \right) = \left\{ \frac{\omega_0}{a_0} \left( 1-M_c \frac{x_1 - \bar{u}t}{\sqrt{1-M_c^2} r^b} \right) + i M_c \frac{x_1 - \bar{u}t}{r^b} \right\} \frac{i \rho_0 a_0 A_0}{4\pi (1-M_c^2) r^b} \exp i\omega^b(t^b - r^b/a_0). \quad (2.31)$$

In the hydrodynamic or aerodynamic near field induced by the source the second of the two terms in curly brackets again dominates the first yielding a particularly simple relationship between the local (quasi-incompressible, pressure and the streamwise velocity fluctuations (Eq. (2.24)),

$$p = \rho_0 a_0 M_c v_1 = -\rho_0 (\bar{c} - \bar{u}) v_1. \quad (2.32)$$

In the radiated far field, on the other hand,

$$\frac{\omega^b}{a_0} \gg \frac{1}{r^b} \quad (2.33)$$

the acoustic pressure field can be written in terms of the observer coordinates as

$$p = \left( 1-M_c \frac{x_1 - \bar{u}t}{\sqrt{1-M_c^2} r^b} \right) \frac{1}{1-M_c^2} \frac{i \rho_0 \omega_0 A_0}{4\pi r^b} \exp \frac{i\omega_0}{1-M_c^2} \left\{ (1-M_c M_c) t + M_c \frac{x_1}{a_0} - \sqrt{1-M_c^2} \frac{r^b}{a_0} \right\} \quad (2.34)$$

$$\text{with} \quad \sqrt{1-M_c^2} r^b = \sqrt{(x_1 - \bar{u}t)^2 + (1-M_c^2)[(x_2 - \bar{x}_2)^2 + (x_3 - \bar{x}_3)^2]}.$$

18-6 In a similar manner one may obtain the sound field of more complicated higher order sources by modifying the solution (2.18) correspondingly. Here it may suffice to derive the various Doppler frequency shifts and convective amplification factors for a simple monopole in the Lorentz coordinates.

### 2.3 The various practical effects of relative motion

Consider a subsonic ( $M_c < 1$ ), straight-line, uniform (i.e. not accelerated) motion between a simple source and the ambient fluid and an arbitrary motion of the observer parallel to the former. Eq. (2.34) then shows some important effects the motion has when compared to the pressure field the same source would generate in the case  $\vec{c} = \vec{u} = 0$ ,

$$p(r, t) = \frac{i\rho_0\omega_0 A_0}{4\pi r} \exp i\omega_0(t - r/a_0). \quad (2.35)$$

Here and in the following  $r$  will denote the instantaneous distance between the observer and the source. If both move relative to each other we have (compare Fig. 2)

$$r = \sqrt{(x_1 - \bar{u}t)^2 + (x_2 - \bar{x}_2)^2 + (x_3 - \bar{x}_3)^2}. \quad (2.36)$$

Two quantities are of particular interest in practical noise problems, the amplitude  $\hat{p}$  and frequency  $\omega$  of the pressure field. The latter is known to undergo a so-called Doppler frequency shift due to the relative motion. Its most general form may be deduced if we define  $\omega$  as the time derivative of the exponential function in Eq. (2.34),

$$\omega = \frac{\omega_0}{1-M_c^2} \left\{ 1 - MM_c - (M_c - M) \frac{x_1 - \bar{u}t}{\sqrt{1-M_c^2} r^b} \right\}.$$

The most convenient form for  $\hat{p}$  and  $\omega$  is probably in terms of  $M$ ,  $M_c$  and the instantaneous angle  $\vartheta(t)$  between  $r(t)$  and the direction  $x_1$  of the relative motion. With

$$\cos \vartheta = \frac{x_1 - \bar{u}t}{r}; \quad \sin \vartheta = \frac{\sqrt{(x_2 - \bar{x}_2)^2 + (x_3 - \bar{x}_3)^2}}{r}; \quad \sqrt{1-M_c^2} r^b = r \sqrt{1-M_c^2 \sin^2 \vartheta} \quad (2.37)$$

and hence

$$p(x_i, t) = \left( 1 - M_c \frac{\cos \vartheta}{\sqrt{1-M_c^2 \sin^2 \vartheta}} \right) \frac{i\rho_0\omega_0 A_0 / \sqrt{1-M_c^2}}{r \sqrt{1-M_c^2 \sin^2 \vartheta}} \exp i\omega_0 \left\{ t - \frac{r}{a_0} \frac{\sqrt{1-M_c^2 \sin^2 \vartheta} - M_c \cos \vartheta}{1-M_c^2} \right\} \quad (2.38)$$

we may define the following, generally time-dependent parameters of relative motion,

$$\frac{\hat{p}}{\hat{p}_0} = \frac{1 - (M_c \cos \vartheta / \sqrt{1-M_c^2 \sin^2 \vartheta})}{\sqrt{1-M_c^2} \sqrt{1-M_c^2 \sin^2 \vartheta}}, \quad \text{with } \hat{p}_0 = \frac{i\rho_0\omega_0 A_0}{r} \quad (2.39)$$

$$\frac{\omega}{\omega_0} = \frac{1}{1-M_c^2} \left\{ 1 - MM_c - (M_c - M) (\cos \vartheta / \sqrt{1-M_c^2 \sin^2 \vartheta}) \right\}. \quad (2.40)$$

Because these are rather complex functions of space and time it may be worthwhile looking into three specific source/observer configurations separately (compare Fig. 4).

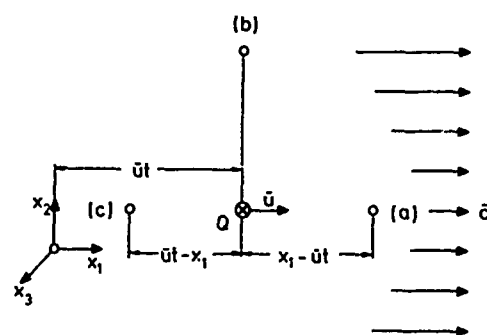


Fig. 4: Source and observer in arbitrary relative motion.

#### (a) Source and observer approaching each other

This special configuration is characterized by

$$\vartheta = 0^\circ, \quad r = x_1 - \bar{u}t = \sqrt{1-M_c^2} r^b$$

and hence Eq. (2.34) reduces to

$$p(r, t) = \quad (2.41)$$

$$= \frac{i\rho_0\omega_0 A_0}{4\pi r} \frac{\sqrt{1-M_c}}{1+M_c} \exp i\omega_0 \frac{1+M}{1+M_c} \left\{ t - \frac{1}{1+M} \frac{x_1}{a_0} \right\}.$$

In this form Eq. (2.41) also indicates the apparent phase velocity and wave length a fixed observer would register. The corresponding parameter ratios were listed along with the amplitude and frequency ratios in Table 1.

#### (b) Source and observer passing each other

This configuration is characterized by

$$\vartheta = 90^\circ, \quad \bar{u}t = x_1, \quad r = \sqrt{(x_2 - \bar{x}_2)^2 + (x_3 - \bar{x}_3)^2} = r^b$$

so that the pressure may be written as



	(c) Departing $\vartheta = 180^\circ$	(b) Passing by $\vartheta = 90^\circ$	(a) Approaching $\vartheta = 0^\circ$
Amplitude $\frac{\hat{p}}{\hat{p}_0}$	$\sqrt{\frac{1+M_c}{1-M_c}}$	$\frac{1}{1-M_c^2}$	$\sqrt{\frac{1-M_c}{1+M_c}}$
Frequency $\frac{\omega}{\omega_0}$	$\frac{1-M}{1-M_c}$	$\frac{1-MM_c}{1-M_c^2}$	$\frac{1+M}{1+M_c}$
Wave length $\frac{\lambda}{\lambda_0}$	$1-M_c$		$1+M_c$
Wave speed $\frac{a}{a_0}$	$1-M$		$1+M$

Table 1: Unified convection effects for specific source/observer configurations as illustrated in Fig. 4.

The above described effects due to source convection hold for any arbitrary values of  $M$  and  $M_c$  as long as

$$|M_c| = |\bar{c} - \bar{u}|/a_0 < 1. \quad (3.44)$$

The corresponding formulae for  $|M_c| > 1$  are easily obtained in a similar manner.

#### 2.4 Three special cases of relative motion

There are several ways of deriving the effects on the sound field due to a uniform convection of the source. It is a characteristic feature of the above described Lorentz transformation approach that the results for the radiated pressure at a fixed point in  $(x_1/t)$ -space are given directly in terms of the moving source position as measured at the time the far field signal is received. As a consequence of this, part of what was identified as convective amplification or attenuation by comparing Equations (2.34) and (2.35) directly can under certain circumstances be simply due to the source/observer distance varying in time rather than to any effect of relative motion.

The alternative retarded-time formulation, which was used almost exclusively in recent aeroacoustic theories (see, e.g., Refs. [3], [4]), accounts, explicitly, for the fact that the sound received at  $t$  was emitted as sound at the retarded time

$$t_r = t - R/a, \quad (2.45)$$

where now  $R$  denotes the wave propagation path the sound has travelled from the source to the observer at a phase speed  $a$ . The latter approach appears to be advantageous when, in particular, the sound propagates in a medium otherwise at rest with then  $a = a_0$ .

##### 2.4.1 Moving-source problem

We now reduce our general analysis of Chap. 2.2 to the more specific case where there is no mean flow present and the source moves at a constant Mach number  $M_s$  in the positive  $x_1$ -direction (see sketch (1) on Table 2), i.e.

$$M \equiv \bar{c}/a_0 = 0; \quad M_c \equiv (\bar{c} - \bar{u})/a_0 = -\bar{u}/a_0 = -M_s. \quad (2.46)$$

Eq. (2.34) may then be rewritten as

$$p = \left(1 + M_s \frac{x_1 - \bar{u}t}{R_1}\right) \frac{i\rho_0\omega_0 A_0 / \sqrt{1-M_s^2}}{4\pi R_1} \exp i\omega_0(t - R/a_0) \quad (2.47)$$

$$\text{with } R_1 = \sqrt{(x_1 - \bar{u}t)^2 + (1-M_s^2)[(x_2 - \bar{x}_2)^2 + (x_3 - \bar{x}_3)^2]} \quad (2.48)$$

and, according to Eqs. (2.45), (2.21), (2.22), and (2.19),

$$R = a_0(t - t_r) = \frac{1}{1-M_s^2} \left\{ M_s(x_1 - \bar{u}t) + R_1 \right\}. \quad (2.49)$$

Introduction of the time-dependent angle of emission relative to the direction of motion,  $\theta$ ,

$$x_1 - \bar{u}t_r = R \cos \theta \quad (2.50)$$

enables us to replace  $x_1 - \bar{u}t$  in Eq. (2.49) by

$$p(r,t) = \frac{i\rho_0\omega_0 A_0}{4\pi r} \frac{1}{1-M_c} \exp i\omega_0 \left( t - \frac{1}{\sqrt{1-M_c^2}} \frac{r}{a_0} \right) \quad (2.42)$$

at that very moment. The amplitude and frequency ratios (according to Eqs. (2.39) and (2.40)) were again listed on Table 1.

##### (c) Source and observer departing from each other

This situation with

$$\vartheta = 180^\circ, \quad r = \bar{u}t - x_1 = \sqrt{1-M_c^2} r^b$$

resembles that of case (a) with

$$p(r,t) = \frac{i\rho_0\omega_0 A_0}{4\pi r} \frac{\sqrt{1+M_c}}{1-M_c} \exp i\omega_0 \frac{1-M_c}{1+M_c} \left( t + \frac{1}{1-M_c} \frac{x_1}{a_0} \right) \quad (2.43)$$

now showing the wave propagation in the negative  $x_1$ -direction. The characteristic parameters were again listed on Table 1.

18-8

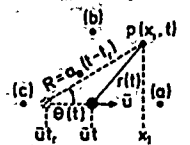
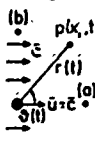
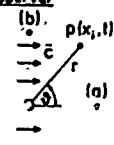
(1) Moving source	(2) Moving observer	(3) Co-moving source and observer
		
(a) $\frac{A}{A_0} = \frac{1 + \bar{u}/a_0}{1 - \bar{u}/a_0} \cdot \frac{a_0}{a_s} = 1$ $\frac{\omega}{\omega_0} = \frac{1}{1 - \bar{u}/a_0} \cdot \frac{\lambda}{\lambda_0} = 1 - \bar{u}/a_0$	$\frac{A}{A_0} = \frac{\lambda}{\lambda_0} = 1$ $\frac{\omega}{\omega_0} = \frac{a_0}{a_s} = 1 + \bar{c}/a_0$	$\frac{A}{A_0} = \frac{1 + \bar{c}/a_0}{1 - \bar{c}/a_0} \cdot \frac{\omega}{\omega_0} = 1$ $\frac{a_0}{a_s} = \frac{\lambda}{\lambda_0} = 1 + \bar{c}/a_0$
(b) $\frac{A}{A_0} = \frac{\omega}{\omega_0} = \frac{1}{1 - (\bar{u}/a_0)^2}$	$\frac{A}{A_0} = \frac{\omega}{\omega_0} = 1$	$\frac{A}{A_0} = \frac{1}{1 - (\bar{c}/a_0)^2} \cdot \frac{\omega}{\omega_0} = 1$
(c) $\frac{A}{A_0} = \frac{1 + \bar{u}/a_0}{1 - \bar{u}/a_0} \cdot \frac{a_0}{a_s} = 1$ $\frac{\omega}{\omega_0} = \frac{1}{1 - \bar{u}/a_0} \cdot \frac{\lambda}{\lambda_0} = 1 + \bar{u}/a_0$	$\frac{A}{A_0} = \frac{\lambda}{\lambda_0} = 1$ $\frac{\omega}{\omega_0} = \frac{a_0}{a_s} = 1 - \bar{c}/a_0$	$\frac{A}{A_0} = \frac{1 + \bar{c}/a_0}{1 - \bar{c}/a_0} \cdot \frac{\omega}{\omega_0} = 1$ $\frac{a_0}{a_s} = \frac{\lambda}{\lambda_0} = 1 - \bar{c}/a_0$

Table 2: Modifications in amplitude, frequency, phase velocity, and wave length due to a uniform motion.

$$x_1 - \bar{u}t = x_1 - \bar{u}t_r - \bar{u}(t - t_r) = R \cos \theta - M_S R = R(\cos \theta - M_S) \quad (2.51)$$

thus yielding

$$R_1 = R(1 - M_S \cos \theta) \quad (2.52)$$

and hence for the pressure field in terms of the source coordinates at the respective time of emission,

$$p = \frac{i\omega_0 \rho_0 A_0}{4\pi(1 - M_S^2)^{3/2}} \frac{1}{R(1 - M_S \cos \theta)^2} \exp i\omega_0(t - R/a_0) \quad (2.53)$$

p is now in a form similar to that in standard textbooks (see, e.g., Morse & Ingard [5], Eq. (11.2.15) or Goldstein [3], Eq. (1.110)). It shows the occurrence of a multiplicative factor in the amplitude function which describes convective amplification as a function of  $\theta$  with

$$C^2 = (1 - M_S \cos \theta)^{-2} = \begin{cases} (1 - M_S)^{-2} & \theta = 0^\circ \\ 1 & \text{for } \theta = 90^\circ \\ (1 + M_S)^{-2} & \theta = 180^\circ \end{cases} \quad (2.54)$$

The Doppler frequency shift, too, may be expressed in terms of the angle of emission,  $\theta$ , if we define  $\omega$  as the time derivative of the phase function in Eq. (2.47),

$$\omega = \frac{d}{dt}[\omega_0(t - R/a_0)] = \omega_0(1 - \frac{1}{a_0} dR/dt) = \omega_0 \left\{ 1 + \frac{1}{1 - M_S^2} \left[ M_S + \frac{M_S(x_1 - \bar{u}t)}{R_1} \right] \right\}$$

C is thus seen to also determine the frequency ratio

$$\frac{\omega}{\omega_0} = C = (1 - M_S \cos \theta)^{-1} = \begin{cases} (1 - M_S)^{-1} & \theta = 0^\circ \\ 1 & \text{for } \theta = 90^\circ \\ (1 + M_S)^{-1} & \theta = 180^\circ \end{cases} \quad (2.55)$$

in full agreement with the formulac for  $\theta = 0^\circ$  in box (1a) and for  $\theta = 180^\circ$  in box (1b) of Table 2. For sound radiation at  $\theta = 90^\circ$ , i.e. normal to the direction of motion, the frequency remains that of the original source fluctuations. Note, however, that the source will have passed the observer by an amount  $\bar{u}(t - t_e)$  until that sound can be received. C is plotted as a function of  $\theta$  in Fig. 5.

While the Doppler frequency shifts at points in or opposite to the direction of motion are independent of the model employed, the apparent upstream amplification and downstream

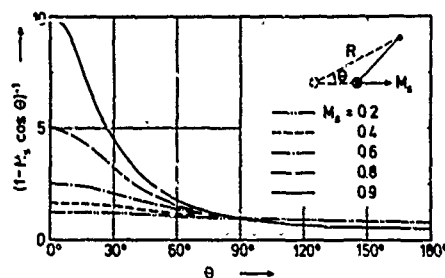


Fig. 5: Convection factor  $C$  due to a uniform motion ( $M_s$ ) of a simple source according to Eq. (2.55).

attenuation depend on the reference source, whether it is thought of as being placed at (i) the real-time position  $\vec{u}$  or (ii) the retarded-time position  $\vec{u}_r$ . The corresponding upstream/downstream pressure amplitude ratios therefore differ for the two models,

(i) symmetric real-time positions (Table 2)

$$\frac{\hat{p}_{00}}{\hat{p}_{180}} = \frac{1+M_s}{1-M_s} \quad (2.56)$$

(ii) symmetric retarded-time positions (Eq. (2.54))

$$\frac{\hat{p}_{00}}{\hat{p}_{180}} = \left( \frac{1+M_s}{1-M_s} \right)^2 \quad (2.57)$$

Both were plotted in Fig. 6 on a logarithmic decibel scale as sound pressure level (SPL) difference

$$\Delta L = 20 \log (\hat{p}_{00}/\hat{p}_{180}) \quad (2.58)$$

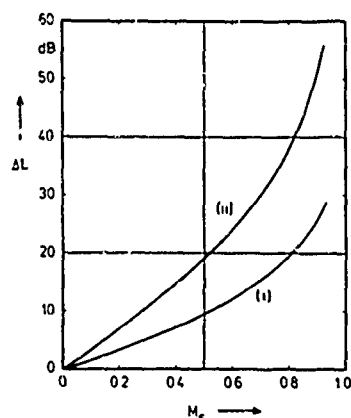


Fig. 6: Upstream/downstream SPL difference for a moving source according to Eqs. (2.56)-(2.58).

In any case, the motion of the source relative to the ambient medium is seen to have a tremendous effect on both the frequency and intensity of its sound field as received by a stationary observer, even at relatively small Mach numbers. For higher order acoustic sources one can, under certain circumstances, imagine an energy concentration in front of the source which even exceeds that illustrated in Fig. 6. The so-called *convective amplification* factor is sometimes written in the form

$$C_n = C^{2n+2} = (1 - M_s \cos \theta)^{-2n-2}; \quad n = \begin{cases} 0, & \text{monopole} \\ 1, & \text{dipole} \\ 2, & \text{quadrupole} \end{cases} \quad (2.59)$$

with  $n$  varying with the specific structure of the source (compare, e.g., Morfey [4], Eq. (7)).

What all convection effects, in this notation, have in common is the invariance with  $M_s$  of the sound field at normal incidence,  $\theta = 90^\circ$ . This is illustrated in Fig. 7 where

$$\Delta L_1 = L_\theta - L_{90} = 20 \log (1 - M_s \cos \theta)^{-2} = 40 \log C \quad (2.60)$$

was plotted as a function of  $\theta$  with  $M_s$  as a parameter.

Although that alternative notation may be less convenient in cases, we may finally write the Doppler frequency shift and amplification factors in terms of the *instantaneous* source-observer angle  $\vartheta$  according to Eqs. (2.39) and (2.40),

$$\frac{\hat{p}}{\hat{p}_0} = \frac{1 + (M_s \cos \vartheta / \sqrt{1 - M_s^2} \sin^2 \vartheta)}{\sqrt{1 - M_s^2} \sqrt{1 - M_s^2} \sin^2 \vartheta} \quad (2.61)$$

$$\frac{\omega}{\omega_0} = \frac{1}{1 - M_s^2} \left\{ 1 + M_s (\cos \vartheta / \sqrt{1 - M_s^2} \sin^2 \vartheta) \right\} \quad (2.62)$$

#### 2.4.2 Moving observer problem

The second, more trivial case where the receiver moves relative to a stationary source and a fluid at rest is physically indistinguishable from that of a source co-moving with the fluid at the same velocity  $\vec{u} = \vec{c}$  relative to the (then fixed) observer (see sketch (2) on Table 2),

$$M \equiv \vec{c}/a_0 = M_0; \quad M_c \equiv (\vec{c} - \vec{u})/a_0 = 0 \quad (2.63)$$

On these simplifying assumptions Eq. (2.38) assumes the following form

$$\hat{p} = \frac{i p_0 \omega_0 A_0}{4 \pi r} \exp i \omega_0 (t - r/a_0) \quad (2.64)$$

with

$$r = \sqrt{(x_1 - a_0 M_0 t)^2 + (x_2 - \bar{x}_2)^2 + (x_3 - \bar{x}_3)^2}.$$

The new Doppler shifted frequency received by the moving observer may, according to Eq. (2.39), be expressed by

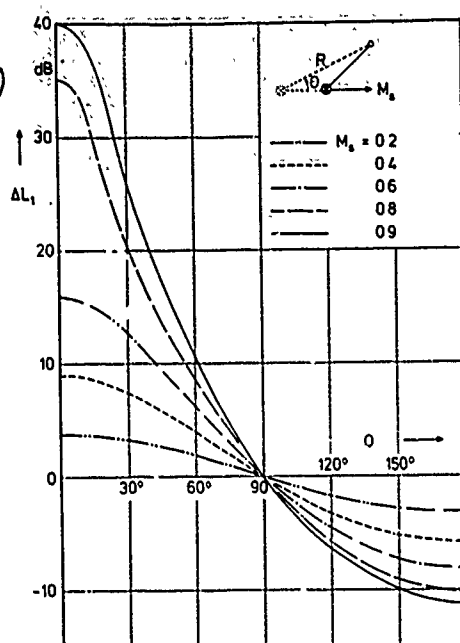


Fig. 7: Effect of a uniform motion ( $M_s$ ) on the directivity pattern of a simple source according to Eqs. (2.53), (2.54), and (2.60).

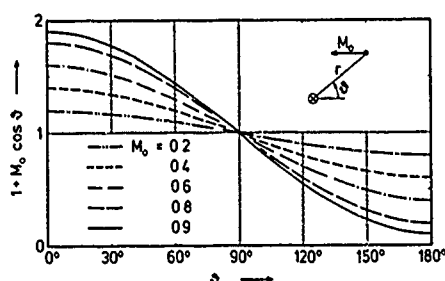


Fig. 8: Doppler frequency shift  $\omega/\omega_0$  as registered by a uniformly moving ( $M_s$ ) observer according to Eq. (2.65).

tivity pattern of the source as compared to its static directivity. For our idealized sound receiver, however, we would expect exactly the same difference to occur when static noise data are compared with directivity patterns measured in fly-over or pass-by tests. Only the frequencies would be Doppler shifted according to case 2.4.2 and the instantaneous source-observer angle  $\theta$  will have to vary during the fly-over test. The amplification and attenuation due to the flight effects, however, can best be described by the logarithm of Eq. (2.67),

$$\Delta L_2 = L - L(M_F = 0) = 20 \log \frac{\hat{P}}{P_s} \quad (2.68)$$

The corresponding directivity patterns depicted in Fig. 9 show several very remarkable features some of which may be worth to be taken into account in standard fly-over or pass-by noise testing procedures:

- The amplification in the upstream direction is equal (in absolute values) to the attenuation in the downstream direction,

$$\Delta L_2(\theta = 0^\circ) = -\Delta L_2(\theta = 180^\circ) \quad .$$

- The direction normal to the flow ( $\theta = 90^\circ$ ) shows a negligible flow effect for vanishing  $M_F \ll 1$  only. Considerable amplification is found at  $\theta = 90^\circ$  for moderate  $M_F$ .

$$\frac{\omega}{\omega_0} = (1 + M_0 \cos \theta) \quad (2.65)$$

where, of course,  $\theta$  is defined by Eq. (2.37) as the instantaneous source/observer angle. The corresponding plots in Fig. 8 show an essential difference when compared to  $\omega/\omega_0$  in case (1) (Fig. 5). This difference becomes negligible only for vanishing Mach numbers  $M_0 \ll 1$ .

This kind of a relative motion has, naturally, no effect on the structure of the source or its radiation field as we have tacitly assumed an idealized (i.e. immaterial) sound receiver throughout in our analysis.

#### 2.4.3 Co-moving source and observer problem

This is another special case incorporated in our more general analysis of Chap. 2.2 When studying the noise of a propulsion system, e.g., a propeller or jet engine on an aircraft, it is often very convenient and has, in fact, become common practice to perform the bulk of the measurements with the whole vehicle or the propulsion system alone on a static test facility. We are then faced with the problem of how these static test data might be converted into those to be expected when the vehicle is in motion.

The inverse problem would be to relate the aircraft noise measured in a fly-over test or the noise of a high speed train while passing by to the corresponding data known from static tests. The principle effects due to this kind of relative motion can be investigated by assuming a simple, acoustically compact source to begin with. Although such a procedure would, in practice, create insurmountable experimental difficulties, we now let the idealized receiver move with this simplified source or (what is physically the same) superimpose a uniform mean flow  $\bar{c}$  on a stationary source/observer constellation (see sketch (3) on Table 2). With

$$M \equiv \bar{c}/a_0 = M_F = M_0 \quad (2.66)$$

we may then rewrite Eqs. (2.39) and (2.40) to obtain

$$\frac{\hat{P}}{P_0} = \frac{1 - (M_F \cos \theta / \sqrt{1 - M_F^2} \sin^2 \theta)}{\sqrt{1 - M_F^2} \sqrt{1 - M_F^2} \sin^2 \theta} \quad (2.67)$$

$$\frac{\omega}{\omega_0} = 1$$

The new convection factor, Eq. (2.67), may tell us the principal difference in the directivity pattern of the source as compared to its static directivity. For our idealized sound receiver, however, we would expect exactly the same difference to occur when static noise data are compared with directivity patterns measured in fly-over or pass-by tests. Only the frequencies would be Doppler shifted according to case 2.4.2 and the instantaneous source-observer angle  $\theta$  will have to vary during the fly-over test. The amplification and attenuation due to the flight effects, however, can best be described by the logarithm of Eq. (2.67),

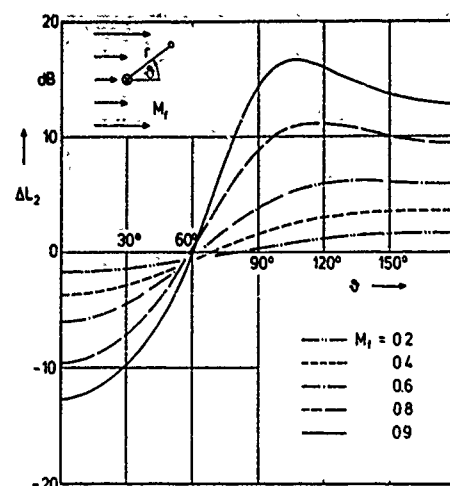


Fig. 9: Effect of a uniform flow ( $M_f$ ) on the directivity pattern of a simple source according to Eq. (2.68).

- While the maximum attenuation occurs always at  $\theta = 0^\circ$  the peak amplification is continuously shifted from  $\theta = 180^\circ$  for  $M_f \ll 1$  towards  $\theta = 90^\circ$  with  $M_f$  approaching unity. 18-11

- All directivity correction curves in Fig. 9 seem to cross in a fairly narrow range of angles around  $\theta = 60^\circ$ . This angle, at which the flow effect is practically absent, whatever the value of  $M_f$ , represents itself as that angle where the intensity of the stationary source can be measured during flight.  $\theta = 60^\circ$  may thus take the role of  $\theta = 90^\circ$  in the moving source problem (compare Fig. 7).

### 3. JET NOISE RADIATED UNDER STATIC AND UNDER FLIGHT CONDITIONS

When looking for examples to illustrate the various Doppler frequency shifts and convective amplification effects of sources in motion relative to the fluid and/or the observer one soon realizes that the corresponding experiments are scarce. One important area of application of the foregoing theoretical considerations is to the aerodynamic near fields of turbulent wave packets travelling downstream in free shear layers. These will be the subject of the ensuing Chaps. 4 and 5.

Here we will try to illustrate the effects of relative motion of aeroacoustic sources on their far field radiation characteristics. For lack of a better example, we may first consider the effect of the downstream convection (or propagation) of the jet flow inhomogeneities generating jet noise. Secondly, the effect of forward motion of the aircraft is illustrated by assuming that the jet flow radiates as one coherent simple source.

#### 3.1 Jet noise source convection effect

Sound generation by an extended turbulent flow like a simple, circular, subsonic jet is an extremely complicated process. The radiated far field as characterized by the

- acoustic intensity level
  - power spectrum density
  - polar directivity pattern
  - azimuthal field structure
- can, at least in principle, be related to a bunch of different source characteristics as there are
- intensity distribution (*strength*)
  - statistical behaviour (*coherence*)
  - spatial scales (*compactness*)
  - azimuthal structure (*modes*)
  - downstream propagation (*convection*).

A complete theory relating the acoustic to the aerodynamic field quantities requires an integration process in which aerodynamic source cancellation and acoustic wave interference mechanisms must be accounted for. As an alternative to such a quantitative jet noise theory, one may study the effects on the far field of the various near field characteristics separately. Here we want to concentrate on the very specific effect source convection has on the acoustic directivity. We assume that all the other source parameters remain entirely unaltered and ask ourselves, what is the effect of the convection Mach number  $M_s$  as typical of the downstream propagation of those jet disturbances that are responsible for the radiated noise (compare Fig. 10).

From published data we take

$$M_s = 0.65 M_j \quad (3.1)$$

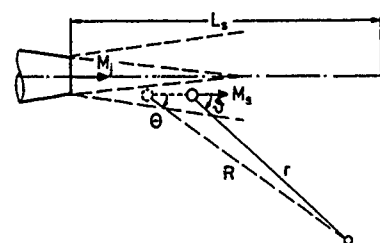


Fig. 10: Sektch illustrating source convection effect.

and assume, for a while, that the axial extent of the total source region,  $L_s$ , be small compared to the far field distance  $r$ ,

$$L_s \ll r \text{ and } R \approx r \text{ (geometric far field).} \quad (3.2)$$

This means, effectively, that the fixed observer in the far field should see all the downstream travelling source elements under the same angle  $\theta$  to the jet axis. The finiteness (as distinct from the above mentioned compactness) of the source region has an important consequence with respect to the source convection effect derived under Sec. 2.4.1: for sound waves to arrive at an arbitrary constant angle  $\theta$  it is necessary that they were emitted at approximately the same angle  $\theta = \theta$  to the jet axis at the

appropriate retarded time  $t_r = t - (R/a_0)$ . Hence the emitting source element has long disappeared before this sound has reached the observer. This particular situation suggests the emission angle  $\theta$  as the only appropriate variable when plotting polar directivity patterns for jet noise as measured on a static test facility.

Next we assume the jet to have a "basic" directivity that is uniform like that of a simple monopole and the whole of the directionality observed in the far field being a result of the source convection only. This admittedly is an oversimplified model of the real situation. Yet, knowing that a higher order source can be composed by a series of simple sources, we may tentatively use the directivities from Fig. 7 for a comparison with measured jet noise data. Since at  $\theta = 90^\circ$  this specific type of convection effect is absent,

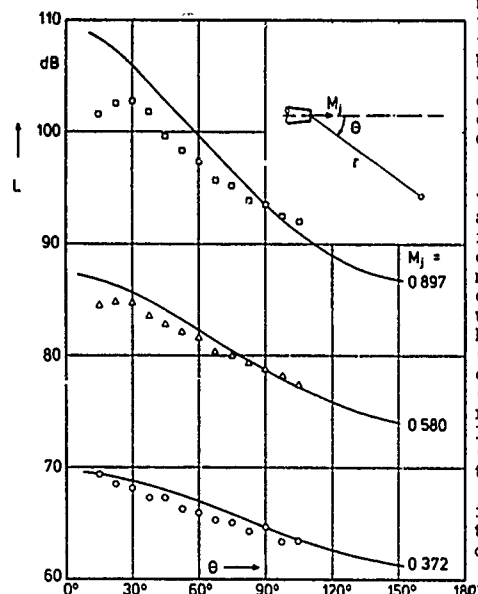


Fig. 11: Polar directivity patterns of jet noise after Ref. [6] and of a convected simple source according to Eq. (2.60).

tortion in field shapes is almost the same as that of a simple monopole convected in the downstream direction.

### 3.2 Jet noise forward speed effect

Fig. 12 illustrates two physically equivalent configurations for studying the effect of forward speed of a vehicle on the far field of the sources moving with it. The superposition of a uniform flow with Mach number  $M_f$  on the assumedly unaltered stationary source (configuration (a)) corresponds to the co-moving source and observer problem of Sec. 2.4.3. It is not easily accomplished experimentally since it requires, among other things, extremely large wind tunnels and in-flow sound measurements [9]. The fact that, in practical situations, the observer moves with the flow would make no difference for the directivity as a function of  $\theta$ , which, in this case, is undoubtedly the most appropriate angle to be chosen whether the observer is co-moving

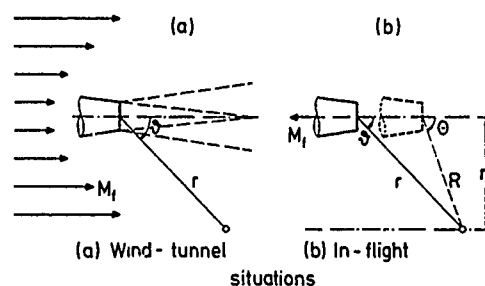


Fig. 12: Sketch illustrating forward speed effect.

with the source or the fluid. The frequency spectra would differ for the two cases but not the intensities as was earlier described in Sec. 2.4.2 (moving observer problem).

The effect of flight on jet noise, e.g., can thus be studied, in a qualitative manner, by adding intensity levels  $\Delta L_2$  according to Eq. (2.68) to the directivities measured under

we have used the sound pressure level measured normal to the jet as the reference point and plotted in Fig. 11 the conjectural directivity patterns along with those experimentally determined by Lush [6]. The field shapes are seen to agree very well at low Mach numbers. At higher values of  $M_j$ , however, the assumed source convection effect overestimates the amplification in the quadrant  $0^\circ < \theta < 90^\circ$ .

Several explanations can be given for this deviation considering all the other aerodynamic and acoustic parameters that might change with varying jet Mach number. The least probable one, however, seems to be that, instead of a simple source model, one should proceed to a higher-order type of a source. A quadrupole model, for instance, would be even worse as it would predict a still higher power of the convection factor in Eq. (2.59). Goldstein [3] in his Figs. 2.14 and 2.15 compared directivity patterns predicted by  $(1 - M_s \cos \theta)^{-1}$  with the sound intensity measurements of Lush [6] and other investigators. But later on (in his Figs. 6.3 and 6.4) he found a  $(1 - M_s \cos \theta)^{-3}$  dependence with  $M_s \approx 0.62 M_j$  to fit the experimental data much better. Jones [7], too, considered different convection factors in an attempt to overcome this discrepancy between measurements and theories based on the specific quadrupole model introduced by Lighthill [8].

Assuming a correspondingly smaller value for  $M_s/M_j$  as was occasionally recommended in the literature does not seem a valid approach either. Here suffice it to state that, due to source convection, sound radiated at acute angles  $\theta$  to the jet axis is amplified whereas that radiated at obtuse angles  $\theta$  is attenuated. The measured dis-

static conditions. This flight correction of the field shapes can be done in the same way for polar or linear plots. The latter has become common practice in static-to-flight comparisons [10, 11, 12].

Such a directivity plot of the static data along a line parallel to the jet axis corresponding to a flight altitude of  $r_0$  was reproduced in Fig. 13. The raw static data were obtained by Brooks [10] with a Rolls-Royce Viper 11 jet engine over a concrete surface along a line parallel to and only 30 m to the side of the engine centre-line. For the flight tests the same engine was installed on a Jet Provost aircraft and the microphone mounted on a tower of a bridge. The actual fly-over tests were then done at  $r_0 = 150$  m with the engine operating conditions maintained constant so far as possible in order to simulate the same noise source conditions as in the static tests. We have modified Brooks's static field shapes in three steps and replotted them in Fig. 13:

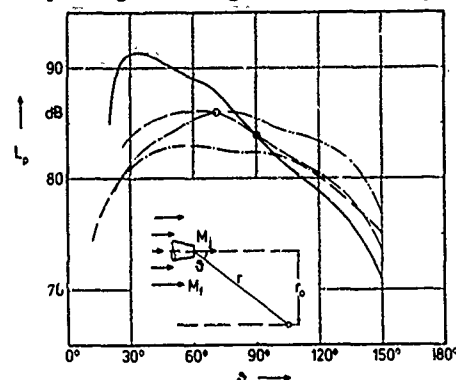


Fig. 13: Qualitative static-to-flight comparison of jet noise linear field shapes.  
 $M_j = 1.07$ ;  $M_s = 0.373$ ,  $r_0 = 150$  m.  
 — Static test (bare Viper 11 engine, Aston Down) [10]  
 - - - Due to modified source convection factor (Eqs. (2.54), (3.3))  
 - . - Due to forward speed effect (Eq. (2.67))  
 . . . Flight test (Jet Provost aircraft, Severn Bridge) [10]

could now try to correct the directivity according to Eq. (2.67) or Fig. 9. The maximum of the new directivity can be seen in Fig. 13 to have been shifted towards  $80^\circ$  with an almost symmetric decay at both sides of this peak. Such field shapes are very typical for jet noise in flight.

(iii) Although this is not clearly stated in Brooks's paper, we take it from a private communication with Prof. J.E. Ffowcs Williams that all the flight data of Ref. [10]

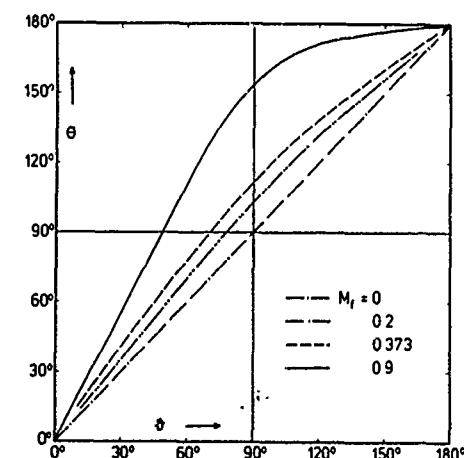


Fig. 14: Emission angle  $\theta$  and observation angle  $\phi$  interdependence according to Eq. (3.4)

At least one might get this impression from most recently published papers on jet noise in flight. The corresponding correction formula in the quadrupole model as originally derived by Ffowcs Williams [13],

$$\frac{\tilde{p}(\theta)}{\tilde{p}(\theta=90^\circ)} = \frac{1}{(1+M_s \cos \theta)^{1/2}} \frac{1}{(1-M_s \cos \theta)^{5/2}} \quad (3.5)$$

(i) Due to the forward speed ( $M_s = 0.373$  in our example) we expect a correspondingly reduced source convection Mach number

$$M_s = 0.65(M_j - M_s) \quad (3.3)$$

to become effective. This modifies the field shape according to Eq. (2.54) and Fig. 7 relative to its value at  $\phi = 90^\circ$ . The correspondingly corrected directivity pattern has its new maximum at  $60^\circ$  to the jet axis.

(ii) In a very crude first approximation, we may take this modified static field shape as a new datum that accounts for the varied aerodynamic conditions only. If the forward speed had no additional effects on the development of the mean flow and the turbulence structure of the jet, we have been plotted as a function of the angle  $\theta$  at the time of emission of the sound. This, however, is simply related to the instantaneous observation angle  $\phi$  by

$$\sin \theta = \sin \phi \sqrt{1 - M_s^2 \sin^2 \phi} + M_s \cos \phi \quad (3.4)$$

which is independent of the side-line distance  $r_0$  (compare sketch (b) of Fig. 12). With the aid of Eq. (3.4) or Fig. 14 we may replot Brooks's flight data and compare it with the modified static directivity characteristic in Fig. 13.

Despite of the very rough assumptions made the two directivities are amazingly similar in shape except for small angles to the jet axis. The philosophy behind our simple model is that we think that the jet flow as a whole should be considered as one more or less coherently radiating sound source as opposed to a model that assumes a large number of statistically uncorrelated and hence independently radiating turbulent eddies. In both models source convection is likely to have an important effect on the far field directivity. The simple source model seems to yield the correct trends for source convection and flight effects whereas the well known quadrupole model was apparently less successful.



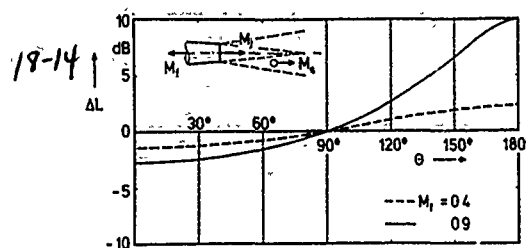


Fig. 15: Flight factor  $(1 + M_f \cos \theta)^{-1/2}$  according to Ref. [13].

seems to have been tried with little success.

The flight factor  $(1 + M_f \cos \theta)^{-1/2}$  is shown for comparison in Fig. 15. For moderate values of  $M_f$ , as in the example treated above, it can only account for a modification by less than 1 dB of the directivity between  $\theta = 60^\circ$  and  $120^\circ$ . The differences between the correction curves in Figs. 15 and 9 are even more pronounced for higher flight Mach numbers. Eq. (2.67) results in a strong amplification of the noise radiated in the forward quadrant (particularly at angles close to  $90^\circ$ ) and similarly strong attenuation in the rearward arc. Both effects were observed in a variety of static-to-flight comparisons but cannot be explained by the conventional correction factors.

So far we have considered the effect of source convection and forward speed on the field shapes only. No attempt was made to also estimate the effect of flight on the absolute intensity at a given point in the far field. This would require a more elaborate inspection of the source integral. Michalke and Michel [14], however, have only recently derived a new jet noise flight correction factor. This enables more than just a qualitative static-to-flight comparison; it also predicts the intensity variations with an unprecedented accuracy.

#### 4. AERODYNAMIC PRESSURE MEASUREMENTS IN TURBULENT FLOW

##### 4.1 The near field induced by convected flow inhomogeneities

Chapter 2 of these lecture notes dealt with linear perturbations of a fluid flow in the most general sense. The basic equations are equally valid for small aerodynamic fluctuations about a steady state as induced, for instance, by a moving source or sink. The laminar flow over a wavy boundary, the flow field induced by an isolated vortex or by a more or less regular vortex street shed from an obstacle in the flow would be some typical examples of unsteady aerodynamic flow fields of practical interest. In the limit of very slow variations in time ( $\omega \rightarrow 0$ ) or the medium being considered as *quasi-incompressible* ( $a_0 \rightarrow \infty$ ) we may concentrate on what was termed near field in the preceding sections.

In the radiated far field (Sections 2.3 and 2.4) we have, for obvious reasons, dealt with the acoustic pressure exclusively. The acoustic particle velocity  $v_p$  in the direction of propagation is always simply related to the local *acoustic pressure* by

$$p(x_1, t) = \rho_0 a_0 v_p(x_1, t) \quad (4.1)$$

(compare Eqs. (2.24), (2.25) and (2.31) for  $x_2 = \bar{x}_2$  and  $x_3 = \bar{x}_3$ ). In the aerodynamic near field, however, the interrelationship between unsteady pressure and velocity fields is far less obvious.

In countless studies of low subsonic ( $M = \bar{c}/a_0 \ll 1$ ), unsteady flow fields it has been assumed as a characteristic property of the *aerodynamic pressure* fluctuation that it is proportional to the *square* of the local velocity fluctuation in contrast to a sound field, in which the acoustic pressure is proportional to the *first power* of the velocity fluctuation (refer, e.g., to Ref. [5], Chap. 11.1, p. 703, and Chap. 11.4, p. 764). A relationship like

$$\bar{p} = \alpha \rho_0 \bar{v}^2, \quad (4.2)$$

where the twiddles denote statistical averages (r.m.s. values) and  $\alpha$  takes on values between 0.58 and unity, may be valid in the very special case of homogeneous, *isotropic* turbulence [15]. As an estimate of the pressure fluctuation in a real flow, however, Eq. (4.2) would require that the turbulent velocity perturbations be convected with the assumedly uniform flow, i.e. Taylor's hypothesis  $\partial/\partial t = -\bar{c}\partial/\partial x$  be strictly satisfied.

It is much more realistic, however, to assume that in real flows we have all kinds of inhomogeneities travelling at convection speeds  $\bar{u}$  which are somehow coupled to but need not be identical with the value of the mean flow speed,  $\bar{c} \neq \bar{u}$ . This is especially true when there is violent vortical motion in a region of high shear rates (as, e.g., in the mixing region of a jet, Fig. 16) which can induce disturbances in (i) the adjacent higher-velocity potential core region or (ii) the lower-velocity entrainment region. This is a situation very similar to that depicted in Fig. 2 of a source  $Q$  moving relative to both the flow and the observer.

In the near field of the source we may, according to Eq. (2.32) of Sec. 2.2, expect a *linear* relationship between the local streamwise velocity and pressure perturbations,

$$p(x_1, t) = -\rho_0 (\bar{c} - \bar{u}) v_1(x_1, t). \quad (4.3)$$

A similar relation would hold if, instead of a simple source, we had one of higher order of complexity and, instead of just a single point source, we had a series of sources, all travelling at the same constant speed  $\bar{u} \neq \bar{c}$  in the direction  $x_1$  of the mean flow  $\bar{c}$ . The pressure and velocity fields of convected vortices were discussed in some detail in Refs. [16] and [17].



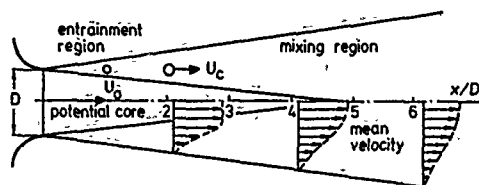


Fig. 16: Circular jet flow configuration.

Fluctuating pressure measurements were mostly restricted to the pressure field at solid flow boundaries where it is measurable with flush-mounted microphones [19].

Pressure probes for measuring the pressure fluctuations within the turbulent flow, on the other hand, have long been suspected of inevitably creating and subsequently receiving additional spurious pressure disturbances due to probe-flow interactions. Considerable efforts have been expended over the past ten years to show that acceptable pressure data may be obtained in a variety of flow configurations,

- Circular model jets [16, 20]
- Conical model jets [21]
- Two-stream plane shear layers [22]
- Two-dimensional wake behind cylinders [23-25]
- Axisymmetric wake behind disks [26]
- Turbulent duct flows [27]

#### 4.2 Possible sources of error in aerodynamic pressure measurements

Most of the above mentioned pressure measurements employed suitably shaped condenser microphone probes. A number of probe/flow interferences are conceivable which may render applications of this technique difficult:

- Acoustic contamination of the flow
- Resolution error due to finite transducer dimensions
- Flow-affected sensitivity of the microphone
- Acceleration response due to probe vibrations
- Probe-flow interaction noise
- Fluctuating cross flow error
- Response to axial velocity fluctuations

Some of these error mechanisms were described in some detail in Refs. [18], [28-30].

The cross-flow error, e.g., is due to the lateral velocity fluctuations  $v_n$  normal to the probe surface causing an unsteady stagnation pressure of the order

$$\bar{p}_e = \frac{1}{2} \rho_0 \bar{v}_n^2 \quad (4.5)$$

Although the magnitude of the error coefficient,  $|\beta|$ , should, according to Ref. [28], never exceed a value of 0.5, Eq. (4.5) confirms earlier suspicions that it is principally impossible to accurately measure pressures of the order  $\rho_0 \bar{v}^2$ . A probe that necessarily disturbs the flow at the measuring point would surely be inadequate for measuring the pressure in an isotropic turbulence field if this were governed by Eq. (4.2).

When dealing with highly anisotropic jet and wake flows, however, a more realistic estimate of the r.m.s. flow pressure can make use of the relation (4.3) yielding

$$\bar{p} = \gamma \rho_0 \bar{v}^2 \quad (4.6)$$

The new coefficient

$$\gamma = |1 - \bar{u}/\bar{c}| = |M_0/M| \quad (4.7)$$

can be estimated to lie between 0.2 and 0.5 corresponding to local convection speeds of the disturbances in the range

$$\frac{\bar{u}}{\bar{c}} = 0.5 - 0.8; \quad \gamma = 0.2 - 0.5 \quad (4.8)$$

depending on the specific flow under investigation. As a result of this relative motion between the flow and the aerodynamic inhomogeneities disturbing it we would not be surprised at all if the pressure coefficient

$$\frac{\bar{p}}{\frac{1}{2} \rho_0 \bar{v}^2} = 2\gamma \left( \frac{\bar{u}}{\bar{c}} \right)^{-1} \quad (4.9)$$

would exceed the critical value around unity by orders of magnitude depending on the local value of the flow turbulence level  $\bar{v}/\bar{c}$  which can be very small indeed!

In the special case of a frozen pattern of turbulence convected past the observer, it would be possible to describe a harmonic Fourier component by

$$v_1(x_1, t) = A \exp i\Omega(t - x_1/\bar{u}) \quad (4.4)$$

i.e. a coherent wave-like perturbation of the flow and obtain Eq. (4.3) from integrating the linearized equation of motion directly [18].

Experiments inside turbulent flows have until recently favoured the measurement of the mean and fluctuating velocity fields with highly sophisticated hot wire and Laser anemometers.

18-16 In order to ensure the validity of a measuring technique employing microphone probes inserted in the flow it is therefore essential to consider, first of all, the locally measured pressure coefficients  $\bar{p}/(1/2 \rho_0 \bar{v}^2)$  for a variety of flow configurations in which we are primarily interested.

#### 4.3 Survey of pressure coefficients measured in various shear flows

For low Mach number flows the aerodynamic pressure coefficient of Eq. (4.9) is always very small compared to the corresponding ratio in an acoustic wave field according to Eq. (4.1).

$$\frac{\bar{p}}{1/2 \rho_0 \bar{v}^2} = 2 \left( \frac{\bar{v}_r}{a_0} \right)^{-1} = 2M^{-1} \left( \frac{\bar{v}_r}{c} \right)^{-1} \quad (4.10)$$

Yet, it will be seen to exceed, by a considerable amount, the values of Sec. 4.1 for isotropic turbulence,

$$\frac{\bar{p}}{1/2 \rho_0 \bar{v}^2} = 2\alpha = 1.2 - 2.$$

The following collection of pressure and velocity data will commence with the results obtained in unbounded free shear layers. It is in this area where pressure measurements are most urgently needed in connection with certain aero-acoustic and turbulent-energy-transport phenomena, but where equally often pressure measuring devices have been suspected of being unreliable. The pressure intensity results will be reproduced as reported by several independent research groups employing highly dissimilar pressure probe geometries and sensing devices.

In each individual case where the r.m.s. pressure  $\bar{p}$  has been measured along with the local mean ( $U$ ) and fluctuating ( $\bar{v}$ ) velocities, the dimensionless pressure coefficient  $\bar{p}/(1/2 \rho_0 \bar{v}^2)$  will be evaluated.  $\rho_0$  is the mean density of the medium, which in all cases will be air at velocities  $U$  varying between 10 and 200 m/s. This pressure coefficient, which may be looked at as the ratio of potential to kinetic aerodynamic energy density, will always be plotted against the local (longitudinal) turbulence level  $\bar{v}/U$ . This way of presentation of the results will enable an easy comparison of the situation in free mixing layers with that in a variety of flow configurations with solid boundaries.

##### 4.3.1 Circular model jets

The first set of data was obtained with a condenser microphone and hot wire placed in the potential core region of a jet issuing from a vortex-filament nozzle with a contraction ratio of 200 cm/14 cm [18]. The results are shown in Fig. 17. The velocity was kept very low during this earlier study, as may be seen from Table 3, which supplements the figure by co-ordinating the symbols with the respective jet parameters. More recently, Armstrong [31] has extended the jet pressure measurements towards higher exit velocities in another jet facility which was also described in Ref. [18]. Only a few of his results are reproduced in Fig. 17, but for Mach numbers not exceeding 0.6 - 0.7 Armstrong found no dramatic changes in either the normalized intensity or structure of the turbulent pressure and velocity fields.

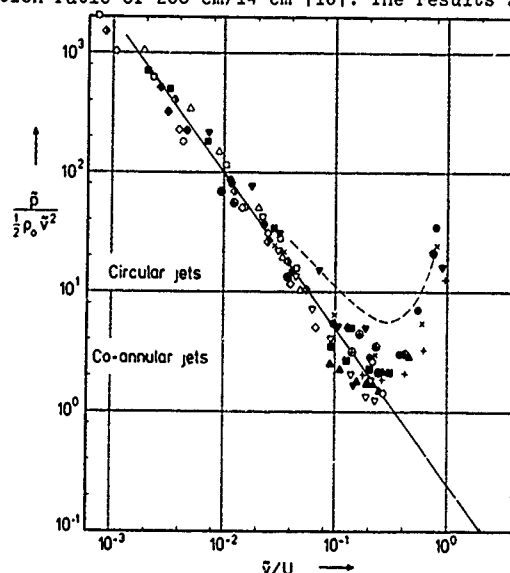


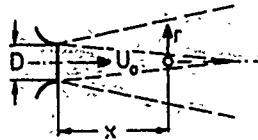
Fig. 17: Aerodynamic pressure coefficient versus local longitudinal turbulence level in circular and co-annular jet flows.

Nevertheless, their data fit quite well into the overall trends depicted in Fig. 17. The dashed line gives an average of their pressure and velocity results from several radial traverses at varying distances  $x$  from the jet exit.

Siddon [28] designed and tested a special pressure probe which enabled him to correct the detected pressure signal for the error due to the fluctuating cross-flow normal to the

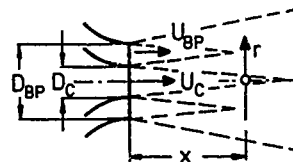
Planchon [20] at the University of Illinois in his jet pressure measurements employed a bleed-type pressure transducer, details of which were given by Spencer and Jones [33]. Although the design and operation of this transducer has little in common with the probe microphones preferred by our group, the results for the intensity and structure of the pressure field look promisingly similar (compare Fig. 17).

Sami et al. [32] appear to not have been convinced themselves that they were measuring the true r.m.s. turbulent pressures with their piezo-electric ceramic probe, which again differs considerably from the probes described above. Nevertheless,



## 1. Circular jets

Fuchs [18] D = 14 cm $10^5 < Re_D < 3 \cdot 10^5$	◇ r = 0 ◇ □ ◆ x = D ■	0.5 D < x < 5 D   0 < r < 0.5 D	U <sub>0</sub> = 10 m/s 20 30 20 30
Armstrong [31] D = 10 cm; Re <sub>D</sub> = 4 · 10 <sup>5</sup>	▽ r = 0	0 < x < 13 D	U <sub>0</sub> = 60 m/s
Planchon [22] D = 6.35 cm Re <sub>D</sub> = 4 · 10 <sup>5</sup>	△ r = 0 ○ 0.5 D ● λ = 1 D × 3 D + 10 D	D < x < 5 D D < x < 10 D 0 < r < 0.67 D 0 < r < 1.1 D 0 < r < 2.5 D	U <sub>0</sub> = 90 m/s
Sami et al. [32] D = 30 cm; Re <sub>D</sub> = 2 · 10 <sup>5</sup>	---	1 D < x < 10 D 0 < r < 1.5 D	U <sub>0</sub> = 10 m/s
Siddon [28] D = 10 cm; Re <sub>D</sub> = 3.3 · 10 <sup>5</sup>	⊞ x = 6 D	0 < r < 0.8 D	U <sub>0</sub> = 50 m/s



## 2. Co-annular jets

Hammersley [21] D <sub>C</sub> = 7.6 cm; D <sub>BP</sub> = 22 cm Re <sub>C</sub> = 7.8 · 10 <sup>5</sup> , 14 cm	▼ x = 1 D <sub>C</sub> ▲ 10 D <sub>C</sub> ⊕ 3 D <sub>C</sub>	0 < r < 2.2 D <sub>C</sub> 0 < r < 3.2 D <sub>C</sub> 0 < r < 1.6 D <sub>C</sub>	U <sub>C</sub> = 135 m/s U <sub>BP</sub> = 54 m/s
---	---	--	--

Table 3: Parameters of circular jets with and without secondary flow (symbols correspond to data points in Fig. 17).

probe's surface. Siddon's result obtained at  $x = 6 D$  for a 10 cm circular jet are also incorporated in Fig. 17 and Table 3.

## 4.3.2 Co-annular model jets

It is well known that a secondary flow passing by the primary flow as an annular jet, considerably modifies all three: the mean flow properties, the distribution of turbulent intensity and, hence, the noise generation. It is interesting to see whether the relative magnitude of the pressure and velocity fluctuations would also be altered by the by-pass flow.

Work done at Illinois University also provides valuable data in this respect. Hammersley [21] reports pressure and velocity data for the core (index C) and by-pass (BP) regions with by-pass ratios  $D_{BP}/D_C$  of the order of 2 or 3, respectively. For a constant velocity ratio  $U_{BP}/U_C$  equal to 0.4 the corresponding pressure coefficients have been plotted against  $v/U$  where  $U$  represents the local mean velocity as in the plain jet case.

The data of the plain and co-axial model jets are seen in Fig. 17 to follow the same overall trend for  $\bar{p}/(1/2 \rho v^2)$  to decrease as  $v/U$  increases from low to high turbulence levels. The pressure coefficient reaches a minimum close to one where the local turbulence reaches its maximum. This typically lies in the middle of the mixing layer of a single jet or in the middle of the two layers in the case of co-axial jets.

#### 4.3.3 Two-stream plane shear layer

18-18

After having discussed axisymmetric shear layers, we now turn to two-dimensional free shear layers. Spencer and Jones [22] have investigated the mixing of two parallel, uniform air streams with  $U_a > U_b$ . For measuring conditions as listed in Table 4, their pressure and velocity data are shown in Fig. 18. On the high-velocity side of the shear layer ( $\eta > 0$ ) the results follow the same trend as in the core region of a circular jet reaching

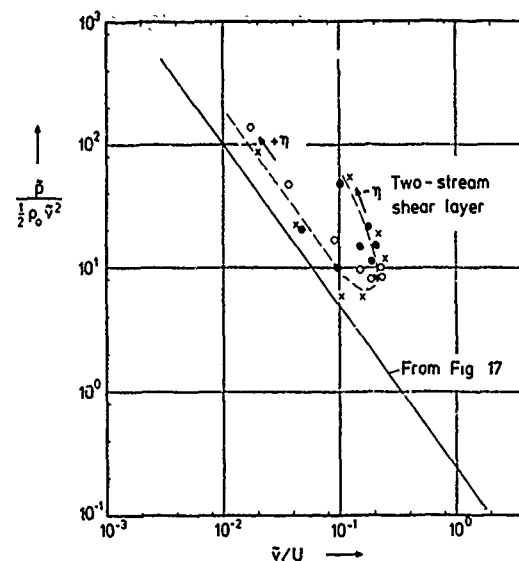


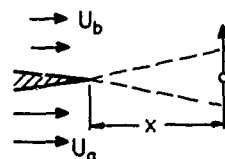
Fig. 18: Aerodynamic pressure coefficient versus local longitudinal turbulence level in free shear layers.

r.m.s. pressure  $\bar{p}$  is by far larger than that anticipated in Eq. (4.2) for isotropic turbulence. The last statement is especially true for measuring positions remote from the axis of symmetry ( $r = 0$ ) in the outer flow region.

pressure coefficients above 100. Again the higher values of  $\bar{p}/(1/2 \rho_0 \bar{v}^2)$  correspond to measuring positions remote from that region where the most intense turbulent mixing takes place. For the normalized lateral distance  $\eta = 0$ , a minimum of  $\bar{p}/(1/2 \rho_0 \bar{v}^2) > 5$  is reached for  $\bar{v}/U$  between 0.15 and 0.20. Similarly, as in the jet experiments, the pressure coefficient increases again on the low-velocity side ( $\eta < 0$ ) of the shear layer reaching values of 50 and more. In contrast to the jet entrainment region, the latter correlate with lower turbulence levels since a slowly decreasing  $\bar{u}$  is divided by  $U$  approaching  $U_b$  instead of  $U$  approaching zero in the jet case.

#### 4.3.4 Axisymmetric wake behind circular disk

Only most recently we have started measuring the aerodynamic pressure field in the wake of a circular disk in a large free jet wind tunnel [26]. The normalized intensity plots in Fig. 19 show quite an amazing similarity with the conditions in jet flows as indicated by the straight line (from Fig. 17). The wake results, so far, look very promising in that they seem to reveal a remarkably different large scale unsteady flow structure when compared to that of turbulent jets. It may suffice here to note that, again, the



Two-stream plane shear layer

Spencer & Jones [22]	$x = 10 \text{ cm}$	$-0.06 < \eta < +0.06$	$U_a = 30 \text{ m/s}$
$U_b/U_a = 0.3$	●	17.8	
	○	127	

Table 4: Parameters of two-dimensional free shear layers (symbols correspond to data points in Fig. 18).

$\bar{p}/(1/2 \rho_0 \bar{v}^2)$  as a function of  $\bar{v}/U$ . The corresponding data points in Fig. 19 lie very close to the results valid for axisymmetric jets and wakes.

This coincidence of the jet and wake situations is confirmed if one replots in our unified form Strasberg's results which he obtained at  $x = 24 D$  where the turbulence level is higher by a factor of two, at least. His result apparently remained constant for considerably varying flow parameters (compare Table 4). These far-wake results 42 D and 24 D downstream may be accomplished by a single measurement of Maekawa et al. [25] close to a cylinder at  $x = 2.3 D$ . All three 2d-wake investigations employed different, partly home-made, probe microphones with a ball-shaped nose and the pressure-sensing holes (or ring slit) about 2.5 (or 5) probe diameters away from the tip.

#### 4.3.6 Fully developed turbulent duct flows

The fully developed turbulent flow in long ducts may be considered as intermediate between free and attached shear layers. Neise [27], when determining the turbulent background noise for sound measurements in hard-walled, circular ventilating ducts, obtained pressure

#### 4.3.5 Two-dimensional wake behind circular cylinders

Kobashi [23], in what is one of the earliest studies of aerodynamic pressure fluctuations, measured intensity profiles at 42 D downstream of a circular cylinder. If, in his Fig. 16,  $k$  is approximately taken as  $\bar{p}$  and the dimensions of this as  $\text{kg/ms}^2 = \text{N/m}^2$  (instead of  $\text{kg/m}^2$  as written at the ordinate), one may again evaluate

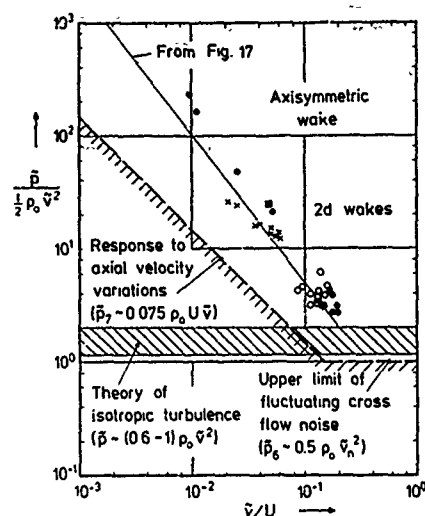


Fig. 19: Aerodynamic pressure coefficient versus local longitudinal turbulence level in axisymmetric and two-dimensional wake flows. For comparison: pressure according to Eqs. (4.5), (4.11), and (4.16).

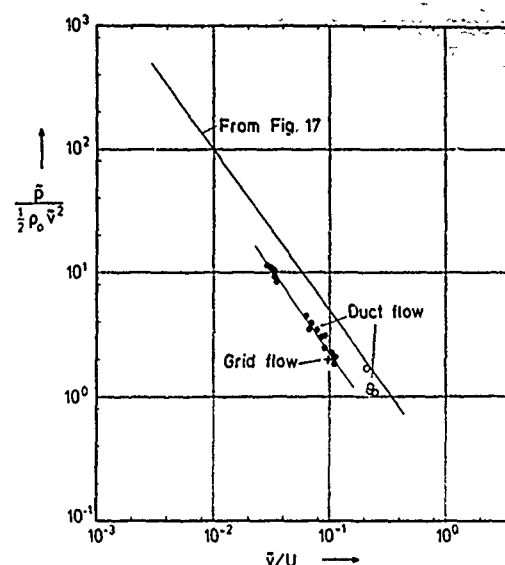
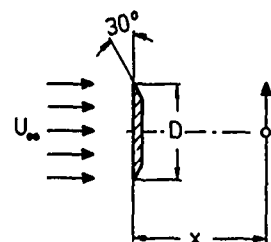
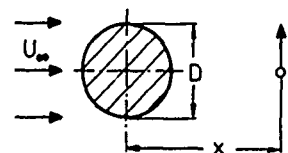


Fig. 20: Aerodynamic pressure coefficient versus local longitudinal turbulence level in various duct flows.



#### 1. Axisymmetric wake behind circular disk

Fuchs et al. [26]	● $x = 3 D$ $0 < r < 2.5 D$	$U_\infty = 15 \text{ m/s}$
$D = 5 \text{ cm}, Re_D = 5 \cdot 10^4$	○ $r = 0$ $0.25 D < x < 7 D$	

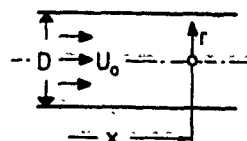


#### 2. Two-dimensional wake behind circular cylinders in a cross flow

Kobashi [23]	× $x = 42 D$ $-4 D < r < +4 D$	$U_\infty = 14 \text{ m/s}$
$D = 1 \text{ cm}, Re_D = 10^4$		
Strasberg [24]	⊠ $x = 24 D$ $r = 0.5 D$	$4 < U_\infty < 24 \text{ m/s}$
$2.5 < D < 10 \text{ cm}, 6 \cdot 10^3 < Re_D < 1.6 \cdot 10^5$		
Maekawa et al. [25]	⊙ $x = 2.3 D$ $r = 1.75 D$	$U_\infty = 9.7 \text{ m/s}$
$D = 2 \text{ cm}, Re_D = 1.3 \cdot 10^4$		

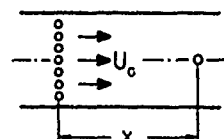
Table 5: Parameters of axisymmetric and of two-dimensional wake flows (symbols correspond to data points in Fig. 19).

and velocity coefficients which are depicted in Fig. 20. Comparison with the jet data indicated by the upper solid line shows that the duct values for  $\bar{p}/(\frac{1}{2} \rho_0 \bar{v}^2)$  lie just a little below the former. This may, according to Eqs. (4.8) and (4.9), be indicative of the convection speeds in duct turbulence to exceed the values of  $\bar{u}/\bar{c}$  in the initial region of a jet.



## 1. Fully developed channel flow

Neise [19]	● $x = 40 D$ $0 < r < 0.5 D$	$U_0 = 40 \text{ m/s}$
$D = 15.3 \text{ cm}$ ; $Re_p = 4 \cdot 10^5$	○ $x = 5 D$	



## 2. Grid generated turbulence

Siddon [10], meshes: $4.5 \times 7 \text{ cm}^2$	$+ x \approx 3 \text{ m}$	$U_0 = 21 \text{ m/s}$
--	---------------------------	------------------------

Table 6: Parameters of ducted flows (symbols correspond to data points in Fig. 20).

## 4.3.7 Grid generated turbulence

Siddon [28] also reported pressure intensity profiles in a rectangular channel flow. The results lie close to Neise's. In addition, Siddon measured aerodynamic pressure and velocity fluctuations in a wind tunnel far downstream of a coarse grid which was especially built into the upstream end of the diffuser section to generate a homogeneous and approximately isotropic turbulence field in the test section. The combination of  $\bar{p}/(1/2\rho_0 v^2) = 2$  and  $v/U \approx 0.1$  lies close to the duct data measured near the walls.

## 4.4 Limitations on measuring techniques employing inserted microphone probes

In the preceding Sec. 4.3 we have plotted normalized pressure and velocity coefficients for a variety of selected flows. For similar plots of data from bounded flows (e.g. wall jets and boundary layers) refer to Ref. [34]. Figs. 17-20 allow a rough estimate of the fluctuating pressure intensity  $\bar{p}$  from what is usually termed "turbulence level",  $v/U$ , and from the respective mean flow velocity  $U$  at the measuring position.

The normalized pressure coefficient  $\bar{p}/(1/2\rho_0 v^2)$  as measured with inserted microphone probes may tentatively be compared with the results in Eqs. (4.6) through (4.9) from our simple linearized analysis of convected flow inhomogeneities. The conjectural coefficient  $\gamma$  comes very close to what one might expect as corresponding convection speeds  $U_c/U \approx |1-\gamma|$  in these flows (compare Table 7). The duct flow estimate,  $0.82 < U_c/U < 0.9$ , agrees very well indeed with measured convection speeds in such turbulent flows. The relatively high

Jet Flows	$0.1 < \gamma < 0.9$	$0.1 < U_c/U < 0.9$
Wake Flows	$0.16 < \gamma < 1.0$	$0 < U_c/U < 0.84$
Duct Flows	$0.1 < \gamma < 0.18$	$0.82 < U_c/U < 0.9$

Table 7: Conjectured convection speeds when results of Figs. 17, 19, and 20 are interpreted as due to convected flow inhomogeneities.

pressure coefficients yielding the extremely low  $U_c/U$  values in Table 7 correspond (i) to the fluctuations in the so-called potential core close to the jet exit and (ii) to the outer flow regions far remote from the wake ( $r = 2.5 D$ ). Inside the actual wake and jet mixing regions the conjectural values for  $U_c/U$  vary between 0.6 and 0.8 in excellent agreement with convection speeds measured there.

It is noted, however, that this oversimplified model can only be regarded as a first, qualitative approach aimed at a better understanding of aerodynamic pressure fields in turbulent flow. It may help explain why pressure intensity levels exceed those expected for isotropic turbulence by orders of magnitude in more realistic flow situations. Before more comprehensive studies of the aerodynamic pressure fields can be undertaken, one would like to know the possible limitations imposed on the probe microphones measuring technique by the error mechanisms discussed under Sec. 4.2:

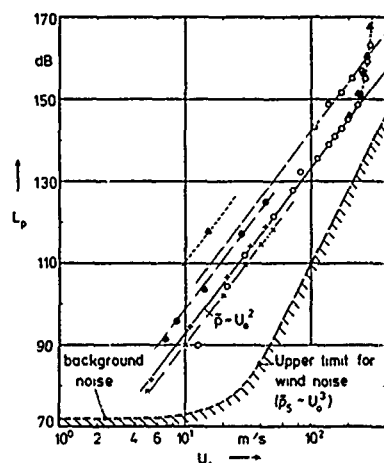
## 4.4.1 Acoustic contamination of the flow

The effects of an externally applied sound field on the flow are twofold. The first is quite obvious; when acoustic pressure disturbances are superimposed, with the flow acting as its carrier in a strictly passive manner, the sound pressure level  $L$  ought to lie sufficiently far (say, 10 dB) below the equivalent aerodynamic flow pressure level  $L_p$ ,

$$L_p = 20 \log \bar{p}/\bar{p}_0, \quad (4.12)$$

where  $\bar{p}_0 = 2 \cdot 10^{-5} \text{ N/m}^2$  is the same reference pressure as for the sound pressure level. Otherwise  $L$  would contribute to  $L_p$  or even mask the pressure fluctuations to be measured.

Fig. 21 may be used for a first estimate of what pressure levels  $L_p$  are to be expected as a function of characteristic flow velocity  $U_0$  in jet, wake, and duct flows mainly considered here. With the equivalent flow pressure levels as high as 97 to 117 dB at a flow velocity as low as 15 m/s, in the present experiments this kind of an acoustic contamination could safely be excluded. Sound pressure levels of the order indicated by Fig. 21 are extremely unlikely even in relatively noisy flow facilities occasionally used in practice.



Armstrong et al. [42]

$D = 5 \text{ cm}$

Lau [39];  $D = 5 \text{ cm}$

Fuchs et al. [26]

Neise [27]

(increased turbulence level)

- $x = 2 D, r = 0$
- $x = 3 D, r = 0.5 D$
- △  $x = 2 D, r = 0$
- ▲  $x = 3 D, r = 0$
- ×  $x = 40 D, r = 0$
- +  $r = 0.25 D$
- $x = 5 D, r = 0.225 D$

Fig. 21: Aerodynamic pressure fluctuation level in various turbulent flows. For comparison: wind noise level according to Eq. (4.13).

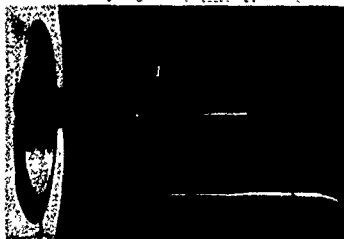


Fig. 22: Fluctuating pressure measuring probes with built-in B&K condenser microphones fitted with nose cones ( $d = 1/4 \text{ in.}$  and  $1/8 \text{ in.}$ )

low. In our own jet and wake experiments [18, 26], where we have preferably used 1/8-inch Bruel & Kjaer condenser microphones fitted with nose cones (Fig. 22), we came to the conclusion that this type of resolution error was practically absent. This may not surprise after these flow fields have been found to be dominated by large-scale coherent turbulence structures.

#### 4.4.3 Flow-affected sensitivity of the microphone

Pressure sensitivity and frequency response of microphones are usually calibrated for sound waves impinging at an individual (or random) angle of incidence to the probe axis with the medium (usually air) otherwise at rest. It is conceivable that these response characteristics are affected in the presence of flow. One knows, e.g., that the acoustic impedance of perforated walls is affected by turbulent grazing flow [36]. Both amplitude and phase of the measured acoustic or aerodynamic pressures could thus be adulterated.

Neise [37] determined exactly how large the effect of flow is on the pressure sensitivity of probe microphones of the kind used for in-flow pressure measurements. He showed that there is a measurable loss in sensitivity due to the air flow. It does, however, not exceed 0.5 dB for low subsonic flow velocities in a frequency range between 40 and 1250 Hz. Fig. 23 shows the results and a schematic of the test set-up in which a reference microphone was mounted flush with the duct wall. Unfortunately, these experiments could not be carried out for flow velocities beyond 40 m/s, a value which is typical of fan noise measurements in ventilating ducts [38].

A second effect of acoustic contamination is far less obvious; the flow, apart from carrying the sound waves, may actively respond to acoustic disturbances however small these may be. This is undoubtedly the case whenever the flow goes through a transition from a laminar to a turbulent state like in a jet at lower Reynolds numbers. Use has, in fact, been made of this in especially devised experiments; a sound field of a certain frequency may be used to trigger the flow disturbances in the initial shear layer near the jet nozzle lip. In these artificially excited aerodynamic pressure waves which then travel downstream in the steadily broadening jet shear layer, the randomness as typical of the naturally occurring fluctuations has been removed. Acoustically seeding or forcing of a jet flow may even, in certain circumstances, facilitate investigations into the aerodynamic pressure field [35].

#### 4.4.2 Resolution error due to finite transducer dimensions

As is well known from wall pressure measurements underneath turbulent boundary layers [19] it is of the utmost importance that the size of the pressure sensing transducer element be sufficiently small to obtain optimum resolution. This is warranted only when the dimensions of the pressure sensing area are small compared with the characteristic scale of the pressure field. Otherwise the pressure is measured too



18-22

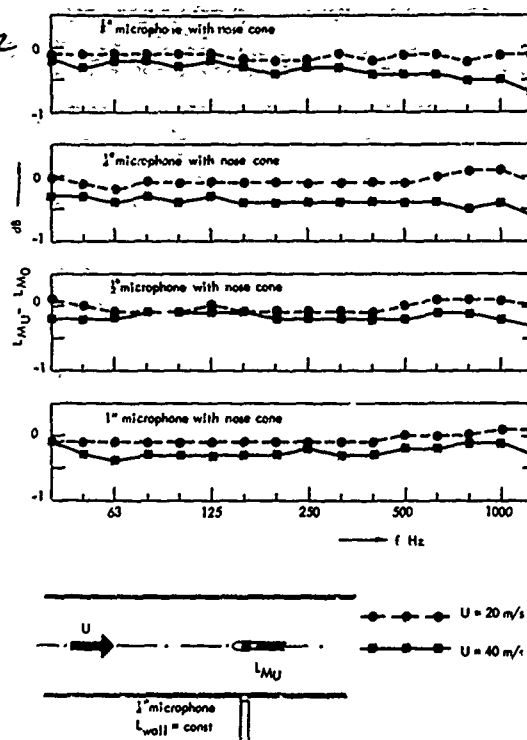


Fig. 23: Change of acoustic sensitivity of microphone probes of the type shown in Fig. 22, after [37].

and aircraft to move the microphone probe through assumedly undisturbed air. None of these, however, is reckoned to have yielded the absolute minimum wind noise level. We conclude this from measurements in one of our high contraction ratio free jet facilities (Fig. 22). A reasonably quiet, low turbulence ( $\bar{v}/U_0 < 0.005$ ), parallel flow is generated in the jet exit plane. If the above described 1/8, 1/4, 1/2, and 1 inch microphone probes are inserted there, they measure pressure levels below those previously reported as wind noise at the respective flow velocities provided the probes are carefully aligned with the flow and fitted with the standard nose cones. Considerably higher noise levels are measured with the nose cones replaced by the standard protection grids. For the time being, we may therefore take these pressure levels as the upper limit for the wind noise for as long as no lower pressure levels are found in, possibly, even quieter flow situations.

The respective signal-to-noise ratio for aerodynamic pressure measurements in jet, wake, and duct flows may, on this basis, be seen in Fig. 21 to deteriorate with the flow velocity. This is because this type of wind noise increases with approximately the third power of  $U_0$ ,

$$\bar{p}_n \sim U_0^3 \quad (4.13)$$

whereas the aerodynamic pressure, from all we know, scales on  $\rho \cdot U_0^2$ ,

$$\bar{p} \sim \rho \cdot U_0^2 \quad (4.14)$$

for not too high flow Mach numbers  $M$ . The reason for the wind noise level in Fig. 21 to level off for  $U_0 < 30$  m/s is the acoustic background noise in the test room contaminating the pressure measurements in the jet exit plane at these very low velocities.

Another, very important probe-flow interaction effect becomes evident at very high subsonic flow velocities. For  $U_0 > 220$  m/s corresponding to  $M_0 > 0.6$  the jet results for  $r = 0$ ,  $x = 2D$  in Fig. 21 show quite a dramatic deviation from the dependence indicated by Eq. (4.14). This effect, which does not occur in the data obtained at  $r = 0.5D$ , was also found by Lau [39] in a completely different jet facility (compare the triangles in Fig. 21).

No really conclusive explanation of this probe-flow interaction effect can be given here. But there is sufficient evidence that when an obstacle like the probe microphone is inserted in the high velocity jet core flow this may generate both additional flow disturbances and noise in excess of what is experienced with the unperturbed jet. The former

#### 4.4.4 Acceleration response due to probe vibrations

Another possible source of error may have its origin in the response of the microphone built into the pressure probe to possible flow-induced probe vibrations. The unsteady flow around the body can in certain cases excite vibrations thus simulating pressure fluctuations in the microphone output. In our own experiments we had no problem avoiding critical probe vibrations by mounting the microphones on fairly rigid home-made holders as seen on Fig. 22. Small lateral oscillations of the probe tips which became visible at higher flow velocities do not seem to have caused spurious pressure signals.

#### 4.4.5 Probe-flow interaction effects

Even if the pressure probes were made ideally rigid and the on-coming flow perfectly laminar, one can still imagine a variety of mechanisms by which pressure perturbations may be created. Two of these mechanisms depend on the geometry and relative motion of the probe alone: Firstly, a wake is formed behind the probe, and secondly, a boundary layer develops along the probe surface. Both flow phenomena may, in principle, induce pressure fluctuations on the probe itself if no other unsteadiness is present. Part of these self-induced disturbances may also be registered as noise by the microphone dependent on the position of the pressure sensor thus limiting the measurement of the wanted aerodynamic or acoustic pressure.

A number of attempts were made to determine this kind of a "wind noise" due to the flow around the probe. They employed rotating booms, ground vehicles



may give rise to upstream travelling pressure waves which, under certain conditions, help building up a feedback loop with the downstream travelling jet instability waves. This phenomenon was thoroughly studied by Neuwerth [40]. The latter effect was occasionally observed in jet noise far field investigations, especially in so-called "causality (near field/far field) correlations" [41].

18-23

It is quite clear from considerations like those in Sec. 2.4.3 that any acoustic disturbances emanating from the probe will be amplified in the upstream direction as was illustrated by Fig. 9. For flow Mach numbers  $M_0$  approaching unity this amplification plus the onset of a strong feedback mechanism may well explain an increase in measured aerodynamic pressure fluctuation levels which is primarily due to the measuring probe sitting in and interacting with the flow around it in a way which becomes critical at  $M_0 > 0.6$ .

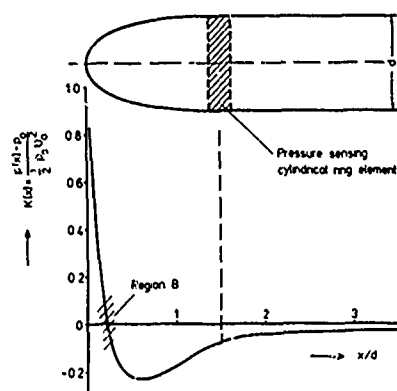
It is, however, pointed out here that a similarly strong probe-flow interaction effect does not occur at  $M_0 < 0.6$  and that measurements at higher jet exit velocities,  $U_0 > 220$  m/s, seem not to have been affected if performed with the probe positioned in the mixing region (the squares in Fig. 21) where the local mean flow Mach number stays below 0.6 even when  $M_0$  approaches unity.

#### 4.4.6 Fluctuating cross flow error

This error mechanism has already been discussed in Sec. 4.2. Let us assume that  $\bar{v}_n$ , the flow velocity fluctuations normal to the probe surface, to be of the same order of magnitude as  $\bar{v}$ , the axial velocity component. We may then conclude from Figs. 17 through 20 that the measured pressure exceeds the critical value of Eq. (4.5) by orders of magnitude except for those flow situations providing conditions for nearly isotropic turbulence (e.g., the in-duct results downstream of a grid or perforated orifice in Fig. 20). In Fig. 19 we have indicated both limits for isotropic turbulence and for the fluctuating cross flow error.

#### 4.4.7 Response to axial velocity fluctuations

We are left with one last possible source of error which may be due to yet another unsteady flow/probe interference effect. To understand this effect in principle, consider a steady (or slowly varying) potential flow about a stream-lined body simulating the



microphone probe as aligned with the mean flow direction (Fig. 24). Only in a limited region B on the surface of the body will the pressure  $p_B$  be approximately equal to the undisturbed static pressure  $p$  in the flow. Exterior to that distinguished area the pressure differs from  $p$  and similarly a fluctuating pressure there cannot in general be expected to equal that at the measuring position in the flow before the insertion of the probe.

The effect of variations in the axial flow velocity on the pressure fluctuations on the probe surface was estimated in Ref. [18] for both acoustic and aerodynamic pressure measurements with inserted microphones. In this analysis the geometry of the probe, particularly its diameter  $d$ , played an important role. In the limit

$$d \ll \lambda_x,$$

where  $\lambda_x$  is the axial scale of the aerodynamic pressure inhomogeneities (or the wave length  $\lambda$  in the case of a sound wave propagating in the axial direction) two special cases may be considered here;

Fig. 24: Pressure distribution for quasi-steady, symmetric flow around the pressure probe [18].

##### (a) Acoustic pressure at the probe tip

$$fd/a_0 = d/\lambda \ll 1; \quad \bar{p}_A/\bar{p} = 1 + M_0. \quad (4.15)$$

For Mach numbers approaching unity the sound pressure level may thus be measured too high by up to 6 dB due to the response of the probe at  $x = 0$  to the acoustic particle velocity of the incident sound wave. At any other point on the probe surface this error would be much less.

##### (b) Aerodynamic pressure at cylindrical ring element (Fig. 24)

One could think of designing a probe with pressure holes located exactly where the mean static pressure  $p_B$  just equals  $p$  in the undisturbed flow. In practical situations with turbulence levels over 10%, however, the instantaneous flow direction would continuously change with time. This would shift the zero crossing of the pressure distribution on the probe surface and result in considerable stagnation pressures in that particular region B. The small negative pressure at the cylindrical ring element shown in Fig. 24, on the other hand, has the advantage of not varying too much with the angle of incidence. For the profile chosen to imitate a standard B&K nose cone, of the old type, the error due to axial velocity variations was roughly estimated in Ref. [18] as

18-24

provided that

$$\frac{\bar{p}_r}{\frac{1}{2} \rho_0 \bar{v}^2} \approx 0.15 \left( \frac{\bar{v}}{\bar{u}} \right)^{-1} \quad (4.16)$$

$$\frac{d}{\Lambda_x} = \frac{f d}{\bar{u}} = \frac{f D}{U_0} \frac{U_0}{\bar{u}} \frac{d}{D} \ll 1 \quad (4.17)$$

and  $\bar{p}$  and  $\bar{v}$  are approximately related according to Eq. (4.6).

The estimate (4.16) was used in Fig. 19 to indicate a possible error response involved in measurements of aerodynamic pressures of the type discussed in Sec. 3. For feasible ways of further minimizing this "nose curvature error", in cases where  $\bar{p}$  should not dominate over  $\bar{v}$ , of Eq. (4.16), refer to Refs. [18, 28].

#### 5. AERODYNAMIC PRESSURE FIELDS IN WAKES AND IN JETS

In Sec. 4.4 we have given a detailed description of the error mechanisms involved in measuring aerodynamic pressure fluctuations with inserted microphone probes. From the survey of pressure data in Figs. 17 through 19 we may conclude that in free shear layers the pressure measurements are most likely unaffected by possible probe-flow interferences. The validity of the measuring technique for practically important jets and wakes has enabled extensive investigations into their unsteady flow fields. These have helped reveal certain large-scale coherent turbulence phenomena which could not be identified in earlier studies employing, e.g., hot-wire probes in the mixing region of turbulent jets. Characteristic structures were found to exist in these flows which do not fit into conventional concepts of turbulent eddies be they small or large. A large portion of the turbulence in circular jets and wakes, for instance, can much better be described by a very pronounced, three-dimensional wave field propagating with the mean flow.

As these, purely aerodynamic, wave structures have recently gained interest in the field of experimental and theoretical aeroacoustics, we may briefly mention how these

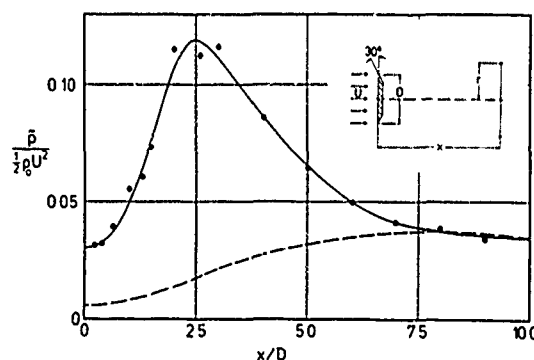


Fig. 25: Normalized pressure intensity  $\bar{p}/(1/2 \rho_0 U^2)$  in a circular wake (—) and jet (---).  $r=0$

waves behave in terms of the r.m.s. pressure associated with them. Fig. 25 shows the downstream development of the pressure level  $\bar{p}/(1/2 \rho_0 U^2)$  along the centre-line of (a) the axisymmetric wake behind a circular disk and (b) the axisymmetric free jet.

Particularly strong pressure pulsation levels of up to 12 % of the (mean) total head pressure  $1/2 \rho_0 U^2$  are realized around  $x = 2.5 D$  in the downstream stagnation point region behind the disk. This amazingly high unsteadiness in the aerodynamic pressure field in a wake becomes an even more important factor in unsteady aerodynamics as we now know that these pressure oscillations occur coherently over the whole of the wake in the lateral as well as in the longitudinal directions [26].

The jet pressure waves show a comparatively smooth increase in the initial

jet region up to a level below 4 % and (not shown in Fig. 25) a gradual decay in the transition region. Far downstream the jet and wake pressure fields seem to be comparable in strength. On the disk surface, on the other hand, the fluctuating pressure remains considerably above that in the jet exit plane (about 3 % as compared to 0.6 %, respectively). This pressure will, of course, exert an unsteady aerodynamic force on the disk and cause the jet thrust to fluctuate, too.

We conclude this short excursion into the field of unsteady aerodynamics with Fig. 26. This shows that for both flows the linear relationships Eqs. (4.6) through (4.8) provide a fairly acceptable model for the pressure and axial velocity fluctuations. One would estimate axial phase velocities of the order

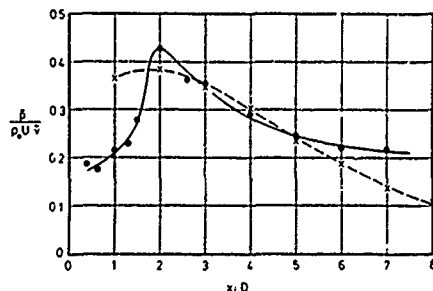


Fig. 26: Dimensionless ratio  $\bar{p}/\rho_0 U \bar{v}$  in a circular wake (—) and jet (---).

$$\frac{\bar{u}}{\bar{U}} = 0.6 - 0.9$$

in rough agreement with corresponding measurements [31]. It is noted, however, that a simple model like that leading to Eq. (4.6) cannot be regarded as a substitute for necessarily more comprehensive studies of the individual pressure field characteristics of the flows so briefly described in Sec. 4.3.

## 6. SOUND PRESSURE MEASUREMENTS IN TURBULENT FLOW

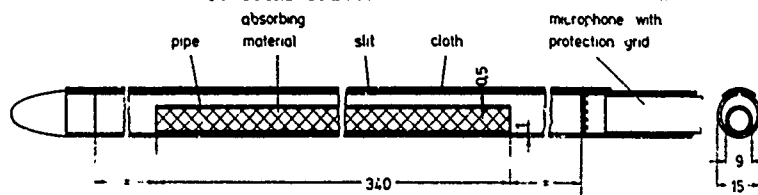


Fig. 27: Schematic of a slit-tube microphone probe for sound measurements in turbulent flow [43].

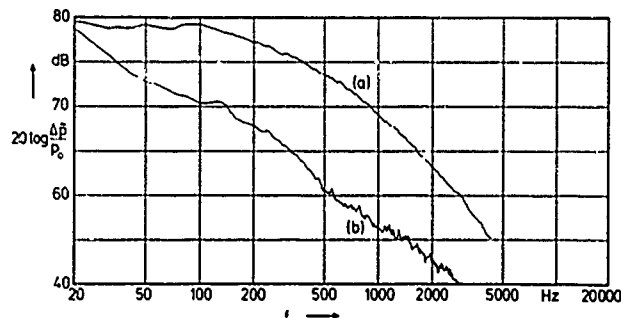


Fig. 28: Turbulent flow pressure spectra measured in a duct by means of a 1/2-in. B&K condenser microphone (a) with nose cone (b) with slit tube [43].  
 $U_0 = 20$  m/s, 15 % turbulence level,  
 $r = 0$ ,  $x = 5 D$ ,  $\Delta f = 10$  Hz.

purpose, Neise [27] has developed a slit-tube microphone probe a cross-sectional view of which is shown in Fig. 27. It enables a suppression of the turbulent flow pressure by more than 12 dB over a broad range of frequencies as long as the duct flow Mach number is low enough (Fig. 28).

Since we have no space here to discuss this important measuring procedure in depth the interested reader may refer to Neise's most recent paper [43]. There he may also find recommendations how one can check the validity of this technique in cases where the flow turbulence level cannot be measured separately.

In Chapters 4 and 5 we have discussed in-flow probe measurements of the true flow pressure field assumed not to be contaminated by any spurious pressure fluctuations as due to internal or external sound sources. Other

aeroacoustic problems require the measurement of sound pressure fields superimposed on a turbulent flow, e.g., in model experiments in wind tunnels or when sound propagation in ventilating ducts is to be studied. It is then necessary to not only avoid any kind of probe/flow interference generating extra noise but also suppress the detection of the above described aerodynamic pressures already present in the flow before the insertion of the probe. The latter can be seen in Fig. 21 to reach remarkably high pressure levels.

To give an example, the in-duct method for determining the sound power generated by turbo-machines [38] requires that the unwanted flow pressure level be reduced as much as possible in order to achieve an optimum signal-to-noise ratio for the sound measurements. For this

purpose, Neise [27] has developed a slit-tube microphone probe a cross-sectional view of which is shown in Fig. 27. It enables a suppression of the turbulent flow pressure by more than 12 dB over a broad range of frequencies as long as the duct flow Mach number is low enough (Fig. 28).

## REFERENCES

- [1] Fuchs, H.V.: "Basic aerodynamic noise theory", AGARD-VKI Lecture Series No. 80 (1977), "Aerodynamic Noise", Paper 2.
- [2] Fuchs, H.V.: "Fluctuations in a uniform moving medium originating from convected sources", Univ. Southampton, ISVR Memo. 280 (1969).
- [3] Goldstein, M.E.: "Aeroacoustics", McGraw-Hill (1976), NASA SP-346 (1974).
- [4] Morfey, C.L.: "The sound field of sources in motion", J.S.V. 23 (1972), 291-295.
- [5] Morse, P.M.; Ingard, K.U.: "Theoretical Acoustics", McGraw-Hill (1968).
- [6] Lush, P.A.: "Measurements of subsonic jet noise and comparison with theory", J. Fluid Mech. 46 (1971), 477-500.
- [7] Jones, I.S.F.: "Aerodynamic noise dependent on mean shear", J. Fluid Mech. 33 (1968), 65-72.
- [8] Lighthill, M.J.: "Sound generated aerodynamically", Proc. Roy. Soc. London, Ser. A, 267 (1962), 147-182.
- [9] Strout, F.G.; Attencio, A.: "Flight effects on JT8D engine jet noise as measured in the NASA AMES 40 x 80-foot wind tunnel", AIAA Paper 76-556 (1976).

- 18-26
- [10] Brooks, J.R.: "Flight noise studies on a turbojet engine using microphones mounted on a 450 ft tower", AIAA-Paper 77-1325 (1977).
  - [11] Drevet, P.; Duponchel, J.P.; Jacques, J.R.: "The effect of flight on jet noise as observed on the Bertin aerotraine", J. Sound Vib. 54 (1977), 173-201.
  - [12] Stone, J.R.: "Prediction of in-flight exhaust noise for turbojet and turbofan engines", Noise Control Engin. 10 (1978), 40-46.
  - [13] Ffowcs Williams, J.E.: "Some thoughts on the effects of aircraft motion and eddy convection on the noise from air jets", Univ. Southampton, U.S.A.A. Rep. 155 (1960).
  - [14] Michalke, A.; Michel, U.: "Relation between static and in-flight directivities of jet noise", J. Sound Vib. 63 (1979), 602-605.
  - [15] Batchelor, G.K.: "Homogeneous turbulence", Cambridge University Press (1953).
  - [16] Lush, P.A.: "The pressure and velocity fields of convected vortices", J. Sound Vib. 27 (1973), 266-270.
  - [17] Fuchs, H.V.: Comments on "The pressure and velocity fields of convected vortices", J. Sound Vib. 30 (1973), 249-251.
  - [18] Fuchs, H.V.: "Measurement of pressure fluctuation within subsonic turbulent jets", J. Sound Vib. 22 (1972), 361-378.
  - [19] Willmarth, W.W.: "Unsteady force and pressure measurements", Ann. Rev. Fluid Mech. 3 (1971), 147-170.
  - [20] Planchon, H.P.: "The fluctuating static pressure field in a round jet turbulent mixing region", Univ. Illinois, Ph. D. Thesis (1974).
  - [21] Hammersley, R.J.: "An experimental investigation of the turbulent characteristics of co-annular jets and their role in aerodynamic noise generation", Univ. Illinois, Ph. D. Thesis (1974).
  - [22] Spencer, B.W.; Jones, B.G.: "Statistical investigation of pressure and velocity fields in the turbulent two-stream mixing layer", AIAA-Paper 71-613 (1971).
  - [23] Kobashi, Y.: "Measurements of pressure fluctuation in the wake of cylinder", J. Phys. Soc. Japan 12 (1957), 533-543.
  - [24] Strasberg, M.: "Measurements of fluctuating 'static' and total-head pressure in turbulent wake", AGARD Rep. 464 (1963).
  - [25] Maekawa, T.: "Pressure fluctuation measuring apparatus with condenser microphones", Proc. 15th Japan Nat. Congr. Appl. Mech. (1965), 159-163.
  - [26] Fuchs, H.V.; Mercker, E.; Michel, U.: "Large scale coherent structures in the wake of axisymmetric bodies", J. Fluid Mech., 93 (1979), 189-211.
  - [27] Neise, W.: "Einfluß der Mikrofonumströmung bei der Messung von Ventilatorgeräuschen im angeschlossenen Kanal", Techn. Univ. Berlin, Dissert. (1973).
  - [28] Siddon, T.E.: "On the response of pressure measuring instrumentation in unsteady flow", Univ. Toronto, UTIAS Rep. 136 (1969).
  - [29] Lau, J.C.; Fisher, M.J.; Fuchs, H.V.: "The intrinsic structure of turbulent jets", J. Sound Vib. 22 (1972), 379-406.
  - [30] Lush, P.A.: "Errors in static pressure measurements by probes in a fluctuating flow", J. Sound Vib. 26 (1973), 429-431.
  - [31] Armstrong, R.R.: "Einfluß der Machzahl auf die kohärente Turbulenzstruktur eines runden Freistrahls", Techn. Univ. Berlin, Dissert. (1977).
  - [32] Sami, S. et al.: "Jet diffusion in the region of flow establishment", J. Fluid Mech. 27 (1967), 231-252.
  - [33] Spencer, B.W.; Jones, B.G.: "A bleed-type pressure transducer for in-stream measurements of static pressure fluctuations", Rev. Scientific Instrum. 42 (1971), 450-454.

- [34] Fuchs, H.V.: "Turbulent pressure data relevant to air frame noise sources", DLR-FB 76-09 (1976).
- [35] Ackermann, U.: "Instabilitätswellen in einem runden, turbulenten Freistrah und ihre Schallabstrahlung", Univ. Göttingen, Dissert. (1976).
- [36] Kompenhans, J.: "Das akustische Verhalten überströmter Öffnungen in Abhängigkeit von der Wandgrenzschicht", Univ. Göttingen, Dissert. (1976).
- [37] Neise, W.: "The change of microphone sensitivity under mean flow conditions", J. Sound Vib. 43 (1975), 53-60.
- [38] "Determination of sound power levels of noise sources - In-duct method", Intern. Organization for Standardization ISO/DIS 5136.
- [39] Lau, J.C.: "The coherent structure of jets", Univ. Southampton, Ph. D. Thesis (1971).
- [40] Neuwerth, G.: "Akustische Rückkopplungserscheinungen am Unter- und Überschall-Freistrah, der auf einen Störkörper trifft", DLR-FB 72-72 (1972).
- [41] Sidcon, T.E.: "Noise source diagnostics using causality correlations", AGARD-CP-131 (1974), Paper 7.
- [42] Armstrong, R.R.;  
Michalke, A.;  
Fuchs, H.V.: "Coherent structures in jet turbulence and noise", AIAA-Journal 15 (1977), 1011-1017.
- [43] Neise, W.;  
Stahl, F.: "The flow noise level of microphones in flow ducts", J. Sound Vib., 63 (1979), 561-579.

## LIST OF SYMBOLS

$a$	sound propagation speed
$a_0$	speed of sound in medium at rest
$A_0$	source strength
$\bar{C}_i$	mean flow velocity vector (Fig. 1)
$C$	source convection factor (Eq. (2.54))
$d$	pressure probe diameter
$f$	frequency
$L$	acoustic pressure fluctuation level (dB)
$L_c$	coherence length scale
$L_p$	aerodynamic pressure fluctuation level (Eq. (4.12))
$L_s$	source length scale
$M$	flow Mach number (Eq. (2.10))
$M_c$	Mach number of relative motion (Eq. (2.11))
$M_r$	Mach number of source and observer in motion (Eq. (2.66))
$M_j$	jet exit Mach number
$M_o$	Mach number of observer in motion (Eq. (2.63))
$M_s$	Mach number of source in motion (Eq. (2.46))
$p$	pressure
$\hat{p}_0$	pressure amplitude radiated by a stationary source in a medium at rest (Eq. (2.39))
$Q$	source
$r_b$	source-observer distance
$r^b$	source-observer distance in Lorentz system (Eq. (2.13))
$R$	source-observer distance at the time of emission
$R_1$	defined in Eq. (2.48)
$t$	time
$t_r$	retarded time (Eq. (2.45))
$\bar{u}$	speed at which source moves (Fig. 2)
$v_i$	particle velocity vector
$x_i$	fixed (Cartesian) coordinates
$x_i^I$	Galilean-transformed coordinates (Eq. (2.2))
$x_i^*$	Lorentz-transformed coordinates (Eq. (2.8))
$x_{i,a}$	flow coordinates (Eq. (2.5))
$x_{i,b}$	specified Lorentz coordinates (Eq. (2.12))
$x_{i,c}$	source coordinates (Eq. (2.16))
$\gamma$	coefficient defined in Eqs. (4.6) and (4.7)
$\theta$	observation angle between $r$ and the direction of motion (Table 2)
$\Theta$	emission angle between $R$ and the direction of motion (Table 2)
$\lambda$	acoustic wave length
$\Lambda_x$	axial scale of a flow inhomogeneity
$\rho_0$	fluid density
$\phi$	velocity potential
$\omega_0$	source frequency
$\omega^b$	frequency in Lorentz system
$\omega, \Omega$	radian frequency

AGARD Report No.686 Advisory Group for Aerospace Research and Development, NATO SPECIAL COURSE ON ACOUSTIC WAVE PROPAGATION Published August 1979 234 pages  The Special Course dealt with the propagation of acoustic waves in inhomogeneous and moving media of both unlimited and finite extent. Recent theoretical and experimental work was reviewed, with particular emphasis on modelling of the phenomena involved and on prediction methods, as well as standardization aspects. The fundamental phenomena treated include: reflection, refraction, scattering, diffraction and P.T.O.	AGARD-R-686  Elastic waves Acoustic scattering Sound transmission Acoustic measurement Atmospheric attenuation Aircraft noise Noise (sound)	AGARD Report No.686 Advisory Group for Aerospace Research and Development, NATO SPECIAL COURSE ON ACOUSTIC WAVE PROPAGATION Published August 1979 234 pages  The Special Course dealt with the propagation of acoustic waves in inhomogeneous and moving media of both unlimited and finite extent. Recent theoretical and experimental work was reviewed, with particular emphasis on modelling of the phenomena involved and on prediction methods, as well as standardization aspects. The fundamental phenomena treated include: reflection, refraction, scattering, diffraction and P.T.O.	AGARD-R-686  Elastic waves Acoustic scattering Sound transmission Acoustic measurement Atmospheric attenuation Aircraft noise Noise (sound)
AGARD Report No.686 Advisory Group for Aerospace Research and Development, NATO SPECIAL COURSE ON ACOUSTIC WAVE PROPAGATION Published August 1979 234 pages  The Special Course dealt with the propagation of acoustic waves in inhomogeneous and moving media of both unlimited and finite extent. Recent theoretical and experimental work was reviewed, with particular emphasis on modelling of the phenomena involved and on prediction methods, as well as standardization aspects. The fundamental phenomena treated include: reflection, refraction, scattering, diffraction and P.T.O.	AGARD-R-686  Elastic waves Acoustic scattering Sound transmission Acoustic measurement Atmospheric attenuation Aircraft noise Noise (sound)	AGARD Report No.686 Advisory Group for Aerospace Research and Development, NATO SPECIAL COURSE ON ACOUSTIC WAVE PROPAGATION Published August 1979 234 pages  The Special Course dealt with the propagation of acoustic waves in inhomogeneous and moving media of both unlimited and finite extent. Recent theoretical and experimental work was reviewed, with particular emphasis on modelling of the phenomena involved and on prediction methods, as well as standardization aspects. The fundamental phenomena treated include: reflection, refraction, scattering, diffraction and P.T.O.	AGARD-R-686  Elastic waves Acoustic scattering Sound transmission Acoustic measurement Atmospheric attenuation Aircraft noise Noise (sound)

<p>attenuation. Measurement techniques and data analysis were also considered. Applications of the material presented occur in aeroacoustics, industrial acoustics and atmospheric propagation.</p> <p>The material assembled was presented at the AGARD-Von Kármán Institute Special Course on Acoustic Wave Propagation presented at the VKI 28 May-1 June 1979.</p> <p>ISBN 92-835-0248-5</p>	<p>attenuation. Measurement techniques and data analysis were also considered. Applications of the material presented occur in aeroacoustics, industrial acoustics and atmospheric propagation.</p> <p>The material assembled was presented at the AGARD-Von Kármán Institute Special Course on Acoustic Wave Propagation presented at the VKI 28 May-1 June 1979.</p> <p>ISBN 92-835-0248-5</p>
<p>attenuation. Measurement techniques and data analysis were also considered. Applications of the material presented occur in aeroacoustics, industrial acoustics and atmospheric propagation.</p> <p>The material assembled was presented at the AGARD-Von Kármán Institute Special Course on Acoustic Wave Propagation presented at the VKI 28 May-1 June 1979.</p> <p>ISBN 92-835-0248-5</p>	<p>attenuation. Measurement techniques and data analysis were also considered. Applications of the material presented occur in aeroacoustics, industrial acoustics and atmospheric propagation.</p> <p>The material assembled was presented at the AGARD-Von Kármán Institute Special Course on Acoustic Wave Propagation presented at the VKI 28 May-1 June 1979.</p> <p>ISBN 92-835-0248-5</p>



8752  
4

# AGARD

NATO OTAN

7 RUE ANCELLE 92200 NEUILLY-SUR-SEINE  
FRANCE

Telephone 745.08.10 - Telex 610176

DISTRIBUTION OF UNCLASSIFIED  
AGARD PUBLICATIONS

AGARD does NOT hold stocks of AGARD publications at the above address for general distribution. Initial distribution of AGARD publications is made to AGARD Member Nations through the following National Distribution Centres. Further copies are sometimes available from these Centres, but if not may be purchased in Microfiche or Photocopy form from the Purchase Agencies listed below.

## NATIONAL DISTRIBUTION CENTRES

### BELGIUM

Coordonnateur AGARD - VSL  
Etat-Major de la Force Aérienne  
Quartier Reine Elisabeth  
Rue d'Evere, 1140 Bruxelles

### CANADA

Defence Scientific Information Service  
Department of National Defence  
Ottawa, Ontario K1A 0Z2

### DENMARK

Danish Defence Research Board  
Østerbrogades Kaserne  
Copenhagen Ø

### FRANCE

O.N.E.R.A. (Direction)  
29 Avenue de la Division Leclerc  
92 Châtillon sous Bagneux

### GERMANY

Zentralstelle für Luft- und Raumfahrt-  
dokumentation und -information  
c/o Fachinformationszentrum Energie,  
Physik, Mathematik GmbH  
Kernforschungszentrum  
7514 Eggenstein-Leopoldshafen 2

### GREECE

Hellenic Air Force General Staff  
Research and Development Directorate  
Holargos, Athens, Greece

### ICELAND

Director of Aviation  
c/o Flugrad  
Reykjavik

### UNITED STATES

National Aeronautics and Space Administration (NASA)  
Langley Field, Virginia 23365  
Attn: Report Distribution and Storage Unit

THE UNITED STATES NATIONAL DISTRIBUTION CENTRE (NASA) DOES NOT HOLD  
STOCKS OF AGARD PUBLICATIONS, AND APPLICATIONS FOR COPIES SHOULD BE MADE  
DIRECT TO THE NATIONAL TECHNICAL INFORMATION SERVICE (NTIS) AT THE ADDRESS BELOW.

### ITALY

Aeronautica Militare  
Ufficio del Delegato Nazionale all'AGARD  
3, Piazzale Adenauer  
Roma/EUR

### LUXEMBOURG

See Belgium

### NETHERLANDS

Netherlands Delegation to AGARD  
National Aerospace Laboratory, NLR  
P.O. Box 126  
Delft

### NORWAY

Norwegian Defence Research Establishment  
Main Library  
P.O. Box 25  
N-2007 Kjeller

### PORTUGAL

Direcção do Serviço de Material  
da Força Aérea  
Rua da Escola Politécnica 42  
Lisboa  
Attn: AGARD National Delegate

### TURKEY

Department of Research and Development (ARGE)  
Ministry of National Defence, Ankara

### UNITED KINGDOM

Defence Research Information Centre  
Station Square House  
St. Mary Cray  
Orpington, Kent BR5 3RE

## PURCHASE AGENCIES

### Microfiche or Photocopy

National Technical  
Information Service (NTIS)  
5285 Port Royal Road  
Springfield  
Virginia 22161, USA

### Microfiche

Space Documentation Service  
European Space Agency  
10, rue Mario Nikis  
75015 Paris, France

### Microfiche

Technology Reports  
Centre (DTI)  
Station Square House  
St. Mary Cray  
Orpington, Kent: BR5 3RE  
England

Requests for microfiche or photocopies of AGARD documents should include the AGARD serial number, title, author or editor, and publication date. Requests to NTIS should include the NASA accession report number. Full bibliographical references and abstracts of AGARD publications are given in the following journals.

Scientific and Technical Aerospace Reports (STAR)  
published by NASA Scientific and Technical  
Information Facility  
Post Office Box 8757  
Baltimore/Washington International Airport  
Maryland 21240, USA

Government Reports Announcements (GRA)  
published by the National Technical  
Information Services, Springfield  
Virginia 22161, USA



Printed by Technical Editing and Reproduction Ltd  
Harford House, 7-9 Charlotte St, London W1P 1HD

ISBN 92-835-0248-5